26
8-8-80

CONF-7910160 Vol. I
PNL-SA-8571

CONF-7910160--(vol. 1)

Waste Isolation Safety Assessment Program

Task 4
Third Contractor Information Meeting
Volume I

MASTER

J. F. Relyea, Chairman

Seattle, Washington
October 14-17, 1979

Prepared for the
Office of Nuclear Waste Isolation
under its Contract with the
U.S. Department of Energy

Pacific Northwest Laboratory
Operated for the U.S. Department of Energy
by Battelle Memorial Institute

Battelle

PNL-SA-8571 Vol. I

DISTRIBUTION OF THIS DOCUMENT IS UNLIMITED

DISCLAIMER

This report was prepared as an account of work sponsored by an agency of the United States Government. Neither the United States Government nor any agency Thereof, nor any of their employees, makes any warranty, express or implied, or assumes any legal liability or responsibility for the accuracy, completeness, or usefulness of any information, apparatus, product, or process disclosed, or represents that its use would not infringe privately owned rights. Reference herein to any specific commercial product, process, or service by trade name, trademark, manufacturer, or otherwise does not necessarily constitute or imply its endorsement, recommendation, or favoring by the United States Government or any agency thereof. The views and opinions of authors expressed herein do not necessarily state or reflect those of the United States Government or any agency thereof.

DISCLAIMER

Portions of this document may be illegible in electronic image products. Images are produced from the best available original document.

NOTICE

This report was prepared as an account of work sponsored by the United States Government. Neither the United States nor the Department of Energy, nor any of their employees, nor any of their contractors, subcontractors, or their employees, makes any warranty, express or implied, or assumes any legal liability or responsibility for the accuracy, completeness or usefulness of any information, apparatus, product or process disclosed, or represents that its use would not infringe privately owned rights.

The views, opinions and conclusions contained in this report are those of the contractor and do not necessarily represent those of the United States Government or the United States Department of Energy.

PACIFIC NORTHWEST LABORATORY
operated by
BATTELLE
for the
UNITED STATES DEPARTMENT OF ENERGY
Under Contract DE-AC06-76RLO 1830

Printed in the United States of America
Available from
National Technical Information Service
United States Department of Commerce
5285 Port Royal Road
Springfield, Virginia 22151

Price: Printed Copy $_____*; Microfiche $3.00

*Pages	NTIS Selling Price
001-025	$4.00
026-050	$4.50
051-075	$5.25
076-100	$6.00
101-125	$6.50
126-150	$7.25
151-175	$8.00
176-200	$9.00
201-225	$9.25
226-250	$9.50
251-275	$10.75
276-300	$11.00

CONF-7910160 Vol. I
PNL-SA-8571

Waste Isolation Safety Assessment Program

TASK 4
THIRD CONTRACTOR INFORMATION MEETING

VOLUME I

J. F. Relyea, Chairman

Held at
Battelle Memorial Institute,
Human Affairs Research Centers
Seattle, Washington 98105
October 14-17, 1979

June 1980

Prepared for
the Office of Nuclear Waste Isolation
under its contract with the
U.S. Department of Energy
DE-AC06-76RLO 1830

DISCLAIMER

This book was prepared as an account of work sponsored by an agency of the United States Government. Neither the United States Government nor any agency thereof, nor any of their employees, makes any warranty, express or implied, or assumes any legal liability or responsibility for the accuracy, completeness, or usefulness of any information, apparatus, product, or process disclosed, or represents that its use would not infringe privately owned rights. Reference herein to any specific commercial product, process, or service by trade name, trademark, manufacturer, or otherwise, does not necessarily constitute or imply its endorsement, recommendation, or favoring by the United States Government or any agency thereof. The views and opinions of authors expressed herein do not necessarily state or reflect those of the United States Government or any agency thereof.

Pacific Northwest Laboratory
Richland, Washington 99352

DISTRIBUTION OF THIS DOCUMENT IS UNLIMITED

EDITORS' NOTE: The views expressed in the papers and discussions remain the responsibility of the authors or participants where identified. Portions of the report have been reproduced directly from the best available copy.

PREFACE

The WISAP Task 4, Third Contractor Information Meeting was held in Seattle, Washington, October 14-17, 1979. The purpose of the meeting was to:

- present an overview of ONWI needs and schedules
- present an overview of WISAP goals and methodology
- reiterate Task 4 objectives
- present technical accomplishments of subcontractors during FY-1979.

We are grateful to Gary Brock of the Battelle Memorial Institute, Human Affairs Research Centers, and John Burlison of Pacific Northwest Laboratory, for careful recording of notes on the discussions, for preparing the transcripts, and for editorial assistance. Sue Gano of Pacific Northwest Laboratory provided additional assistance.

We also wish to thank Jody Marshall and Jolene Kitzerow of Battelle for their help in conference organization and logistical support. We are grateful to the rest of the Battelle-Seattle conference staff who were responsible for lodging, food, and audio-visual services.

Finally, the effort of guest speakers and attendees--whose participation led to lively discussions and program redirection and guidance--is much appreciated.

This research was supported by the Waste Isolation Safety Assessment Program (WISAP) conducted by Pacific Northwest Laboratory. This program was sponsored by the Office of Nuclear Waste Isolation, which is managed by Battelle Memorial Institute under contract DE-AC06-76RLO 1830 with the U.S. Department of Energy.

THIS PAGE

WAS INTENTIONALLY

LEFT BLANK

CONTENTS

VOLUME I

PREFACE iii

INTRODUCTION ix

AGENDA xi

ABSTRACTS xv

TECHNICAL REPORTS . . . . . .

STATISTICAL INVESTIGATION OF THE MECHANICS CONTROLLING RADIONUCLIDE SORPTION. Anthony N. Mucciardi, Thomas C. Johnson, Julia Saunier, Adaptronics, Inc. 1

QUESTIONS AND ANSWERS 69

TRANSPORT OF RADIONUCLIDES IN GEOLOGIC MEDIA. M. G. Seitz, P. G. Rickert, R. A. Couture, J. Williams, N. Meldgin, S. M. Fried, A. M. Friedman, and M. J. Steindler, Argonne National Laboratory 77

QUESTIONS AND ANSWERS 149

SURFACE MIGRATION OF RADIOACTIVE WASTE MATERIALS BY PARTICULATE TRANSPORT. Geoffrey G. Eichholz and T. F. Craft, editors, Georgia Institute of Technology 155

QUESTIONS AND ANSWERS 245

THEORETICAL AND EXPERIMENTAL EVALUATION OF WASTE TRANSPORT IN SELECTED ROCKS. R. J. Silva, L. V. Benson, A. W. Yee and G. A. Parks, Lawrence Berkeley Laboratory 249

QUESTIONS AND ANSWERS 353

GEOCHEMICAL STUDIES OF SORPTION AND TRANSPORT OF RADIONUCLIDES IN ROCK MEDIA. David G. Coles, Homer C. Weed, John D. Tewhey, Lawrence Livermore Laboratory. 357

QUESTIONS AND ANSWERS 423

LABORATORY STUDIES OF RADIONUCLIDE DISTRIBUTION BETWEEN SELECTED GROUNDWATERS AND GEOLOGIC MEDIA. B. R. Erdal, Los Alamos Scientific Laboratory 435

QUESTIONS AND ANSWERS 523

VOLUME II

PREFACE iii

INTRODUCTION ix

AGENDA xi

ABSTRACTS xv

TECHNICAL REPORTS . . . . . .

SYSTEMATIC STUDY OF NUCLIDE ADSORPTION ON SELECTED GEOLOGIC MEDIA. R. E. Meyer, Oak Ridge National Laboratory 1

QUESTIONS AND ANSWERS 75

SORPTION-DESORPTION OF LONG-LIVED RADIONUCLIDE SPECIES ON GEOLOGIC MEDIA. C. W. Francis and E. A. Bondietti, Oak Ridge National Laboratory 81

QUESTIONS AND ANSWERS 133

LABORATORY STUDIES OF Pu-237 SORPTION ON SELECTED MINERALS UNDER ANOXIC CONDITIONS. J. F. Relyea, R. J. Serne, R. W. Fulton, C. D. Washburne and W. J. Martin, Pacific Northwest Laboratory . . 135

EFFECTS OF HYDROGEN PEROXIDE PRETREATMENT OF CLAY MINERALS ON THE ADSORPTION OF Sr-85 AND Tc-95m UNDER ANOXIC CONDITIONS. J. F. Relyea and C. D. Washburne, Pacific Northwest Laboratory . . 159

SORPTION BEHAVIOR OF ^{85}Sr, ^{137}Cs AND ^{95m}Tc UNDER NORMAL ATMOSPHERIC AND REDUCED OXYGEN LEVELS. J. F. Relyea, C. D. Washburne and R. W. Fulton, Pacific Northwest Laboratory 173

QUESTIONS AND ANSWERS 207

INTERACTION OF PLUTONYL (VI) WITH SOIL MINERALS. Dhanpat Rai, R. J. Serne, D. A. Moore, Pacific Northwest Laboratory 213

SOLUBILITY OF PLUTONIUM COMPOUNDS AND THEIR BEHAVIOR IN SOILS. Dhanpat Rai, R. J. Serne, D. A. Moore, Pacific Northwest Laboratory 235

QUESTIONS AND ANSWERS 257

THE KINETICS AND REVERSIBILITY OF RADIONUCLIDE SORPTION REACTIONS WITH ROCKS. G. Scott Barney, Glenda E. Brown, Rockwell Hanford Operations 261

QUESTIONS AND ANSWERS 309

GENERAL DISCUSSION 317

APPENDIX A - PARTICIPANT LIST A.1

APPENDIX B - OVERVIEW OF WRIT PROGRAM B.1

THIS PAGE

WAS INTENTIONALLY

LEFT BLANK

INTRODUCTION

The Contractor Information Meeting (October 14-17, 1979) was part of the FY-1979 effort of Task 4 of the Waste Isolation Safety Assessment Program (WISAP): "Sorption/Desorption Analysis." The objectives of this task are to:

- evaluate sorption/desorption measurement methods and develop a standardized measurement procedure
- produce a generic data bank of nuclide-geologic interactions using a wide variety of geologic media and groundwaters
- perform statistical analysis and synthesis of these data
- perform validation studies to compare short-term laboratory studies to long-term in situ behavior
- develop a fundamental understanding of sorption/desorption processes
- produce X-ray and gamma-emitting isotopes suitable for the study of actinides at tracer concentrations
- disseminate resulting information to the international technical community
- provide input data support for repository safety assessment.

To accomplish these objectives, the experimental program initiated in FY-1977 is continuing with the assistance of ten scientific groups at national laboratories and private institutions.

The purpose of the Contractor Information Meeting was to:

- present an overview of ONWI needs and schedules
- present an overview of WISAP goals and methodology
- reiterate Task 4 objectives
- present technical accomplishments of subcontractors during FY-1979
- encourage information and idea exchange with other representatives of related programs
- solicit program critiques and peer review.

Conference participants included those subcontracted to WISAP Task 4, representatives and independent subcontractors to the Office of Nuclear Waste Isolation, representatives from other waste disposal programs, and experts in the area of waste/geologic media interaction.

Since the meeting, WISAP has been divided into two programs: Assessment of Effectiveness of Geologic Isolation Systems (AEGIS) (modeling efforts) and Waste/Rock Interactions Technology (WRIT) (experimental work). The WRIT program encompasses the work conducted under Task 4.

This report contains the information presented at the Task 4, Third Contractor Information Meeting. Technical Reports from the subcontractors, as well as Pacific Northwest Laboratory (PNL), are provided along with transcripts of the question-and-answer sessions. The agenda and abstracts of the presentations are also included. Appendix A is a list of the participants. Appendix B gives an overview of the WRIT program and details the WRIT work breakdown structure for 1980.

AGENDA

Sunday (October 14)

6:00-9:00 p.m.	Registration/Dinner

Monday (October 15)

8:00-9:00 a.m.	Overview of ONWI/WISAP/Task 4 R. J. Serne Session I: Experimental Methodology and Data Acquisition; Subtasks 4.1 and 4.2
9:00-9:45 a.m.	(1a) "Effects of Hydrogen Peroxide Pretreatment of Clay Minerals on the Adsorption of Sr-85 and Tc-95m Under Anoxic Conditions." J. F. Relyea and C. D. Washburne, PNL (1b) "Laboratory Studies of Pu-237 on Selected Minerals Under Anoxic Conditions." J. F. Relyea, R. J. Serne, R. W. Fulton, C. D. Washburne, and W. J. Martin, PNL
9:45-10:05 a.m.	(2) "Cesium Sorption on SiO_2 and Smectites." R. J. Silva, LBL
10:05-10:15 a.m.	Break
10:15-10:45 a.m.	(3) "Transport of Radionuclides in Geologic Media: Methods. P. Rickert, ANL
10:45-11:15 a.m.	(4) "Systematic Study of Nuclide Adsorption on Selected Geologic Media; Experimental Methodology and Data Acquisition." R. E. Meyer, ORNL
11:15-11:45 a.m.	(5a) "Strontium, Technetium, and Tritium Transport in Tuff and Sandstone Cores." H. C. Weed, LLL (5b) "Observations on a Batch Kd Technique Using Filtration at Various Stages." D. G. Coles, LLL
11:45-12:15 p.m.	Discussion
12:15-1:15 p.m.	Lunch
1:15-1:45 p.m.	(6) "Sorption of Technetium on Geologic Media Under Anoxic Conditions." C. W. Francis and E. A. Bondietti, ORNL

1:45-2:15 p.m.	(7) "The Kinetics and Reversibility of Radionuclide Reactions with Basalt, Granite, and Argillite." G. S. Barney, RHO
2:15-2:30 p.m.	Break
2:30-3:30 p.m.	(8a) "Sorption of Salt Dome Materials: Uranium (VI) and Technetium (VII)." B. R. Erdal, D. P. Bayhurst, S. J. DeVilliers, F. O. Lawrence, and E. N. Vine, LASL
	(8b) "Effects of Anoxic Conditions and Water Composition on Sorption-Desorption." S. J. DeVilliers, D. P. Bayhurst, W. R. Daniels, B. R. Erdal, F. O. Lawrence, and E. N. Vine, LASL
	(8c) "Behavior of Plutonium and Americium." W. R. Daniels and F. O. Lawrence, E. N. Vine, P. Q. Oliver, and S. Maestas, LASL
	(8d) "Dynamic (Column) Studies of Radionuclide Migration Rates." E. N. Vine, LASL
3:30-4:00 p.m.	Discussion
	Session II: Data Synthesis; Subtask 4.3
4:00-5:00 p.m.	(9) "Statistical Investigation of the Mechanics Controlling Radionuclide Sorption." T. C. Johnson and A. N. Mucciardi, Adaptronics
5:00-5:30 p.m.	Discussion

Tuesday, (October 16)

	Session III: Verification Studies; Subtask 4.4
8:00-8:40 a.m.	(10) "Testing a Site-Binding Electrical Double-Layer Model for Predicting Kd Values." L. W. Benson and R. J. Silva, LBL; G. A. Parks, Stanford University
8:40-8:55 a.m.	(11) "Calculation of Chemical Equilibrium Between Aqueous Solution and Minerals: The EQ3/6 Software Package." T. J. Wolery, LLL
8:55-9:15 a.m.	Discussion
	Session IV: Mechanism Studies; Subtask 4.5
9:15-9:55 a.m.	(12a) "Adsorption of Plutonyl by Aerated Soil Minerals." D. Rai, D. A. Moore, and R. J. Serne, PNL

	(12b) "Solubility of Plutonium Compounds and Their Behavior in Soils." D. Rai, R. J. Serne, and D. A. Moore, PNL
9:55-10:05 a.m.	Break
10:05-10:40 a.m.	(13) "Transport of Radionuclides in Geologic Media--Mechanisms." M. G. Seitz, ANL
10:40-11:10 a.m.	(14) "Systematic Study of Nuclide Adsorption on Selected Geologic Media-Mechanisms of Adsorption." R. E. Meyer, ORNL
11:10-11:40 a.m.	(15) "Sorption of Americium and Neptunium on Geologic Media." G. W. Beall and B. Allard, ORNL
11:40-12:00 noon	(16) "A Systematic Study of the Kd Values for 15 Sandstones Having a Wide Range of Mineralogical Composition." D. G. Coles, LLL
12:00-1:00 p.m.	Lunch
1:00-1:20 p.m.	(17) "Sorption of Radionuclides on Weathered Rocks." G. E. Brown, G. S. Barney, RHO
1:20-1:50 p.m.	(18) "Microautoradiographic Studies of Rock Thin-Sections and Cores." J. L. Thompson, W. R. Daniels, and S. Maestas, LASL
1:50-2:40 p.m.	(19) "Subsurface Migration of Radioactive Waste Materials by Particulate Transport." G. G. Eichholz, GIT
2:40-3:00 p.m.	(20) "The Valence States of the Actinides in Natural Waters and Sorption on Geologic Media Under Anoxic Conditions." B. Allard and G. W. Beall, ORNL
3:00-3:20 p.m.	Discussion
3:20-3:35 p.m.	Break
3:35-6:00 p.m.	Guest Speakers and Discussion (Sandia, USGS, Atomic Energy of Canada)
6:00 p.m.	Dinner

<u>Wednesday (October 17)</u>

8:00-12:00 noon	General Discussion of WISAP Task 4

THIS PAGE

WAS INTENTIONALLY

LEFT BLANK

ABSTRACTS

(1a) Effects of Hydrogen Peroxide Pretreatment of Clay Minerals on the Adsorption of Sr-85 and Tc-95m Under Anoxic Conditions. J. G. Relyea*, and C. D. Washburne, Pacific Northwest Laboratory.

Treatment of three clay minerals with hydrogen peroxide affects the observed adsorption behavior of technetium relative to untreated clay under anoxic conditions. A possible adsorption mechanism of Tc is the reduction of TcO_4 to a more positively charged species. Oxidation of the clay by H_2O_2 would hinder the reduction of the TcO_4 by buffering the clay-water system at a higher Eh value.

(1b) Laboratory Studies of Pu-237 Sorption on Selected Minerals Under Anoxic Conditions. J. F. Relyea*, R. J. Serne, R. W. Fulton, C. D. Washburne, and W. J. Martin, Pacific Northwest Laboratory.

Plutonium Kd values were generally higher under anoxic conditions than ambient conditions in both 5.13N NaCl and 0.03N $CaCl_2$. Lower values for Kd(Pu) were observed in 0.03N $NaHCO_3$ under anoxic than in an ambient atmosphere and no significant differences were found in Kd(Pu) values in 0.03N NaCl for the two oxygen levels. Sorption of Pu was greatest on the phyllosilicates (illite, montmorillonite, vermiculite, and biotite).

The blank-corrected batch Kd method is not well suited for measuring low Kd values when the tracer nuclide is sorbed by the blank container. Measurement of the amount of nuclide sorbed by the blank container can be used to correct calculated Kd values; however, the process doubles the radioanalytical counting requirements over the normal blank-corrected batch method. Containers which do not adsorb tracer nuclides should be used, if possible.

(2) Cesium Sorption on SiO_2 and Smectites. R. J. Silva*, Lawrence Berkeley Laboratory.

No abstract available.

(3) Transport of Radionuclides in Geologic Media-Methods. Paul Rickert*, Argonne National Laboratory.

(1) Nuclide migration by infiltration versus that predicted by batch Kd, (2) batch experiments that reproduce column geometry, (3) analyses of radionuclides on particles by dialyses techniques, (4) leach-migration experiments, and (5) our new rock column holders with pressurized Teflon sleeves.

(4) Systematic Study of Nuclide Adsorption on Selected Geologic Media - Experimental Methodology and Data Acquisition. R. E. Meyer*, Oak Ridge National Laboratory.

Distribution coefficients have been determined as a function of solution variables for a variety of adsorption systems. Last year, we concentrated on studies of adsorption of a number of ions on clay minerals at low pH values where complications due to hydroloysis and precipitation are minimized. We also showed in the systems tested that essentially identical results were obtained using all three of our methods of measuring distribution coefficients, batch, column, and axial filtration. This year we have concentrated on extending adsorption studies to higher pH ranges more characteristic of natural systems, usually from about 4 to 10. The nuclides studies were Cs(I), Sr(II), Eu(III), I^-, Tc(VII), Am(III), Np(V), and U(VI) in various NaCl solutions and a simulated groundwater, all as a function of pH. Clay minerals included montmorillonite, kaolinite, illite, and attapulgite, and hydrous oxides included chromatographic alumina, Corundum, Gibbsite, and Hematite.

Iodide adsorption was studied in a variety of solutions for a number of minerals and rocks including most of the controlled sample rocks. The work on actinide adsorption (supported in part by the Division of Nuclear Sciences/BES) included studies of the adsorption of Am, Np(V), and U(VI) as a function of pH on a large number of rock-forming minerals. Strong increases with pH were observed for a number of systems including Sr(II) and Eu(III) on the hydrous oxides and Am(III) on many of the rock-forming minerals. For some cases, for example, Sr(II) on montmorillonite, little or no dependence on pH was found.

(5a) Strontium, Technetium, and Tritium Transport in Tuff and Sandstone Cores. H. C. Weed*, Lawrence Livermore Laboratory.

Radionuclide transport experiments have been conducted at room temperature and 10MPa confining pressure on cores of Thirsty Canyon tuff with tuff-equilibrated water and St. Peter sandstone with sandstone-equilibrated water. The radionuclides are Sr-85, Tc-95m, and T as HTO. Results will be presented in the form of concentration profiles for the cores, concentration vs. time curves for the effluent solutions, and sorption ratio values derived from these measurements.

(5b) Observations on a Batch Kd Technique Using Filtration at Various Stages in the Procedure. David G. Coles*, Lawrence Livermore Laboratory.

Simulated groundwater that has been equilibrated with various radiotracers is first filtered through an 0.4 μm pore size filter before contacting it with the geologic media being studied. Implications to the final Kd value derived using this technique are discussed. In particular, filtration is compared to simple centrifugation as a phase separation method.

(6) Sorption to Tc on Geologic Media Under Anoxic Conditions. C. W. Francis*, and E. A. Bondietti, Oak Ridge National Laboratory.

The influence of time, temperature, pH, Eh, Fe^{+2}, and Tc concentrations on the sorption-desorption of Tc on a basalt, granite, and shale was investigated. Loss of the TcO_4^- anion from the solution phase appears not to be due to sorption of the anion on the solid phase matrix, but rather due to the reduction to a lower oxidation state; probably TcO_2 which is highly water-insoluble. Loss of TcO_4^- increased with time. There appears to be an interaction between the reduction of TcO_4^- and temperature, viz, increasing temperature enhanced the initial reduction rate, but the rate exponentially decayed at high temperatures (72 vs. 22°C). Basalt significantly reduced TcO_4^- faster and in greater quantities than the granite or shale samples. On the order of 10^6 more Tc-99 was retained on anoxic basalt columns than Tc-95m; however, the apparent distribution coefficients (0.64 and 3.54 ml/g) were not appreciably different. The additions of Fe^{+2} prior to TcO_4^- additions did not affect TcO_4^- reduction; however, additions of Fe^{+2} to TcO_4^- suspensions readily reduced TcO_4^-. The reduced form of Tc is slowly oxidized to the TcO_4^- under oxic conditions. In Eh-pH monitored stirred suspensions, the most important variables influencing the loss of TcO_4^- are Eh and the solution to solid ratio of the suspension.

(7) The Kinetics and Reversibility of Radionuclide Reactions with Basalt, Granite, and Argillite. G. S. Barney*, Rockwell Hanford Operations.

Observations of sorption-desorption reactions of Cs, Sr, Np, Am, and Pu on basalt, granite, and argillite were extended to 218 days. Equilibrium concentrations of radionuclides in batch experiments were not reached for most radionuclides even after this lengthy equilibration time. In addition, reactions of the crushed rock with groundwaters (dissolution, hydrolysis, precipitation, etc.) did not reach equilibrium after 150 days. The dissolution of

basalt is accompanied by the formation of colloidal particles which contain Si, Fe, Ca, and Al. These colloids sorb Cs, Sr, Am, and Pu during equilibration experiments. Some of the colloids pass through 0.3 μm filters (some are not retained even on 0.01 m filters) and therefore cause calculated Kd values to be too low.

Additional experiments were performed to determine the effects of radionuclide concentration on Kd values and to measure the reversibility of radionuclide sorption. Several improvements were incorporated into these experimental procedures. Spiked solutions were filtered to eliminate precipitation of tracers before equilibration and dried tracers were added to groundwater solutions to prevent alteration of solution composition by the tracer stock solution.

(8a) Sorption of Salt Dome Materials, Uranium(VI), and Technetium(VII).
B. R. Erdal*, B. P. Bayhurst, S. J. DeVilliers, F. O. Lawrence, and E. N. Vine.

Studies of the sorption of strontium, cesium, barium, cerium, europium, uranium, and americium on Hainesville salt dome materials were made under aerobic and anaerobic (less than 0.2 ppm oxygen) conditions. Results using a dilute brine and a bicarbonate water will be presented.

Results from investigations of the sorption-desorption of uranium (VI) and technetium(VII) on various Nevada Test Site (NTS) materials under aerobic and anerobic conditions, at ambient and elevated (70°C) temperature, will also be presented.

(8b) Effects of Anoxic Conditions and Water Composition on Sorption-Desorption. S. J. DeVilliers*, B. P. Bayhurst, W. R. Daniels, B. R. Erdal, F. O. Lawrence, and E. N. Vine.

The sorption-desorption behavior of several radionuclides under conditions of very low oxygen concentration (less than 0.2 ppm), as may be present in deep geologic formations, was studied using the batch technqiue. Samples of argillite, granite, and Yucca Mountain tuff from the NTS were used. Comparisons will be made between these measurements and those made earlier using the same materials.

The effect of groundwater composition on the measured sorption-desorption behavior for strontium, cesium, barium, cerium, and europium was studied using two groundwaters having rather different ionic strengths. The geologic materials used were argillite, granite, and tuff from the NTS, all ground to the same particle size. The dependence of the Rd values on the groundwater composition will be discussed.

(8c) Behavior of Plutonium and Americium. W. R. Daniels*, F. O. Lawrence, P. Q. Oliver, and S. Maestas.

The behavior of Pu and Am during batch sorption ratio measurements was studied. A multiple-centrifuging technique resulted in aqueous solutions of Pu which were not altered by subsequent filtration, even through membranes as small as 0.05 μm. This result implies that the particulates present in these solutions (pH = 8) were smaller than 0.05 μm and that the Pu species present did not sorb on the filter membranes, at least during the time required for filtration. Results for Am indicate that solutions prepared in the same way as the Pu still contain Am species which are removed by filtration.

The effects of passing various soloutions involved in the batch sorption ratio measurements through polycarbonate membranes were studied by a microautoradiographic technique.

The results from sorption-desorption studies on granite, argillite, and tuff will also be discussed.

(8d) Dynamic (Column) Studies on Radionuclide Migration Rates. E. N. Vine*.

The migration rates of radionuclides in columns of crushed material from three types of geologic media (argillite, granite, and tuff from the NTS), and some of the parameters affecting these rates, will be discussed and compared to data previously obtained by a static (batch) technique.

(9) Statistical Investigation of the Mechanics Controlling Radionuclide Sorption. A. N. Mucciardi*, Adaptronics, Inc.

Nonlinear, adaptive learning network (ALN) models were synthesized that predict Kd for seven radionuclides (Tc, Sr, Cs, Np, Am, I, Pu) as a function of solid adsorbent, contacting solution and nuclide properties. Factors that were considered in this year's work included: (1) analysis of reversibility (adsorption versus desorption Kd's), (2) comparison of the Kd predictor equation on dilute waters versus salt brine, (3) comparison of Kd predictor equations on individual adsorbents versus groups of adsorbents, (4) analysis of the ORNL Ion Exchange data base, and (5) identification of the key variables controlling Kd for each radionuclide. Results of the predictor equations on data not used for model synthesis will be presented.

(10) Testing a Site-Binding Electrical Double-Layer Model for Predicting Kd Values. L. V. Benson*, and R. J. Silva, Lawrence Berkeley Laboratory; and G. A. Parks, Stanford University.

No abstract available.

(11) Calculation of Chemical Equilibrium Between Aqueous Solution and Minerals: The EQ3/6 Software Package. Thomas J. Wolery*, Lawrence Livermore Laboratory.

The newly developed EQ3/6 software package computes equilibrium models of aqueous geochemical systems. The package contains two principal programs: EQ3 performs distribution-of-species calculations for natural water compositions; EQ6 uses the results of EQ3 to predict the consequence of heating and cooling aqueous solutions and of irreversible reaction in rock-water systems. The programs are valuable for studying such phenomena as the formation of ore bodies, scaling and plugging in geothermal development, and the long-term disposal of nuclear waste.

(12a) Adsorption of Plutonyl by Aerated Soil Minerals. Dhanpat Rai*, D. A. Moore, and R. J. Serne, Pacific Northwest Laboratory.

Plutonyl(VI) was added to aerated mineral suspensions (1 g mineral and 34 ml of 10 meq $CaCl_2$) maintained at pH 4. The concentration of Pu in 0.015 m filtered solutions was determined at different time intervals.

The maximum adsorption occurred within the first two hours. The minerals differed considerably in their adsorption capacities. The minerals in an increasing order of adsorption were: gibbsite < kaolinite < montmorillonite << vermiculite $\leq$ biotite. In order to understand this difference in behavior

of various minerals, cation exchange capacity, surface area, chemical nature of the surfaces, and the chemical makeup of the minerals were determined. The results showed that the very high adsorption of plutonyl by vermiculite and biotite was largely due to the presence of ferrous iron in their structure which reduced plutonyl to very highly adsorbable species [Pu(III) and/or Pu(IV)].

(12b) Solubility of Plutonium Compounds and Their Behavior in Soils. Dhanpat Rai*, R. J. Serne, and D. A. Moore, Pacific Northwest Laboratory.

The solubilities of $^{239}PuO_2(s)$ and $^{239}Pu(OH)_4(s)$ under natural environmental conditions were determined. These data were then used to predict the 1) nature of the solid phases present in contaminated soils, and 2) total concentration of Pu that can be expected in soil solutions when these Pu solids are present.

Based upon solubility measurements, an estimated value of the log K° (equilibrium constant) for the dissolution of $^{239}PuO_2(s)$ [$PuO_2(s) \rightleftharpoons PuO_2$] + e^- was found to be -14.8. The estimated value of the log K° for the dissolution of $^{239}Pu(OH)_4(s)$ [$Pu(OH)_4(s) \rightleftharpoons PuO_2 + 2\ H_2O + e^-$] was found to be -12.8.

Comparison of Pu concentration, in solutions in equilibrium with contaminated Hanford soils, with the $PuO_2(s)$ and $Pu(OH)_4(s)$ solubility lines indicated that $Pu(OH)_4(s)$ was absent from all the samples and that two of the samples contained $PuO_2(s)$. The presence of $PuO_2(s)$ was also confirmed by X-ray diffraction of Pu particles isolated from one of the samples.

(13) Transport of Radionuclides in Geologic Media - Mechanisms. Martin G. Seitz*, Argonne National Laboratory.

(1) Non-linear adsorption isotherms related to concentration expected in groundwater after leaching solidified waste, (2) rock loadings and limits they place on nuclide immobilization, (3) competing cation effects, Rb-Cs as an example and (4) recommendations for more detailed groundwater analysis to serve the need of the repository designer.

(14) Systematic Study of Nuclide Adsorption on Selected Geologic Media: Mechanisms of Adsorption. R. E. Meyer*, Oak Ridge National Laboratory.

The adsorption experiments at low pH values (4 to 5) were designed to test the applicability of ideal ion exchange equations to the data. These equations predict that at loadings small compared to the capacity, slopes of plots of the logarithm of the distribution coefficient versus the logarithm of the sodium chloride concentration should be -2 for divalent ion adsorption, -3 for trivalent ion adsorption, etc. Such slopes were observed for a number of cases, especially at low pH, but, in general, slopes were somewhat less than the ideal values. For other adsorption systems, e.g. Eu(III) on montmorillonite at intermediate to high pH, little or no salt dependency was found. For some systems the logarithm of the distribution coefficient increased approximately linearly with pH. Loading studies show many cases where adsorption follows an essentially linear isotherm from trace to intermediate loadings and expected decreases in distribution coefficient as loading becomes significant with respect to the capacity. In other cases, more complicated dependencies of the distribution coefficient with loading was found. Various explanations for this loading behavior and the pH dependence of adsorption are considered with respect to our data.

(15) Sorption of Americium and Neptunium on Geologic Media. G. W. Beall* and B. Allard, Oak Ridge National Laboratory.

No abstract available.

(16) A Systematic Study of the Kd Values for 15 Sandstones Having a Wide Range of Mineralogical Composition. David G. Coles*.

Kd measurements have been made on 15 sandstones using a simulated brine as the aqueous phase. These sandstones were chosen for their wide range of mineralogical compositions and have been extensively characterized both physically and mineralogically. The effects of the Kd's for Se-75, Sr-85, Sb-125, Cs-137, Ce-144, and Pu-237 are discussed in terms of size fraction and mineralogical variation.

(17) Sorption of Radionuclides on Weathered Rocks. G. E. Brown*, Rockwell Hanford Operations.

Samples of crushed basalt, granite, and argillite were artificially "weathered" by continuous leaching with distilled water for six months. The leaching was performed both in air and in an oxygen-free stream of nitrogen gas. The "weathered" rock was then characterized to determine surface area, cation exchange capacity, and composition of the weathered surface of the rock. Comparisons were made of radionuclide sorption (after 14 days) on fresh rock, rock weathered in air, and rock weathered in N_2. Although there are some exceptions, sorption on rocks weathered in N_2 is less than rock weathered in air. This is possibly due to the lack of an $Fe(OH)_3$ coating on the rock weathered in N_2. The $Fe(OH)_3$ is known to scavenge cations and silica from solution. Sorption of Cs, Am, and Pu is strongly affected by weathering basalt and argillite.

However, the cation exchange capacity is changed very little. This suggests that ion exchange plays a minor role in sorption of these radionuclides.

(18) Microautoradiographic Studies of Rock Thin-Sections and Cores. J. L. Thompson*, W. R. Daniels, and S. Maestas.

Characteristics of Pu-239 and Np-237 sorption on alluvium, tuff, granite, and argillite thin-sections as determined by microautoradiography will be discussed. Also several experiments will be described in which Sr-85 or U-238 was infused into solid rock cores, yielding sorption data which may be compared with that obtained by batch and column methods. Microautoradiographic examination of these rock cores will also be discussed.

(19) Subsurface Migration of Radioactive Waste Materials by Particulate Transport. G. G. Eichholz*, Georgia Institute of Technology.

The objective of this work is the study of the uptake of dissolved radionuclides leached from waste material by water onto suspended colloidal particulates and their subsequent transport through permeable media. Vertical column packed with basalt, limestone and other media have been set up to observe the migration of labeled particles. It has been shown that such particles do, in fact, migrate and are absorbed to a degree depending on the type of particle and bed medium rather than physical hindrance. The attachment on waste ions on such particles has been observed from distilled water, rock-equilibrated and saline waters and, as expected, depends on concentration, competition with other dissolved ions, pH and effective surface area. The latter does not necessarily stay constant since agglomeration of kaolin particles occurs in brines. The implication of this on migration in salt beds and in adjacent strata is also being studied.

(20) The Valence States of the Actinides in Natural Waters and Sorption on Geologic Media Under Anoxic Conditions. B. Allard* and G. W. Beall, Oak Ridge National Laboratory.

No abstract available.

TECHNICAL REPORTS

VOLUME I

ADI Ref. 548

ANNUAL REPORT

STATISTICAL INVESTIGATION OF THE MECHANICS CONTROLLING RADIONUCLIDE SORPTION

Anthony N. Mucciardi
Thomas C. Johnson
Julia Saunier

December 1979

Submitted to:

BATTELLE-PACIFIC NORTHWEST LABORATORIES
P.O. Box 999
Richland, WA 99352
Attention: Mr. Jeff Serne

Special Agreement No. B-70741-A-K

Submitted by:

ADAPTRONICS, INC.
1750 Old Meadow Road
McLean, VA 22102

THIS PAGE

WAS INTENTIONALLY

LEFT BLANK

FOREWORD

This annual report documents results of the project entitled "Investigation of the Mechanics Controlling Radionuclide Sorption," conducted for Battelle Memorial Institute, Pacific Northwest Laboratories. This report covers work performed during the period March 15, 1979 through September 30, 1979.

The Project Manager for Adaptronics was Dr. Anthony N. Mucciardi.

The authors thank Mr. Jeff Serne and Dr. John Relyea of Battelle for their guidance throughout this year's efforts.

ABSTRACT

The focus of this year's work was to resynthesize ALN predictive K_d models using a larger set of solid/solution variables, especially solid chemistry and mineralogy. Empirical predictive models were developed for each of seven nuclides (Tc, Sr, Cs, Np, Am, I, Pu) measured on 16 solid adsorbents (12 minerals and 4 rocks) in contact with four solutions (1 brine and 3 dilute). A sensitivity (i.e., partial derivative) analysis was then conducted to establish a rank-ordering of the importance of each solid/ solution variable for predicting the K_d of a given nuclide. A minimal and rank-ordered set of key solid/solution variables has been constructed for each nuclide/solid/solution system studied.

The feasibility of constructing a solid adsorbent K_d model from a weighted sum of individual mineral or mineral group K_d models was established for certain nuclide/solid/solution systems. The advantage of this approach is that the potential exists for computing an approximate value of K_d for a new solid/ solution system without conducting experiments.

It is shown that the ALN modeling protocol has the capability of "rediscovering" the classical ion exchange equation when this form of the transport equation is appropriate for a given nuclide/bulk ion system. In systems where this is not the most appropriate form, the ALN equation produced an "improved" transport equation.

1. INTRODUCTION

1.1 PROJECT OBJECTIVE

The primary objective of this year's statement of work was described in the Battelle Purchase Order as "Analysis of PNL Data Base...Adaptronics will be supplied an experimental data base consisting of the K_d adsorption and K_d desorption of seven elements (Tc, Sr, Cs, Np, Am, I, Pu) measured on 16 solid adsorbents in contact with four solutions. Of paramount importance will be analysis of the data to produce a mathematical model employing adaptive learning network (ALN) protocol describing K_d as a function of solid adsorbent, contacting solution and nuclide properties as performed on previous data sets [3,4]."

1.2 WORK TASKS

The following work tasks were established to accomplish the project objectives:

(1) Univariate Statistical Results - correlate the effects of some of the independent variables on one another

(2) Adsorption-Desorption Reversibility - compare the adsorption and desorption K_d's to establish if the reaction is reversible

(3) K_d Predictive ALN Models - synthesize empirical ALN K_d models that are a nonlinear function of solid and solution variables

(4) Solid/Solution Variable Importance - after model synthesis, perform a sensitivity analysis on the variables selected per model to rank-order their effect on K_d

(5) Dilute Waters vs. Salt Brine Comparison - compare the ALN K_d models synthesized for each solution type to find differences

(6) Individual vs. Group Adsorbent Models - establish feasibility of constructing a solid K_d adsorbent model from a weighted sum of individual mineral or mineral group models

(7) Ion Exchange Data Base Analysis - compare ALN models to classical ion exchange (transport) models for common isotope/bulk ion systems.

1.3 REPORT ORGANIZATION

The data base and its format used for Tasks (1) - (6) is summarized in Section 2. The remaining sections are organized as:

Report Section	Work Task(s)
3	(1)
4	(2)
5	(3),(4),(5)
6	(6)
7	(7)

2. RADIONUCLIDE K_d DATA BASE

2.1 INTRODUCTION

A data base was required to synthesize the empirical K_d models. The results of a series of experiments to measure the K_d of several nuclides in various geological media were provided by Pacific Northwest Laboratory (PNL) [1,3,4].

2.2 CHARACTERISTICS OF THE DATA BASE

Experiments utilizing different approaches were performed by PNL to obtain the K_d for various geological materials and solutions. Seven radionuclides were studied, each in media comprised of combinations of 16 solid adsorbents and four solutions as shown in Table 2.1. The K_d was measured three times over an interval of 30 days (although only the results at the 30-day interval were used in this study [3,4]). Each nuclide-mineral-solution experiment was repeated three times. In addition, many of the experiments were run under aerobic and anerobic (i.e., anoxic) conditions. The experimental data base was then transmitted to Adaptronics. The data base summary form is shown in Tables 2.1 and 2.2.

The 16 solids can be classified into four groups as shown in Table 2.3. Most of the analyses in the remainder of the report are discussed as a function of this grouping.

Both adsorption and desorption experiments were conducted. Adsorption results were obtained for all nuclide-mineral group-solution combinations, but desorption data were only obtained selectively. That is, desorption experiments were not conducted on the Group 4 Rocks for any nuclide. Also, some of the adsorption or desorption data were rather sparse for a particular nuclide-mineral-solution combination due to experimental equipment problems, etc. Table 2.4 shows the data that were used in these analyses.

The soil chemistry and mineralogy data were obtained from Ames [1].

TABLE 2.1: DESCRIPTION OF BATTELLE EXPERIMENTAL DATA BASE

3 Experiments x 7 Isotopes x 4 Solutions x 16 Solids

ISOTOPES		SOLUTIONS	
Tc	Technetium	5130 Meq/l NaCl	Salt Brine
Sr	Strontium	30 Meq/l $CaCl_2$	Calcium Dominated
Cs	Cesium	30 Meq/l NaCl	Dilute Brine
Np	Neptunium	30 Meq/l $NaHCO_3$	Bicarbonate Dominated
Am	Americium		
I	Iodine		
Pu	Plutonium		

SOLIDS

Illite
Kaolinite
Montmorillnite
Vermiculite
Biotite
Quartz
Albite
Anorthite
Microcline
Hornblende
Enstatite
Augite
Argillaceous Shale
Westerly Granite
Oolitic Limestone
Sentinal Gap Basalt

TABLE 2.2: FORMAT OF EACH 66-WORD DATA RECORD

1. RECORD NUMBER
2. ADSORPTION/DESORPTION FLAG (0 = A, 1 = D)
3. ISOTOPE (Tc, Sr, Cs, Np, Am, I, Pu) (= 1 - 7)
4. SOLID (= 1 - 16)
5. SOLUTION (5.13 N NaCl, 0.03 N $CaCl_2$, 0.03 N NaCl, 0.03 $NaHCO_3$) (= 1 - 4)
6. DAYS (NUMBER OF DAYS OF EXPERIMENT)
7. REPLICATION (1, 2, 3)
8. K_D
9. Q (CHARGE)
10. R (IONIC RADIUS)
11. Q/R (IONIC POTENTIAL)
12. V (VALENCE)
13. pH (ACID-BASE BALANCE)
14. Eh (OXIDATION-REDUCTION POTENTIAL, Eh(0) = Eh + 59 pH IS THE CORRECTED Eh)
15. SA (ETHYLENE GLYCOL SURFACE AREA)
16. BET (SURFACE AREA)
17. CEC (CATION EXCHANGE CAPACITY)

TABLE 2.2 (CONT'D)

SOLID CHEMISTRY IN PERCENTAGE

18. SiO_2
19. TiO_2
20. Al_2O_3
21. FeO
22. CaO
23. MgO
24. K_2O
25. Na_2O
26. MnO
27. P_2O_5
28. CO_2

IONIC CONCENTRATIONS

54. CO_3
55. HCO_3
56. Cl
57. SO_4
58. Al
59. Ca
60. Fe
61. K
62. Mg
63. Na
64. Sr
65. Si
66. AEROGNOSY (1 = AEROBIC, -1 = ANEROBIC)[1/]

SOLID MINERALOGY IN PERCENTAGE

29. ILLITE (ILL)
30. KAOLINITE (KAO)
31. MONTMORILLINITE (MON)
32. VERMICULITE (VER)
33. BIOTITE (BIO)
34. QUARTZ (QTZ)
35. MICROCLINE (MIC)
36. HORNBLENDE (HOR)
37. ENSTATITE (ENS)
38. ILMENITE (ILM)
39. OLIGOCLASE (OLIG)
40. MUSCOVITE (MUS)
41. CALCITE (CAL)
42. GARNET (GAR)
43. MAGNETITE (MAG)
44. SALITE (SAL)
45. RUTILE (RUT)
46. ANDESINE (AND)
47. ENDIOPSIDE (END)
48. PLAGIOCLASE (PLA)
49. CLAYS (CLY)
50. PYROXENES (PYR)
51. GROUNDMASS (GRM)
52. METALLIC OXIDES (MET)
53. HEMATITE (HEM)

[1/] ANEROBIC AND ANOXIC ARE USED INTERCHANGEABLY IN THIS REPORT.

TABLE 2.3: MINERAL GROUPS

Group 1 - Phyllosilicates

Illite
Kaolinite
Montmorillinite
Vermiculite
Biotite

Group 2 - Tektosilicates

Quartz
Albite
Anorthite
Microcline

Group 3 - Inosilicates

Hornblende
Enstatite
Augite

Group 4 - Rocks

Argillaceous Shale
Westerly Granite
Oolitic Limestone
Sentinal Gap Basalt

TABLE 2.4: TOTAL USABLE EXPERIMENTAL DATA 1/ 2/

ADSORPTION

ISOTOPE	ALL GROUPS	GROUP 1 PHYLLOSILICATES	GROUP 2 TEKTOSILICATES	GROUP 3 INOSILICATES	GROUP 4 ROCKS
TECHNETIUM	X	X	X	X	X
STRONTIUM	X	X	X	X	X
CESIUM	X	X	X	X	X
NEPTUNIUM	X	X	X	X	
AMERICUM	X	X	X	X	
IODINE	X	X	X	X	
PLUTONIUM	X	X	X	X	

DESORPTION

ISOTOPE	ALL GROUPS	GROUP 1 PHYLLOSILICATES	GROUP 2 TEKTOSILICATES	GROUP 3 INOSILICATES	GROUP 4 ROCKS
TECHNETIUM	X	X	X	X	
STRONTIUM	X	X	X	X	
CESIUM	X	X	X	X	
NEPTUNIUM	X	X	X	X	
AMERICIUM	X	X	X	X	
IODINE	X	X	X		
PLUTONIUM					

1 AN "X" MEANS THAT DATA WERE USABLE.

2 EACH OF THE ABOVE USABLE EXPERIMENTS WAS RUN UNDER AEROBIC AND ANEROBIC CONDITIONS.

3. UNIVARIATE STATISTICAL RESULTS

This section contains the results of a small series of univariate correlation results required in Task 1.4 of the Work Statement; the correlation coefficients are:

(a) BET surface area vs. ethylene glycol surface area -- not performed due to only four BET surface area values (for the rocks) in the entire data base.

(b) BET surface area vs. cation exchange capacity -- same as in (a).

(c) Ethylene glycol surface area vs. cation exchange capacity -- 0.870 (for 7 isotopes, 4 solutions and 16 solids).

(d) Ion content of water vs. Eh -- 0.083.

(e) K_d dependence on Eh when Fe^{+} in solution is greater than 0.1 ppm -- -0.039.

There were approximately 50 observations used for the computation in (c), (d), and (e). Part (c) is statistically significant at a level greater than 0.001.

4. ADSORPTION-DESORPTION REVERSIBILITY

The objective of this task was to establish the sorption reversibility for various isotope-mineral-solution combinations. A t-test was employed to determine the statistical significance of the following hypothesis: that the adsorption and desorption K_d's were derived from the same population (H_0) versus the alternative hypothesis that the two sets of K_d's were derived from different populations (H_1). Acceptance of the H_0 (termed the null hypothesis) implies that the reaction is reversible; rejection of the first hypothesis (i.e., acceptance of H_1) implies that the reaction is irreversible.

For each mineral and isotope tested, a t-value for the adsorption and desorption K_d's was computed as:

$$t = \frac{\bar{K}_d(D) - \bar{K}_d(A)}{\sigma(2/N)^{1/2}}$$

where,

$$\sigma^2 = \frac{(N-1)\sigma_A^2 + (N-1)\sigma_D^2}{2(N-1)}$$

$\bar{K}_d(D)$ = desorption mean K_d

$\bar{K}_d(A)$ = adsorption mean K_d

The computed t-value was compared to tabular values [2] using a two-sided test: the absolute value, $|t|$, was taken; to determine whether or not the difference was significant so as to reject the reversible hypothesis, the absolute t-value was found in the table and compared to the computed value.

The table contains confidence limits that the null hypothesis should be rejected, i.e., a vote in favor of irreversibility. The criteria used were as follows: If the computed t-value exceeded the 95% confidence limit, the reaction was declared to be nonreversible; if t was less than the 95% confidence level and greater than the 75% confidence level limit, the reaction was declared to be weakly reversible; otherwise, if t was less than the 75% limit, the reaction was declared to be reversible.

The t-test was performed for K_d as well as for $\log_{10} K_d$ values. The reason for the latter transformation was to not bias the t value by a few very large K_d values (thereby biasing the means). The logarithmic transformation was:

$$\log K_d = \begin{cases} \log K_d, & K_d \geq 1 \\ 0, & K_d < 1 \end{cases}$$

Also, the t values for each nuclide and solid were computed over all four solutions and for both aerobic and anerobic cases.

Tables 4.1 and 4.2 show the t-values, number of observations, (N), and significance level of the computed t value. Tables 4.3 and 4.4 summarize the results of the above analyses.

TABLE 4.1: t-VALUES, (NUMBER OF OBSERVATIONS) AND CONFIDENCE LEVEL FOR K_d

MINERAL	ISOTOPE Tc	Sr	Cs	Np	Am	I
Group 1 PHYLLOSILICATES						
ILLITE	-2.8815 (12) <.05	-2.3094 (12) <.05	-3.2047 (8) <.05	-0.0900 (8) >.25	-1.5232 (8) .05<p<.25	1.1777 (8) .05<p<.25
KAOLINITE	-0.9189 (12) >.25	-2.5272 (12) <.05	-1.1208 (8) .05<p<.25	0.7302 (8) .05<p<.25	-1.8956 (8) <.05	1.2084 (8) .05<p<.25
MONTMORILLONITE	3.4261 (12) <.05	-3.4115 (12) <.05	-2.7141 (8) <.05	0.6864 (8) >.25	-2.3635 (8) <.05	1.2245 (8) .05<p<.25
VERMICULITE	-0.1592 (12) .05<p<.25	-3.4624 (12) <.05	-2.4387 (8) <.05	0.7501 (8) .05<p<.25	-2.1670 (8) <.05	1.2038 (8) .05<p<.25
BIOTITE	-2.4317 (12) <.05	-2.0379 (12) <.05	0.7898 (8) .05<p<.25	1.1759 (8) .05<p<.25	0.5010 (8) >.25	1.1876 (8) .05<p<.25
Group 2 TEKTOSILICATES						
QUARTZ	-2.3989 (12) <.05	-2.5490 (12) <.05	-3.0495 (8) <.05	0.9926 (8) .05<p<.25	-2.7869 (8) <.05	1.2002 (8) .05<p<.25
ALBITE	-3.1529 (12) <.05	-2.3302 (12) <.05	-3.0491 (8) <.05	0.6185 (8) >.25	-2.1623 (8) <.05	1.2039 (8) .05<p<.25
ANORTHITE	-2.9689 (12) <.05	-2.9057 (12) <.05	-1.8015 (8) .05<p<.25	0.7496 (8) .05<p<.25	-2.5789 (8) <.05	1.2198 (8) .05<p<.25
MICROCLINE	3.2788 (12) <.05	-2.7021 (12) <.05	-2.9916 (8) <.05	0.8400 (8) .05<p<.25	-3.5766 (8) <.05	-
Group 3 INOSILICATES						
HORNBLENDE	-1.3401 (12) .05<p<.25	-2.4397 (12) <.05	-3.2552 (8) <.05	0.7183 (8) .05<p<.25	-2.2974 (8) <.05	-
ENSTATITE	0.8616 (12) .05<p<.25	-3.0468 (12) <.05	-0.1866 (8) >.25	0.3338 (8) >.25	-1.1956 (8) .05<p<.25	-
AUGITE	-2.2163 (12) <.05	-2.3196 (12) <.05	-1.5587 (8) .05<p<.25	0.8400 (8) .05<p<.25	-2.1715 (8) <.05	-

TABLE 4.2: t-VALUES, (NUMBER OF OBSERVATIONS) AND CONFIDENCE LEVEL FOR LOG_{10} K_d

MINERAL	ISOTOPE Tc	Sr	Cs	Np	Am	I
GROUP 1 PHYLLOSILICATES						
ILLITE	-5.3172 (12) <.05	-5.6046 (12) <.05	-7.1663 (8) <.05	-2.4048 (8) <.05	-4.7815 (8) <.05	0.4949 (8) >.25
KAOLINITE	-4.5424 (12) <.05	-3.9027 (12) <.05	-3.4763 (8) <.05	-0.4698 (8) >.25	-4.9712 (8) <.05	1.0400 (8) .05<p<.25
MONTMORILLONITE	-8.1128 (12) <.05	-5.9942 (12) <.05	-4.2351 (8) <.05	-1.9011 (8) <.05	-5.9297 (8) <.05	1.5675 (8) .05<p<.25
VERMICULITE	-5.1369 (12) <.05	-6.2368 (12) <.05	-5.8475 (8) <.05	-2.0363 (8) <.05	-5.3645 (8) <.05	1.1333 (8) .05<p<.25
BIOTITE	-6.4619 (12) <.05	-3.8084 (12) <.05	-1.3931 (8) .05<p<.25	-0.5746 (8) >.25	-1.7562 (8) .05<p<.25	0.6000 (8) >.25
Group 2 TEKTOSILICATES						
QUARTZ	-4.3045 (12) <.05	-6.3359 (12) <.05	-4.0006 (8) <.05	-0.9175 (8) .05<p<.25	-5.4800 (8) <.05	1.2036 (8) .05<p<.25
ALBITE	-4.5181 (12) <.05	-6.0442 (12) <.05	-4.0674 (8) <.05	-1.4858 (8) .05<p<.25	-4.9826 (8) <.05	1.0728 (8) .05<p<.25
ANORTHITE	-4.4563 (12) <.05	-6.0175 (12) <.05	-3.2103 (8) <.05	-1.4839 (8) .05<p<.25	-4.5967 (8) <.05	1.7251 (8) .05<p<.25
MICROCLINE	-4.6629 (12) <.05	-7.1862 (12) <.05	-7.8513 (8) <.05	-1.9027 (8) <.05	-7.4446 (8) <.05	-
Group 3 INOSILICATES						
HORNBLENDE	-6.6542 (12) <.05	-5.4721 (12) <.05	-3.9075 (8) <.05	-1.8439 (8) .05<p<.25	-4.9667 (8) <.05	-
ENSTATITE	-5.4807 (12) <.05	-5.7851 (12) <.05	-2.2370 (8) <.05	-2.5027 (8) <.05	-4.3116 (8) <.05	-
AUGITE	-8.3720 (12) <.05	-6.5128 (12) <.05	-2.8046 (8) <.05	-1.9027 (8) <.05	-4.7193 (8) <.05	-

TABLE 4.3: SUMMARY OF RESULTS FROM TABLE 4.1 (K_d - Form)

Mineral	ISOTOPE					
	Tc	Sr	Cs	Np	Am	I
PHYLLOSILICATES						
ILLITE	N-R	N-R	N-R	R	W-R	W-R
KAOLINITE	R	N-R	W-R	W-R	N-R	W-R
MONTMORILLONITE	N-R	N-R	N-R	R	N-R	W-R
VERMICULITE	W-R	N-R	N-R	W-R	N-R	W-R
BIOTITE	N-R	N-R	W-R	W-R	R	W-R
TEKTOSILICATES						
QUARTZ	N-R	N-R	N-R	W-R	N-R	W-R
ALBITE	N-R	N-R	N-R	R	N-R	W-R
ANORTHITE	N-R	N-R	W-R	W-R	N-R	W-R
MICROCLINE	N-R	N-R	N-R	W-R	N-R	L
INOSILICATES						
HORNBLENDE	W-R	N-R	N-R	W-R	N-R	L
ENSTATITE	W-R	N-R	R	R	W-R	L
AUGITE	N-R	N-R	W-R	W-R	N-R	L

R = Reversible
N-R = Not Reversible
W-R = Weakly Reversible
L = Lack of Data

TABLE 4.4: SUMMARY OF RESULTS FROM TABLE 4.2 ($Log_{10} K_d$ - Form)

Mineral	ISOTOPE					
	Tc	Sr	Cs	Np	Am	I
PHYLLOSILICATES						
ILLITE	N-R	N-R	N-R	N-R	N-R	R
KAOLINITE	N-R	N-R	N-R	R	N-R	W-R
MONTMORILLONITE	N-R	N-R	N-R	N-R	N-R	W-R
VERMICULITE	N-R	N-R	N-R	N-R	N-R	W-R
BIOTITE	N-R	N-R	W-R	R	W-R	R
TEKTOSILICATES						
QUARTZ	N-R	N-R	N-R	W-R	N-R	W-R
ALBITE	N-R	N-R	N-R	W-R	N-R	W-R
ANORTHITE	N-R	N-R	N-R	W-R	N-R	W-R
MICROCLINE	N-R	N-R	N-R	N-R	N-R	L
INOSILICATES						
HORNBLENDE	N-R	N-R	N-R	W-R	N-R	L
ENSTATITE	N-R	N-R	N-R	N-R	N-R	L
AUGITE	N-R	N-R	N-R	N-R	N-R	L

R = Reversible
N-R = Not Reversible
W-R = Weakly Reversible
L = Lack Of Data

5. K_d PREDICTIVE ALN MODELS

5.1 MODEL SYNTHESIS

Adaptive learning network (ALN) K_d predictive models were created for each nuclide that were valid for all 16 solids, adsorption and desorption, aerobic and anerobic, and particular solutions. A new ALN model synthesis algorithm, recently developed by Adaptronics, was used to obtain the predictive equations. This new algorithm does not require the use of training and test sets to control overfit -- a major improvement over previous algorithms. Also, the stop criteria has been made more adaptive and data-tailored.

The models were divided into three categories, depending upon the solution:

(I) Brine solution
(II) Dilute solution
(III) All (i.e., brine plus dilute) solutions.

These three K_d predictive equations are presented for each nuclide. The logarithm of the solution concentrations was taken in order to reduce the spread from the 30 to 5130 Meq/liter values. Also, the K_d's for most of the isotopes had ranges of values of several orders of magnitude, so a "modified" log function of the K_d's was modeled as the dependent variable. The modified log function was an approximation of a natural logarithm to allow for negative and small values of K_d:

$$K_d' = f(K_d) = \begin{cases} 1 + \ln K_d, & \text{if } K_d > 1 \\ K_d, & \text{if } -1 < K_d < 1 \\ -1 - \ln |K_d|, & \text{if } K_d < -1 \end{cases}$$

This approximation of a log function is linear between $K_d = \pm 1$. (The effect of negative K_d's is slight because there were very few and their values were close to zero.)

Eh was corrected according to:

$$Eh(0) = Eh(m) + 59\ pH(m)$$

where "m" means measured. Eh(0) and pH(m) were used for modeling purposes.

5.2 SENSITIVITY ANALYSIS

All model inputs and outputs were linearly scaled to zero mean and unit standard deviation to allow an evaluation of relative variable importance by comparison of coefficient magnitudes. The predominant mathematical terms of the models, in unitized partial derivative form, are shown below along with the ALN block diagrams. These partial derivatives are quantitative estimates of the relationships between variables. The derivatives were computed as follows:

(a) each variable was normalized by dividing it by the spread (or standard deviation) of all the measurements made on that variable, and,

(b) the percentage change in the network output was computed for a given percentage change in each input.

The assumption in this normalization procedure is that the range of variable values within the data base is indicative of the expected range of values which will be encountered in the physical system. (If this assumption is not true, the relative importance measures will be misleading and, in addition, the ALN models cannot be considered to be fully representative models since there were regions of "input space" which were not adequately fitted in the training process.) Each relative importance, then, is determined by experimentally testing the network to find that a 1% change on variable i leads to a p_i% change in the output K_d and that a 1% change on variable j leads to a p_j% change in K_d. The p_i's and p_j's can be viewed as partial derivatives of the network functions which indicate sensitivities of K_d to the input variables. The magnitudes of the sensitivities -- termed "normalized RMS sensitivity" and "normalized mean sensitivity" -- provide an approximate indication of the relative importance of each of the variables.

Since the networks are nonlinear, a 1% change on variable i will, in general, result in a different percentage change in K_d depending upon the initial value of the variable i and upon the values of all the other network inputs. Thus, for each variable, partial derivatives are taken at representative points throughout the input space and the results are averaged to obtain an overall sensitivity for that variable.

5.3 K_d PREDICTIVE EQUATIONS

The models for each of the seven nuclides are shown in Figures 5.1 through 5.7, respectively. Each figure consists of three parts -- one for each of the three solution cases described in Section 5.1 above.

Also shown in each ALN figure are the range of values over which the models were trained, the mean and standard deviation of the data, the model performance and a rank-ordering of the variables selected for each model (only those variables with a contribution of greater than 5% to the sensitivity measure are listed). Two correlation coefficients (between the true and estimated log K_d values) are given for model performance: one obtained on the data used for model synthesis, and the other is that which is <u>expected</u> on new data which were <u>not</u> used for model synthesis. The expected value is a measure of the accuracy of model predictions for new, previously unseen data.

5.4 RANK-ORDERING OF SOLID/SOLUTION VARIABLES

The variable rank-ordering was accomplished by the sensitivity anlysis procedure described above and is shown in Figures 5.1 through 5.7. The results of this analysis, as encoded in the figures, are summarized in Table 5.1. The table can be read either by variable (horizontally) or by nuclide (vertically). (The designations "strong," "moderate" and "weak" are arbitrary and relate to the relative normalized mean sensitivities.) For example, the variable Kaolinite (wt. %) has the following influence: (1) moderate negative and weak negative for Np and Pu, respectively, in brine, (2) large positive, large negative and moderate negative for Tc, Np and I, respectively, in the dilute solutions, and (3) moderate negative and weak negative for Tc and Cs, respectively in all four solutions. Continuing down the Tc column the

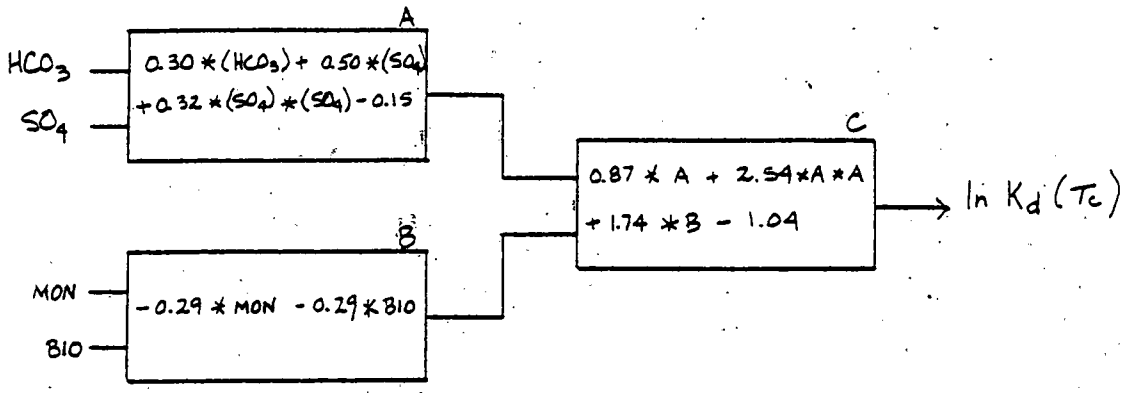

Range of Sorption Data (Log Form)

Min.	-4.38	Mean	3.280
Max.	10.47	St. dev.	3.130

Model Performance (based on predicting the log of sorption)

Correlation Coefficient for Data Used in Training	0.876
Expected Correlation Coefficient for New Data	0.807

Rank Ordered Variables

Variables	Normalized RMS Sensitivity	Normalized Mean Sensitivity
SO_4	22.812	6.138
HCO_3	5.926	1.604
Mon	1.637	-0.464
Bio	1.631	-0.463

FIGURE 5.1(a): PREDICTIVE MODEL FOR TECHNETIUM IN BRINE SOLUTIONS

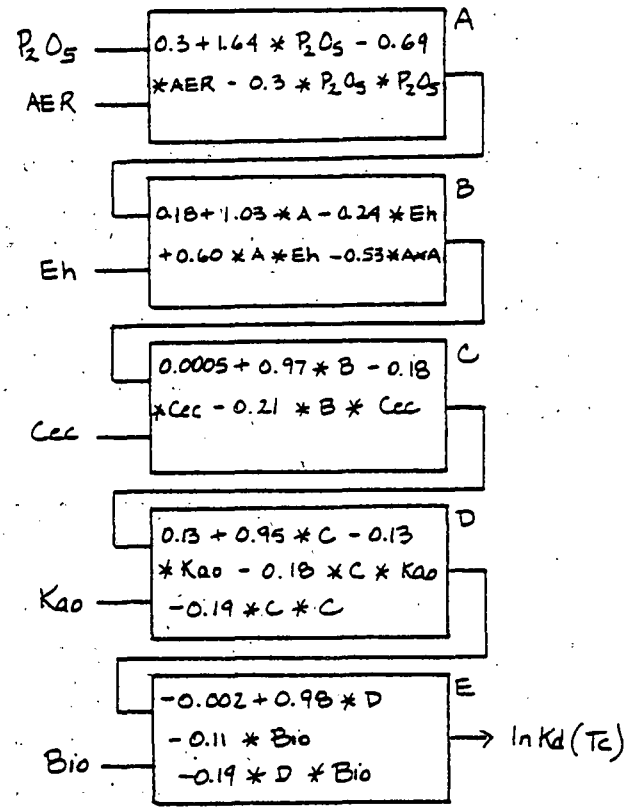

Range of Sorption Data (Log Form)

Min.	-6.35	Mean	2.380
Max.	9.28	St. dev.	3.578

Model Performance (based on predicting the log of sorption)

Correlation Coefficient for Data Used in Training	0.847
Expected Correlation Coefficient for New Data	0.791

Rank Ordered Variables

Variables	Normalized RMS Sensitivity	Normalized Mean Sensitivity
P_2O_5	22.200	8.365
Eh	18.964	4.903
Bio	18.286	4.405
Cec	17.989	4.127
AER	17.870	3.952
Kao	17.823	3.214

FIGURE 5.1(b): PREDICTIVE MODEL FOR TECHNETIUM IN DILUTE SOLUTIONS

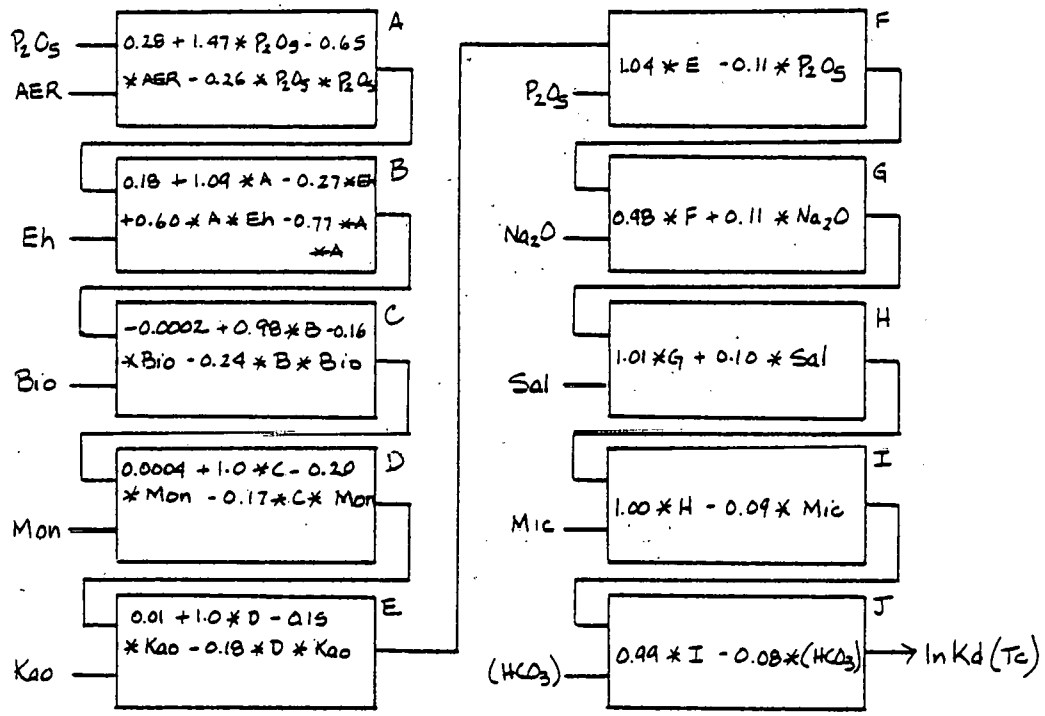

Range of Sorption Data (Log Form)

Min.	-6.35	Mean	2.609
Max.	10.47	St. dev.	3.492

Model Performance (based on predicting the log of sorption)

Correlation Coefficient for Data Used in Training	0.837
Expected Correlation Coefficient for New Data	0.783

Rank Ordered Variables

Variables	Normalized RMS Sensitivity	Normalized Mean Sensitivity
P_2O_5	8.273	2.668
AER	3.312	-1.096
Bio	1.351	-0.586
Mon	1.343	-0.584
Kao	1.155	-0.501
Na_2O	0.420	0.190
Sal	0.379	0.171
Eh	0.372	-0.149
Mic	0.329	0.137
HCO_3	0.295	-0.133

FIGURE 5.1(c): PREDICTIVE MODEL FOR TECHNETIUM IN ALL SOLUTIONS

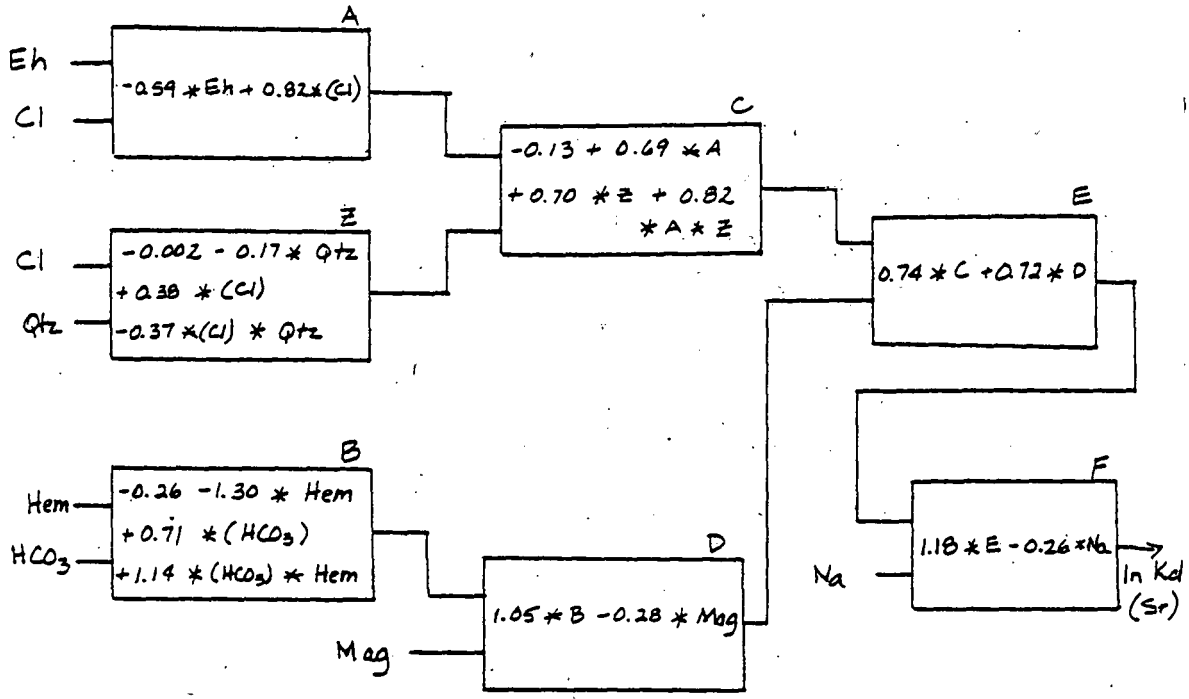

Range of Sorption Data (Log Form)

Min.	-3.57	Mean	1.674
Max.	5.92	St. dev.	2.184

Model Performance (based on predicting the log of sorption)

Correlation Coefficient for Data Used in Training	0.816
Expected Correlation Coefficient for New Data	0.669

Rank Ordered Variables

Variables	Normalized RMS Sensitivity	Normalized Mean Sensitivity
Hem	24.963	-9.025
Eh	24.898	-8.790
Qtz	24.886	-8.695
Na	24.528	-8.552
Mag	24.505	-8.531
HCO_3	23.974	-7.818
Cl	23.085	-7.086

FIGURE 5.2(a): PREDICTIVE MODEL FOR STRONTIUM IN BRINE SOLUTIONS

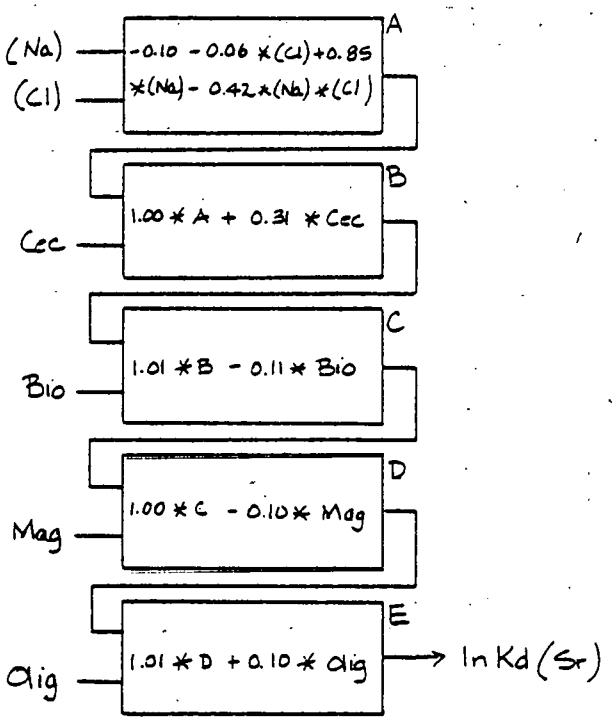

Range of Sorption Data (Log Form)

Min.	-3.17	Mean	4.838
Max.	10.34	St. dev.	2.501

Model Performance (based on predicting the log of sorption)

Correlation Coefficient for Data Used in Training	0.907
Expected Correlation Coefficient for New Data	0.877

Rank Ordered Variables

Variables	Normalized RMS Sensitivity	Normalized Mean Sensitivity
Na	4.190	2.004
Cl	0.937	-0.506
Cec	0.935	0.443
Bio	0.319	-0.168
Mag	0.300	-0.158
Olig	0.285	0.150

FIGURE 5.2(b): PREDICTIVE MODEL FOR STRONTIUM IN DILUTE SOLUTIONS

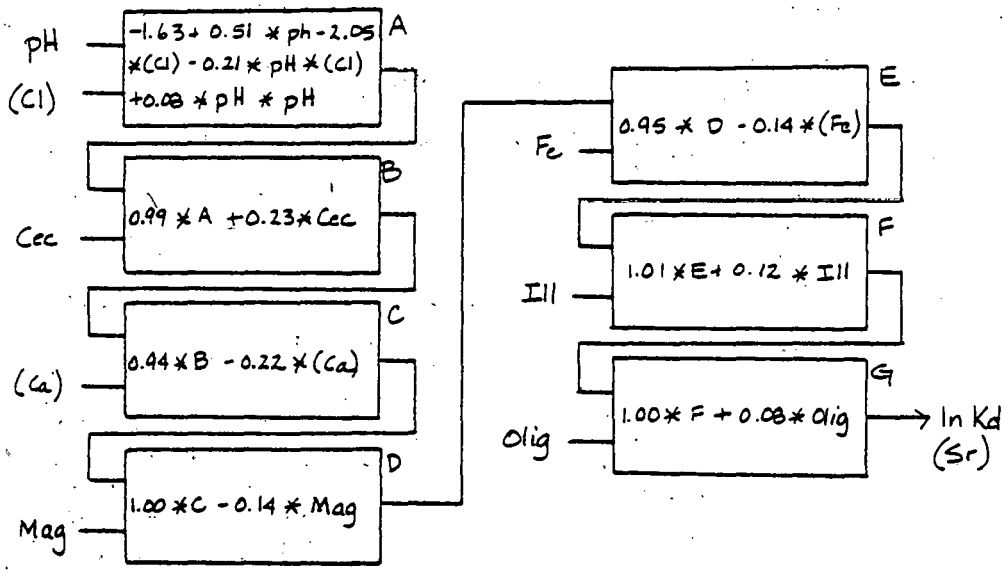

Range of Sorption Data (Log Form)

Min.	-3.57	Mean	4.033
Max.	10.34	St. dev.	2.783

Model Performance (based on predicting the log of sorption)

Correlation Coefficient for Data Used in Training	0.858
Expected Correlation Coefficient for New Data	0.824

Rank Ordered Variables

Variables	Normalized RMS Sensitivity	Normalized Mean Sensitivity
Cl	10.609	-4.441
pH	2.410	0.992
Ca	0.651	-0.277
Cec	0.644	0.274
Fe	0.433	-0.184
Mag	0.414	-0.176
Ill	0.364	0.155
Olig	0.247	0.105

FIGURE 5.2(c): PREDICTIVE MODEL FOR STRONTIUM IN ALL SOLUTIONS

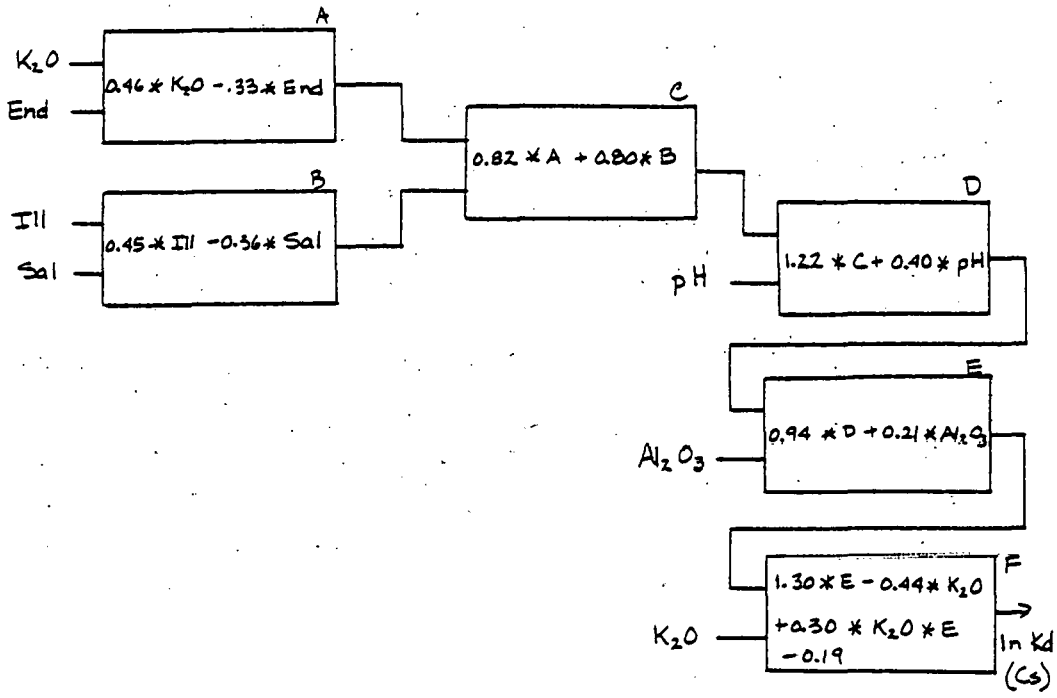

Range of Sorption Data (Log Form)

Min.	-3.51	Mean	3.418
Max.	8.73	St. dev.	2.884

Model Performance (based on predicting the log of sorption)

Correlation Coefficient for Data Used in Training	0.912
Expected Correlation Coefficient for New Data	0.811

Rank Ordered Variables

Variables	Normalized RMS Sensitivity	Normalized Mean Sensitivity
K_2O	2.310	0.652
Ill	2.041	0.615
pH	1.817	0.548
Sal	1.596	- 0.481
End	1.493	- 0.450
Al_2O_3	0.998	0.301

FIGURE 5.3(a): PREDICTIVE MODEL FOR CESIUM IN BRINE

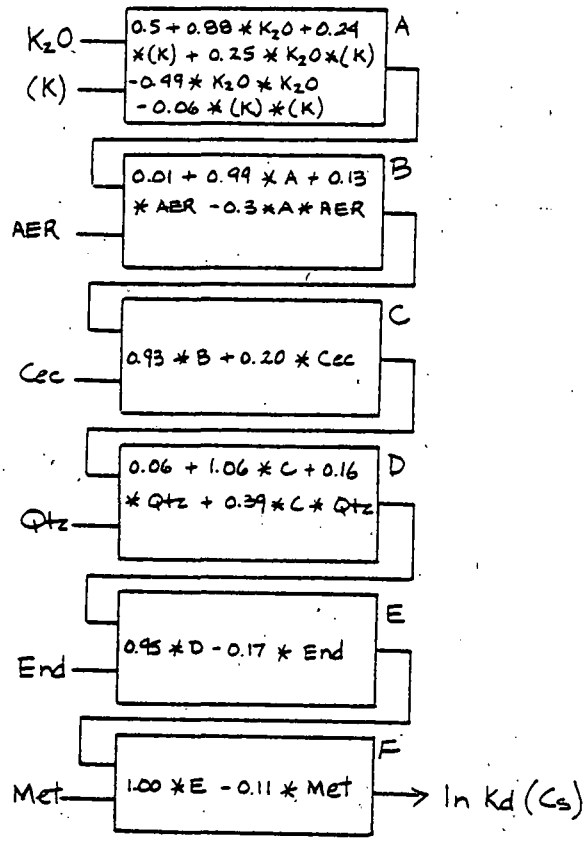

Range of Sorption Data (Log Form)

Min.	1.99	Mean	7.542
Max.	12.98	St. dev.	2.217

Model Performance (based on predicting the log of sorption)

Correlation Coefficient for Data Used in Training	0.743
Expected Correlation Coefficient for New Data	0.691

Rank Ordered Variables

Variables	Normalized RMS Sensitivity	Normalized Mean Sensitivity
K_2O	2.321	0.595
Qtz	2.035	0.592
AER	0.548	0.170
K	0.446	0.159
Cec	0.413	- 0.159
END	0.405	- 0.143
MET	0.253	- 0.099

FIGURE 5.3(b): PREDICTIVE MODEL FOR CESIUM IN DILUTE SOLUTIONS

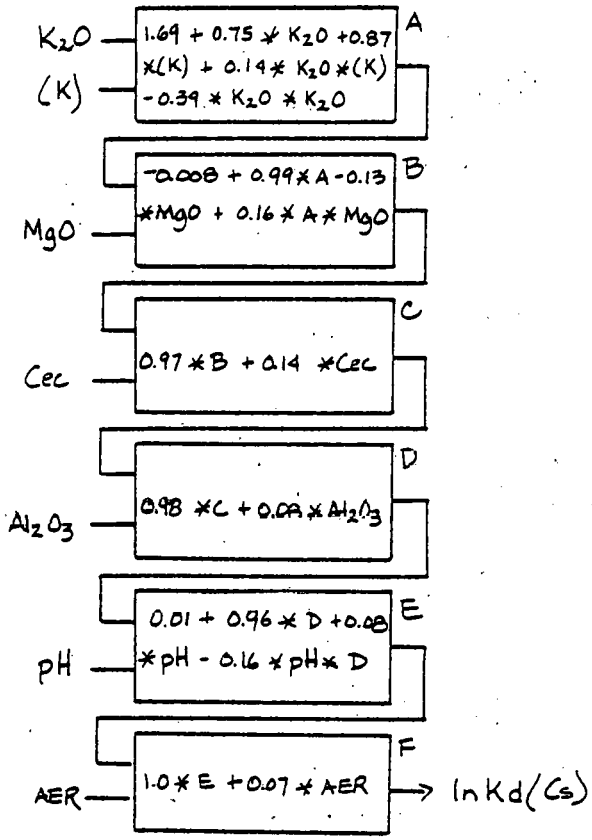

Range of Sorption Data (Log Form)

Min.	-3.51	Mean	6.498
Max.	12.98	St. dev.	3.004

Model Performance (based on predicting the log of sorption)

Correlation Coefficient for Data Used in Training	0.833
Expected Correlation Coefficient for New Data	0.795

Rank Ordered Variables

Variables	Normalized RMS Sensitivity	Normalized Mean Sensitivity
K	7.352	1.801
K_2O	0.714	0.178
pH	0.669	-0.119
Cec	0.431	0.107
MgO	0.339	0.065
Al_2O_3	0.264	0.057
AER	0.227	0.053

FIGURE 5.3(c): PREDICTIVE MODEL FOR CESIUM IN ALL SOLUTIONS

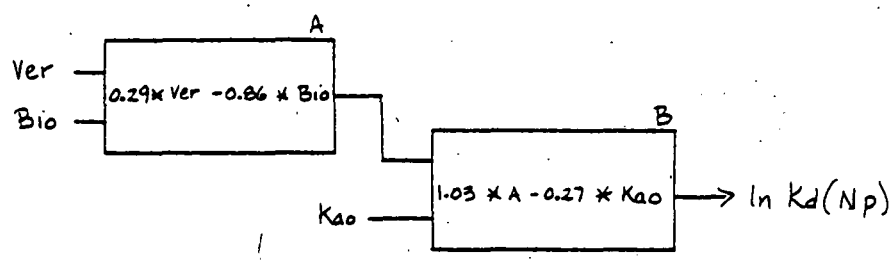

Range of Sorption Data (Log Form)

Min.	-4.10	Mean	4.760
Max.	6.22	St. dev.	2.226

Model Performance (based on predicting the log of sorption)

Correlation Coefficient for Data Used in Training	0.883
Expected Correlation Coefficient for New Data	0.798

Rank Ordered Variables

Variables	Normalized RMS Sensitivity	Normalized Mean Sensitivity
Bio	4.853	-4.463
Ver	1.687	1.551
Kao	1.511	-1.390

FIGURE 5.4(a): PREDICTIVE MODEL FOR NEPTUNIUM IN BRINE SOLUTIONS

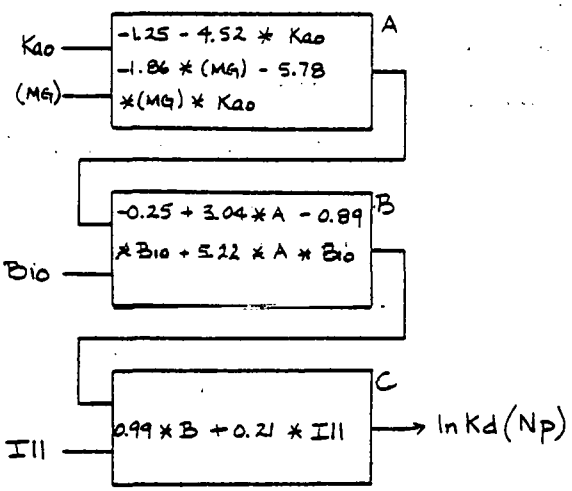

Range of Sorption Data (Log Form)

Min. -4.69 Mean 4.289

Max. 7.21 St. dev. 1.760

Model Performance (based on predicting the log of sorption)

Correlation Coefficient for Data Used in Training 0.812

Expected Correlation Coefficient for New Data 0.754

Rank Ordered Variables

Variables	Normalized RMS Sensitivity	Normalized Mean Sensitivity
Kao	19.329	-12.005
MG	18.251	-4.767
Bio	3.760	- 0.574
Ill	0.616	0.501

FIGURE 5.4(b): PREDICTIVE MODEL FOR NEPTUNIUM IN DILUTE SOLUTIONS

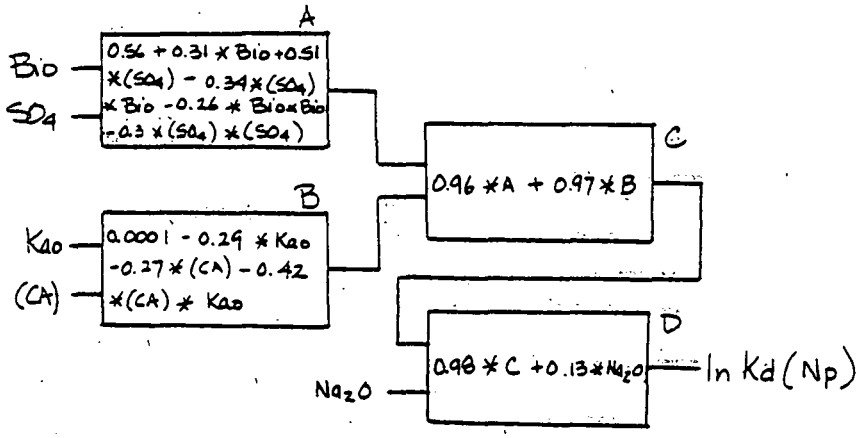

Range of Sorption Data (Log Form)

Min.	-4.69	Mean	4.407
Max.	7.21	St. dev.	1.899

Model Performance (based on predicting the log of sorption)

Correlation Coefficient for Data Used in Training	0.809
Expected Correlation Coefficient for New Data	0.743

Rank Ordered Variables

Variables	Normalized RMS Sensitivity	Normalized Mean Sensitivity
SO4	1.404	0.545
Ca	0.856	0,511
Bio	0.833	-0.435
Kao	0.482	-0.294
Na_2O	0.370	0.273

FIGURE 5.4(c): PREDICTIVE MODEL FOR NEPTUNIUM IN ALL SOLUTIONS

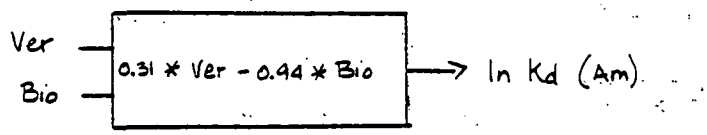

Range of Sorption Data (Log Form)

Min.	-4.89	Mean	5.560
Max.	8.76	St. dev.	3.133

Model Performance (based on predicting the log of sorption)

Correlation Coefficient for Data Used in Training	0.954
Expected Correlation Coefficient for New Data	0.901

Rank Ordered Variables

Variables	Normalized RMS Sensitivity	Normalized Mean Sensitivity
Bio	8.673	-8.235
Ver	2.906	2.760

FIGURE 5.5(a): PREDICTIVE MODEL FOR AMERICIUM IN BRINE SOLUTIONS

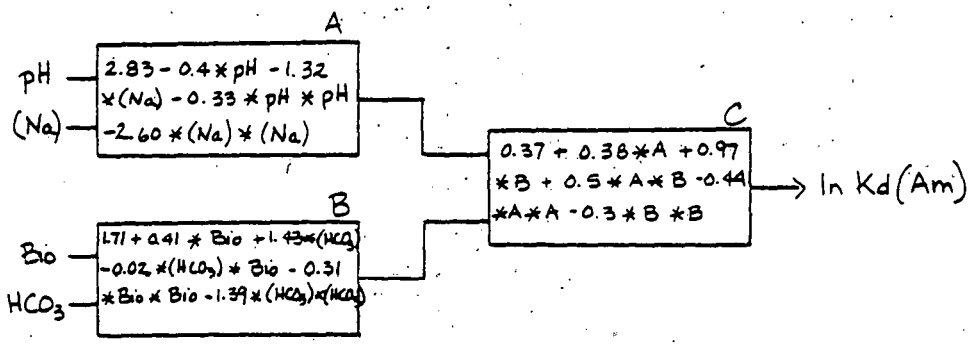

Range of Sorption Data (Log Form)

Min.	-4.05	Mean	8.078
Max.	12.69	St. dev.	2.213

Model Performance (based on predicting the log of sorption)

Correlation Coefficient for Data Used in Training	0.880
Expected Correlation Coefficient for New Data	0.810

Rank Ordered Variables

Variables	Normalized RMS Sensitivity	Normalized Mean Sensitivity
Na	6.329	-1.809
HCO_3	3.417	-0.830
Bio	1.047	0.450
pH	0.997	-0.295

FIGURE 5.5(b): PREDICTIVE MODEL FOR AMERICIUM IN DILUTE SOLUTIONS

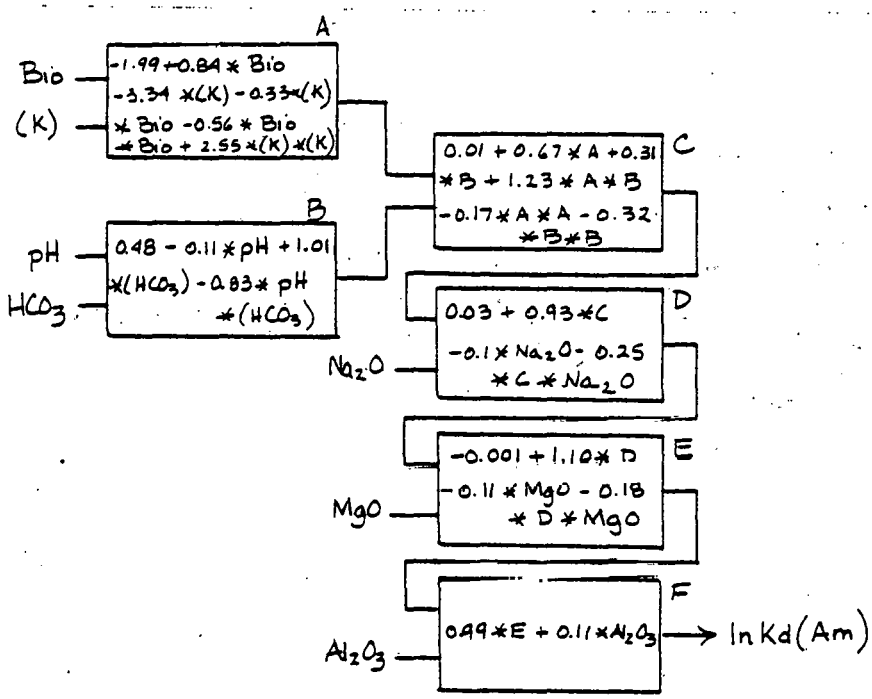

Range of Sorption Data (Log Form)

Min.	-4.77	Mean	7.447
Max.	12.69	St. dev.	2.704

Model Performance (based on predicting the log of sorption)

Correlation Coefficient for Data Used in Training	0.897
Expected Correlation Coefficient for New Data	0.827

Rank Ordered Variables

Variables	Normalized RMS Sensitivity	Normalized Mean Sensitivity
K	35.449	-9.810
Bio	10.897	2.862
pH	2.210	- 0.687
Na_2O	1.274	- 0.385
MgO	0.962	- 0.299
HCO_3	0.490	0.184
Al_2O_3	0.311	0.106

FIGURE 5.5(c): PREDICTIVE MODEL FOR AMERICIUM IN ALL SOLUTIONS

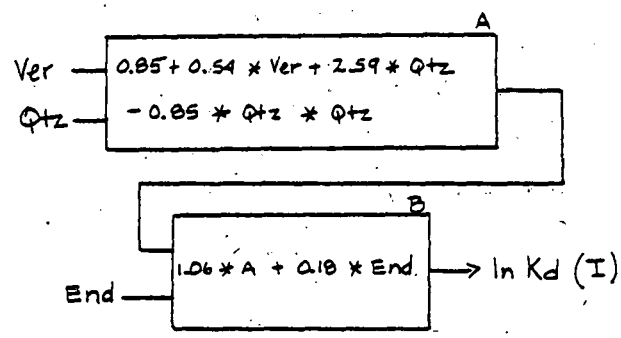

Range of Sorption Data (Log Form)

Min.	-5.61	Mean	-0.749
Max.	6.32	St. dev.	3.396

Model Performance (based on predicting the log of sorption)

Correlation Coefficient for Data Used in Training	0.651
Expected Correlation Coefficient for New Data	0.574

Rank Ordered Variables

Variables	Normalised RMS Sensitivity	Normalized Mean Sensitivity
Qtz	11.962	8.026
Ver	1.974	1.522
End	0.630	0.487

FIGURE 5.6(a): PREDICTIVE MODEL FOR IODINE IN BRINE SOLUTIONS

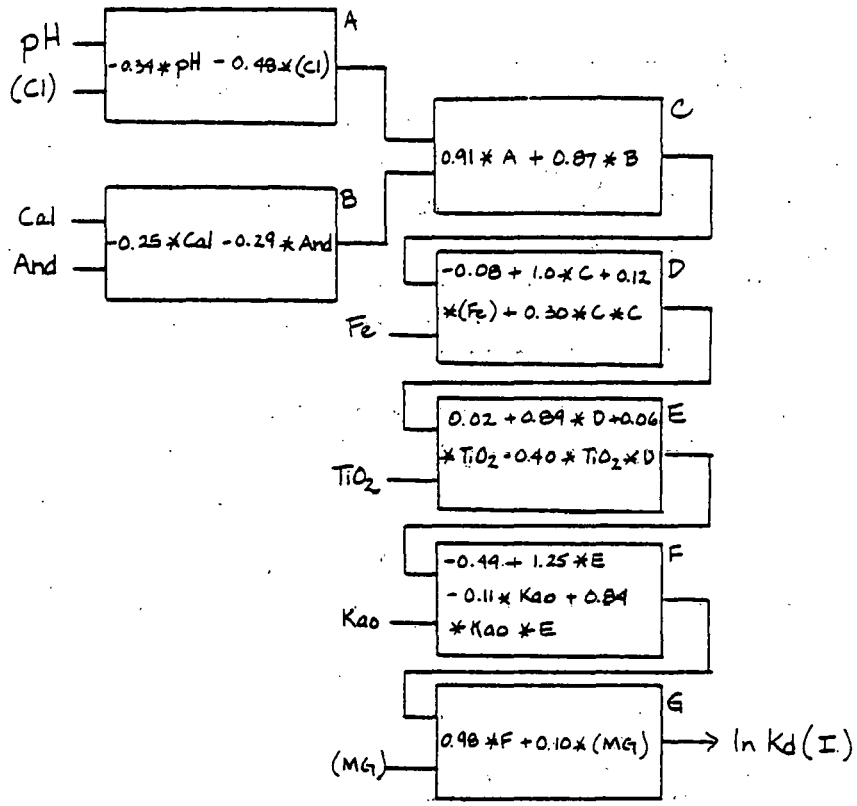

Range of Sorption Data (Log Form)

Min.	-6.53	Mean	0.481
Max.	6.66	St. dev.	3.203

Model Performance (based on predicting the log of sorption)

Correlation Coefficient for Data Used in Training	0.576
Expected Correlation Coefficient for New Data	0.501

Rank Ordered Variables

Variables	Normalized RMS Sensitivity	Normalized Mean Sensitivity
Cl	3.062	-1.262
Kao	2.315	-0.822
pH	1.848	-0.666
And	1.497	-0.573
Cal	1.290	0.349
TiO_2	1.290	0.275
Fe	0.543	-0.256
MG	0.348	0.210

FIGURE 5.6(b): PREDICTIVE MODEL FOR IODINE IN DILUTE SOLUTIONS

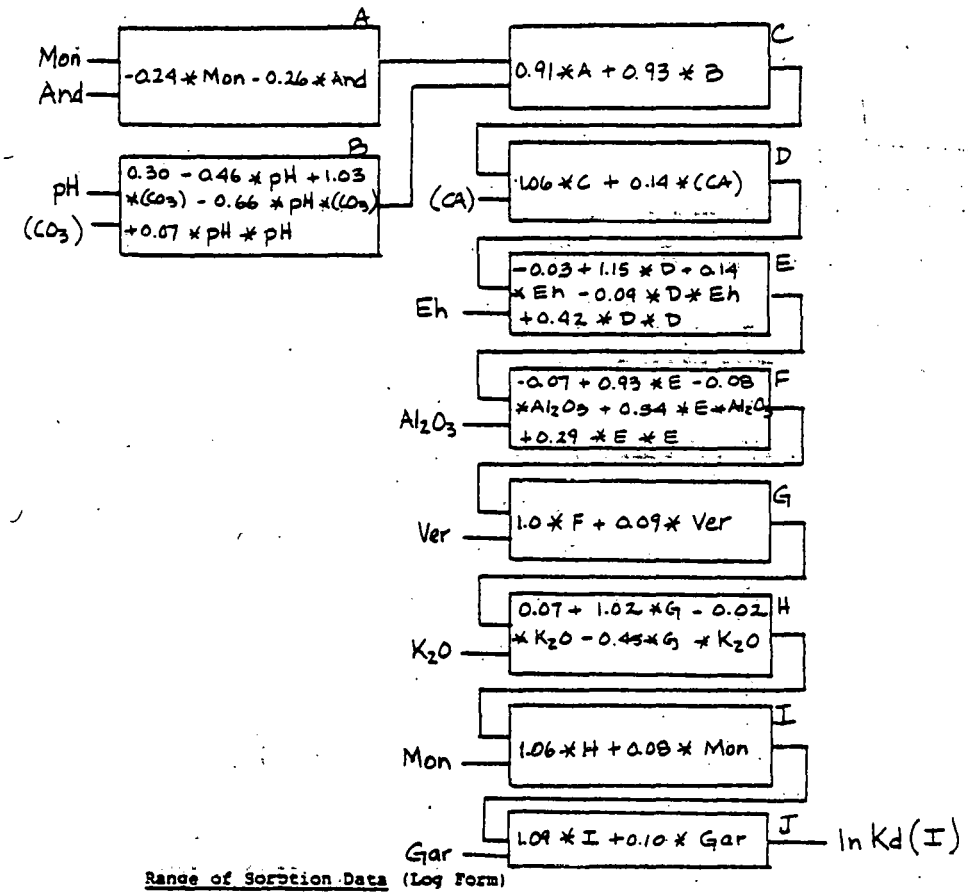

Range of Sorption Data (Log Form)

Min.	-6.53	Mean	0.174
Max.	6.32	St. dev.	3.295

Model Performance (based on predicting the log of sorption)

Correlation Coefficient for Data Used in Training	0.610
Expected Correlation Coefficient for New Data	0.513

Rank Ordered Variables

Variables	Normalized RMS Sensitivity	Normalized Mean Sensitivity
pH	18.761	-3.563
CO_3	11.913	3.365
And	3.455	-0.808
Mon	2.820	-0.631
Al_2O_3	2.723	0.447
K_2O	2.148	-0.431
Ca	1.923	0.361
Eh	1.825	0.285
Ver	0.419	0.125
Gar	0.368	0.118

FIGURE 5.6(c): PREDICTIVE MODEL FOR IODINE IN ALL SOLUTIONS

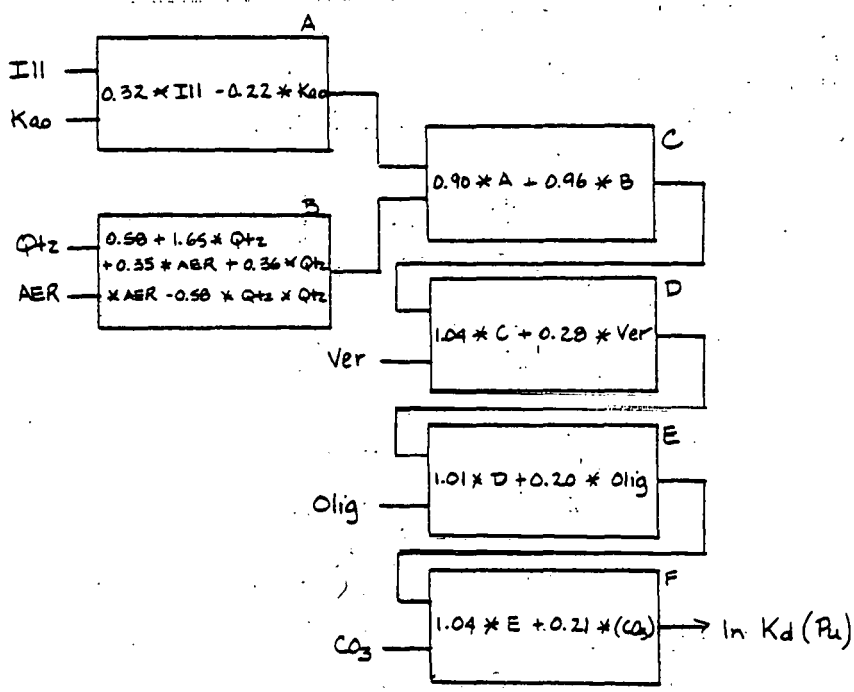

Range of Sorption Data (Log Form)

Min. 5.83 Mean 7.637

Max. 8.92 St. dev. 0.680

Model Performance (based on predicting the log of sorption)

Correlation Coefficient for Data Used in Training 0.796

Expected Correlation Coefficient for New Data 0.648

Rank Ordered Variables

Variables	Normalized RMS Sensitivity	Normalized Mean Sensitivity
Qtz	3.196	2.352
AER	0.918	0.508
Ill	0.474	0.425
Ver	0.435	0.388
Kao	0.323	- 0.288
CO_3	0.321	0.286
Olig	0.318	0.283

FIGURE 5.7(a): PREDICTIVE MODEL FOR PLUTONIUM IN BRINE SOLUTIONS

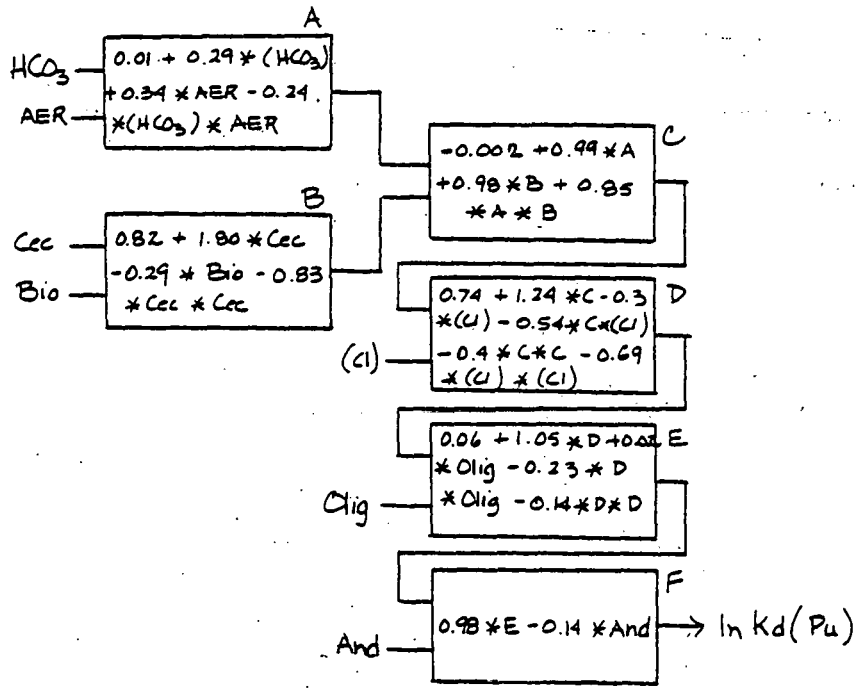

Range of Sorption Data (Log Form)

Min. 2.79 Mean 7.957

Max. 10.06 St. dev. 1.244

Model Performance (based on predicting the log of sorption)

Correlation Coefficient for Data Used in Training 0.822

Expected Correlation Coefficient for New Data 0.744

Rank Ordered Variables

Variables	Normalized RMS Sensitivity	Normalized Mean Sensitivity
Cec	3.156	1.489
Cl	1.303	-0.270
Olig	0.580	0.258
HCO_3	0.494	-0.175
Bio	0.400	0.157
AER	0.271	-0.144
And	0.228	-0.133

FIGURE 5.7(b): PREDICTIVE MODEL FOR PLUTONIUM IN DILUTE SOLUTIONS

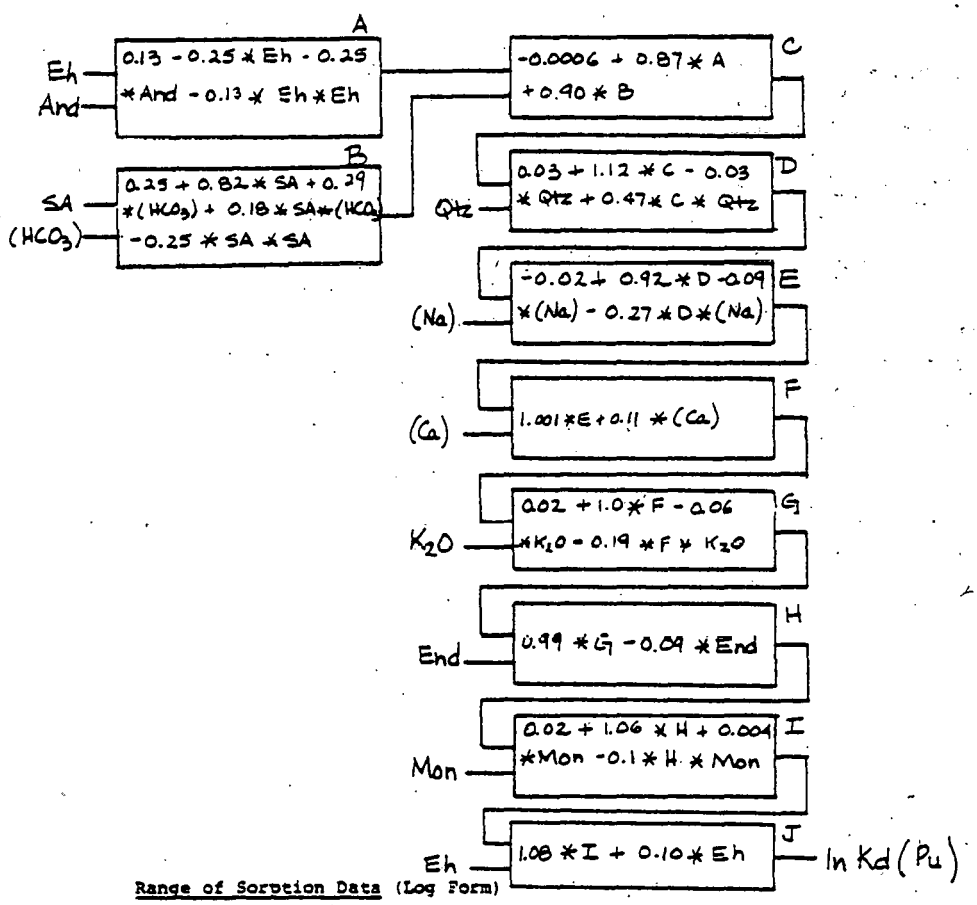

Range of Sorption Data (Log Form)

Min.	2.79	Mean	7.876
Max.	11.06	St. dev.	1.136

Model Performance (based on predicting the log of sorption)

Correlation Coefficient for Data Used in Training	0.705
Expected Correlation Coefficient for New Data	0.632

Rank Ordered Variables

Variables	Normalized RMS Sensitivity	Normalized Mean Sensitivity
SA	1.787	0.902
Qtz	1.055	0.388
HCO_3	0.778	-0.272
Na	0.666	0.254
K_2O	0.501	-0.253
And	0.418	-0.193
Mon	0.253	0.135
Eh	0.251	-0.110
Ca	0.186	-0.074
End	0.151	-0.067

FIGURE 5.7(c): PREDICTIVE MODEL FOR PLUTONIUM IN ALL SOLUTIONS

following variables are seen to influence the K_d(Tc) in the brine solution: montmorillonite and biotite (moderate negative), HCO_3 and SO_4 (strong positive).

The following observations generally summarize the results in Table 5.1:

(1) K_d depends strongly on all five minerals in Group 1 (Phyllosilicates). The overall trend is mainly (-). Groups 2 (Tektosilicates) and 3 (Inosilicates) show much less sensitivity.

(2) The effect of minerals and other variables on:
Sr (Brine) - all strongly (-)
Tc (Dilute) - all strongly (+)
I (Brine) - all (+), less strong

Other isotope solutions are divided between (+) and (-) effects of variables.

(3) Montmorillonite and Brine:
Occur together, both indicating moderate (-) for Tc (Brine) and Tc (all solutions). A strong (+) occurs for Biotite in Tc (Dilute).

(4) Kaolinite and Biotite:
Occur together, indicting moderate-to-strong (-) for Np (Brine) and Np (Dilute).

(5) Magnetite and Cl:
Occur together indicating (-) trend for Sr.

Table 5.2 is a list of variables (from Table 5.1) that showed strong trends in predicting Kd for a given nuclide and solution.

TABLE 5.1: INFLUENCE OF THE SOLID/SOLUTION VARIABLES ON THE SEVEN NUCLIDE K_d's FOR EACH OF THREE SOLUTIONS

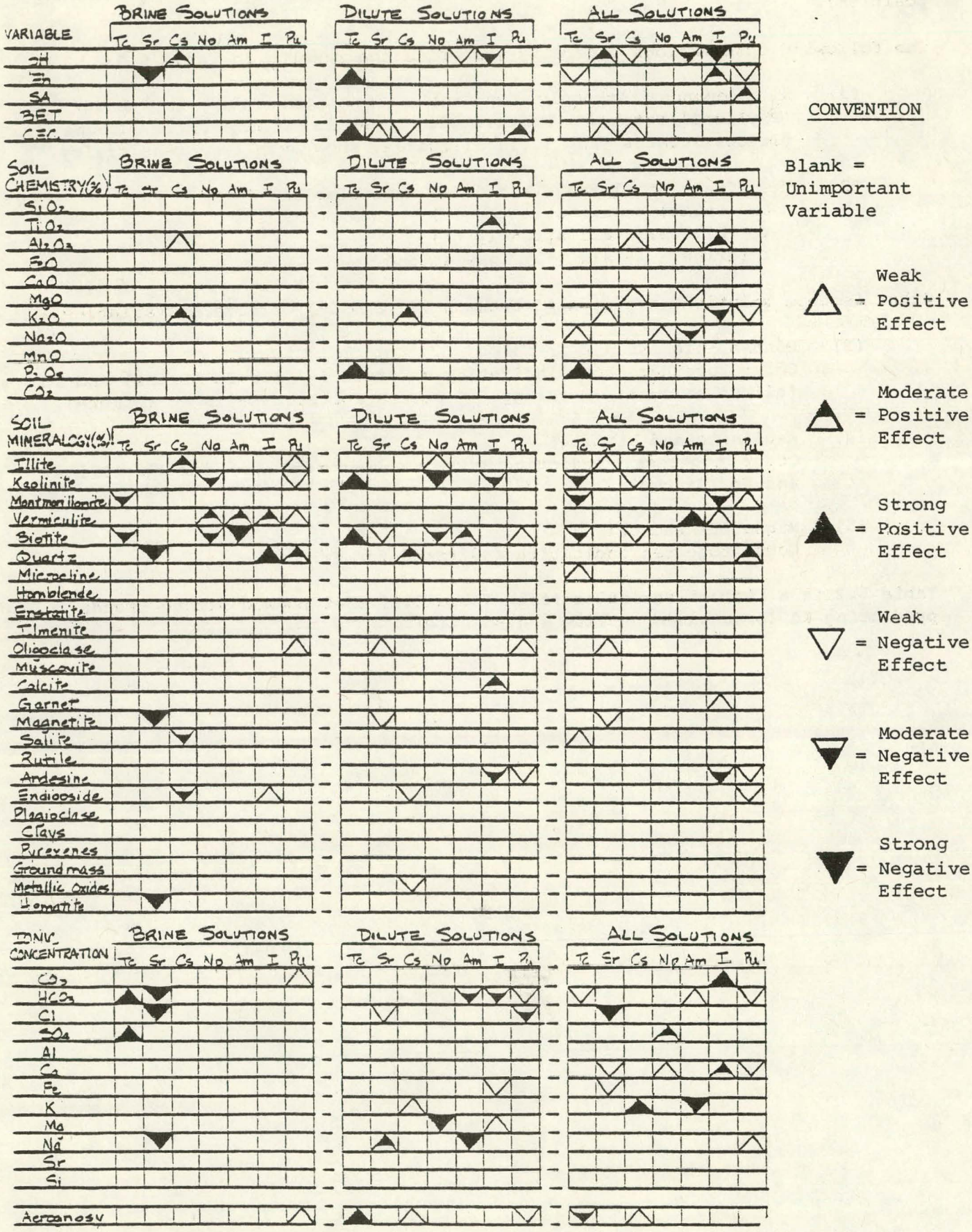

CONVENTION

Blank = Unimportant Variable

△ = Weak Positive Effect

▲ = Moderate Positive Effect

▲ = Strong Positive Effect

▽ = Weak Negative Effect

▼ = Moderate Negative Effect

▼ = Strong Negative Effect

TABLE 5.2: VARIABLES WITH STRONG TRENDS

CEC	Mostly (+)
PH	Mostly (-)
$Al_2 O_3$	All (+)
$P_2 O_5$	Strongly (+)
Illite	All (+), but not strong
Kaolinite	Mostly (-)
Vermiculite	All (+), strong
Montmorillonite	Mostly (-)
Biotite	Mostly (-)
Oligoclase	All (+), not strong
Magnetite	All (-), all in Sr
Andesine	All (-), (present in I and Pu)
HCO_3	Mostly (-)
Cl	All (-), strong for Sr
SO_4	All (+)
Na	Mostly (-)
Aerobic/Anerobic	Effects only Tc, Cs & Pu

6. INDIVIDUAL VS. GROUP ADSORBENT MODELS

6.1 INTRODUCTION

It would be highly desirable to generate the K_d predictor equation for a new geologic medium as a function of equations already developed. For example, if a rock consists of 50% phyllosilicates, 25% tecktosilicates and 25% inosilicates, the rock K_d predictor equation could be estimated as a weighted sum of the three silicate groups models, if they already existed. Further, if a K_d predictor equation existed for a number of minerals, the rock model could be estimated as a weighted sum of the individual mineral models.

This concept was tested by using a weighted-sum-of-models approach. The idea is illustrated in Figure 6.1. A separate ALN model was synthesized for each silicate group for each of two nuclides -- Sr and Tc -- by combining all the minerals in each silicate group (Table 2.3) along with all four solutions into one data base, respectively. Now, given a new solid (i.e., one of the four rocks), the variables (Table 2.2) for the solid were input into each of the three models to yield three K_d value. Each K_d value was then weighted by the weight percentage of its associated silicate group in the solid. The predicted K_d was then the resultant weighted sum. The predicted value was compared to the true, experimental value to establish the feasibility of the approach.

6.2 RESULTS FOR Sr

The results for the Sr models are given in Figure 6.2 for the four rocks. It can be seen that for shale, the weighted sum results compare favorably to experimental values for two of four solutions. The results for the brine and calcium solution are in error due to the tektosilicate model. If this were ignored, the results would be quite close (i.e., compare the phyllosilicate result to the true value).

There is reasonable agreement for granite, except for the calcium solution.

The results for basalt are quite good.

6.3 RESULTS FOR Tc

The Tc weighted sum results (Figure 6.3) are not in good agreement with experimental values except for one case -- basalt and the brine solution.

6.4 DISCUSSION

This task was intended to test the feasibility of constructing group adsorbent models from individual adsorbent models. The approach used was based on the assumption that mixtures of minerals and/or mineral groups would react linearly when combined in a rock. The results suggest that this is generally time for Sr and generally false for Tc.

A more global approach may be to adapt a nonlinear combination assumption. The ALN model, which can identify any nonlinear interactions, could be used to construct one, overall model instead of the individual models as shown in Figure 6.1.

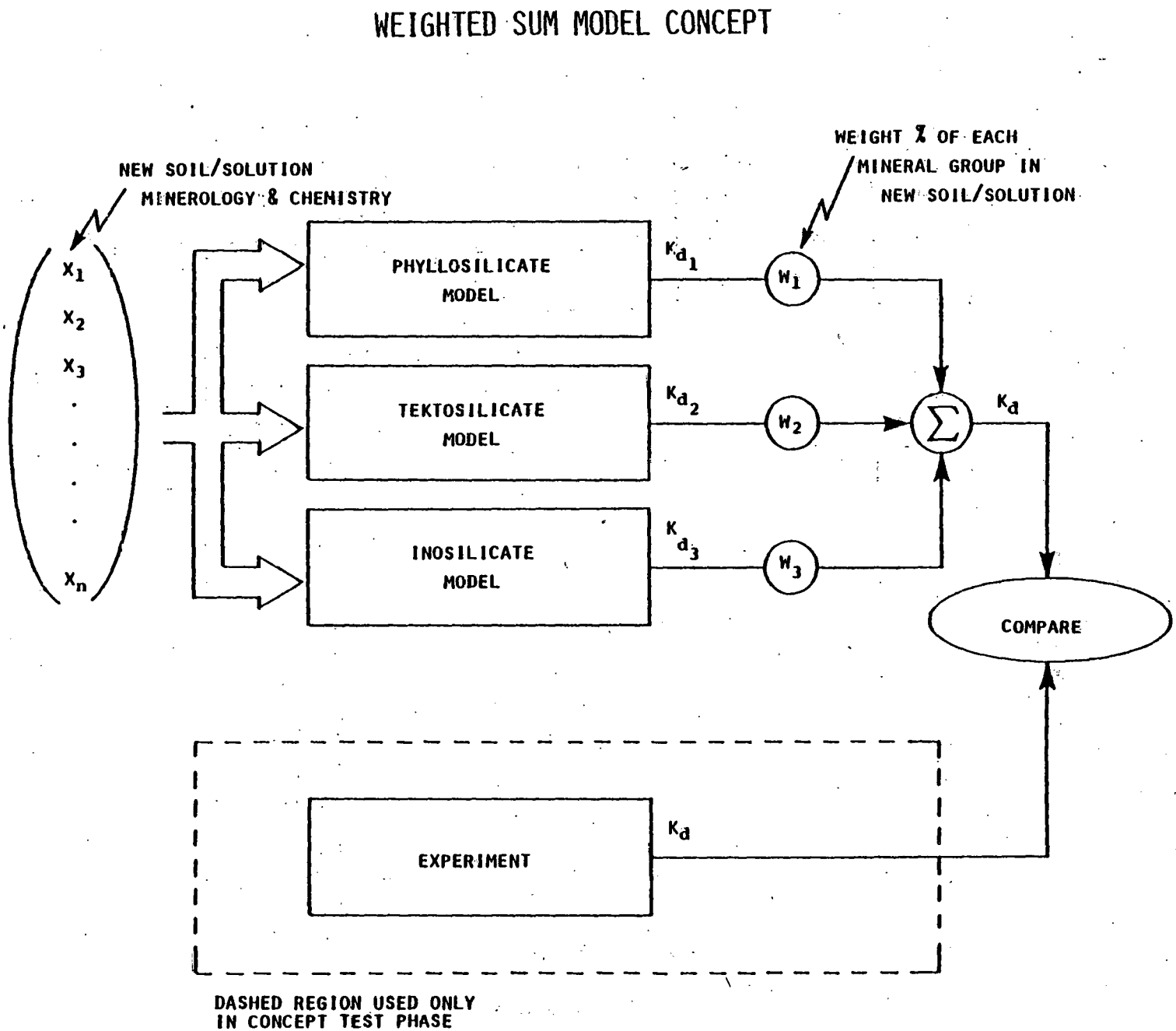

FIGURE 6.1: WEIGHTED SUM MODEL CONCEPT

SR: WEIGHTED SUM RESULTS

ROCK	SOLUTION	PHYLLOSILICATE		INOSILICATE		TEKTOSILICATE		OTHER	WGTD. SUM	TRUE
		K_D	Wt %	K_D	Wt %	K_D	Wt %	Wt %	K_D	K_D
Shale	5.13N NaCl	3.2	85	0.4	0	1.8×10^5	12	3	4.2×10^4	3.4
	0.03N $CaCl_2$	9.0	85	2.3	0	4.1×10^4	12	3	4.5×10^3	12.2
	0.03N NaCl	85.0	85	58.0	0	1.1	12	3	74.0	83.4
	0.03N $NaHCO_3$	350.0	85	300.0	0	-2.2	12	3	303.3	398.7
Granite	5.13N NaCl	1.4	5	0.6	0	24.0	92	3	23.0	1.6
	0.03N $CaCl_2$	4.5	5	2.1	0	1.4×10^4	92	3	1.3×10^4	4.1
	0.03N NaCl	32.3	5	57.0	0	62.7	92	3	61.3	26.4
	0.03N $NaHCO_3$	146.7	5	300.0	0	2.2	92	3	9.6	33.3
Limestone	5.13N NaCl		0		0		0	100		22.5
	0.03N $CaCl_2$		0		0		0	100		5.5
	0.03N NaCl		0		0		0	100		99.8
	0.03N $NaHCO_3$		0		0		0	100		1.01×10^4
Basalt	5.13N NaCl	1.5	0	0.3	32	2.3	44	24	1.5	0.7
	0.03N $CaCl_2$	4.2	0	1.9	32	2.0	44	24	2.0	3.6
	0.03N NaCl	25.0	0	59.0	32	7.6	44	24	29.0	71.4
	0.03N $NaHCO_3$	196.7	0	310.0	32	3.4	44	24	130.0	104.0

FIGURE 6.2: SR: WEIGHTED SUM RESULTS

TC: WEIGHTED SUM RESULTS

ROCK	SOLUTION	PHYLLOSILICATE		INOSILICATE		TEKTOSILICATE		OTHER	WGTD. SUM	TRUE
		K_D	WT %	K_D	WT %	K_D	WT %	WT %	K_D	K_D
SHALE	5.13N NaCL	1.3	85	0.9	0	1.3	12	3	1.2	84.5
	0.03N $CaCL_2$	1.0	85	$1.1x10^{10}$	0	0.6	12	3	0.9	78.7
	0.03N NaCL	0.6	85	-1.6	0	-0.7	12	3	0.4	82.7
	0.03N $NaHCO_3$	-0.1	85	-63.0	0	-2.2	12	3	-0.4	70.1
GRANITE	5.13N NaCL	-0.1	5	0.9	0	0.2	92	3	0.2	9.4
	0.03N $CaCL_2$	-0.2	5	$1.3x10^{9}$	0	-1.2	92	3	-1.1	74.0
	0.03N NaCL	-0.3	5	-6.2	0	-1.9	92	3	-1.8	78.7
	0.03N $NaHCO_3$	-0.8	5	-65.0	0	-5.8	92	3	-5.4	27.5
LIMESTONE	5.13N NaCL		0		0		0	100		7.3
	0.03N $CaCL_2$		0		0		0	100		75.4
	0.03N NaCL		0		0		0	100		77.6
	0.03N $NaHCO_3$		0		0		0	100		65.8
BASALT	5.13N NaCL	0.1	0	0.9	32	2.3	44	24	1.3	1.42
	0.03N $CaCL_2$	-0.2	0	$9.9x10^{6}$	32	0.6	44	24	$3.2x10^{6}$	50.4
	0.03N NaCL	-0.2	0	-51.0	32	0.3	44	24	-16.0	48.3
	0.03N $NaHCO_3$	-0.9	0	-56.0	32	-1.1	44	24	-19.0	49.0

FIGURE 6.3: TC: WEIGHTED SUM RESULTS

7. ION EXCHANGE DATA BASE ANALYSIS

7.1 INTRODUCTION

The purpose of this task was to develop ALN models based on data generated at Oak Ridge National Laboratory on the adsorption of Sr, Cs and Ba into montmorillonite clay vs. salt brine concentration and to compare these ALN models to classical ion exchange equations such as:

$$\log K_d = -C \log Na^+$$

$$\log K_d = -C \log Ca^{2+}$$

where

$$C = \frac{\text{tracer element valence}}{\text{bulk ion in water valence}}$$

As stated in [5], the ion exchange equation form:

$$\log K_d = -C \log X \qquad (5.1)$$

is actually the derivative result:

$$\frac{d(\log K_d)}{d(\log X)} = -C \qquad (5.2)$$

so that a more rigorous form of equation (5.1) includes the constant of integration, Q:

$$\log K_d = -C \log X + Q \qquad (5.3)$$

where Q has the intepretation of an equilibrium constant.

7.2 ALN MODEL

The ORNL data base consisted of a series of experiments, each of which treated one tracer element K^+, Na^+, Cs^+, Ba^{2+}, Sr^{2+}, Eu^{3+} -- and one bulk ion -- Na^+, Ca^{2+}. If the bulk ion is represented as "X", each experiment in the data base can be represented as a two-column set of values:

X	vs	K_d
-		-
-		-
-		-
-		-

Then four ALN candidate inputs were powers of the bulk ion concentration, X: X, X^2, X^3, X^4; the output was $\log_e K_d$. So, for each entry in the above two columns, these four "independent" values were generated.

This choice of input variable form was motivated by examination of Equation 5.1. The log X term can be expanded in a power series:

$$\log_e X = (X-1) - 1/2(X-1)^2 + 1/3(X-1)^3 - \ldots \quad (5.4)$$

which is valid for $0 < X < 2$ (which is the case for most of the bulk ion concentrations). Expanding 5.4, and retaining two terms, gives the quadratic:

$$\log_e X = (X-1) - 1/2(X-1)^2 \quad (5.5)$$
$$= -1.5 + 2X - 0.5X^2$$

while retaining three terms gives the cubic:

$$\log_e X = (X-1) - 1/2(X-1)^2 + 1/3(X-1)^3$$
$$= -1.833 + 2.5X - 1.5X^2 + 0.333X^3 \quad (5.6)$$

Thus, the ion exchange equation (5.1) can be written:

$$\log K_d = -C \log X$$
$$= -C\,[-1.5 + 2X - 0.5X^2] \quad (5.7)$$

or,

$$= -C\,[-1.833 + 2.5X - 1.5X^2 + 0.333X^3] \quad (5.8)$$

Equations 5.7 and 5.8 were the reason for selecting the terms X, X^2, X^3, X^4 as the ALN input variables.

So, the protocol followed was to: (1) develop an ALN model for each ORNL experiment, (2) list the terms of the polynomial model formed by the ALN, and (3) compare the model to Equations 5.7 and 5.8, depending on whether a quadratic or cubic ALN model was formed.

7.3 RESULTS

Figures 7.1 through 7.6 list, for each experiment respectively:

(1) ORNL data
(2) ion exchange equation (Equation 5.1)
(3) ALN equation
(4) true vs. predicted K_d's by each model
(5) graphical representation of the true vs. K_d values from both models.

It can be seen in the figures that of the two transport equations, Equation 5.3 would be a better fit to the data in all cases except for Figure 7.5; i.e., the slope of the transport line is generally accurate, but the intercept needs adjustment. (This form of Equation 5.3 was made available to the authors after Figure 7.1 - 7.6 had been drawn.)

There is some nonlinearity exhibited between the true K_d and the bulk ion concentration observed in all the figures, especially in Figure 7.6. The ALN model generally fits the data quite well. The resulting equations shown in Figures 7.1 - 7.6 are summarized in Table 7.1. The ion exchange column was

(2 PREWASHES, 5 CC EACH, pH ~ 5, K^+ INITIAL = 1.25×10^{-4}M, SHAKING FOR 18 HOURS)

TRANSPORT EQUATION: $\ell_N (K_D) = -1 \ell_N [N_A]$

ALN EQUATION: $\ell_N (K_D) = 4.06 - 2.523 [N_A] + 0.451 [N_A]^2$

	K_D (cc/gm)		
$[N_A]$ (M)	TRUE	TRANSPORT	ALN
4.01	2.9	0.2	3.3
2.01	4.1	0.5	2.2
1.01	6.1	1.0	7.2
0.51	9.0	2.0	18.0
0.26	16.0	3.8	31.0
0.11	33.0	9.1	44.1
0.06	43.0	16.7	49.8
0.035	75.0	28.6	53.0
0.02	74.0	50.0	55.0
0.01	130.0	100.0	56.5

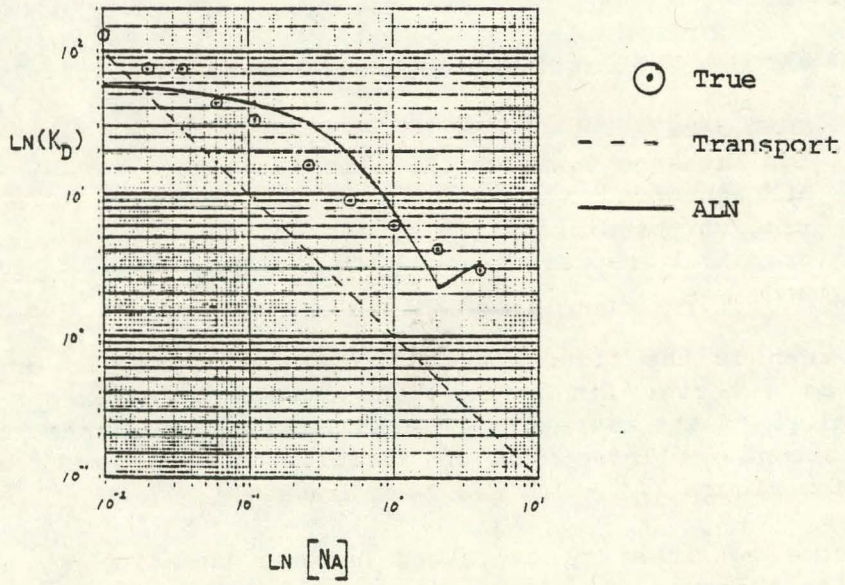

FIGURE 7.1: K^+/Na EXCHANGE ON Na FORM OF PURIFIED Na - MONTMORILLONITE

(2 PREWASHES, 5 CC EACH, Na^+ INITIAL = 1.25×10^{-4} M, SHAKING FOR 45 HOURS)

TRANSPORT EQUATION: $\ell_N (K_D) = -0.5 \ell_N [C_A]$

ALN EQUATION: $\ell_N (K_D) = 2.421 - 1.570 [C_A] + 0.325 [C_A]^2$

	K_D (cc/gm)		
$[C_A]$ (M)	TRUE	TRANSPORT	ALN
2.01	1.7	0.7	1.8
1.01	4.1	1.0	3.2
0.51	4.9	1.4	5.5
0.26	5.6	2.0	7.7
0.11	7.7	3.0	9.5
0.06	11.0	4.1	10.3
0.035	13.0	5.3	10.7
0.02	13.0	7.1	10.9

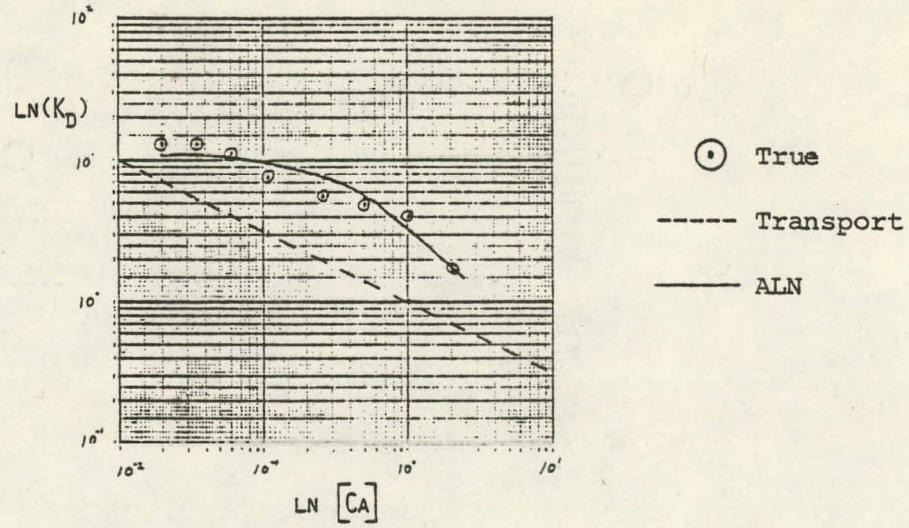

FIGURE 7.2(a): Na^+/Ca^{2+} EXCHANGE ON Ca FORM OF PURIFIED Na - MONTMORILLONITE

(3 PREWASHES, 5CC EACH, pH ~5, Na^+ INITIAL = 1.25×10^{-4}M,

SHAKING FOR 140 HOURS)

TRANSPORT EQUATION: $\ell_N(K_D) = 0.5\, \ell_N [C_A]$

ALN EQUATION: $\ell_N (K_D) = 2.485 - 1.91 [C_A] + 0.268 [C_A]^2$

	K_D (cc/gm)		
$[C_A]$ (M)	TRUE	TRANSPORT	ALN
2.1	3.1	0.7	3.2
1.1	5.2	1.0	4.5
0.6	6.1	1.3	6.5
0.25	7.7	2.0	9.1
0.20	8.8	2.2	9.6
0.1	10.0	3.2	10.7
0.05	11.0	4.5	11.3
0.025	13.0	6.3	11.6
0.01	14.0	10.0	11.8

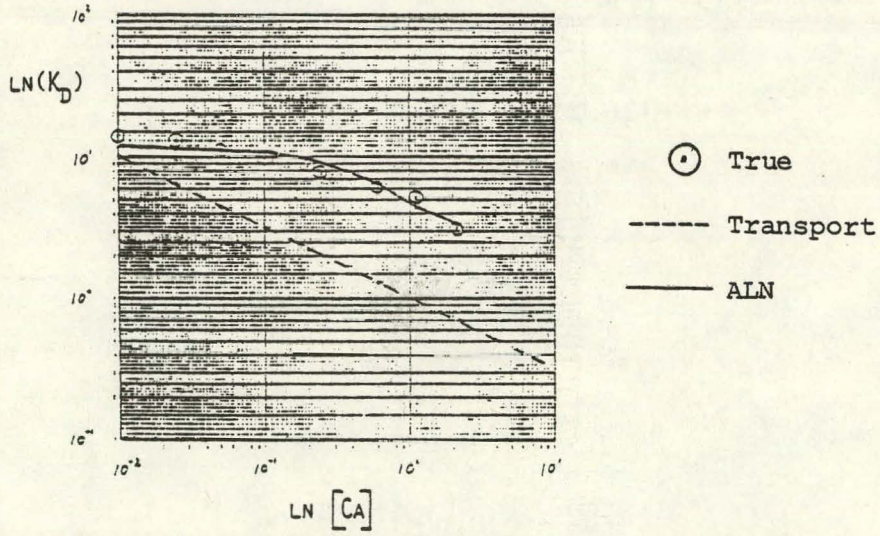

FIGURE 7.2(b): Na^+/Ca^{2+} EXCHANGE ON Ca FORM OF PURIFIED Na - MONTMORILLONITE

(pH ~ 5, Na^+ INITIAL = 1.25×10^{-4} M)

TRANSPORT EQUATION: $\ell_N (K_D) = -0.5\, \ell_N [C_A]$

ALN EQUATION: $\ell_N (K_D) = 2.419 - 3.417 [C_A] + 1.888 [C_A]^2$

$[C_A]$ (M)	K_D (cc/gm)		
	TRUE	TRANSPORT	ALN
1.01	2.4	1.0	2.5
0.51	3.6	1.4	3.2
0.26	5.0	2.0	5.2
0.11	6.5	3.0	7.9
0.06	8.4	4.1	9.2
0.035	11.0	5.3	10.0
0.02	11.0	7.1	10.5
0.01	12.0	10.0	10.8

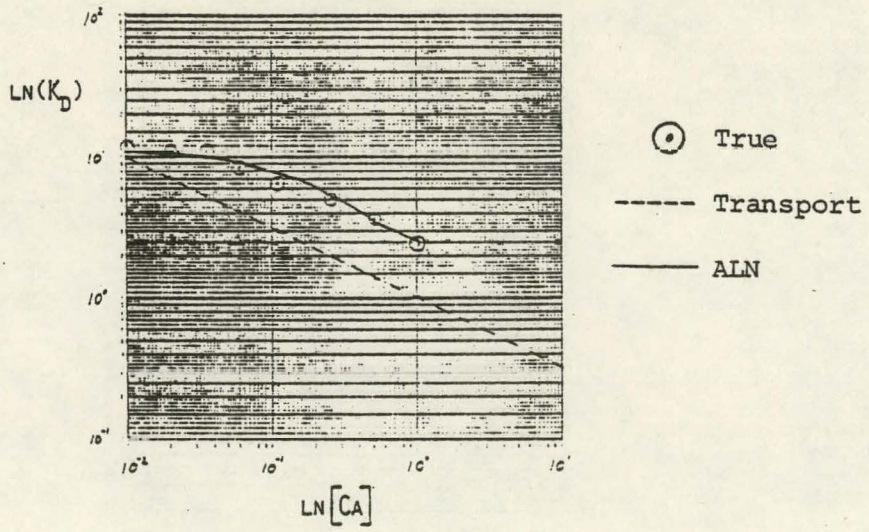

FIGURE 7.2(c): Na^+/Ca^{2+} EXCHANGE ON Ca FORM OF PURIFIED Na - MONTMORILLONITE

(No prewashes, pH ~ 5, Cs^+ initial - 1.25×10^{-4} M,
shaking for 12 hours)

Transport Equation: $\ell_N (K_D) = -0.5 \ell_N [C_A]$

ALN Equation: $\ell_N (K_D) = 6.424 - 1.234 [C_A] + 0.383 [C_A]^2$

$[C_A]$ (M)	K_D (cc/gm) TRUE	TRANSPORT	ALN
2.01	239.0	0.7	242.7
1.01	286.0	1.0	262.2
0.51	337.0	1.4	363.2
0.26	422.0	2.0	459.4
0.11	561.0	3.0	541.3
0.06	556.0	4.1	573.6
0.035	632.0	5.3	591.1
0.01	621.0	10.0	609.7

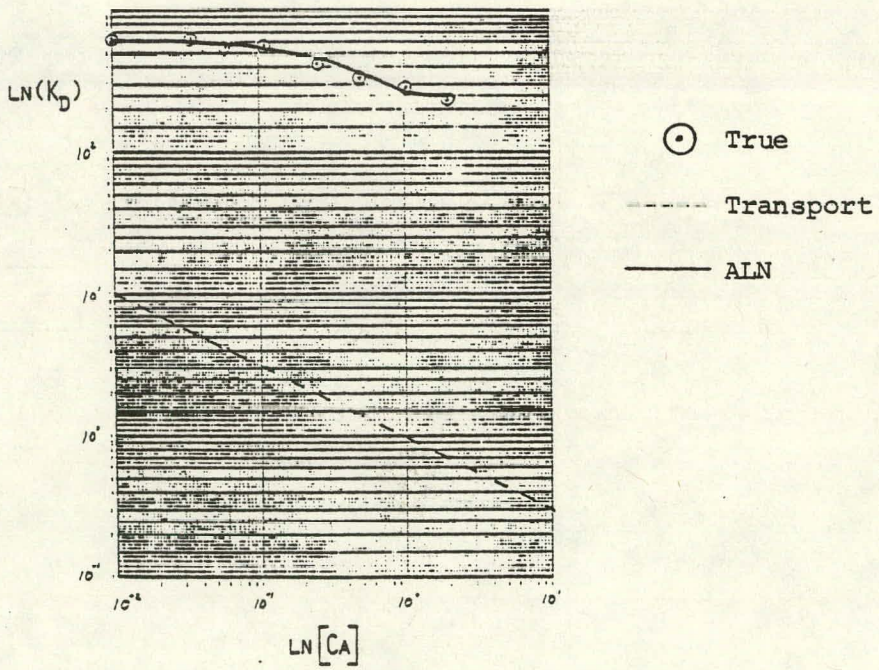

FIGURE 7.3(a): Cs^+/Ca^{2+} EXCHANGE ON Ca FORM OF PURIFIED Na - MONTMORILLONITE

(NO PREWASHES, pH ~ 5, Cs^+ INITIAL = 5×10^{-5} M,
SHAKING FOR 37 HOURS)

TRANSPORT EQUATION: $\ell_N (K_D) = -0.5\, \ell_N [C_A]$

ALN EQUATION: $\ell_N (K_D) = 6.896 - 1.674 [C_A] + 0.669 [C_A]^2$

$[C_A]$ (M)	K_D (cc/gm) TRUE	TRANSPORT	ALN
1.01	326.0	1.0	360.7
1.01	386.0	1.0	360.7
0.51	599.0	1.4	501.2
0.26	575.0	2.0	669.8
0.11	720.0	3.0	829.6
0.06	825.0	4.1	896.9
0.035	905.0	5.3	933.6
0.02	1100.0	7.1	956.2
0.01	1100.0	10.0	972.6

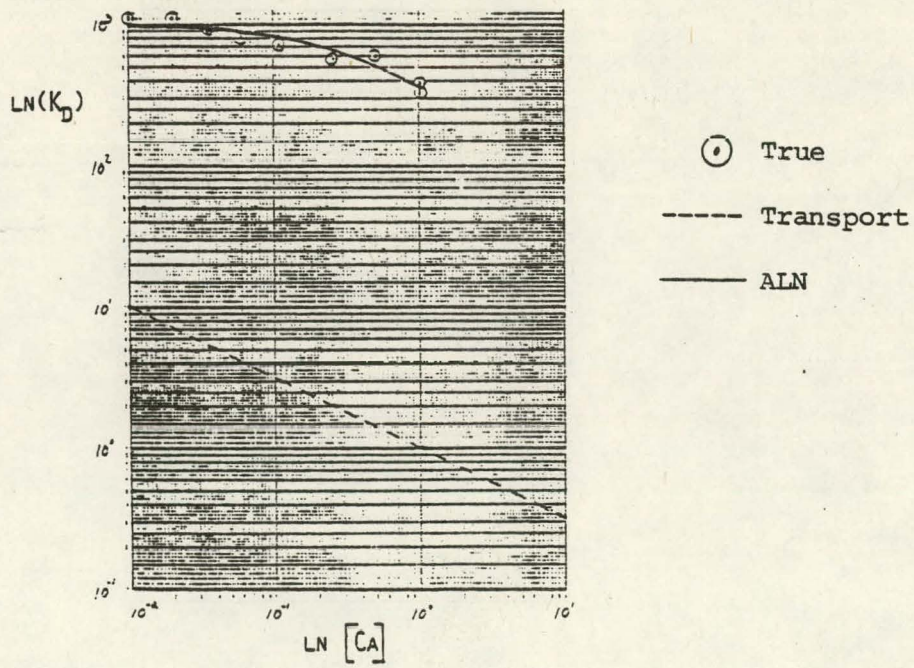

FIGURE 7.3(b): Cs^+/Ca^{2+} EXCHANGE ON A Ca FORM OF PURIFIED Na - MONTMORILLONITE

(NO PREWASHES, pH ~ 5, Cs^+ INITIAL = 2×10^{-5} M,
SHAKING FOR 36 HOURS)

TRANSPORT EQUATION: $\ell_N (K_D) = -0.5 \ell_N [C_A]$

ALN EQUATION: $\ell_N (K_D) = 7.093 - 1.736 [C_A] + 0.589 [C_A]^2$

	K_D (cc/gm)		
$[C_A]$ (M)	TRUE	TRANSPORT	ALN
2.01	387.0	0.7	397.0
1.01	434.0	1.0	380.3
0.51	534.0	1.4	578.8
0.26	704.0	2.0	797.9
0.11	968.0	3.0	1002.2
0.06	954.0	4.1	1086.8
0.035	1150.0	5.3	1133.4
0.02	1310.0	7.1	1163.3
0.01	1350.0	10.0	1183.2

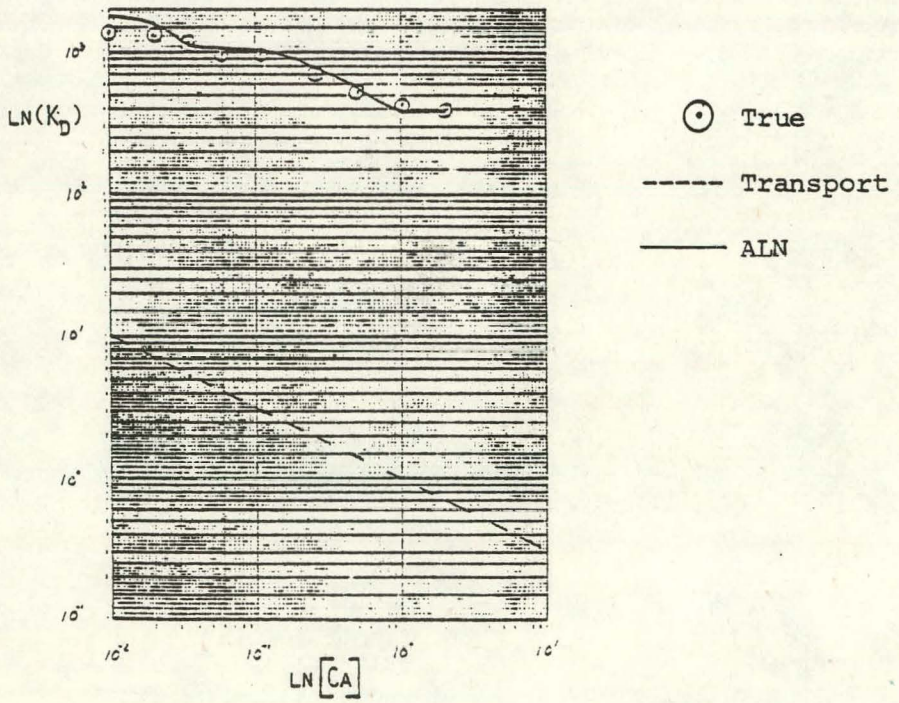

FIGURE 7.3(c): Cs^+/Ca^{2+} EXCHANGE ON Ca FORM OF PURIFIED Na - MONTMORILLONITE

(3 PREWASHES, 5cc EACH, pH ~ 5, TRACE Cs^+,
SHAKING FOR 140 HOURS)

TRANSPORT EQUATION: $\ell_N (K_D) = 0.5 \ell_N [C_A]$

ALN EQUATION: $\ell_N (K_D) = 9.280 - 4.641 [C_A] + 2.354 [C_A]^2$

$[C_A]$ (M)	K_D (cc/gm)		
	TRUE	TRANSPORT	ALN
1.01	1070.0	1.0	1100.0
0.51	2150.0	1.4	1861.2
0.26	3310.0	2.0	3766.9
0.11	6670.0	3.0	6621.0
0.06	6940.0	4.1	8176.3
0.035	7980.0	5.3	9136.2
0.02	8360.0	7.1	9769.3
0.01	16200.0	10.0	10229.2

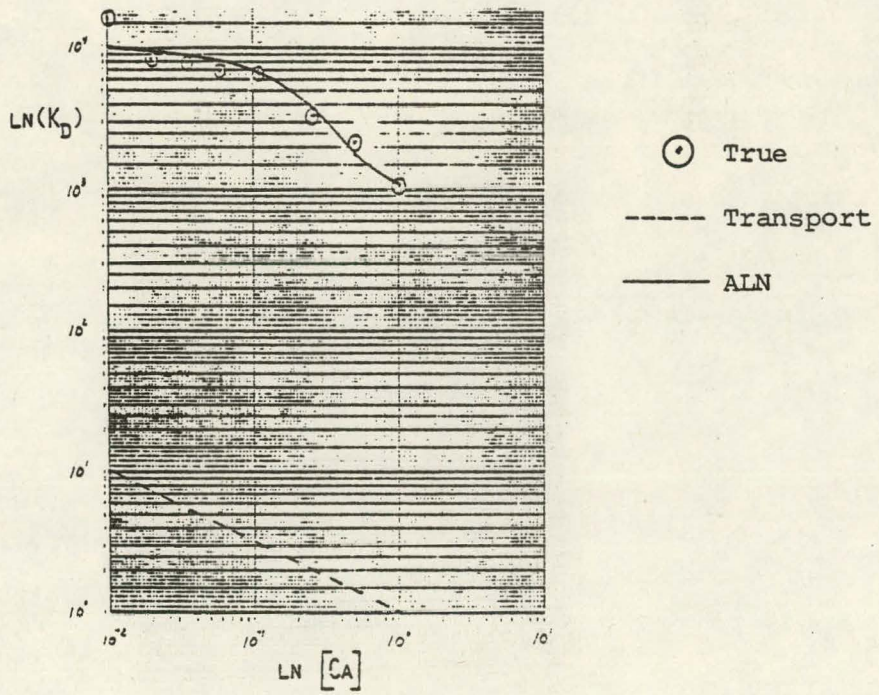

FIGURE 7.3(d): Cs^+/Ca^{2+} EXCHANGE ON Ca FORM OF PURIFIED Na - MONTMORILLONITE

(No prewashes, pH ~ 5, Ba^{2+} initial = 1.25×10^{-4} M, shaking for 30-36 hours)

Transport Equation: $\ell_N (K_D) = -1 \ell_N [Ca]$

ALN Equation: $\ell_N (K_D) = 4.546 - 5.088 [Ca] + 1.770 [Ca]^2$

	K_D (cc/gm)		
$[Ca]$ (M)	TRUE	TRANSPORT	ALN
2.01	3.2	0.5	4.4
2.01	4.9	0.5	4.4
1.01	4.8	1.0	3.4
1.01	6.1	1.0	3.4
0.51	8.1	2.0	11.2
0.51	11.0	2.0	11.2
0.26	17.0	3.8	28.4
0.26	17.0	3.8	28.4
0.11	30.0	9.1	55.1
0.11	31.0	9.1	55.1
0.06	61.0	16.7	70.1
0.06	53.0	16.7	70.1
0.035	85.0	28.6	79.3
0.035	83.0	28.6	79.3
0.02	117.0	50.0	85.4
0.02	145.0	50.0	85.4
0.01	146.0	100.0	89.8
0.01	194.0	100.0	89.8

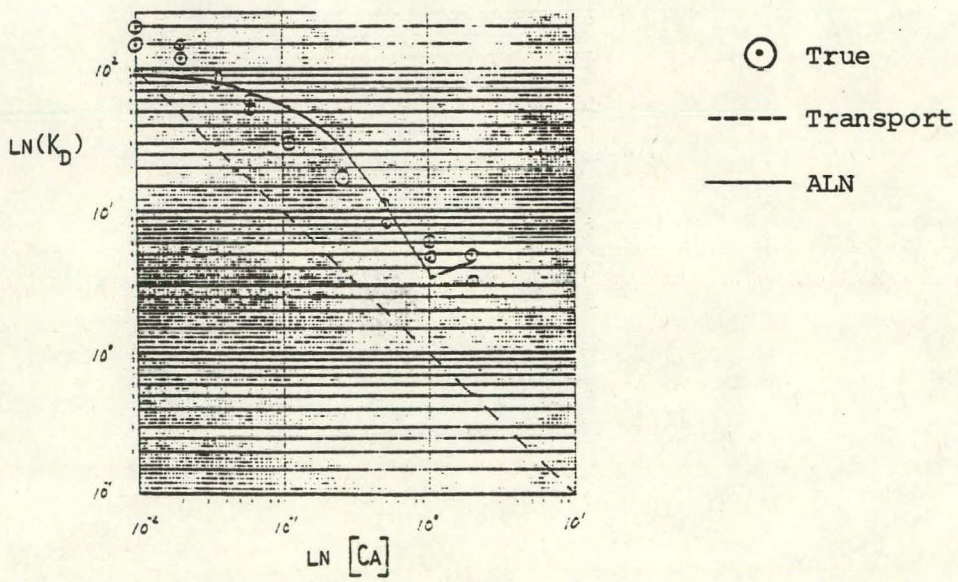

FIGURE 7.4: Ba^{2+}/Ca^{2+} EXCHANGE ON Ca FORM OF PURIFIED Na - MONTMORILLONITE

Sr^{2+}/Ca^{2+} EXCHANGE ON Ca FORM OF PURIFIED Na - MONTMORILLONITE

(No prewashes, pH ~ 5, Sr^{2+} initial = 1.25×10^{-4} M, shaking for 36 hours)

Transport Equation: $\ell_N (K_D) = -1 \ell_N [Ca]$

ALN Equation: $\ell_N (K_D) = 3.201 - 6.198 [Ca] + 2.190 [Ca]^2$

	K_D (cc/gm)		
[Ca] (M)	TRUE	TRANSPORT	ALN
2.01	0.6	0.5	0.7
1.01	0.7	1.0	0.4
0.51	1.7	2.0	1.8
0.26	3.1	3.8	5.7
0.11	6.8	9.1	12.8
0.06	13.0	16.7	17.1
0.035	18.0	28.6	20.0
0.02	35.0	50.0	21.8
0.01	54.0	100.0	23.1

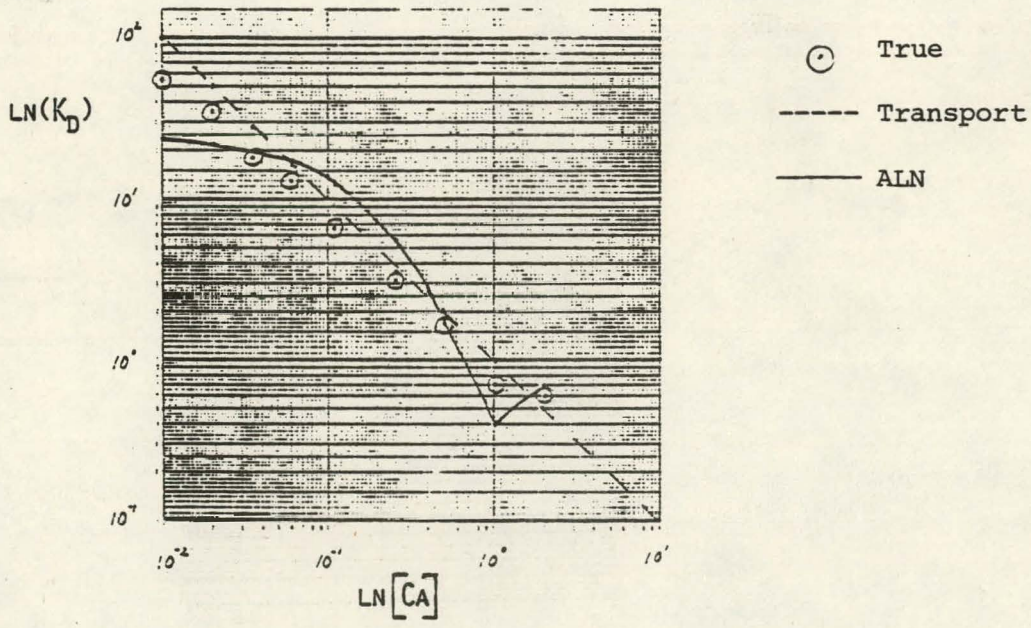

FIGURE 7.5(a): Sr^{2+}/Ca^{2+} EXCHANGE ON Ca FORM OF PURIFIED Na - MONTMORILLONITE

(No prewashes, pH ~ 5, Sr^{2+} initial = 5×10^{-4} M, shaking for 66 hours)

Transport Equation: $\mathcal{L}_N (K_D) = -1 \mathcal{L}_N [C_A]$

ALN Equation: $\mathcal{L}_N (K_D) = 2.917 - 6.561 [C_A] + 2.351 [C_A]^2$

$[C_A]$ (M)	K_D (cc/gm) TRUE	TRANSPORT	ALN
2.01	0.4	0.5	0.5
1.01	0.5	1.0	0.3
0.51	1.1	2.0	1.2
0.26	1.8	3.8	3.9
0.11	4.2	9.1	9.2
0.1	6.1	10.0	9.8
0.05	14.0	20.0	13.4
0.025	24.0	40.0	15.7
0.01	56.0	100.0	17.3

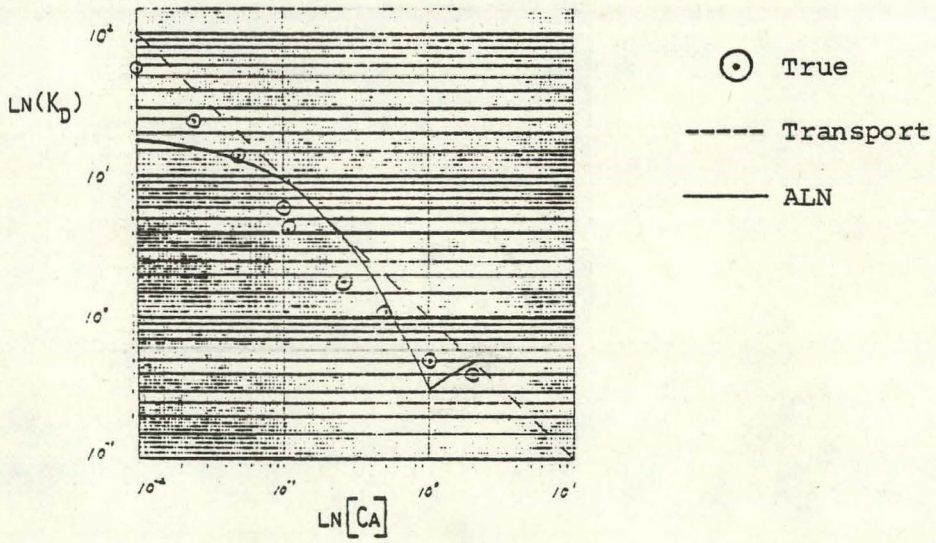

FIGURE 7.5(b): Sr^{2+}/Ca^{2+} EXCHANGE ON Ca FORM OF PURIFIED Na - MONTMORILLONITE

(No prewashes, pH ~ 5, Eu^{3+} initial ~ 5×10^{-4} M, shaking for 70 hours)

Transport Equation: $\ell_N (K_D) = -1.5\, \ell_N [C_A]$

ALN Equation: $\ell_N (K_D) = 4.714 - 21.587 [C_A] + 24.493 [C_A]^2 - 7.189 [C_A]^3$

$[C_A]$ (M)	K_D (cc/gm) TRUE	TRANSPORT	ALN
2.1	2.3	0.3	2.3
1.1	2.5	0.9	2.8
0.35	2.4	4.8	0.9
0.2	2.9	11.2	3.7
0.2	2.5	11.2	3.7
0.1	5.7	31.6	16.3
0.05	21.0	89.5	40.2
0.025	70.0	252.9	66.0
0.01	360.0	1000.2	90.1

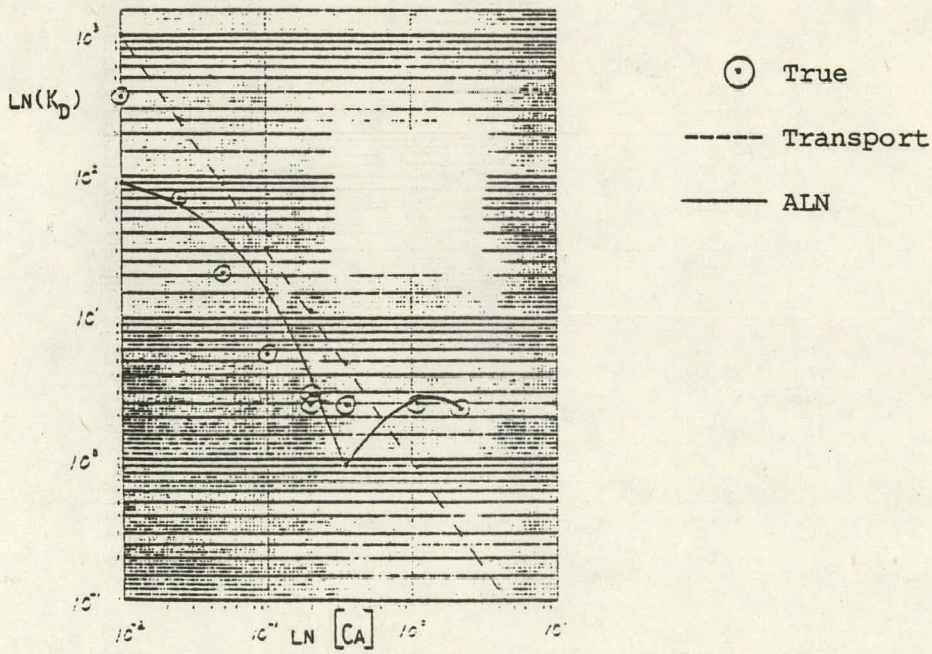

FIGURE 7.6(a): Eu^{3+}/Ca^{2+} EXCHANGE ON Ca FORM OF PURIFIED Na - MONTMORILLONITE

(No prewashes, pH ~ 5, Eu^{3+} initial ~ 5×10^{-4} M, shaking for 118 hours)

Transport Equation: $\ell_N (K_D) = -1.5 \ell_N [Ca]$

ALN Equation: $\ell_N(K_D) = 4.517 - 18.338 [Ca] + 21.047 [Ca]^2 - 6.261 [Ca]^3$

[Ca] (M)	K_D (cc/gm) TRUE	TRANSPORT	ALN
2.1	2.4	0.3	2.3
1.1	2.9	0.9	4.4
0.6	2.3	2.2	0.8
0.35	1.3	4.8	1.5
0.2	3.4	11.2	5.2
0.1	5.5	31.6	17.9
0.05	17.0	89.5	38.6
0.025	58.0	252.9	58.6
0.01	490.0	1000.2	76.3

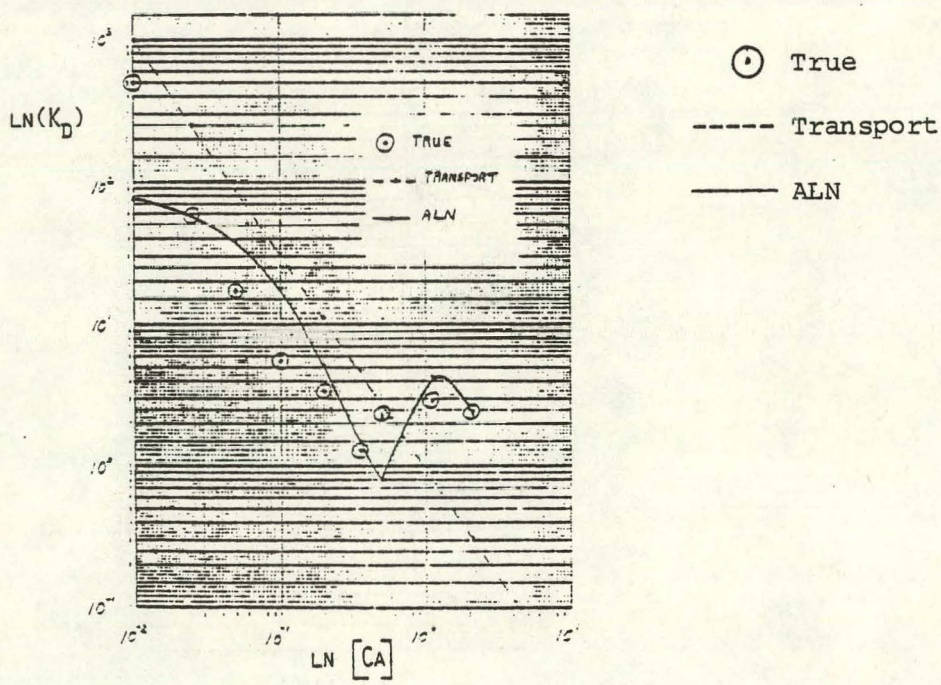

FIGURE 7.6(b): Eu^{3+}/Ca^{2+} EXCHANGE ON Ca FORM OF PURIFIED Na - MONTMORILLONITE

TABLE 7.1: ION EXCHANGE AND ALN EQUATION FOR VARIOUS TRACER/BULK ION EXPERIMENTS

SYSTEM	CONDITIONS	TRANSPORT EQUATION	
		ION EXCHANGE	ALN
K^+/Na^+	$K_o^+ = 1.25 \times 10^{-4}$ M	$1.5-2Na+0.5Na^2$	$4.1-2.5Na+0.5Na^2$
Na^+/Ca^{2+}	BATCH/t=4.5h	$0.8-1Ca+0.3Ca^2$	$2.4-1.6Ca+0.3Ca^2$
Na^+/Ca^{2+}	BATCH/t=140	$0.8-1Ca+0.3Ca^2$	$2.5-1.9Ca+0.3Ca^2$
Na^+/Ca^{2+}	COLUMN/t=0	$0.8-1Ca+0.3Ca^2$	$2.4-3.4Ca+1.9Ca^2$
Cs^+/Ca^{2+}	$Cs_o^+=1.25 \times 10^{-4}$	$0.8-1Ca+0.3Ca^2$	$6.4-1.2Ca+0.4Ca^2$
Ca^+/Ca^{2+}	$Cs_o^+=5 \times 10^{-5}$	$0.8-1Ca+0.3Ca^2$	$6.9-1.7Ca+0.7Ca^2$
Cs^+/Ca^{2+}	$Cs_o^+=2 \times 10^{-5}$	$0.8-1Ca+0.3Ca^2$	$7.1-1.7Ca+0.6Ca^2$
Cs^+/Ca^{2+}	$Cs_o^+ \simeq 0$	$0.8-1Ca+0.3Ca^2$	$9.3-4.6Ca+2.4Ca^2$
Ba^{2+}/Ca^{2+}	Dup. Exper.	$1.5-2Ca+0.5Ca^2$	$4.6-5.0Ca+1.8Ca^2$
Sr^{2+}/Ca^{2+}	$Sr_o^{2+} = 1.25 \times 10^{-4}$	$1.5-2Ca+0.5Ca^2$	$3.2-6.2Ca+2.2Ca^2$
Sr^{2+}/Ca^{2+}	$Sr_o^{2+} = 5 \times 10^{-4}$	$1.5-2Ca+0.5Ca^2$	$2.9-6.6Ca+2.4Ca^2$
Ea^{3+}/Ca^{2+}	t=70h	$2.7-3.8Ca+2.3Ca^2-0.5Ca^3$	$4.7-21.6Ca+24.5Ca^2-7.2Ca^3$
Ea^{3+}/Ca^{2+}	t=118h	$2.7-3.8Ca+2.3Ca^2-0.5Ca^3$	$4.5-18.3Ca+21.1Ca^2-6.3Ca^3$

obtained by expanding Equation 5.1 in either a quadratic or cubic, depending on the form of the ALN model synthesized.

7.4 DISCUSSION

It can be seen that the ion exchange and ALN equations generally agree well in all coefficients but the constant term for the K^+/Na^+, Na^+/Ca^{2+} and Cs^+/Ca^{2+} systems. The addition of the equilibrium constant Q in Equation 5.3 could make a difference in this coefficient. There is more disagreement between the two models for the Ba^{2+}/Ca^{2+}, Sr^{2+}/Ca^{2+} and Eu^{3+}/Ca^{2+} systems. Since the ALN model gave better results in this case, and since modification of the intercept term would not dramatically improve the transport results, it appears that an "improved" transport equation has been synthesized by the ALN.

8. CONCLUSIONS

The major conclusions from this year's work are:

(1) The ALN K_d predictive equations are quite accurate, with good generalizing capability for new data.

(2) The important solid and solution variables -- and their interactions -- have been identified for each isotope studied.

(3) The important solid and solution variables have been rank-ordered, based on their relative importance in predicting K_d for each isotope.

(4) An analysis of reversibility was conducted.

(5) The feasibility of constructing a solid K_d predictive model as a weighted sum of silicate group models was established for some isotope/solid/solution conditions.

(6) Good agreement was shown between the classical ion exchange and ALN models for the ORNL data base for most of the isotope/bulk ion systems studied; in the other cases, the ALN model produced an "improved" ion exchange equation.

9. REFERENCES

1. Ames, L.L., Controlled Sample Program Publication No. 1: Characterization of Rock Samples, Battelle-Pacific Northwest Laboratories Report PNL-2797, October 1978.

2. CRC Handbook of Tables for Probability and Statistics, W. H. Beyer (ed.), 1966, p. 226.

3. Mucciardi, A.N. et. al., Statisitcal Investigation of the Mechanics Controlling Radionuclide Sorption, Part II, Adaptronics, Inc. Final Technical Report to Battelle-Pacific Northwest Laboratories under Contract No. B-56067-A-P, December 1978 (Revised April 1978).

4. Orr, E.C. and A. N. Mucciardi, Statistical Investigation of the Mechanics Controlling-Radionuclide Sorption, Adaptronics, Inc. Final Technical Report to Battelle-Pacific Northwest Laboratories under Contract No. B-38119-A-K. October 1977.

5. Triolo, R. and M. H. Lietzke, Adsorption on Mixtures of Ion Exchangers, Oak Ridge National Laboratory Report No. ORNL-5527, April 1979.

QUESTIONS AND ANSWERS

MUCCIARDI

Kd Modeled as Logarithmic Function

Q: When you write Kd as one of your variables, do you really mean Kd, or the model Kd? I mean, the difference between 10,000 and 11,000 is surely less significant than between 1,000 and 1,100.

A: Mostly the model using log Kd. In this particular case we're using the Kd value besides.

Q: I wonder if that distorts your information?

A: Percentage-wise there is no difference between large and small Kds.

Ion Exchange Equation Model

Q: There is one thing missing. You need a constant in there as well. We've assumed that all equilibrium constants are unity, but this is not so when x = unity. Take the last equation below the line. Kd is equal to 1/X C. X is, say, the sodium concentration. X is equal to unity, then we will find that Kd has to be unity. But in reality the specificity of the absorbent has to come in. There has to be an additional constant in there. The ion exchange equation only gives the derivative, the change in the distribution coefficient with composition, but not the absolute value. That has to be met in addition.

A: So you're saying that if Na is unity here, the log of Kd....

C: Right. You're making all equilibrium constants automatically equal to unity. And that is not correct.

A: You're right.

Sensitivity of Coefficients to Data

Q: Is there any way you can establish the sensitivity of the coefficients to the range of values that might have arisen for basically comparable conditions to see whether or not you need to modify your values? For example, by feeding them a weighted input which might be the weighted mean of the literature value.

A: Yes, exactly.

Q: You plan to do something about this now?

A: Could be done. We, in fact, have a hint of that since these experiments were triplicated. There was a fair difference between the three replicates. Last year we reported on instances in which we used only one or two of the values and predicted the third. The errors averaged out about the same, but there were still considerable differences. One way to do it would be to include all three as part of the science so the model would learn the variance as well and account for that.

Variation of Real and Predicted Kds

Q: Can you dial in the error of the measurement?

A: Yes.

Q: Do you have the same conclusions as you would otherwise? The Kd is not a hard and fast number. It's a 5±3. What would your program do in that case? Would it still get the same conclusions or would it say there is an 85% chance that it's false but certain relations exist and 15% is outside of it. Does it do those things? Or what?

A: It could. You could introduce the noise by deliberately adding noise to the experiment. For instance, if you had only run one experiment, you would run three or four or more so that you would get a certain range of observation. Furthermore, you also know more or less what the range of sensitivity on your experimental conditions were. One of the inputs was pH and you were measuring it with a glass electrode. You know that, from experience, it would be off by such an amount. You could actually take that one experiment and perturbate each of the inputs throughout your range so you could artifically generate several experiments from it and then use the data as if they were actually raw. Consequently, the system would have to learn to cope with noise, actually, find a surface that would operationally go through those noise values. If you have the actual data in the literature, then go ahead and use those, as well.

Missing Data

Q: What I want to ask is not in any way a criticism of the model. I think it is a fascinating approach, but I would I ask a question of the data base manager. You showed that there are some systems with large holes; for example, the basalt system had 24% others. I saw three classes of silicates there--phyllosilicates, inosilicates and tectosilicates. I didn't see any ortho-silicates. In many of the basalts I've seen olivine occurred. Now are we shortchanging this gentleman by not giving him the whole story maybe? Using olivine just as an example?

A: If I were going to look at the Hanford basalt and look at the adsorption data that exist for it, one of the larger experiments, conducted inadvertently but which resulted in a large sorption, did not rely on olivine. I think that much of the sorption capacity in that rock type is...may not be well included here. I'm not sure what materials are on the fracture surfaces, perhaps some others have done that.

Q: I've been wondering if some other basalts have been considered besides Hanford basalt.

C: I think the general comment can be made that an experiment as we see it, or as it's reported, may be deficient in vital pieces of information that may allow us to relate that experiment with other data. I think that's generally true, although there may be exceptions.

Reversibility

Q: Did you get results from any of the reversibility studies, or did you miss something?

A: I haven't analyzed it. In last year's report, for four of the seven isotopes and twelve minerals for which adsorption and desorption were available, we've run the data but we just haven't looked at it yet.

Q: What would happen if you took data for cesium or strontium where there is relatively good agreement rather than using one lab? Have you ever tried that?

A: I believe that's what we're going to be doing this year, just to incorporate the other lab data. In fact, we hoped to last year, but it just wasn't available.

Other Variables (Too Many or Not Enough)

C: Several of these talks today have made an excellent point of how sensitive these data are to loading terms, which is not a factor in this analysis at all. Another point is how time dependent many of these observations are. Yet all of these discussions use constant times--30 days. So there are at least two variables and I think probably more than that have been discussed today that are not a factor in this analysis.

C: That's true. The data for loading are available. You can calculate the loading since you have the cations exchange capacity, and all of the other parameters. It may even turn out that mathematically the loading is implicit. But it hasn't been explicitly called out in the key variable and we can certainly do that.

C: We saw orders of magnitude variations today which arise from this factor alone.

C: Right. There is potential that mathematically and implicitly within some of those 66 characteristics loading is already there. But we can certainly draw from there and explicitly create a 67th characteristic called loading, plug that back in and use it as an extra variable.

C: You want to redo your 66 and see if all of them still qualify. It may be that you can eliminate some.

Computer Time

Q: How much computer time does it take to make a run on these types of data?

A: Only a few minutes; we're running on a big computer--cyber 176. Most of the time is involved in interpreting the data and in preparation.

Q: You seem to be getting good agreement as long as you stay with Kd values, but you never examined the high values. The high values tended to dominate your final results. Can you see any way of getting around that problems?

A: Are you referring to those tables I had?

Q: Yes, where you had 10^5 which clearly dominated everything else. Is there a way of averaging?

A: I haven't really studied as to why that's the case. You take a rock that might have 10% of one silicate group. You could very well be extrapolating in that case. Everything is really blowing up. Even though you're multiplying it with a low weight, it doesn't really compensate; 0.10×10^4 is still a large number.

Q: I think it might make some sense to take the logarithm of the Kd before multiplying by the weight. Weight = the logarithm of Kds....

A: Yes, but the theoretical equation of the combination, unfortunately in this case, is linear, if there is no interaction between the various solids. That is not always true. Then, the observed distribution coefficient should be the weighted sum of the individual distribution coefficients, unfortunately not the logarithm.

A: Just looking at the data I can knock out the extreme sensitivity for the higher numbers.

Q: You may have to impose some limits on your calculations.

A: Clearly the input variables are different in the case of, say, the inosilicates in a model than true inosilicates in their own model. Something is clearly out of whack.

Q: Another thing you could do is choose only the modeling parameters that were reasonably comparable before you do the individual models, for each of these three silicate groups or anything else. This method may be artificial, but it certainly would be a way of stabilizing the answer. There is a report by Striodle and Beatski on what the most simple theory is on how to combine these various solids.

A: The simple theory is known, and they have several curves computed for different combinations.

Q: Does anybody know why it would work better with strontium than technetium?

A: Those reactions are more linear.

Q: Well, technetium can exist in multiple valence states as an anion, for example, so you've got 2 or 3 different oxidation states or components that you may be dealing with. Anion adsorption capacity is generally very low so you're probably dealing with saturated sites, multiple sites adsorption. Strontium generally is dealt with in calcium-dominated waters where it can enhance with the calcium. And it doesn't exchange very strongly so you can put high concentrations without getting non-linear effects.

C: I'd like to make a comment. Point 1 is in your 66 factors you have mentioned. One is the surface area. Now it is well known that surface area measurement can widely vary if you measure with BET, ethylene/glycol or some other methods. I would caution you that you should know which method is used because it is going to make a difference. Also, to go from minerals to a rock you're skipping one step. You need to look at the adsorption of, say, Kd measurements of the state of the nuclides on the number of minerals, combine these minerals in a pot as small particles, and then measure Kd to see if that is a number you can calculate. If so, then go on to the next step. I think that by going directly from

Kd measurements on a particular number of minerals and then to a rock is to simply go one step too far. Instead, look at the measurement of cesium, say, adsorption on a sample which contains 20% quartz and 40% plagioclase and so on.

THIS PAGE

WAS INTENTIONALLY

LEFT BLANK

TRANSPORT OF RADIONUCLIDES IN GEOLOGIC MEDIA
Annual Report

M. G. Seitz, P. G. Rickert, R. A. Couture, J. Williams
N. Meldgin, S. M. Fried, A. M. Friedman, and M. J. Steindler

October 15, 1979

Prepared for the
Office of Waste Isolation Safety Assessment Program
with the U.S. Department of Energy

Argonne National Laboratory
9700 South Cass Avenue
Argonne, Illinois 60439

THIS PAGE

WAS INTENTIONALLY

LEFT BLANK

TRANSPORT OF RADIONUCLIDES IN GEOLOGIC MEDIA
Annual Report

October 1978 to September 1979

by

M. G. Seitz, P. G. Rickert, R. A. Couture, J. Williams,
N. Meldgin, S. M. Fried, A. M. Friedman, and M. J. Steindler

ABSTRACT

Experimental results obtained this year confirm the results obtained in previous years--that nuclides migrating by fluid flow in rock often exhibit complex behavior not predicted by simple chromatographic-type models.

A phenomenon found to lead to complex behavior for leached radionuclides is that the amount of adsorbed nuclide was not proportional to the nuclide concentration in solution (nonlinear adsorption isotherm). For cesium adsorption on limestone and on basalt, nonlinear isotherms were found to occur in the range of initial cesium concentrations in the groundwater of about 10^{-3} to 10^{-9}M. Because cesium concentrations in this range can readily be attained by the leaching of solid waste by groundwater, the effects of nonlinear isotherms are germane to nuclide migration. This dependence of cesium migration on the leached concentration of cesium emphasizes the importance of treating the leaching and migration processes simultaneously. The nonlinear adsorption properties of cesium were confirmed by results of column-infiltration experiments in which cesium migration through limestone and basalt was found to be sensitive to the amount of cesium in solution. The existence of nonlinear isotherms precludes the use of a single partition coefficient (K_d) to describe cesium migration at an arbitrary cesium concentration above 10^{-9}M. Nonetheless, nonlinear isotherms can be studied experimentally (e.g., to give K_d as a function of concentration) and effects of nonlinear adsorption predicted quantitatively.

Comparison of results from column and batch tests suggests that in addition to nonlinear adsorption, kinetic effects need to be considered in predicting nuclide migration from partition coefficients measured in batch tests.

The ability to understand complicating effects such as nonlinear adsorption and to treat kinetic effects suggests that considerably more rigor than has been used previously is possible in the modeling of nuclide migration in geologic bodies.

I. INTRODUCTION

A. OBJECTIVE OF PROGRAM

Disposal of radioactive waste in geologic formations offers a practical method of permanently isolating the waste from the biosphere. Of the many barriers that would restrict movement of the disposed waste, the final barrier between the waste and the biosphere would be the geologic formation itself. The purpose of this work is to define, as quantitatively as possible, the geologic formation as a barrier to the movement of radio-waste elements. The work is part of the larger Task 4 Waste Isolation Safety Assessment Program to evaluate the potential for migration of radionuclides from a breached repository. Previous efforts in this program have been reported by Serne (Serne, 1979).

B. PROGRESS REPORTED PREVIOUSLY

Previous results from our work indicate that many geologic formations are barriers to the movement of waste elements in flowing groundwater. However, reactions that retard element migration are varied and do not lend themselves to simplified description. Nuclides migrating by fluid flow in rock often exhibit complex behavior (bleeding, dispersion of nuclide velocities, etc.) not predicted by simple chromatographic-type models.

The work performed last year focused on the incomplete water-nuclide-rock reactions and quantitatively treated the effects of slow reaction kinetics on nuclide migration. A kinetic factor derived from the experimental results for strontium migration through glauconite (a hydrous silicate) was expressed in terms of the linear flow rate of solution and can be used to predict migration due to solution flow at rates from 0 to about 12 cm/min (60 km/y).

Continuous-flow infiltration experiments with americium in fissures gave results that are predicted by a migration model that includes kinetic factors measured in experiments with static fluids. The results suggest that kinetic

factors are as important as equilibrium adsorption parameters in predicting nuclide migration (Rickert).

Successful treatment of kinetic effects and the ability to sort out complicating effects (such as nonlinear adsorption isotherms) suggested last year that considerably more rigor is possible in the modeling of nuclide migration in geologic bodies than had been achieved previously.

C. EXPERIMENTAL OBJECTIVES

In safety evaluations of a waste repository, the concept of a partition coefficient, K_d, is widely used to predict the migration velocity of a radionuclide through rock. The distribution coefficient expresses the amount of a radionuclide partitioned onto a solid phase per mass of solid and per amount of the radionuclide in solution. Among the many possible reasons for failure of a prediction of migration velocity from a partition coefficient are (1) the radionuclide may not be locally in equilibrium with the rock and solution because of slow reaction kinetics; (2) the fraction of radionuclide adsorbed by the rock may depend upon the nuclide concentration; and (3) adsorption reaction invoked experimentally to measure a partition coefficient (such as adsorption on the surfaces of crushed rock) may not represent the adsorption reactions required for prediction (such as adsorption on pores or fissures of rock).

In spite of these limitations, interest in partition coefficients to predict nuclide velocity through a rock formation continues (1) because of the ease with which a coefficient for any nuclide-rock pair is measured and (2) because of the mathematical simplification that such an approach affords. Because there is a wealth of partition coefficient data available and the amount of data continues to grow, we have conducted experiments to establish the relationship between migration observed experimentally in columns of rock material and migration predicted by partition coefficients measured with the same material. This work is considered the first of several steps required for successful prediction of nuclide migration in geologic formations from partition coefficients measured in the laboratory. An integral part of this

study is the examination of the dependence of nuclide adsorption on the concentrations of the nuclide in the solution (at low nuclide concentrations).

Since radiation can affect the solute ions and the solid substrate, radiation can affect nuclide migration. In an initial examination of radiation effects on migration, batch-partitioning experiments to study the adsorption of cesium, rubidium, and strontium from irradiated solutions onto nonirradiated and irradiated rock material were performed.

Increasing interest is being focused on the nuclide equilibration process in which nuclides penetrate to deeper layers of solid rock with increasing time. Because solid diffusion rates for radionuclides through minierals are low, pores, intracrystalline boundaries, crystal defects, etc. must provide access to the deep regions of rock material. One tool for measuring the extent of fine pores in solids is the high-pressure porosimeter. This instrument was employed to examine pore size distributions of rock materials for which adsorption of nuclides at deep sites was suspected because of the release behavior of adsorbed radionuclides.

Leach-migration experiments which treat leaching and migration processes simultaneously are continuing. A newly designed, chemically inert, rock-column holder permits leach-migration experiments with solid or fractured rock cores under high pressures.

II. THEORETICAL CONSIDERATIONS

A. CONCENTRATION DEPENDENCE OF TRACE ELEMENT MIGRATION

The concept of the distribution coefficient, K_d, to express the distribution of a solute between solution and a solid phase is widely used to predict the migration velocity of a radionuclide through rocks, sediments, and soils. However, K_d is observed in this work to vary at very low trace element concentrations, preventing prediction by this method.

In this section, the principles of adsorption behavior expected at low trace element concentrations and the consequences of that behavior are examined briefly. For several systems, we have calculated under what conditions

appreciable loading of ion exchange sites can be expected to occur and have compared these calculations with observations. Nonlinear isotherm behavior (nonconstant K_d) is shown to be a feature expected for many water-rock systems, making inappropriate the concept of a single K_d value to represent adsorption that is independent of concentration.

1. Use of the Partition Coefficient

The partition coefficient expresses the amount of the element partitioned onto a solid phase per unit of substrate and per unit of concentration of the element in solution (solute). For ion exchange, there is generally a region at low solute concentration at which the partition coefficient is constant. Under certain conditions, the mean velocity of a solute through a packed column, relative to the velocity of solvent, can be predicted approximately by knowing the partition coefficient, the porosity of the column, and the density of the solid. Prediction is based on the principle that the relative velocity is equal to the fraction of the solute in solution.

Of several possible reasons for failure of such a prediction of migration velocity, only nonconstant partition coefficients are of concern in this discussion. Aside from the obvious case in which the partition coefficient is not constant because a solute has precipitated (as, for example, PuO_2), the partition coefficient can vary with solute concentration once the solute populates a large fraction of the ion exchange or adsorption sites. The following analysis is useful for determining the stage in the adsorption process at which nonlinear behavior is virtually certain.

2. Ion Exchange Equations

An example of simple ion exchange illustrates the basic principle. The following equations, modified from (Wahlberg and Fishman, 1962) and (Wahlberg, Baker, Vernon and Dewar, 1965), have been shown to be an approximate representation in many cases of ion exchange data on clay minerals. Consider Cs^+-Na^+ exchange on a substrate whose exchange positions are denoted by "X".

$[CsX]$, $[NaX]$ = concentrations in the substrate.

$[Cs^+]$, $[Na^+]$ = concentrations in solution.

λ_{CsX} , λ_{NaX} = activity coefficients in the substrate.

γ_{Cs^+} , γ_{Na^+} = activity coefficient in the liquid.

K = equilibrium constant.

According to the mass action law, the equilibrium constant is expressed by

$$K = \frac{\lambda_{CsX}\,[CsX]}{\lambda_{NaX}\,[NaX]} \cdot \frac{\gamma_{Na^+}\,[Na^+]}{\gamma_{Cs^+}\,[Cs^+]} \qquad (1)$$

By rewriting Eq. 1, the partition coefficient for cesium can be expressed by

$$K_d = \frac{[CsX]}{[Cs^+]} = K\frac{\lambda_{NaX}\,[NaX]\,\gamma_{Cs^+}}{\lambda_{CsX}\,[Na^+]\,\gamma_{Na^+}} \qquad (2)$$

Since cesium is a rare element, the ratio of cesium to sodium in most natural systems is small. Thus, $[CsX] \ll [NaX]$; *i.e.* most of the exchange sites will be occupied by sodium. Thus, $[NaX]$ is nearly constant (and equal to the ion exchange capacity), and λ_{NaX} and λ_{CsX} are constant. The standard state is defined here so that $\lambda_{NaX} = 1$. At a given ionic strength, $\gamma_{Cs^+}/\gamma_{Na^+}$ is constant and generally near unity. Thus, in this case

$$K_d = \frac{[CsX]}{[Cs^+]} \approx K' \frac{[NaX]}{[Na^+]}\,, \qquad (3)$$

where K' is the selectivity coefficient, approximately equal to K/λ_{CsX} at low loading, and $[NaX]$ equals the ion exchange capacity. Thus, in this simple system, the distribution of cesium between solid and liquid depends on $[Na^+]$ but not on $[Cs^+]$.

However, if there is an appreciable concentration of cesium in the exchange positions, $[NaX]$ < exchange capacity and K_d is proportionately diminished, according to Eq. 2. Equation 3 is obeyed only if the ratio $[CsX]/[NaX]$ is small. A rough estimate of this ratio can be obtained from Eq. 2 by ignoring activity coefficients, so that

$$\frac{[CsX]}{[NaX]} \approx K' \frac{[Cs^+]}{[Na^+]}\,. \qquad (4)$$

Analogous equations can be written for other ions. For Ca^+-Cs^+ exchange, the equation would be

$$\frac{[CsX]}{2[CaX_2]} \approx \frac{1}{2}\left(\frac{K'}{\gamma_{Ca^{++}}[Ca^{++}]\,[CaX_2]}\right)^{1/2} \cdot \gamma_{Cs^+}[Cs^+], \quad (5)$$

where

$$K' = \frac{[CsX]^2\,[Ca^{++}]}{[Cs^+]^2\,[CaX_2]}$$

In section 4 below, we apply these and analogous equations to typical groundwaters.

3. Nonequivalent Ion-Exchange Sites

Any rock may have two or more types of nonequivalent ion-exchange sites. The most obvious example is a multi-mineral rock, in which each mineral is selective for a different solute. In fact, pure minerals and synthetic compounds also are known to have nonequivalent bonding sites (Garrels and Christ, 1956), (Kraus *et. al.* 1958), (Lieser and Kluge, 1967), (Schroeder, 1965). The implication is that a trace element might saturate its preferred bonding sites at concentrations on the substrate far below the determined ion-exchange capacity. In this case, the partition coefficient might be very dependent on trace-element concentration, as section 4 (below) shows.

4. Cs^+-Ca^{++} Exchange in Natural Systems

Because most groundwaters are dilute and because Ca^{++} is generally the most common dissolved cation in groundwater (White, Hem and Waring, 1963), Ca^{++} is generally the most abundant exchangeable ion on clays (Sayles and Mogelsdorf, 1977). (Sodium ion can be the dominant exchangeable ion in arid environments--especially desert soils--and in brines--but such groundwaters are not considered in this discussion). We have estimated the amount of exchangeable cesium in Ca-montmorillonite.

Table 1 shows values of K' for Cs^+-Ca^{++} exchange calculated from the literature and also shows the cesium concentrations in solution at 50% loading of the exchange sites, estimated for typical groundwaters. For this calculation and succeeding calculations, we have assumed a Ca^{++} concentration of 2.5×10^{-4} M, which is a typical value for sandstones and igneous rocks (White, Hem and Waring, 1963). We used the Debye-Hückel law to estimate activity coefficients of the ions in solution.

Table 1 shows that the affinity of clay minerals for Cs^+ is highly dependent on the type of exchange site. Cs^+ is not highly hydrated and therefore has a low hydration energy and a relatively low affinity for the aqueous phase (in comparison to other alkali metal ions and alkaline earth metal ions). Evidently, it fits very well into some exchange sites and may be bound by the lattice in certain cases. The combination of the two factors evidently leads to a large variation in exchange constants for different clay minerals.

The data in Table 1 suggests that distribution of cesium on some clays may be quite sensitive to the cesium concentration at cesium concentrations as low as 10^{-5} or 10^{-6}M in typical groundwaters. In fact, the distribution coefficient may be mush more sensitive to concentration than is implied in Table 1. Meyer (Meyer, 1978) reported a 30% decrease in the partition coefficient between 0 and 0.01% loading! This strongly suggests that more than one type of site is responsible for absorption. Apparently, the site with the greatest affinity for Cs^+ is present in very small abundance--on the order of 0.1% or less. This is no small effect: it could cause an error of one order of magnitude or more in an estimate of the coefficient for a given set of conditions.

TABLE 1. Cesium Concentrations in Groundwater at which Clay Minerals are Estimated to be Approximately 50% Loaded with Cs^+

Mineral	Reference	K', mL/mg	Ion Exchange Capacity, equiv/kg	$[Cs^+]$ in solution at 50% Loading of Clay M
Montimorillonite 21	Wahlberg, 1962	3100	1.3	5×10^{-4}
Kaolinite 4	Wahlberg, 1962	730	0.10	3×10^{-4}
Halloysite 12	Wahlberg, 1962	1.7×10^6	0.19	7×10^{-6}
Montmorillonite	Meyer, 1978	6×10^6 to 3×10^7	0.76	8×10^{-6} to 3×10^{-6}

The second site may be present as a discrete mineral impurity, such as illite. Or it may be related to the pretreatments used to remove carbonates and iron oxides from the clay. In contrast, Wahlberg (Wahlberg and Fishman, 1962) apparently used no pretreatment. Perhaps a small amount of iron was removed from the lattice by Meyer's pretreatment creating a charge deficit which acts as an exchange site. Or perhaps the second site was present before treatment.

5. Sr^{++}-Ca^{++} Exchange in Natural Systems

The above calculation was repeated for Sr^{++} in Ca^{++}-dominated groundwater. The results are shown in Table 2. Since Sr^{++} is not greatly favored over Ca^{++} in ion exchange on clay minerals, a large concentration of dissolved Sr^{++} ($\sim 2 \times 10^{-4}$ M) would be required to cause substantial loading (and, therefore, nonlinear adsorption effects). Substantial loading is unlikely because of the low solubility of $SrCO_3$ and the rarity of strontium (compared to calcium) in nature.

The above conclusion also applies to calcite, the dominant mineral in limestone, and to dolomite as substrates. Sr^{++} is unlikely to be favored over Ca^{++} on ion-exchange sites of calcite and dolomite because it does not fit into the structure (or onto the surface) as well as Ca^{++}. Sr^{++} is a larger ion than Ca^{++}, and the differences of crystal structure of $SrCO_3$ and calcite hinders accommodating the larger ion. Thus, loading of ion-exchange sites with Sr^{++} is unlikely except at unusually high dissolved Sr^{++} concentrations.

TABLE 2. Strontium Concentrations in Groundwater at which Clay Minerals are Estimated to be Approximately 50% Loaded with Sr^{++}. From (Wahlberg, Baker, Vernon and Dewar, 1965).

Mineral	K', mL/mg	$[Sr^{++}]$ in Solution at 50% Loading of Clay, M
Montomorillonite 21	1.1	2×10^{-4}
Illite 35	1.1	2×10^{-4}
Kaolinite 4	0.9	3×10^{-4}
Kaolinite 7	1.2	2×10^{-4}

6. Eu^{3+} - Ca^{++} Exchange In Natural Systems

Partitioning of actinide and lanthanide +3 ions on montmorillonite in NaCl solutions was studied by (Meyer *et al.* 1978). Results were very similar for all ions. Also studied was partitioning of Eu^{3+} ions on montmorillonite in calcium acetate solutions.

The results are probably typical of results for the other lanthanide and actinide +3 ions. At 50% equivalent loading of the clay, the concentration of Eu^{3+} in the groundwater is estimated to be 2×10^{-6}M. However, after correction of that value for acetate complexing in the experiment, the concentration of Eu^{3+} at 50% loading is estimated to be 3×10^{-7} to 7×10^{-7}M, or perhaps less.

Thus, a concentration dependence of sorption by lanthanide and actinide 3+ ions similar to that found for Cs^{+} would not be surprising. Very few data are available to evaluate this speculation--we merely intend to alert experimenters to the problem. In fact, in some cases hydrolysis of the actinide ions may increase sorption so that the concentration dependence is observable at even lower concentrations than estimated here (James and Healy, 1972).

7. Discussion

One might assume that nonlinear isotherms are most likely for rocks and minerals which have a low ion-exchange capacity, such as limestone. However, our analysis suggests that this is not the case. The shape of the isotherm (that is, the amount adsorbed plotted against the solution concentration) depends on the equilibrium constant; it does not necessarily depend on the ion-exchange capacity. In sorption experiments, a high exchange capacity leads to low solution concentrations, which helps to reduce the tendency toward nonlinear behavior. However, we note that montmorillonite (which has a high exchange capacity) showed a very great deviation from linearity.

The implications of these findings on waste disposal are not necessarily severe. Fortunately, nonlinear behavior is greatest for ions which are bound most tightly, and so it is not likely to portend a substantial release of radioactive material from a repository. The danger lies in the difficulty which nonlinear isotherms pose in obtaining accurate and representative data.

If nonlinear isotherms are not understood, there might be substantial errors in evaluating releases from repositories or a lack of confidence in experimental results.

Fortunately, the problem can be dealt with merely by determining the shape of the isotherm. Also, another benefit, often overlooked, of determining the entire isotherm is that the transition from adsorption to precipitation because of increased solute concentration ought to be readily recognized by the unusual shape of an "apparent" isotherm. Other workers have had difficulty in distinquishing between adsorption and precipitation of oxides and hydroxides. Systematic study of final solute concentrations with increased substrate loading is one direct way of removing this experimental ambiguity.

Nonlinear adsorption isotherms have been commonly encountered in laboratory and industrial processes and substrates are generally selected to avoid nonlinear effects. Some natural clays and zeolites may exhibit linear adsorption even after loading with solutions containing high concentrations of the exchanging solute ion [e.g. 10^{-3}M cesium as reported by (Faucher, Southworth and Thomas, 1952)]; such materials have been studied extensively and are attractive for use in chemical porcesses. The important point in this discussion is that geologic materials, in contrast to commercially used clays or zeolites, exhibit nonlinear adsorption at very low concentrations of exchanging solute ions.

The solute concentrations at which nonlinear effects occur are readily achieved in groundwater in contact with solid waste. For example, groundwater (1 mL) in contact for 1 min with 1 cm^2 of solid waste glass at 80°C can acquire a cesium concentration of 3×10^{-7}M (this report). This is a concentration at which cesium exhibits nonlinear behavior for adsorption on limestone and basalt. Therefore, nonlinear behavior can affect the migration of radionuclides leached from solid waste.

B. KINETIC FACTORS IN NUCLIDE MIGRATION

Geochemical processes are not governed solely by chemical reactions that reach equilibrium. For example, at least two rate-determining mechanisms

must be considered for any generalized treatment of adsorption exchange processes in a geologic setting. First, solute ions must transfer from the groundwater to the rock and back again. The rate of ion transfer is governed by the extent to which the rock and groundwater phases are in contact. Secondly, diffusion may proceed within crevices, along crystal boundaries, or through crystalline defects and so that with time, more of the rock becomes available for adsorption. [These mechanisms are the same as the step-wise kinetic process and the diffusional transport process discussed by (Giddings, 1965) in regards to chromotography.] Diffusion as a rate-controlling process in radionuclide adsorption is discussed by (Neretnieks, 1979).

Either of these mechanisms may operate alone to limit a reaction between groundwater and rock, or the two mechanisms may operate together. Each mechanism is most easily studied in a system in which it operates alone.

Previous work in this program has shown that strontium adsorption on glauconite, a hydrous alumina silicate, is probably controlled by ion transfer at the solution-solid interface, as evidenced by the agreement of experimental results with the theory that makes ion transfer the rate-limiting process (Seitz et al., 1979). Actual elution curves obtained for strontium migration through glauconite are shown in Fig. 1. Figure 1A illustrates the behavior for the solution flow rate slow enough that near-equilibrium condition, on a local scale, exist between the solution and the substrate. Fig. 1B illustrates the effect of increasing the flow rate so that the solution and substrate, even on a local scale, are not in equilibrium. Because diffusion is not rate limiting, the radionuclide is presumed always to be uniformly distributed in the substrate particles as illustrated in Fig. 1A and Fig. 1B.

Prediction of diffusion, coupled with exchange processes, requires a complex mathematical treatment that is not readily solved [(Thomas, 1949), (Crank, 1975)]. Therefore, an intuititive approach to predicting the effect of this mechanism is attempted here. The first curves in Fig. 2A at the left illustrate the distribution of a radionuclide within a porous particle when diffusion within the pores is rapid and nearly complete transfer of ions from the solution to the rock is rapid. These conditions lead to simple

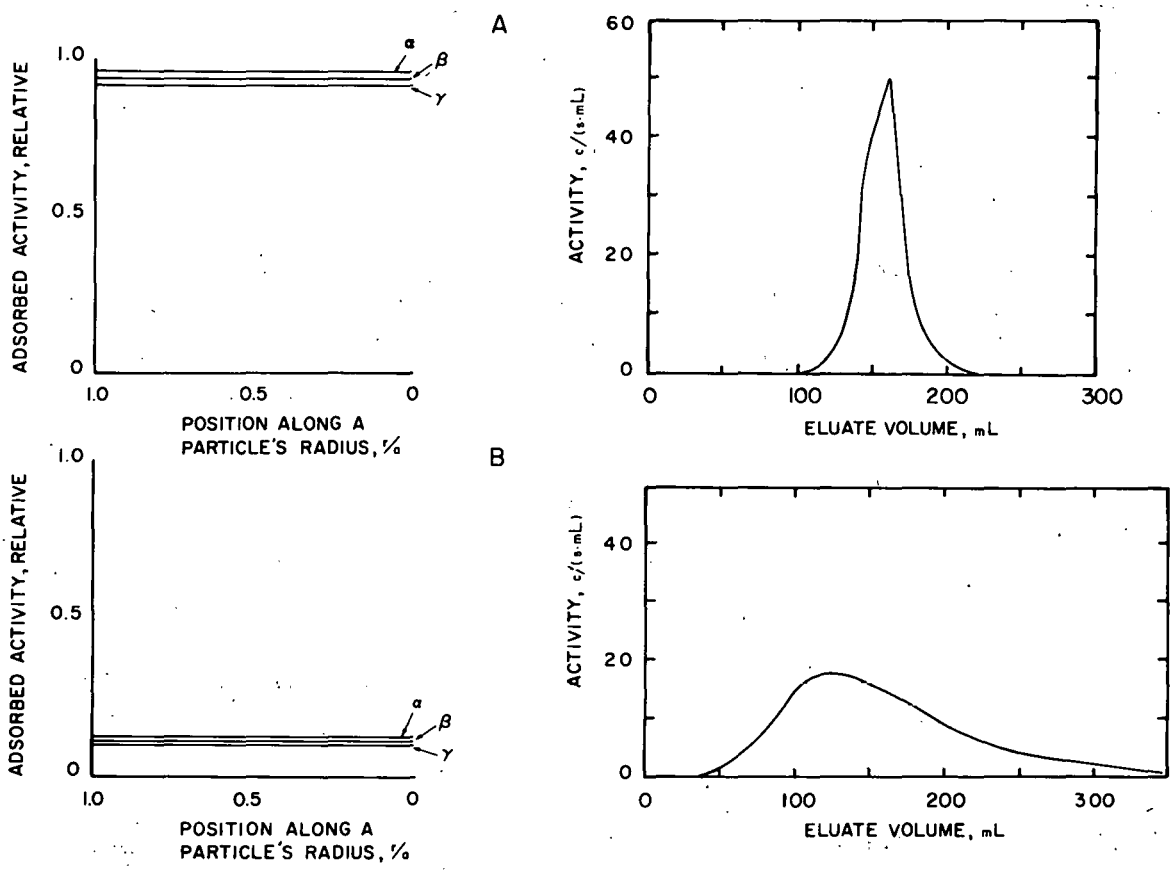

FIGURE 1. Distribution of a Radionuclide (radiostrontium) in a Porous Rock Particle (glauconite) and the Corresponding Elution Curve for Equilibrium Conditions (Fig. 1A) and Nonequilibrium Conditions (Fig. 1B). Solute interaction is controlled by ion transfer at the solid-solution interface. Curve α represents the nuclide distribution in a rock particle after initial adsorption. Curves β and γ represent the distribution after two sequential desorption steps. a = radius; r = distance along the radius of the individual particles.

migration of the ion through the rock column, as represented by hypothetically derived sharp elution peak in Fig. 2A (and in Fig. 1A). Illustrated in Fig. 2B is the behavior expected when the diffusion rate within the rock particles is low and the curve is hypothetical. Under this condition, the radionuclide is eluted more rapidly because of its restricted uptake on the rock particles. However, removal of the activity adsorbed is likewise restricted by the low diffusion rate, and a long asymmetric tail forms on the elution peak. It is

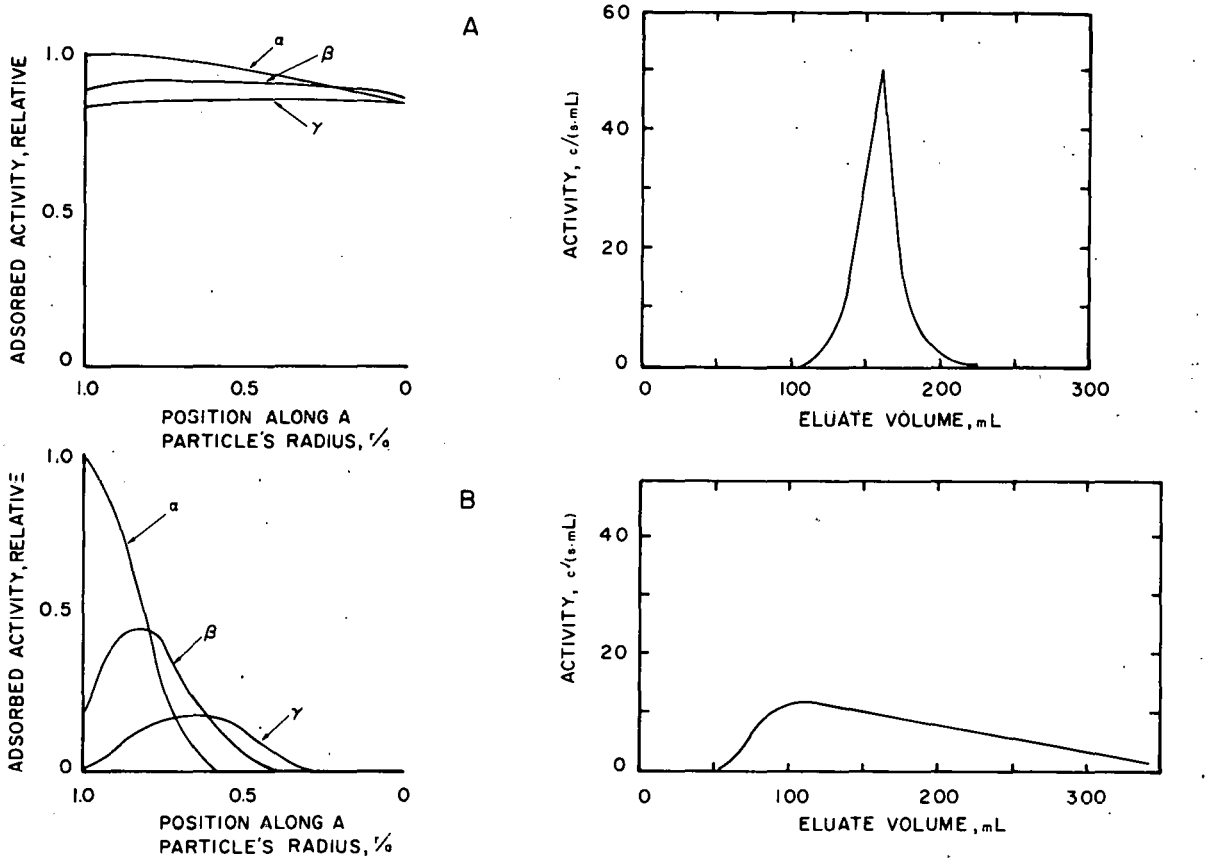

FIGURE 2. Distributions of a Radionuclide in a Rock Particle and the Corresponding Elution Curve for Near-Equilibrium Conditions (Fig. 2A) and for Nonequilibrium Conditions (Fig. 2B). Solute interaction is controlled by diffusion within the rock particle. Curve α represents the nuclide distribution in the rock particle after initial adsorption. Curves β and γ are the nuclide distributions after two sequential desorption steps.

possible, because of this condition, that much of the radionuclide would not appear in the main elution peak, per se, but would occur, rather, in the asymmetrical tail.

In this evaluation of the diffusion process, we assumed that the adsorption sites on the rock particles were occupied by stable isotope of the migrating elements prior to introduction of the radioisotope so that no net adsorption or desorption of an element occurred. The diffusion process would be considerably more complicated than is described here if, as is the more

general case, adsorption of an element exhibiting a nonlinear adsorption isotherm occurred simultaneously with diffusion.

Diagenetic processes in which rock is altered by water are expected to proceed simultaneously with nuclide adsorption and diffusion mechanisms. These diagenetic processes are time-dependent, can increase adsorption capacity, and therefore can generate effects not unlike that proposed for nuclide diffusion within rock pores. Effects of diagenesis can be distinguished from effects of diffusion by reversal and time-dependent adsorption studies.

III. EXPERIMENTAL PROGRAM

A. CESIUM CONCENTRATIONS IN LIMESTONE-EQUILIBRATED WATER

Exhibited in previous studies (Seitz et. al. 1979) has been the important role the concentration of a trace element can play in its propensity to migrate in flowing groundwater. Therefore, this study is focused on measuring cesium concentrations in groundwater solutions used in laboratory experiments.

Three solutions subjected to cesium analyses were obtained from the experiments performed to study cesium migration in oolitic limestone. The solutions are (1) a rock-equilibrated water (REW) prepared by reacting oolitic limestone with distilled water, (2) an eluant formed by passing the REW solution containing ^{134}Cs through a limestone column and, (3) a leachate formed by passing the REW solution over a solidified waste glass (McElroy, 1977) at 80°C.

A solution used as a standard in the analyses was prepared to have a cesium concentration of 9.25×10^{-6} M (as determined by atomic absorption spectroscopy) by adding $CsNO_3$ to distilled water.

The cesium analyses of the solutions were performed by neutron-activation analyses with thermal neutron and resonance-neutron fluxes. The results of the analyses, are listed in Table 3, indicate that a low but measurable concentration of cesium exists in REW solutions to which no cesium had been added. The REW solution leached a considerable quantity of cesium from the waste glass, as indicated by the high concentration of cesium in the leachate (Solution No. 3).

TABLE 3. Analyses of Cesium (Activated to ^{134}Cs) in Experimental Solutions by Resonant-Neutron Activation.

Solution No.[a]	^{134}Cs Activity in Solution, dpm			Stable Cesium Concentration,[b] M
	After Neutron Activation	Before Neutron Activation	Net	
1	2.5×10^3	$<1.0 \times 10^2$	2.5×10^3	3.6×10^{-8}
2	2.2×10^3	5.3×10^2	1.7×10^3	2.4×10^{-8}
3	2.2×10^4	7.2×10^2	2.1×10^4	3.0×10^{-7}

[a]No. 1 solution is 2 mL of REW solution made by reacting distilled water with limestone. REW, or rock-equilibrated water, is a synthetic groundwater solution typically prepared by stirring 10 g of a powdered rock in 1 L of distilled water for four weeks and filtering the solution through a 0.45μm Millipore filter. No. 2 solution is 2 mL of REW solution with added radioactive cesium that was eluted through ∿3 cm of limestone rock. No. 3 solution is 2 mL of REW solution that had leached cesium from a solid waste glass.

[b]The results are based on a standard containing 9.25×10^{-6} M cesium, giving a derived specific activity of 2.65×10^2 dpm/ng cesium.

B. NONLINEAR ADSORPTION ISOTHERM--ADSORPTION OF CESIUM

1. Cesium Adsorption on Limestone

To establish the adsorption dependence of cesium on cesium concentration, batch partitioning experiments* with cesium adsorption on limestone were performed, using synthetic groundwater solutions containing different concentrations of cesium. The batch partitioning experiments were done using materials and procedures described in the Waste Isolation Safety Assessment Program (WISAP) Controlled Sample Program (Relyea, and Serne, 1979).

The synthetic groundwater solution (consisting of 92.5 mg $Ca(OH)_2$, 18 mg $MgSO_4$, 5.8 mg NaCl, and 0.8 mg KCl per liter of distilled water) was used after being filtered through a 0.4-μm pore membrane filter. Solutions

*In a batch-partitioning experiment, a small sample of particulate rock is agitated with an aqueous solution in a test tube for several days or weeks. The partitioning of an element between solution and rock is then determined.

having different concentrations of cesium (ranging from ∿2 x 10^{-9} to 1 x 10^{-3}M) were prepared from the synthetic groundwater solution for use in the experiments. Some solutions contained stable cesium, some radioactive ^{137}Cs and some both.

The 20 to 50 mesh size aggregate of oolitic limestone supplied for this controlled sample program was wet sieved on a 60-mesh screen then dried for use in the batch experiments. Characteristics of this material are described by (Ames, 1978).

For each batch experiment, ∿3.0 g of limestone was placed in a 15 mL polystyrene centrifuge tube and was rinsed three times with synthetic groundwater solution containing cesium. Each rinse was done with 10 mL of solution in the capped centrifuge tube. The tube was rotated end-over-end six times a minute for 24 h, after which the limestone was allowed to settle and the wash solution was decanted. The centrifuge tubes with limestone aggregate were weighed before and after washing to determine the weight of residual wash solution remaining with the limestone (as prescribed in the controlled sample procedure). Also test tubes not containing limestone were rinsed in a similar manner. These tubes were used as blanks (as prescribed in the procedures). Solutions used in the third rinses of the limestone and test tubes were analyzed by flame atomic absorption and flame emission techniques with analyses given in Table 1A of the appendix.

Triplicate batch adsorption experiments were run with the washed limestone and with seven solutions having different cesium concentrations (that matched the concentrations in the wash solutions) and containing ^{137}Cs. These solutions, containing ^{137}Cs, are described in Table 2A of the appendix. Blank tests run with the rinsed test tubes and with the solutions listed in Table 2A (again matching the solutions by cesium concentrations to the test tubes rinsed with solutions of differing cesium concentration).

All test tubes were capped and rotated end over end six times a minute for three days. Seven tubes with limestone and solutions having seven different initial cesium concentrations were centrifuged, and the solutions were filtered through 0.4 μm-pore membrane filters and counted for cesium

activity. The solutions in the test tubes without limestone were filtered and counted after the fourth day. The remaining tubes were agitated periodically (twice daily for 1 h periods) and were centrifuged after either seven or eight days of contact of the radioactive solutions with the limestone.

Results of the batch tests are listed in Table 3A (Appendix) and show that cesium adsorption by limestone depends very strongly on the cesium concentration of the solution. With the highest cesium concentration, there was very little radiocesium adsorbed or exchanged with cesium on the limestone. With the lowest cesium concentration, virtually all of the radiocesium had been adsorbed by the limestone or exchanged with cesium on the limestone. Very little of the radiocesium adsorbed onto the test tubes as indicated by the activity of cesium in the solution from the test tubes without limestone being nearly equal to the activity in the solutions at the start of the experiments. [Radionuclide adsorption on test tube walls can occur even in the presence of rock material (Seitz et al, 1979A), in which case, corrections for adsorption obtained from blank tests in the absence of rock material are inadequate.]

The data given in Table 3A cannot be used by themselves to construct an adsorption isotherm because the concentrations of stable cesium in the solutions of low cesium content are not known from the radiochemical counting data alone. These solutions probably contain cesium that was derived from the limestone as does REW groundwater that was prepared by reacting water with the limestone (see Section III. A of this report).

The radiochemical counting data was combined with analyses of cesium in rinse solutions and with calculations of the amount of cesium that could be derived from limestone in order to determine the final cesium concentration in the solution with radiocesium. The analyses of the rinse solutions given in Table 1A of the appendix indicate that no net cesium was adsorbed during the third rinse of the limestone (considering the cesium concentrations in the test-tube rinses to be the initial cesium concentration of the rinse solution) and that, therefore, the limestone samples had adsorbed enough cesium from the two previous rinses to be compatible with the rinse solutions

having added cesium. Only an upper limit of 3.8×10^{-9} M cesium was determined for cesium in the rinse solution with no added cesium. This concentration is close to that indicated by the following calculation and was close to the initial concentration of the radioactive solution that contacted the limestone.

A calculation indicated that the six rinse solutions with added cesium were effective in saturating the limestone samples with cesium (saturation for the particular cesium concentration of the rinse solution) but that the solution with no added cesium would acquire a concentration of 5.9×10^{-9} M cesium by contact with the solution. For this calculation, we assumed that the limestone was in equilibrium with groundwater having $\sim 3.6 \times 10^{-8}$ M cesium and that it contained $\sim 1.6 \times 10^{-9}$ mol. cesium per gram of rock that was exchangeable with solution. The amount of cesium on the rock was calculated using a partition coefficient of 50 mL/g which is consistent with the results of these batch experiments.

Under these conditions, the limestone would gain cesium from the wash solutions containing greater than 3.6×10^{-9} M cesium and would loose cesium to wash solutions containing less than this concentration of cesium. The discrepancy between the measured and calculated values of the lowest cesium concentration may be due to the wet sieving and washing of the limestone with loss of cesium that preceded the experiments.

The curve in Fig. 3 was drawn from the measured radiochemical data (for 8 days of contact, given in Table 2A) using the final concentration of cesium in the radioactive solutions equal to the initial concentration. (As justified above).

2. Cesium Adsorption on Basalt

To establish whether or not there exists an adsorption dependence on concentration for cesium adsorption by basalt, batch partitioning experiments were performed with synthetic groundwater solutions containing six different concentrations of cesium and with Sentinel Gap basalt. The batch partitioning experiments were run using materials and procedures described in the Waste Isolation Safety Assessment Program (WISAP) Controlled Sample Program (Relyea and Serne, 1979).

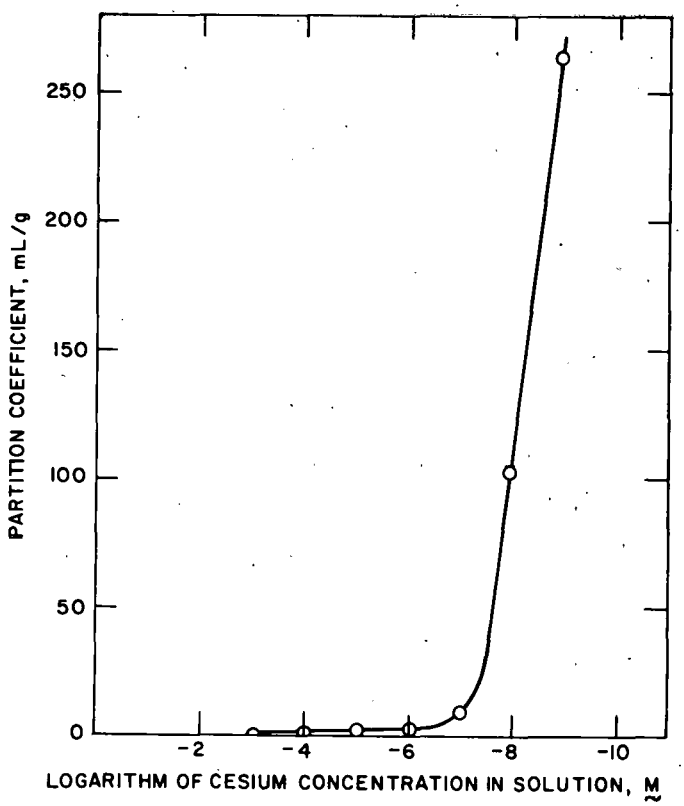

FIGURE 3. Dependence of Cesium Adsorption by Limestone on Cesium Concentration in the Groundwater Solution

A synthetic groundwater solution was prepared (with 79.8 mg $NaHCO_3$, 24.85 mg Na_2SO_4, 14.91 mg KCl, 14.42 mg $CaCl_2$, 4.81 mg $MgSO_4$, 4.76 mg $CaSO_4$, and 2.32 mg KF per liter of distilled water) and was filtered through a 0.4-μm pore membrane filter. Solutions with six different concentrations of cesium (added as CsCl), ranging from $\sim 2.6 \times 10^{-9}$ to 1×10^{-4} M, were prepared from the synthetic groundwater solution for use in the experiments. These solutions contained either radioactive ^{137}Cs or radioactive ^{137}Cs and stable cesium.

The 20-50 mesh size aggregate of Sentinel Gap basalt supplied for the controlled sample program was used in the experiments. Characteristics of this material are described by (Ames, 1978).

For each batch experiment, ∿0.8 g of basalt was placed in a 15-ml polystyrene centrifuge tube and was washed twice with synthetic groundwater solution. The contact time for the first wash was 16 days, and the contact time for the second wash was 14 days. Each wash was done with 10 mL of solution in the capped centrifuge tube. The centrifuge tubes were agitated on a rotary mixer. The centrifuge tubes with basalt aggregate were weighed before and after washing to determine the weight of residual wash solution remaining with the basalt.

Four batch adsorption experiments were run with each of six solutions having different cesium concentrations and containing radioactive ^{137}Cs. For each cesium concentration, two experiments had contact times of 15 days and two experiments had contact times of 28 days. The centrifuge tubes were tumbled on a rotary mixer to ensure thorough mixing.

After the solution was centrifuged and filtered through 0.4-μm pore size membrane filter, the concentration of radioactive cesium remaining in solution was determined for each experiment.

The results of the batch tests are listed in Table 4A (Appendix). The results show that cesium adsorption by basalt depends strongly on the cesium concentration in solution. The partition coefficients determined after 28 days of contact are larger than the partition coefficients determined after 15 days of contact. This implies that equilibrium was not attained in 15 days of contact. Equilibrium is probably not attained in 28 days either, but the contact times (15 and 28 days) are much greater than the solution residence times that will be used in column infiltration experiments with 20-50 mesh basalt.

An adsorption curve for cesium adsorption by basalt (28-day contact) is plotted in Figure 4. It was constructed using the assumption that the basalt did not contain enough exchangeable cesium to be a significant source of cesium in these experiments.

Cesium adsorption on basalt shows significant dependence on cesium concentration in the range, 1×10^{-5} to $\sim 8 \times 10^{-11}$ M.

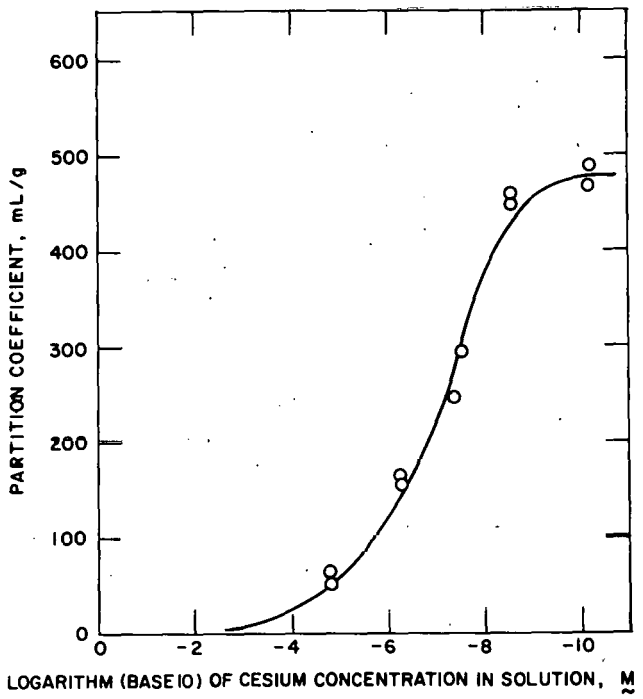

FIGURE 4. Dependence of Cesium Adsorption by Basalt (28-day contact) on Cesium Concentration.

C. RADIATION EFFECTS ON NUCLIDE MIGRATION

Ionizing radiation from radioactive wastes can modify the nuclide species in solution or the adsorption sites on the rock surface and thus can affect nuclide migration. Two different sets of experiments were done to investigate the effect of radiation on nuclide migration. In the first set of experiments, groundwater solutions containing strontium were irradiated, then exposed to limestone rock to test if radiation can affect adsorption downstream outside of the radiation field. In the second set of experiments, the solutions and rock were irradiated while cesium and rubidium adsorption was proceeding. Adsorption near the solidified radioactive waste is simulated by this type of experiment. Because nuclide concentration can play such an important role in nuclide adsorption, the experiments were done with solutions having various known concentrations of radionuclides.

1. Strontium Adsorption by Limestone from Irradiated Solutions

Batch partitioning experiments were performed with strontium on oolitic limestone, using synthetic groundwater solutions containing four different concentrations of strontium. Fractions of the four solutions were irradiated in the radiation field of a ^{60}Co source prior to the batch tests to determine whether the radiolysis would affect subsequent adsorption of strontium onto the limestone.

A synthetic groundwater used in the experiments was prepared, using reagent grade chemicals mixed with distilled water (92.3 mg $Ca(OH)_2$, 18.1 mg $MgSO_4$, 7.6 mg NaCl, and 0.9 mg KCl per liter of water (Relyea and Serne, 1978) and filtered (after two weeks of mixing) through a 0.45 μm pore pleated membrane filter). Strontium was added to aliquots of the groundwater solution in quantities to produce solutions containing 1.03×10^{-6}, 0.91×10^{-7}, and 0.9×10^{-8} M strontium. These solutions, together with the original groundwater solution (with no added strontium), were used to wash the oolitic limestone and were also used, after the addition of radioactive ^{90}Sr, in the batch experiments.

The range of strontium concentrations was chosen to be as wide as possible without causing precipitation of a strontium compound. Strontium carbonate has a solubility product of 1.6×10^{-9} M at 25°C. With a bicarbonate concentration in the solution of $\sim 2 \times 10^{-3}$ M (Seitz et al., 1979A) and an assumed concentration of carbonate ion equal to the bicarbonate ion, the solubility limit for Sr^{++} is $\sim 1 \times 10^{-6}$ M. Therefore, solutions at or below this concentration were used in the experiments.

Oolitic limestone, of 20 to 50 mesh sized aggregate, was wet sieved on a 60 mesh screen and was dried for use in the experiments. The material is described by (Ames, 1978).

For each batch experiment, 3.0 g of limestone was placed in a 15-mL polystyrene centrifuge tube and was rinsed three times with one of the four groundwater solutions (which contained different concentrations of strontium but no radioactive ^{90}Sr. Each rinse used 10 mL of solution in the capped centrifuge tube. To promote reaction of the solution with the rock material,

the tubes were rotated, end-over-end at six revolutions per minute for one continuous hour out of every six hours. Each rinse was continued for ~4 days, whereupon the limestone was allowed to settle, and the rinse solution was decanted. The centrifuge tubes that contained limestone were weighed before and after rinsing to determine the weight of residual rinse solution remaining with the limestone.

A trace quantity of radioactive ^{90}Sr was added to each of the four solutions containing different concentrations of strontium. The four solutions were each halved and placed in borosilicate Erlenmeyer flasks. One set of these solutions was irradiated in a ^{60}Co gamma field of 7.5×10^5 rad/h for 100 h.

The radiation field was measured by the change of absorbance of cobalt glass dosimeters at a light wavelength at 450λ. The solutions were then used in experiments 72 h after irradiation was terminated. The concentration of strontium in the solutions and the activities of the solutions (counted with 0.5-and 1.0-mL aliquots of solution in 15 mL of scintillation liquid) are given in Table 5A (Appendix).

Triplicate batch experiments were run with each groundwater solution by adding 10 mL of an irradiated or a nonirradiated solution to limestone which had been washed with a groundwater solution having the same strontium content as the added solution. Blank tests to evaluate strontium adsorption on the test tube walls were performed by placing aliquots of the solutions in centrifuge tubes not containing limestone.

The test tubes were again rotated (the same as for the rinsing). A set of the tubes with solutions having different strontium concentrations was removed from the rotator after 7, 14 and 21 days. The solutions were filtered through 0.4 μm pore membrane filters, and were counted by scintillation detection 3, 10, and 17 days after preparation (to establish decay equilibrium between ^{90}Sr and ^{90}Y).

Results of the batch experiments are listed in Table 6A (Appendix). The measured partition coefficients are listed in Table 4. The results indicate that strontium adsorption is sensitive to neither the irradiation of solu-

tions by gamma rays under the condition to which we exposed the solutions nor the strontium concentration in the concentration range explored. The amount of strontium adsorbed increased from 7 to 14 days of adsorption time but not from 14 to 21 days.

2. Cesium and Rubidium Adsorption by Limestone in a Radiation Field

Batch partitioning experiments were performed with cesium on oolitic limestone, using synthetic groundwater solutions containing seven different concentrations of rubidium. Cesium adsorption is sensitive to cesium concentration and is likely to be sensitive to rubidium concentration as well. In nature, rubidium, being about thirty times more abundant than cesium, may interact more with radiocesium during migration than does natural cesium.

The solutions and rock materials were irradiated while adsorption took place, and so represent the adsorption that may occur in the radiation field near the solidified waste.

The experiments were performed like the other batch experiments described in this section. In each experiment, 3.0 g of limestone in a 15-mL polystyrene centrifuge tube was rinsed three times with one of the seven groundwaters containing stable rubidium. To promote the reaction of solution with rock material, each tube was rotated end-over-end--both during the rinses and during the exchange of radioactive rubidium and cesium. One set of test tubes was irradiated in a ^{60}Co gamma field during exchange of the radioactive species. The other set of tubes was placed outside the radiation field and served as controls. For both the irradiated and non-irradiated samples, adsorption proceeded for sixteen days. The test tubes remained still and in the same laboratory environment (no ^{60}Co radiation field) for three to 5 h before individual five mililiter aliquots were filtered through 0.4μm-pore sizes Gelman membranes. Gamma detection for rubidium and cesium was done on these solutions later.

The radiation field at 15 points occupied by the test tube rack was measured by the change in absorbance of cobalt glass dosimeters at a light wavelength of 450 μm. The gamma radiation for the irradiated experiment had a ^{60}Co source. Differences in the dose of radiation varied throughout the area of the test tube rack (from 2.0×10^5 to 3.4×10^5 rads/h). An average

TABLE 4. Partition Coefficients Measured for Strontium Adsorption on Limestone from Irradiated and Nonirradiated Solutions

Strontium Concentration In Solution, M	Measured Partition Coefficient, mL/g	
	Irradiated[a]	Nonirradiated
First Series (Contact for 7 days)		
1.00×10^{-11}	5.2	4.8
0.90×10^{-8}	4.6	6.7
0.91×10^{-7}	4.2	3.9
1.03×10^{-6}	4.2	4.4
Second Series (Contact for 14 days)		
1.00×10^{-11}	7.7	7.0
0.90×10^{-8}	6.5	8.9
0.91×10^{-7}	5.5	5.7
1.03×10^{-6}	6.5	6.5
Third Series (Contact for 21 days)		
1.00×10^{-11}	6.4	7.4
0.90×10^{-8}	5.5	8.1
0.91×10^{-7}	5.5	6.4
1.03×10^{-6}	5.4	6.4

[a]The strontium-bearing solutions were exposed in a ^{60}Co gamma field of 7.5×10^5 rad/h for 100 h.

dose for the samples was taken to be the amount received at the central point of the middle radial plane ($\sim 1.02 \times 10^8$ rads). This dose may be related to radiation surrounding a waste canister and viewed as follows: (1) The dose accumulated in one year at a distance of one foot from the center of

an original 5000 W Canister containing ten years old waste. (2) The dose accumulated in ten years at a distance of 1.4 feet from the center of an original 5000 W canister containing ten years old waste. Waste canisters have an inside diameter of 6 in., steel wall thickness of 0.25 in., and a height of 8 feet (Blomeke, 1971).

The partition results obtained by radiochemically counting the solutions are given in Table 5. Lower partition coefficients for cesium and rubidium are generally the case for the irradiated batch experiment versus those found in the nonirradiated experiment. However, the differences may not be from the gamma radiation, but rather, from differences in temperature of the two test tube racks. The nonirradiated experiment had a temperature of 22°C to 24°C. The irradiated experiment had a temperature of 29 to 32°C (30° ave). Cesium partition coefficient dependence on temperature was shown by Couture, Seitz and Steindler, 1978) and (Seitz and Couture, 1979). In those experiments kaolinite was found to posses a high affinity for cesium over sodium, but this diminished by two orders of magnitude between 25°C and 170°C. (Eichholz, 1979) has also shown the dependence of cesium partition coefficients on temperature with both kaolin and shale batch experiments, and how this effect interfered with interpretation of radiation effect experiments. Eichholz found that the partition coefficients for cesium, under conditions of increasing temperature, decrease in the present of kaolin but increase in the presence of shale.

Figure 5 presents cesium partition coefficients measured in the presence of rubidium. From Figure 5, varying the amount of rubidium in solution can be seen to have the same effect on cesium adsorption as varying the amount of cesium in solution (compare to Figure 4).

D. ROCK-INFILTRATION EXPERIMENTS

Rock-infiltration experiments have the advantage that nuclide migration by fluid flow in intact rock is measured directly. The results include the effects of kinetics, Donnan exclusion, multiple speciation of a radionuclide and other factors that are important under flow conditions and that are not measured in a static experiment.

TABLE 5. Partition Coefficients for Rb and Cs from Irradiated and Nonirradiated Batch Tests.

Molarity of Rb Initial Wash Solution, M.	CESIUM Irradiated Kd Values mL/g	Average	CESIUM Nonirradiated Kd Values mL/g	Average	RUBIDIUM Irradiated Kd Values mL/g	Average	RUBIDIUM Nonirradiated Kd Values mL/g	Average
4.1×10^{-8}[a]	3.4		11.4		2.0		4.9	
	3.7		11.5		2.2		4.9	
	3.4	3.54	11.7	12.	2.0	2.1	5.1	5.0
1.52×10^{-7}[a]	3.6		9.9		2.1		4.6	
	3.6		9.7		2.1		4.4	
	3.7		10.4	10.	2.3	2.2	4.6	4.5
8.4×10^{-7}	1.7		3.8		1.3		2.8	
	1.8		3.7		1.4		2.6	
	1.8	1.79	3.6	3.7	1.4	1.4	2.5	2.6
1.1×10^{-5}	0.31		0.59		-0.3		1.2	
	0.45		0.64		0.6		1.2	
	0.46	0.41	0.60	0.61	0.7	0.03	1.2	1.2
9.8×10^{-5}	0.63		0.8		0.002		0.3	
	0.67		0.08		0.07		0.3	
	0.67	0.67	0.08	8.3	0.1	0.06	0.2	0.3
8.8×10^{-4}	-0.003		0.007		-0.2		-0.04	
	nd[b]		0.02		nd[b]		0.04	
	0.0001	∿0.0	0.008	0.01	-0.2	∿0.0	-0.005	∿0.0
9.7×10^{-3}	0.006		0.003		-0.03		0.07	
	0.002		0.005		-0.02		0.1	
	0.007	∿0.0	0.005	0.004	-0.03	∿0.0	0.08	0.09

[a]The rubidium concentrations of these solutions were below the detectable limits of atomic absorption spectrophotometry.

[b]The rubidium concentrations were calculated from the specific activity of the ^{86}Rb (6.9 m Ci/mg at 12:00 a,n,m August 23, 1979) and from pipetting solution, of known formulated rubidium concentrations.

nd indicated that the value was not determined because the test tube stopper leaked and the solution was lost during the irradiation.

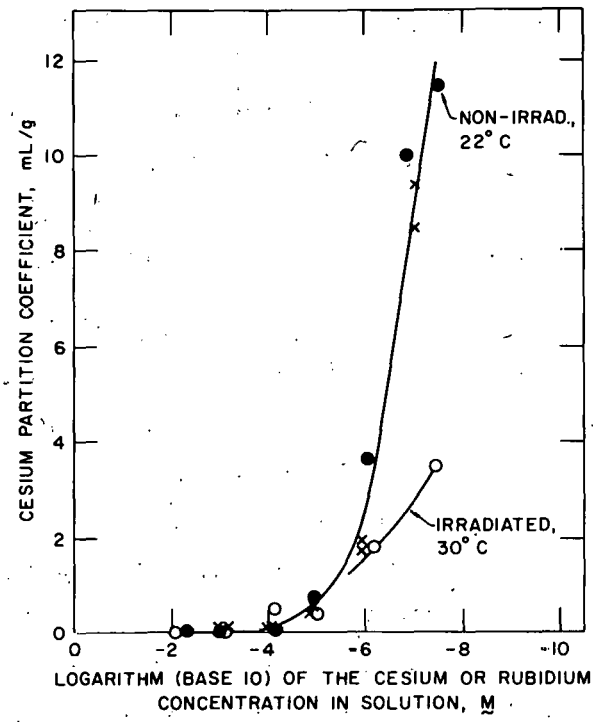

FIGURE 5. Cesium Partition Coefficients for Different Concentrations of Cesium or Rubidium. Crosses (+) are data with varied concentrations of cesium in solution, 7 and 8 days contact time, with a temperature of ∿22°C. Solid circles (●) are data with varied concentrations of rubidium in solution, 16 days contact, and a temperature of ∿22°C. Open Circles (○) are data with varied concentrations of rubidium in solution, 16 days contact, a temperature of 30°C and irradiation field of ∿2.6×10^5 rads/h.

1. Cesium Concentration in the Groundwater as a Controlled Variable in Infiltration Experiments

Four infiltration experiments were performed to measure the migration of cesium in limestone at different concentrations of cesium in solution. A limestone column, 1 cm in diameter and 3.8 cm long, mounted with epoxy and confined in stainless steel tubing, was used in the experiments. Solution flow rate was controlled by a solution metering pump. The oolitic limestone REW solution used in the experiments was prepared by stirring water with powdered limestone for ∿30 days and filtering the resulting solution

(solutions prepared in this manner are unsaturated with respect to $CaCO_3$). Cesium concentrations were varied from $\sim 3.6 \times 10^{-8}$ M (that measured to be in the oolitic limestone REW) to $\sim 1.4 \times 10^{-3}$ M. The higher concentrations of cesium were obtained by adding $CsNO_3$ to the oolitic groundwater solutions. Each experiment was performed by injecting a small quantity (20 μL) of solution containing ^{134}Cs in the solution stream above the limestone column and monitoring the activity in the solution exiting from the column. The experiments were run sequentially, using solutions of increasingly higher concentrations and the same limestone column A for each experiment (Table 6).

Upon changing to higher cesium concentrations, cesium activity bound on the column from the previous experiment was released and appeared in the new eluate. Therefore, prior to performing each experiment, the column was washed with the solution to be used in the experiment until the cesium activity of the wash solution was comparable to or below the counting background. Most of the released activity appeared in the initial 10 mL of eluate, but since some appeared in subsequent eluate, several hundred milliliters of solution were required for the wash. The groundwater solution was pumped through the column at a nominal rate of 0.1 mL/min (~0.07 mL/min actual flow rate, corresponding to a linear flow rate of 0.5 cm/min or ~2 km/y).

The most striking change caused by higher cesium concentrations in the solution is the increased amount of radioactive cesium eluted in a given volume of eluate. This change is evident in column 4 of Table 6, which gives the activity in the first 10 mL of eluate. This change is also illustrated graphically in Figure 6, where the cumulative amounts of activity for experiments (Expt. 148-49, 148-61, and 148-66) using solutions with different cesium concentrations are plotted against the eluate volume.

Figure 6 contains activities for only two solution fractions from experiments 148-49. The complete results from this experiment are listed in the Appendix (Table 7A). Also plotted in Figure 6 is a region that is estimated to encompass the migration behavior of leachate containing 3.0×10^{-7} M cesium. This concentration of cesium was determined to enter the groundwater solution in leach-migration experiments during the leaching process. (The glass used in the experiments contained 1.03% CsO and had a ^{134}Cs activity of 1.38×10^{6}

TABLE 6. Conditions and Results of Experiments Used to Measure the Behavior of Cesium in Limestone at Different Concentrations in Solution

Expt. No.	Cesium Concentration of Solution, M	Size of Fraction, mL	Activity of Cesium[a] Recovered in the First 10 mL of Eluate, c/s
148-49	3.6×10^{-8}[b]	7.4	16
148-61	1.42×10^{-4}	1.3	46
157-14	1.82×10^{-4}	7.4	49
148-66	1.44×10^{-3}	1.3	58

[a]The activity of cesium recovered in the first 10 mL of solution is for the 605-KeV gamma ray present in 98% of the cesium-134 decay and is a fraction of the 94.6 c/s introduced in each experiment. The activities were counted on 1.3-mL samples or were activities of larger samples adjusted to reflect counting of 1.3-mL samples.

[b]The cesium concentration was found by neutron activation analysis.

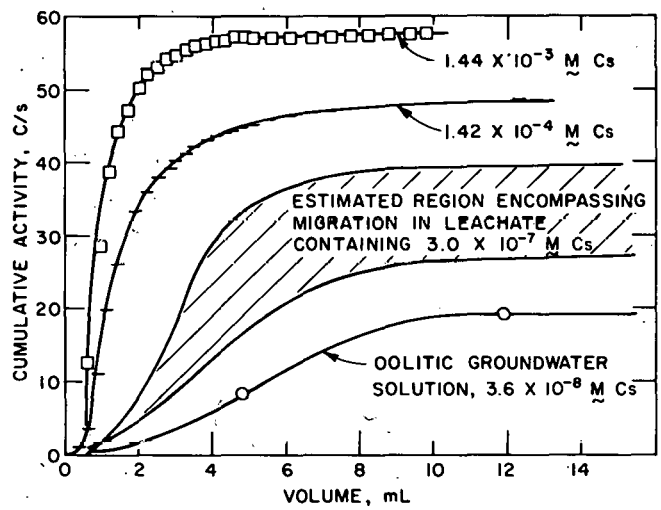

FIGURE 6. Cumulative Activity of Cesium Eluted Through Limestone with Groundwater Solutions Containing Various Amounts of Cesium. Total activity applied in each experiment (and therefore for each curve) was 95 c/s. Pore volume of the column was 0.68 mL (as measured by tritium elution).

d/(s)(g) og glass. The activity of the leachate was ∿14 d/(s)(mL), giving a concentration of cesium in the leachate of 0.10 μg/mL solution or 7.6 x 10^{-7} M cesium from the leached glass).

2. Dependence of Cesium Migration in Granulated Basalt on Cesium Concentration

Rock columns were made from granulated Sentinel Gap basalt placed in 1-cm-ID 316-type stainless steel tubing with metal frits at the ends. The hydrodynamic characteristics of the columns were measured at all flow rates used in subsequent experiments by flowing a small amount of tritiated water through the columns and recording the tritium elution peak. The tritium elution peaks indicated that the volume subject to fluid flow was 3.26 mL for the first column used in the experiments.

For each experiment, cesium-137 was injected into groundwater solution stream which then passed through a column of granulated basalt. A relatively high flow rate, ∿5 km/y, was used so that the series of experiments could be completed within the year with another series with flow rates of ∿55 m/y. The effluent from the column was sampled and analyzed for cesium-137. A first series of six experiments was performed with a 9.88-cm-long rock column and with six different concentrations of nonradioactive cesium, each flowing sequentially at the same rate through the same column. The curves of activities in the eluates for the first series of experiments are illustrated in Figures 7 to 12. From the curves, cesium is seen to migrate through the basalt more rapidly in solutions of higher cesium concentrations. Detailed analyses of these column results and comparison with predictions from results of batch K_D experiments are given in Section E and F of this report.

3. Strontium Migration in Los Alamos Tuff

A rock infiltration experiment was preformed to determine the contribution of longitudinal dispersion to the broad elution peak observed for the migration of strontium through an intact core of Bandelier tuff by groundwater transport under conditions of saturated flow.

For the experiment, a core of tuff 3.89 cm long by 1.98 cm in diameter was sealed with wax in a column arrangement. Groundwater was percolated through the core for several days prior to the experiment to wash any mobile particles out of the core. Groundwater was prepared by treating distilled

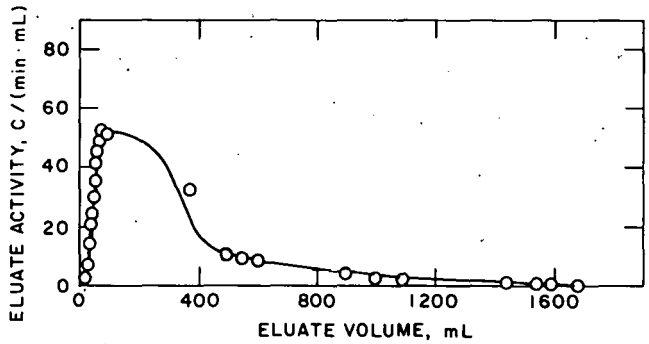

FIGURE 7. Elution of ^{137}Cs (0.1 μCi) Through a Column of Granulated Basalt. The solution contained 1 x 10^{-4}M Cs and flowed at a velocity of 4.9 km/y. Pore volume of the column (subject to fluid flow) was measured to be 3.36 mL. Experiment 148-126.

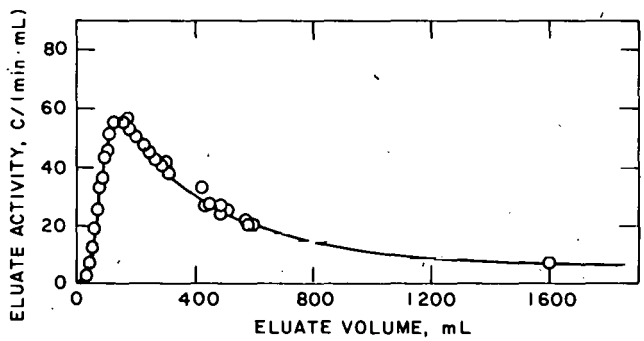

FIGURE 8. Elution of ^{137}Cs (0.2 μCi) Through a Column of Granulated Basalt. The solution contained 1 x 10^{-5}M Cs and flowed at a velocity of 5.0 km/y. Pore volume of the column was 3.36 mL. Experiment 148-133.

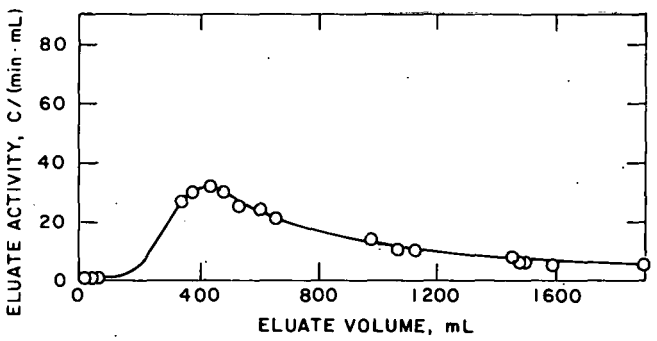

FIGURE 9. Elution of ^{137}Cs (0.2 μCi) Through a Column of Granulated Basalt. The solution contained 1 x 10^{-6}M added Cs and flowed at a velocity of 5.0 km/y. Pore volume of the column was 3.36 mL. Experiment 148-138.

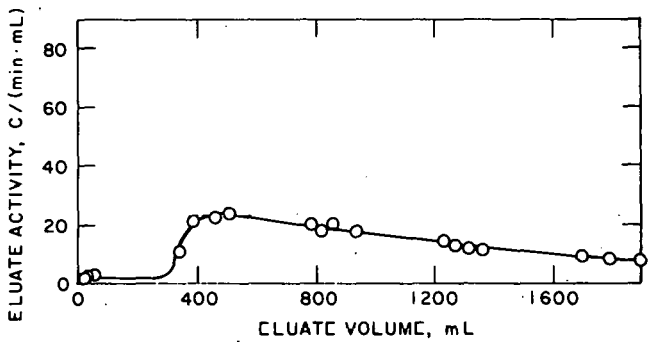

FIGURE 10. Elution of ^{137}Cs (0.2 μCi) Through a Column of Granulated Basalt. The solution contained 1 x 10^{-7}M added Cs and flowed at a velocity of 5.0 km/y. Pore volume of the column was 3.36 mL. Experiment 148-141.

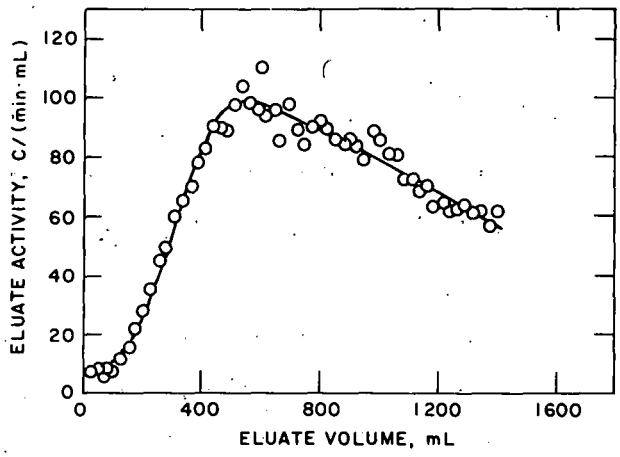

FIGURE 11. Elution of ^{137}Cs (1.0 μCi) Through a Column of Granulated Basalt. The solution contained 1 x 10^{-8}M added Cs and flowed at a velocity of 5.2 km/y. Pore volume of the column was 3.36 mL. Experiment 148-147.

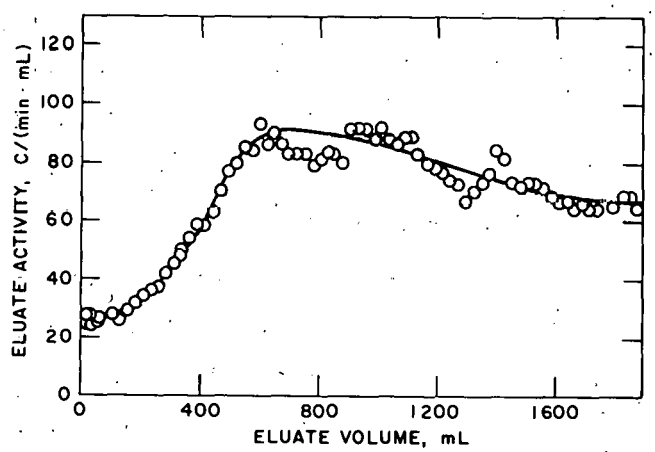

FIGURE 12. Elution of ^{137}Cs (1.0 μCi) Through a Column of Granulated Basalt. Cesium (~2 x 10^{-11}M) was added to the solution for radiochemical analyses. The solution flowed at a velocity of 5.2 km/y. Pore volume of the column was 3.36 mL. Experiment 164-2.

water with powdered Bandelier tuff for period of ∿14 days. An analysis of groundwater prepared in this manner can be found in (Seitz et al., 1979A). Before use, the groundwater was filtered through 0.4 μm-pore-size membrane filters. The pH of the groundwater was measured to be 5.9.

The nonadsorbing ion, iodide, was used in the experiment to measure the longitudinal dispersion. A radioactive solution was prepared by dissolving in the groundwater $SrCl_2$ and NaI containing radioactive ^{85}Sr and ^{131}I. The radioactive solution was filtered through a 0.015-μm-pore membrane filter before use.

A 50-μL portion of the radioactive solution was applied to the top of the tuff core (saturated with groundwater). The radioactive solution was allowed 4 min to be adsorbed by the core; then groundwater was continuously applied to the core at a rate of ∿0.102 mL/min. The effluent was collected in a series of vials, and the ^{131}I and ^{85}Sr contents were determined. The experiment was continued until all of the ^{131}I applied to the column. The specific activity of the strontium at the commencement of the experiment was 0.58 mCi/mg. Approximately 0.38 μg of strontium was applied.

Figure 13 is the plot of iodine activity in the eluate versus the eluate volume obtained for the transport of I^- through the tuff core. Figure 14 shows the curve of strontium activity versus eluate volume obtained for the transport of Sr^{2+} through the tuff core. Both curves account for nearly all (95% and 102%, respectively) of the activity administered to the core.

In Figure 13, the peak of the nonadsorbing iodide species occurred at an eluate volume of 4.55 mL. This volume of solution represents one free volume of the rock or, in other words, the volume of solution that is required to advance the water front a distance of 3.89 cm (i.e. the length of the rock core). The average fluid velocity, v_f, through the column was 0.087 cm/min or 458 m/y. The first observation of ^{131}I in the effluent came at 1.84 mL, at which point 0.041% of the applied iodine concentration was detected in a collection volume of 0.22 mL. Because of the uniform shape of the peak and the absence of other iodine peaks (e.g. due to iodate, periodate, etc.), we assumed that the iodide was the only iodine species present and that the shape of the curve was due only to longitudinal dispersion within the rock core.

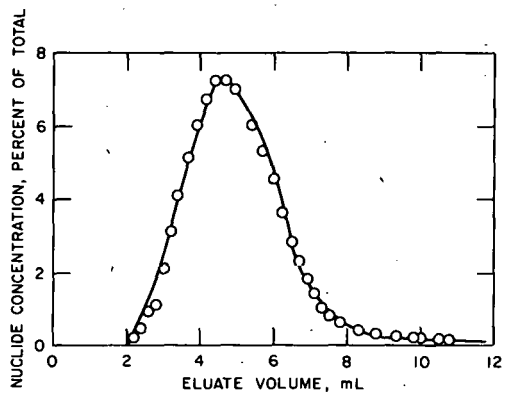

FIGURE 13. Iodine Activity in Eluate Versus Eluate Volume After Elution Through a 3.89-cm-long Core of Bandelier Tuff.

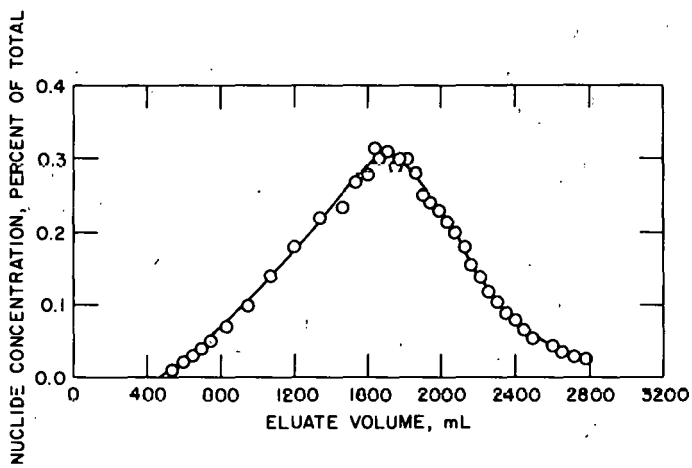

FIGURE 14. Strontium Activity in Eluate After Elution Through a 3.89-cm-long Core of Bandelier Tuff.

From Figure 14, the adsorbing Sr^{2+} is seen to have a retention volume of 1710 mL, which corresponds to an average velocity of 2.3×10^{-4} cm/min. The migration rate for strontium in Bandelier tuff relative to the velocity of water (under conditions of this experiment i.e., solution composition, pH, concentration of Sr, etc.) is 2.66×10^{-3}. This parameter is commonly called the retardation factor and is referred to by the symbol R_f.

Due to tailing observed in both the I^- and Sr^{2+} elution curves, the best comparison of the curve shape for strontium caused by longitudinal dispersion to the experimental strontium curve is a comparison of the full widths at half maximums of the two curves. The experimental curve for strontium has a full width at half maximum of 1040 mL, which corresponds, in a linear dimension, to a width of 890 cm. The experimental curve for iodide in the tuff core at half maximum is 4.55 ± 1.45 mL. To compare the dispersion in the iodide curve to the dispersion in the strontium curve, the iodide curve needs to be projected to the position (in eluate volume) of the strontium curve. This is done by dividing the volumes on the iodide curve by the retardation factor, R_f. The lower and upper volumes at half maximum for the projected curve can be obtained by dividing the retention volumes at half maximum for the iodide curve by the R_f for strontium. This yields a low retention volume of 1165 mL and a high retention volume of 2256 mL for a difference of 1091 mL. This difference is the full width of half maximum for the projected iodide curve attributable to longitudinal dispersion and corresponds in linear dimension to a width of 932 cm.

It is apparent that longitudinal dispersion is the primary cause of strontium peak broadening in this experiment.

E. FORM OF CESIUM IN SOLUTIONS

Differences in results of leach-migration and column-infiltration experiments for cesium migration were once postulated (Seitz et. al., 1979) to arise because of cesium adsorbed on finely divided particles that remained suspended in solution and did not interact with rock. Now, nonlinear adsorption isotherms exhibited by cesium are suspected of being the major cause for the different results seen in the experiments [see (Seitz et. al., 1979) for a discussion of the problem and its resolution]. Nevertheless, it is instructive to examine the extent to which radionuclides may be adsorbed in

extent to which radionuclides may be adsorbed in particles in order to estimate the complication to results that this phenomenon may cause. This section describes equilibrium dialysis techniques that are generally applicable to the analyses of radionuclides associated with particles or colloids suspended in solutions.

1. Analysis of Solutions for Suspended Particles

The reason postulated for the behavior of cesium differing in leach-migration and infiltration experiments centered on the premise that cesium added as a cesium chloride solution to groundwater was ionic while cesium leached from a solid waste form was a particle nature being tightly bound to residues of the leached glass suspended in the groundwater. Therefore, these two types of solutions were examined for suspended particles. In addition, a solution in which cesium was dissolved was passed through a limestone column and then tested to see if suspended particles containing cesium had been added or removed from solution by the limestone. Cesium-bearing particles might be added to the solution--for example, by adsorption of cesium on the surface of the limestone, followed by abrasion of the surface. Alternatively, the limestone might filter from the solution the particles on which cesium was adsorbed. Also, the concentrated cesium chloride solution used to make the radioactive groundwater solutions was tested for suspended particles by dialysis.

a. Filtration of Solutions through 0.4-and 0.1-μm-Pore Membrane Filters

Activities of solutions before and after being filtered through 0.4-μm and 0.1-μm-pore membrane filters (Nuclepore plycarbonate membranes) are given in Table 8A (Appendix). Only three of the four solutions were tested by filtration. The results in Table 8A indicate that very little if any cesium in these solutions was associated with 0.1-μm or larger particles.

b. Equilibrium Dialysis of Solutions

A dialysis membrane permits molecules of low molecular weight to transfer between solutions on either side of the membrane while keeping molecules of high molecular weight isolated in one of the solutions. Seamless, regenerated cellulose tubing, 2.7-cm diameter (obtained from Scientific

Products), was used in the studies. The tubing has a nominal transmission cutoff at a molecular weight of 5000 (nominal pore size of 0.0014 μm). Equilibrium dialysis studies were performed by placing solutions bearing radioactive cesium in a dialysis tube and immersing the tube in a solution containing no radioactive cesium. The light molecules in the solutions then exchanged between the solutions after which the cesium activities in the solutions inside and outside the dialysis tube were measured. If cesium were adsorbed onto particles but if it could freely exchange with cesium in solution, then it could pass through the membrane and readsorb onto a particle outside the dialysis tubing. In this case, the cesium would be "percieved" in both the dialysis experiments and in the column infiltration experiments as having an ionic character and the cesium association with particles in leaching experiments could not be envoked to explain its difference in behavior with cesium in spike experiments.

In an experiment, 25 mL of radioactive solution was placed inside the tube; 100 mL of a nonradioactive solution (with a composition comparable to that of the radioactive solution) was placed in the vessel surrounding the tube and stirred with a small, 0.7-cm long, stirring bar. In this configuration, it was found that the solution outside the tubing attained, in 2 h, 82% of the cesium activity that could be expected from complete mixing with the solution inside the bag. Dialyses was continued for at least 6 h to ensure an equilibrium concentration of the transferable cesium in the outer solution (<99% equilibrium concentration).

Results of the equilibrium dialyses studies for four solutions are given in Table 7. In one of the solutions was any measurable amount of cesium retained by the dialysis membrane. Therefore, it is considered that in these solutions cesium is not bound to particles larger than ∿0.0014 μm. Although it is possible that cesium's association with small particles (<0.0014 μm) in some solutions accounts for the behavior of cesium observed in column studies, it is probable that cesium is present as ions in all solutions.

F. DISTRIBUTION OF PORE SIZES

The capability of a rock to absorb radionuclides depends on the amount of surface area available for adsorption and is related to the type of rock porosity (pore-size distribution, pore morphology, open or closed pores, etc.).

TABLE 7. Equilibrium Dialysis of Solutions Containing Cesium-134.

Sample	Net Activity of Dialysis Samples,[a] counts/s·mL		
	Diluted Sample[b]	Solution Inside Dialysis Tubing	Solution Outside Dialysis Tubing
Cesium-Spiked Groundwater, Expt. 148-22	0.07	0.05[c]	0.07[c]
Groundwater Eluate from Expt. 148-22	0.07	0.08[c]	0.06[c]
Leachate from Simulated Waste[d]	0.31	0.28[e]	0.027[e]
Concentrated Radio-Cesium Chloride Solution	1.42	1.09[f]	1.14[f]

[a]Activity is for the 0.796-MeV gamma ray from the decay of cesium-134. Background correction was ∿0.29 c/s·mL.

[b]Activity of the sample diluted by the equilibrating solution was calculated from the measured activity of the initial solution and the solution volumes after equilibration. Approximately 10% of the solution was lost (by evaporation) in a 20-h period.

[c]Uncertainty (σ) from counting statistics is ∿25%.

[d]Solidified Waste was irradiated 76-68 glass composed of one part Pw-8a-3 calcine and two parts of 76-101 glass as described by (McElroy, 1977).

[e]Uncertainty (σ) from counting statistics is ∿9%.

[f]Uncertainty (σ) from counting statistics is ∿5%. Less than 7% of the radioactive cesium was found to be absorbed by the dialysis tubing.

To gain some knowledge of rock porosity, an Aminco 30,000-psi porosimeter was employed to examine pore size distributions for pores with diameters smaller than 20 μm for (1) a Columbia River basalt (mesh ranges of 16-20, 30-40, and 50-70), (2) Sentinel Gap basalt (20-50 mesh), and (3) oolitic limestone (20-50 mesh). The Columbia River basalt samples were used in a previous study of americium adsorption on different mesh ranges of basalt (Seitz et.al., 1978). The oolitic limestone and Sentinel Gap basalt samples were

used in the Controlled-Sample Program (Relyea and Serne, 1979) and were included in this study because no accurate porosity data had been gathered on either. A specific objective of the analuses was to test for porosity that had been postulated to account for penetration of americium into basalt to a depth of approximately 500 μm in batch adsorption experiments (Seitz et.al., 1978).

1. Pore Size Measurements

The Aminco porosimeter enables one to quantitatively measure the volumes of pores of different sizes by intruding mercury at increasingly higher pressures into pores of progressively smaller diameters. Pores at the surface of rock grains resist penetration by mercury. The amount of pressure required to infiltrate these pores varies inversely with the diameter of the opening and directly with the surface tension and the contact angle between the pore and mercury as follows:

$$p = \frac{-4\phi\cos\theta}{d}$$

where: p is the mercury pressure at the pore opening
d is the pore diameter
ϕ is the surface tension of mercury
and θ is the contact angle

Surface tension and contact angle are assumed to remain constant during a test and are equal to 473 dynes/cm (mercury surface tension at 25°C) and 130°, respectively, so that the relationship between pore diameter and mercury pressure is

$$d = 1.216/p$$

where d is the pore diameter in micrometers (μm) and
p is the mercury pressure in pascals (Pa)

At a pressure of 2.1×10^8 Pa (30 000 psia, the working limit for the porosimeter used), the pore diameter of the smallest pore filled with mercury is calculated with the equation to be 0.006 μm. Surface tension and contact angle depend on the material being contacted with mercury and, therefore, would depend on pressure since, in the general case, pore sizes would be different in the different minerals and the different contacts within a rock. Pore size distributions measured with the porosimeter should be

viewed with this limitation in mind.

In the operation of the porosimeter, a dry solid sample is placed in a penetrometer cell, which is evacuated and then filled with mercury to 31 kPa (4.5 psia). The glass penetrometer stem is removed from the mercury supply, and pressure in the cell is increased up to atmospheric pressure by admitting air to the bottom of the stem. The mercury pressure is determined by reading a 0 to 15 psi-range guage. The position of the mercury meniscus in the penetrometer stem is determined by eye.

The penetrometer cell, now filled with mercury, is then transported to the high-pressure test apparatus for porosimeter measurements from 103 kPa to 2.1×10^5 kPa. Pressure is read from a 0-30,000 psi range gauge. The lower pressure readings (below 3 MPa) are adjusted to account for the pressure from the column of mercury in the stem of the porosimeter (which is approximately 20 Pa). As the pressure rises, the volume of mercury displaced is measured by a thin wire which moves up the penetrometer stem and acts as an electrical lead, ceasing motion each time connection is made with the mercury. The porosity measurements are then corrected by use of a blank to negate the effect of the compressibility of mercury on the final results. The pressures and corresponding stem readings for a test of the 30-40 mesh Columbia River basalt are listed in Table 9A (Appendix).

Corrected penetrometer readings are plotted against absolute pressure in Figures 15, 16, and 17. The initial positive slope of these graphs up to a plateau at approximately the 20-μm-diameter pore level is produced by mercury infiltration of the interstitial grain voids. The amount of pore space (porosity) equals the difference between pore volumes measured in cm^3/g at the highest pressure run and at the pressure at which interstitial grain filling stops, times the density of the sample tested. The interstitial void volume is greater for smaller sized material of the same weight, as graphically illustrated in Figure 15.

The oolitic limestone was found to have a density of 2.6 g/cm^3 by displacement of water in a graduated cylinder. This compact limestone has a measured porosity for pores smaller than 20-μm diameter just below 0.25%. If a density of 3.1 g/cm^3 is assumed for Sentinel Gap basalt, the porosity determined by the porosimeter method is 0.03%.

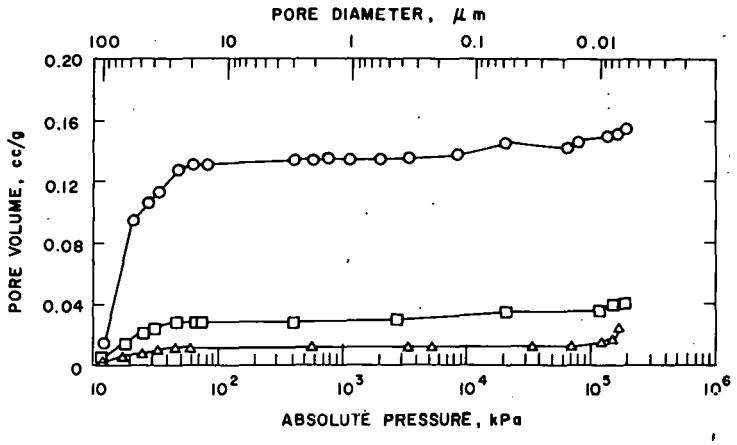

FIGURE 15. Integrated Pore Volume Versus Pore Diameter for Three Fractions of Columbia River Basalt. Circles are for the 50 to 70 mesh material, squares for the 30 to 40 mesh material, and triangles for the 16 to 20 mesh material.

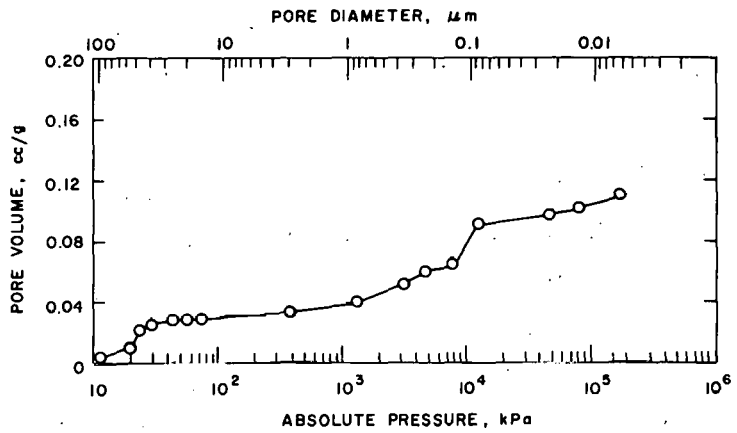

FIGURE 16. Integrated Pore Volume Versus Pore Diameter for 20 to 50 Mesh Oolitic Limestone. Porosity due to pores smaller than 20 μm is 0.25%.

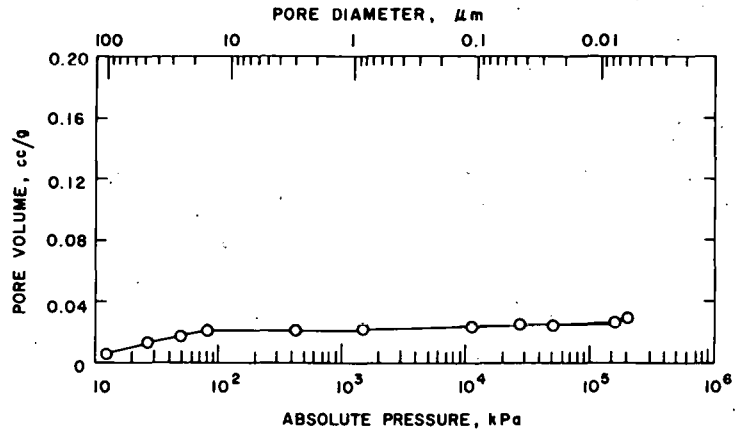

FIGURE 17. Integrated Pore Volume Versus Pore Diameter for 20 to 50-Mesh Sentinel Gap Basalt. Porosity due to pores smaller than 20 μm is ∿0.03%.

The density of the Columbia River basalt (30-40 mesh size) was found to be 3.1 g/cm^3. Using this value, the Columbia River basalt samples have the following measured porosities: 16-20 mesh size = 0.04%, 30-40 mesh size = 0.03% and 50-70 mesh size = 0.06%.

For the basalt samples, the correction due to the compressibility of mercury was a 0.02 % porosity reduction. If this correction is approximately the error associated with the measurements, the differences in porosities for the three mesh ranges of Columbia River basalt may not be significant.

2. Estimated Pore-Surface Area of Columbia River Basalt

All samples have small (and with the analytical uncertainly, possibly, zero) porosities from pores below 20 μm in size. But to judge the possible significance of even a small porosity to adsorption phenomena, the surface area of the pores was estimated by assuming that the pores are tubes, ∿500 μm in length [a length suggested by the apparent penetration depth obtained by adsorption of americium, (Seitz et.al., 1978)] and ∿0.008 μm in diameter as suggested by the porosimeter results described above).

The ratio of the pore-surface area to the particle surface area (assuming nonporous spheres) is given in Table 8 for the three mesh fractions of Columbia River basalt. Because the estimated pore surface areas greatly exceed the areas of the rock particles (calculated for nonporous spheres), we

TABLE 8. Estimates of Pore Surface Areas of Particles of Columbia River Basalt and the Ratios of Pore Surface Area to Surface Area of the Particles

Mesh Size	Opening Width in μm for the screen at each mesh range	Porosity of 0.008-μm dia. pores, %	Surface Area of pores,[a] m^2/g	Ratio of Pore Surface to Particle Surface[b]
16-20	850 to 1180	0.04	0.06	34
30-40	425 to 595	0.03	0.05	13
50-70	212 to 300	0.06	0.10	13

[a]Surface areas were calculated assuming that the pores were tubes 500 μm long and 0.008 μm in diameter.

[b]Particle surface area was calculated by assuming nonporous spheres having diameters equal to the average mesh size openings.

conclude that small pores in the basalt may be important to nuclide adsorption, even though they constitute only a fraction of a percent of the rock volume. This conclusion is not sensitive to pore morphology that is used in the calculation. If porosity is assumed to be hemispheres at the particle surfaces rather than long cylinders, the numbers in the last two columns of Table 8 are reduced only by a factor of 6.

G. APPARATUS DEVELOPMENT

An experimental apparatus was constructed to study the leach-migration characteristics of radionuclides in rock. The apparatus is similar to previous experimental devices used to incorporate rock in a fluid stream (Seitz et.al., 1979). The major change in equipment design is that a solid rock core is held in a pressurized Teflon sleeve (see Figure 18). Concentrations of gases dissolved in the solution to be pumped through the rock core are regulated using a gas sparging apparatus described previously (Seitz et.al., 1979). The apparatus is currently in use in leach migration experiments with a solid waste glass (No 76-68) hypothesized for Nuclear Fuel Services Waste (Bradley, 1979).

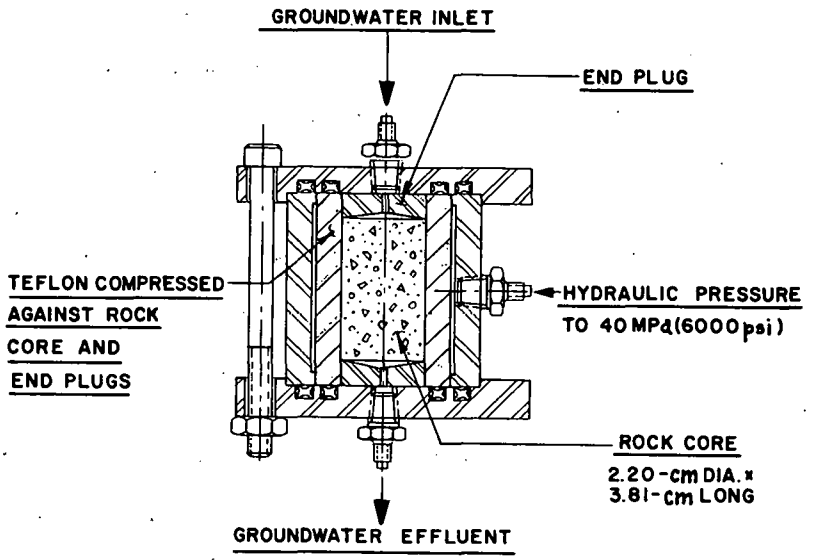

FIGURE 18. Rock-Column Holder with Pressurized Teflon Jacket

H. PREDICTION OF MIGRATION VELOCITIES FROM PARTITION COEFFICIENTS: CESIUM IN BASALT

For a comparison reported here for the column-infiltration experiments and a batch-partitioning experiments with basalt, the partition coefficients (illustrated in Figure 4 listed in Table 4A) were used to calculate the relative velocities of cesium, V_{Cs}/V_W (the velocity of the cesium relative to the velocity of the water front) at the different cesium concentrations by the equation

$$V_{Cs}/V_W = \frac{1}{1+K_d(p/\varepsilon)} \quad \frac{1}{1+K_d(\rho/\varepsilon)}$$

where ρ is the bulk density of the rock column and ε is the porosity of the rock column. The principle used to derive this equation is that the relative velocity of cesium is equal to the fraction of cesium in solution.

Relative velocities from column infiltration experiments and calculated from results of batch experiments are given in Table 9. The concentrations of cesium in solutions are also given in the Table 9. For column infiltration experiments, the concentrations are for solutions used to elute the cesium during the experiments. For batch-partitioning experiments, the concentrations were determined from the amounts of cesium added to the solutions and from the amounts of ^{137}Cs remaining in solution after adsorption. We assumed there was only a negligible quantity of cesium in the basalt and in the chemicals (except the CsCl) used to make the groundwater solution.

The results from both experiments are comparable in that they show a dependence of migration velocity on cesium concentration as observed in previous studies (Seitz et.al., 1979). Only at concentrations below 4.4×10^{-8}M cesium may the migration velocity be independent of the cesium concentration. Because of the dependence of migration velocity on trace-element concentration, any comparison of results from different experiments must be done at controlled (and known) radionuclide concentrations or any agreement observed may be considered fortuitous or any disagreement may be assumed to result simply from differences in trace element levels.

The results from the two experimental procedures disagree in that at similar cesium concentrations, consistently higher relative velocities are obtained from infiltration experiments. This disagreement may be due to slow reaction kinetics that affect infiltration experiments most profoundly, with the reactions controlled principally by diffusion of the ion being adsorbed through rock pores or cracks. A qualitative treatment of this phenomena, given in the theoretical section of this report, suggests a curve shape for the eluted radionuclide similar to that seen experimentally. The effect is more rapid elution of a diminutive radionuclide peak, with a major fraction of the radionuclide retained by the rock and eluted (only after considerable solution flow) as an elongated tail of the early radionuclide peak.

TABLE 9. Relative Velocities of Cesium in Basalt From Column-Infiltration Experiments and Calculated From Partition Coefficients Measured in Batch-Partitioning Experiments

Cesium Concentration in Solution,[a] M	Relative Velocity of Cesium	
	Column Infiltration[b]	Batch Partitioning[c]
1.0×10^{-4}[d]	0.04	--
1.8×10^{-5}[e]	--	0.006
1.0×10^{-5}[f]	0.02	--
1.0×10^{-6}[g]	0.008	--
7.8×10^{-7}[e]	--	0.003
1.0×10^{-7}[h]	0.008	--
4.4×10^{-8}[e]	--	0.001
1.0×10^{-8}[i]	0.006	--
3.4×10^{-9}[e]	--	0.001
3.8×10^{-10}[e]	--	0.0009
3.0×10^{-11}[k]	--	0.0009
3.0×10^{-11}[j]	0.0054	--

[a] Cesium concentrations were known from the amounts of cesium added to the solutions and from the amounts of ^{137}Cs remaining in solution after adsorption. It was assumed that no cesium was present (1) in the chemical used to make the solutions (except where explicitly stated) or (2) in the basalt.

[b] Solution flow at a rate of 5.0 km/y was used in the column-infiltration experiments.

[c] A column density of 1.41 g/cm^3 and a porosity of 0.42 were used to calculate the relative velocities from results of batch-partitioning experiments. The porosity was measured by tritium elution and is significantly different from the value of 0.51 measured by water saturation. Uncertainty in the porosity value could contribute to the discord in the comparison.

[d] Data was obtained from elution curve illustrated in Figure 7.

[e] Migration rate was obtained from data given in Table 4A and footnote C in this table.

[f] Data was obtained from elution curve illustrated in Figure 8.

[g] Data was obtained from elution curve illustrated in Figure 9.

[h] Data was obtained from elution curve illustrated in Figure 10.

[i] Data was obtained from elution curve illustrated in Figure 11.

[j] Data was obtained from elution curve illustrated in Figure 12.

[k] Recently obtained data was not presented elsewhere in this report.

It is concluded that results of batch tests can be used to predict migration as observed in column infiltration tests reasonably well provided the materials relevant to the infiltration tests are used in the batch tests and that detailed consideration of the migrating element's concentration (and that of any competing trace element) is taken. A more refined prediction of migration from partition coefficients would require consideration of reaction kinetics. In general, it is seen from this comparison that the relationship of a partition coefficient, K_d, to migration in a specified rock material with a specified solution is not simple but may be related by diffusional effects within dead-end pores, and trace element concentration of the groundwater and, possibly, to other complicating effects.

IV. APPLICATIONS AND IMPLICATIONS OF EXPERIMENTAL RESULTS

A. CONCENTRATION DEPENDENCE OF NUCLIDE ADSORPTION BY LIMESTONE AND SENTINEL GAP BASALT

The results of batch partitioning experiments described in this report clearly demonstrate the dependence of cesium adsorption on cesium concentration in groundwater solutions.

Adsorption that is not linear with concentration is not unexpected and has been observed with exchange resins, purified minerals in acetate solutions, abyssal red clays and so forth. What were unexpected in the results reported here are the low trace element concentrations at which nonlinear effects occur for geologic materials. We conclude from the experimental results that nonlinear effects are important to repository safety consideration and that nonlinear phenomena, without being suspected, have profoundly affected results reported previously in the WISAP program. The view that nonlinear affects are important to repository considerations contrasts with a recently published conclusion (Shiao et.al, 1979) that concern regarding applicability of adsorption data obtained at finite concentration compared with true "trace" condition is unfounded.

1. Nonlinear Adsorption in Infiltration Experiments

The concentration dependence of adsorption such as that listed in Tables 3A and 4A of the Appendix and illustrated in Figures 3 and 4, is probably the origin of cesium behavior differing in leach-migration and conventional infiltration experiments performed in this program (Seitz et.al., 1979). In the conventional infiltration experiments, small quantities of radiocesium (2.0×10^{-4} µg or $\sim 1.5 \times 10^{-12}$ mol cesium) were introduced into solution streams essentially devoid of cesium (cesium concentration was determined by neutron activation analyses to be $\sim 3 \times 10^{-8}$ M in limestone REW solution). Therefore, based on the results of the batch partitioning experiments, the radiocesium dispersed in ~1 mL or more of REW solution would be expected to be strongly adsorbed. This what was seen experimentally in the filtration experiments.

On the other hand, in leach-migration experiments, leaching of the glass introduces $\sim 3 \times 10^{-7}$ M cesium into the solution. At this cesium concentration, based on the results illustrated in Figure 3, most of the cesium would be expected to be readily transmitted through limestone. Experimentally, we have seen that all but 1 to 2% of the leached cesium was transmitted through limestone (Seitz et.al., 1979).

The data in Figure 6 for cesium migration in limestone show that concentration dependences but also reveal a phenomenon not suggested by the batch experiment data. Although cesium migration rate is increased by higher cesium concentrations (as suggested by the batch tests), a significant fraction of the cesium (40% in a 1.4×10^{-3} M cesium solution in limestone, more at lower cesium concentration) is held up in the rock column after passage of the main cesium peak. This effect may be due to cesium diffusing into intergranular sites in the bulk of the rock material and appears to be a very significant effect in the retardation of cesium in flowing groundwater. A discussion of this mechanism is given in Section II B of this report.

Dependence of cesium migration on cesium concentration in the groundwater solution is expected from results of batch experiments (Figure 4) and is seen clearly from results of column infiltration experiments on basalt (Figures 7 to 12).

2. Nonlinear Effects in the Controlled-Sample Program

We can understand previously unexplained results of the controlled-sample program in the WISAP task 4 program in the light of results reported here. In the controlled-sample program, investigators in nine different laboratories reported partition coefficients for cesium on limestone ranging from 1.3 to 880 mL/g (Relyea and Serne, 1979) and for cesium on basalt ranging from 31 to 450 mL/g (Relyea and Serne, 1979). In contrast, reported partition coefficients for strontium adsorption on limestone and basalt were much less varied and ranged for dilute groundwater from 1.4 to 15 mL/g for adsorption on limestone and from 40 to 90 mL/g for adsorption on basalt. In the results reported here adsorption of cesium depended sensitively on solute concentration where adsorption of stronium did not. Furthermore, from theoretical consideration (Section II A of this report) we expect that the adsorption of cesium will depend on its concentration, much more so than the adsorption of strontium.

The cesium concentrations were not reported in the controlled-sample program and could have varied sufficiently between laboratories to be responsible for the large discrepancies in reported partition coefficients for cesium. Only radiocesium concentrations were reported, not the total cesium concentrations, in the solutions from which these measurements were made. Not all radiocesium concentrations were reported and of those that were, most concentrations were upper limits which ranged from $<1 \times 10^{-6}$ to $\leq 6 \times 10^{-12}$ M. Based on the range of reported upper limits for radiocesium, radiocesium concentration used in the different laboratories are likely to have been different.

Like the radiocesium concentrations, the total cesium concentrations of the solutions formulated in the different laboratories are likely to differ. In a set of experiments done in a given laboratory, cesium concentrations greatly in excess of the reported radiocesium levels could have occurred because of cesium added as a carrier, as an impurity in chemicals used to make the synthetic groundwater solution, or as a constituent of the limestone itself (cesium from the limestone itself will produce solutions containing $\sim 3.6 \times 10^{-8}$ M cesium).

Based on the data in Figure 3, the radiocesium concentrations augmented by stable cesium could result in the partition coefficients reported in the controlled-sample program for cesium adsorption on limestone over the entire range measured (1.3 to 800 mL/g). Similarly, on the basis of data in Figure 4 for basalt, different cesium concentrations, all below $\sim 1 \times 10^{-6}$ M, would produce the measured partition coefficients (ranging from 31 to 450 mL/g) reported in the controlled-sample program for cesium adsorption on basalt. Although variations in other experimental parameters may have contributed to the range of partition coefficients, only the dependence of cesium adsorption on its concentration below 10^{-6} M needs to be invoked to explain the diversity of results obtained for cesium adsorption in the controlled-sample program.

Nuclide adsorption can be affected by trace concentrations of other solute ions. Cesium adsorption, for example, is sensitive to the concentration of rubidium in solution. Because rubidium is thirty times more abundant than cesium in nature, interference from rubidium may be the major influence to consider in cesium adsorption.

From theoretical considerations (Section II A, this report) we expect lanthanite 3+ ions or any strongly adsorbed ions to show strong concentration dependences on adsorption. So, variations in concentrations may be responsible, in part, for the large variations in partition coefficients reported for plutonium adsorption on limestone and basalt (Relyea and Serne, 1979). However, with plutonium, precipitation with the formation of tiny colloids or filterable solids has to be suspected as also contributing to the large variation in reported values.

3. Implications of Nonlinear Isotherms to Nuclide Migration

In this report, the existence of nonlinear isotherms is predicted, theoretically, to be a general phenomenon for radionuclides forming singly charged or triply charged ions and any other strongly adsorbed ion. In the experimental work reported here, nonlinear behavior for cesium adsorption on two widely different types of rock was found. Because the phenomenon exists at cesium concentrations that are readily generated when a solid waste form is leached by groundwater, it is relevant to safe confinement of nuclear

waste in a repository. Linear-adsorption behavior is also relevant in some cases (weakly adsorbed nuclide, solutions of high ionic strength) to repository conditions. The point to be made here is that linear adsorption cannot be assumed to be relevant for all cases.

From the isotherms depicted in Figures 3 and 4, we would expect that most cesium leached in concentrations of $\sim 10^{-7}$ M from a solid waste form would move with the leachate away from the repository because of weak adsorption. However, as the concentration of the leachate is lowered by some adsorption of cesium on the rock and by dilution of the leachate with other groundwater, cesium adsorption would be expected to increase until the cesium concentration was that of the unperturbed groundwater. In groundwater of low cesium (and rubidium) concentration, this condition would result in a very low net migration rate for cesium. Thus, the existence of nonlinear adsorption of cesium is not necessarily detrimental to nuclide immobilization. It is, however, a complication that must be treated for accurate representation of cesium migration.

4. Implications of Results to Experimental Technique

Many experimental techniques used to obtain adsorption data are inappropriate when performed with nuclides exhibiting nonlinear adsorption isotherms. For example, an adsorption-desorption experiment, as it is commonly performed to test for nuclide sorption reversibility, results in a changing and unknown concentration of the nuclide throughout the experiment because of the "fresh" solutions which are periodically introduced. Results from such experiments are likely to be affected by the changing radionuclide concentration as well as by any genuine irreversibility.

Nuclide adsorption has often been reported by experimenters to depend on the amounts of solution and rock used in experiments. Such behavior can be postulated to originate from nonlinear adsorption behavior if radionuclide concentration in solutions were not controlled. Nonlinear adsorption can either increase or decrease the measured partition coefficient with varied solution to rock ratios depending on the specific procedures used in the experiments (e.g. a constant amount of radionuclide being adsorbed from increasing volumes of solution would lead to an increased partition coefficient with increased solution to rock ratio; on the other hand, use of a solution

with an established radionuclide concentration would lead to a decreased partition coefficient with increased solution to rock ratio).

In general, an appreciation of the effects of nonlinear isotherms must be included in the design of experiments and in the interpretation of experimental results.

B. CONCLUSIONS

Results of batch partitioning experiments and column infiltration experiments described in this report clearly demonstrate the dependence of cesium adsorption and of cesium migration on cesium concentration in groundwater solution. Because nonlinear effects occur at cesium concentrations that are readily attained by leaching of a solid waste form, the effect is considered relevant to safety assessments of waste repositories. Nonlinear behavior was generalized by theory and is exepected for all nuclides that are adsorbed strongly from dilute groundwater solutions.

Nonlinear behavior is thought to be responsible for many previously unexplained results and discrepant data that were reported to describe nuclide migration. In general, more appreciation of the effects of nonlinear isotherms than has heretofore been practiced must be included in the design of experiments and in the interpretation of experimental results for a comprehensive understanding of nuclide migration.

REFERENCES

Ames, L. L., 1978. Controlled Sample Program, Publication No. 1, Characterization of Rock Samples, PNL-2797. Battelle Pacific Northwest Laboratories, Hanford, WA.

Blomeke, J. L., E. Sonder, J. P. Nichols, S. Lindenbaum, R. S. Dillon, E. D. Arnold, and H. F. Soard, 1971. An Analysis of Energy Storage and Its Effects in the Proposed National Radioactive Waste Repository, ORNL-TM-3403. Oak Ridge National Laboratory, Oak Ridge, TN.

Bradley, D. J., 1979. Personal Communication to D. Lam, January 3, 1979.

Couture, R. A., M. G. Seitz and M. J. Steindler, 1978. Experimental Trace-Element Transport by Fluid Flow at Elevated Temperatures: Ion Exchange on Kaolinite. Amer. Geophys. Union, Transaction 59, p. 1225.

Crank, J., 1975. The Mathematics of Diffusion, Second Edition. Clarendon Press, Oxford, England.

Eichholz, G. G., T. F. Craft, B. G. Wahlig, P. D. Simpson, M. D. Mathenz, E. B. Shingelton, K. A. Will, and R. J. Titolo, 1979. Subsurface Migration of Radionuclide Waste Materials by Particulate Transport, Annual Report of the WISAP Contractors, Seattle, WA, R. J. Serne, Editor. PNL-

Faucher, J. A., R. W. Southworth, and H. C. Thomas, 1952. "Adsorption Studies on Clay Minerals I. Chromatography on Clays." J. Chem Phys. 20 (1): 157-160.

Fried, J. J., 1975. Groundwater Pollution. Elsevier, New York.

Garrels, R. M., and C. L. Christ, 1956. "Application of Cation-Exchange Reactions to the Beidellite of the Putnam Silt Loam Soil." J. Sci. 254: 372.

Giddings, J. C., 1965. Dynamics of Chromatography Part 1 Principles and Theory, Marcel Dekker, Inc., New York.

James, R. O. and T. W. Healy, 1972. "Adsorption of Hydrolyzable Metal Ions at the Oxide-Water Interface: I. Cobalt (II) Adsorption on Silicon Dioxide as Model Systems." J. Colloid Interface Sci. 40: 43-52.

Kraus, K. A., H. O. Phillips, T. A. Carlson, and J. S. Johnson, 1958. "Ion-Exchange Properties of Hydrous Oxides," Proc. Second United Nations International Conference on the Peaceful Uses of Atomic Energy, Vol. 28, p. 3-16, United Nations, Geneva.

Lieser, K. H., and E. Kluge, 1967, "Abtrennung von Reinem Francium-223 aus Actinium-227 auf Eines Trennsaule," Sonderdruck aus Radiochim Acta 7, 3-9.

McElroy, J. L., 1977. Quarterly Progress Report, Research and Development Activities, Waste Fixation Program, Oct-Dec 1976 Report, PNL-2264. Battelle Pacific Northwest Laboratories, Hanford, WA.

Meyer, R. E., 1978. "Systematic Study of Nuclide Adsorption on Selected Geologic Media," App. D., in Waste Isolation Safety Assessment Program Quarterly Technical Progress Report for Oct-Dec 1978, A. Brandstetter, Ed.

Neretnieks, I., 1979. Diffusion in the Rock Matrix-An Important Factor in Radionuclide Retardation? Report in The KBS Series KBS-79-xx Technical Report.

Relyea, J. F., and R. J. Serne, 1979. Controlled-Sample Program, Publication No. 2, Interlaboratory Comparison of Batch K_d Values. PNL-2872 Battelle Pacific Northwest Laboratory. Hanford, WA.

Rickert, P. G., R. G. Strickert, and M. G. Seitz, 1979. "Nuclide Migration in Fractured or Porous Rock," ACS Symposium Series, No. 100, Radioactive Waste in Geologic Storage, Sherman Fried, Editor, American Chemical Society.

Sayles, F. L., and P. C. Magelsdorf, Jr., 1977. "The Equilibration of Clay Minerals with Seawater: Exchange Reaction," Geochim. Cosmochim. Acta 41: 951-960.

Schroeder, H. J., 1962. "Trennung Naturlicher Radionuklide mittels Ammonium Molybdatophosphat," Radiochim Acta 1 (1): 29-31.

Seitz, M. G., P. G. Rickert, S. M. Fried, A. M. Friedman, and M. J. Steindler, 1979. Studies of Nuclear-Waste Migration in Geologic Media, Annual Report October 1977 to September 1978. ANL-79-30.

Seitz, M. G., P. G. Rickert, S. M. Fried, A. M. Friedman, and M. J. Steindler, 1979A. Transport Properties of Nuclear Wastes in Geologic Media, Annual Report for the Waste Isolation Safety Assessment Program, for period October 1, 1977 to September 30, 1978, R. Serne, Chairman, PNL-SA-7352.

Seitz, M. G., P. G. Rickert, S. M. Fried, A. M. Friedman, and M. J. Steindler, 1979B. "Migratory Properties of Some Nuclear Waste Elements in Geologic Media," Nucl. Technol. 44: 284-296.

Seitz, M. G., and R. Couture, 1979. Transport in Lithic Material by Fluid Flow at High Temperatures. QRT RPT July-Sept. ANL-79-6.

Seitz, M. G., P. G. Rickert, S. M. Fried, A. M. Friedman, and M. J. Steindler, 1978. Studies of Nuclear-Waste Migration in Geologic Media, Annual Report November 1976 to October 1977, ANL-78-8.

Serne, R. J., Chairman, 1979. Waste Isolation Safety Assessment Program, Task 4. Contractor Information Meeting Proceedings, Sept. 20-23, 1977, PNL-SA-6957 (1978) and the Second Contractor Meeting Proceeding, Oct. 2-5, 1978, PNL-SA-7352. Battelle Pacific Northwest Laboratories.

Shiao, S. Y., P. Rafferty, R. E. Meyer, and W. J. Rogers 1979 "Ion-Exchange Equilibria between Montmorillonite and Solutions of Moderate-to-High Ionic Strength" in Radioactive Waste in Geologic Storage S. Fried Ed. ACS Symposium Series 100 ACS, Washington, D.C.

Thomas, H.C., 1949. Kinetics of Fixed-Bed Ion Exchange in Ion Exchange Theory and Application. F. C. Nachod, Editor. Academic Press Inc., New York, NY.

Wahlberg, J. S., and M. J. Fishman, 1962. Adsorption of Cesium on Clay Minerals, U.S. Geol. Survey Bull. 1140-A, 30 pp.

Wahlberg, J. S., J. H. Baker, R. W. Vernon, and R. S. Dewar, 1965. Exchange Adsorption of Strontium on Clay Minerals, U.S. Geol. Survey Bull. 1140-C, 26 pp.

White, D. E., J. D. Hem, and G. A. Waring, 1963. Chemical Composition of Subsurface Waters, Data of Geochemistry (6th ed.): U.S. Geol. Survey Prof. Paper 440-F, pp. F-1 to F-67.

APPENDIX

EXPERIMENTAL DATA FROM BATCH AND INFILTRATION EXPERIMENTS

TABLE 1A. Cesium Concentrations of Solutions Used for the Third Rinse of Test Tubes (Blanks) and Limestone in Preparation for the Batch Adsorption Tests with Cesium.

Solution	Cesium Concentration by Pipetting,[a] M	Final Cesium Concentration,[b] M
Test Tube Rinses		
W-7	0.0	$<3.8 \times 10^{-9}$
W-6	1.02×10^{-8}	7.5×10^{-8}
W-5	1.02×10^{-7}	1.4×10^{-7}
W-4	1.04×10^{-6}	9.6×10^{-7}
W-3	1.04×10^{-5}	9.7×10^{-6}
W-2	1.05×10^{-4}	9.6×10^{-5}
W-1	1.04×10^{-3}	1.0×10^{-3}
Limestone Rinses		
W-7	0.0	$<3.8 \times 10^{-9}$
W-6	1.02×10^{-8}	6.8×10^{-8}
W-5	1.02×10^{-7}	1.1×10^{-7}
W-4	1.04×10^{-6}	1.4×10^{-6}
W-3	1.04×10^{-5}	9.0×10^{-6}
W-2	1.05×10^{-4}	9.4×10^{-5}
W-1	1.04×10^{-3}	9.9×10^{-4}

[a] Cesium concentrations were determined from the volumes of cesium-bearing solution added to known volumes of recipe groundwater solution.

[b] Solutions containing less than 9.0×10^{-6} M cesium and the solution containing 9.7×10^{-6} M were analyzed using flame emission techniques. The other solutions were analyzed using flame atomic absorption spectroscopy techniques.

TABLE 2A. Cesium Concentrations and Activities of Solutions Used in the Batch-Partitioning Experiments.

Solution	Added Cesium, Concentration in M[a]	Activity[b] From ^{137}Cs, c/(s)(mL)
S-7	1.63×10^{-9}	131.1
S-6	1.19×10^{-8}	129.2
S-5	1.04×10^{-7}	131.1
S-4	1.04×10^{-6}	130.6
S-3	1.04×10^{-5}	131.5
S-2	1.04×10^{-4}	131.3
S-1	1.04×10^{-3}	128.7

[a]Stable cesium was added to the solutions as dissolved $CsNO_3$. The only cesium added to solution S-7 was ^{137}Cs with 66% carrier. The synthetic groundwater solution, before addition of cesium, was found by flame emission analyses to contain less than 3.8×10^{-9}M cesium and was assumed for these calculated concentrations to contain no cesium.

[b]The efficiency for the counting geometry employed (5 mL of solution in a test tube placed in a NaI well crystal) was determined to be 0.18 for the 0.662-MeV gamma ray from ^{137}Cs decay.

TABLE 3A. Activities of Solution and Partition Coefficients Measured in Batch Experiments for Cesium Adsorption on Oolitic Limestone.

Batch Experiment Number[a]	Cesium Concentration in Solution,[b] M	Volume of ^{137}Cs-Bearing Solution, mL	Volume of Residual Wash Solution, mL	Activity of Solution After Contact,[c] c/(s)(mL)	Measured Partition Coefficient[d] mL/g
First Series (contact for 3 days)					
1	1.6×10^{-9}	9.93	1.14	2.43	170.
2	1.2×10^{-8}	9.95	1.22	5.58	74.
3	1.0×10^{-7}	9.94	1.18	38.3	7.6
4	1.0×10^{-6}	9.93	1.12	85.0	1.4
5	1.0×10^{-5}	9.97	1.21	100.0	0.6
6	1.0×10^{-4}	10.00	1.22	106.8	0.3
7	1.0×10^{-3}	9.94	1.18	113.5	0.1
Second Series (contact for 7 days)					
8	1.6×10^{-9}	9.65	1.19	1.53	265.
9	1.2×10^{-8}	9.98	1.12	3.82	104.
10	1.0×10^{-7}	9.92	1.18	33.0	9.4
11	1.0×10^{-6}	9.93	1.20	76.9	1.9
12	1.0×10^{-5}	9.90	1.17	99.8	0.6
13	1.0×10^{-4}	9.94	1.21	108.4	0.2
14	1.0×10^{-3}	9.92	1.28	112.9	0.1
Third Series (contact for 8 days)					
15	1.6×10^{-9}	9.92	1.15	1.55	268.
16	1.2×10^{-8}	9.91	1.21	3.55	119.
17	1.0×10^{-7}	9.94	1.18	35.50	8.5
18	1.0×10^{-6}	9.96	1.16	76.66	1.9
19	1.0×10^{-5}	9.99	1.17	100.8	0.6
20	1.0×10^{-4}	9.99	1.17	109.9	0.2
21	1.0×10^{-3}	9.94	1.22	123.7	0.0

TABLE 3A. (Cont.)

Batch Experiment Number[a]	Cesium Concentration in Solution, M	Volume of ^{137}Cs-Bearing Solution,[b] mL	Volume of Residual Wash Solution, mL	Activity of Solution After Contact,[c] c/(s)(mL)	Measured Partition Coefficient[d] mL/g
Fourth Series (Tests without rock material)					
22	1.6×10^{-9}	9.90	0.0	115.6	-
23	1.2×10^{-8}	9.94	0.0	121.3	-
24	1.0×10^{-7}	10.01	0.0	122.2	
25	1.0×10^{-6}	9.96	0.0	124.2	-
26	1.0×10^{-5}	9.95	0.0	127.0	-
27	1.0×10^{-4}	10.01	0.0	130.1	-
28	1.0×10^{-3}	9.95	0.0	127.1	-

[a]Experiments 1 to 21 were each performed with 3/g of 20-50 mesh oolitic limestone (actual amount varied from 2.99 to 3.03 g). Experiments No. 22 to 27 were blank tests performed with no limestone present.

[b]The cesium-bearing solutions used are those listed in Table 1A.

[c]Solutions were filtered through 0.4-μm pore-size membrane filters before being counted.

[d]The partition coefficients were calculated assuming that no activity was adsorbed by the centrifuge tube walls.

TABLE 4A. Fractionation of Cesium and Partition Coefficients for Cesium Adsorption on Sentinel Gap Basalt Batch Experiments.

Initial Molarity of CsCl in Solution	Contact Time, days	Final Molarity of Cs in Solution[a]	Adsorbed Cs mol/g	Distribution Vs Partition Coefficient[b]
2.5×10^{-9}	15	8.3×10^{-11}	3.2×10^{-11}	380 ± 6
2.5×10^{-9}	15	7.3×10^{-11}	3.1×10^{-11}	420 ± 7
2.5×10^{-9}	28	7.0×10^{-11}	3.3×10^{-11}	470 ± 10
2.5×10^{-9}	28	6.3×10^{-11}	3.1×10^{-11}	490 ± 10
1.2×10^{-8}	15	3.6×10^{-10}	1.5×10^{-10}	420 ± 7
1.2×10^{-8}	15	3.8×10^{-10}	1.5×10^{-10}	420 ± 7
1.2×10^{-8}	28	3.2×10^{-10}	1.6×10^{-10}	500 ± 10
1.2×10^{-8}	28	3.3×10^{-10}	1.6×10^{-10}	480 ± 10
9.8×10^{-8}	15	3.5×10^{-9}	1.2×10^{-9}	350 ± 6
9.9×10^{-8}	15	3.4×10^{-9}	1.3×10^{-9}	370 ± 6
9.9×10^{-8}	28	2.8×10^{-9}	1.3×10^{-9}	450 ± 9
1.0×10^{-7}	28	2.8×10^{-9}	1.3×10^{-9}	450 ± 9
9.7×10^{-7}	15	4.4×10^{-8}	1.2×10^{-8}	260 ± 4
9.7×10^{-7}	15	4.8×10^{-8}	1.2×10^{-8}	250 ± 4
9.7×10^{-7}	28	4.1×10^{-8}	1.2×10^{-8}	300 ± 5
9.7×10^{-7}	28	4.0×10^{-8}	1.2×10^{-8}	300 ± 6
9.7×10^{-6}	15	7.8×10^{-7}	1.1×10^{-7}	145 ± 2
9.7×10^{-6}	15	8.2×10^{-7}	1.1×10^{-7}	141 ± 2
9.7×10^{-6}	28	7.1×10^{-7}	1.2×10^{-7}	165 ± 3
9.7×10^{-6}	28	7.1×10^{-7}	1.2×10^{-7}	164 ± 3
9.7×10^{-5}	15	1.9×10^{-5}	1.0×10^{-6}	56.5 ± 0.5
9.7×10^{-6}	15	1.8×10^{-5}	1.0×10^{-6}	56.5 ± 0.5
9.7×10^{-5}	28	1.6×10^{-5}	1.0×10^{-6}	65.4 ± 0.6
9.7×10^{-5}	28	1.6×10^{-5}	1.1×10^{-6}	67.3 ± 0.7

[a] The pH of each solution was measured after contact. The range was 7.3-7.6.

[b] The partition coefficients were calculated assuming that no cesium was adsorbed by the test tube walls.

TABLE 5A. Strontium Concentrations and Activities of Solutions Used to Investigate Radiation Effects on Strontium Adsorption by Oolitic Limestone

Solution	Added Strontium Concentration, M	Solution Irradiated	Solution Activity, c/(m)(mL)	
			1.0-mL Aliquot Counted	0.5-mL Aliquot Counted
1	1.03×10^{-6}	No	199020	195680
2	0.91×10^{-7}	No	203990	185890
3	0.90×10^{-8}	No	196400	202310
4	1.0×10^{-11}[a]	No	199920	205120
5	1.03×10^{-6}	Yes	197740	208030
6	0.91×10^{-7}	Yes	197730	204830
7	0.90×10^{-8}	Yes	198170	203070
8	1.0×10^{-11}[a]	Yes	198170	210490

[a]The concentration of strontium in this solution is that added as radiotracer ^{90}Sr containing 38% stable ^{88}Sr.

Table 6A. Results of Batch Partitioning Experiments for Strontium Adsorption on Oolitic Limestone (Section II-B-1)

Strontium Concentration in Solution M	Batch Experiment Number	Solution Irradiated	Volume of ^{90}Sr Bearing Solution mL	Volume of Residual Wash Solution mL	Activity of Residual Wash After Contact[a] c/m·mL	Measured Partition Coefficient, mL/g
First Series (Contact for 7 days)						
1.0×10^{-11}	1	No	9.96	1.20	77740	4.8
0.90×10^{-8}	2	No	9.99	1.19	62440	6.7
0.91×10^{-7}	3	No	10.04	1.21	88870	3.9
1.03×10^{-6}	4	No	9.96	1.19	80520	4.4
1.0×10^{-11}	9	Yes	10.05	1.19	74430	5.2
0.90×10^{-8}	10	Yes	10.00	1.22	79510	4.6
0.91×10^{-7}	11	Yes	9.98	1.25	82550	4.2
1.03×10^{-6}	12	Yes	10.02	1.22	83470	4.2
Second Series (Contact for 14 days)						
1.0×10^{-11}	5	No	10.02	1.18	62380	7.0
0.90×10^{-8}	6	No	10.00	1.21	51650	8.9
0.91×10^{-7}	7	No	10.01	1.23	71960	5.7
1.03×10^{-6}	8	No	10.01	1.28	64420	6.5
1.0×10^{-11}	13	Yes	10.06	1.19	58100	7.7
0.90×10^{-8}	14	Yes	10.00	1.19	64660	6.5
0.91×10^{-7}	15	Yes	9.98	1.21	71010	5.5
1.03×10^{-6}	16	Yes	9.98	1.16	64360	6.5
Third Series (Contact for 21 days)						
1.0×10^{-11}	17	No	10.04	1.21	59940	7.4
0.90×10^{-8}	18	No	9.99	1.19	55160	8.1
0.91×10^{-7}	19	No	9.98	1.19	67360	6.4
1.03×10^{-6}	20	No	9.98	1.20	65130	6.4
1.0×10^{-11}	29	Yes	10.00	1.19	65020	6.4
0.90×10^{-8}	30	Yes	9.99	1.23	71480	5.5
0.91×10^{-7}	31	Yes	10.00	1.19	71340	5.5
1.03×10^{-6}	32	Yes	9.99	1.29	71810	5.4
1.0×10^{-11}	21	No	10.03	0.0	195520	--
0.90×10^{-8}	22	No	10.04	0.0	184360	--
0.91×10^{-7}	23	No	9.98	0.0	199080	--
1.03×10^{-6}	24	No	10.00	0.0	189820	--
1.0×10^{-11}	25	Yes	10.01	0.0	193200	--
0.90×10^{-8}	26	Yes	10.01	0.0	194450	--
0.91×10^{-7}	27	Yes	9.99	0.0	197100	--
1.03×10^{-6}	28	Yes	10.00	0.0	196170	--

[a]Solutions were filtered through 0.4 m pore sized membrane filters . Solutions in Series 1 were counted in vials containing 1 mL of solution and 15 mL of scintillation liquid. Solutions in Series 2, 3, and 4 were counted in vials containing 0.5 mL of solution and 15 mL of scintillation liquid

TABLE 7A. Sampling Data and ^{134}Cs Activities of Eluate from Experiment 148-49

Fraction	Volume of Fraction, mL	Cumulative Volume, mL	Specific Activity,[a] c/s·mL	Net Activity,[a] c/s	Cumulative Net Activity,[a] c/s
1	4.8	4.8	1.65	7.93	7.9
2	7.1	11.9	1.58	11.21	19.2
3	7.5	19.4	0.16	1.19	20.4
4	4.9	24.3	0.06	0.27	20.6
5	7.0	31.3	0.06	0.42	21.0
6	7.0	38.3	0.06	0.43	21.5
7	7.0	45.3	0.06	0.42	21.9
8	7.0	52.3	0.06	0.40	22.3
9	7.0	59.3	0.05	0.37	22.7
10	7.0	66.3	0.06	0.42	23.1
11	7.0	73.3	0.05	0.37	23.4
12	7.0	80.3	0.05	0.36	23.8
13	7.1	87.4	0.05	0.39	24.2
14	7.1	94.5	0.07	0.5	24.7
15	7.0	101.5	0.05	0.3	25.0
16	7.1	108.6	0.05	0.3	25.3
17	7.1	115.7	0.06	0.4	25.7
18	7.1	122.8	0.05	0.4	26.1
19	7.0	129.8	0.05	0.4	26.5
20	7.1	136.9	0.04	0.3	26.8
21	7.1	144.0	0.05	0.3	27.1
22	7.1	151	0.07	0.5	27.6
23	7.0	158	0.03	0.2	27.8
24	7.1	165	0.04	0.3	28.1
25	7.1	172	0.02	0.1	28.2
26	7.1	179	0.05	0.3	28.6
27	7.0	186	0.04	0.3	28.9
28	7.1	194	0.05	0.3	29.2

TABLE 7A. (Cont.)

Fraction	Volume of Fraction, mL	Cumulative Volume, mL	Specific Activity,[a] c/s•mL	Net Activity,[a] c/s	Cumulative Net Activity,[a] c/s
29	7.0	201	0.04	0.3	28.9
30	7.3	208	0.04	0.3	29.8
31	7.1	215	0.04	0.2	30.1
32	7.1	222	0.03	0.2	30.4
33	7.2	229	0.03	0.2	30.6
34	7.1	236	0.04	0.3	30.8
35	7.0	243	0.04	0.3	31.1
36	7.0	250	0.03	0.2	31.3
37	7.0	257	0.04	0.3	31.6
38	7.1	265	0.04	0.3	31.9
39	7.0	272	0.04	0.3	32.2
40	7.4	279	0.03	0.2	32.4
41	7.1	286	0.04	0.3	32.7
42	7.1	293	0.05	0.3	33.0
43	7.1	300	0.02	0.1	33.2
44	7.1	307	0.03	0.2	33.4
45	0	307	0.00	0.0	33.4
46	0	307	0.00	0.0	33.4
47	0	307	0.00	0.0	33.4
48	0	307	0.00	0.0	33.4
49	6.5	314	0.05	0.3	33.7
50	0	314	0.00	0.0	33.7
51	6.4	320	0.05	0.3	34.1
52	0	320	0.00	0.0	34.1
53	6.5	327	0.02	0.1	34.2
54	0	327	0.00	0.0	34.2
55	0	327	0.00	0.0	34.2
56	6.5	333	0.03	0.2	34.4

TABLE 7A. (Cont)

Fraction	Volume of Fraction, mL	Cumulative Volume, mL	Specific Activity,[a] c/s·mL	Net Activity,[a] c/s	Cumulative Net Activity,[a] c/s
57	0	333	0.00	0.0	34.4
58	0	333	0.00	0.0	34.4
59	6.4	340	0.05	0.3	34.7
60	7.1	347	0.04	0.25	35.0

[a]Net activity was determined from the total counts per unit time obtained for the 605-KeV gamma peak from the decay of ^{134}Cs by subtracting background (0.49 c/s) and correcting for variations in sample size of each fraction. The net activity was calculated to be the activity measured in 1.3 mL of solution. The relative counting efficiency versus solution volume is plotted in Appendix, Figure 1. Solution fractions were counted for 400 s (except Fractions 11, 12, 13), and some fractions were recounted for 4000 s (Fractions 1-13). The specific activity was calculated from the net activity and the volume of each fraction.

TABLE 8A. Radioanalyses of Solutions Before and After Filtering.

Sample	Net Activity[a] of Cesium counts/s•mL		
	Initial Solution	Filtrate Passing Through 0.4-μm-Pore Membrane	Filtrate Passing Through 0.1-μm-Pore Membrane
Cesium-spiked Groundwater, Expt. 148-22[b]	0.36	0.33	0.34
Groundwater Eluate from Expt. 148-22[b]	0.21	0.23	0.22
Leachate from Simulated Waste	1.40	1.38	1.36

[a]Activity is for the 0.605-MeV gamma ray from the decay of cesium-134. Background correction was ∿0.32 c/s•mL. Uncertainty (σ) from counting statistics was ∿7%.

[b]Equilibrium dialysis experiment, Table 6.

TABLE 9A. Pressures, Corresponding Stem Readings, and Corrected Volumes of Infiltrated Mercury for a Test with 0.4 g of 30 to 40-Mesh Columbia River Basalt.

Pressure,	Penetrometer Stem Reading, mL	Corrected Penetrometer Reading, mL
0.012	0.0020	0.0020
0.019	0.0070	0.0070
0.026	0.0090	0.0090
0.033	0.0100	0.0100
0.047	0.0110	0.0110
0.061	0.0110	0.0110
0.079	0.0110	0.0110
0.424	0.0116	0.0116
1.46	0.0116	0.0116
2.15	0.0119	0.0118
2.84	0.0125	0.0124
3.52	0.0129	0.0128
5.27	0.0131	0.0128
8.72	0.0133	0.0131
13.9	0.0136	0.0132
20.8	0.0146	0.0141
34.6	0.0148	0.0141
69.0	0.0154	0.0142
86.2	0.0160	0.0144
103.5	0.0165	0.0147
120.7	0.0170	0.0149
137.9	0.0180	0.0157
155.1	0.0190	0.0165
193.0	0.0195	0.0167

QUESTIONS AND ANSWERS

ANL

Column Flow Rates and Residence

Q: What were your column velocities? Also, the differences you observed between the batch and the column work seem to be the same for both types of minerals. Could that be due to the column set ups (tubing and how you collected the samples and how you derived the numbers and plotted).

A: In the case of basalts, the flow rate in the column experiments were about 3 km/yr, and in the case of the tuff experiments, the flow rate was 600 m/yr.

Q: Could the experimental technique make any difference?

A: It's possible that's it's just the column capacity or a porosity effect. In the batch experiment all the surface area of the ground material was being contacted with the solution. In the column experiments the porosities are about 40%, and in the tuff experiment, about 30%.

Q: There is a point that Rick was trying to make there with the flow velocity and the batch Kd. There is a residence time effect, and, I believe, your residence time in the column was about an order of magnitude lower than the residence in the batch Kd. And I believe the residence times in the LASL columns were on the order of 2 weeks for strontium instead of 2 days.

Crushed Versus Intact Rock for Columns

Q: In one case you have a column of crushed material and in the other case tuff. Both cases compared the migration with a Kd. Now the Kd on the tuff was a crushed material.

A: The material was disaggregated and sieved on a 60 mesh screen.

Q: But how do you relate them to a chunk of tuff which is really a phase integration?

A: That's the reason I chose the Bandolier tuff from Los Alamos, because it disaggregates...it's such a problem that disaggregating it you're not really, I'd say, disturbing the surface area or the volume ratio that would be contacted by solution. The porosity of the materials in the batch experiment would not be that different from the porosity of the column. Did you check out porosity by a permeability measurement?

A: No, not the column.

Tracer Spike Versus Constant Concentration

Q: In the case of the crushed material you ran a spike through and you have a spike out. In the case of the tuff you ran a constant concentration through.

A: Right.

Q: Why didn't you do them both the same way?

A: There's one more experiment I want to do with the tuff column. I'll just start from the beginning. In the basalt column we saturated the column with cesium of various molarities and then we ran the spike through. In the tuff, like you said, we started with spiked influent solution and loaded the column with cesium-137 and found column capacity at the various molarities of cesium. The next experiment I want to do will show the columns are still running and I want to spike those columns with a small amount of cesium-134 at the same molarities and find out if the spike comes through as a representative Kd that would be predicted from the batch experiment and from the column experiment where we load up column capacities.

Mineral Pretreatment

Q: Regarding the round robin sentinal gap basalt that was distributed, it had been dry sieved. Did you wet sieve yours before you used it?

A: Yes, I cleaned mine.

Nuclide Concentration Affects Kd

C: On the conversion from distribution coefficient for the shaking and column experiments, I believe the equations everybody else is using only apply in the linear isotherm range. To get a distribution coefficient if you are eluting in the non-linear isotherm range is not so simple. People in chromotography have been worrying about this for many years.

A: By loading the column in a certain concentration and then determining the exchange at that concentration using the same molar solution as the spike going through the column.

Q: Yes, but you have a whole range of distribution coefficients over the band.

A: No, but we only have one range then, and then when we go to a different concentration we're looking at a second range. You're right. We find an anomaly adsorption isotherm, but we take it out and load the column in a certain concentration. The capacity at a certain concentration is different from what it would be at another concentration.

Q: Yes, and the shape itself, each point really has its own distribution coefficient. That's why tailing occurs.

C: I think the misconception there is the way that Paul did his column. He was running the concentration of say 10^{-4} molar cesium through and, if I'm right, I think that in the spike was a cesium-137 that was several orders of magnitude lower.

A: No, it was the same concentration. We took stock solution at 1×10^{-4}, spiked that with cesium-137, not altering the molarities of cesium, took 20 ml of that and ran through the column. We're looking at 10^{-4} molar solution going through a column that has been equilibrated with 10^{-4} molar cesium in solution.

Q: So you're not changing the solution concentration?

A: No.

C: I was just going to emphasize that point. We look at individual concentrations at the adsorption population at that concentration, so there are to tailing effects in these experiments.

C: That worried me, too, because your breakthrough curve shot straight into one rather than bending over in kind of an asymptote.

A: I'm sorry I didn't bring that out.

C: It's not a concentration dependent effect because we're using iso-concentrate solutions in these experiments. I might emphasize that point about concentration. Missing from this morning's discussion on tracer levels of cesium or tracer loadings was consideration of the cesium indigenous to rock materials. In the control sample program, for example, cesium was probably leached from some of the materials like limestone and the basalt. If you're looking at a 10^{-9} or 10^{-10} molar cesium solution, the tracer may be overwhelmed by the amount of cesium in the natural materials.

Nuclide Concentrations

Q: What are the concentrations of the materials used in these experiments? Are these concentrations anywhere approaching what you would guess to be the concentrations in materials in the outer repository? How realistic are these observations? Does anybody know that?

Q: Do you mean out of the repository or off the waste form?

A: Out of the repository.

A: Tomorrow I'll be discussing some results of where we're looking at leachates and looking at concentrations of nuclides in solutions and looking at subsequent migration of those nuclides. I'll show that the migration is very dependent on the concentration of these radionuclides in solution.

Cs Isotherms or Nuclide Concentrations

Q: Did you use a rock core or a column of crushed limestone?

A: We used a rock core and, therefore, the experiment was not completely analagous to the granulated materials used in the batch experiments. That's another explanation as to why the isotherm that was measured there was not directly applicable to our column or core work.

Nuclide (Non R.A.) from Rocks

C: There are reasons to believe that the source of the cesium is the repository. As the ground water disperses in the rock, some of the cesium is absorbed and diluted by ground water. The cesium concentration is lowered and the partitioning is stronger. The implication is that the formations could not absorb that cesium concentration. In fact, that concentration comes from the formation itself. And we can't expect concentrations lower than those values either.

Q: Do you pre-equilibrate your spike before you inject it into your pre-equilibrated solution?

A: The spike was made with cesium chloride. The sodium cesium chloride was dissolved in the rock equilibrated water.

Q: It was the tracer?

A: Yes, it was a tracer. The cesium was part of the rock equilibrated ground water to start with. In fact, the natural cesium from the rock itself overwhelmed the amount of radiocesium that we added to the solution.

Q: But you didn't have any acid added to that?

A: No.

Batch Versus Column or Cs Isotherm

Q: What was the purpose of doing experiments? Will you know when they agreed or why they didn't agree?

A: Yes. In the past, we've conducted a number of experiments with the columns and we were unable to obtain agreeable results between batch and column. We determined what might be the cause of the discrepancies and studied, specifically, a concentration of nuclides in solution. By observing the concentration dependence on adsorption, we were able to get closer results between our column experiments and our batch experiments.

Annual Report
Subcontract No. B-23171-A-H
Prime Contract EY-76-C-06-1830

SUBSURFACE MIGRATION OF RADIOACTIVE WASTE MATERIALS BY PARTICULATE TRANSPORT

Revised Annual Progress Report 1978-1979

Edited by

Geoffrey G. Eichholz

and

T. F. Craft

Prepared for Office of Nuclear Waste Isolation,
Battelle Memorial Institute
under its Contract with U.S. Department of Energy

September 1979

Revised

February 1980

School of Nuclear Engineering
Georgia Institute of Technology
Atlanta, Georgia 30332

THIS PAGE

WAS INTENTIONALLY

LEFT BLANK

NOTICE

This report was prepared as an account of work sponsored by the United States Government. Neither the United States nor the Department of Energy, nor any of their employees, nor any of their contractors, subcontractors, or their employees, makes any warranty, expressed or implied, or assumes any legal liability or responsibility for the accuracy, completeness, or usefulness of any information, apparatus, product, or process disclosed, or represents that its use would not infringe privately owned rights.

ABSTRACT

The objective of this work is the study of the uptake of dissolved radionuclides leached from waste material by water onto suspended colloidal particulates and their subsequent transport through permeable media. Vertical columns packed with basalt, limestone and other media have been set up to observe the migration of labeled particles. It has been shown that such particles do, in fact, migrate, but are subject to some retardation or deposition depending on the type of particle and the porous medium. Physical hindrance does not appear to be a very significant factor under the conditions investigated. The attachment of waste ions on such particles has been observed from distilled water, rock-equilibrated, and saline waters and, as expected, depends on concentration, competition with other dissolved ions, pH, and effective surface area. The latter does not necessarily stay constant since agglomeration of kaolin particles occurs in brines. The implication of this on waste migration from salt beds and in adjacent strata is also being studied.

I. INTRODUCTION

The safe disposal of high-level radioactive wastes, whether in the form of reprocessed purified material or as unprocessed burnt-up elements, requires an understanding of any long-range effects that may cause redissolution or remobilization of any portion of the stored wastes and may control their subsequent movement through subsurface aquifers, resulting eventually, hypothetically, in their possible emergence on surface.

Most of the processes that are known or believed to be significant in this situation are under investigation by various teams within the WISAP Project. The particular project reported here is concerned specifically with the transport of leached high-level waste products by fine suspended particulates that may exist in subsurface aquifers. Such particulates may arise from erosion of rock material by stress or decrepitation, hydraulic effects or thermal cycling, by mobilization of fine clay particles, by suspension of fine sand grains during passage of the water through other strata, and finally by surface spalling of the waste matrix itself.

The existence of suspended matter in subsurface water has been observed widely. Previous research, particularly at Georgia Tech (1,2), has served to demonstrate the capability of particulates to serve as carriers of adsorbed radionuclides. Although the experimental work has involved several different radionuclides, under field conditions the transuranium elements are the most important.

Four different processes are involved in the transport of radioactivity by particulates and are being investigated in this project:

1. Adsorption of dissolved radionuclides on particles of different constitution;
2. Competition between moving particles and surrounding rock surfaces for adsorbed ions;
3. Interaction effects between particles and rock surfaces that may control particle motion ; and
4. Competition with other dissolved ions in the water for accessible adsorption sites.

It may be assumed that the adsorption-desorption processes do not depend on the (slow) motion of the particles and, also, that the rock-particle interactions are not significantly affected by the presence of any adsorbed trace ion on the particle surface. For this reason, adsorption tests with radioactive tracers can be conducted almost independently of tracer tests on particle movement in a long column, and this has resulted in designing the project plan along two parallel lines.

Two major variables must be taken into account in such test work. One is the composition of the water; that is, whether it is distilled water, has been conditioned by lengthy exposure to rock surfaces, or contains added components such as sodium chloride. The oxygen and carbon dioxide content of the water is also of prime importance. The other variable is the condition of the bed matrix surfaces; they can consist of freshly fractured particles, oxidized surfaces, or surfaces modified by diagenesis. There seems to be no clear consensus on what one may reasonably expect at great depth, and the present project was planned to progress from "fresh" surfaces and deoxygenated distilled water to increasingly weathered material and waters of different composition with various gas contents to determine the importance of these factors in the present context.

Table I lists the principal experimental parameters that may be involved in the migration process and the proposed radiotracers employed in the study. Some of the tracers, such as Pu-237, Np-235, and Tc-95m are available only in limited quantity and work with them has to be planned to fit into supply availability.

The work has been conducted in parallel with a related study sponsored by the U.S. Nuclear Regulatory Commission and the results of both investigations will be presented here jointly.

TABLE 1. Experimental Parameters

Liquid Medium	Dissolved Gas	Bed Material	Suspended Material	Tracers
Deionized Water	None	Sand	Kaolin	Na-24
"Conditioned" Water	Air	Basalt	Vermiculite	Cs-137
Saline Water	CO_2	Granite	Limestone	Cr-51
	N_2	Limestone	Sand	Pu-237
		Shale	Bacteria	Np-235
		Sandstone		Tc-95m
				Sr-90
				Zr-95
				Ce-144

II. OBJECTIVES OF THE PROJECT

The goal of the project is the study of the mechanisms by which movement of radioactive waste products by attachment to suspended particles may contribute to total migration rates of leached waste products and to evaluate the significance of this pathway as compared to the movement of dissolved waste ions. This is being accomplished by investigating the movement of labeled particles through packed columns of minerals representing geological media of types that may occur near actual depository sites. Work to date has involved crushed material to maximize the surface area and sorptive effects. Later experiments are planned to investigate fractured or intact rock surfaces if sufficient suitable material can be obtained. If possible, limits of probable nuclide transport by particulates will be estimated.

III. REVIEW OF EXPERIMENTAL WORK

Several distinct processes are involved in particulate migration. Some of these can be considered fairly independent of each other and can be studied separately; others operate synergistically and yet others are highly site-specific. The progression in the work plan has been to study phenomena in a fairly qualitative fashion initially, both to assess the magnitude of effects involved and to demonstrate the reality of the postulated particulate migration process. The next stage requires more quantitative measurements on adsorption rates, migration ranges and retardation effects and this stage has been begun during the past summer. The final stage on more site-specific conditions cannot be started until a preliminary selection of potential sites has occurred, but in any case is not expected to be feasible before 1980.

The work conducted during the year can be categorized under these general headings:

A. Characterization of materials and conditions;
B. Sorption experiments; and
C. Particulate migration experiments.

The following sections will discuss the principal activities under those headings.

A. CHARACTERIZATION OF MATERIALS AND CONDITIONS

a. MINERALS

As Table I indicated, mineral samples are required to simulate both the suspended particulates and the rock matrix bounding the aquifer or the depository. For the particulates, suspensions have been prepared using Georgia kaolinite, oolitic limestone, and vermiculite. Coarse mineral bed

samples were prepared from specimens of basalt, limestone, dolomite and shale obtained through the WISAP program and fully characterized (Ames[4]). Batch Kd values on these materials have also been reported by Relyea and Serne.[5] Table 2 lists the source of the mineral samples.

Coarse material was crushed and ground as needed in the Mineral Engineering Labs at Georgia Tech. Suspensions were prepared in large carboys to provide an adequate supply of material of consistent composition and concentration. No direct particle size distributions have been obtained so far. Centrifuged and dried samples have been examined by electron microscopy; such observations on kaolin particles will be reviewed later. Concentrations of suspended particles were controlled mainly by turbidity and optical transmission tests. Attempts are under way to standardize size distributions by comparison with calibrated latex suspensions.

The basalt with which we have been working is a very tough material and there is a potential for contamination by wear from the surfaces of the crushing equipment. The basalt was received in the form of chunks, fist-sized and slightly larger. Early samples were broken by hand with a hammer and then crushed between heavy cast steel rollers which were set successively closer together. The crushed material was fractionated by screening. Some of the finer sizes were also produced by ball milling fractions larger than 15 mesh in a ceramic jar with alumina balls. This also produces contamination; visible wear occurred on the jar. It is believed, however, that the ball and jar material was removed later as very fine particles when the subsequently screened fractions were repeatedly washed until no turbidity could be seen in the wash water. The basalt was then dried for storage until use. Subsequent samples have been precrushed with a jaw crusher.

b. PHYSICAL AND CHEMICAL CONDITIONS OF DEEP GROUNDWATER

To establish realistic test conditions an appropriate choice of experimental parameters is important. Three areas of specific importance to the present work are the nature and concentration of carbon dioxide in deep waters, the influence of diagenesis, and the effects and importance of "equilibration" of water with surrounding minerals.

TABLE 2. Rocks Utilized in the 20 to 50 Mesh Size Range in Task 4 Studies (from Ref. 4)

Rock	Source	Donor
Westerly Granite	New England	Lawrence Livermore Labs Hugh Heard
Argillaceous Shale (Green)	New York State	Wards Natural Science Establish. Cat. No. 47W7400
Oolitic Limestone	Indiana	Wards Natural Science Establish. Cat. No. 47W4670
Sentinel Gap Basalt	Washington State Hiway 243 Road outcrop between Beverly and Mattawa, WA	Pacific Northwest Laboratory, L. L. Ames
Conasauga Shale	Core Well No. OWI-OR-8 depth 16 to 100 ft	Oak Ridge National Lab L. R. Dole
Climax Stock "Granite"	Pile driver tunnel complex, 1367 ft below the collar of shaft 1501 Nevada State N901, 147 E 677,016	Lawrence Livermore Lab L. D. Ramspott
Anhydrite	Core Well AEC 8 depth 3080.9 - 3083.5 ft Los Medanos, N. Mexico	Sandia Laboratories D. W. Powers
Magenta Dolomite Rustler Formation	Roadcut along N.M. Hiway 31 near entrance to IMC mine Sec 1, T22S, R29E	Sandia Laboratories D. W. Powers
Culebra Dolomite Rustler Formation	Roadcut along N.M. Hiway 62/180 about 7 miles South of Carlsbad airport, Sec 4, T24S, R26E	Sandia Laboratories D. W. Powers

Estimates of the concentrations of dissolved CO_2 in deep water seem to vary appreciably. I. W. Marine at Savannah River Labs has analyzed deep groundwater samples and reported concentrations of 10-40ppm.[6] Though the source of water may be different in different candidate depository formations, that range of CO_2 concentrations will be used in upcoming tests in the present project. Canadian measurements on the Lac Du Bonnet batholith[7] report CO_2 concentrations of 13 and 45ppm. Various ways of attaining such concentrations have been examined, based on the known reaction constants for the CO_2-carbonate system in water. No water with added CO_2 has been used so far.

There has been disagreement among investigators as to the validity of data obtained using freshly crushed rock when extrapolation is to be made to the actual conditions existing in the rock in situ. Surfaces in contact with groundwater for significant periods of time are subject to diagenesis and alteration of surface properties and characteristics. Obtaining and studying material with sufficient natural surface has not been possible within the limitations of our work, so ground material has been used. "Equilibrated" water has been used in some instances to provide at least a more stable situation between the composition of the mineral surface and the liquid in contact with it.

"Equilibrated" water has been prepared by keeping deionized water in contact with sizable portions of the mineral for extended periods (weeks or months). In some instances stirring was employed, and in others the water was gently refluxed. The equilibrated water is passed through a Millipore filter before use. Some properties of these waters are listed in Table 3.

c. PROPERTIES OF THE PARTICULATES

The behavior of kaolin particles in columns of crushed basalt has been studied, using deionized water as the carrier.

The kaolin suspension had been prepared about two months before use by stirring kaolin in water and allowing it to stand. Samples were removed from the top for use. The suspension was prepared for use by centrifuging, decanting the supernatant, resuspending in water by ultrasonic agitation,

TABLE 3. Preparation and Properties of Equilibrated Water

Mineral	Method of Production*	pH	Conductivity ($\mu\Omega$/cm)
Basalt	Refluxed	7.59	55
Basalt	Stirred	7.10	94
Shale	Refluxed	6.96	630
Limestone	Refluxed	8.74	450
Magenta dolomite	Refluxed	8.62	1600
Culebra dolomite	Stirred	8.54	265

*Water and mineral in contact for 60 days or more.

and then repeating this sequence again. The resulting sol was activated by irradiation in the Georgia Tech Research Reactor for one hour at a flux of 10^{13} neutrons/cm^2/sec. Sodium is the only easily activable constituent of the kaolin and the resulting Na-24 has been used to follow the movement of the kaolin particles.

The initial problem was to obtain enough of the particles from their respective suspensions to effectively wash and label them. 50 ml samples of suspension were placed in centrifuge tubes and "spun down," out of suspension. With the water drained off, it was a simple matter to transfer the solid material at the bottom of the tubes (the particles) into a single test tube. Particles from 1 liter of suspension of each type were grouped into one tube.

After the concentration was made, a 4:1 buffer to peroxide ratio was used to fill the tubes containing the particles. This mixture was then boiled for about 10 minutes to wash the particle surfaces. The buffer solution was used to negate the acidic quality of peroxide that becomes apparent when it is boiled. The particles were then spun down, resuspended and rinsed in water, spun down, rinsed, and finally spun down for good. In this state, they were ready for absorption of the tracer isotope.

All of the tubes with the particles were diluted with 50 ml of distilled and deionized H_2O. All of the percent transmittances were measured at λ = 3200 A. The highest percent transmittance was kept as a standard and the others were diluted to this value ($\pm 5\%$). These diluted solutions of particles and H_2O will be called "rock solution."

The morphology of the particulates was determined from electron micrographs. The particles shown on the electron micrographs were counted on a Zeiss counter and a probability plot (Fig. 1) was prepared. The mean particle size was found to be 0.125 ± 0.03 micron. It was assumed initially that with particles this small, little mechanical entrapment due to physical hindrance or interstitial straining will occur in a 40/50 mesh medium unless particle agglomeration occurs; any radioactivity deposited in the column will, therfore, be due to particle immobilization by other mechanisms or by transfer of radioactivity to the bed material. Figure 2 shows a typical

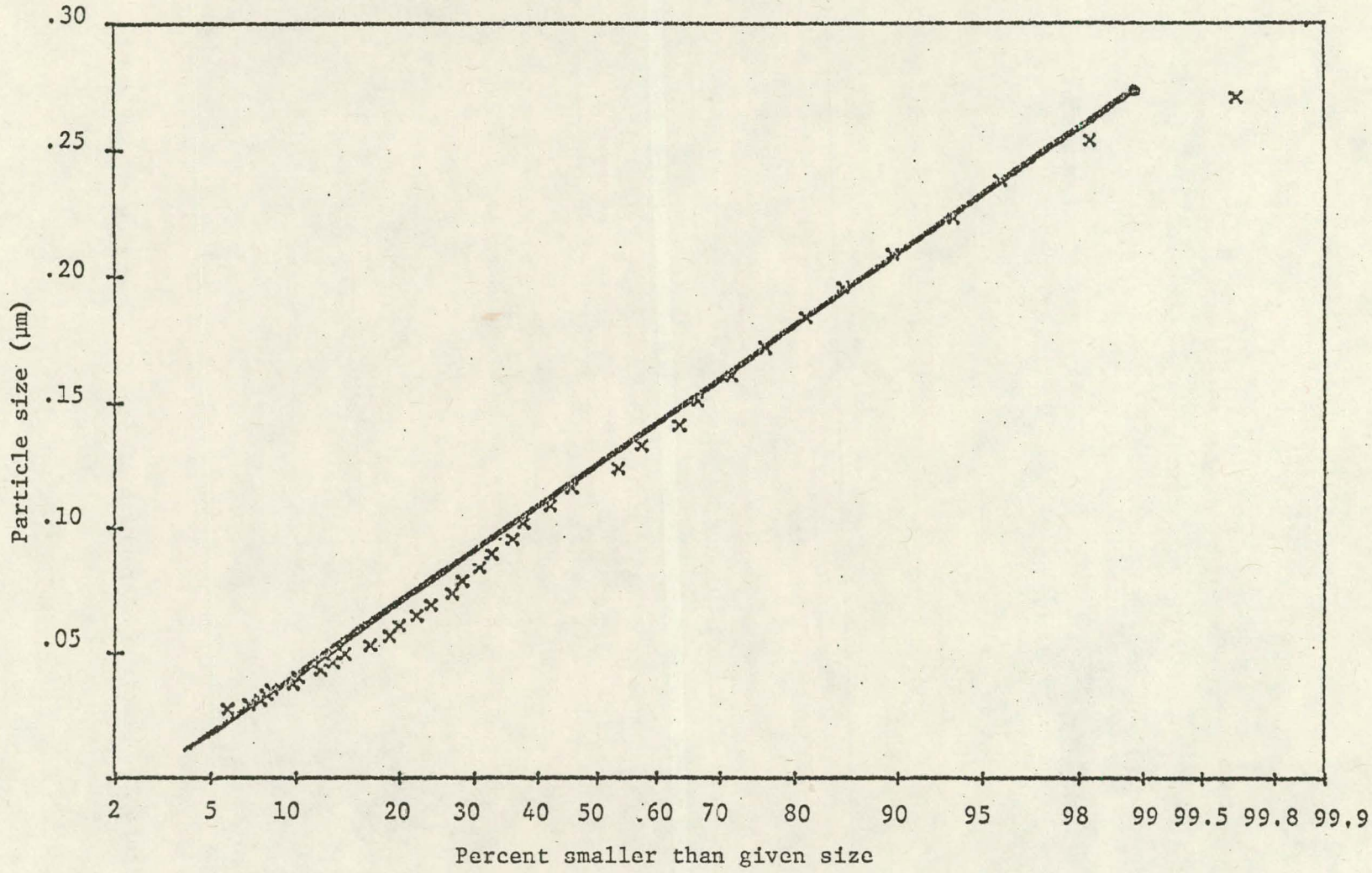

FIGURE 1. Kaolin Particle Size Distribution

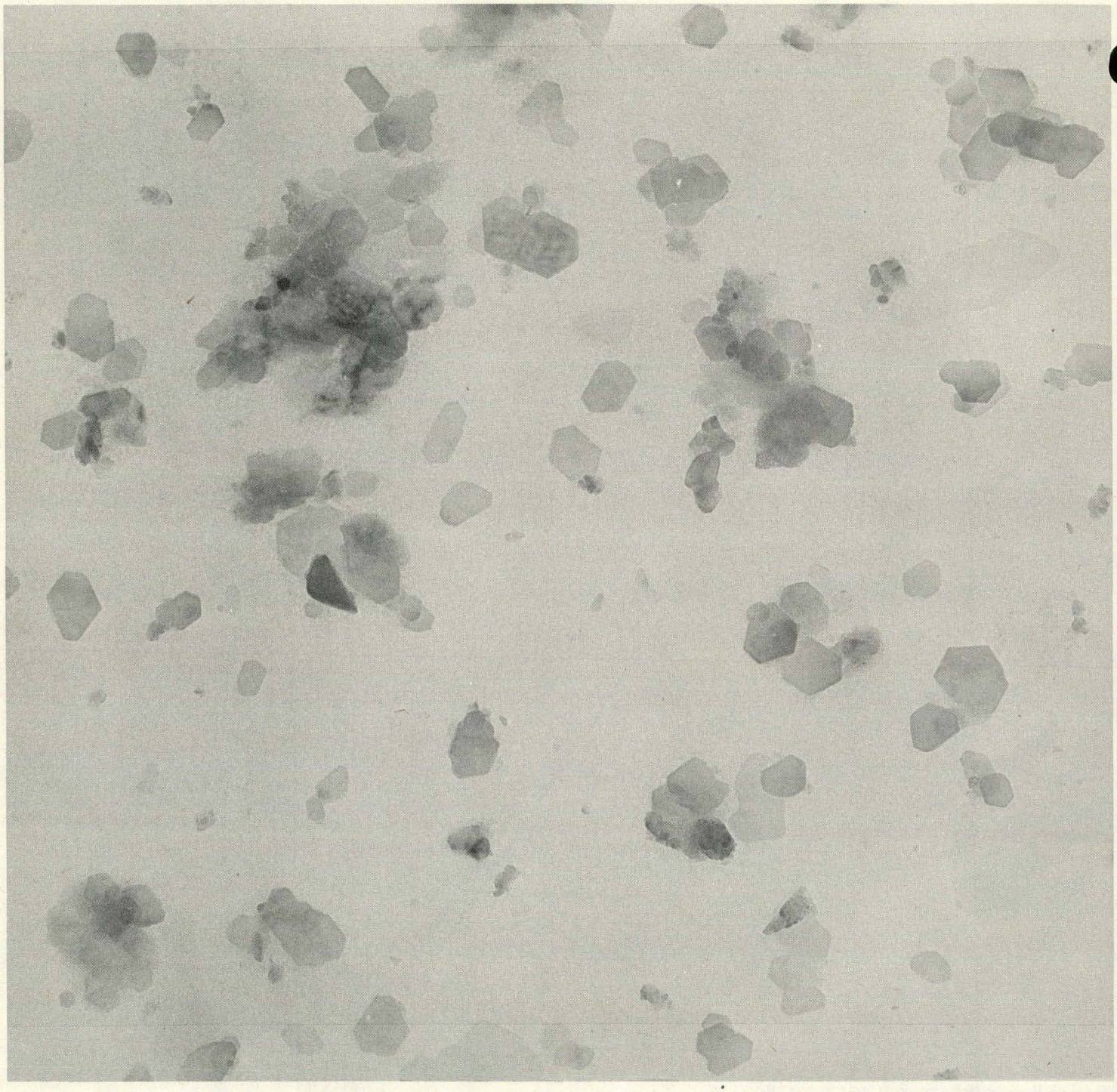

Figure 2. Electron Micrograph of Kaolin Dispersion

electron micrograph of the kaolin particles from a suspension. They are seen to be well-formed polygonal platelets, with some natural conglomeration occurring even in deionized water. So far no satisfactory method has been found for the measurement of effective surface areas of these particles.

B. SORPTION EXPERIMENTS

Particulate vectors contribute to radionuclide migration only to the extent that direct spallation of the waste solid occurs, or that dissolved atoms adsorb on the dispersed particles present in the first place and stay on them as they pass through various aquifers under conditions of varying pH, salinity, hardness, and mineral boundaries. For that reason it is important to investigate the adsorption by particulates of representative trace elements, any desorption effects, and transfer processes from particles to bed surface.

a. ADSORPTION TESTS ON COARSE PARTICLES

One of the principal mechanisms of interest is the attachment of radioactive waste ions onto the suspended particulates. In order to simulate this effect, sorption measurements were done under static conditions with coarse particles exposed to tracer solutions of varying strength and condition. Absorption studies have been conducted to determine the relative distribution of radiotracers between solid and liquid phases.

The initial step in the study of the competitive forces has been to determine the distribution of Cs^{137} and Pu^{237} in different liquid-solid systems. The presumed lack of free oxygen in subsurface formations has led to a series of experiments under deoxygenated conditions.

The general technique is to place 100 ml of the liquid in a flask with a known amount (usually 1 gram) of the mineral to be studied, and to add a known amount of radionuclide. Samples of the solid and liquid are separated at intervals and the radioactivity of each fraction is measured. The deoxygenated system consisted of flasks connected in series by flexible tubing

through which a slow flow of water-saturated nitrogen was maintained. Each flask was provided with a Teflon-coated stirring bar and a magnetic stirrer. It was soon found that strong continuous stirring leads to a disintegration of the mineral and/or stirring bar. The tough, abrasive particles of basalt, in particular, are very effective in grinding from the stirring bar fine particles of Teflon which float to the surface. The stirring regime was therefore changed and in subsequent runs the deoxygenated flasks have been stirred for only a few minutes at the time about twice a day. In those cases where no attempt to exclude oxygen was made, the flasks have been swirled by hand. Under these circumstances the mineral contacts all parts of the liquid, but there is no attritional change in the size of the particles.

Several variations have been employed, including equilibration of the Cs^{137} solution with the flasks, to avoid uncertainties due to absorption on the surface of the flask. Some unstirred flasks have also been included, but the true significance of this effect has not been well established due to the small volume of liquid involved, and the amount of inadvertent mixing caused by handling and sampling. It now appears, however, that stirring is not a factor of concern in these experiments. The presence or absence of oxygen also did not seem to cause any significant difference in the Cs^{137} results, although our system of oxygen exclusion was admittedly less than absolute. The nitrogen gas used is known to contain a few parts per million of oxygen, but based on its partial pressure, the dissolved oxygen in the water was obviously quite low. Table 4a summarizes the results obtained in several different runs of four weeks duration. In each instance, only the radioactivity of the liquid is given, as determination of the activity of the solid will require termination of the experiment. Each liquid sample is centrifuged and decanted before counting. From this table it is seen that sand has the least affinity for Cs^{137} and basalt has the greatest, although it is to be noted that both sand samples were much coarser than the other minerals. The intermediate value given by the liquid from the basalt-kaolin combination (#9) is believed due to incomplete removal of the kaolin from the sample which retained a visible turbidity.

In another set of experiments (see Table 4b) the effects of deionized water and brine were compared in the absorption of Cs^{137} on basalt and

TABLE 4a. Summary of Cesium Adsorption Tests on Various Rock Types

	Description	Oxygen	Stir	Initial	4 weeks	Kd,ml/g
1.	Sand(60-140 Mesh)	No	Yes	13,985	8,265	1.4
2.	Magenta(325-500)	No	Yes	17,175	1,245	13
3.	Basalt(325-500)	No	Yes	19,060	464	40
4.	Shale(250-270)	No	Yes	17,238	892	18
5.	Culebra(250-270)	No	Yes	18,441	483	37
6.	Limestone(200-250)	No	Yes	19,357	1,644	11
7.	Basalt(325-500)	Yes	Yes	18,341	423	42
8.	Basalt(325-500)	Yes	No	19,540	409	47
9.	Basalt(325-500) + Kaolin	Yes	Yes	16,526	1,306	12
10.	Sand(35-60)	Yes	No	17,525	11,442	0.53

*Kaolin that did not settle out after 3 days left in. Liquid was definitely turbid. Cs on particles accounts for elevated value over 3, 7, and 8.

Each sample contains 1.00 gram of the specified sample in 100 ml of Cs-137 solution containing 0.028 Ci/ml activity.

TABLE 4b. Cesium-137 Adsorption Tests

Description	Residual cpm/ml after equilibration
Basalt in deionized water	579
Basalt in saturated salt water	13,049
Kaolin in deionized water	1,367
Kaolin in saturated salt water	12,972

in each case 5 gm/100 ml (0.0276 Ci/ml)

kaolin. Kaolin coagulated rapidly in the presence of salt water due to interference with the normal repulsive forces which would keep it in suspension. The results shown in Table 4 lead to the conclusion that if basalt is first brought to equilibrium with saturated brine its sorptive capacity for Cs^{137} is greatly reduced. This is probably due to having most of the active sites on the surfaces filled by sodium ions. Similar results are seen for kaolin, although the effect of surface area reduction due to coagulation is yet to be fully explored.

The mineral substrates investigated in this series were Sentinel Gap basalt, Conasauga shale, oolitic limestone, magenta dolomite, and Culebra. The results are summarized in Table 5.

It has also been observed that virtually identical quantities of Pu^{237} are absorbed by basalt in contact with brine and with equilibrated water.

The general pattern of these results shows that increasing ionic strength of the liquid phase reduces the sorption of cesium on the mineral. This effect is probably due to competition between ions for the limited number of absorption sites on the surface of the substrate. The absence of oxygen in distilled, deionized water had little, if any, effect except in the case of limestone, where sorption was greatly increased in the absence oxygen. Oxygen was excluded from the sodium chloride solutions in only one instance (with basalt) where a significant decrease in sorption was observed.

The ion competition concept is supported by other observations. It was noted that there was a very wide difference in the level of radioactivity found in the initial liquid samples, although the same quantity of Cs^{137} had been added to each flask. While manipulative techniques and counting statistics can explain some variation, clearly other factors were involved as shown by the data of Table 6. There appears to be some difference between the distilled, deionized samples depending on the presence of oxygen, but there is an unmistakable difference between equilibrated and distilled deionized waters. The highest counts were obtained in the 1.0 M sodium chloride solutions, which were much higher in ionic strength than any of the other

TABLE 5. Percent Removal of Cs-137 from Liquids in Contact with Mineral Particles

Liquid phase	Solid: Basalt	Shale	Limestone	Magenta	Culebra
Distilled, deionized water	81.5	95.1	29.7	90.1	92.1
Distilled, deionized, deoxygenated water	82.4	90.4	71.5	90.0	90.3
Equilibrated water heated (a)	75.8	92.0	12.3	79.5	----
Equilibrated water stirred (b)	82.4	----	----	----	72.7
1.0 M NaCl	39.2	84.7	14.7	57.0	22.8
1.0 M NaCl deoxygenated	15.2	----	----	----	----

(a) Prepared from distilled, deionized water refluxed in contact with the corresponding mineral for several weeks.

(b) Same as (a), except stirred instead of refluxed.

TABLE 6. One-Minute Counts of Liquids to Which Equal Amounts of Cs-137 had been Added

	Distilled Deionized Water	Distilled Deionized Deoxygenated Water	Equilibrated Water (Refluxed)	Equilibrated Water (Stirred)	1.0M NaCl	1.0M NaCl Deoxygenated
	6053	6889	9323[a]	11065[a]	21403	18747
	7519	7398	11154[b]	8477[d]	15936	
	7960	6144	12926[c]		16332	
	6991	5120	13604[e]		17742	
	7902	6386			16280	
	6743				15897	
Average	7195	6387	11752	9771	17265	18747

a) Basalt
b) Shale
c) Limestone
d) Culebra
e) Magenta

liquids. It is not possible to determine from the single value given whether deoxygenation of the 1.0 M NaCl solution causes any differences.

To determine if beaker wall adsorption affected the activity, some flasks were first treated by filling with a 0.01 M solution of non-radioactive cesium chloride for three days prior to use. In most instances the results were very similar to those obtained in untreated flasks, and it was concluded that pretreatment is not necessary. The actual figures obtained are given in Table 7.

The ease with which the sorption equilibrium can be shifted was demonstrated by the addition of 10 ml of 6.2 M sodium chloride solution to each of the flasks used in the experiments of Table 5. The added salt displaces some of the adsorbed activity, increasing the activity in the liquid phase, as clearly shown by the data of Table 8. These data include a correction for dilution by the added liquid. It is evident that tracer adsorption is less from equilibrated water, with its concentration of competing dissolved ions, and in the presence of NaCl than in deionized water.

Because of the appreciable effect the presence of salt has on ion adsorption on particulates, an additional series of tests was carried out on saline solutions, in the same manner as previously. The results are summarized in Table 9 and Fig. 3. Except for limestone, increased salt concentration clearly decreased available adsorption sites, as expected. In all cases adsorption on limestone was appreciably less than in other minerals; however, because of the friable nature of limestone, for flow in limestone higher concentrations of fine particulates may be available as carriers, compensating for lower specific uptake.

b. ADSORPTION ON SUSPENDED PARTICLES

The adsorption of radioisotopes on the very small particles that constitute the mobile solids has also been investigated. The procedure was essentially the same as that used with the granular material of much larger particle size, but some manipulative refinements were required. In order to obtain enough solids with which to work, it was necessary to centrifuge the normally stable sols that are used in this work. Kaolin, vermiculite, and basalt particles were concentrated in this manner. The kaolin was treated

TABLE 7. Percent Reduction of Cs-137 Activity in Flasks with and without Prior Treatment with Cesium Chloride Solution

	Mineral Substrate	Liquid phase	Pretreated flask	Kd* (ml/g)	Untreated flask	Kd* (ml/g)
1.	Basalt	Distilled, deionized water	88	7.3	82	4.6
2.	Basalt	Equilibrated water	81	4.3	76	3.2
3.	Basalt	1.0 M NaCl	26	0.35	40	0.67
4.	Limestone	Distilled, deionized water	16	0.19	30	0.43
5.	Limestone	Equilibrated water	0	---	12	---
6.	Limestone	1.0 M NaCl	18	0.22	15	0.18
7.	Shale	Distilled, deionized water	93	13.3	95	19.0
8.	Shale	Equilibrated water	94	15.7	92	11.5
9.	Shale	1.0 M NaCl	86	6.1	85	5.7

TABLE 8. Change in Cs-137 Adsorption Following Sodium Chloride Addition

Mineral Substrate	Liquid phase (Water)	Relative activity detected			
		Initial	After mineral addition	After NaCl addition	Kd, ml/g
1. Basalt	Distilled, deionized deoxygenated	1190	98	1534	---
2. Basalt	1.0M NaCl, deoxygenated	3364	2798	2535	0.33
3. Basalt	Distilled, deionized	1066	148	1189	---
4. Basalt	Equilibrated (refluxed)	1649	312	1887	---
5. Basalt	Equilibrated (stirred)	1990	295	1770	0.12
6. Basalt	1.0M NaCl	3841	2169	2265	0.70
7. Shale	Distilled, deionized deoxygenated	1254	86	240	4.2
8. Shale	Distilled, deionized	1425	12	183	6.8
9. Shale	Equilibrated (stirred)	2018	46	265	6.6
10. Shale	1.0M NaCl	2693	349	306	7.8
11. Limestone	Distilled, deionized deoxygenated	984	231	1242	---
12. Limestone	Distilled, deionized	1181	763	1412	---
13. Limestone	Equilibrated (stirred)	2249	1863	2596	---
14. Limestone	1.0M NaCl	3001	2495	2569	0.17
15. Culebra	Distilled, deionized deoxygenated	905	49	602	0.50
16. Culebra	Distilled, deionized	1385	67	878	0.58
17. Culebra	Equilibrated (stirred)	1413	413	1516	---
18. Culebra	1.0M NaCl	2826	2015	907	2.1
19. Magenta	Distilled, deionized deoxygenated	1127	52	449	1.5
20. Magenta	Distilled, deionized	1170	101	553	1.1
21. Magenta	1.0M NaCl	2726	987	1111	1.4

TABLE 9. Adsorption of Cs-137 for Sodium Chloride Solutions of Different Concentrations

	NaCl Concentrations	Basalt	Limestone	Shale	Magenta
	M Mole/l				
1.	0.0	89.5%	48.0%	96.2%	95.7%
2.	5.0	90.1	29.2	95.5	89.8
3.	10.0	88.3	25.9	94.5	91.2
4.	15.0	87.3	35.4	93.2	89.3
5.	25.0	82.6	28.5	92.1	89.6
6.	50.0	77.6	29.2	91.2	84.1
7.	100.0	71.0	33.0	90.5	78.4
8.	500.0	51.8	29.0	86.7	66.1
9.	1000.0	30.2	18.0	84.8	50.9

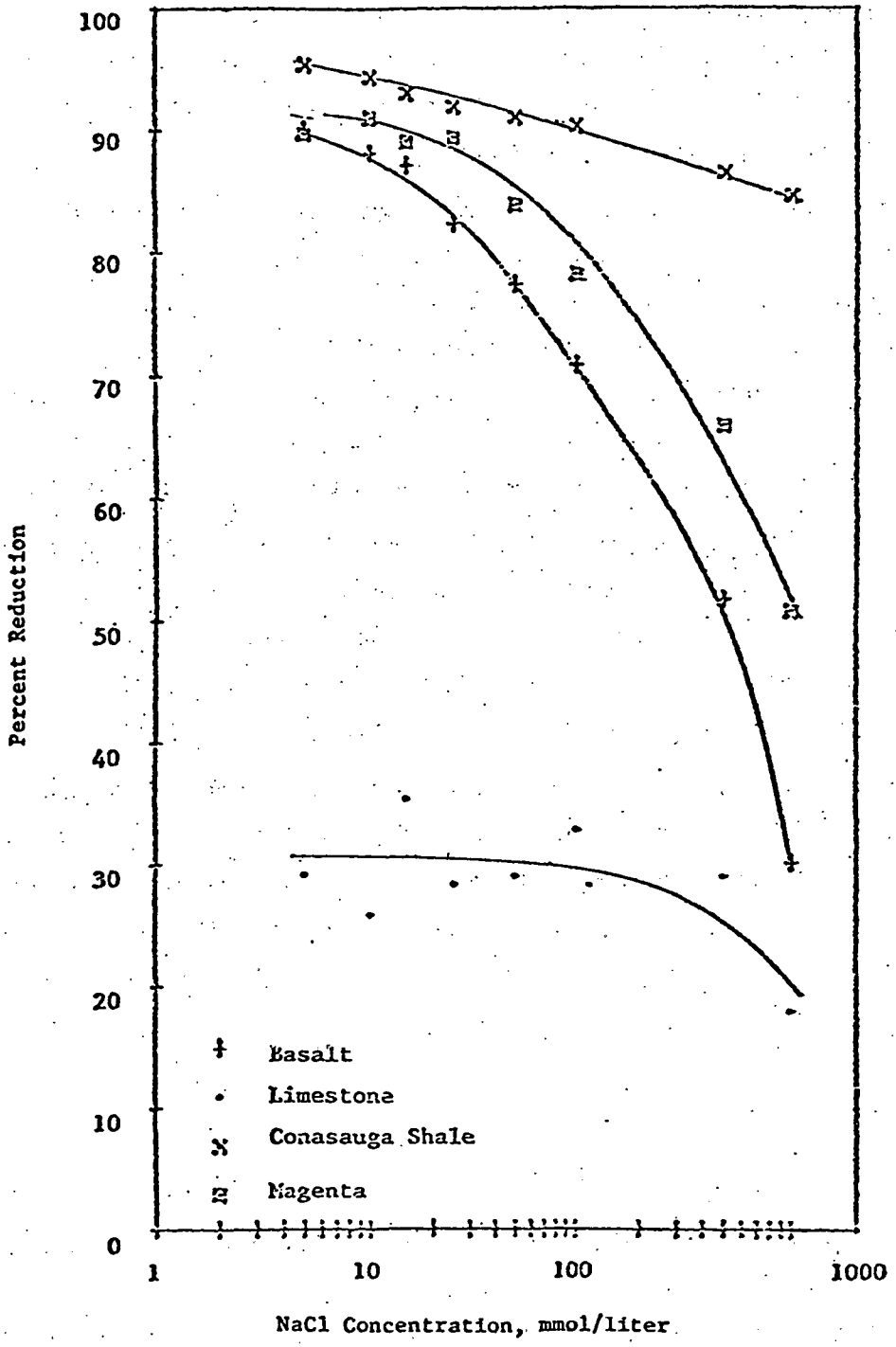

Figure 3. Percent Reduction in Cs-137 concentration vs. NaCl content

with hydrogen peroxide in a buffer solution in order to oxidize any organic matter present which could exert absorptive capability disproportionately to its quantity. Excess peroxide and other extraneous solubles were removed by washing and centrifuging several times.

The concentration of particles was approximately equalized by dilution with water until the suspension of all three minerals showed the same percent transmission of light when measured spectrophotometrically. Experiments were then carried out with these suspensions in which the variables were quantity of suspension, Cs^{137} concentration, sodium chloride concentration, and pH. Table 10 shows the matrix of variables. Three tubes of each permutation were required; one each for vermiculite, kaolin, and basalt.

It is seen that the tracer concentration has little bearing on the fraction adsorbed. The amount adsorbed levels off with increasing particle concentration to an equilibrium partition factor; this is shown in Fig. 4. Adsorption on vermiculite is clearly above the others; again quantitative evaluation must await surface area determination.

The effect of salt in solution is most striking and significant. Except for vermiculite at low salt concentrations, NaCl appears to pre-empt adsorption sites and to interfere with tracer uptake. (Note: Other work reported later indicates, however, that for related reasons, any particle that does carry waste adsorbents is likely to have a longer migration range in brines than in deionized water.)

Experimental Details

The initial problem was to obtain enough of the particles from their respective suspensions to effectively wash and label them. 50 ml samples of suspension were placed in centrifuge tubes and "spun down," out of suspension. With the water drained off, it was a simple matter to transfer the solid material at the bottom of the tubes (the particles) into a single test tube. About 1 liter of suspended particles of each type were grouped into one tube.

TABLE 10: Cs-137 Adsorption on Suspended Particles

A) Effect of particulate concentration

Suspended Mineral	Concentr. (ml of susp.)	Initial Count (cpm)	Final Count (cpm)	Residual activ. in solution (%)	Percent uptake (%)	Kd (ml/g)
Vermiculite	3.0	14815	9376	63.3	36.7	0.58
	2.5	15358	12280	80.0	20.0	0.25
	2.0	14646	9970	68.1	31.9	0.47
	1.5	14548	10430	71.7	28.3	0.39
	1.0	13657	11295	82.7	17.3	0.21
Kaolin	3.0	17403	12441	71.5	28.5	0.40
	2.5	14340	13020	87.0	13.0	0.15
	2.0	15833	13478	85.1	14.9	0.18
	1.5	15187	14382	94.7	5.3	0.056
	1.0	14840	13840	93.3	6.7	0.072
Basalt	3.0	13387	12734	95.1	4.9	0.052
	2.5	14746	12825	87.0	13.0	0.15
	2.0	14527	12906	88.8	11.2	0.13
	1.5	14324	12798	89.3	10.7	0.12
	1.0	13588	13555	99.8	0.2	0.0020

B) Effect of Cs-137 concentration

Suspended Mineral	Cs-137 added (ml)	Initial Count (cpm)	Final Count (cpm)	Residual activ. in solution (%)	Percent uptake (%)	Kd (ml/g)
Vermiculite	0.050	7569	3961	52.3	47.7	0.91
	0.075	11459	---	---	---	---
	0.150	22888	18570	81.1	18.9	0.23
	0.250	40822	35126	86.0	14.0	0.16
Kaolin	0.050	6708	5527	82.4	17.6	0.21
	0.075	10602	9663	91.1	8.9	0.098
	0.150	22121	21540	98.7	1.3	0.013
	0.250	38431	38400	99.9	0.1	0.0010
Basalt	0.050	6464	5306	82.0	18.0	0.22
	0.075	9187	8687	94.6	5.4	0.057
	0.150	26637	25752	96.7	3.3	0.034
	0.250	38394	40173	105.0	---	---

TABLE 10. Cs-137 Adsorption on Suspended Particles (continued)

C) Effect of NaCl concentration

Mineral	Amount of NaCl added (g)	Initial Count (cpm)	Final Count (cpm)	Residual activ. in solution (%)	Percent uptake (%)	Kd (ml/g)
Vermiculite	0.005	16419	14184	86.4	13.6	0.16
	0.010	15060	13936	92.5	7.5	0.081
	0.020	14820	13833	93.3	6.7	0.072
	0.050	15169	16382	108.0	---	---
	0.100	15788	16819	107.0	---	---
Kaolin	0.005	15526	17381	112.0	---	---
	0.010	13468	16746	124.0	---	---
	0.020	15172	17744	117.0	---	---
	0.050	16284	18436	113.0	---	---
	0.100	15966	18760	118.0	---	---
Basalt	0.005	15813	21742	138.0	---	---
	0.010	15173	17970	118.0	---	---
	0.020	13975	17026	122.0	---	---
	0.050	15698	18084	118.0	---	---
	0.100	15460	18084	117.0	---	---

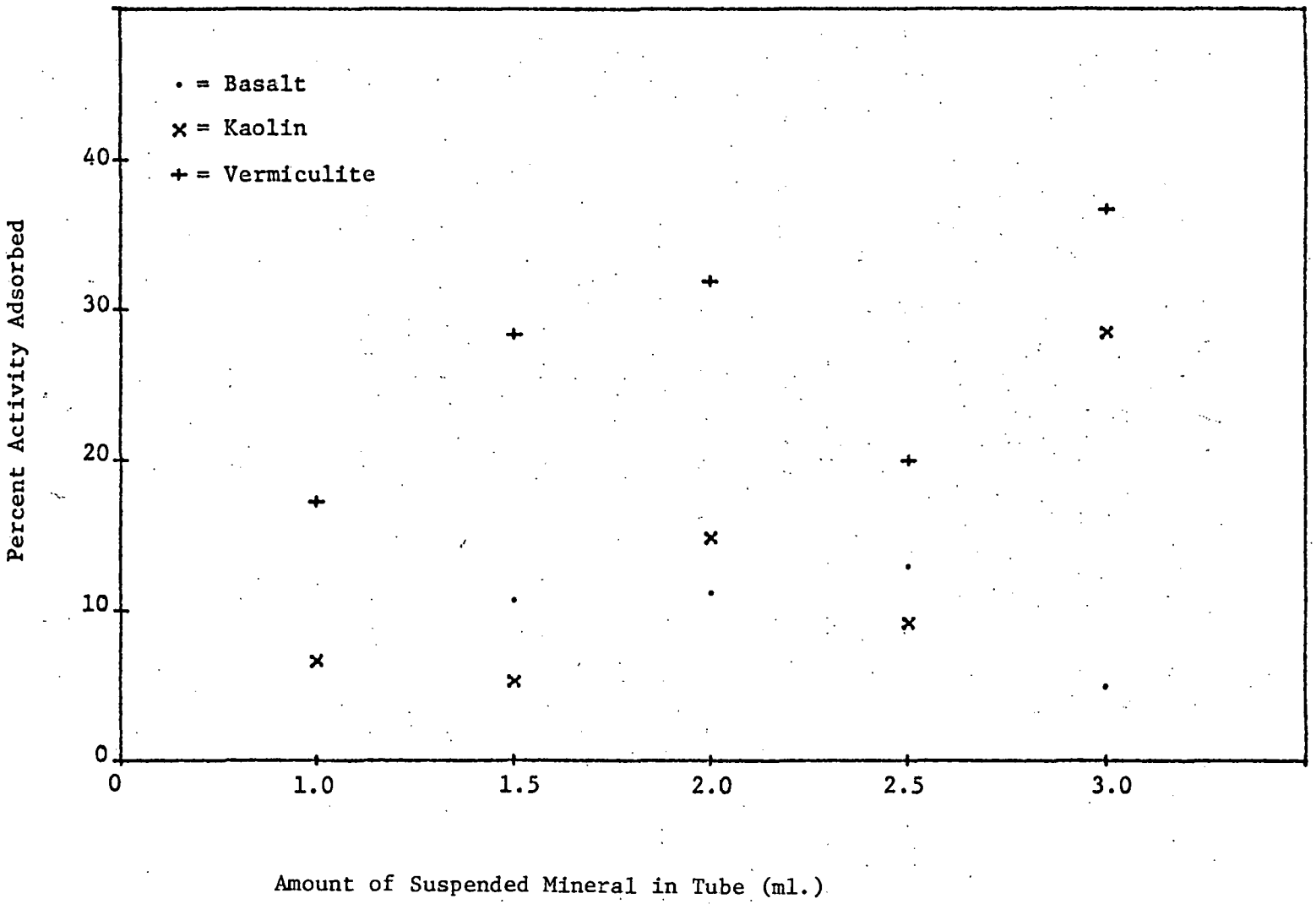

Figure 4. Plot of Percent Activity Adsorbed vs. Amount of Suspended Mineral

After the concentration was made, a 4:1 buffer to peroxide ratio was used to fill the tubes containing the particles. This mixture was then boiled for about 10 minutes to wash the particle surfaces. The buffer solution was used to negate the acidic quality of peroxide that becomes apparent when it is boiled. The particles were then spun down, resuspended and rinsed in water, spun down, rinsed, and finally spun down for good. In this state, they were ready for absorption of the tracer isotope.

The concentration of particles was equalized in an approximate manner by use of an spectrophotometer. By dilution of the more concentrated samples, all samples were brought to about the same percent of light transmittance. It is recognized that transmittance is affected by the character of the particulate, but any differences were not significant for the purpose of this experiment. The exact procedure was as follows: All of the tubes with the particles were diluted with 50 ml of distilled and deionized water. All of the percent transmittances were measured at λ= 3200 A. The highest percent transmittance was kept as a standard and the other two were diluted to this value ($\pm$ 5%). These diluted suspensions of particles and water will be called "rock solution."

The purpose of the experiment was to vary three parameters for each rock. With a constant volume of 15 ml per test, varying amounts of rock solution, Cs^{137} solution, and NaCl were used. Equilibration periods of two weeks were used in this set of experiments.

c. TRANSFER OF ACTIVITY FROM PARTICLES TO BED MATERIALS

A preliminary experiment has been carried out in an attempt to determine the degree of transfer of Cs^{137} from small kaolin particles to larger particles of shale. Poor counting geometry accounts for the somewhat anomalous results actually recorded, but the general findings are at least indicative.

The work was performed by adding Cs^{137}-labeled kaolin particles to small flasks containing shale of four different mesh sizes plus distilled deionized water. After vigorous shaking, the flasks were allowed to stand undisturbed for a week. Each flask was then counted with a sodium iodide

crystal detector to obtain a total count of the entire flask contents. The shale was then washed nominally free of kaolin particles which were counted separately. Each flask was then counted empty, and with the shale returned after three washes with distilled, deionized water. This was followed by three additional, vigorous washes and a final counting in a new flask. The results are summarized in Table 11.

d. EFFECTS OF RADIATION AND TEMPERATURE ON ADSORPTION

In determining the adsorption of radioisotopes by various substrates, the question arose as to possible effects of a high radiation field on the liquid/solid distribution of the radioisotope. A slurry of kaolin in water was prepared and Cs^{137} was added. The mixture was divided among 12 test tubes and placed in a 12,000 Ci Cesium-137 irradiator. Upon removal from the irradiator, each tube was centrifuged, and a sample removed for counting. The values observed were compared with samples collected prior to irradiation. The findings are shown in Table 12 and Fig. 5.

Exact doses were not measured, but only the two tubes closest to the source showed any significant variation from the average of the other 10 tubes. The maximum dose was approximately 1.5 megarad. It was also noted that the temperature of the two deviant tubes was appreciably higher than that of the others, thereby leaving unanswered the question of whether the radiation or the higher temperature produced the observed effect.

To resolve the question if temperature played any part in the uptake observed, additional experiments were performed in which temperature was the variable. Tubes were prepared containing Cs^{137} and water as before, but each was brought to a selected temperature before the kaolin was added. After 175 minutes contact, each tube was centrifuged, a sample was removed, and compared with initial samples. Although the tubes return to near room temperature during the period of centrifugation, it is clear from the results presented in Table 13 and Fig. 6 that there was definitely a temperature effect as expected; increasing temperature decreases the adsorption of Cs^{137} on kaolin by increased solubility in solution. It is also concluded that

TABLE 11. Activity* of Components of Shale/Kaolin Experiment

Shale Mesh Size	Flask + contents	Washed out particulates	Flask Only	Flask+Shale 3 washes	New Flask+Shale 3 more washes
<50	4510	2800	300	4540	4620
25-50	5060	960	310	5580	5390
14-25	6200	1280	400	6050	5730
>14	5840	1200	350	5760	5770

*Counts per minute (rounded)

TABLE 12. Effect of Gamma Irradiation on Cs Uptake on Kaolin

Position to Source (#1=closest, #10=farthest)	First Sample Activity (cpm)	Second Sample Activity (cpm)	% Activity on Kaolin	Kd (ml/g)
1. (1.5 MR)	17342	7144	58.8	1.4
2.	16716	7211	56.9	1.3
3.	16684	5393	67.8	2.1
4.	16544	5081	69.3	2.3
5.	16264	4444	72.7	2.6
6.	16508	5314	67.8	2.1
7.	16783	5836	65.2	1.9
8.	15904	5480	65.5	1.9
9.	16161	4614	71.4	2.5
10.	15263	5193	70.0	1.9
Standard #1*	14239	5198	63.5	1.7
Standard #2	15531	5178	66.7	2.0

*"Standards" were not irradiated

TABLE 13. Temperature Effect on Cs Adsorption on Kaolin

Tube #	Temperature (°C)	First Sample (cpm)	Second Sample (cpm)	% Absorbed on Kaolin	Kd (ml/g)
1	0°C	21594	10195	52.8	1.1
2	23°C (room temp.)	21369	8782	58.9	1.4
3	51°C	21526	11814	45.1	0.83
4	56°C	20958	10889	48.0	0.91
5	65°C	22469	13738	38.8	0.63
6	81°C	23800	16553	30.5	0.43

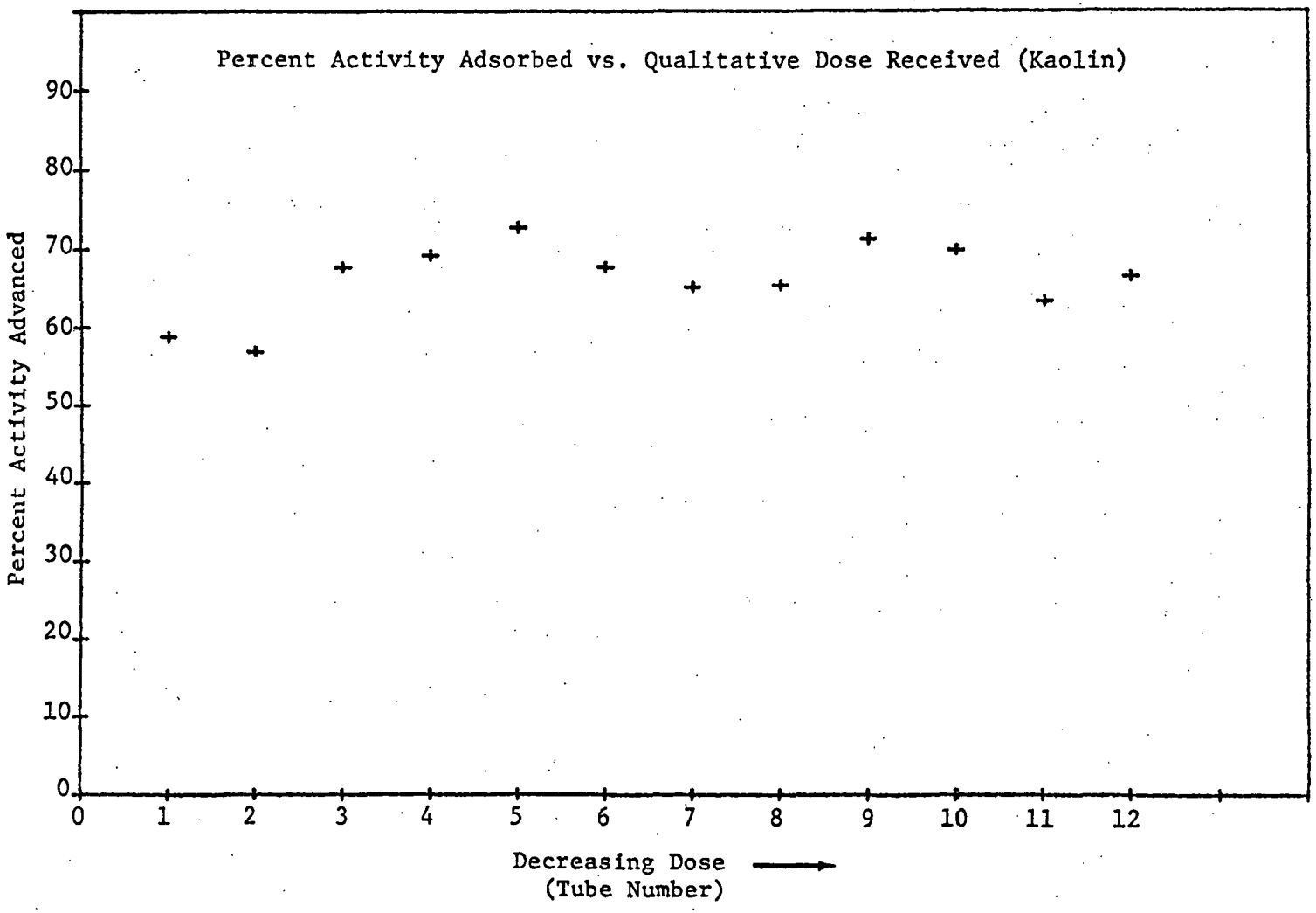

Figure 5. Effect of Gamma Radiation on Cs-137 Uptake on Kaolin

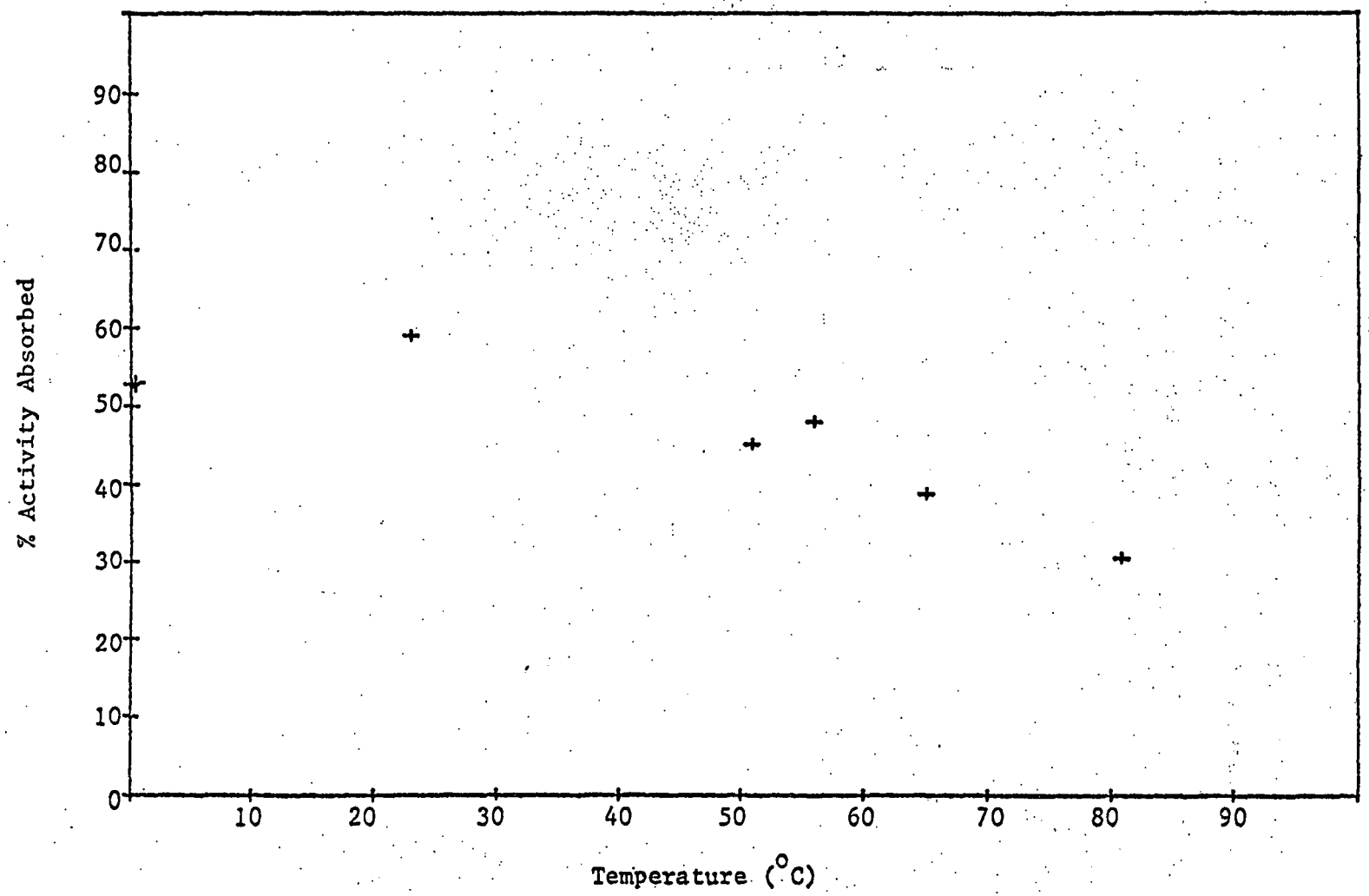

Figure 6. Effect of Temperature on Cs Adsorption on Kaolin

radiation had no effect on the adsorption, as the effects observed in the radiation exposure can be explained by the difference in temperature.

A further study was made of the temperature effect, utilizing shale in place of kaolin. The experiment was carried out as before and the results are displayed in Table 14 and Fig. 7. The clear finding is that adsorption increased as the temperature rises, the opposite effect of that observed with kaolin.

TABLE 14. Temperature Effect on Adsorption of Cs-137 on Shale

Tube #	Temperature (°C)	First Sample Activity	Second Sample Activity	% on Shale
1	0.0	14166	7109	49.82
2	23.1	13762	6331	54.00
3	34.0	14790	2086	85.9
4	46.0	15495	1509	90.3
5	61.5	14416	1187	91.6

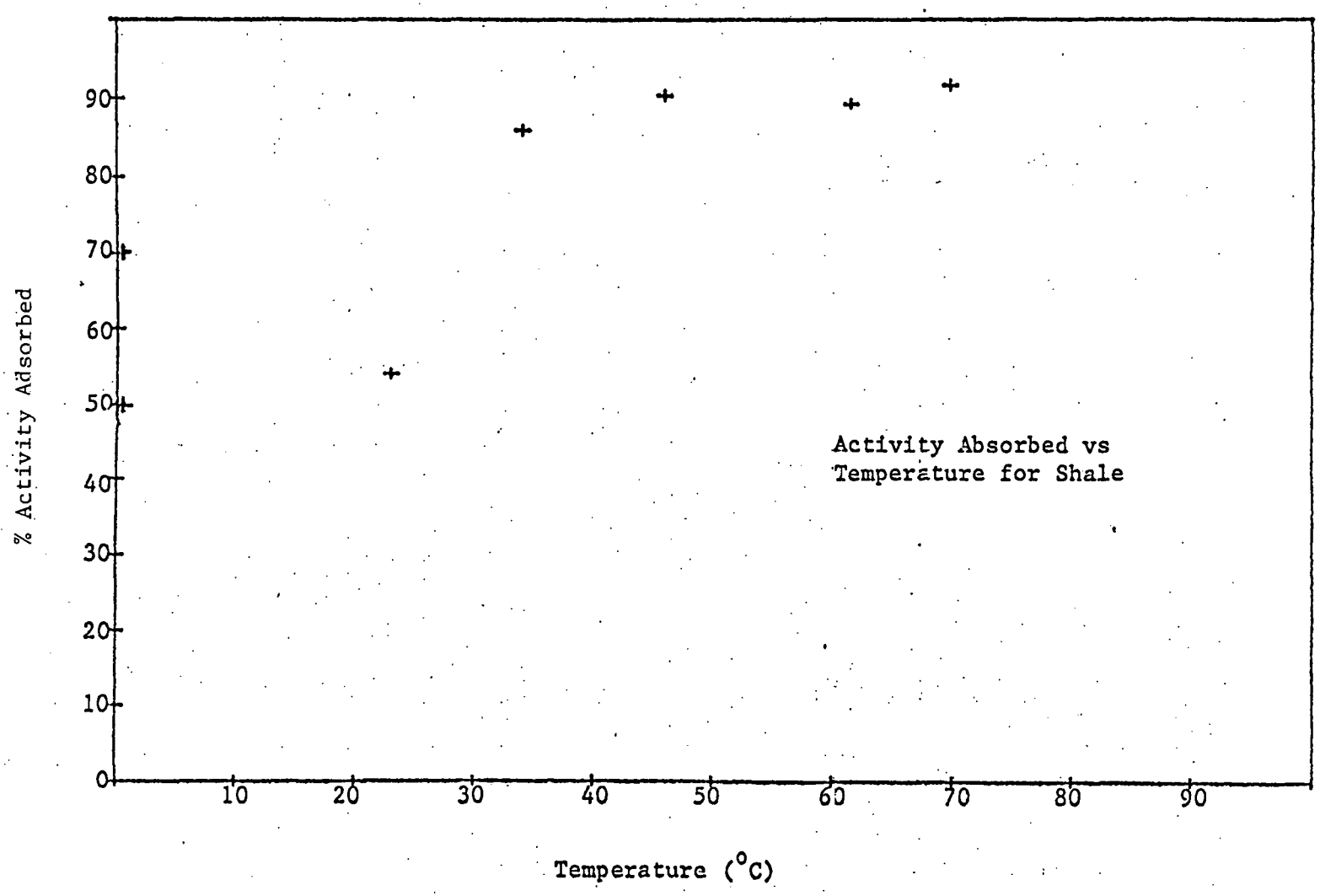

Figure 7. Effect of Temperature on Cs Adsorption on Shale

C. PARTICULATE MIGRATION EXPERIMENTS

The second major portion of the project effort has been devoted to the area of particle behavior in crushed rock columns. Tests this year have all used kaolin clay, because of the prevalence of clay in natural systems, its ease of preparation, and its convenience of use. Future tests are planned with other kinds of particles.

a. EXPERIMENTAL DETAILS

MATERIALS

Crushed Rock

The rock used in these initial tests was Sentinel Gap basalt as distributed to all subcontractors. This material was broken in a jaw crusher, screened, and washed. The 40-50 mesh (355-425 μm) fraction was used for column packing.

Repeated washing removed obvious foreign bodies from the basalt, but some magnetic particles remained. These impurities were not discovered until recently and are relatively rare. Furthermore, many of them are apparently mineral. (Basalt contains appreciable magnetite.) Since redox conditions are not expected to be important in particle behavior, it has not been thought worthwhile to attempt to remove the few metallic slivers at the cost of removing a substantial portion of the magnetite.

Clay Suspension

In July, 1977 a stable suspension of clay particles was prepared by the prolonged ball milling of Hydraglos kaolin obtained from the J. M. Huber mine and production facility at Wrens, Georgia. The size distribution of these particles was determined in October 1978 by the analysis of photomicrograph (prepared by the Engineering Experiment Station at Georgia Tech) using an optical Zeiss counter (School of Chemical Engineering). This distribution is shown in Fig. 1. The mean particle size is found to be 0.125 μm. No

explanation is apparent for the observed normal size distribution (when log-normal was expected), other than the relatively small number of particles (277) analyzed in its preparation. The suspension has appeared to be stable over the reporting period and no further size determinations have been made.

Prior to use in the columns, kaolin was concentrated from 80-100 ml of the stored suspension by centrifugation until the supernatant was visually clear. The supernatant was discarded. The clay was resuspended in a H_2O_2 solution buffered to pH 5 with acetic acid and potassium hydroxide. The suspension was then lightly boiled for 15-30 minutes to remove organic contaminants and to place the surfaces as much as possible in potassium form. Multiple rinses followed. Kaolin processed in this manner has been termed "treated kaolin". Irradiation for 1-2 hours at 10^{13} neutrons/cm/sec in the Georgia Tech Research Reactor results in the activation of sodium in the clay structure to 15.0-hr Na^{24}. The strong gamma rays from this radionuclide are used to trace the position of kaolin particles in the columns and their arrival in the effluent.

COLUMNS

Several refinements in column design have been made during this year, although their basic configuration has remained unchanged. About ten standardized columns have been fabricated, and a typical one is shown in Fig. 8. Although the prototypes were constructed of acrylic plastic tubing, the superior strength of polycarbonate tubing of the same size has led to its use in the current columns. End flanges and caps are acrylic plastic and flow fittings are polyethylene.

A vertical tube with a gas sparger was included between the water reservoir and the column. Nitrogen flows through the sparger during experiments when oxygen is to be excluded. In future experiments, carbon dioxide or other gases may be introduced in this manner. During operation a constant head is maintained on the column by adjusting the flow from the main reservoir to match the rate of flow from the vertical tube. In-line flow meters are used to measure flow rates which can reach 10 or 15 ml/min when all valves are opened, although typical flow rates are around 1 ml/min. Details of the set-up for experiments involving flow through columns are shown in Fig. 9.

The actual bed is contained in the 0.5 inch (1.3 cm) diameter x 24 inch (61 cm) cylindrical volume defined by the tubing, flanges, and the fine-mesh polyethylene screen cemented to the end caps. Thus, for the largest (425 μm) particles, the ratio of column to particle diameter is ~ 30:1. It has been found experimentally[8] that this ratio is sufficient to insure uniform flow of water through the bed cross-section, within ± 10%. This is confirmed by the results of our void volume determinations made by two methods: the volume of water required to fill the bed (which clearly includes all the bed voids), and the volume of water required to carry a non-interacting tracer through the bed agree within ± 2%, implying the absence of channeling at the walls. The sharpness of the tracer peak observed provides reassurance that no portion of the flow in the bed is significantly slower, either.

In early experiments, flow was induced by the force of gravity from an elevated carboy (~2 m head). Within the last quarter a multichannel tubing

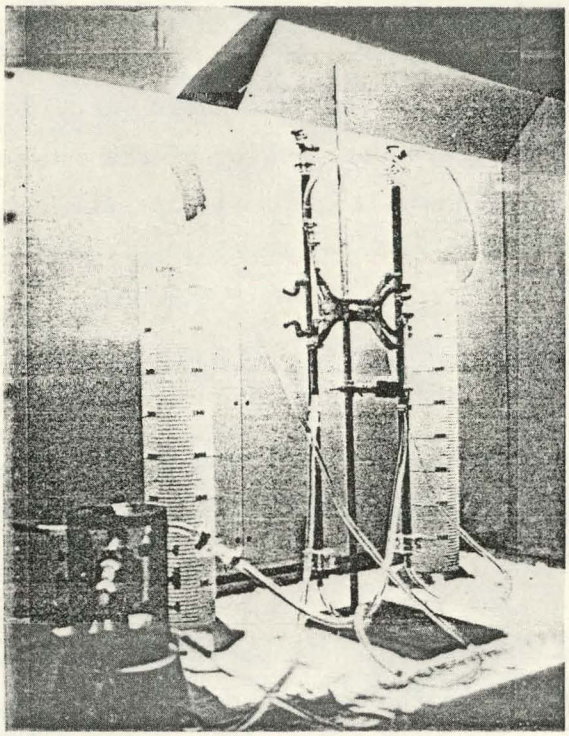

Figure 8. View of Adsorption Columns

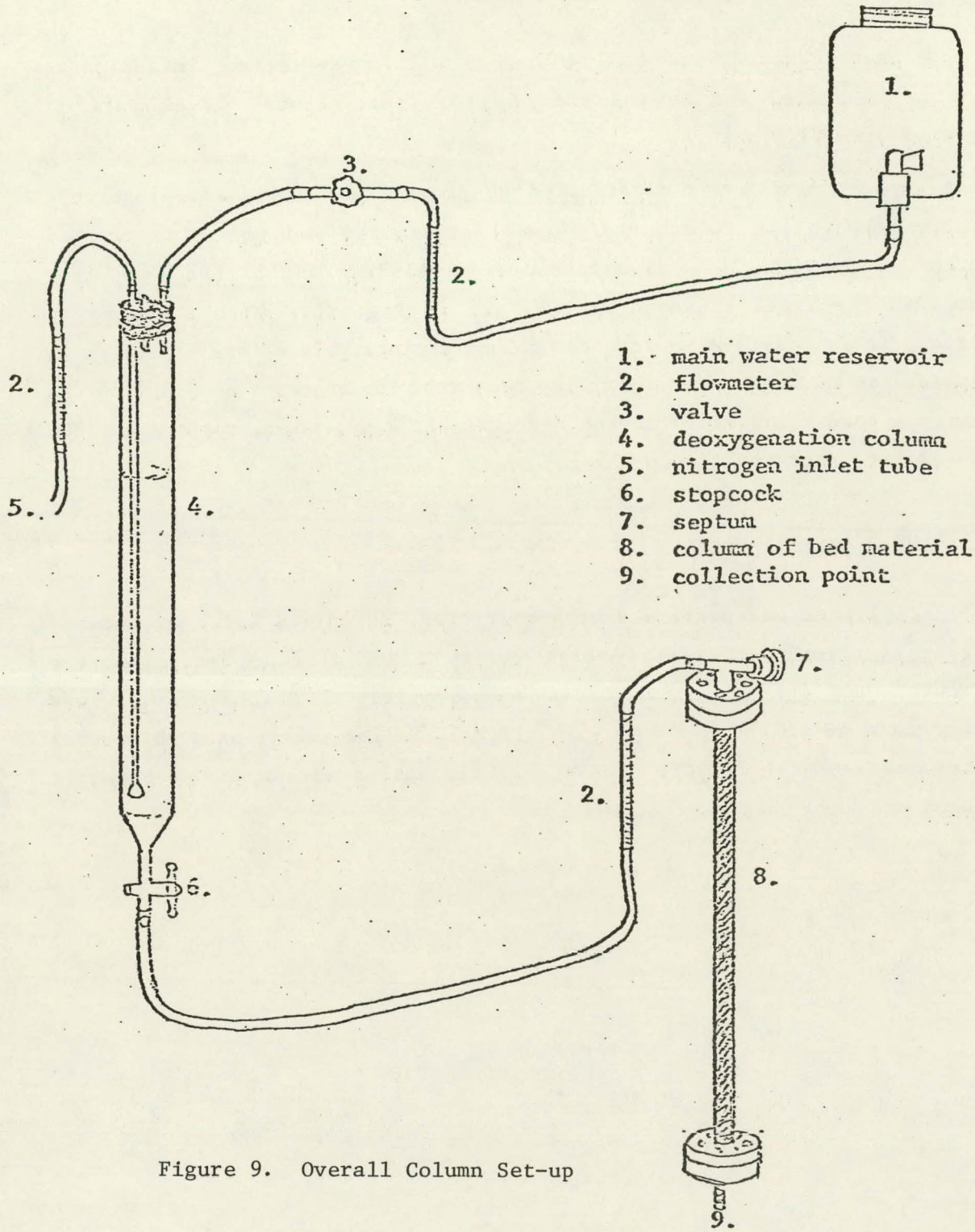

Figure 9. Overall Column Set-up

pump has been acquired, and will be used in all future tests. Pulsation in the flow is damped out by the use of flow restrictions. Flow rate is monitored with flow meters.

A support system was constructed to provide a fixed and reproducible geometry between the column and a small collimated sodium iodide crystal detector. The detector was attached to a sliding shelf that fits into grooves in the frame as shown on the left in Fig. 10. With a column in position, it is possible to scan the column at intervals as small as 6 mm to determine the pattern of radioactivity deposited (or at least present) in the column. A lead collimator for the detector was made, which employs a 3/32" slit and fits half way around the column.

Mobilizing Solutions

Initial work was performed with distilled, deionized water as the mobilizing solution. Its fairly high purity makes routine determinations difficult, but its resistivity was approximately 2 megohm-cm, and was usually about pH 4.5. Later work with slightly saline waters used this water and weighed amounts of NaCl. These slightly saline waters are much better balanced and have near neutral pH.

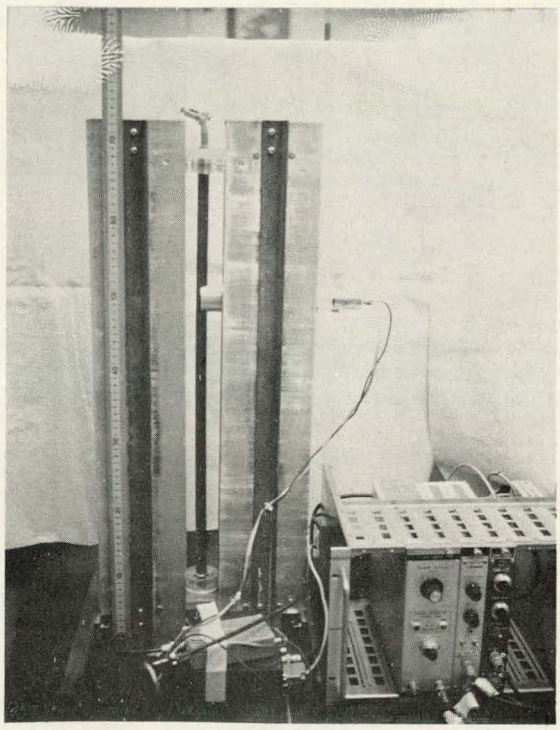

Figure 10. Support Frames for Collimated Detectors

PROCEDURES

Physical Characterization of Columns

It is naturally important to have a measure of the basic physical and hydraulic characteristics of each bed. Void volume and hydraulic conductivity are measured, from which porosity, effective pore size, and pore flow velocity may be calculated.

The total capacity of the column could be easily calculated, but it was also necessary to measure the void space or porosity of the packed bed. Two methods were used to make this determination and they agreed very closely. The direct method consisted of weighing the column and the filling material, and then weighing the filled water saturated column. The difference in weight was due to the water added. It was believed that this procedure would give the maximum value, as it would take into account all water in the column, including any stagnant volumes that might not be involved in any method involving flow.

The routine method of void volume measurement has employed injection of a presumed non-interacting tracer (Cr^{51}-tagged chromic acid) and the determination of its γ-ray count rate in successive effluent samples. Curve fitting and interpolation of the discrete data points allows the computation of volume at the point where the specific activity peaks, corresponding to the void volume. Recently EDTA-complexed Cr^{51} has been used to insure the unimpeded passage of the tracer, and the tracer recovery of (> 98%) and peak sharpness (full-width at 0.1 of maximum $\sim$ 0.2 void volumes) have been so satisfactory that its continued use is anticipated. (Earlier tests with uncomplexed Cr resulted in less-satisfactory recoveries.) Porosity is then calculated from the known volume of the bed envelope (77.2 cc), and was usually of the order of $\pm$ 50%. (The divergence of this from the porosity (36%) of a hexagonal close-packed structure which would be anticipated if the bed grains were spherical, is explained by the fact that the grains are in fact more like jagged slivers.) Pore velocity is $\sim$1.6 cm/min.

The values obtained from chromium tests were in excellent agreement with parallel determinations by the other method, leading to the conclusion that little (if any) of the liquid in the column is not accessible to the general flow. Since the tracer method is much more convenient and may be repeated during the use of the column, it was made the routine method. A typical chromium tracer void volume determination (from which a void volume of 39.56 ml was deduced) is shown in Fig. 11. About 99% of the injected tracer was recovered.

Hydraulic conductivity is determined by the treatment of the entire column as a falling-head permeameter. The conductivities so measured generally fall between 0.07 and 0.095 cm/sec, and average $\sim$ 0.085 cm/sec. From the Carman-Kozeny equation[9] one can then calculate the mean hydraulic radius of pores in the bed as $\sim$ 14.6 μ m. The diameter of such a theoretical pore would be 4 x this value, or $\sim$ 58 μ m. Thus, the average pore is about 250 times the size of the 99th percentile kaolin particle.

Tracer Test Procedure

Following column characterization, the main tracer tests were done. Regardless of whether the tracer is ionic or particulate, the same procedures were followed.

Samples are collected in polyethylene containers or planchets, which are weighed when full and after drying. All effluent from the column is so collected. Following drying on a steam heater the samples are counted using a 2-inch NaI(Tl) detector and a single channel analyzer. With the weights of the standard and of the injected tracer known, the sample count rates can be normalized to provide information about the fraction of the tracer in each sample and about the fraction of the tracer per unit volume in each sample. In all cases this is recorded with the void volume of the particular column as the unit to allow comparison of results between columns whose void volumes are different.

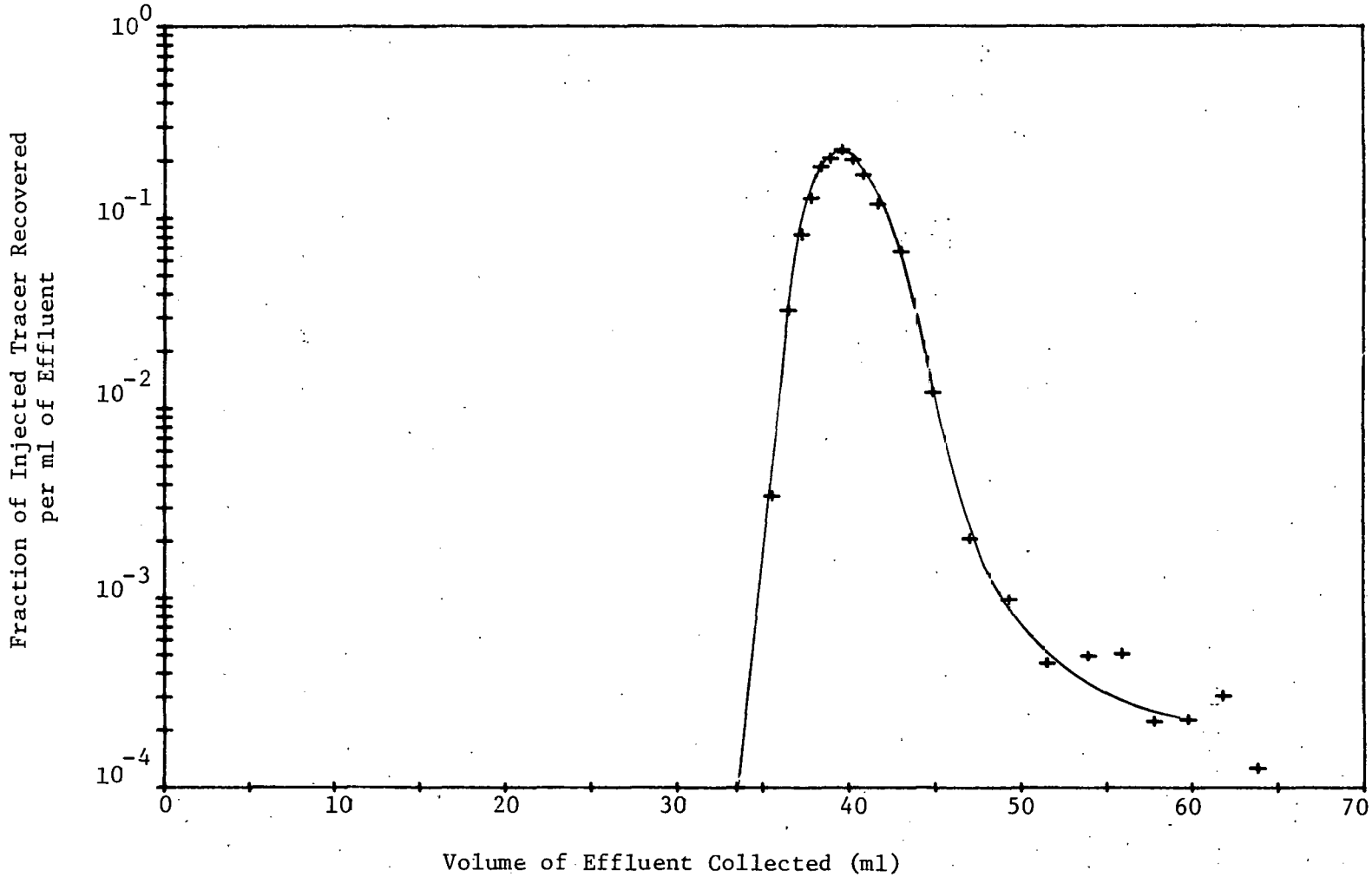

Figure 11. Typical Void Volume Determination

b. COLUMN TESTS

The initial run was made in a 40-50 mesh basalt column using activated kaolin as the tracer. Activated kaolin sol (1.629 grams of solution), which showed typically a count rate of 305,323 cpm, was injected into the column and washed through with distilled, deionized water at a rate of 2-3 ml/minute. This rate of injection gives a Darcy velocity of 3.4-4.5 cm/min or an actual pore velocity of 8.5-11.4 cm/min.

The column effluent was caught in approximately 6 ml fractions on planchets which were weighed, the liquid evaporated, and then reweighed. The planchets were then counted on the sodium iodide crystal detector. The results are given in Fig. 12, which shows the relation of recovered tracer to flow through the column. A total of 5 column volumes of water was collected and this was found to contain 14.96% of the total injected tracer. At this point the effluent contained about 0.5% of the total activity in each portion, but the quantity was decreasing. The appearance of air bubbles in the column (later found due to a crack in the column) terminated the experiment, leaving about 85% of the activity in the column.

The column was then clamped off and placed in the holder for scanning of activity. The distribution curve obtained was similar to that from an uncollimated detector moving along the total length of a line source. This led to further tests of collimator resolution. A thin Co^{60} source was used in a variety of positions around the collimator and it was concluded that collimation was quite adequate for all low-energy tracers. However, sufficient collimator penetration occurred with the 2.75 MeV photons from Na^{24} to affect the distribution curve in that case.

To test the competitive effect of complexing, attempts were made to remove the remaining activity by rinsing with water containing a high-phosphate detergent, but this resulted in the removal of only 22.66% of the initial activity. The results are illustrated by Fig. 13. In considering these findings, it appeared possible that particle deposition might be occurring with simultaneous loss from the particles of active sodium ions which would continue through the column. To test this hypothesis, a solution of

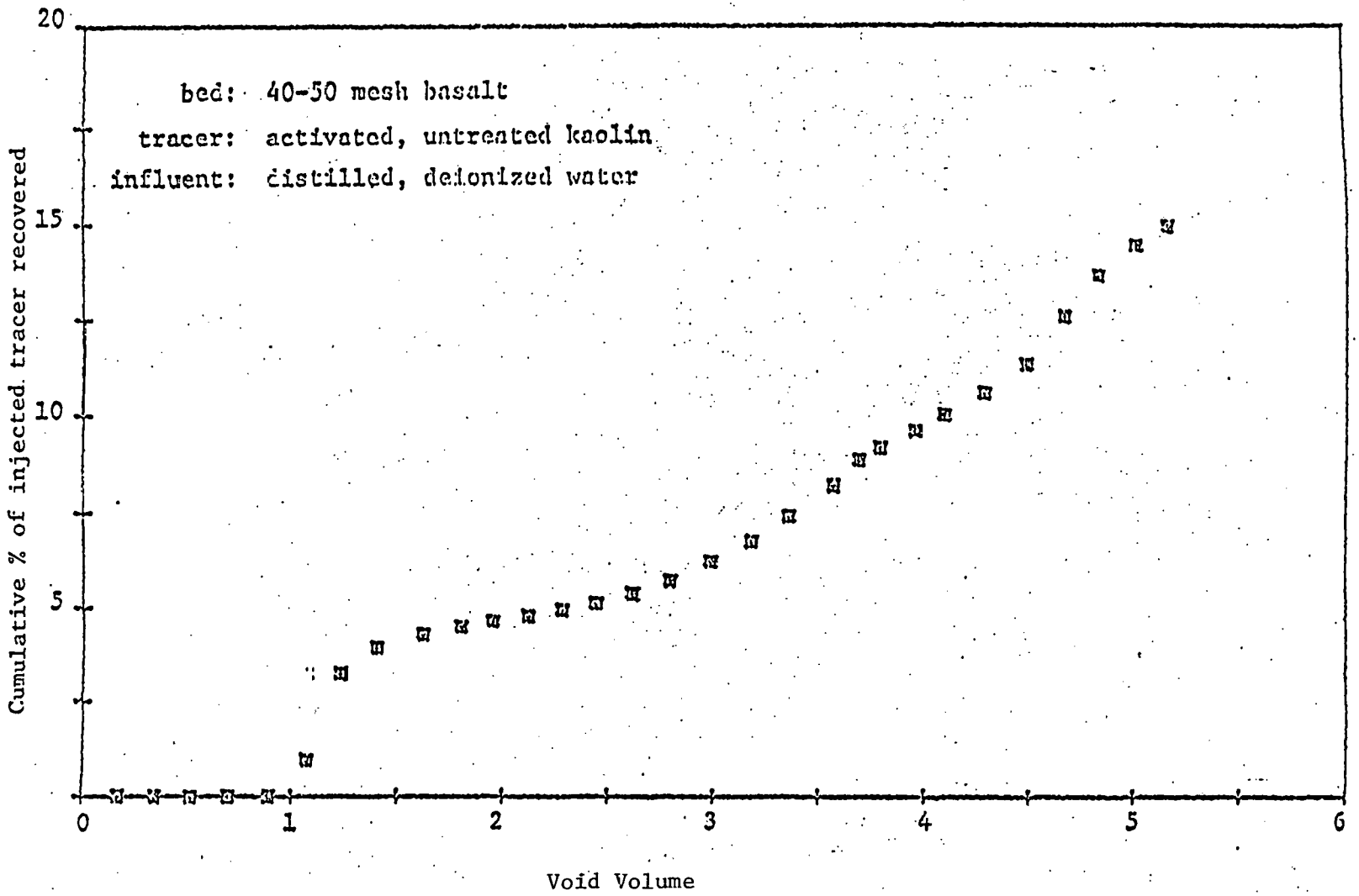

Figure 12. Tracer Recovery

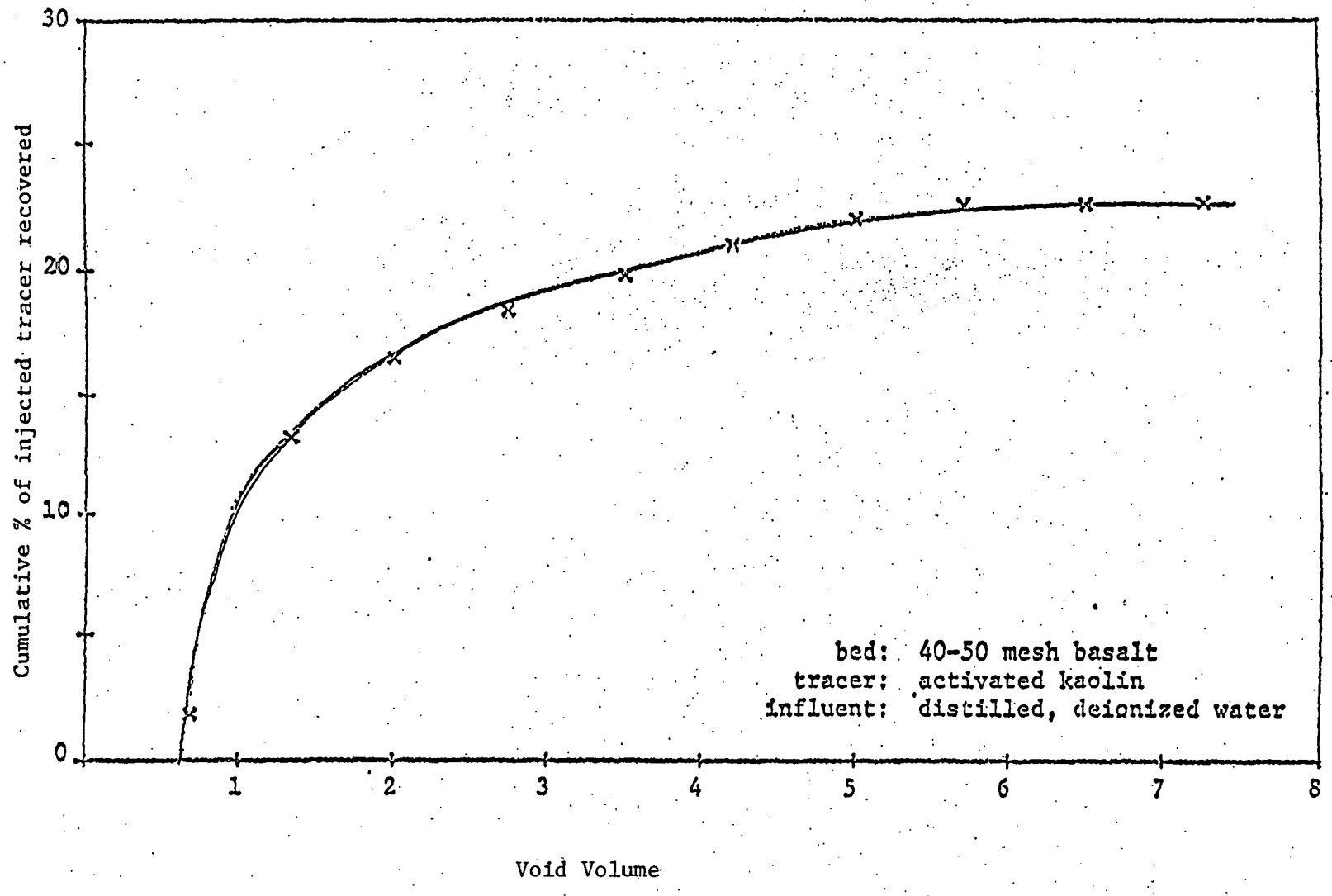

Figure 13. Tracer Recovered by Detergent Rinsing

sodium ion was activated and injected into the column. Figure 14 shows the outcome--virtually no retardation of the sodium and 90% recovery within one void volume of effluent. Full recovery was made within three void volumes.

In another column run, activated kaolin was used but was first treated to replace any loosely held sodium ions by potassium ions. Flow was stopped after 15 column volumes had passed through, with only about 1.5% of the total activity in the final volume. A total of 29% of the activity passed through, and these results are given in Fig. 15.

Comparison with Fig. 12, illustrating results with untreated kaolin, shows some differences. At 1.5 column volumes, nearly 5% of the injected tracer had been collected in the effluent as compared to only 2.5% of the potassium-treated kaolin. At 5 column volumes, the values were 17.5% and 5% respectively. It is therefore assumed that with untreated kaolin, ionic sodium (separated from the kaolin particles) was a major contributor to the activity which passed through the column. The two plots (Figs. 12 and 15) are similar, and both reveal a second point of inflection at which the rate of activity recovery in the effluent increases.

A scan of the column following the treated kaolin run is given in Fig. 16 and is different from that of the untreated kaolin. The evidence of the treated material is that the immobilized activity is highest at (or near) the top of the column and decreases steadily toward the bottom. This curve, although subject to considerable fluctuations due to the low count rate involved, is more typical of the deposition pattern of particles in a porous medium.

Additional work on the use of kaolin particles with sorbed tracers is under way. An experiment has been performed in which kaolin particles were allowed to stand in contact with Cs^{137} for 3 days. They were then washed and prepared in the usual manner and used in a column run. The activity of the labeled particles was found to be too low for good counting statistics. Using a non-collimated detector, it was found that the highest level of residual activity in the column was at the top, and this fell off to background levels a few centimeters down the column. This experiment is being repeated using a higher concentration of Cs^{137} solution to obtain a higher specific activity in the kaolin particles.

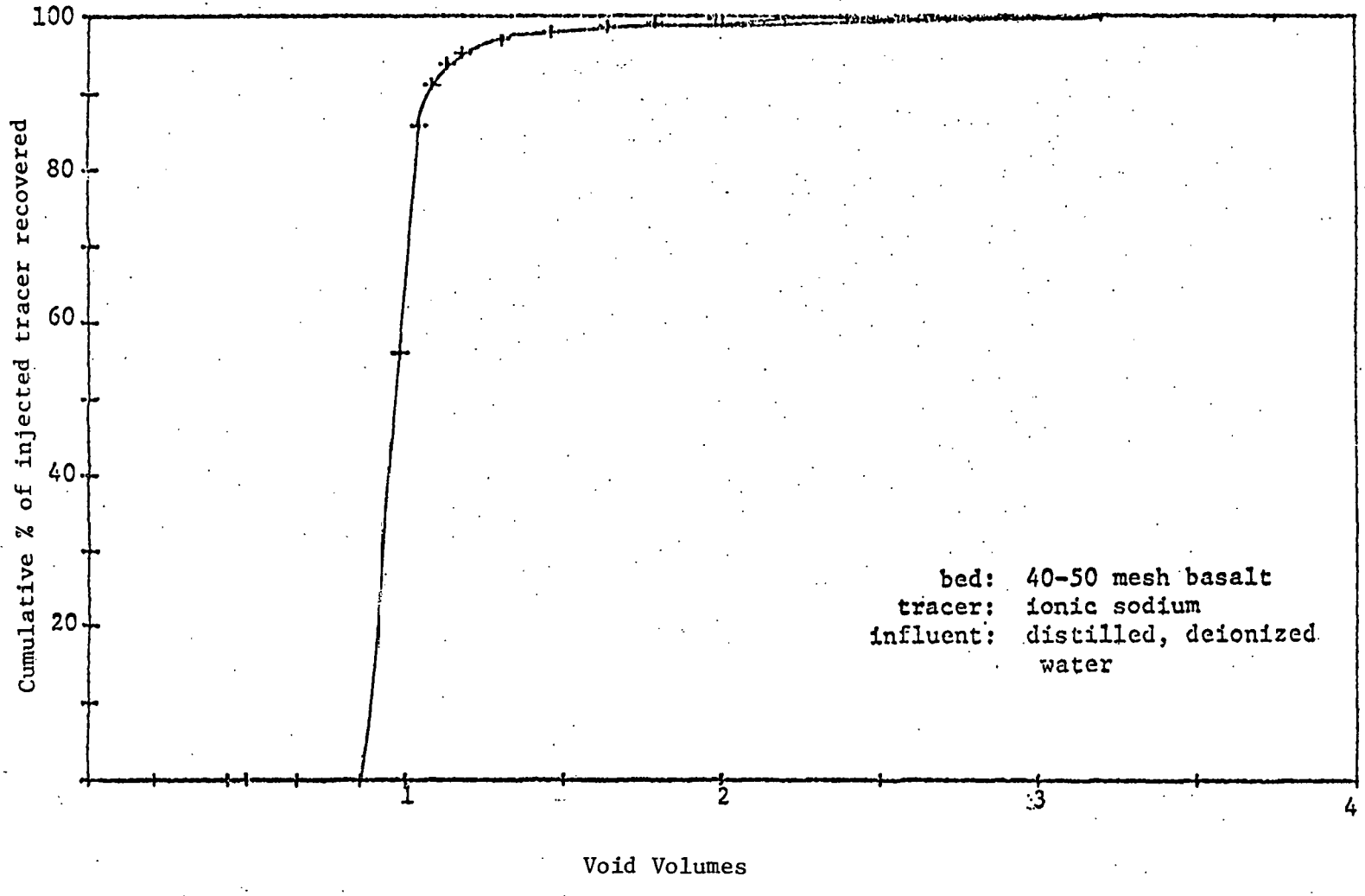

Figure 14. Ionic Sodium Recovery

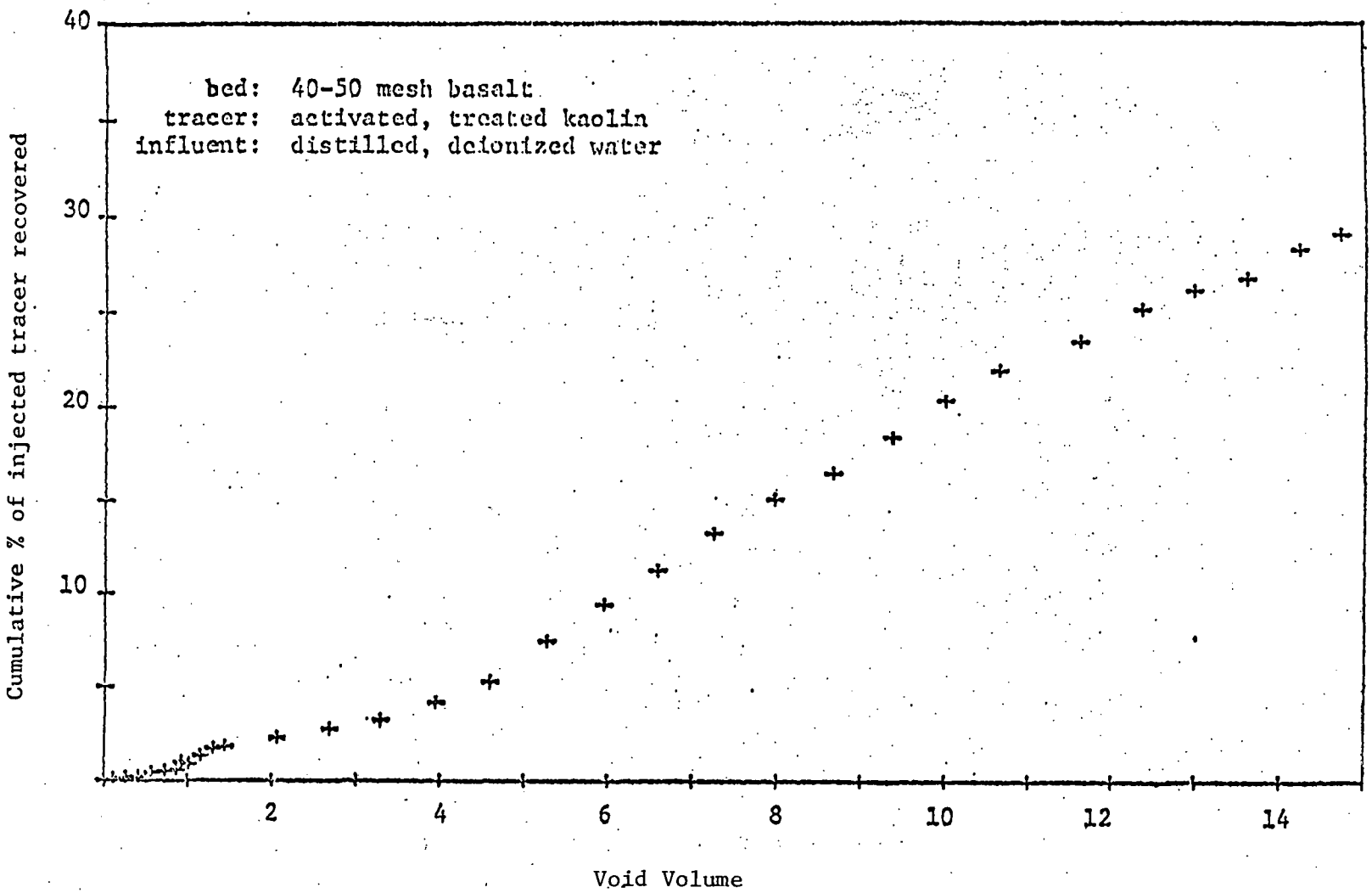

Figure 15. Kaolin Throughput for K-treated Particles

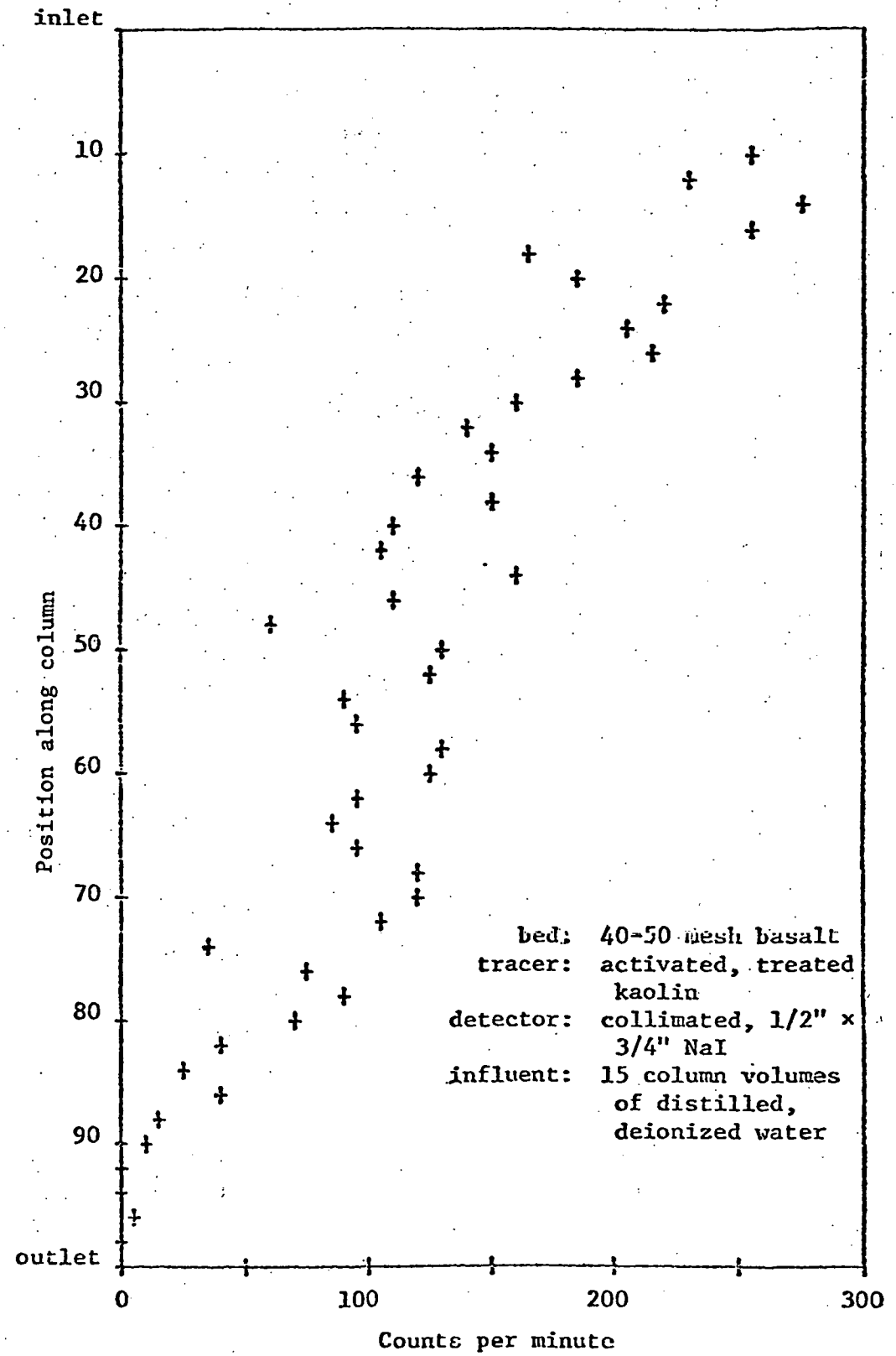

Figure 16. Distribution of Tracer Throughout Column

In order to monitor more closely the radioactivity of column effluents during long runs at low flow rates, a continuous flow system was assembled as shown in Fig. 17. It was tested with runs involving dissolved Cs^{137} introduced into a basalt column. No radioactivity was observed in the effluent during the following 60 hours during which 20 void volumes passed through the system. Higher flow rates and the injection of 30 ml of 0.1 M NaCl solution resulted in no observable activity in the effluent, but activity was observed after 60 ml of saturated ($\sim$ 6.2 M) sodium chloride solution was passed through the system. The eluted isotope amounted to about 1.4% of the quantity injected. A scan of the column showed that the balance of the activity was still in the column, concentrated in the top 10 cm. A small amount of a brownish, fluffy precipitate was observed in the final collection flask. It was found to contain iron (thiocyanate test) and is believed to have been iron oxide/hydroxide/hydrated oxide that originated in the basalt itself, as there was no metallic iron in contact with the liquid anywhere else in the system. The importance of the precipitate is at present unevaluated, but clearly could be of significance as a particulate carrier of radioisotopes. (Closer investigation of this point will occur during the subsequent quarter.)

Of particular interest was a series of column runs with ^{235}Np-labeled kaolin particles. Two parallel columns, one filled with basalt and the other with limestone, were observed over an 11-day period during which flow rate varied from 0.4 to 1.0 ml/min. 67% of injected activity was recovered after passing through the basalt column, whereas only 2% was recovered from the limestone column. Figure 18 shows the distribution of the ^{235}Np activities in the two columns. It is evident that in limestone most of the activity was retained near the top of the column, though only weakly, whereas in basalt there was an almost uniform distribution (the apparent rise in activity near the middle of the column is due to insufficient collimation, adopted to obtain adequate count rates). The neptunium activity itself is unlikely to affect the retention of the kaolin particles.

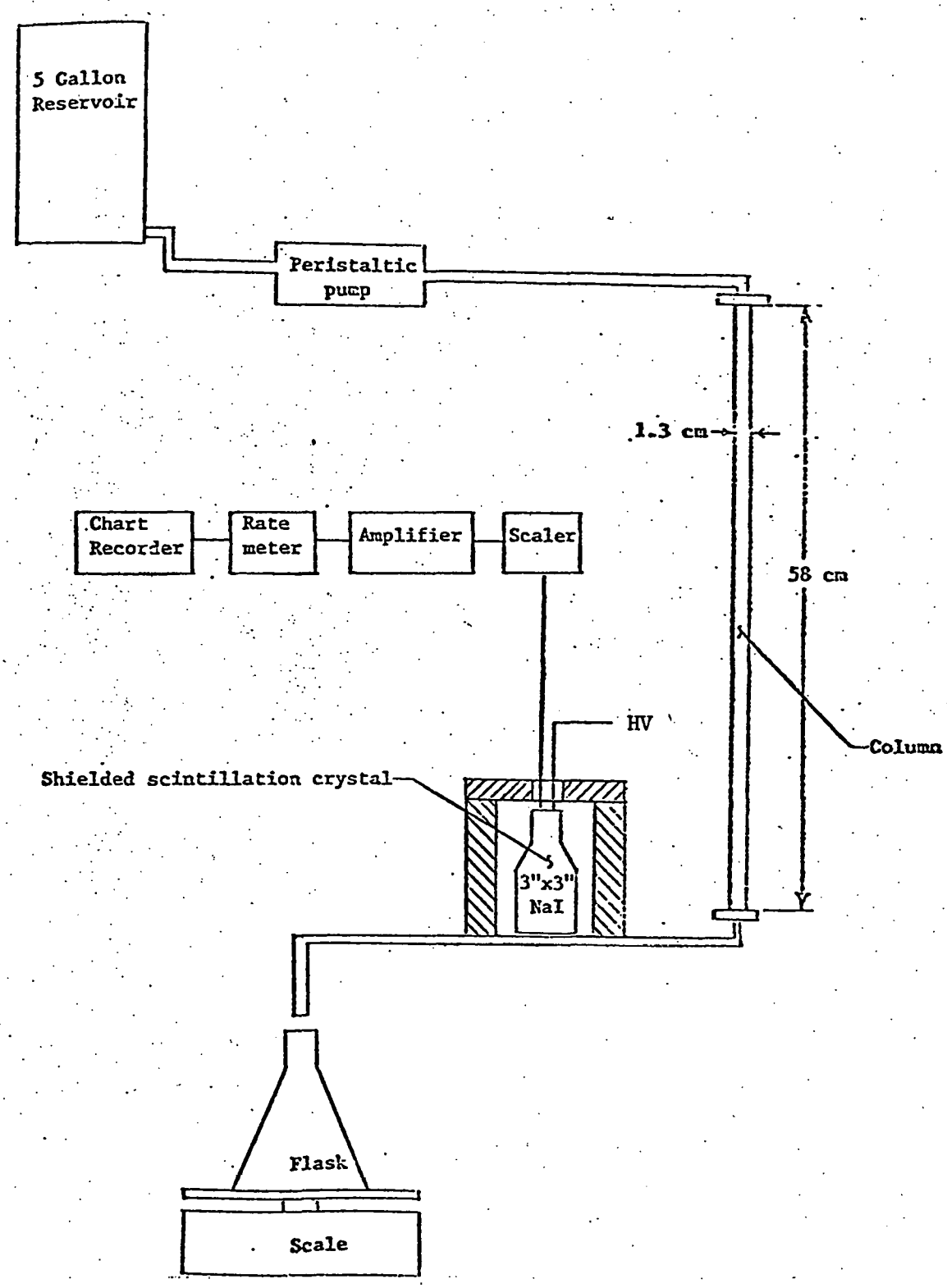

Figure 17. Continuous Flow System

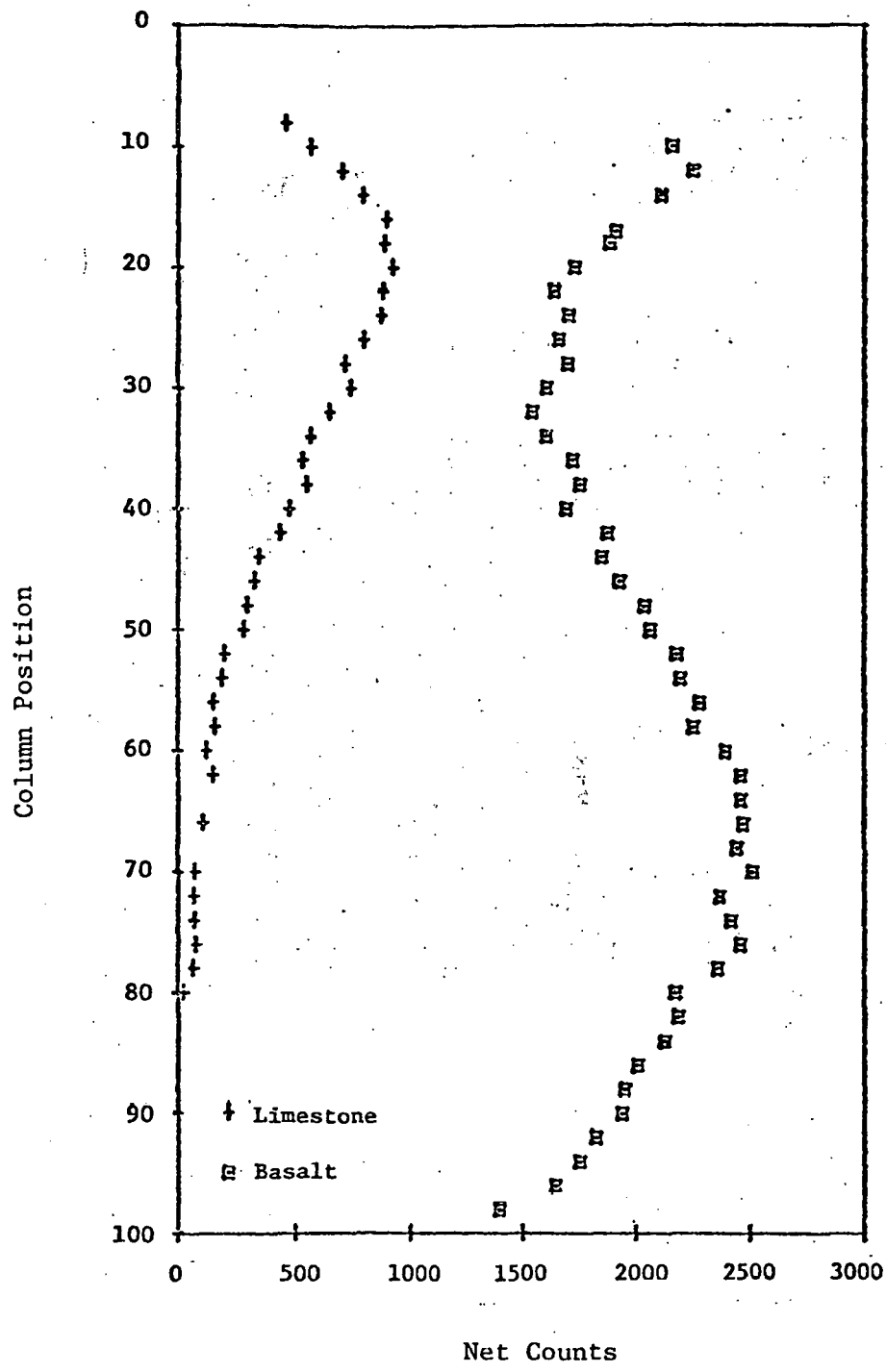

Figure 18. Distribution of Np-labeled Kaolin Particles in Basalt and Limestone Columns

A major concern in this work is to identify what particles pass through the bed and what characteristics determine their range of migration. Effluent from the column is quite clear to the unaided eye, but in order to determine if any of the injected particles pass completely through the column, electron micrographs were made of effluent samples. The samples were collected after 1 1/2, 2, 2 1/2, 3, and 3 1/2 void volumes of water had passed through. Figure 19 shows two examples of particles in the effluent. Particles of kaolin are easily recognized and found in all samples. It was noted that the particles appeared in clumps of varying shapes and sizes. Although there is a slight possibility that this clumping was caused by the technique used to prepare the samples for examination under the electron microscope, earlier electron micrographs taken of other samples of the same kaolin showed numerous individual platelets.

The very low density of particles in the effluent, particularly in the final sample, does not provide any good statistics, but the number of clumps observed were in the approximate ratios as follows:

Void volumes passed	Relative number of clumps
1½	50-100
2	50-100
2½	5
3	5
3½	0.5

Additional investigation is planned to ascertain if there is any change in size of the eluted clumps or their component individual particles as flow through the column continues. From the limited data now available, the clump size seems quite variable; the colloidal aggregates seem to form in planar rather than globular assemblies and this may have a bearing on the quantity of radioactive matter transported.

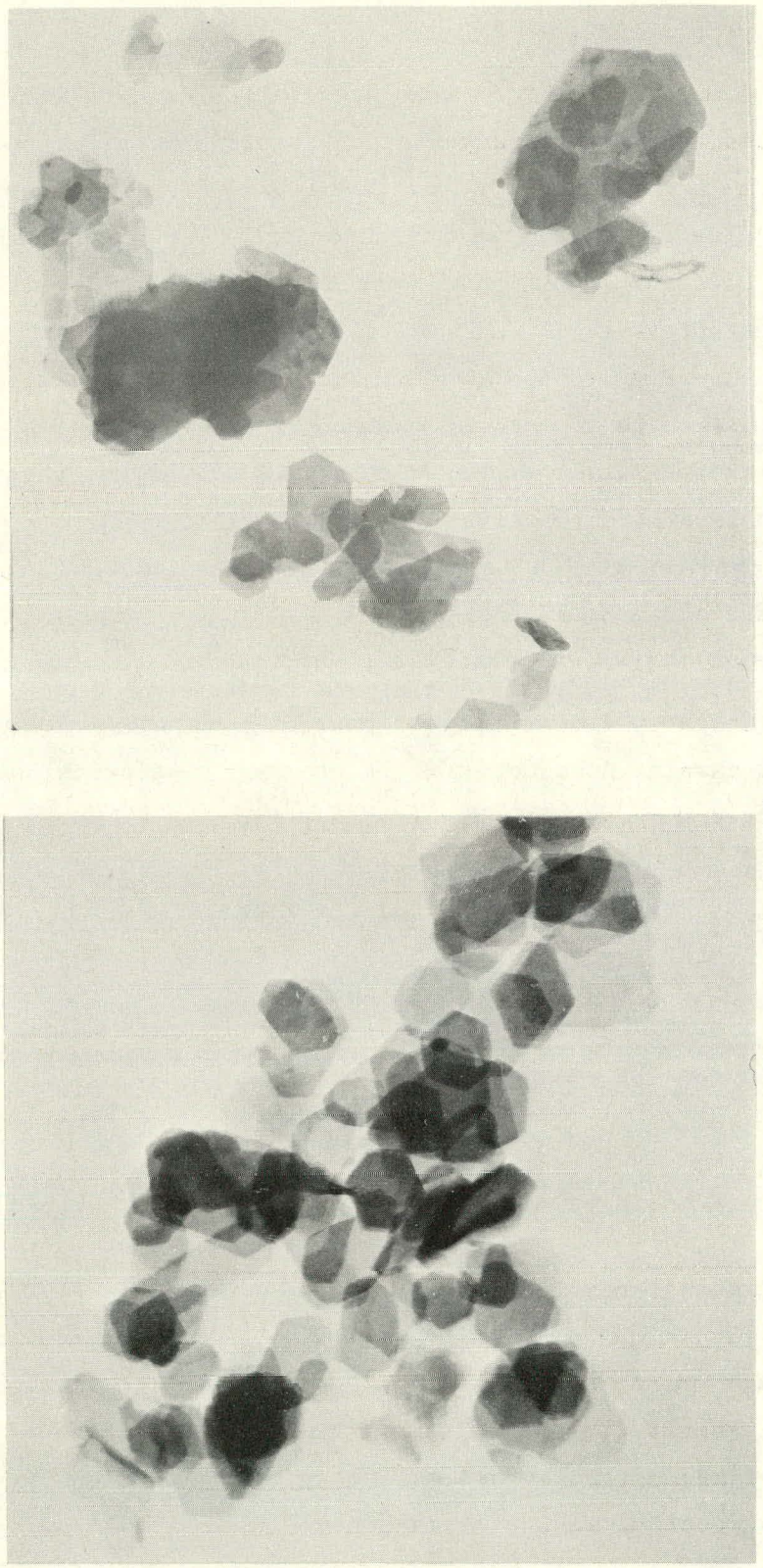

Figure 19. Examples of Kaolin Particle Agglomerates in the Column Effluent

Effect of Saline Water

Tests performed with the columns were of two types; movement of ionic sodium and of activated particles. In the ionic sodium test, 0.094 M $^{24}Na_2CO_3$ was prepared and injected. Its appearance in the effluent was monitored by collection of the effluent in successive planchets, drying, and counting of the characteristic gamma ray peaks with a NaI(Tl) system.

In one of the activated particle tests, involving columns of basalt, 20 mg of kaolin particles were prepared as previously described. Treatment with H_2O_2 in a KOH-acetic acid buffer not only served to remove extraneous organic matter, but placed the particle surfaces in K^+ form prior to irradiation. Since the activity detected in the particle tests was also ^{24}Na, it is clear that the particles themselves were being detected and not ions bound on, or released from, their surfaces. Through a fortunate accident, the tests were not performed in the same order on the two columns. For Column A, the particle test was performed before the ion test. For Column B, the particle test was performed after the ion test, and was followed by another ion test. This change had a profound effect on the results. In each case approximately 6 mg of kaolin particles were injected.

In neither particle test was significant kaolin carried through the crushed rock column. The sample count rates fluctuated near background for both columns, showing a carry-through of $\sim 0.1\%$ of the injected activity carried out to approximately 20 column volumes, no other counts were registered above twice the standard deviation of the background. In fact, for Column B all the counts, including the small initial peak, fell below σ_B.

In the sodium ion test performed before the particle test on Column B, essentially all (98%) the ^{24}Na was recovered in the first 1.5 column volumes after injection, with the peak appearing at precisely 1.0 column volumes after injection (Fig. 20); that is, the sodium ions were nearly unaffected by their passage through the column. The ion tests carried out after the particle tests showed behavior which was both similar in some respects and radically different from the before-particle ionic sodium test. The elution profiles are shown in Fig. 21. Total recovery of the ^{24}Na was much smaller than in the earlier case. For each column, the initial one-column-volume

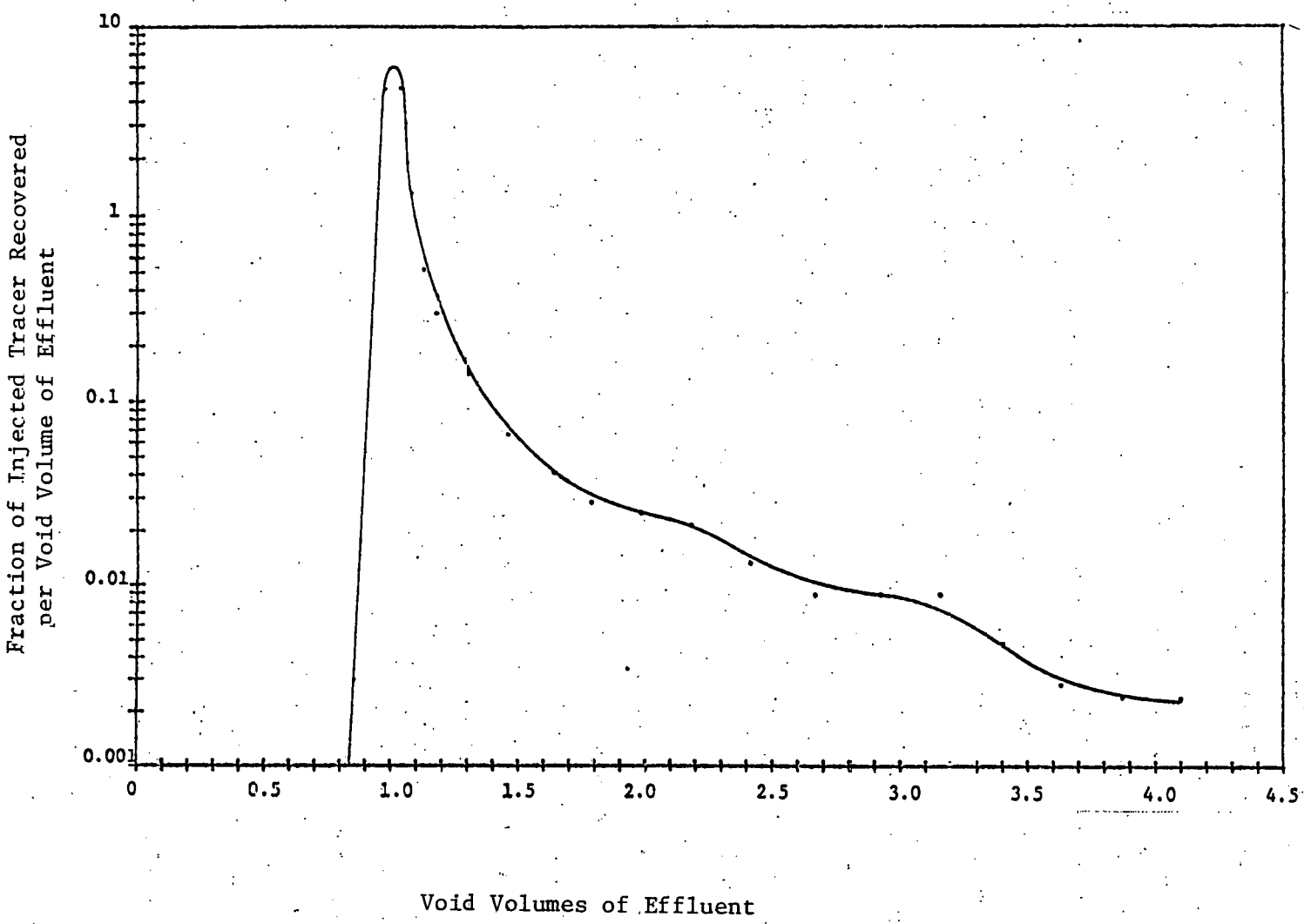

Figure 20. Sodium Ion Test Before Particle Test

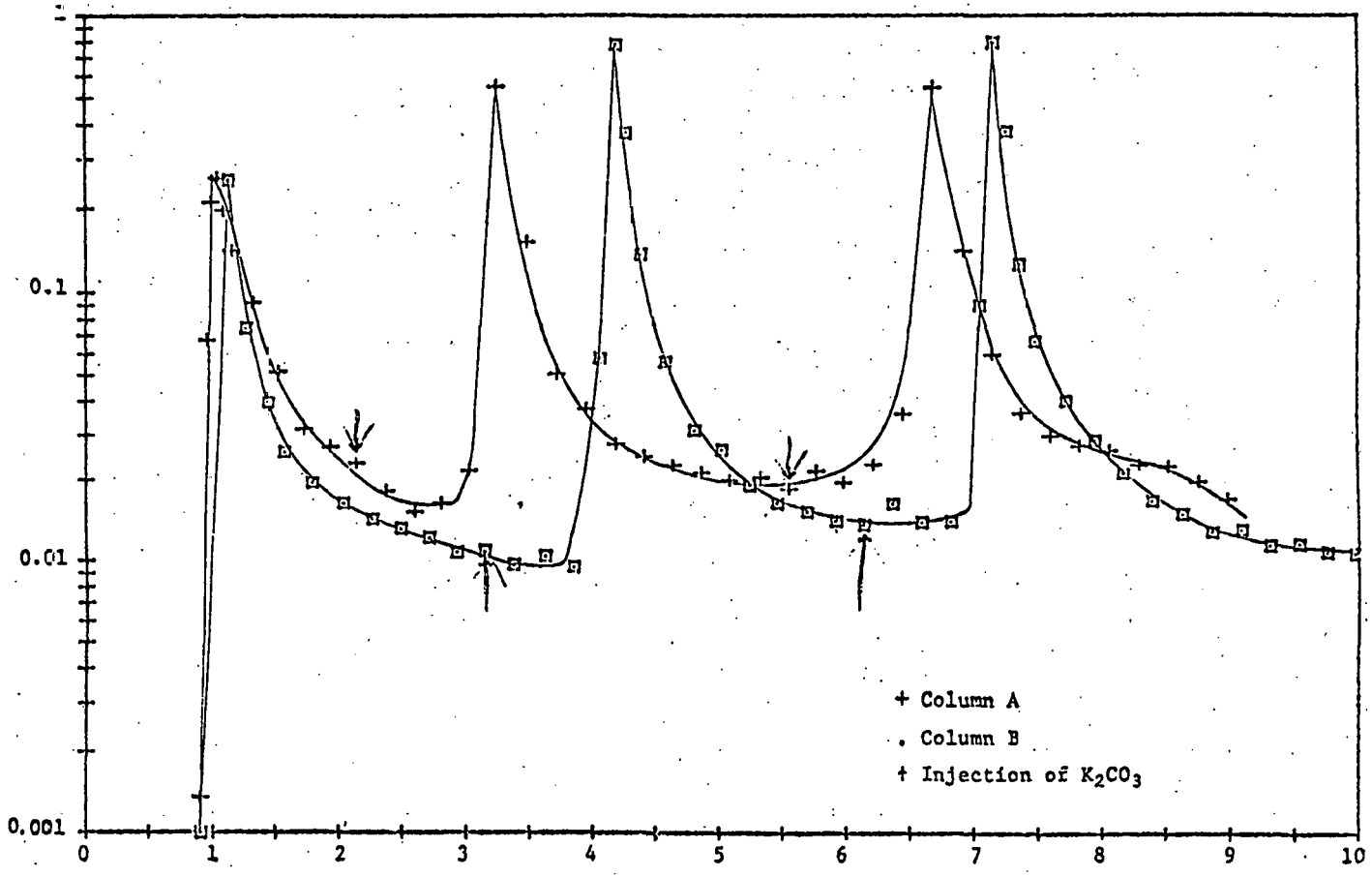

Figure 21. Sodium Ion Tests After Particle Tests

peak contained only ± 10% of the injected activity. Scanning the columns with a G-M survey meter showed the activity to be concentrated in the topmost few centimeters--the same area as the kaolin particles had been in at the end of the particle tests. This suggested that the kaolin particles sorbed on the basalt were acting as an ion exchange medium for the migrating sodium.

K_2CO_3 of the same molarity as the initial injection of Na_2CO_3 was prepared and injected. After the peak from this injection had passed, the K_2CO_3 injection was repeated, again with the same number of moles as the initial Na_2CO_3 injection. Each of these injections removed one-fifth to one-fourth of the initial activity in a peak which appeared about 1.1 column volumes after the injection. After each treatment, the remaining ^{24}Na activity in the column was observed to have moved farther along the column length, again suggesting a simple ion exchange.

IONIC AND PARTICULATE TRACER TESTS

Ionic Sodium

Despite the pretreatment of the kaolin particles to place their surfaces in potassium form, it is still possible that some sodium ions could remain on their surfaces only to be released in the columns and complicate the observed effects. Thus, it was worthwhile to briefly explore the behavior of Na ions in basalt beds.

A typical elution curve for a sodium ion test is shown in Fig. 22. The columns were each injected with about 1 ml of 0.094 M $^{24}Na_2CO_3$ and the distribution of the tracer in the effluent was monitored by collection of the effluent and counting of the emitted gamma rays with a NaI(Tl) system. Distilled, deionized water was the driving solution.

In several replicates of this test, 9.8 ± 1.5% of the ^{24}Na appeared in the first three void volumes of effluent (first peak in Fig. 22). The effect of K_2CO_3 as an eluting agent was tested by the injection of about 1 ml of 0.094 M K_2CO_3 after the first peak had passed. This removed 17.7 ± 2.5% of the remaining activity from the columns in the following two void volumes of

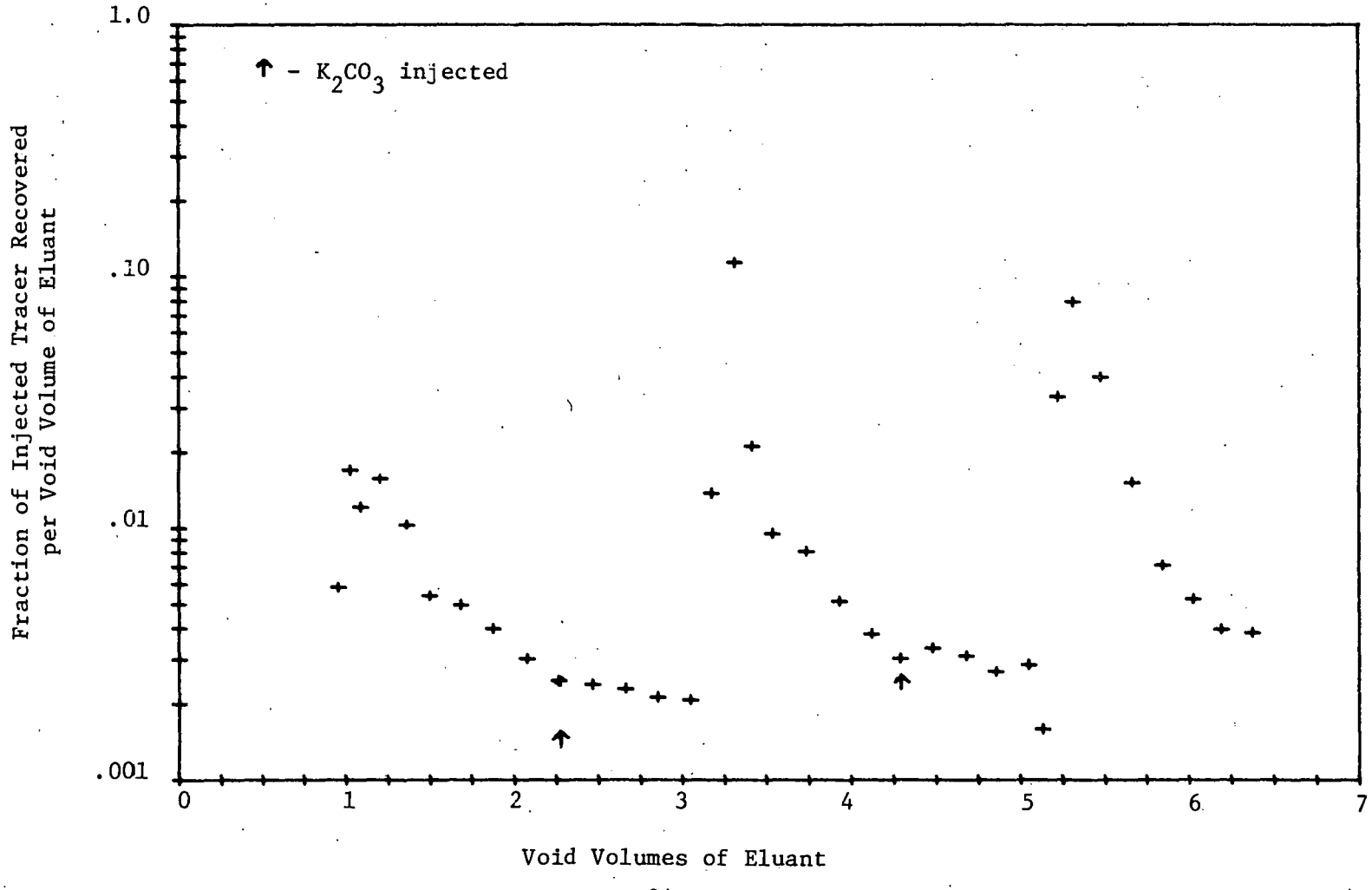

Figure 22. Typical $^{24}NaCO_3$ Elution Curve

effluent (second peak in Fig. 22). Repetition with a similar amount of K_2CO_3 eluted 30 ± 5% of the activity then remaining (third peak in Fig. 22).

One may then conclude that sodium ions are only moderately bound by basalt and are readily eluted by the passage of a front of potassium ions in otherwise low-conductivity water. Similar behavior of sodium ions was observed whether or not inactive kaolin particles were also present in the columns (as residue from previous activated particle tests). This latter result is not surprising since the cation exchange capacities of kaolin and this basalt are both a few meg/100g, but there is a much greater mass of basalt than of kaolin.

Activated Kaolin

The main item of interest in this portion of the project was the behavior of particles in the beds, and this has now been observed for kaolin in basalt, where the carrying solution was of four different salinities. In all cases, the data quoted are averages of two or more replicates performed under the given conditions.

1. Distilled, Deionized Water

A typical elution profile for treated kaolin in distilled, deionized water is shown in Fig. 23. Note that the peaks are 10 times lower for the kaolin particles than for the ionic sodium as a fraction of injected tracer. In each case, a small peak appeared at 1 void volume (VV), containing approximately 1% of the injected activity. In tests carried out to more than 15 VV of effluent, there was only a steady decline in sample specific activity with no other peaks appearing spontaneously.

The effect of K_2CO_3 on the particles was examined as it had been with the ions. Since so much less sodium was present in the particulate tests, the effect of K_2CO_3 might be expected to be profound if the assumed particulate activity were in fact ionic. This was not observed. As the second the third peaks in the figure show, injection of the same amount of K_2CO_3 as had been used in the ionic tests succeeded in removing less than 0.5% of the remaining activity either time. It was noted however, that the longer-term

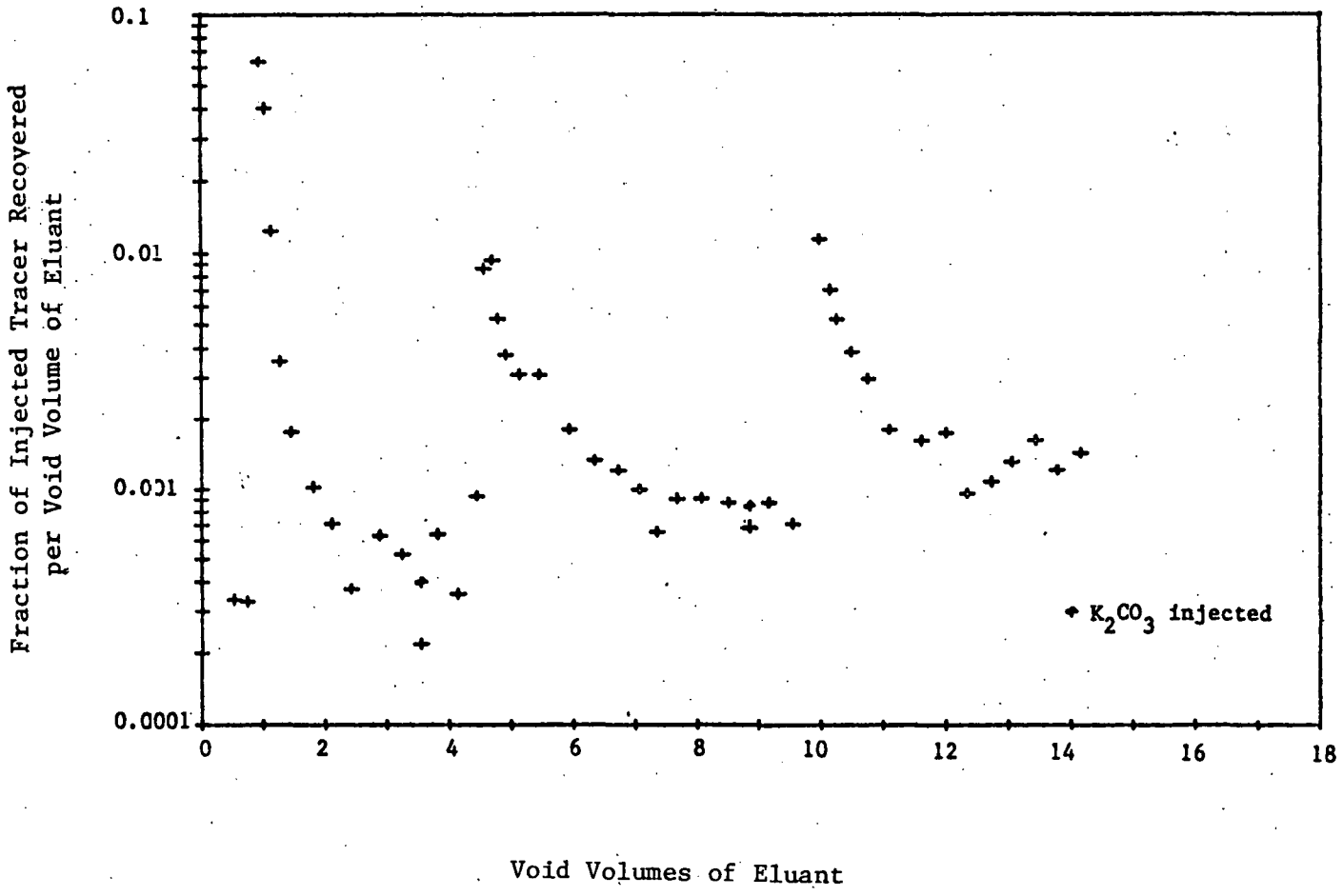

Figure 23. Elution of Kaolin in Distilled, Deionized Water

elution rate following an injection was about twice as high as prior to the injection, although it declined slowly.

It is apparent from these tests that kaolin particles are strongly trapped in a crushed basalt bed in low-conductivity water and are quite resistant to leaching. This is in profound contrast to the ionic sodium behavior discussed in the previous section, and provides confirmation that the activated particle tests will show behavior which is characteristic of the particles themselves, and not of any remaining surface sodium ions.

2. 500 mg/l (∿0.008 M) NaCl Solution

The critical coagulation concentration for kaolin in water was measured here as ∿ 1000 mg/l. It was desirable to measure kaolin behavior both above and below this value, so the first value chosen was 500 mg/l. The specific conductivity of this solution is ∿ 10,000 mS/m (1000 mho/cm), which is not out of order for any deep waters. The columns were pre-equilibrated with 40 VV of this solution over 3 days before the test.

The observed behavior is shown for one column in Fig. 24. In each case the very sharp, small peak at 1 VV contained only about 0.6% of the injected activity. But in this case a low, broad peak appeared spontaneously, beginning (on the average) at ∿ 3.6 VV, peaking at ∿ 5.9 VV, and trailing off beyond 15 VV. This peak contained 80-90% of the injected activity. The result of injecting a small volume of concentrated salt solution was insignificant compared to the main peak, eluting only ∿1% of the remaining activity (small peak near 9 VV). The cumulative tracer recovery curve is shown in Fig. 25 (combined data for two runs). The point of 50% recovery is near 6.5 VV.

3. 750 mg/l (0.013 M) Salt Solution

In view of the interesting behavior outlined above, a similar series of tests was performed at a second salt concentration, but one still below the CCC, 750 mg/l NaCl. The columns were equilibrated with this solution by flowing ∿ 20 VV of it through them over a period of 4 days.

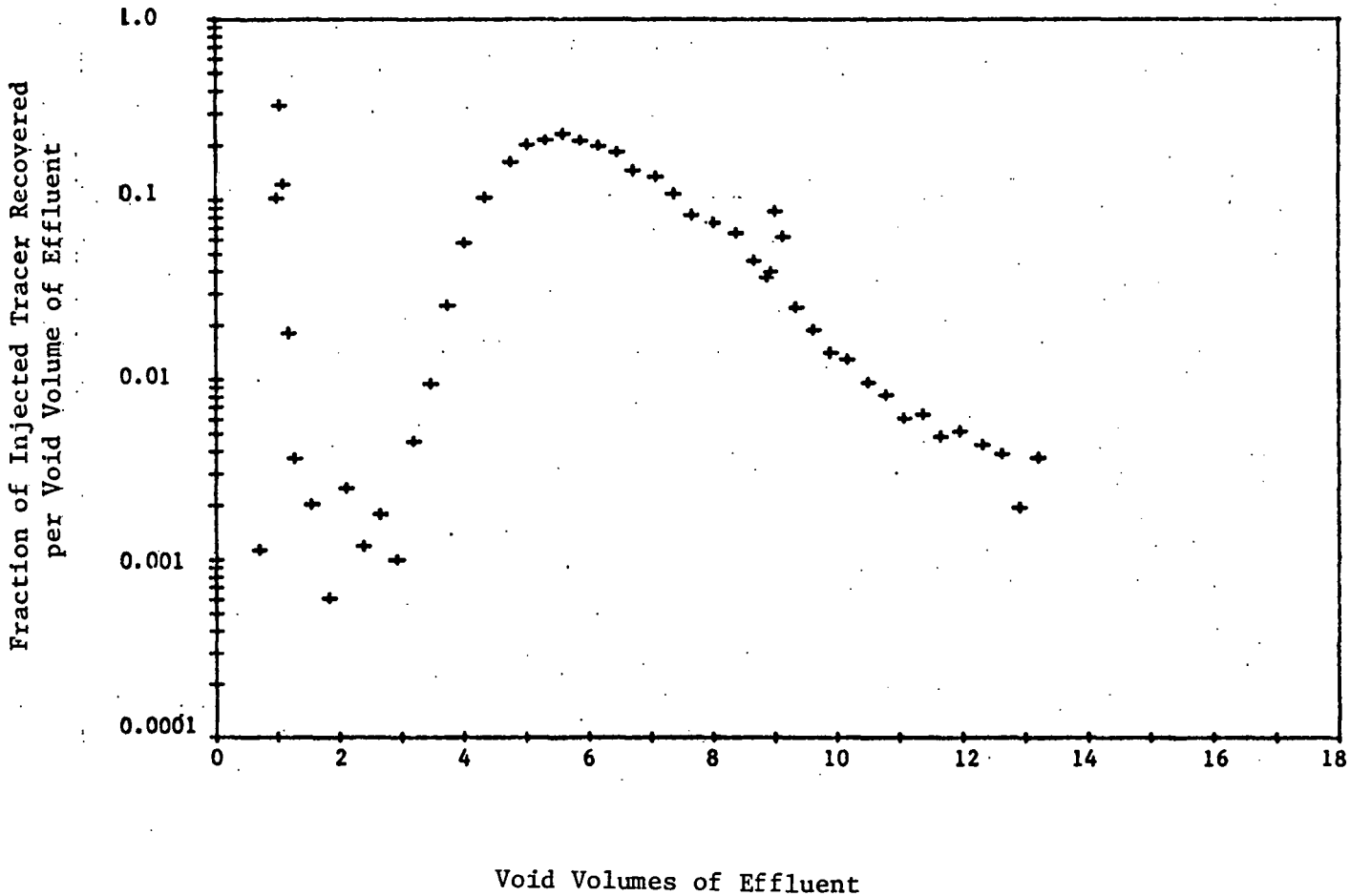

Figure 24. Elution of Kaolin in 500 mg/l NaCl Solution

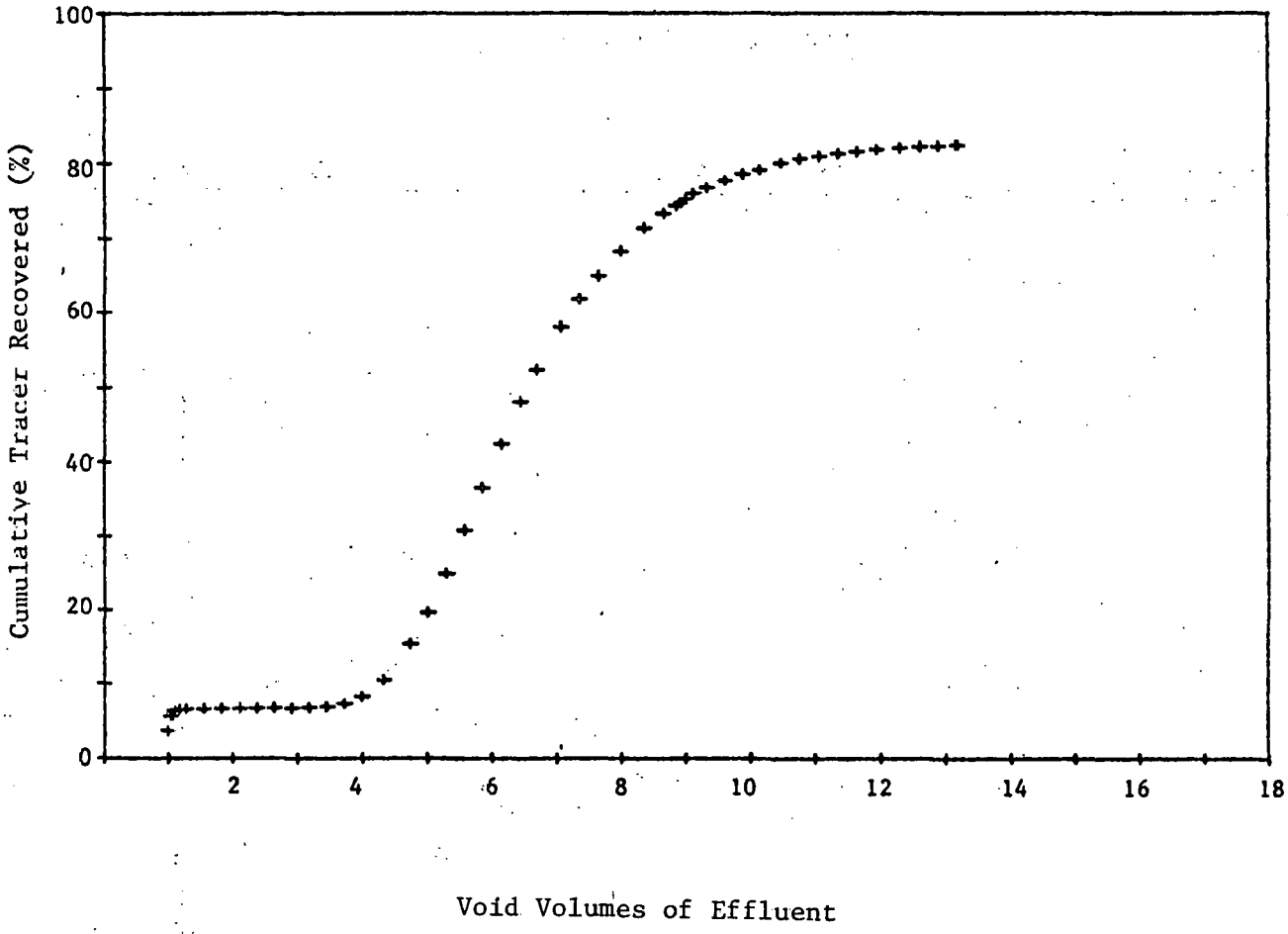

Figure 25. Cumulative Recovery of Kaolin in 500 mg/l NaCl Solution (Average for Two Columns)

It was only in these tests (performed on the same day with tracer from the same batch) that significant activity was observed in the 1 VV peak. Figure 26 (averaged data for 2 columns) shows this peak, in which $\sim$ 28% of the injected activity appeared.

A secondary peak was also observed beginning at 3.1 VV, peaking at 5.4 VV, and returning to zero near 12 VV. It contained about 15% of the originally injected activity, or 20% of the activity remaining in the column at its appearance. This is also clearly visible in Fig. 26.

It is not known at this time whether the high activity of the 1 VV peak is a real effect, or is attributable to some unrecognized difference in particle preparation for these particular tests. Repetition of this experiment is planned.

4. 1250 mg/l (0.021 M) Salt Solution

Two runs were also made at 1250 mg/l NaCl, which is well above the CCC for kaolin. Each column was again equilibrated with the new influent by the passage of $\sim$ 30 VV over a period of 4 days.

Figure 27 shows the average elution behavior under these circumstances. As usual (except in 750 mg/l tests), the 1 VV peak contains $\sim$ 1% of the activity. The secondary peak begins earlier still ($\sim$ 2.1 VV), peaks near 3.6 VV, and returns to 0 near 8 VV. It contains $\sim$ 15% of the injected activity.

Since there was only moderate migration of the particulate activity in this test, one column was subjected to an additional 10 VV of influent at 500 mg/l to determine whether the kaolin trapping would be reversed by what had been a condition very favorable to migration. No effect was observed as the count rate for all samples was statistically identical to background.

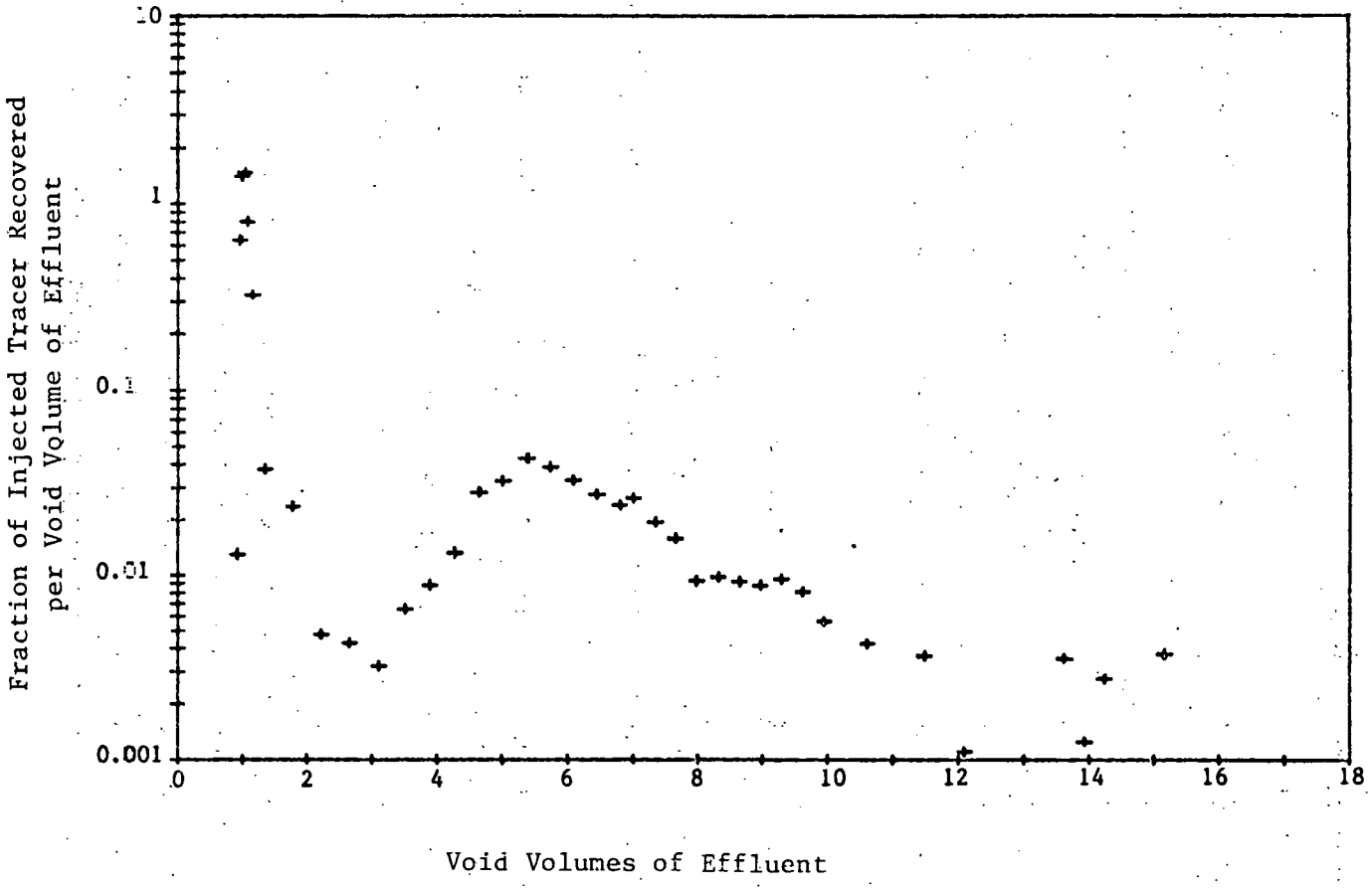

Figure 26. Elution of Kaolin in 750 mg/l NaCl Solution
(Average for Two Columns)

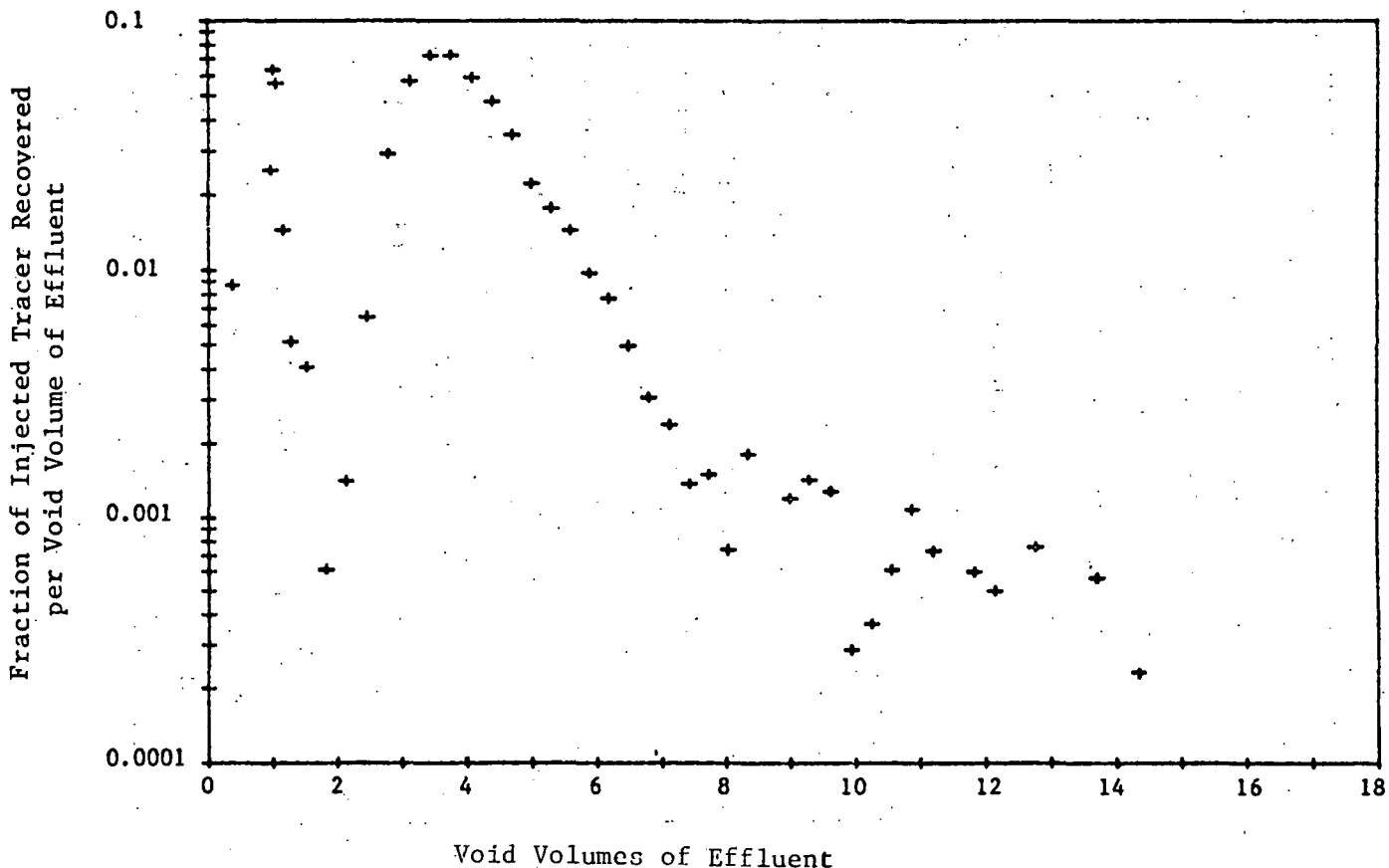

Figure 27. Elution of Kaolin in 1250 mg/l NaCl Solution
(Average for Two Columns)

c. AGGLOMERATION

It is well known that suspended clay particles can be coagulated by the addition of dissolved salts in sufficiently high concentration. It is therefore possible that mobile particles in a porous medium could become immobilized through agglomeration by contact with saline water. The concentration of salt at which agglomeration occurs is known as the Critical Coagulation Concentration (CCC) and is different for different salts and for particles of different composition. Experiments have, therefore, been carried out to determine the CCC of sodium chloride for kaolin, vermiculite, and basalt particles which are used as representative mobile solids in this study.

Effect of NaCl Concentration

By definition, particles remain in suspension at salt concentrations below the critical value, and coagulate and settle out rapidly at concentrations above the critical point. The tests, therefore, consisted of adding increasing amounts of sodium chloride to test tubes containing suspensions of the solids. After mixing, the tubes were allowed to stand overnight and were then visually inspected. Results of the kaolin and vermiculite tubes were easily determined, but because of the small variations occurring in the basalt tubes, their contents were examined spectrophotometrically. For a more quantitative evaluation of the kaolin results, they were also examined spectrophotometrically at these different wavelengths (350, 450, 550 nm). The results are displayed in Fig. 28.

As is clear from an examination of Fig. 28, under these circumstances the CCC is not a sharp point, but consists of a range of sodium chloride concentrations over which there is a rather rapid change in the population of suspended particles. It is concluded that the CCC ranges for each material are as follows:

Kaolin	15-20 millimoles NaCl/l of suspension
Vermiculite	30-40
Basalt	30-50

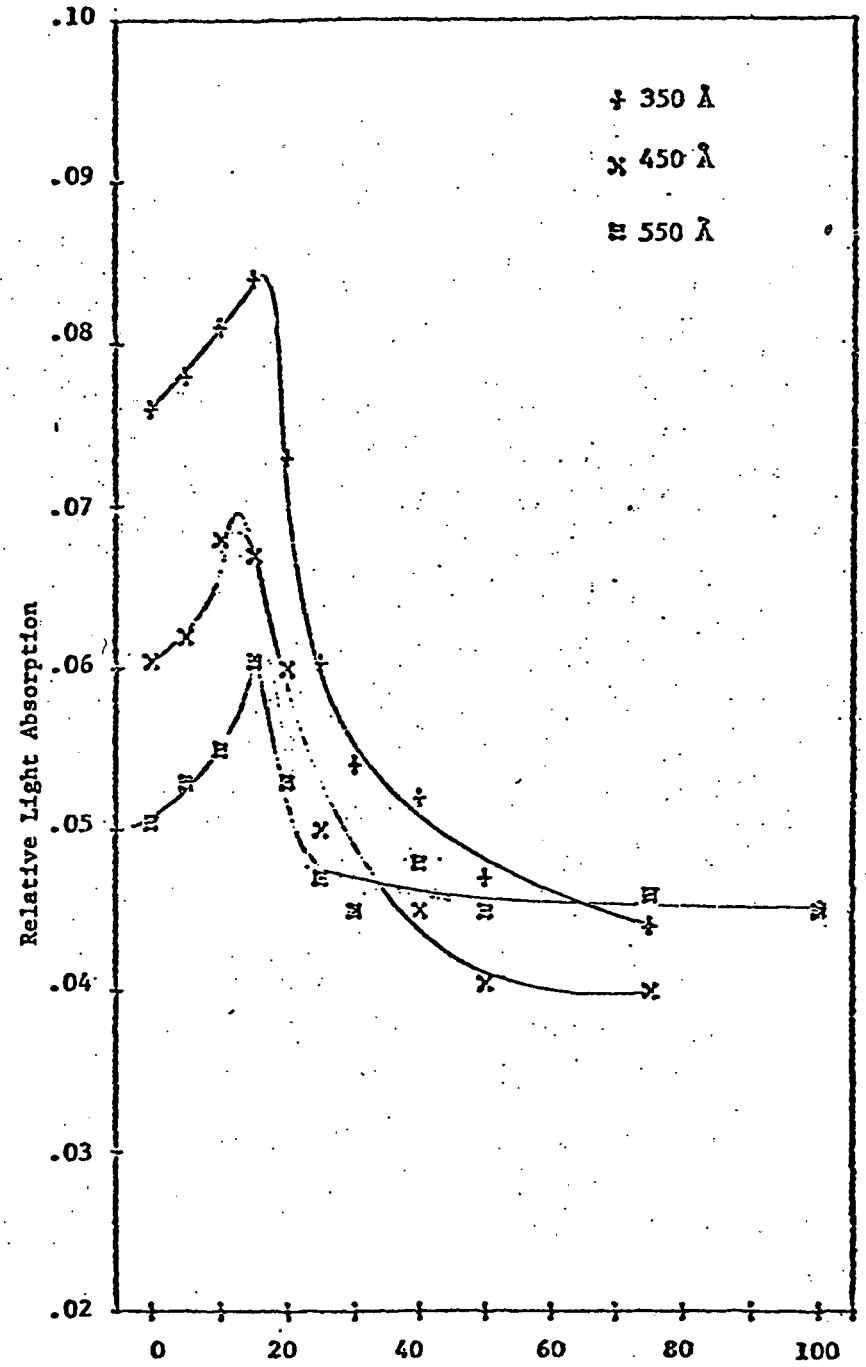

Figure 28. Turbidity of Kaolin Suspension as a Function of Wavelengths of Light

The effect of pH on the possible coagulation of kaolin was also investigated. Buffer solutions in the range of pH 4.0 to pH 10 in increments of 2.5 units were prepared. Equal amounts of kaolin were added, the containers mixed, and allowed to stand. Observations after 24 and 48 hours revealed no difference in the appearance of the suspensions. It is therefore concluded that pH alone is not a significant factor in the coagulation of small kaolin particles in this range of pH values. A similar test, involving shale, was conducted to look for variations in adsorption with agglomeration at different pH levels.

The procedure was as follows:

1. To 150 ml of distilled, deionized water was added 9.4 μCi of Cs^{137}.
2. The carefully and thoroughly mixed solution was divided into 10 aliquots, and allowed to stand two days for equilibration with the walls of the glass flasks.
3. Initial samples were withdrawn for counting.
4. One gram of clean 25-40 mesh shale was added to each flask, and mixed by swirling thoroughly.
5. Samples were withdrawn at selected intervals.
6. All samples were counted.

The results of this experiment are shown in Table 15 together with the calculated values for the distribution coefficient. Since about one-third of the activity was adsorbed by the shale during the first hour, a second experiment was performed to examine more closely the events of the first hour. The same procedure was followed as before, except plastic containers were used instead of glass flasks. The results of the second experiment are tabulated in Table 16 together with the data of the longer-term experiment.

Effect of Radiation

Because in the vicinity of the waste depository high radiation fields would be expected to affect adsorption and coagulation processes, the possible effect of a high dose of gamma radiation on the stability of a vermiculite sol has also been investigated. A portion of the sol was divided into

TABLE 15. Adsorption of Cs-137 by Shale at pH 5.2

Time Elapsed Since Addition of Shale	Fraction of Activity in Solution	Fraction of Activity on Rock (Assumed)	Kd (ml/g)
1.0 hours	0.67	0.33	7.5
2.5 hours	0.70	0.30	6.4
4.0 hours	0.35	0.65	28
7.5 hours	0.25	0.75	45
28.0 hours	0.16	0.84	77
48.25 hours	0.14	0.86	91
100.0 hours	0.06	0.94	233
168 hours	0.03	0.97	443

TABLE 16. Short Term Adsorption of Cs-137 by Shale of pH 5.6

Minutes Since Addition of Shale	Fraction of Activity in solution	Fraction of Activity on Rock	Kd (ml/g)
1	0.94	0.06	2.6
3	0.96	0.04	1.7
5	0.83	0.17	8.0
15	0.64	0.36	23
30	0.66	0.34	21
60	0.61	0.39	26

parts, one of which was retained under ambient laboratory conditions. The other part was placed near a 100,000 curie Co-60 source in a hot cell of the Georgia Tech Neely Nuclear Research Center. After receiving a dose of approximately 200 megarads, it was removed and compared with the non-irradiated sol. Light transmission was the same for the two liquids (within experimental error) and it was concluded that, under the conditions tested, there was no significant change in agglomeration conditions due to the radiation field.

d. Discussion

An outline of the data accumulated on the behavior of kaolin particles in beds of crushed basalt is contained in Table 17.

It is likely that two effects control the retardation and capture of particles by the bed: interstitial straining or trapping of large particles, and van der Waals bonding-double layer effects in small particles. Changes in solution salt concentration will affect both mechanisms. If the 1 VV peak in the 750 mg/l tests is considered suspect for the reasons outlined above, theoretical considerations will provide a qualitative understanding of the data.

Champlin[3] has calculated the curves shown in Fig. 29 for various concentrations of NaCl. Dotted lines correspond to repulsive energy, while the solid diagonal is the attractive van der Waals energy. The van der Waals energy is independent of the type of salt in solution; the repulsive energy depends on the valence (v) of the positive ion in solution according to $(ve^{v})^{-1}$. Thus, use of a divalent cation such as Ca^{++}, would lower the repulsive energy curves by a factor of $\pm$ 14.8. Although the curves were calculated for interactions of two kaolin plates, similar curves would apply for any other two particles of like charge in water. (Kaolin acquires a negative charge in water, as do most minerals.) He also showed that a fine particle is more strongly attracted to a thick grain (such as the basalt which composes the columns) than it is to another particle of the same size as itself at the same distance.

TABLE 17. Summary of Data on Kaolin Behavior in Basalt

Added Salt in Influent (mg/l)	First Peak %of Tracer Recovered	Second Peak Begins (VV)	Second Peak Peaks (VV)	Second Peak Ends (VV)	% of Remaining Tracer Recovered
0	1	N/D*			
500	0.6	3.6	5.9	15	83
750	25	3.1	5.4	12	20
1250	1	2.1	3.6	8	15

*N/D - Not Detected

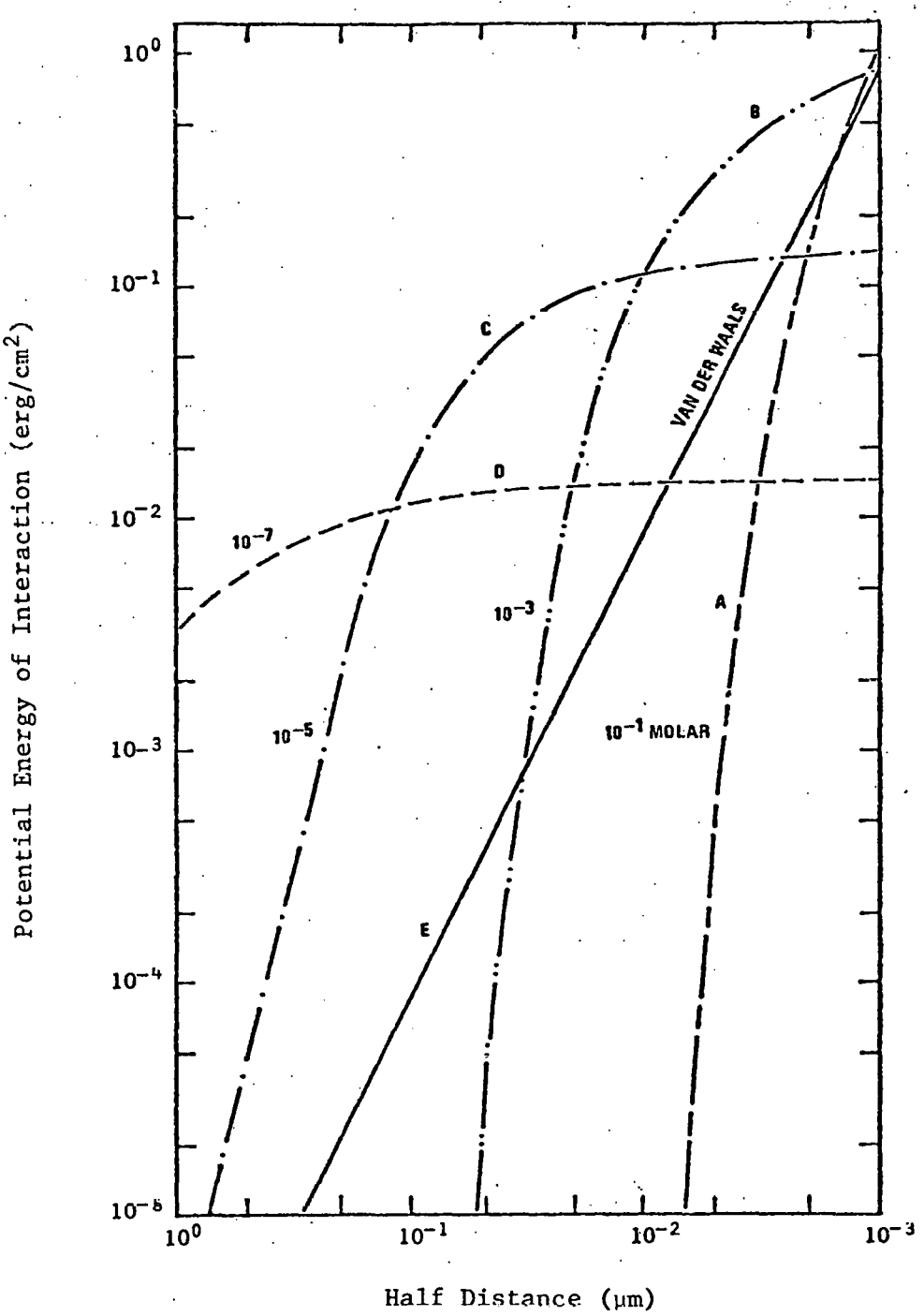

Figure 29. Energy of Interaction Between Kaolin in Plates at Various Concentrations of NaCl

These data may be qualitatively transformed into the more familiar potential energy-distance curves of the type shown in Fig. 30[10]. At high solution concentrations van der Waals attraction overcomes double layer repulsion at all distances which are greater than the particle-particle distance at contact. At lower concentrations, there is a substantial activation energy which must be supplied by Brownian motion or kinetic energy of flow in order for irreversible sorption in the primary minimum to occur. At low and intermediate concentrations, there also occurs a secondary minimum in the potential energy curve. Depending on the solution concentration, the distance at which this secondary minimum begins will be 0.01-100 m. The lower the concentration, the greater the distance at which the secondary minimum begins.

One may then explain the effect of changing salt concentrations on particles already captured by the bed. Most particles that are captured rather than delayed will probably be bound in the deep or primary well, where they are most stably held. From Fig. 30, one would expect that once the particles are already trapped, an increase in salt concentration will release only a few of them; these would be some of those nearest the outside edge of the well where Brownian collisions could provide the (small) activation energy required for them to escape. This was observed when small amounts of concentrated solutions were applied to columns in which particles had been trapped at 0 and 500 mg/l added salt: there was a small but finite release of particles. (Although a similar effect of release of Na ions might be anticipated under these conditions, it was shown above that the prepared kaolin tracer behaves very differently from ionic ^{24}Na tracer; thus, it is inferred that the activity released is indeed particulate.)

On the other hand, decreasing the salt concentration once the particles are trapped in the primary well will make them more firmly bound, since the activation energy for escape will increase. No particles should therefore be released. This was observed when particles trapped at 1250 mg/l salt concentration were treated with a large volume of 500 mg/l solution; there was no statistically significant release. (Again, it should be noted that a similar

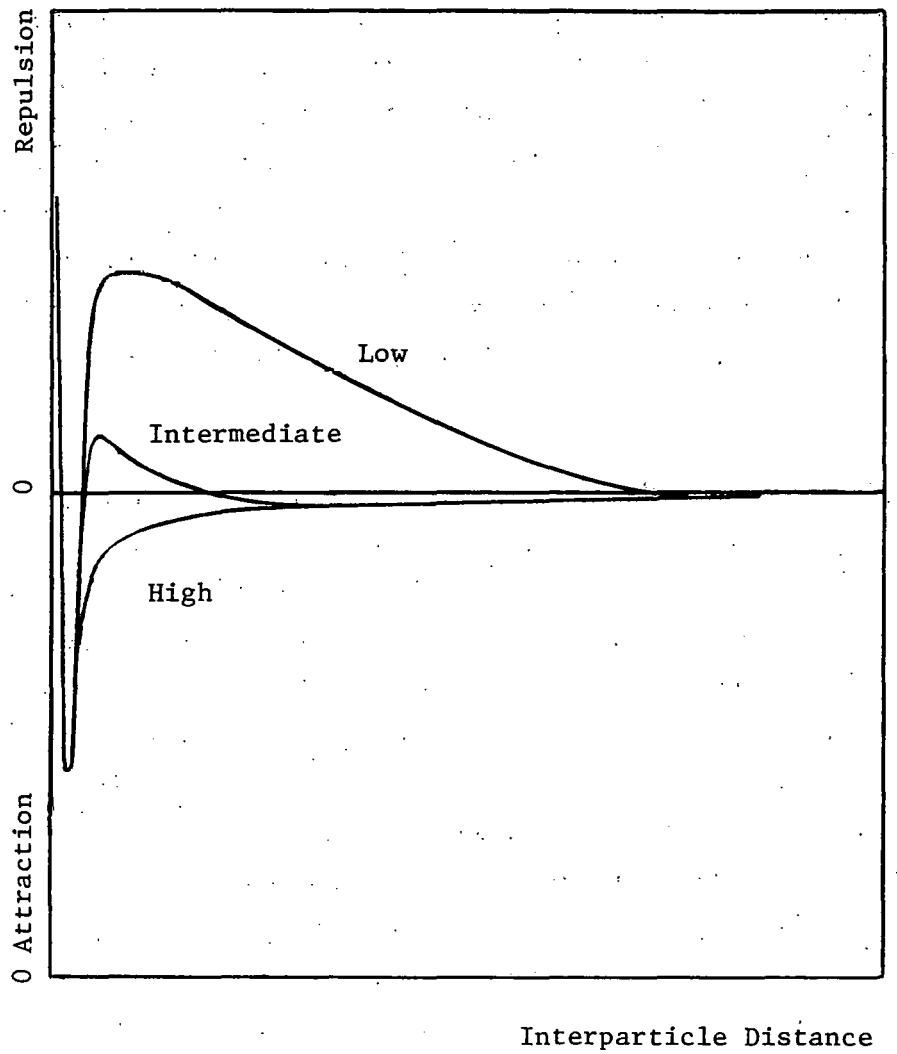

Figure 30. Potential Energy for Two Isolated Particles at Three Solution Ion Concentrations

effect would be observed for Na ions, but there is no reason to suspect the presence of free radioactive Na ions in the beds.)

A particle passing through fine pores in a packed bed does not experience forces from only one bed grain as Fig. 30 implies. Rather, it experiences forces from all the (three or more) grains which form the walls of the pore. If the grains are of the same size and shape (as is roughly the case in the current work), there will always exist an area at the center of the pore where the net force on the particle is zero and its potential energy with respect to each of the surrounding grains is also zero. Brownian interactions will displace particles randomly from this zero-force region, but it may be expected that some (few) particles will spend most or all of their time in this neutral zone. These are the particles which will comprise the 1 VV peak in the elution curve.

Figure 31 shows the subtractive superposition of Fig. 30-type curves for bed grains on opposite sides of a pore. The width of the "neutral zone" is not very dependent on solution concentration. Therefore, it is expected that the fraction of injected kaolin in the 1 VV peak will be roughly independent of the solution concentration. This was observed except in the case of the suspect 750 mg/l experiments.

At intermediate concentrations, Fig. 31 shows a small region near the center of the pore where attraction in the secondary well predominates. Since this well is rather shallow, most particles which pass through it would be expected to be delayed rather than captured, since their flow kinetic energy could pull them free. Particles which spend most of their time in this well are those which form the secondary peak.

Concentration effects on this secondary peak would then be rather complex. At low solution concentrations the secondary well will begin at a distance too great to be contained by our 50 μm pores, and so will not be observed. At high concentrations no secondary well exists at any distance from an isolated grain, so none is observed in the pore. Thus, the secondary peak is expected to appear only at intermediate concentrations. It should be most delayed at some concentration where the well is deepest and should be less delayed at higher and lower salt concentrations.

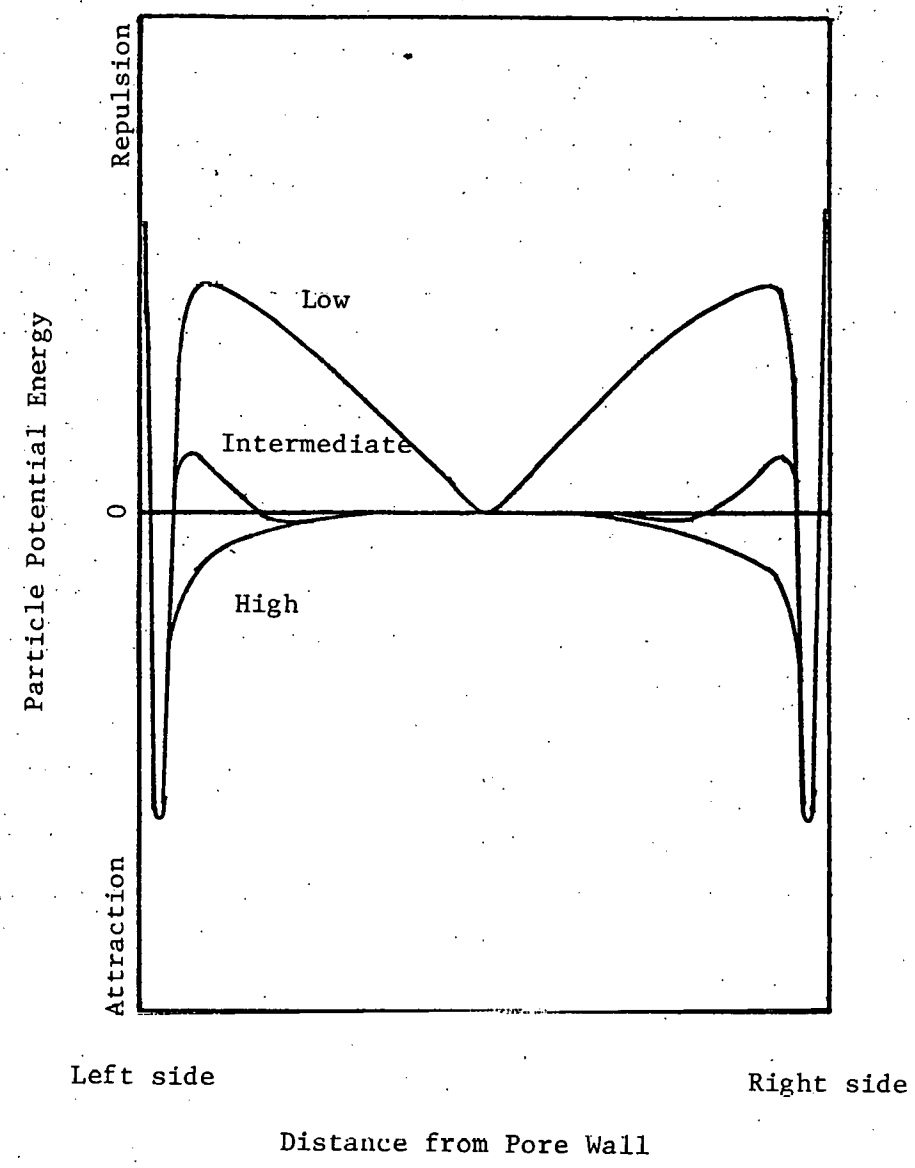

Figure 31. Particle Potential Energy within a Pore at Three Solution Ion Concentrations.

In the current work, we have observed the absence of a secondary peak at very low added salt concentrations and the decline in its delay at relatively high concentrations. This hypothesis predicts that experimentation in the 0-500 mg/l region will reveal some point at which the secondary peak appears, and that tests in the > 1250 mg/l range will show a gradual fadeout of the secondary peak. These predictions will be tested.

We have also observed a portion of the predicted delay time behavior. The experiments in the > 1250 mg/l range would be expected to show a continuation of the decline in delay of the secondary peak. In the 0-500 mg/l range, it is anticipated that some maximum delay will be found, and, that at lower concentrations, the second peak will be progressively less delayed.

Finally, it is anticipated that the fraction of injected kaolin recovered in the secondary peak will parallel the extent of its delay. When the well is deepest and delay is longest, more particles should be found in it. This prediction will also be readily tested by the higher and lower concentration tests.

It should also be noted that one other mechanism will favor retardation of particles in solutions $\geq$ 0.02 M in NaCl. Coagulation of kaolin particles accelerates markedly above this concentration, and the resulting larger particles will be more easily strained out of the migrating solution. This would be most likely to occur in regions where two bed grains are in contact or near contact, leaving a small area with low flow between them. A decrease in salt concentration following particle coagulation produces only slow resuspension in the absence of physical agitation.

Until the range of concentrations is identified over which the particles can be expected to be delayed but not wholly retained, the consequences of clay particle transport for a mined geologic repository will be unclear. Since the concentrations of groundwaters vary over a considerable range, it may well be that some formations will be materially better in this regard than will others.

IV. CONCLUSIONS

While the work so far has been rather qualitative, mainly because of problems in determining the surface areas of dispersed colloids, it has resulted in several significant results. It can be concluded that fine suspended particles are likely to occur in deep waters that may impinge on a depository site. Their size and shape depend on water quality; in particular, in high salt concentration colloidal aggregation occurs though not to an extent to interfere severely the migration of the particles. In "old" water which contains appreciable concentrations of mineral ions, these may tend to preempt adsorption sites that may otherwise attract the disperse particulates; consequently, they may travel greater distances than they would in "pure" water.

The adsorption of dissolved radionuclides onto the suspended particles also occurs in competition with other ions in solution and, as expected, is very sensitive to variations in pH and temperature. Most of the work so far has been devoted to cesium. Adsorption of transuranium atoms, Pu and Np in particular, will require considerably more study. Investigations on technetium using Tc-95m as the tracer are only just getting under way and should be useful in showing the migration probability of anionic waste products by particulate transport.

The differences in retention characteristics of limestone, basalt, and shale columns will become particularly important in site-related studies on the migration properties of wastes beyond the immediate vicinity of the depository itself. Though the presence of air does not appear to have an appreciable effect on particle uptake and mobility, this factor, and the effect of other dissolved gases, will require some further attention.

REFERENCES

1. J. B. F. Champlin and G. G. Eichholz. 1968. "The Movement of Radioactive Sodium and Ruthenium through a Simulated Aquifer." Water Resources Research. 4:147-158.

2. J. B. F. Champlin and G. G. Eichholz. 1976. "Fixation and Remobilization of Trace Contaminants in Simulated Subsurface Aquifers." Health Phys. 30: 215-219.

3. J. B. F. Champlin. 1971. "The Physics of Fine-particle Movement through Permeable Aquifers." J. Soc. Petroleum Eng. 11:367-373.

4. L. L. Ames. 1978. Characterization of Rock Samples, Controlled Sample Program Publication No. 1. Report PNL-2797. Battelle Pacific Northwest Lab.

5. J. F. Relyea and R. J. Serne. 1979. Interlaboratory Comparison of Batch Kd Values, Controlled Sample Program Publication No. 2. Report PNL-2872. Battelle Pacific Northwest Lab.

6. I. W. Marine. 1976. Geochemistry of Ground Water at the Savannah River Plant. Report DP-1356. Savannah River Lab., Aiken, S.C.

7. Anon. 1979. Chemical Analysis of the Initial Groundwater Samples from the Lac du Bonnet Batholith. Technical Record TR21. Atomic Energy of Canada Ltd. Pinawa, Man.

8. W. A. Gray. 1968. The Packing of Solid Particles. Chapman and Hall Ltd. London.

9. M. Muskat. 1937. The Flow of Homogeneous Fluids through Porous Media. McGraw-Hill. New York.

10. H. van Olphen. 1977. An Introduction to Clay Colloid Chemistry. John Wiley and Sons. New York.

THIS PAGE

WAS INTENTIONALLY

LEFT BLANK

QUESTIONS AND ANSWERS

GIT

EICHHOLTZ DISCUSSION

Ground-water Particles in situ

Q: If you look in situ in the host rock, how much particulate matter do you think is travelling, for example, into a well drilled into the host rock?

A: I can suggest that the drilling process, itself, will result on considerable decrepitation material, i.e., material from fractured rock produced by the drilling.

Q: Yes, but doesn't it clarify?

A: Not entirely; that is the point. The coarse materials will certainly settle out, but there is always a finite fraction that is fine and will stay in suspension. In addition, any mechanism that involves eruption of water into the sites typically follow with gross and various suspended clay materials. And so a number of mechanisms have been suggested to produce this kind of particulate concentration, in addition to the colloid formations. There appears to be evidence for this point. For instance, in the Swedish mine, investigators have looked at decrepitation products and several are attributable to the drilling activity.

Column Design

Q: In the up-flow versus down-flow column, is there any kind of possibility of channeling in the down-flow?

A: We don't think so. The general idea is that the columns are small (column diameter > than 34 x particle size) so that the wall effects are essentially negligible. We haven't found any channeling - it certainly would appear quickly in terms of the activity distribution in the effluent.

C: It was interesting that the horizontal flow in this instance reproduced the down-flow.

A: I have to say the later tests don't show this effect, but I think it's a good sign, and the principle, "Don't throw out anything until you understand what went wrong" applies. At this time we aren't sure what went wrong.

Column Flow Rate

Q: Did you say that the flow rate was a milliliter per minute?

A: Yes.

Q: Why? Isn't that somewhat fast?

A: Yes, but there is a problem of getting enough activity in a reasonable time through this column, and so it seems like a reasonable compromise. We've used slower rates too -- in fact we've done a rate of about 2 ml/hr. It doesn't seem to make a great deal of difference. We are looking at the effect of flow rate. We hope that all these flow rates are low enough that we don't get any settling effect in the tests one way or another. Several of the tests have been taken down much lower. Some of the tests have been conducted over a period of 11 to 14 days.

Particle Versus Solute Movement

Q: I'm not sure how you differentiate between the movement of what I'll call a hot particle, the desorption of the tracer from the particle, and sorption on something in the bed.

A: Well, you see, we can test the particles by themselves by activating them, before anything ever gets sorbed. So we look for the ^{24}Na activity.

Q: So it's the sodium ...

A: No, this is structural Na that we are activating, not surface activation.

C: O.K., but much of your data indicate 900 will absorb cesium.

A: In the case of absorbed cesium, yes. There may be some of both, but, by and large, in the type of run we've had, there seems to be very little transfer of the cesium to the column. Now there has been some adsorption and desorption. But certainly it looks so far that the post-bed surface effect on the particles can clearly be separated from any transfer of absorbed activity from the particles to the solution.

THIS PAGE

WAS INTENTIONALLY

LEFT BLANK

WASTE ISOLATION SAFETY ASSESSMENT PROGRAM

TASK 4: COLLECTION AND GENERATION OF TRANSPORT DATA .

THEORETICAL AND EXPERIMENTAL EVALUATION OF WASTE TRANSPORT IN SELECTED ROCKS

ANNUAL PROGRESS REPORT

OCTOBER 1, 1978 - SEPTEMBER 30, 1979

R. J. SILVA, L. V. BENSON, A. W. YEE
and G. A. PARKS (STANFORD UNIVERSITY)

SEPTEMBER 30, 1979

BATTELLE/ONWI SUBCONTRACT NO. 45901AK

LAWRENCE BERKELEY LABORATORY
UNIVERSITY OF CALIFORNIA
BERKELEY, CALIFORNIA 94720

This report was prepared by Lawrence Berkeley Laboratory under Subcontract 45901AK with Battelle Memorial Institute, Project Management Divsion, under Contract EY-76-C-06-1830 with the Department of Energy. The subcontract was administered by the Office of Nuclear Waste Isolation.

THIS PAGE

WAS INTENTIONALLY

LEFT BLANK

NOTICE

This report was prepared as an account of work sponsored by the United States Government. Neither the United States nor the Department of Energy, nor any of their employees, nor any of their contractors, subcontractors, or their employees, makes any warranty, express or implied, or assumes any legal liability or responsibility for the accuracy, completeness, or usefulness of any information, apparatus, product, or process disclosed, or represents that its use would not infringe privately owned rights.

THIS PAGE

WAS INTENTIONALLY

LEFT BLANK

THEORETICAL AND EXPERIMENTAL EVALUATION OF WASTE TRANSPORT IN SELECTED ROCKS

R. J. Silva
L. V. Benson
A. W. Yee
G. A. Parks

ABSTRACT

The objective of the program is to establish a basis for the prediction of radionuclide sorption in geologic environments. In FY 79, experimental and theoretical efforts were concentrated on a study of the sorption of cesium on the solid substrates Min-u-sil (quartz) and Belle Fourche clay (montmorillonite).

Cesium sorption isotherms were obtained for the two substrates at 26°C as a function of initial Cs concentration in solution (10^{-3}M to 10^{-9}M), pH (5 to 10) and supporting electrolyte concentration (0.002M, 0.01M, 0.1M, and 1M NaCl and a simulated basalt groundwater in batch-type experiments using crushed material. Characterization of the solid phases included measurements of chemical compositions, particle sizes, surface areas, and cation-exchange capacities. In addition, potentiometric acid/base titrations of the solid phases were conducted in order to determine the acid dissociation and electrolyte exchange constants of the surfaces. Preliminary analysis of the sorption data indicated that while the clay data could be explained by simple mass-action expressions, the quartz data could not.

Theoretical efforts were aimed at developing and testing an electrolyte binding electrical double-layer model to predict sorption isotherms. A computerized version of the model, MINEQL, which simultaneously considers surface and solution chemical equilibria, was brought to operational status. Input parameters required by MINEQL were determined and sorption isotherms for Cs on the Belle Fourche clay were calculated over the same range of parameters as the experimental measurements. Comparisons showed that the model was able to simulate the isotherms quite well except at the lowest pH values for the 0.002M and 0.01M NaCl solutions.

INTRODUCTION

The licensing procedure for the storage of nuclear waste in underground geologic media will involve a safety assessment of the proposed site. Since the time scale being considered is one hundred thousand to a million years, predictions based on realistic modeling studies provide the main avenue of assessment. Modeling studies are only as reliable as the data on which they are based. For the prediction of radionuclide migration in geologic media, it is essential that the systems involved be well understood. Without this information, arguments regarding subsurface storage lack credibility.

The specific goal of Task 4 is the development of quantitative data and methods to describe the radionuclide-geologic media interactions that control the aqueous transport of radionuclides. The method must quantify the relationships of the independent variables to the observed sorption phenomena and develop into a predictive model which is capable of estimating the interaction (i.e., distribution coefficients) of any given radionuclide with a variety of geologic materials and groundwater types. The resultant predictive model can then be incorporated into a more general radionuclide transport model (WISAP Task 3), which includes hydrologic, geosphere and biosphere transport. The general model will be used for the hazards assessment of subsurface storage for any proposed site.

This report covers the FY 79 activities of the Geosciences Group of the Earth Sciences Division, Lawrence Berkeley Laboratory, by R. J. Silva, L. V. Benson, and A. W. Yee in support of Task 4 of the Waste Isolation Safety Assessment Program with contributions from Professor G. A. Parks, consultant from Stanford University.

OBJECTIVE OF PROGRAM

The objective of the program is to develop quantitative data and methods to describe the interactions that control the transport of radionuclides in geologic environments anticipated for terminal radioactive waste storage facilities. It covers a theoretical and experimental evaluation of the physical and chemical processes which govern the sorption phenomena with the goal of

establishing a basis on which distribution coefficients might be reliably predicted for any given radionuclide with a variety of geologic materials and groundwater types.

The migration behavior of a radionuclide is strongly dependent on its chemical properties. Therefore, the effects of oxidation state, speciation and concentration of the radionuclide on the rock-nuclide interactions, i.e., distribution coefficients, need to be determined and any realistic model should include them as input parameters. This means reliable data on the solubilities of radionuclide compounds and complexation constants of radionuclide ions that might form under geologic conditions, e.g., carbonates, hydroxides, phosphates, etc., is needed. In addition, the conditions for oxidation and reduction should be considered.

Further, the chemical and physical properties of the sorbing substrates need to be known in detail since the sorptive properties depend on sorption site densities, effective areas, surface charges, pH, concentration of radionuclide in the liquid phase, concentration and nature of the supporting electrolyte, etc. The effects of these parameters on the rock-nuclide interaction need also to be studied and should be included in the model.

It was concluded that the most effective means of securing information relevant to the migration of radionuclides was to proceed with a study aimed at defining the principle controls on the migration of any radionuclde, including the properties of the substrates as well as the radionuclides, and to attempt to develop a model for predicting distribution coefficients, k_d's based on these relationships. It is believed that by focusing the research effort, results in a usable form will be available in time to meet the licensing requirements of a high level waste terminal storage repository.

PROGRESS REPORTED PREVIOUSLY

The first year of this program, fiscal 1977, was devoted to a review of the literature on the thermodynamic data for aqueous complexes and solid phases of Pu, Np, Am and Cm likely to form in the natural environment and on the transport mechanisms of radionuclides in water-saturated rocks. An

assessment of factors influencing the radionuclide-rock interactions for conditions expected in a terminal storage facility was made. This work was reported in the WISAP Task 4 Contractor Information Meeting Proceedings, September 20-23, 1977 (Apps et al., 1977).

During FY 78, a theoretical and experimental program was developed with the purpose of identifying the most important parameters governing the transport of five actinides (U, Np, Pu, Am and Cm) in the three rock types Umtanum basalt (Hanford), Eleana shale (NTS), and Climax quartz monzonite (NTS). The work demonstrated that the behavior of the actinides in groundwater and their sorption on rocks was dependent on the oxidation state of the actinide and on the solubility of stable precipitates such as oxides, hydroxides, and carbonates. Furthermore, it was determined that secondary alteration phases such as clays and zeolites, appeared to sorb actinides preferentially over other rock-forming minerals such as silica and feldspars. This work was reported in detail in the WISAP Task 4 Contractor Information Meeting Proceedings, October 2-5, 1978 (Silva et al., 1978).

OBJECTIVES FOR FY 79

In FY 79, experimental and theoretical efforts were concentrated on a study of the sorption of cesium on the substrates quartz and montmorillonite - two representative geologic materials that are widely distributed and frequently coat weathered surfaces - in order to begin to delineate the principle parameters in sorption processes. Cesium was chosen for these beginning studies because it exhibits rather simple chemical behavior under most solution conditions. Thermodynamic data (Sillen and Martell 1964; Smith and Martell 1976; Seidell and Linke 1958) indicate that the compounds of cesium likely to form under geologic conditons, i.e., carbonates, hydroxides, chlorides, sulfates, etc., are quite soluble and it is not expected to hydrolize or complex to any extent, except at very high ligand concentrations, and should exist mainly as Cs^+ ion in solution.

The experimental effort was aimed at (1) characterization of the solid phases, (2) a study of the surface chemistry of the solid phases, and (3) the

measurement of Cs sorption isotherms on the two substrates over a wide range of Cs concentrations, pH, and concentration of supporting electrolyte. Sodium chloride was selected as the supporting electrolyte because of the current interest in salt domes as a waste repository. In addition, one mixed electrolyte of a composition similar to the groundwaters from Columbia River basalts was selected to simulate a natural system.

The theoretical effort was aimed at developing and testing an advanced sorption model to predict K_d values. This model is reasonably complete in that physical and chemical interactions are considered simultaneously in the calculation of surface and solution equilibria for major electrolyte ions and dilute solutes and has been successfully used to describe the uptake of metal ions and complexes on solid surfaces. The model requires a rather complete knowledge of the thermodynamic properties of the solid surfaces as well as the solute, e.g., sorption site density, solute solubility and complexation constants, sorption isotherms, etc. However, once a system has been characterized, the model can be used to quantitatively predict sorption effects for other aqueous systems having different compositions for the solute and substrate. It was desired that a computerized version of the model, called MINEQL, be brought to full operational status at LBL. Data from the experimental effort could then be input to the computer code, the sorption isotherms for Cs on the two substrates simulated, and the ability of the model to predict K_d values for this system tested. Discrepancies between the simulated and measured quantities would provide the basis for corrections to the model.

THE ELECTROLYTE BINDING ELECTRICAL DOUBLE LAYER MODEL

INTRODUCTION

Electrical charge acquired by colloid or solid surfaces in aqueous systems plays a significant role in determining the properties of the surfaces. Therefore, methods for predictively modelling the behavior of charged surfaces are important for an understanding of adsorption behavior.

A particle or surface which acquires charge, or an electrical potential different from the solution, accumulates counter charges in order to preserve electrical neutrality. The countercharge may consist simply of a rather loosely bound, diffuse atmosphere of counter ions or a compact layer of bound charge near or at the surface plus a diffuse atmosphere. The surface, compact and diffuse charges together have been called the electrical double layer (e.d.l.). The compact layer counterions are unlikely to approach the surface more closely than some distance, β, probably close to the ionic radii of anions and the hydrated radii of cations (James and Parks 1979). For calculational purposes, the surface charge, σ_0, is taken to be at the surface (s-plane), the compact charge, σ_β, at some distance β from the surface (β-plane) and the diffuse charge, σ_d, at the boundary between the compact and diffuse regions (d-plane).

Gouy and Chapman (Gouy 1910; Chapman 1913; Gouy 1917) derived equations for describing the diffuse distribution of counter ions accumulated near a charge surface; Stern and Grahame (Grahame 1947) extended the model to include specific adsorption or binding of counter ions close to the surface, i.e., the compact layer in addition to the diffuse layer. In recent years, several lines of research and model development involving a variety of surfaces as different as metallic mercury, insoluble oxides, silver halides, proteins, polystyrene latexes, and clays (James and Parks 1979), have converged. For colloids and hydrosols which contain acidic, basic, and amphoteric functional groups at their surfaces, a single, conceptually simple model capable of predictively modeling the development of surface charge and potential, electrolyte adsorption densities and other related properties has emerged, the electrolyte binding electrical double layer model (Yates, Levine and Healy 1974; Davis, James and Leckie 1978).

DESCRIPTION OF MODEL

In order to develop a description of the e.d.l., it is necessary to formulate the reactions for the development of surface charge on the solid surfaces. A variety of acidic, basic, and amphoteric hydroxyl groups are present on oxides, hydroxides, and silicates. It is generally considered that the

surface charging mechanism for oxides is the adsorption of protons or hydroxyl ions by ionizable surface groups to form positive or negative sites. The resulting surface charge, which depends on an excess of one type of charge site or the other, is a function of the solution pH. For this reason, H^+ and OH^- are considered the potential determining ions, p.d.i.

Clays and zeolites contain OH sites, but, in addition, their surface charge properties may be dominated by less localized charge distributions. The structure consists of SiO_4, AlO_6 and AlO_4 groups, bonded together by varying degrees of oxygen sharing. In many resulting structures, there is a net deficiency of positive charges which may be associated with a particular AlO_4 group but not with any particular oxygen ion. Such charge may not be best described as an ionizable site, in the same sense as a particular OH group, but this interpretation has been applied with reasonable success (James and Parks 1979).

As part of the development of the model, it is customary to write local equilibrium reactions and intrinsic (thermodynamic) constants for simple ionization reactions of the surface sites (S), i.e.,

$$SOH_2^+ \rightleftarrows SOH + H_s^+; \quad K_{a_1}^{int} = \frac{(SOH)(H^+)_s}{(SOH_2^+)} \tag{1}$$

$$SOH \rightleftarrows SO^- + H_s^+; \quad K_{a_2}^{int} = \frac{(SO^-)(H^+)_s}{(SOH)} \tag{2}$$

where the subscript, s, denotes at the surface. The first reaction dominates at high acid concentrations while the second dominates in near neutral and alkaline solutions.

In addition to reactions involving protons and hydroxyl ions, electrolyte counter ions could interact directly with the surface and adsorb to neutralize specific sites. The formation of surface complexes readjust the acid-base equilibrium and affects the proton balance. To account for specific adsorption

of electrolyte ions, e.g., Na^+ and Cl^-, the formation of ion pairs or surface complexes at the charged sites is assumed, i.e.,

$$SO^- + Na_s^+ \rightleftarrows SO^-Na^+; \quad K_{Na^+}^{int} = \frac{(SO^-Na^+)}{(SO^-)(Na^+)_s} \tag{3}$$

$$SOH_2^+ + Cl_s^- \rightleftarrows SOH_2^+Cl^-; \quad K_{Cl^-}^{int} = \frac{(SOH_2^+Cl^-)}{(SOH_2^+)(Cl^-)_s} \tag{4}$$

The protons involved in the surface reactions are assumed to be in the surface plane and the electrolyte ions to lie in the compact layer at a distance β from the surface. The protons in the suface plane and the Na^+ and Cl^- ions in the β plane are distinguished from those in the bulk solution because the difference in the electrical potentials between the surface and bulk solution, Ψ_o, and the β plane and solution, Ψ_β, result in a difference in the chemical potential of the ions. Their activities are modified by the electrical work necessary to bring them from the bulk solution to the plane in which they react. Hence, the activities at the surface are related to the activities in solution by (Stumm and Morgan 1970),

$$(H^+)_s = (H^+)_{aq}\exp(-e\Psi_o/kT) \tag{5}$$

$$(Na^+)_s = (Na^+)_{aq}\exp(-e\Psi_\beta/kT) \tag{6}$$

$$(Cl^-)_s = (Cl^-)_{aq}\exp(+e\Psi_\beta/kT) \tag{7}$$

where the subscripts s and aq refer to activities at the surface and in the bulk solution, respectively, e is the unit electronic charge, k is the Boltzmann constant, and T is the absolute temperature.

The intrinsic constants are related to operational reaction quotients, Q, through the modification of equations (1)-(4) using equations (5)-(7), i.e.,

$$Q_{a_1} = \frac{(SOH)(H^+)_{aq}}{(SOH_2^+)} = K_{a_1}^{int} \exp(+e\Psi_o/kT) \quad (8)$$

$$Q_{a_2} = \frac{(SO^-)(H^+)_{aq}}{(SOH)} = K_{a_2}^{int} \exp(+e\Psi_o/kT) \quad (9)$$

$$Q_{Na^+} = \frac{(SO^-Na^+)}{(SO^-)(Na^+)_{aq}} = K_{Na^+}^{int} \exp(-e\Psi_\beta/kT) \quad (10)$$

$$Q_{Cl^-} = \frac{(SOH_2^+Cl^-)}{(SOH_2^+)(Cl^-)_{aq}} = K_{Cl^-}^{int} \exp(+e\Psi_\beta/kT) \quad (11)$$

These latter reactions, 10 and 11, may be written as exchange reactions which are more useful for analyses of surface charge data, i.e.,

$$SOH + Na_s^+ \rightleftarrows SO^-Na^+ + H^+_s \quad (12)$$

The corresponding intrinsic exchange constants, ${}^*K^{int}$, and exchange reaction quotients, ${}^*Q$, are:

$${}^*Q_{Na^+} = \frac{(SO^-Na^+)(H^+)_{aq}}{(SOH)(Na^+)_{aq}} = {}^*K_{Na^+}^{int} \exp \frac{e\Psi_o - e\Psi_\beta}{kT} \quad (13)$$

and

$${}^*Q_{Cl^-} = \frac{(SOH)(H^+)_{aq}(Cl^-)_{aq}}{(SOH_2^+Cl^-)} = {}^*K_{Cl^-}^{int} \exp \frac{e\Psi_o - e\Psi_\beta}{kT} \quad (14)$$

Thus, because of the surface charge and double layer potential, the distribution of ions between surface and solution are not given by a simple equilibrium constant but by a variable activity or concentration quotient. This quotient is the product of an intrinsic constant applicable when the surface charge and potential are zero and a variable Boltzman term which depends on the state of

charge or potential of the surface. In principle, the intrinsic constants and reaction quotients are determined by the activities of the reacting species. However, since there is no theory for calculating the activity coefficient of the surface species SOH, SO^-, SO^-Na^+, and $SOH_2^+Cl^-$, the practice has been to substitute the concentrations of these species for their activities in calculations (see for example, equations 22, 25, 27, and 30).

Additional solute ions are handled in a similar manner as for NaCl with similar sets of equilibrium equations and intrinsic exchange constants. The solute cations are allowed to compete with H^+ and Na^+ for surface sites. It is also possible to include simultaneously in the model other ionizable adsorption sites which exhibit different intrinsic ionization and exchange constants. However, the relative amounts of the different types of sites need to be known.

SURFACE CHARGE

The surface charge, σ_o, represents the net number of protons released or consumed by all surface reactions including electrolyte ion binding reactions as well as ionization of the surface to form the species SO^- and SOH_2^+. Hence, surface charge is determined by the concentration of reacted sites,

$$\sigma_o = B([SOH_2^+] + [SOH_2^+Cl^-] - [SO^-] - [SO^-Na^+]) \quad (15)$$

and the charge due to specific adsorption is given by,

$$\sigma_\beta = B([SO^-Na^+] - [SOH_2^+Cl^-]) \quad (16)$$

where B is a factor for conversion from concentrations, moles/liter, to surface charge, μ coulombs/cm^2.

$$B = \frac{10^6 F}{A}$$

where F = Faraday constant and A = surface area (cm^2/ℓ) of the solid substrate

containing the sites. For the species (SO^-Na^+) and ($SOH_2^+Cl^-$), the SO^- and SOH_2^+ are considered to be at the surface and contribute charge to the S-plane, while the Na^+ and Cl^- are in the compact layer and contribute charge to the β-plane.

The surface species are distributed among the total number of sites available. The total number of sites is then

$$N_s = [SOH] + [SOH_2^+] + [SOH_2^+Cl^-] + [SO^-] + [SO^-Na^+] \tag{17}$$

Electrical neutrality requires that

$$\sigma_o + \sigma_\beta + \sigma_d = 0 \tag{18}$$

The generalized relationship between diffuse layer charge and Ψ_d for a $z_+ : z_-$ electrolyte at 25°C is (Hunter and Wright 1971),

$$\sigma_d = -0.0587 \sqrt{C}\left[\frac{\Psi_d}{|\Psi_d|}\right]\left[\frac{1}{z_+}\left(\exp\left(-z_+ e \frac{\Psi_d}{kT}\right) - 1\right) - \frac{1}{z_-}\left(\exp\left(-z_- e \frac{\Psi_d}{kT}\right) - 1\right)\right]^{1/2} \tag{19}$$

where

C = electrolyte concentration

Ψ_d = mean potential at the start of the diffuse layer

e = unit electronic charge

There are two planes of fixed charge, the surface plane, σ_o, and the plane of bound counter ions, σ_β. The separation of charge allows the use of conventional molecular capacitor models (Grahame 1947) to relate charge density to potential gradient, i.e.,

$$\Psi_o - \Psi_\beta = \frac{\sigma_o}{C_1} \qquad \Psi_\beta - \Psi_d = -\frac{\sigma_d}{C_2} \tag{20}$$

where C_1, and C_2 are the integral capacitances of the surface to β and the β to d portions of the compact layer, respectively.

DETERMINATION OF INTRINSIC SURFACE IONIZATION AND EXCHANGE CONSTANTS

The intrinsic acid ionization and exchange constants needed for the model are not amenable to direct measurement since the surface activities of the reacting ions, e.g., $(H^+)_s$ and $(Na^+)_s$, are not directly measurable. However, the constants can be estimated from experimental acid-base titration data obtained on aqueous suspension of the solid material over a wide range of pH at several different electrolyte concentrations.

During acid and/or base titrations, a surface charge may be acquired by the solid surfaces if the transfer of positive and negative potential determining ions, e.g., $[H^+]$ and $[OH^-]$, is nonstoichiometric. The total net surface charge is the difference in the concentrations of the positive and negative sites, i.e.,

$$\sigma_o = B([C_A - C_B] - [C_H - C_{OH}]) \tag{21}$$

C_A and C_B are the total hydrogen ion and/or hydroxyl ion concentrations added to reach a point on the titration curve and C_H and C_{OH} are the measured concentrations of H^+ and OH^- at that point. For amphoteric surfaces, a point of zero charge (PZC) should be observed corresponding to zero net charge on the solid surface. Curves of pH versus amount of acid and/or base added for each of several electrolyte concentrations should intersect at a unique pH, the pH of the PZC. At lower pH values, the next charge is positive corresponding to the formation of an excess of positively charged surface sites, e.g., SOH_2^+ and $SOH_2^+Cl^-$, while at higher pH values the net charge is negative corresponding to an excess of negatively charged sites, e.g., SO^- and SO^-Na^+. At the PZC, the concentration of positive and negative sites are equal. Their concentrations are usually small but depend on the actual ionization and exchange constants of the sites. Furthermore, σ_o is dominated by uncomplexed species when the electrolyte concentration is very low and by complexed species when the electrolyte concentration is high. Thus, by selection of the appropiate range of pH and electrolyte concentrations, the experimental σ_o provides an estimate of the surface concentrations of one of four possible species that is dominant.

Surface Ionization Constants

At low electrolyte concentrations, the surface charge may be approximated as being due to simple acid dissociation, i.e., reactions (1) and (2). For pH values less than the PZC, the positive sites, SOH_2^+, are dominant and

$$(SOH_2^+) \cong \frac{\sigma_o}{B}, \quad (SOH) \cong \frac{N_s - \sigma_o}{B} \tag{22}$$

where total number of sites, N_s, is expressed in terms of charge/cm^2. Substitution in equation (8) gives

$$K_{a_1}^{int} \cong \frac{\frac{N_s - \sigma_o}{B} (H^+)_{aq}}{\frac{\sigma_o}{B}} \exp(-e\psi_o/kT) \cong Q_{a_1} \exp(-e\psi_o/kT) \tag{23}$$

In negative logarithmic form

$$pK_{a_1}^{int} = pH + \log \frac{\alpha_+}{1 - \alpha_+} + \frac{e\psi_o}{2.3kT} = pQ_{a_1} + \frac{e\psi_o}{2.3kT} \tag{24}$$

where

$$\alpha_+ = \text{fractional ionization of the positive site} \cong \frac{\sigma_o}{N_s}$$

Since the surface ionization constants are functions of both the surface ionization (or degree of ionization) and the electrolyte concentration, plots of pQ_{a_1} versus σ_o (or α_+) for each electrolyte concentration are first made. Smooth curves through the experimental points can be extrapolated to $\sigma_o = \alpha_+ = 0$ and provisional $pK_{a_1}^{int}$ values obtained for each electrolyte concentration. These provisional $pK_{a_1}^{int}$ values are then plotted as a function of electrolyte concentration, C, and extrapolation to C = 0 results in an estimate of $pK_{a_1}^{int}$.

As previously mentioned, zero surface charge does not mean zero concentration of charged sites but only equal concentrations of positively and

negatively charged sites, e.g., $SOH_2^+ = SO^-$. Thus, the approximation,

$$\left[SOH_2^+\right] \cong \frac{\sigma_o}{B}$$

is not valid for small values of σ_o and the calculated pQ_{a_1} diverges to infinity. Extrapolation to $\sigma_o = 0$ is made assuming a smooth, continuous variation of pQ_{a_1} with σ_o and the sharp divergence of the calculated pQ_{a_1} at small σ_o is ignored. This is a reasonable assumption since the function,

$$pK_{a_1}^{int} = pQ_{a_1} + \frac{e\Psi_o}{kT}$$

is a well behaved and a slowly varying linear function of σ_o at small values of σ_o.

Similar considerations for the region pH > PZC, where σ_o is negative, give

$$(SO^-) \cong \frac{|\sigma_o|}{B}, \quad (SOH) \cong \frac{N_s - |\sigma_o|}{B}, \text{ and } \alpha_- \cong \frac{|\sigma_o|}{N_s} \tag{25}$$

yields

$$pK_{a_2}^{int} \cong pH - \log \frac{\alpha_-}{1 - \alpha_-} + \frac{e\Psi_o}{2.3kT} \cong pQ_{a_2} + \frac{e\Psi_o}{2.3kT} \tag{26}$$

Again plots of pQ_{a_2} versus σ_o or α_- can be extrapolated to zero surface charge and electrolyte concentration to estimate $pK_{a_2}^{int}$

Exchange Constants

At high electrolyte concentrations, surface complexes dominate the contribution to surface charge formation, i.e, $SOH_2^+Cl^-$ and SO^-Na^+. For the region pH > PZC, SO^-Na^+ is assumed dominant and

$$(SO^-Na^+) \cong \frac{|\sigma_o|}{B}, \quad (SOH) \cong \frac{N_s - |\sigma_o|}{B} \quad \alpha_- \cong \frac{|\sigma_o|}{N_s} \tag{27}$$

Substitution of these equations into equation (13) yields

$$ {}^{*}K^{int}_{Na^+} \cong \frac{(H^+)_{aq}(\alpha_-)}{(Na^+)_{aq}(1 - \alpha_-)} \exp \frac{e\Psi_\beta - e\Psi_o}{kT} \cong {}^{*}Q_{Na^+} \exp \frac{e\Psi_\beta - e\Psi_o}{kT} \quad (28) $$

In negative logarithmic form,

$$ p^{*}K^{int}_{Na^+} \cong pH - \log \frac{\alpha_-}{1 - \alpha_-} + \log(Na^+) + \frac{e(\Psi_o - \Psi_\beta)}{2.3kT} \quad (29) $$

$$ \cong p^{*}Q_{Na^+} + \frac{e(\Psi_o - \Psi_\beta)}{2.3kT} $$

Similar considerations for the region pH < PZC at high electrolyte concentration, where

$$ (SOH_2^+Cl^-) \cong \frac{\sigma_o}{B}, \quad (SOH) \cong \frac{N_s - \sigma_o}{B}, \quad \text{and} \quad \alpha_+ \cong \frac{\sigma_o}{N_s}, \quad (30) $$

give

$$ p^{*}K^{int}_{Cl^-} \cong pH + \log \frac{\alpha_+}{1 - \alpha_+} - \log(Cl^-) + \frac{e(\Psi_o - \Psi_\beta)}{2.3kT} \quad (31) $$

$$ \cong p^{*}Q_{Cl^-} + \frac{e(\Psi_o - \Psi_\beta)}{2.3kT} $$

Again, plots of $p^{*}Q_{Na^+}$ and $p^{*}Q_{Cl^-}$ versus σ_o (or α_- and α_+) can be extrapolated to zero surface charge (or α) and high electrolyte concentration (usually taken as 1M) and the intrinsic exchange constants estimated.

THE COMPUTER PROGRAM MINEQL

DESCRIPTION

The components of water solutions are more often than not distributed among many species. The calcium in hard water, for instance, is likely to be present as bicarbonate and sulfate complexes in addition to free $Ca^{2+}(aq)$.

In an unsaturated solution of $CaSO_4$, exposed to atmospheric CO_2, for example, the components of the solution and species among which they are distributed are

H_2O: H^+OH^-

Ca^{2+}: Ca^{2+}, $CaHCO_3^+$, $CaCO_3^o$ (aq), $CaSO_4^o$ (aq)

SO_4^{2-}: SO_4^{2-}, HSO_4^-, $CaSO_4^o$ (aq)

CO_3^{2-}: CO_3^{2-}, HCO_3^-, $H_2CO_3^o$ (aq), $CaHCO_3^+$, $CaCO_3^o$ (aq)

If the analytical concentration of each component is known, the concentration of all eleven species can be calculated, since all are related through mass balances for each component, stability constants for each complex, and dissociation constants for water and the weak acids. Even in this simple system, simultaneous solution of the set of constraining equations is tedious.

MINEQL is a computer code designed to accept a list of components of a solution and their total analytical concentrations, solve the appropriate set of mass balance and equilibrium constant expressions, and produce a list of the identities and concentrations of all species formed by interaction among the components and between them and/or water.

An internal data set, THRM.DAT, contains the compositions and stability constants for most complexes (and solid precipitates) likely to form from commonly encountered components. MINEQL scans for possible interactions and searches THRM.DAT to select those for which stability constants are available. It is not

necessary to instruct the program that complexes will form if the data exist in THRM.DAT. (It is a simple matter to add new complexes or to edit stability constants through the input data set as well.)

The minimum essential input data set includes the list of components and total concentrations, a measure of total hydrogen and hydroxyl ions and the fixed pH and an ionic strength (assumed fixed in most current versions of MINEQL). Data processing involves reading the input solution composition, identifying the complexes expected, fetching the required stability constants, connecting the stability constants to the ionic strength imposed, and deriving the appropriate mass balance expressions. The resulting set of stability and mass balance expressions is solved by the Newton Raphson method, using satisfaction of the mass balances as the criterion of successful solution. The mathematical methods have been described in detail (Westall, Zachary and Morel 1976)

Precipitation and dissolution of solids can be included by extending the mass balance expressions to include solids. The output then includes the mass of precipitates formed or dissolved. Redox reactions are included as well by including the electron as a "component". Changes in computational constraints appropriate for the presence of solids or occurrence of redox reactions are part of the program; they are triggered by flags entered with the input information.

Simple sorption can be incorporated by writing the reaction as complexation with a surface site, or more specifically, if S: represents an sorption site, adsorption of $Hg^{++}(aq)$ could be represented as

$$Hg^{++}(aq) + S: = Hg:S \qquad (32)$$

If Hg actually adsorbs the dihydroxo complex, the reaction would be written

$$Hg(OH)_2(aq) + S: = Hg(OH)_2 : S \qquad (33)$$

For convenience in programming, this reaction would be written in the equivalent form,

$$Hg^{++}(aq) + 2\,H_2O + S: = S:Hg(OH)_2 + 2\,H^+ \qquad (34)$$

Any reaction can be incorporated into MINEQL if the reaction stoichiometry and equilibrium constants are known.

Ion exchange by clay can be introduced by treating the clay surface as a weak acid, SOH, which can dissociate,

$$SOH \rightleftarrows SO^- + H_s^+; \quad K_{a_2}^{int} = \frac{(SO^-)(H^+)_s}{(SOH)} \qquad (2)$$

or adsorb Na^+ in exchange for H^+,

$$SOH + Na_s^+ \rightleftarrows SO^-Na_s^+ + H_s^+; \quad {}^*K^{int}_{Na^+} = \frac{(SO^-Na^+)(H^+)_s}{(SOH)(Na^+)_s} \qquad (12)$$

$$SOH + Cs_s^+ \rightleftarrows SO^-Cs^+ + H_s^+; \quad {}^*K^{int}_{Cs^+} = \frac{(SO^-Cs^+)(H^+)_s}{(SOH)(Cs^+)_s} \qquad (35)$$

The MINEQL input data includes a new component, SOH, and the total concentration of SOH in the system. This concentration is equivalent to the cation exchange capacity of the system. The input must also include the information in equations 2, 12, and 35 including stoichiometry and equilibrium constants, since THRM.DAT includes no adsorption or exchange information.

Through manipulation of the input information, any of the common modes of describing cation exchange can be simulated. If the clay is assumed totally saturated with either Na^+ or Cs^+ at all times (SO^- and SOH << SO^+Na^+ or SO^-Cs^+), $K_{a_2}^{int}$ can be set arbitrarily small (SOH made a strong acid) and ${}^*K^{int}_{Na^+}$ and ${}^*K^{int}_{Cs^+}$ set >> $K_{a_2}^{int}$ with the absolute values arbitrary but ${}^*K^{int}_{Cs^+}/{}^*K^{int}_{Na^+}$ equal to the Cs/Na exchange constant. The exchange constant which describes the reaction

$$SO^-Na_s^+ + Cs_{aq}^+ \rightleftarrows SO^-Cs_s^+ + Na_{aq}^+$$

must be determined experimentally. For calculational purposes, the selectivity coefficient corrected for activities in solution, $K^{a}_{Cs/Na}$, is usually used.

Experimental values of $K^{a}_{Cs/Na}$ are often sensitive to pH and the ratio of Cs^+ to Na^+ on the clay, i.e.,

$$\frac{[SO^-Cs^+]}{[SO^-Na^+]} \quad \text{or} \quad \frac{[SO^-Cs^+]}{[SO^-Cs^+] + [SO^-Na^+]}$$

pH dependence can be introduced by experimental determination of $K^{int}_{a_2}$ as well as of $*K^{int.}_{Na+}$

Sensitivity to loading requires a solid-state activity correction which is beyond the state-of-the-art. A regular solution model has been described (Truesdell and Christ 1968; Garrels and Christ 1956) through which a semi-empirical solid state activity coefficient is introduced. This has not yet been used in MINEQL (to our knowledge).

Particles in water are electrically charged through partial dissociation of SiOH or AlOH groups or release of exchangeable ions. A correction for the effect of surface charge on the equilibrium constants of reactions near surfaces has been incorporated into MINEQL (Davis, James and Leckie 1978), i.e., the electrical double layer model.

Surface Charge Effects

If surface charge is finite, there must be a potential difference between the surface and the bulk solution. The resulting difference in activities of the ions near the surface and far from the surface is the work that must be done to bring the ion from zero potential to the surface potential, i.e. $Z_i e^{\Psi}_o/kT$, where Z_i is the charge on the ion. These corrections have been discussed previously, e.g., equations 5, 6 and 7.

Equation 8 can be written:

$$K^{int}_{a_1} = \frac{(SOH)(H^+)_{aq}}{(SOH^+_2)} \exp(-e^{\Psi}_o/kT)$$

The exponential term plays the same algebraic role as do the chemical species, thus the surface charge correction can be incorporated into MINEQL by including $\exp(-Ze\Psi_o/kT)$ as a component and including that "component" in defining the composition of complexes. A positive site produced by adsorption of H^+ onto SOH would be composed of one each of three components,

$$(SOH),\ (H^+),\ \left(\exp \frac{e\Psi_o}{kT}\right),$$

for example.

In the version of MINEQL developed by Davis, James and Leckie, to incorporate the surface charge correction, the Gouy-Chapman-Stern Grahame model of electrical double layer development is adopted. The equation relating surface charge, area, and potential are added to the chemical constraints and solved simultaneously. Charge is assumed to develop by ionization of surface sites; and potential develops in response to charge as required by the electrical double layer constraints. Adsorbing ions are assumed to approach the surface less closely than protons and a smaller potential is used in the exponential term which corrects for their altered chemical potential.

Input for computations involving electrochemical adsorption must include surface area, total site concentration, and the reaction and equilibrium constants responsible for charge development and adsorption in addition to the composition of the solution phase (Davis, James and Leckie 1978).

EXPERIMENTAL METHODS AND RESULTS

PREPARATION OF SOLUTIONS AND SOLID PHASES

Solutions

In order to investigate the effects of pH and supporting electrolyte concentration on the Cs sorption process, four solutions were first prepared with concentrations of 0.002M, 0.01M, 0.1M, and 1M in NaCl. In addition, a synthetic groundwater (SGW) was prepared with the chemical composition given

in Table 1 and had an ionic strength of 0.003M. The composition was similar to the groundwaters within Columbia River basalts and allowed a comparison of the effects of a mixed electrolyte of a more natural composition with the NaCl.

TABLE 1. Chemical Composition of Synthetic Groundwater

Component	Na	K	Ca	Mg	Fe	Al	HCO_3	Cl	SO_4	SiO_2
Concentration (mg/l)	30.0	5.0	10.0	5.0	0.1	0.01	65.0	27.8	24.0	25.0

Care was taken in the preparation of solutions so as not to introduce contaminants. All solutions were prepared with doubly-distilled deionized water from which CO_2 had been removed by boiling for about one hour followed by flushing with Ar. Ultrapure salt, obtained from Alfa Division of Ventron Corp., was used for preparing the NaCl solutions; analytical grade $NaHCO_3$, $CaSO_4 \cdot 2H_2O$, $CaCl_2$, KCl, $MgSO_4 \cdot 7H_2O$, $AlCl_3 \cdot 6H_2O$, $FeCl_2 \cdot 4H_2O$, and H_4SiO_4, from Mallinckrodt Inc., were used to prepare the synthetic groundwater.

Six portions of each of the five electrolyte solutions had their pH adjusted to 5, 6, 7, 8, 9, or 10 with ultrapure NaOH, from Alfa Division of Ventron, and were placed in an argon filled, inert atmosphere box. Since the effect of dissolved CO_2, i.e., HCO_3^- and CO_3^{2-} ions, on the sorptive properties of the solid substrates was unknown, it was decided to exclude CO_2 from the system. A final pH adjustment was made in the inert box just prior to use in the Cs sorption experiments.

Solid Phases

Min-u-sil

The Min-u-sil (SiO_2) was obtained from the Pennsylvania Glass Sand Corporation in the form of a fine powder (nominal 5 micron particle size). It was prepared from natural quartz sand from Berkeley Springs, West Virginia, by grinding in a silica lined ball mill using silica pebbles. Selection of

particle size was by air separation in a cyclone separator. The silica was first boiled twice in a 6M HNO_3-HCl mixture to dissolve and remove any iron contaminant introduced in the manufacturing process. After settling each time, the very finely suspended material was decanted off. The remaining leached material was filtered out on a fine glass frit and washed repeatedly with first 0.1M HCl and then deionized-distilled water. The material was then washed with 2M NaOH followed by 0.5M NaCl to produce the sodium form and repeatedly washed with deionized-distilled water to remove the excess salt. Each water wash was tested for residual chloride by adding $AgNO_3$. The washing was continued until no AgCl precipitate formed. The purified silica was then dried in an oven at 110°C, heated to 450°C for 12 hours to destroy organic material, and stored in a desiccator.

Belle Fourche Clay

The Belle Fourche clay (montmorillonite #27) was obtained from Ward's Natural Science Establishment, Inc., Rochester, N. Y. Three hundred grams of clay were first soaked in 8 liters of deionized water overnight with gentle stirring using an electric stirrer. The suspension was then filtered through a 350 mesh stainless steel screen to remove the coarse particles. The viscous filtrate was then diluted to a total volume of 16 liters and divided equally into four 4-liter beakers. The clay suspension was allowed to stand undisturbed for 48 hours. At the end of 48 hours the unsettled clay suspension was carefully decanted and the settled material discarded. The clay suspension was placed in 8-oz plastic bottles and centrifuged at 5,000 rpm for ten minutes using a Sorval high-speed preparative centrifuge. Particles less than 1 micron remained in the supernatant and were discarded (Jackson 1975, p.110).

To remove the iron and aluminum oxides on the clay, extraction with acid ammonium oxalate was selected (McKeague and Day 1966). This method was used in preference to the citrate-dithionite method because of less possible structural alteration of the clay. The clay particles were stirred in 8 liters of 0.2M ammonium oxalate solution and the pH adjusted to 4.0 using 1.0N HCl. At the end of 24 hours, the clay suspension was centrifuged and rinsed twice with deionized water. To remove the amorphous silica imbedded between the layers

of the clay particles, hot caustic extraction was employed (Jones and Bower 1977, p.197). To each of the plastic centrifuge bottles containing the clay, 0.5M NaOH was added. The mixtures were stirred and placed in a 95°C water bath for 1 hour. At the end of the extraction period, they were centrifuged and washed. To fully convert the clay particles into the sodium form, the solid phase was rinsed twice with 0.5M NaCl and then once with deionized water to remove the excess salt before dialysis. The sodium clay, still containing large amounts of salt, was placed in a cellulose acetate dialysis bag and dialyzed against deionized water in a 4-liter beaker with constant agitation (Keren, Gast and Barnhisel 1977). To shorten the dialysis time, frequent 30-minute water changes were necessary. The silver nitrate method was used to monitor the progress of dialysis. When no cloudy precipitate was formed on addition of 0.1N $AgNO_3$ to the dialysate, dialysis was considered to be complete. The purified clay suspension was then removed from the dialysis bag and diluted with deionized water and stored in a plastic container for subsequent experiments.

Characterization of Solid Phases

Chemical Analyses

In order to check the purity of the samples, both the Min-u-sil and the Belle Fourche clay were sent to John Husler of the University of New Mexico for chemical analyses.

Silica was determined gravimetrically by fusion with Na_2CO_3, dehydration with HCl, and weighing as SiO_2. Sulfur was determined on the filtrate by precipitation with $BaCl_2$ and weighing as $BaSO_4$ (Koltoff, Sandell, Meeham and Bruckenstein 1969, p.602). Total Fe, Al, Mg, Ca, Na, K, Ti, Mn, and Sr were determined by atomic absorption spectrophotometry by a method developed by Husler (Husler 1972). The P was determined by a colorimetric method (Husler 1972). The H_2O^- was determined by weight loss at 110°C and the loss on ignition, H_2O^+, was determined by weight loss from 110°C to 1000°C. The Fe^{2+} was determined by volumetric titration with standardized $K_2Cr_2O_7$ (Koltoff, Sandell,

Meeham and Bruckenstein 1969, p.839). In addition, trace element analysis of the clay was done by Helen Michels of LBL by neutron activation analysis. The results of the analyses are given in Table 2.

The chemical composition of the clay was typical for a smectite and very similar to a reported composition of smectite from Upon, Wyoming (Grim 1968, p.578). The K concentration in our sample was considerably less than the Upon clay (0.6%) however, probably due to replacement by Na during the processing of our clay. There was no evidence for Cs of sufficient concentration to interfere with the subsequent sorption measurements.

The Min-u-sil contained considerably larger amounts of Fe, Mg, Ca, Na, K, and Al than is usually found in pure quartz; these elements are usually present in the few parts per million range (Deer, Howie, and Zussman 1963. p.191). Our results are consistent with the analyses supplied by the manufacturer, i.e., 99.6% SiO_2, 0.10% Al_2O_3, 0.019% TiO_2, and 0.023% Fe_2O_3. Apparently most of the iron was surface or particulate contamination and was removed during our processing. The proportions of the cations suggest the presence of a small amount (a few tenths of a percent) of other silicate minerals.

Particle Size

Scanning electron microscopy was used by Barry Scheetz of Pennsylvania State University to measure the particle sizes and size distributions of the Min-u-sil and Belle Fourche clay samples. Summarizing the data, the average particle size for the Belle Fourche clay was 1.14 microns with 90% of the particle sizes in the range 0.5 - 2.0 microns; the average size for the Min-u-sil was 2.42 microns with 90% in the range 0.28 - 4.56 microns.

Surface Areas

Total surface area is required in the calculation of layer charges and potentials. Surface area measurements of the purified clay and quartz were performed by the nitrogen adsorption technique, i.e., the BET method (Jackson 1975, p.335). For the clay, approximately 2 milliliters of the stock suspension

TABLE 2. Chemical Composition of Solid Substrates.

Component[1]	Chemical Analysis (%) Min-u-sil	Belle Fourche Clay	Component	Activation Analysis[2] Belle Fourche Clay
SiO_2	98.92	55.73	Al	11.0 ± 0.1 %
Al_2O_3	0.20	22.17	Mg	2.2 ± 0.7 %
Fe_2O_3	0.006	3.71	Ca	< 1.0 %
FeO	--	0.02	Ti	700 ± 320
MgO	0.007	2.18	V	< 37
CaO	0.004	0.65	Dy	2.37 ± 0.05
Na_2O	0.006	2.70	Mn	8.0 ± 0.6
K_2O	0.014	0.023	Na	1.99 ± 0.03 %
H_2O^+	0.22	6.08	K	0.17 ± 0.13 %
H_2O^-	0.04	6.61	Sr	82 ± 36
TiO_2	< 0.05	0.14	U	1.03 ± 0.03
P_2O_5	< 0.01	< 0.01	Th	3.62 ± 0.18
MnO	<0.001	0.002	Sm	3.42 ± 0.02
SrO	<0.003	0.013	La	18.4 ± 0.02
SO_3	<0.1	--	Nd	16.1 ± 1.0
			Mo	1.1 ± 0.5
Total	99.42	100.03	W	2.8 ± 1.4
			Ba	< 12
			Co	0.50 ± 0.06
			Sc	6.12 ± 0.03
			Fe	2.62 ± 0.04 %
			Cr	2.41 ± 0.59
			Rb	3.5 ± 2.4
			Cs	< 0.28
			Ce	32.9 ± 0.7
			Hf	7.56 ± 0.09
			Ta	2.56 ± 0.03
			Yb	1.17 ± 0.02
			Eu	0.23 ± 0.01

1 Reported as shown.
2 ppm except when stated %.

were carefully introduced into a weighed sample holder with the aid of a syringe fitted with teflon tubing. The sample was then freeze-dried. After drying, the sample tube was kept in a 100°C oven overnight to prevent surface adsorption of moisture. The tube was weighed and the actual weight of the clay obtained by subtracting the weight of the sample holder. The surface area determined by this method was 18.1 m^2/gram. For the quartz, 0.5 g samples of the dried material were used. The measured surface area for the Min-u-sil by this method was 3.03 m^2/g.

The value obtained for the clay was considerably lower than the theoretical value of ~800 m^2/g from unit cell dimensions (Grim 1968, p.464; van Olphen 1977, p.254). However, the BET method measures only the exposed external surface area of the particles and not the interlayer surface areas (Grim 1968, p.464). Further, the exposed external surface area of the clay varies with the degree of aggregation, i.e., face-to-face association. Therefore, surface areas obtained by the BET method show a wide variation for clay, e.g., values in the range of 30 - 150 m^2/g (Alymore 1977, p.148). Water vapor adsorption methods are thought to measure both internal and external surface areas for montmorillonite and give values of 150 - 250 m^2/g (Grim 1968, p.265). Aggregation seems also to effect the values. Alternative methods to determine total internal and external surface areas are based on the adsorption of polar organic compounds from the liquid phase, e.g., adsorption of cetyl pyridinium bromide has been used and gave 800 m^2/g (Greenland and Quirk 1962) while ethylene glycol adsorption has been found to give values of 700 - 800 m^2/g for montmorillonite (Morin and Jacobs 1964). Methods based on adsorption of negative ions yielded values of 470 - 560 m^2/g (Edwards and Quirk 1962). With these methods, difficulties are encountered due to surface changes produced by heating and drying, surface contamination, and in obtaining only monolayers of adsorbed molecules. For our modeling calculations, the theoretical value of 800 m^2/g is probably the most appropriate and reliable.

The B.E.T. method does appear to be reliable for the measurement of external surface areas of simple materials such as silica. In fact, some form of silica is frequently used as a standard for calibration.

Cation Exchange Capacities

Cation exchange capacities, CEC, are needed for calculating loading fractions used in data evaluation as well as for measurement of site density for modeling calculations. The Na, K, Ca, Cs, and NH_4 cation exchange capacities were determined for the Belle Fourche smectite and the Min-u-sil. For the clay, the procedure of M. L. Jackson (Jackson 1975, p.253) was closely followed. The method involved washing an accurately weighed sample in a tared centrifuge tube with a 0.5M solution of the chloride salt of the cation to be loaded on the clay. This was followed by five washings with 0.01M salt solution. After centrifugation and removal of the solution phase, the excess 0.01M solution remaining with the sample was determined by again weighing the tube. To desorb Na, K, or Cs, the sample was rinsed with 0.5M NH_4Cl five times with centrifugation between rinsings. For Ca and NH_4 desorption, 0.5M $MgCl_2$ and 0.5M NaCl solutions, respectively, were used. The combined rinse was diluted and the concentration of Na, K, Cs, or Ca determined by atomic absorption using a Perkin Elmer model 306 spectrophotometer. To determine ammonia, three methods were tested. For samples with high cation exchange capacities and therefore high concentrations of ammonium ion, a simple macro-kjeldahl determination could be used directly on the mineral sample. For samples with low exchange capacities, either Nessler's method (Hawk, Oser, and Summerson 1965, p.878) or the Ninhydrin method (Hawk, Oser, and Summerson 1965, p.892) could be used. Nessler's method is about thirty times more sensitive than the Kjeldahl method and can detect NH_3 down to the 1 ppm level. The Ninhydrin method is even more sensitive and can detech NH_3 down to the 10^{-9}M level. Both Nessler's and the Ninhydrin methods involve the formation of colored complexes that can be quantitatively detected spectrophotometrically.

In order to avoid the loss of particles during decantation in processing of the Min-u-sil, the procedure was modified to placement of the samples in a column with a glass fritted disk at the outlet. The weight of the column was determined by weighing. The salt solution used to load the sample with the appropriate cation was poured through the column slowly (~30 ml/hr). The saturated solid was then rinsed with the 0.01M salt solution and the excess solution remaining on the column determined by weighing as before. To elute the

cations, the appropriate desorption solution (given above) was passed through the column. The eluate was collected and the concentrations of cations determined as before. The results of the cation exchange capacity measurements for duplicate samples are given in Table 3.

TABLE 3. Cation Exchange Capacities (meq/100g)

Cation	Na^+	K^+	Ca^{2+}	Cs^+	NH_4^+
Min-u-sil	0.22	0.26	1.25	0.45	0.95 (N)
Belle Fourche Clay	120	131	146	119	91.4 (NH)
					97.2 (K)

N = Nessler, K = Kjeldahl, NH = Ninhydrin

Cation exchange capacities of a given mineral vary with a number of factors, e.g., source, pretreatment, etc. A range of 80 - 150 milliequivalents (meq) per 100 g has been reported (Grim 1968, p.189) for smectite. It was expected that all of the cations used in the CEC determinations would give about the same value for the clay (van Olphen 1977, p.255) i.e., 90 - 95 meq/100 g. The discrepancy between NH_4 and the other monovalent ions is bothersome since it was originally felt that the methods for determining ammonia were more reliable than those for the other ions.

The total surface site concentration, N_S, is an input parameter for the calculations using MINEQL, e.g., equations 22, 25, 27, and 30. In the case of clays, the experimental CEC appears to be a good measure of N_S, i.e., nearly all of the hydrogen on the sites has been exchanged for the electrolyte cations (James and Parks 1979). However, for SiO_2, standard methods for measuring CEC underestimate the total number of sites considerably (Allen, Matijevic and Meites 1971). For example, at pH 7 and 1M NaCl electrolyte concentration (typical conditions for loading cations in CEC measurements), only about 10% of the sites may have been converted from the hydrogen form to the sodium form. Calculated site concentrations based on measured surface areas appear to give

a more accurate estimate for N_s (Yates 1975) and it is N_s that is needed as input to MINEQL. Yates has estimated a site density for SiO_2 of 5 sites/nm^2 from structural considerations. Using this value and our measured surface of 3.03 m^2/g, a site concentration of 2.52 meq/100 g was calculated assuming one equivalent is equal to Avogadro's number of sites.

DETERMINATION OF INTRINSIC SURFACE IONIZATION AND EXCHANGE CONSTANTS

Potentiometric Titrations

Potentiometric acid/base titration of a sol provides a direct measure of surface charge, σ_0, through equation 21. From a mass balance of the potential determining hydrogen and hydroxyl ions added to the sol compared to the measured amounts in the solution, the concentration of excess or the deficiency of H^+ ions on the surface can be calculated. As described in the section on the electrolyte binding electrical double layer model, σ_0 can be used to approximate the concentrations of different surface species, i.e., SO^-, SO^-Na^+, SOH_2^+, and $SOH_2^+Cl^-$ under certain conditions of pH and supporting electrolyte concentration. Using this information and the total site density, estimates of the intrinsic surface ionization and exchange constants can be made for input to the computer program MINEQL. Since the surface charge is a function of surface ionization itself, as well as supporting electrolyte concentration, a series of titrations over a wide range of pH and electrolyte concentrations are needed.

Procedures

Titrations were carried out on the acid forms of the Min-u-sil and the Belle Fourche clay. The acid form of the quartz was prepared by washing a few grams in a glass column with 0.1M HCl followed by doubly distilled deionized water to remove the excess acid. In the case of clay, it has been reported that it is nearly impossible to prepare a clay in which all the exchange sites are occupied by hydrogen ions, since Al^{3+} moves from the lattice to exchange positions before saturation with H^+ is completed (Grim 1968, p.210). It was suggested that a better method for preparing the hydrogen form of the clay is by

cation exchange with the hydrogen form of an organic ion exchange resin (Grim 1968, p.210). In our case, an aqueous suspension of the clay (0.02 g/ml) was passed through a 2.5 cm diameter by 14 cm long column of 100 - 200 mesh Dowex 50 x 8 cation exchange resin.

A small polyethylene cell (~200 ml capacity) was used to carry out the titrations under an inert atmosphere of argon and at a temperature of 26°C. Acid/base titrations of the purified water and the NaCl solutions to be used in the quartz and clay titrations were first made in order to detect and eliminate any contaminants in the system that could produce titration errors, e.g., carbon dioxide or acid-base impurities from the reagents. Cyclic titrations with first 0.05M HCl followed by 0.05M NaOH were conducted for two cycles over the pH region 3 - 11. A shift in the equivalence point between cycles of less than the volume of titrant used between successive titration points, 50 microliters, was considered adequate. It was found that the argon (99.998%) obtained from the standard manufacturer's cylinders needed to be purified. The purification system consisted of a CO_2 trap, dilute H_2SO_4 scrubber, a water scrubber, and a drying trap. Slightly improved results were also obtained when ultrapure grades of acid, base, and NaCl were used.

The first step in the titration of the sol was the determination of the pH of 100 ml of CO_2-free, purified water or salt solution, i.e., the initial H^+ ion concentration of the aqueous phase. Then, either 1 gram of clay or 10 grams of quartz was added to the aqueous phase and the pH again measured after stirring for ~ 5 minutes with a magnetic stirrer. For Min-u-sil, small portions, usually 50 microliters, of 0.05M HCl were added in steps until the pH was reduced to about 3.5. The suspension was then back-titrated in steps with 0.05M NaOH until the pH reached 8 - 9. At each step in the titration the resulting pH was measured. It usually required from 5 - 20 minutes for the readings to stabilize after stirring was stopped.

After addition of the clay to the water or NaCl solutions, the pH dropped to 3 or less. Because of the danger of structural alteration, further reduction of the pH with acid was omitted. Therefore, the clay was titrated only with base from the starting pH to pH ~ 11.

Results.

The results of a series of titrations of the Min-u-sil for 6.5 x 10^{-5}M, 0.001M, 0.01M, and 0.1M concentrations of NaCl are shown in Figure 1. The first value was the residual Na concentration in the sample with no sodium chloride added as determined by atomic absorption. For clarity, only the back titrations with base are shown. The curves for the four electrolyte concentrations converge at low pH values and cross at a pH of about 3.9, i.e., the point of zero charge.

The results obtained for the Belle Fourche clay at several electrolyte concentrations are shown in Figure 2. The residual Na concentration in the clay sample with no sodium chloride added was 0.0002M. A PZC was not observed in the pH range investigated. The titration curves appear to be made up of more than one component. One site being neutralized from the initial pH to pH ~ 5.5 and the other from pH ~ 5.5 to ~ 11. To distinguish between the two sites, the first is frequently called SOH sites and the second TOH sites. This is typical behavior for montmorillonite and is usually interpreted as resulting from the successive neutralization of two energetically different exchange sites with differing acid constants (Garrels and Christ 1956).

Figure 3 shows the surface charge as a function of pH calculated for Min-u-sil from the titration data, while Figure 4 is a similar plot for the Belle Fourche clay. The surface charge was calculated for each titration point using equation 21, i.e.,

$$\sigma_o = \frac{10^6 F}{A}\left[(H^+)_o - (OH^-)_o\right]\frac{V_o}{\gamma_o} + C_A V_A - C_B V_B - \left[(H^+)_1 - (OH)_1\right]\frac{V_1}{\gamma_1} \quad \mu C/cm^2. \tag{36}$$

F = Faraday constant, coulombs/equivalent

A = total surface area of sample, cm^2

$(H^+)_o$, $(OH^-)_o$ = measured H^+ and OH^- ion activities of the starting electrolyte solution of starting volume V_0 (liters)

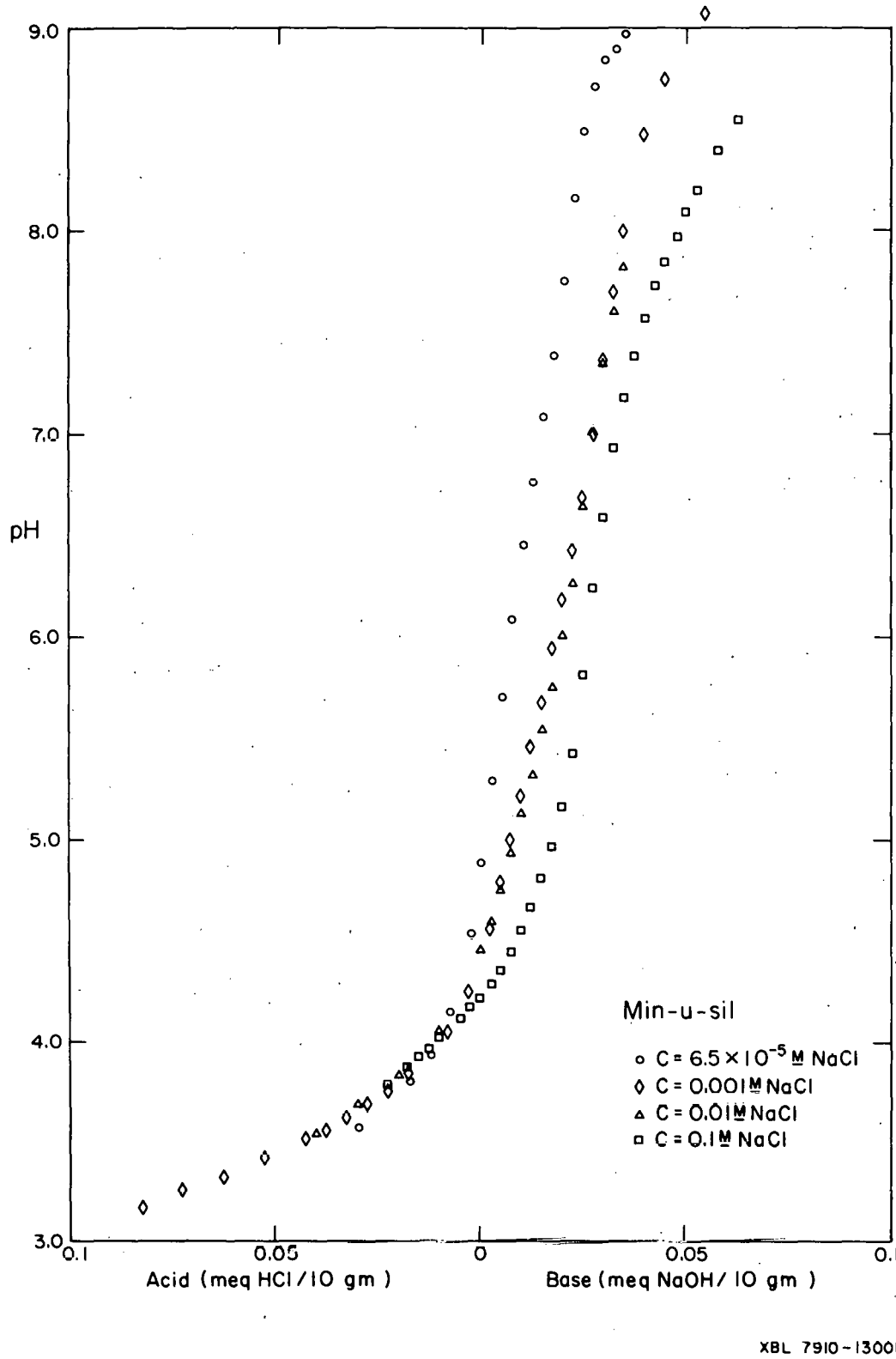

FIGURE 1. Potentiometric acid/base titration curves for Min-u-sil in aqueous suspension as a function of NaCl electrolyte concentration.

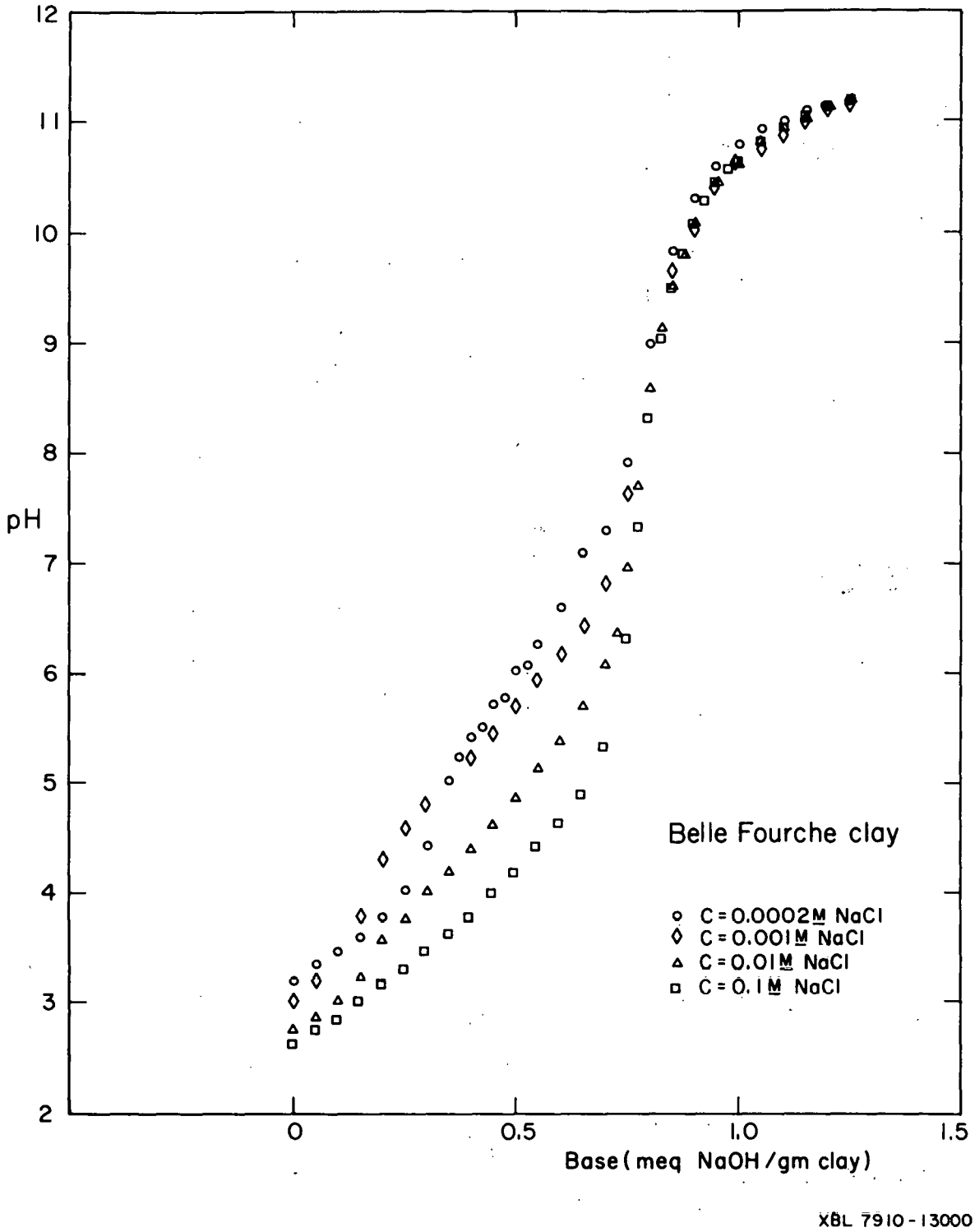

FIGURE 2. Potentiometric base titration curves for Belle Fourche clay in aqueous suspension as a function of NaCl electrolyte concentration.

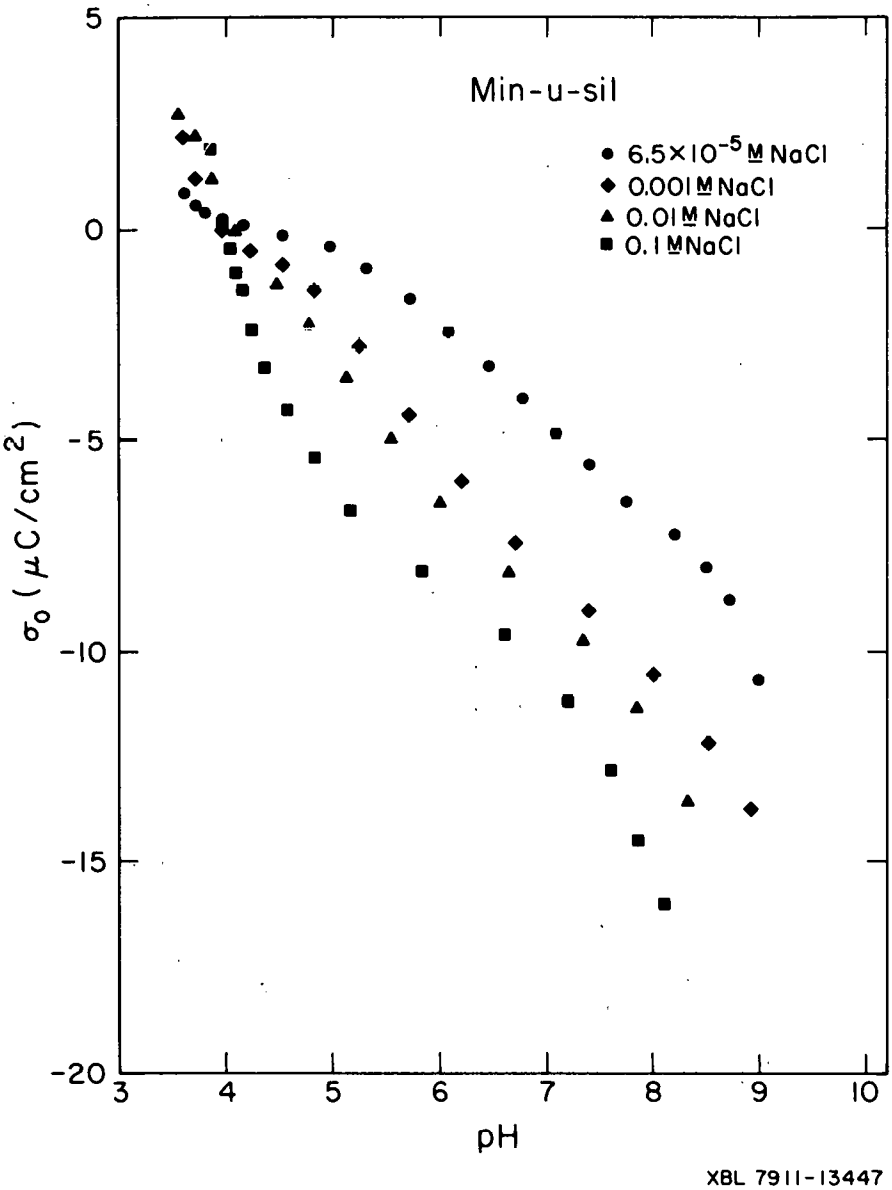

FIGURE 3. The surface charge, σ_0, of Min-u-sil in aqueous suspension as a function of pH and NaCl electrolyte concentration. Calculated from titration data.

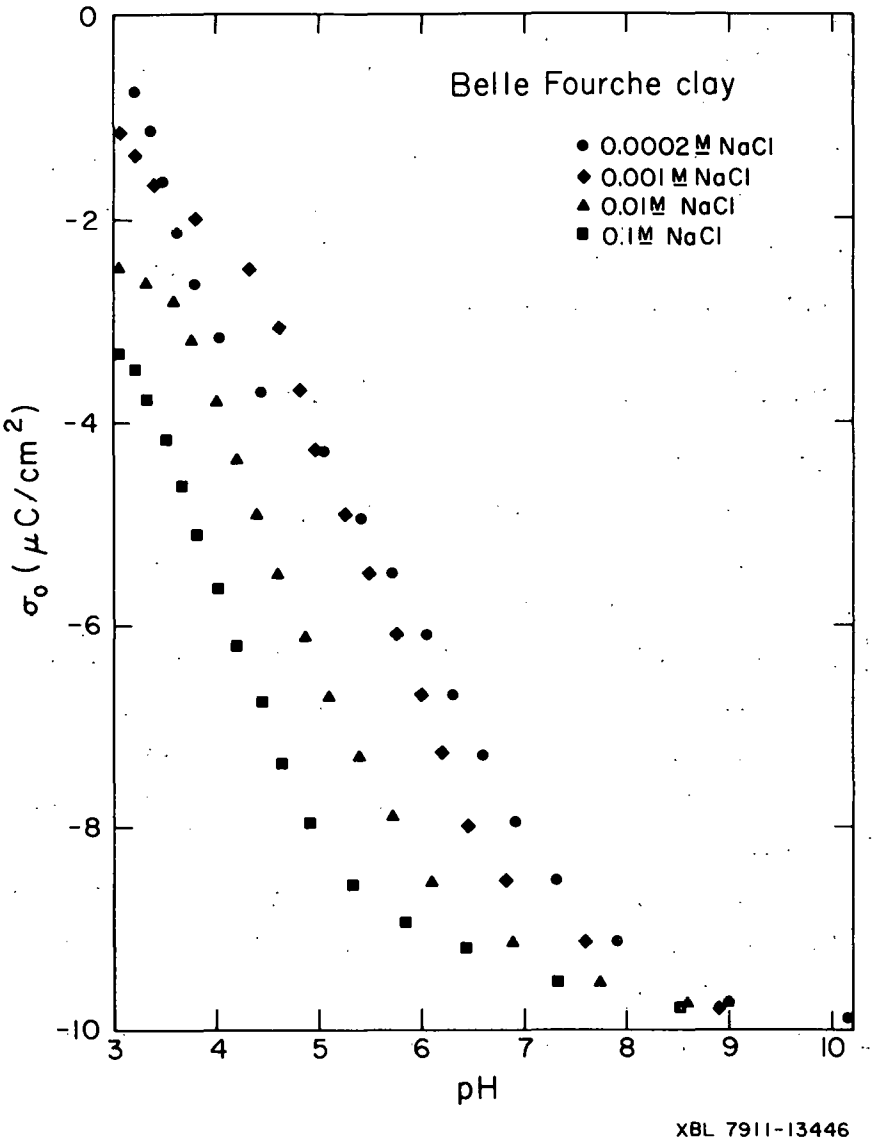

FIGURE 4. The surface charge, σ_o, of Belle Fourche clay in aqueous suspension as a function of pH and NaCl electrolyte concentration. Calculated from titration data.

C_A, C_B = molar concentration of acid and base used for titration

V_A, V_B = volume of acid and/or base used to reach a given point 1 on titration curve, liters

$(H^+)_1$, $(OH^-)_1$ = measured H^+ and OH^- ion activities at a given point on titration curve

V_1 = total volume at a given point on titration curve, $V_o+V_A+V_B$

γ_o, γ_1 = activity coefficients of H^+ and OH^- used to convert activities to concentrations. Calculated using Davies equation (Butler 1964, p.437).

Estimates of Intrinsic Constants by Double Extrapolation

Estimates of the intrinsic surface ionization and exchange constants can be made using the surface charge information derived from the titration data. Since the Cs sorption isotherms were measured over a pH range of 5 - 10, i.e., pH >> PZC, the surface charge is always negative and the constants of interest are K_{a2}^{int} and $^*K_{Na^+}^{int}$. The approximations that are used and the appropriate equations, 25, 26, 27 and 29, were given previously in the section describing the e.d.l. model. Since the intrinsic constants are functions of both the degree of ionization of the surface or surface charge and the concentration of supporting electrolyte, C, a double extropolation procedure has been developed (James, Davis and Leckie 1978). For the estimates of pK_{a2}^{int}, pQ_{a2} is plotted versus $\alpha_- + \sqrt{C}$. The square root of C is used rather than C itself to spread the data more evenly and conveniently for graphic extrapolations. The shapes of the curves depend upon α_-. The $\sqrt{C}$ only shifts the curves relative to each other.

Figure 5 shows plots of the pQ_{a2} versus $\alpha_- + \sqrt{C}$ for Min-u-sil for the several different electrolyte concentrations. The fractional ionizations, α_-, for Min-u-sil were calculated using the estimated value of 0.0252 meq/g for the total site concentration, N_s, or 80.2 $\mu C/cm^2$ in terms of charge. For each NaCl concentration, a smooth curve through the experimental points is drawn and the nearly linear, decreasing portion at low values of α_- is extrapolated to intersect the vertical line $\alpha + \sqrt{C} = \sqrt{C}$. At this point α_o is zero. These

extrapolations produce the open symbols in Figure 5. A smooth curve is then drawn through these points and extrapolated to $\alpha_- + \sqrt{C} = 0$, where both α_0 and C are zero. This intercept is taken as an estimate for pK_{a2}^{int}.

For an estimate of $p^*K_{Na^+}^{int}$, it is convenient to plot $p^*Q_{Na^+}$ versus $\alpha_- - 1/10 \log C$. Figure 6 shows such plots for Min-u-sil for the different electrolyte concentrations. Extrapolation of smooth curves through the points to $\alpha_- - 1/10 \log C = -1/10 \log C$ yields the open symbols. Extrapolation of a smooth curve through the open symbols to $\alpha_- - 1/10 \log C = 0$ yields a value for $p^*Q_{Na^+}$ for C = 1M. This value is customarily taken as an estimate for $p^*K_{Na^+}^{int}$

There is some arbitrariness involved in the extrapolations. However, this method is useful for obtaining a first-estimate for the intrinsic constants. These values can then be starting values for input to MINEQL. By fitting calculated titration curves using MINEQL with the experimentally determined ones, refinements in the values of the intrinsic constants can be made.

Application of the double extrapolation method to the clay did not produce reliable results. At the starting point of the titration, the SOH sites are already 20 to 30% ionized depending on the salt concentration, i.e., $\alpha_- = 0.2$ to 0.3. Plots of pQ_{a2} or $p^*Q_{Na^+}$ versus a_- (or a_- plus the appropriate function of C) did not produce regions of points where a smooth curve could be drawn and extrapolated to $\alpha_- = 0$ with any confidence as for Min-u-sil. As an example, a plot of pQ_{a2} versus $\alpha_- + \sqrt{C}$ for the SOH sites is shown in Figure 7. For the TOH sites, a similar problem in the extrapolations occurs. A surface charge builds up during the titration of the SOH sites and the effect on the subsequent ionization of the TOH is not known. Extrapolation to $\alpha_- = 0$ in this case does not mean $\sigma_0 = 0$. Plots of pQ_{a2} or $p^*Q_{Na^+}$ versus some function of σ_0 seem appropriate, however, extrapolation from the data points for the TOH sites to $\sigma_0 = 0$ is quite long, from 4 - 5 $\mu c/cm^2$ to 0, and rather meaningless. Therefore, estimates of the intrinsic constants from fitting curves calculated by MINEQL to the experimental titration curves is probably the best recourse. Simpler methods of reliably estimating the intrinsic constants from the titration data are being explored.

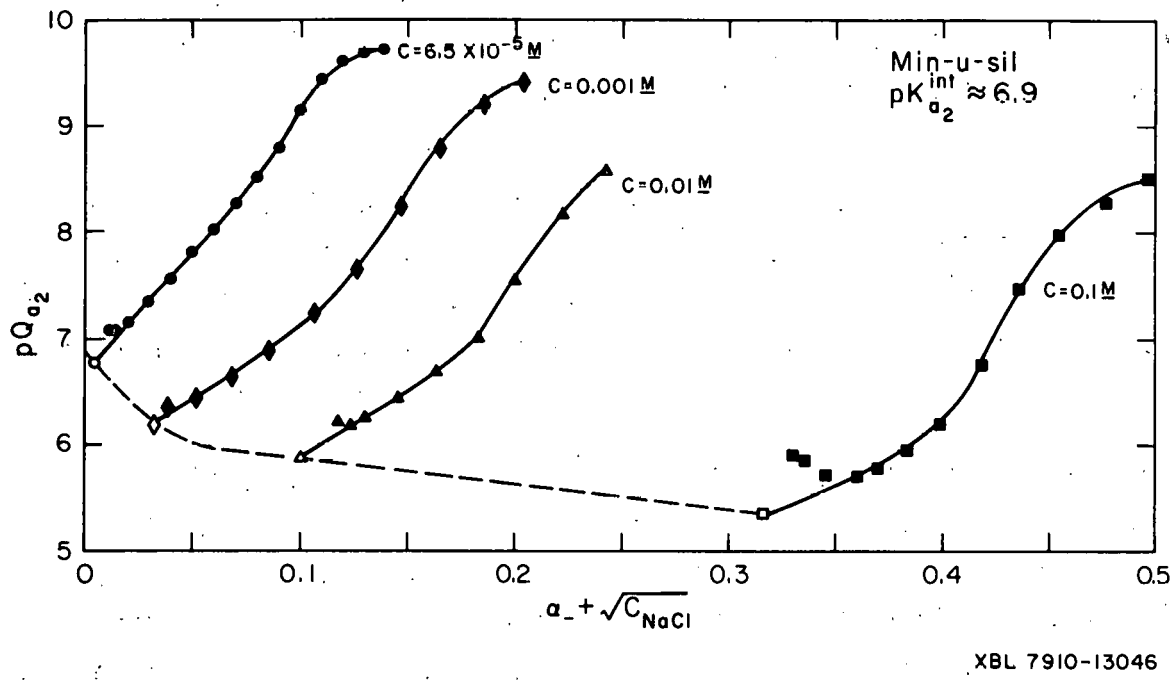

FIGURE 5. Double extrapolation plot for the estimation of pK_{a2}^{int} showing the variation of the surface acidity quotient, pQ_{a2}, for the dissociation of the negative sites on Min-u-sil in aqueous suspension at 26°C with the fractional ionization, α_-, and the NaCl electrolyte concentration.

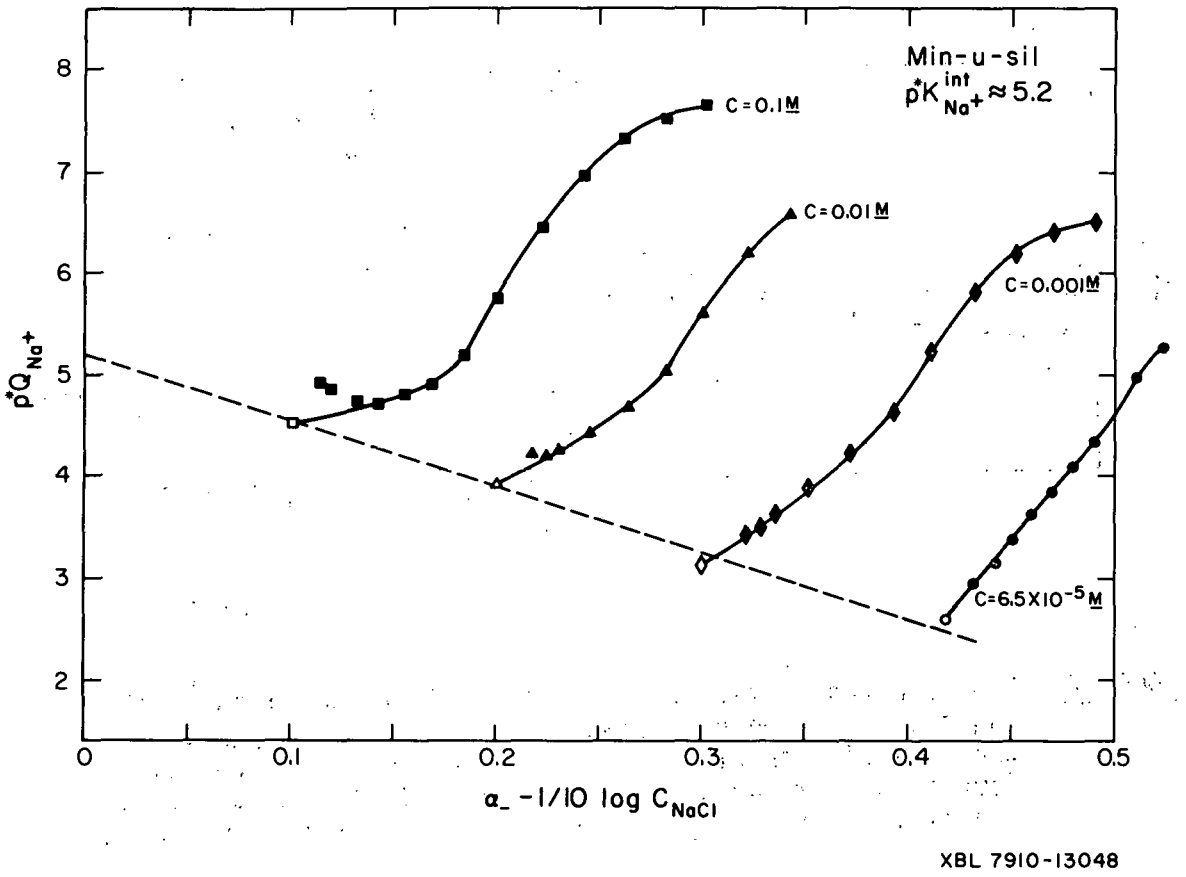

FIGURE 6. Double extrapolation plot for the estimation of $p^{*int}K_{Na^+}$ showing the variation of the Na exchange quotient, $p^*Q_{Na^+}$, for the negative sites on Min-u-sil in aqueous suspension at 26°C with the fractional ionization, α_-, and the NaCl electrolyte concentration.

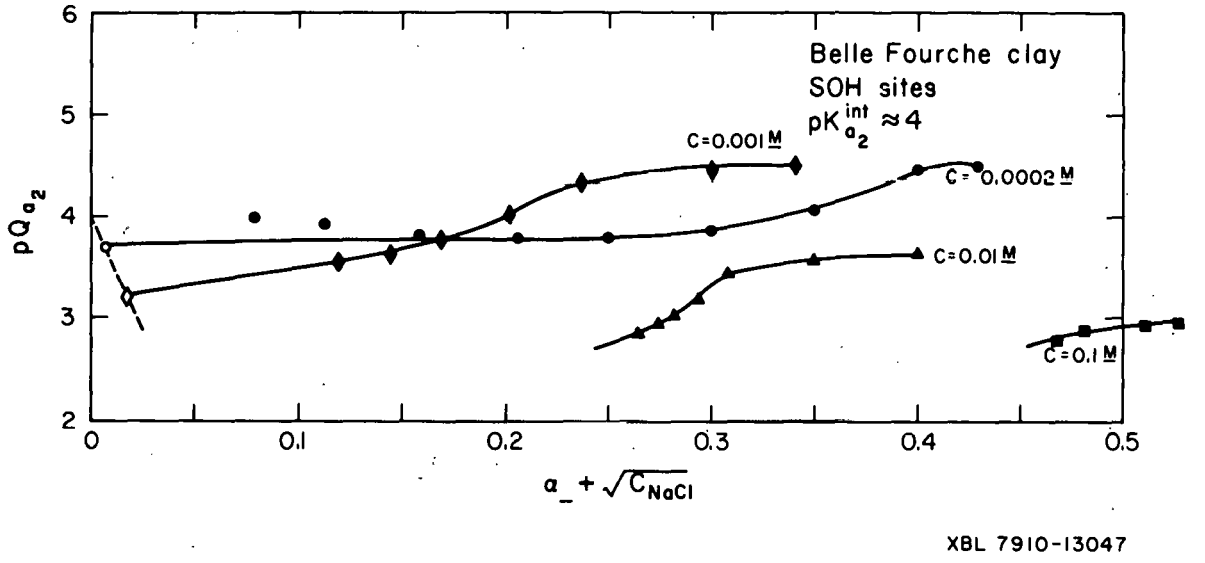

FIGURE 7. Double extrapolation plot for the estimation of pK_{a2}^{int} showing the variation of surface acidity quotient, pQ_{a2}, for the dissociation of the negative SOH-type sites on Belle Fourche clay in aqueous suspension at 26°C with the fractional ionization, α_-, and the NaCl electrolyte concentration.

DETERMINATION OF Cs SORPTION ISOTHERMS

Procedures

Cesium sorption isotherms using the sodium form of the Belle Fourche clay and Min-u-sil were obtained as a function of Cs concentration, pH, and supporting electrolyte concentration in batch-type experiments. The initial Cs concentrations ranged from 10^{-3}M to 10^{-9}M for the clay and 10^{-4}M to 10^{-9}M for the quartz; pH values were 5, 6, 7, 8, 9, and 10; electrolyte solutions were 0.002M, 0.01M, 0.1M, and 1M NaCl and the simulated groundwater.

Clay and quartz suspensions of approximately 500 ml volumes were made up to each of the five different electrolyte concentrations. The pH of 75 ml portions of each of these suspensions was adjusted to a given value with microliter amounts of 0.05M HCl or 0.05M NaOH and the solutions were transferred to the inert box. Just prior to the sorption measurements, the pH of the solutions were checked and readjusted if necessary. Ten ml portions of each of these solutions of a given pH were placed in polyethylene bottles and 10 microliter aliquots of different concentrations of stock Cs solutions, "spiked" with ^{137}Cs tracer, were also added. The solutions were agitated for 15 - 20 minutes. The sorption of Cs as a function of time was investigated in separate experiments and no detectable increase in sorption was measured after 15 minutes. Approximately 3 ml of the suspensions were then centrifuged for 3 minutes at 12,000 rpm. The supernates were filtered through 0.2 micrometer pore size filters. Exactly one ml portions of the filtrates were analyzed for ^{137}Cs content by γ-ray counting using a 3" x 3" NaI crystal.

Results

Since the concentration (and radioactivity) of the influent Cs solutions had previously been measured, the determinations of the ^{137}Cs radioactivities (and thus total Cs concentrations) in the effluent solutions allowed the calculation of K_d's.

$$K_d = \frac{1 - f}{f} \cdot \frac{v}{w} \qquad (37)$$

where

f = fraction of influent Cs remaining in solution
v = volume of solution (ml)
w = weight of clay or quartz (g)

The results of the Cs sorption isotherm measurements at 26 ± 2°C are summarized in Tables 4 - 15. Also shown are the final Cs concentrations in solution, C_f, and on the substrate, L_{Cs}. The assigned errors result from a consideration of errors associated with counting and sampling. Duplicates were run on only about 10% of the samples and agreements were within the estimated error.

The equation for the exchange of the monovalent cations Cs^+ and Na^+ between the solid surface, s, and the aqueous solution, a, may be written as

$$SO^-Na_s^+ + Cs_a^+ \rightleftarrows SO^-Cs_s^+ + Na_a^+ \tag{38}$$

The mass action expression for the thermodynamic equilibrium constant is

$$K_{Cs/Na} = \frac{[SO^-Cs^+]_s[Na^+]_a}{[SO^-Na^+]_s[Cs^+]_a} \cdot \frac{\gamma_{Na^+}\ \gamma_{SO^-Cs^+}}{\gamma_{Cs^+}\ \gamma_{SO^-Na^+}} \tag{39}$$

where the first term is expressed in concentrations of ions on the surface and in the solution phases and the second term contains the corresponding activity coefficients. The latter equation can be written as (Helfferich 1962, p.154)

$$K_{Cs/Na} = K^a_{Cs/Na}\ \frac{\gamma_{SO^-Cs^+}}{\gamma_{SO^-Na^+}} \tag{40}$$

The Cs/Na selectivity coefficient corrected for activities in solution, $K^a_{Cs/Na}$, can be determined experimentally since it is made up of quantities that can be measured or estimated. In logarithmic form with rearrangement,

$$\log\frac{(SO^-Cs^+)_s}{(SO^-Na^+)_s} = \log K^a_{Cs/Na} + \log\frac{(Cs^+)_a}{(Na^+)_a} \cdot \frac{\gamma_{Cs^+}}{\gamma_{Na^+}} \tag{41}$$

TABLE 4. Cs SORPTION ISOTHERM DATA ON BELLE FOURCHE CLAY AT 26 ± 2°C

Supporting Electrolyte	pH = 5				
Final Cs Conc.(M), C_f					
Cs Loading (mmoles/gm), L_{Cs}	Initial Cs Concentration (M)				
Distribution Coefficient (ml/gm), K_d	0.93×10^{-3}	1.00×10^{-4}	1.00×10^{-5}	1.01×10^{-7}	1.04×10^{-9}
0.002M NaCl					
C_f	$5.48\pm0.27\times10^{-5}$	$5.26\pm0.26\times10^{-6}$	$4.25\pm0.21\times10^{-7}$	$4.26\pm0.22\times10^{-9}$	$4.65\pm0.24\times10^{-11}$
L_{Cs}	$8.79\pm0.46\times10^{-2}$	$9.48\pm0.50\times10^{-3}$	$9.58\pm0.50\times10^{-4}$	$9.67\pm0.50\times10^{-6}$	$9.94\pm0.53\times10^{-8}$
K_d	1606±92	1801±102	2253±127	2271±129	2138±121
0.01M NaCl					
C_f	$1.05\pm0.05\times10^{-4}$	$8.77\pm0.44\times10^{-6}$	$9.11\pm0.46\times10^{-7}$	$9.11\pm0.46\times10^{-9}$	$1.11\pm0.06\times10^{-10}$
L_{Cs}	$8.29\pm0.46\times10^{-2}$	$9.12\pm0.50\times10^{-3}$	$9.00\pm0.50\times10^{-4}$	$9.19\pm0.50\times10^{-6}$	$9.30\pm0.53\times10^{-8}$
K_d	790±47	1040±61	998±59	1009±59	843±50
0.1M NaCl					
C_f	$4.69\pm0.23\times10^{-4}$	$4.80\pm0.24\times10^{-5}$	$4.09\pm0.20\times10^{-6}$	$4.30\pm0.22\times10^{-8}$	$4.44\pm0.22\times10^{-10}$
L_{Cs}	$4.66\pm0.46\times10^{-2}$	$5.25\pm0.50\times10^{-5}$	$5/92\pm0.50\times10^{-4}$	$5.81\pm0.50\times10^{-6}$	$5.96\pm0.52\times10^{-8}$
K_d	99.2±10.2	108±11	145±13	135±12	134±12
1M NaCl					
C_f	$8.85\pm0.44\times10^{-4}$	$9.04\pm0.45\times10^{-5}$	$8.61\pm0.43\times10^{-6}$	$8.93\pm0.45\times10^{-8}$	$9.67\pm0.49\times10^{-10}$
L_{Cs}	$4.93\pm4.78\times10^{-3}$	$9.55\pm5.00\times10^{-5}$	$1.39\pm0.50\times10^{-4}$	$1.17\pm0.51\times10^{-6}$	$7.34\pm5.22\times10^{-9}$
K_d	5.6 ±5.3	10.6 ±5.5	16.1 ±5.8	13.1 ±5.7	7.6 ±5.4
SGW					
C_f	$6.91\pm0.35\times10^{-5}$	$5.59\pm0.28\times10^{-6}$	$5.08\pm0.26\times10^{-7}$	$4.66\pm0.24\times10^{-9}$	$5.30\pm0.27\times10^{-11}$
L_{Cs}	$8.65\pm0.47\times10^{-2}$	$9.44\pm0.50\times10^{-3}$	$9.49\pm0.50\times10^{-4}$	$9.65\pm0.50\times10^{-6}$	$9.88\pm0.53\times10^{-8}$
K_d	1251±72	1690±96	1867±106	2069±117	1863±106

TABLE 5. Cs SORPTION ISOTHERM DATA ON BELLE FOURCHE CLAY AT 26 ± 2°C

Supporting Electrolyte	pH = 6				
Final Cs Conc.(M), C_f					
Cs Loading (mmoles/gm), L_{Cs}	Initial Cs Concentration (M)				
Distribution Coefficient (ml/gm), K_d	0.93×10^{-3}	1.00×10^{-4}	1.00×10^{-5}	1.01×10^{-7}	1.04×10^{-9}
0.002M NaCl					
C_f	$4.25\pm0.21\times10^{-5}$	$3.70\pm0.19\times10^{-6}$	$3.26\pm0.16\times10^{-7}$	$3.24\pm0.16\times10^{-9}$	$3.45\pm0.18\times10^{-11}$
L_{Cs}	$8.92\pm0.46\times10^{-2}$	$9.62\pm0.50\times10^{-3}$	$9.67\pm0.50\times10^{-4}$	$9.78\pm0.52\times10^{-6}$	$1.05\pm0.05\times10^{-7}$
K_d	2098±118	2602±146	2986±166	3022±169	2916±164
0.01M NaCl					
C_f	$1.04\pm0.05\times10^{-4}$	$1.00\pm0.50\times10^{-5}$	$9.81\pm0.49\times10^{-7}$	$8.59\pm0.43\times10^{-9}$	$9.53\pm0.21\times10^{-10}$
L_{Cs}	$8.30\pm0.41\times10^{-2}$	$9.00\pm0.50\times10^{-3}$	$9.02\pm0.50\times10^{-4}$	$9.24\pm0.50\times10^{-6}$	$8.75\pm0.53\times10^{-8}$
K_d	801±48	897±53	919±54	1076±63	992±58
0.1M NaCl					
C_f	$4.47\pm0.22\times10^{-4}$	$4.49\pm0.25\times10^{-5}$	$4.17\pm0.21\times10^{-6}$	$4.12\pm0.21\times10^{-8}$	$4.13\pm0.21\times10^{-10}$
L_{Cs}	$4.87\pm0.46\times10^{-2}$	$5.51\pm0.50\times10^{-3}$	$5.83\pm0.50\times10^{-6}$	$5.98\pm0.50\times10^{-6}$	$6.28\pm0.52\times10^{-8}$
K_d	109±11	123±11	140±12	145±13	152±13
1M NaCl					
C_f	$8.57\pm0.43\times10^{-4}$	$9.32\pm0.47\times10^{-5}$	$9.09\pm0.45\times10^{-6}$	$8.99\pm0.45\times10^{-8}$	$9.50\pm0.48\times10^{-10}$
L_{Cs}	$7.70\pm4.67\times10^{-3}$	$6.79\pm5.00\times10^{-4}$	$9.17\pm5.00\times10^{-5}$	$1.11\pm0.51\times10^{-6}$	$9.05\pm5.14\times10^{-9}$
K_d	9.0 ±5.5	7.3 ±5.4	10.1 ±5.5	12.3 ±5.6	9.5 ±5.5
SGW					
C_f	$5.63\pm0.28\times10^{-5}$	$4.96\pm0.25\times10^{-6}$	$4.45\pm0.22\times10^{-7}$	$4.28\pm0.22\times10^{-9}$	$4.79\pm0.24\times10^{-11}$
L_{Cs}	$8.77\pm0.48\times10^{-2}$	$9.55\pm0.50\times10^{-3}$	$9.54\pm0.50\times10^{-4}$	$9.67\pm0.50\times10^{-6}$	$9.92\pm0.52\times10^{-8}$
K_d	1559±89	1917±109	2148±121	2260±127	2069±117

TABLE 6. Cs SORPTION ISOTHERM DATA ON BELLE FOURCHE CLAY AT 26 ± 2°C

Supporting Electrolyte Final Cs Conc.(M), C_f Cs Loading (mmoles/gm), L_{Cs} Distribution Coefficient (ml/gm), K_d	pH = 7 Initial Cs Concentration (M) 0.93×10^{-3}	1.00×10^{-4}	1.00×10^{-5}	1.01×10^{-7}	1.04×10^{-9}
0.002M NaCl					
C_f	$3.53\pm0.18\times10^{-5}$	$2.97\pm0.15\times10^{-6}$	$2.70\pm0.14\times10^{-7}$	$2.57\pm0.13\times10^{-9}$	$2.78\pm0.14\times10^{-11}$
L_{Cs}	$8.97\pm0.47\times10^{-2}$	$9.71\pm0.50\times10^{-3}$	$9.73\pm0.50\times10^{-4}$	$9.84\pm0.52\times10^{-6}$	$1.01\pm0.05\times10^{-7}$
K_d	2548±143	3267±182	3726±207	3839±214	3645±204
0.01M NaCl					
C_f	$9.36\pm0.47\times10^{-5}$	$9.49\pm0.48\times10^{-6}$	$8.16\pm0.41\times10^{-7}$	$8.52\pm0.43\times10^{-9}$	$8.06\pm0.41\times10^{-11}$
L_{Cs}	$8.40\pm0.47\times10^{-2}$	$9.05\pm0.50\times10^{-3}$	$9.18\pm0.50\times10^{-4}$	$9.25\pm0.50\times10^{-6}$	$9.60\pm0.53\times10^{-8}$
K_d	898±53	953±56	1126±66	1085±63	1190±69
0.1M NaCl					
C_f	$4.12\pm0.21\times10^{-4}$	$4.30\pm0.21\times10^{-5}$	$3.88\pm0.19\times10^{-6}$	$3.87\pm0.19\times10^{-8}$	$4.17\pm0.21\times10^{-10}$
L_{Cs}	$5.22\pm0.47\times10^{-2}$	$5.75\pm0.50\times10^{-3}$	$6.12\pm0.50\times10^{-4}$	$6.23\pm0.50\times10^{-6}$	$6.24\pm0.52\times10^{-8}$
K_d	127±12	133±12	157±13	161±13	150±13
1M NaCl					
C_f	$8.32\pm0.42\times10^{-4}$	$8.96\pm0.45\times10^{-5}$	$8.59\pm0.43\times10^{-6}$	$8.63\pm0.43\times10^{-8}$	$9.43\pm0.47\times10^{-10}$
L_{Cs}	$1.01\pm0.47\times10^{-2}$	$1.04\pm0.50\times10^{-3}$	$1.40\pm0.50\times10^{-4}$	$1.40\pm0.50\times10^{-6}$	$9.74\pm0.52\times10^{-9}$
K_d	12.5 ±5.6	11.7 ±5.6	16.6 ±5.8	17.7 ±5.9	10.3 ±5.5
SGW					
C_f	$4.79\pm0.24\times10^{-5}$	$3.81\pm0.19\times10^{-6}$	$3.71\pm0.19\times10^{-7}$	$3.48\pm0.18\times10^{-9}$	$3.63\pm0.18\times10^{-11}$
L_{Cs}	$8.86\pm0.47\times10^{-2}$	$9.62\pm0.50\times10^{-3}$	$9.62\pm0.50\times10^{-4}$	$9.76\pm0.52\times10^{-6}$	$1.00\pm0.05\times10^{-7}$
K_d	1851±105	2528±143	2594±146	2799±157	2765±155

TABLE 7. Cs SORPTION ISOTHERM DATA ON BELLE FOURCHE CLAY AT 26 ± 2°C

Supporting Electrolyte Final Cs Conc.(M), C_f Cs Loading (mmoles/gm), L_{Cs} Distribution Coefficient (ml/gm), K_d	pH = 8 Initial Cs Concentration (M) 0.93×10^{-3}	1.00×10^{-4}	1.00×10^{-5}	1.01×10^{-7}	1.04×10^{-9}
0.002M NaCl					
C_f	$3.12\pm0.16\times10^{-5}$	$2.55\pm0.13\times10^{-6}$	$2.23\pm0.11\times10^{-7}$	$2.22\pm0.11\times10^{-9}$	$2.25\pm0.12\times10^{-11}$
L_{Cs}	$9.02\pm0.47\times10^{-2}$	$9.74\pm0.50\times10^{-3}$	$9.78\pm0.50\times10^{-4}$	$9.88\pm0.52\times10^{-6}$	$1.02\pm0.05\times10^{-7}$
K_d	2891±162	3824±213	4384±244	4450±248	4529±254
0.01M NaCl					
C_f	$8.44\pm0.42\times10^{-5}$	$8.27\pm0.42\times10^{-6}$	$7.41\pm0.37\times10^{-7}$	$7.69\pm0.39\times10^{-9}$	$7.68\pm0.39\times10^{-11}$
L_{Cs}	$8.50\pm0.47\times10^{-2}$	$9.17\pm0.50\times10^{-3}$	$9.26\pm0.50\times10^{-4}$	$9.34\pm0.50\times10^{-6}$	$9.64\pm0.53\times10^{-8}$
K_d	1006±59	1109±65	1250±72	1250±72	1256±73
0.1M NaCl					
C_f	$4.02\pm0.20\times10^{-4}$	$4.09\pm0.21\times10^{-5}$	$3.98\pm0.20\times10^{-6}$	$3.83\pm0.19\times10^{-8}$	$3.92\pm0.20\times10^{-10}$
L_{Cs}	$5.32\pm0.47\times10^{-2}$	$5.92\pm0.50\times10^{-3}$	$6.01\pm0.50\times10^{-4}$	$6.28\pm0.50\times10^{-6}$	$6.48\pm0.52\times10^{-8}$
K_d	132±12	145±12	151±13	164±14	165±14
1M NaCl					
C_f	$8.12\pm0.41\times10^{-4}$	$9.09\pm0.46\times10^{-5}$	$8.59\pm0.43\times10^{-6}$	$8.52\pm0.43\times10^{-8}$	$9.01\pm0.45\times10^{-10}$
L_{Cs}	$1.21\pm0.47\times10^{-2}$	$9.12\pm5.00\times10^{-4}$	$1.40\pm0.50\times10^{-4}$	$1.58\pm0.50\times10^{-6}$	$1.39\pm0.53\times10^{-8}$
K_d	15.0 ±5.8	10.0 ±5.5	16.4 ±5.8	18.5 ±5.9	15.4 ±5.8
SGW					
C_f	$4.33\pm0.22\times10^{-5}$	$3.49\pm0.18\times10^{-6}$	$3.14\pm0.16\times10^{-7}$	$3.14\pm0.16\times10^{-9}$	$3.18\pm0.16\times10^{-11}$
L_{Cs}	$8.90\pm0.47\times10^{-2}$	$9.65\pm0.50\times10^{-3}$	$9.68\pm0.50\times10^{-4}$	$9.79\pm0.52\times10^{-6}$	$1.01\pm0.05\times10^{-7}$
K_d	2058±116	2767±155	3095±173	3157±174	3174±178

TABLE 8. Cs SORPTION ISOTHERM DATA ON BELLE FOURCHE CLAY AT 26 ± 2°C

Supporting Electrolyte	pH = 9				
Final Cs Conc.(M), C_f					
Cs Loading (mmoles/gm), L_{Cs}	Initial Cs Concentration (M)				
Distribution Coefficient (ml/gm), K_d	0.93×10^{-3}	1.00×10^{-4}	1.00×10^{-5}	1.01×10^{-7}	1.04×10^{-9}
0.002M Nacl					
C_f	$2.82\pm0.14\times10^{-5}$	$2.55\pm0.13\times10^{-6}$	$2.08\pm0.11\times10^{-7}$	$2.21\pm0.11\times10^{-9}$	$2.49\pm0.13\times10^{-11}$
L_{Cs}	$9.06\pm0.47\times10^{-2}$	$9.74\pm0.50\times10^{-3}$	$9.79\pm0.50\times10^{-4}$	$9.88\pm0.52\times10^{-6}$	$1.02\pm0.05\times10^{-8}$
K_d	3212±179	3826±212	5707±260	4451±246	4775±268
0.01M NaCl					
C_f	$8.87\pm0.46\times10^{-5}$	$8.23\pm0.41\times10^{-6}$	$6.54\pm0.33\times10^{-7}$	$6.84\pm0.34\times10^{-9}$	$7.00\pm0.35\times10^{-11}$
L_{Cs}	$8.46\pm0.47\times10^{-2}$	$9.18\pm0.50\times10^{-3}$	$9.35\pm0.50\times10^{-4}$	$9.42\pm0.50\times10^{-4}$	$9.70\pm0.53\times10^{-8}$
K_d	953±56	1115±65	1429±82	1377±79	1386±80
0.1M NaCl					
C_f	$4.03\pm0.20\times10^{-4}$	$4.03\pm0.20\times10^{-5}$	$3.69\pm0.18\times10^{-6}$	$3.81\pm0.19\times10^{-8}$	$3.81\pm0.19\times10^{-10}$
L_{Cs}	$5.30\pm0.47\times10^{-2}$	$5.98\pm0.50\times10^{-3}$	$6.74\pm0.50\times10^{-4}$	$6.29\pm0.50\times10^{-6}$	$6.59\pm0.52\times10^{-8}$
K_d	132±12	148±13	171±14	165±14	173±14
1M NaCl					
C_f	$8.41\pm0.42\times10^{-4}$	$9.03\pm0.45\times10^{-5}$	$8.43\pm0.42\times10^{-6}$	$8.69\pm0.43\times10^{-8}$	$9.09\pm0.46\times10^{-10}$
L_{Cs}	$9.29\pm4.67\times10^{-3}$	$9.71\pm5.00\times10^{-4}$	$1.57\pm0.50\times10^{-4}$	$1.40\pm0.50\times10^{-6}$	$1.31\pm0.52\times10^{-8}$
K_d	11.1 ±5.6	10.8 ±5.5	18.6 ±5.9	16.2 ±5.8	14.4 ±5.7
SGW					
C_f	$4.11\pm0.21\times10^{-5}$	$3.36\pm0.17\times10^{-6}$	$3.37\pm0.17\times10^{-7}$	$3.19\pm0.16\times10^{-9}$	$3.01\pm0.15\times10^{-11}$
L_{Cs}	$8.93\pm0.47\times10^{-2}$	$9.66\pm0.50\times10^{-3}$	$9.66\pm0.50\times10^{-4}$	$9.78\pm0.50\times10^{-6}$	$1.01\pm0.05\times10^{-8}$
K_d	2174±122	2875±160	2869±160	3070±171	3352±188

TABLE 9. Cs SORPTION ISOTHERM DATA ON BELLE FOURCHE CLAY AT 26 ± 2°C

Supporting Electrolyte	pH = 10				
Final Cs Conc.(M), C_f					
Cs Loading (mmoles/gm), L_{Cs}	Initial Cs Concentration (M)				
Distribution Coefficient (ml/gm), K_d	0.93×10^{-3}	1.00×10^{-4}	1.00×10^{-5}	1.01×10^{-7}	1.04×10^{-9}
0.002M NaCl					
C_f	$2.73\pm0.14\times10^{-5}$	$2.55\pm0.13\times10^{-6}$	$2.19\pm0.11\times10^{-7}$	$2.06\pm0.10\times10^{-9}$	$2.08\pm0.11\times10^{-11}$
L_{Cs}	$9.07\pm0.47\times10^{-2}$	$9.74\pm0.50\times10^{-3}$	$9.78\pm0.50\times10^{-4}$	$9.90\pm0.50\times10^{-6}$	$1.02\pm0.05\times10^{-8}$
K_d	3327±185	3824±212	4474±247	4807±264	4899±275
0.01M NaCl					
C_f	$8.66\pm0.43\times10^{-5}$	$8.07\pm0.41\times10^{-6}$	$6.94\pm0.35\times10^{-7}$	$6.87\pm0.35\times10^{-9}$	$7.52\pm0.38\times10^{-11}$
L_{Cs}	$8.47\pm0.47\times10^{-2}$	$9.19\pm0.50\times10^{-3}$	$9.31\pm0.50\times10^{-4}$	$9.41\pm0.50\times10^{-6}$	$9.65\pm0.53\times10^{-8}$
K_d	979±58	1139±66	1341±77	1371±79	1284±74
0.1M NaCl					
C_f	$3.64\pm0.18\times10^{-4}$	$3.80\pm0.19\times10^{-5}$	$3.95\pm0.20\times10^{-6}$	$3.61\pm0.18\times10^{-8}$	$3.74\pm0.19\times10^{-10}$
L_{Cs}	$5.70\pm0.47\times10^{-2}$	$6.20\pm0.50\times10^{-3}$	$6.05\pm0.50\times10^{-4}$	$6.49\pm0.50\times10^{-6}$	$6.66\pm0.52\times10^{-8}$
K_d	157±13	163±14	153±13	180±14	178±14
1M NaCl					
C_f	$8.12\pm0.41\times10^{-4}$	$8.60\pm0.43\times10^{-5}$	$8.80\pm0.44\times10^{-6}$	$8.41\pm0.44\times10^{-8}$	$9.29\pm0.46\times10^{-10}$
L_{Cs}	$1.22\pm0.47\times10^{-4}$	$1.40\pm0.52\times10^{-3}$	$1.20\pm0.50\times10^{-4}$	$1.69\pm0.50\times10^{-6}$	$1.11\pm0.52\times10^{-8}$
K_d	15.1 ±5.8	16.3 ±5.8	13.6 ±5.7	20.1 ±6.0	12.0 ±5.6
SGW					
C_f	$4.03\pm0.20\times10^{-5}$	$3.10\pm0.16\times10^{-6}$	$3.09\pm0.16\times10^{-7}$	$2.75\pm0.14\times10^{-9}$	$3.12\pm0.16\times10^{-11}$
L_{Cs}	$8.94\pm0.47\times10^{-2}$	$9.70\pm0.50\times10^{-3}$	$9.67\pm0.50\times10^{-4}$	$9.83\pm0.50\times10^{-6}$	$1.01\pm0.05\times10^{-7}$
K_d	2219±125	3128±174	3132±174	3575±198	3238±182

TABLE 10. Cs SORPTION ISOTHERM DATA ON Min-u-Sil at 26 ± 2°C

Supporting Electrolyte	pH = 5					
Final Cs Conc.(M), C_f						
Cs Loading (mmoles/gm), L_{Cs}	Initial Cs Concentration (M)					
Distribution Coefficient (ml/gm), K_d	1.05×10^{-4}	1.05×10^{-5}	1.05×10^{-6}	1.06×10^{-7}	1.07×10^{-8}	1.09×10^{-9}
0.002M NaCl						
C_f	$8.29\pm0.41\times10^{-5}$	$6.24\pm0.62\times10^{-6}$	$3.16\pm0.16\times10^{-7}$	$4.06\pm0.21\times10^{-9}$	$8.77\pm0.46\times10^{-11}$	$6.74\pm0.40\times10^{-12}$
L_{Cs}	$2.10\pm0.50\times10^{-4}$	$4.05\pm0.51\times10^{-5}$	$6.97\pm0.51\times10^{-6}$	$9.68\pm0.51\times10^{-7}$	$1.01\pm0.05\times10^{-7}$	$1.03\pm0.06\times10^{-8}$
K_d	2.54±0.60	6.73±0.82	22.1 ±1.6	238±13	1150±65	1527±96
0.01M NaCl						
C_f	$8.77\pm0.44\times10^{-5}$	$7.62\pm0.38\times10^{-6}$	$4.95\pm0.25\times10^{-7}$	$1.28\pm0.06\times10^{-8}$	$3.49\pm0.18\times10^{-10}$	$2.53\pm0.13\times10^{-11}$
L_{Cs}	$1.65\pm0.50\times10^{-4}$	$2.75\pm0.51\times10^{-5}$	$5.28\pm0.51\times10^{-6}$	$8.84\pm0.51\times10^{-7}$	$9.83\pm0.53\times10^{-8}$	$1.01\pm0.05\times10^{-8}$
K_d	1.88±0.57	3.60±0.66	10.6 ±1.0	69.2 ±4.2	282±16	399±22
0.1M NaCl						
C_f	$9.89\pm0.49\times10^{-5}$	$9.59\pm0.48\times10^{-6}$	$7.60\pm0.38\times10^{-7}$	$4.05\pm0.20\times10^{-8}$	$2.93\pm0.15\times10^{-9}$	$1.13\pm0.06\times10^{-10}$
L_{Cs}	$5.76\pm4.97\times10^{-5}$	$8.65\pm4.97\times10^{-6}$	$2.77\pm0.51\times10^{-6}$	$6.20\pm0.51\times10^{-7}$	$7.37\pm0.51\times10^{-8}$	$9.28\pm0.53\times10^{-9}$
K_d	0.58±0.50	0.90±0.62	3.63±0.66	15.4 ±1.3	25.1 ±1.9	82.5 ±4.9
1M NaCl						
C_f	$1.00\pm0.05\times10^{-4}$	$1.02\pm0.06\times10^{-5}$	$9.73\pm0.49\times10^{-7}$	$7.35\pm0.37\times10^{-8}$	$5.43\pm0.27\times10^{-9}$	$5.65\pm0.28\times10^{-10}$
L_{Cs}	$4.44\pm4.97\times10^{-5}$	$3.26\pm4.97\times10^{-6}$	$7.37\pm4.97\times10^{-7}$	$3.10\pm0.44\times10^{-7}$	$5.08\pm0.44\times10^{-8}$	$4.97\pm0.46\times10^{-9}$
K_d	0.44±0.50	0.32±0.59	0.77±0.51	4.19±0.69	9.21±0.95	8.91±0.94
SGW						
C_f	$9.17\pm0.46\times10^{-5}$	$6.96\pm0.35\times10^{-6}$	$3.81\pm0.19\times10^{-7}$	$6.85\pm0.34\times10^{-9}$	$2.79\pm0.14\times10^{-10}$	$2.25\pm0.12\times10^{-11}$
L_{Cs}	$1.27\pm0.50\times10^{-4}$	$3.37\pm0.51\times10^{-5}$	$6.36\pm0.51\times10^{-6}$	$9.44\pm0.51\times10^{-7}$	$9.90\pm0.51\times10^{-8}$	$1.01\pm0.05\times10^{-8}$
K_d	1.38±0.55	4.83±0.72	16.7 ±1.4	137±08	354±20	450±25

TABLE 11. Cs SORPTION ISOTHERM DATA ON Min-u-Sil at 26 ± 2°C

Supporting Elcctrolyte	pH = 6					
Final Cs Conc.(M), C_f						
Cs Loading (mmoles/gm), L_{Cs}	Initial Cs Concentration (M)					
Distribution Coefficient (ml/gm), K_d	1.05×10^{-4}	1.05×10^{-5}	1.05×10^{-6}	1.06×10^{-7}	1.07×10^{-8}	1.09×10^{-9}
0.002M NaCl						
C_f	$5.94\pm0.30\times10^{-5}$	$3.91\pm0.20\times10^{-6}$	$1.77\pm0.09\times10^{-7}$	$3.12\pm0.16\times10^{-9}$	$8.22\pm0.43\times10^{11}$	$6.17\pm0.38\times10^{-12}$
L_{Cs}	$4.33\pm0.51\times10^{-4}$	$6.27\pm0.51\times10^{-5}$	$8.29\pm0.51\times10^{-6}$	$9.79\pm0.51\times10^{-7}$	$1.01\pm0.05\times10^{-7}$	$1.03\pm0.06\times10^{-8}$
K_d	7.30±0.85	16.0 ±1.3	46.9 ±3.0	313±17	1227±70	1669±107
0.01M NaCl						
C_f	$8.59\pm0.43\times10^{-5}$	$5.93\pm0.30\times10^{-6}$	$3.50\pm0.17\times10^{-7}$	$9.24\pm0.46\times10^{-9}$	$2.54\pm0.13\times10^{-10}$	$1.77\pm0.09\times10^{-11}$
L_{Cs}	$1.81\pm0.51\times10^{-4}$	$4.34\pm0.51\times10^{-5}$	$6.64\pm0.51\times10^{-6}$	$9.20\pm0.51\times10^{-7}$	$9.91\pm0.51\times10^{-8}$	$1.02\pm0.05\times10^{-8}$
K_d	2.12±0.58	7.32±0.74	19.0 ±1.5	99.5 ±6.1	391±22	577±32
0.1M NaCl						
C_f	$1.01\pm0.05\times10^{-4}$	$9.66\pm0.48\times10^{-6}$	$6.83\pm0.34\times10^{-7}$	$3.30\pm0.17\times10^{-8}$	$1.41\pm0.07\times10^{-9}$	$1.09\pm0.06\times10^{-10}$
L_{Cs}	$3.89\pm4.97\times10^{-5}$	$8.10\pm4.36\times10^{-6}$	$3.50\pm0.51\times10^{-6}$	$6.95\pm0.51\times10^{-7}$	$8.82\pm0.44\times10^{-8}$	$9.33\pm0.46\times10^{-9}$
K_d	0.39±0.49	0.83±0.52	5.09±0.74	21.0±1.6	62.7 ±3.8	85.8 ±5.1
1M NaCl						
C_f	$1.03\pm0.05\times10^{-4}$	$9.58\pm0.48\times10^{-6}$	$9.32\pm0.47\times10^{-7}$	$7.30\pm0.37\times10^{-8}$	$5.53\pm0.28\times10^{-9}$	$5.46\pm0.27\times10^{-10}$
L_{Cs}	$1.58\pm4.97\times10^{-5}$	$8.76\pm4.97\times10^{-6}$	$1.13\pm0.50\times10^{-6}$	$3.17\pm0.51\times10^{-7}$	$4.91\pm0.50\times10^{-8}$	$5.15\pm0.52\times10^{-9}$
K_d	0.15±0.48	0.91±0.52	1.21±0.54	4.29±0.70	8.89±0.94	9.46±0
SGW						
C_f	$8.35\pm0.42\times10^{-5}$	$5.96\pm0.35\times10^{-6}$	$3.01\pm0.15\times10^{-7}$	$5.41\pm0.27\times10^{-9}$	$2.38\pm0.12\times10^{-10}$	$2.08\pm0.11\times10^{-11}$
L_{Cs}	$2.04\pm0.50\times10^{-4}$	$4.31\pm0.44\times10^{-5}$	$7.11\pm0.51\times10^{-6}$	$9.55\pm0.51\times10^{-7}$	$9.92\pm0.51\times10^{-8}$	$1.02\pm0.05\times10^{-8}$
K_d	2.45±0.60	7.24±0.85	23.7 ±1.7	176±10	418±23	490±28

TABLE 12. Cs SORPTION ISOTHERM DATA ON Min-u-Sil at 26 ± 2°C

Supporting Electrolyte	pH = 7					
Final Cs Conc. (M), C_f	Initial Cs Concentration (M)					
Cs Loading (mmoles/gm), L_{Cs}						
Distribution Coefficient (ml/gm), K_d	1.05×10^{-4}	1.05×10^{-5}	1.05×10^{-6}	1.06×10^{-7}	1.07×10^{-8}	1.09×10^{-9}
0.002M NaCl						
C_f	$5.60\pm0.28\times10^{-5}$	$2.32\pm0.12\times10^{-6}$	$1.15\pm0.06\times10^{-7}$	$2.17\pm0.11\times10^{-9}$	$6.52\pm0.35\times10^{-11}$	$6.13\pm0.37\times10^{-12}$
L_{Cs}	$4.73\pm0.51\times10^{-4}$	$7.77\pm0.51\times10^{-5}$	$8.89\pm0.51\times10^{-6}$	$9.86\pm0.51\times10^{-7}$	$1.01\pm0.06\times10^{-7}$	$1.03\pm0.06\times10^{-8}$
K_d	8.31±0.91	33.5 ±2.3	77.3 ±4.6	454±25	1549±89	1679±108
0.01M NaCl						
C_f	$8.47\pm0.42\times10^{-5}$	$5.10\pm0.26\times10^{-6}$	$3.05\pm0.15\times10^{-7}$	$7.34\pm0.37\times10^{-9}$	$2.27\pm0.12\times10^{-10}$	$1.90\pm0.10\times10^{-11}$
L_{Cs}	$1.93\pm0.50\times10^{-4}$	$5.15\pm0.51\times10^{-5}$	$7.08\pm0.51\times10^{-7}$	$9.37\pm0.51\times10^{-7}$	$9.97\pm0.53\times10^{-8}$	$1.02\pm0.05\times10^{-8}$
K_d	2.28±0.59	10.1 ±0.9	23.2 ±1.7	128±7	440±24	536±30
0.1M NaCl						
C_f	$1.00\pm0.05\times10^{-4}$	$9.41\pm0.47\times10^{-6}$	$6.67\pm0.33\times10^{-7}$	$3.21\pm0.16\times10^{-8}$	$1.57\pm0.08\times10^{-9}$	$1.08\pm0.05\times10^{-10}$
L_{Cs}	$4.58\pm0.50\times10^{-5}$	$1.03\pm0.50\times10^{-5}$	$3.65\pm0.51\times10^{-6}$	$7.07\pm0.51\times10^{-7}$	$8.69\pm0.57\times10^{-8}$	$9.33\pm0.53\times10^{-7}$
K_d	0.46±0.50	1.10±0.53	5.46±0.76	21.9 ±1.6	55.4 ±3.4	86.7 ±5.1
1M NaCl						
C_f	$1.01\pm0.05\times10^{-4}$	$1.01\pm0.06\times10^{-5}$	$9.65\pm0.48\times10^{-7}$	$6.91\pm0.35\times10^{-8}$	$5.80\pm0.29\times10^{-9}$	$5.45\pm0.27\times10^{-10}$
L_{Cs}	$1.03\pm0.50\times10^{-4}$	$4.82\pm0.51\times10^{-5}$	$7.24\pm0.51\times10^{-6}$	$9.57\pm0.51\times10^{-7}$	$9.94\pm0.51\times10^{-8}$	$1.02\pm0.05\times10^{-8}$
K_d	0.36±0.49	0.35±0.59	0.84±0.52	5.08±0.74	8.04±0.89	9.50±0.97
SGW						
C_f	$8.19\pm0.41\times10^{-5}$	$5.42\pm0.27\times10^{-6}$	$2.88\pm0.14\times10^{-7}$	$5.37\pm0.27\times10^{-9}$	$2.36\pm0.12\times10^{-10}$	$1.86\pm0.10\times10^{-11}$
L_{Cs}	$1.03\pm0.50\times10^{-4}$	$4.82\pm0.51\times10^{-5}$	$7.24\pm0.51\times10^{-6}$	$9.57\pm0.51\times10^{-7}$	$9.94\pm0.51\times10^{-8}$	$1.02\pm0.05\times10^{-8}$
K_d	2.68±0.62	8.90±0.94	25.2±1.8	181±10	421±23	547±31

TABLE 13. Cs SORPTION ISOTHERM DATA ON Min-u-Sil at 26 ± 2°C

Supporting Electrolyte	pH = 8					
Final Cs Conc. (M), C_f	Initial Cs Concentration (M)					
Cs Loading (mmoles/gm), L_{Cs}						
Distribution Coefficient (ml/gm), K_d	1.05×10^{-4}	1.05×10^{-5}	1.05×10^{-6}	1.06×10^{-7}	1.07×10^{-8}	1.09×10^{-9}
0.002M NaCl						
C_f	$5.67\pm0.28\times10^{-5}$	$1.81\pm0.09\times10^{-6}$	$8.14\pm0.41\times10^{-8}$	$1.65\pm0.08\times10^{-9}$	$6.63\pm0.36\times10^{-11}$	$5.05\pm0.33\times10^{-12}$
L_{Cs}	$4.58\pm0.51\times10^{-4}$	$8.27\pm0.51\times10^{-5}$	$9.20\pm0.51\times10^{-6}$	$9.90\pm0.50\times10^{-7}$	$1.01\pm0.06\times10^{-7}$	$1.03\pm0.07\times10^{-8}$
K_d	8.09±0.89	45.9 ±2.9	113±7	601±33	1523±88	2041±139
0.01M NaCl						
C_f	$8.12\pm0.41\times10^{-5}$	$4.57\pm0.23\times10^{-6}$	$2.64\pm0.13\times10^{-7}$	$6.48\pm0.33\times10^{-9}$	$2.34\pm0.12\times10^{-10}$	$1.84\pm0.10\times10^{-11}$
L_{Cs}	$2.27\pm0.51\times10^{-4}$	$5.63\pm0.61\times10^{-5}$	$7.48\pm0.51\times10^{-6}$	$9.46\pm0.51\times10^{-7}$	$9.94\pm0.53\times10^{-8}$	$1.02\pm0.05\times10^{-8}$
K_d	2.79±0.62	12.3 ±1.1	28.3 ±2.0	146±8	425±24	554±31
0.1M NaCl						
C_f	$9.96\pm0.50\times10^{-5}$	$8.77\pm0.44\times10^{-6}$	$6.29\pm0.31\times10^{-7}$	$3.50\pm0.17\times10^{-8}$	$1.48\pm0.07\times10^{-9}$	$1.07\pm0.05\times10^{-10}$
L_{Cs}	$2.53\pm4.97\times10^{-5}$	$2.18\pm4.97\times10^{-3}$	$1.06\pm0.50\times10^{-6}$	$3.53\pm0.51\times10^{-7}$	$5.10\pm0.51\times10^{-8}$	$5.41\pm0.53\times10^{-9}$
K_d	0.52±0.50	1.87±0.57	6.35±0.80	19.3 ±1.5	59.1 ±3.6	87.2 ±5.2
1M NaCl						
C_f	$1.02\pm0.05\times10^{-4}$	$1.03\pm0.06\times10^{-5}$	$9.39\pm0.47\times10^{-7}$	$6.88\pm0.34\times10^{-8}$	$5.33\pm0.27\times10^{-9}$	$5.21\pm0.26\times10^{-10}$
L_{Cs}	$2.53\pm4.97\times10^{-5}$	$2.18\pm4.97\times10^{-3}$	$1.06\pm0.50\times10^{-6}$	$3.53\pm0.51\times10^{-7}$	$5.10\pm0.51\times10^{-8}$	$5.41\pm0.53\times10^{-9}$
K_d	0.25±0.49	0.21±0.58	1.13±0.53	5.13±0.74	9.56±0.97	10.4 ±1.0
SGW						
C_f	$8.10\pm0.42\times10^{-5}$	$5.45\pm0.27\times10^{-6}$	$2.57\pm0.13\times10^{-7}$	$6.84\pm0.34\times10^{-9}$	$2.14\pm0.11\times10^{-10}$	$1.80\pm0.09\times10^{-11}$
L_{Cs}	$2.04\pm0.50\times10^{-4}$	$4.80\pm0.51\times10^{-5}$	$7.55\pm0.51\times10^{-6}$	$9.44\pm0.51\times10^{-7}$	$9.97\pm0.51\times10^{-8}$	$1.02\pm0.05\times10^{-8}$
K_d	2.43±0.60	8.81±0.93	29.3 ±3.0	138±8	466±26	566±32

TABLE 14. Cs SORPTION ISOTHERM DATA ON Min-u-Sil at 26 ± 2°C

Supporting Electrolyte	pH = 9					
Final Cs Conc.(M), C_f						
Cs Loading (mmoles/gm), L_{Cs}	Initial Cs Concentration (M)					
Distribution Coefficient (ml/gm), K_d	1.05×10^{-4}	1.05×10^{-5}	1.05×10^{-6}	1.06×10^{-7}	1.07×10^{-8}	1.09×10^{-9}
0.002M NaCl						
C_f	$4.26\pm0.21\times10^{-5}$	$1.74\pm0.09\times10^{-6}$	$7.42\pm0.37\times10^{-8}$	$1.60\pm0.08\times10^{-9}$	$4.51\pm0.25\times10^{-11}$	$4.55\pm0.31\times10^{-12}$
L_{Cs}	$5.94\pm0.51\times10^{-4}$	$8.32\pm0.51\times10^{-5}$	$9.28\pm0.51\times10^{-6}$	$9.90\pm0.51\times10^{-7}$	$1.02\pm0.05\times10^{-7}$	$1.03\pm0.07\times10^{-8}$
K_d	13.9 ±1.2	47.7 ±3.0	125±7	621±35	2244±134	2267±161
0.01M NaCl						
C_f	$7.95\pm0.40\times10^{-5}$	$3.88\pm0.19\times10^{-6}$	$2.15\pm0.11\times10^{-7}$	$6.03\pm0.30\times10^{-9}$	$2.18\pm0.11\times10^{-10}$	$1.71\pm0.09\times10^{-11}$
L_{Cs}	$2.42\pm0.51\times10^{-4}$	$6.29\pm0.51\times10^{-5}$	$7.94\pm0.51\times10^{-6}$	$9.50\pm0.51\times10^{-7}$	$9.97\pm0.52\times10^{-8}$	$1.02\pm0.05\times10^{-8}$
K_d	3.06±0.63	16.2 ±1.3	37.0 ±2.4	157±9	457±25	595±34
0.1M NaCl						
C_f	$9.80\pm0.49\times10^{-5}$	$8.68\pm0.43\times10^{-6}$	$6.07\pm0.30\times10^{-7}$	$3.48\pm0.17\times10^{-8}$	$1.41\pm0.07\times10^{-9}$	$1.09\pm0.05\times10^{-10}$
L_{Cs}	$6.64\pm4.97\times10^{-5}$	$1.72\pm0.50\times10^{-5}$	$4.20\pm0.51\times10^{-6}$	$6.78\pm0.61\times10^{-7}$	$8.02\pm0.51\times10^{-8}$	$9.33\pm0.53\times10^{-9}$
K_d	0.68±0.50	1.99±0.58	6.93±0.83	19.5±1.5	62.5 ±3.8	94.8 ±5.6
1M NaCl						
C_f	$9.76\pm0.49\times10^{-5}$	$1.00\pm0.06\times10^{-5}$	$9.49\pm0.48\times10^{-7}$	$7.03\pm0.35\times10^{-8}$	$5.64\pm0.28\times10^{-9}$	$4.96\pm0.25\times10^{-10}$
L_{Cs}	$7.04\pm4.97\times10^{-5}$	$4.55\pm4.97\times10^{-6}$	$9.61\pm4.36\times10^{-7}$	$3.39\pm0.51\times10^{-7}$	$4.80\pm0.51\times10^{-8}$	$5.65\pm0.53\times10^{-9}$
K_d	0.72±0.51	0.45±0.60	1.01±0.53	4.83±0.72	8.54±0.92	11.4 ±1.1
SGW						
C_f	$7.30\pm0.37\times10^{-5}$	$4.64\pm0.23\times10^{-6}$	$2.35\pm0.12\times10^{-7}$	$4.82\pm0.24\times10^{-9}$	$2.17\pm0.11\times10^{-10}$	$1.84\pm0.10\times10^{-11}$
L_{Cs}	$3.04\pm0.51\times10^{-4}$	$5.57\pm0.51\times10^{-5}$	$7.74\pm0.51\times10^{-6}$	$9.61\pm0.51\times10^{-7}$	$9.91\pm0.51\times10^{-8}$	$1.02\pm0.05\times10^{-8}$
K_d	4.17±0.69	12.0 ±1.1	33.0 ±2.2	200±11	458±25	553±31

TABLE 15. Cs SORPTION ISOTHERM DATA ON Min-u-Sil at 26 ± 2°C

Supporting Electrolyte	pH = 10					
Final Cs Conc.(M), C_f						
Cs Loading (mmoles/gm), L_{Cs}	Initial Cs Concentration (M)					
Distribution Coefficient (ml/gm), K_d	1.05×10^{-4}	1.05×10^{-5}	1.05×10^{-6}	1.06×10^{-7}	1.07×10^{-8}	1.09×10^{-9}
0.002M NaCl						
C_f	$3.60\pm0.18\times10^{-5}$	$1.92\pm0.10\times10^{-6}$	$5.03\pm0.25\times10^{-8}$	$1.30\pm0.07\times10^{-9}$	$5.44\pm0.30\times10^{-11}$	$4.51\pm0.31\times10^{-12}$
L_{Cs}	$6.58\pm0.51\times10^{-4}$	$8.14\pm0.51\times10^{-8}$	$9.50\pm0.51\times10^{-6}$	$9.94\pm0.53\times10^{-7}$	$1.01\pm0.05\times10^{-7}$	$1.03\pm0.06\times10^{-8}$
K_d	18.1 ±1.4	42.6 ±2.7	189±11	768±42	1860±107	2286±162
0.01M NaCl						
C_f	$7.14\pm0.36\times10^{-5}$	$5.09\pm0.25\times10^{-6}$	$1.96\pm0.10\times10^{-7}$	$6.27\pm0.31\times10^{-9}$	$2.34\pm0.12\times10^{-10}$	$1.82\pm0.10\times10^{-11}$
L_{Cs}	$3.19\pm0.51\times10^{-4}$	$5.15\pm0.51\times10^{-5}$	$8.12\pm0.51\times10^{-6}$	$9.48\pm0.51\times10^{-7}$	$9.94\pm0.51\times10^{-8}$	$1.02\pm0.05\times10^{-8}$
K_d	4.48±0.71	10.1 ±1.0	41.5 ±3.2	151±9	424±24	560±32
0.1M NaCl						
C_f	$9.51\pm0.48\times10^{-5}$	$7.6\pm0.38\times10^{-6}$	$5.37\pm0.27\times10^{-7}$	$3.13\pm0.16\times10^{-8}$	$1.30\pm0.07\times10^{-9}$	$8.60\pm0.43\times10^{-11}$
L_{Cs}	$9.46\pm4.97\times10^{-5}$	$2.75\pm0.51\times10^{-5}$	$4.00\pm0.51\times10^{-6}$	$7.08\pm0.51\times10^{-7}$	$8.93\pm0.51\times10^{-8}$	$9.53\pm0.53\times10^{-9}$
K_d	0.99±0.52	3.61±0.66	9.08±0.95	22.7±1.7	68.5 ±4.1	111±6
1M NaCl						
C_f	$1.01\pm0.05\times10^{-4}$	$9.69\pm0.58\times10^{-6}$	$8.27\pm0.41\times10^{-7}$	$5.97\pm0.30\times10^{-8}$	$5.00\pm0.25\times10^{-9}$	$4.32\pm0.22\times10^{-10}$
L_{Cs}	$0.99\pm4.97\times10^{-5}$	$7.70\pm4.97\times10^{-6}$	$2.12\pm0.50\times10^{-6}$	$4.40\pm0.51\times10^{-7}$	$5.41\pm0.51\times10^{-8}$	$6.27\pm0.53\times10^{-9}$
K_d	0.10±0.48	0.79±0.61	2.56±0.61	7.37±0.86	10.8±1.0	14.5 ±1.3
SGW						
C_f	$6.54\pm0.33\times10^{-5}$	$4.89\pm0.25\times10^{-6}$	$2.27\pm0.11\times10^{-7}$	$5.24\pm0.26\times10^{-9}$	$2.38\pm0.12\times10^{-10}$	$2.05\pm0.11\times10^{-11}$
L_{Cs}	$3.76\pm0.51\times10^{-4}$	$5.32\pm0.51\times10^{-5}$	$7.81\pm0.51\times10^{-6}$	$9.51\pm0.51\times10^{-7}$	$9.94\pm0.51\times10^{-8}$	$1.02\pm0.06\times10^{-8}$
K_d	5.76±0.77	10.8 ±1.0	34.4 ±2.3	183±10	417±23	496±28

Plots of the first term versus the third term should produce straight lines of slope n = 1 for exchange of monovalent ions from which $K^a_{Cs/Na}$ can be obtained.

For low Cs loadings of the surface, $(SO^-Na^+)_s$ can be approximated by the sodium CEC and $(Na^+)_a$ by the electrolyte concentration. The concentrations of Cs on the surface can be calculated from the initial and final Cs concentrations in solution. The values of γ_{Cs^+} and γ_{Na^+} can be estimated for the different electrolyte solutions from extended Debye-Hückel theory (Butler 1964, p.438). Figures 8 - 19 show the logarithmic plots for the Belle Fourche clay and for Min-u-sil for the six pH values and the four NaCl solutions studied. The solid lines were calculated from a linear least squares fit to the points. The corresponding slopes, n, and Cs/Na exchange constants, $K^a_{Cs/Na}$, are also shown in the figures.

The plots of the clay data do result in straight lines of slope nearly equal to one. The $K^a_{Cs/Na}$ values increase slowly with pH from about 6 to 10. Apparently the sorption of Cs by the clay can be expressed as a simple exchange of Cs for Na and the mass-action equations are applicable over the range of pH and NaCl concentrations studied.

The plots of the Min-u-sil data also result in straight lines but slopes of from 0.55 to 0.64 were obtained with increasing pH. The values of $K^a_{Cs/Na}$ also varied over a factor of 6, from 0.78 to 5 with increasing pH. The simple mass action expression for the exchange of Cs for Na is not adequate to predict the Cs sorption. For the concentration of Na on the quartz, $(SO^-Na^+)_s$, we assumed the Na CEC value measured at pH 7 for all pH values in the analysis. Since the Na CEC may vary appreciably with pH for quartz (Allen, Matijevic and Meites 1971), using a constant value for $(SO^-Na^+)_s$ could cause the apparent variation of $K^a_{Cs/Na}$ with pH. Also, the results of the chemical analysis of the quartz suggest the presence of a small amount of a contaminating mineral or minerals. If this material has a high CEC, e.g., like mica or clay, it could make a measurable contribution to the sorption. The apparent slope, n, could then be the result of more than one component, one from the quartz and one or more from the contaminants, and thus the slope could differ from unity.

However, deviations from a single mass-action law expression were also observed by Allen et al. in investigations of the exchange of Na^+ for H^+ on silica (Allen, Matijevic and Meites 1971). They attempted to explain the deviations as being due to the presence of two distinct types of sites or silica phases with sufficiently different reactivities that one site nearly completely fills before the second site begins to fill. They also suggest that the apparent equilibrium constant for the exchange at a single type of site changes with the surface composition. It is not known at present whether the deviations from simple behavior we observe are due to experimental problems or are intrinsic to the quartz (or a combination of both).

Figures 20 - 25 show the variation of K_d with Cs loading, L_{Cs}, and electrolyte concentration for the clay for each of the pH values. The K_d values rapidly approach a constant value with decreasing loading for all pH values and electrolyte concentrations, as would be expected from the mass-action expression. The K_d values for the synthetic groundwater solutions behave similarly and the magnitudes are close to those of the NaCl solution of nearly the same ionic strength, i.e., the 0.002M NaCl solutions. An average K_d value was calculated for each electrolyte concentration over the range of loading where the K_d appears to be constant, i.e., L_{Cs} less than 10^{-3}, and these values are plotted as a function of pH in Figure 26. There does appear to be a small increase in K_d with decreasing hydrogen ion concentration, particularly for the lower electrolyte concentrations.

Figures 27 - 32 show the variation of K_d with Cs loading and electrolyte concentration for the quartz for each of the pH values. There is a rather large variation of K_d with loading for all electrolyte concentrations at all pH values, however, the K_d values appear to approach constant values at the lowest loadings. Figures 33, 34, and 35 show the variation of K_d with pH for the different electrolyte concentrations at fixed values of cesium loading of 2×10^{-4}, 2×10^{-6}, and 2×10^{-8}. The K_d values were estimated by drawing smooth curves through the points in the K_d versus L_{Cs} plots and slicing through the curves at the desired loading values. Except for L_{Cs} of 2×10^{-8}, the large errors in K_d values for the 1M NaCl solutions precluded a reliable

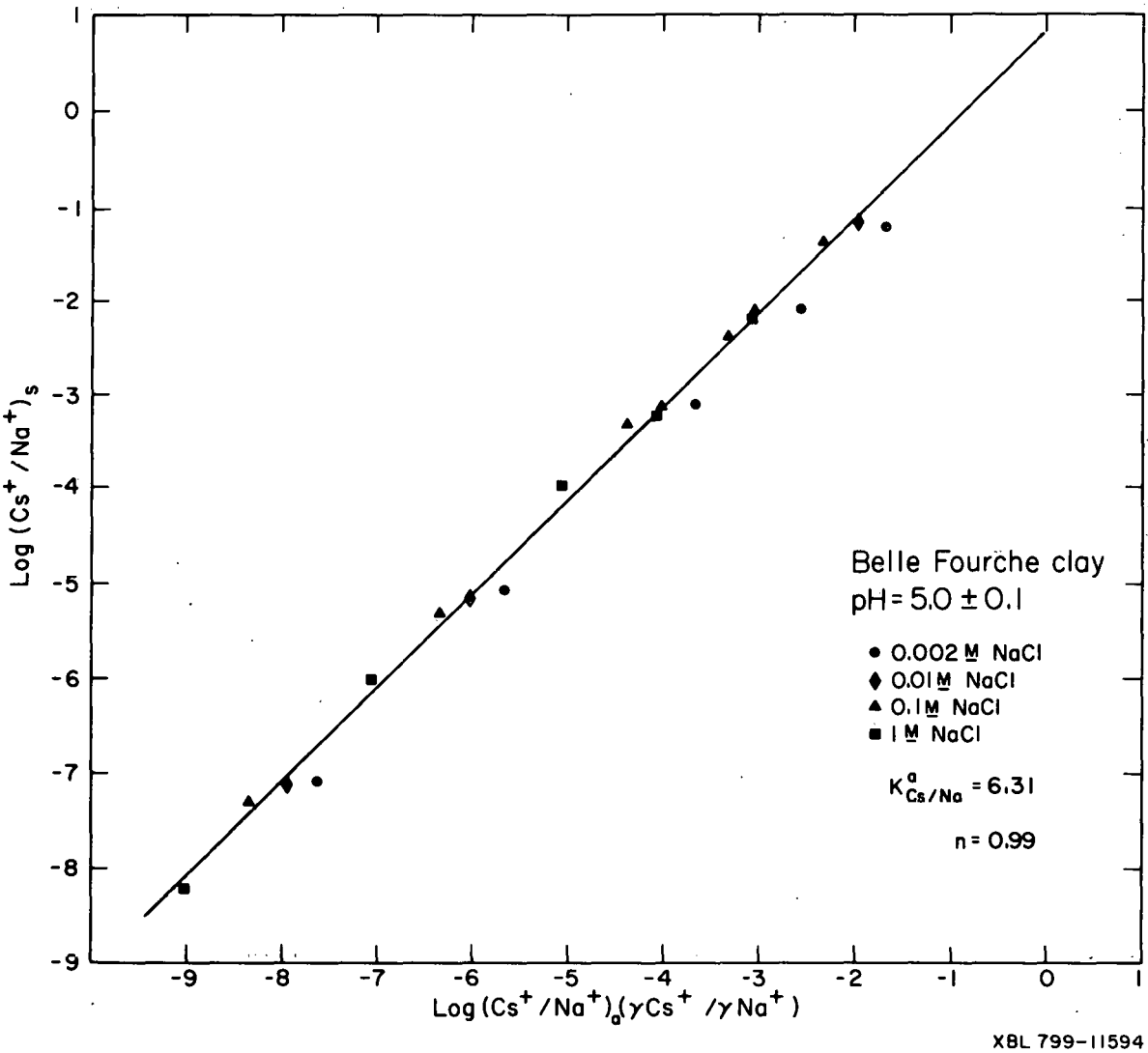

FIGURE 8. Mass-action law representation (equation 41) of the exchange of Cs^+ for Na^+ on the Belle Fourche clay at pH 5 and several NaCl electrolyte concentrations. The solid line is a least squares fit to the experiment points from which an estimate of the Cs/Na exchange constant, $K^a_{Cs/Na}$, can be obtained. The slope, n, should be 1 for the exchange of monovalent ions.

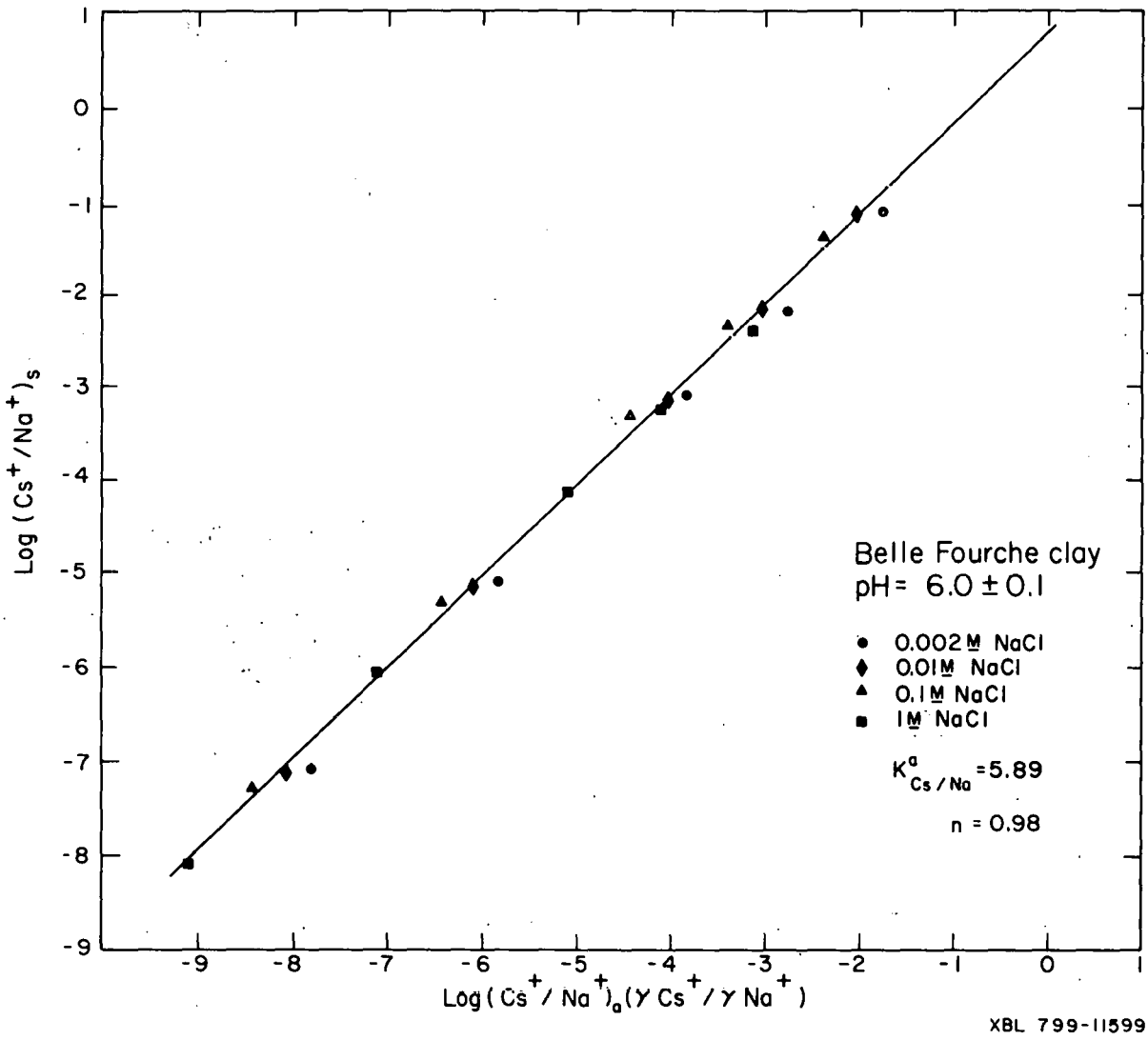

FIGURE 9. Mass-action law representation (equation 41) of the exchange of Cs^+ for Na^+ on the Belle Fourche clay at pH 6 and several NaCl electrolyte concentrations. The solid line is a least squares fit to the experimental points from which an estimate of the Cs/Na exchange constant, $K^a_{Cs/Na}$, can be obtained. The slope, n, should be 1 for the exchange of monovalent ions.

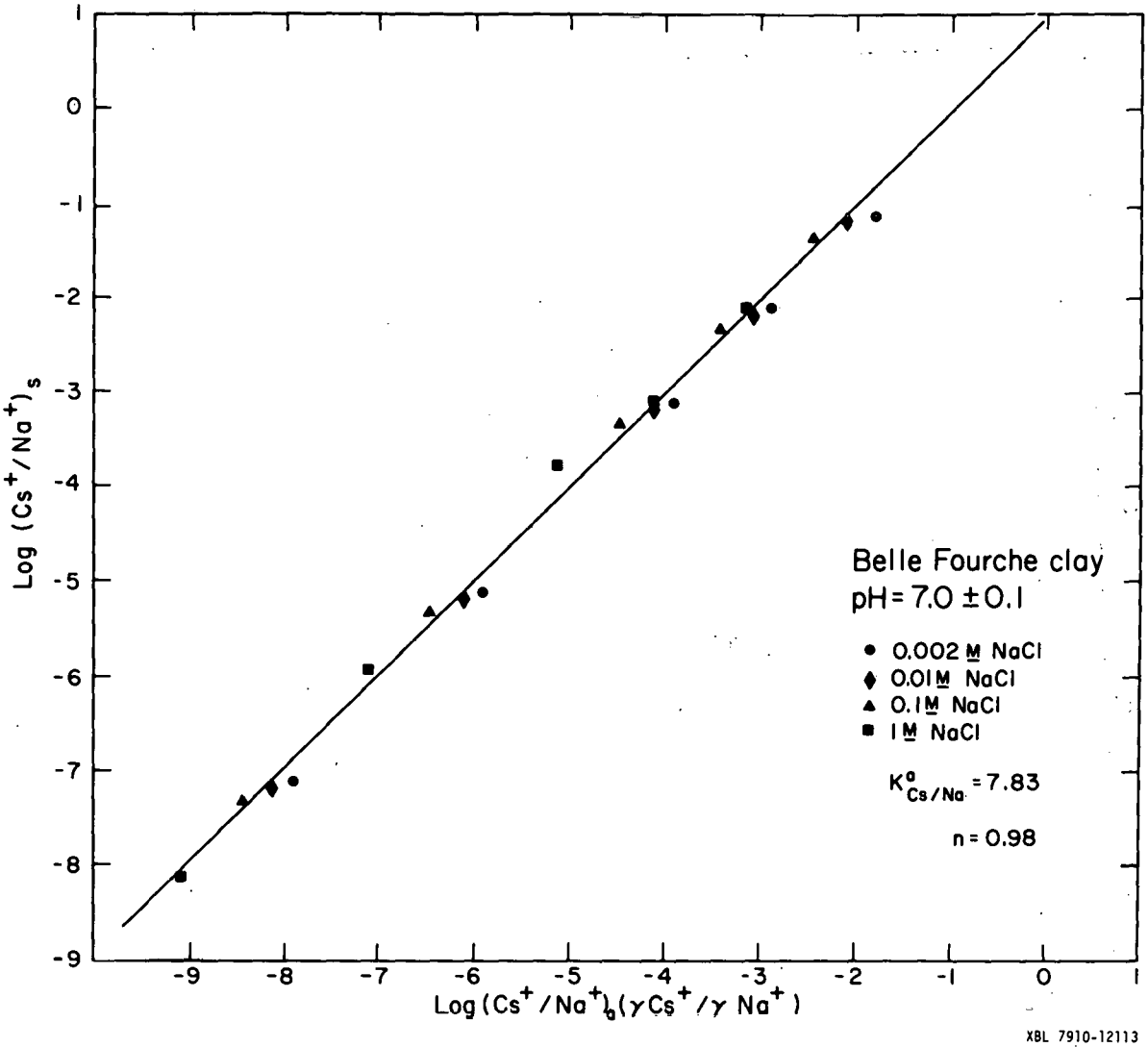

FIGURE 10. Mass-action law representation (equation 41) of the exchange of Cs^+ for Na^+ on the Belle Fourche clay at pH 7 and several NaCl concentrations. The solid line is a least squares fit to experimental points from which an estimate of the Cs/Na exchange constant, $K^a_{Cs/Na}$, can be obtained. The slope, n, should be 1 for the exchange of monovalent ions.

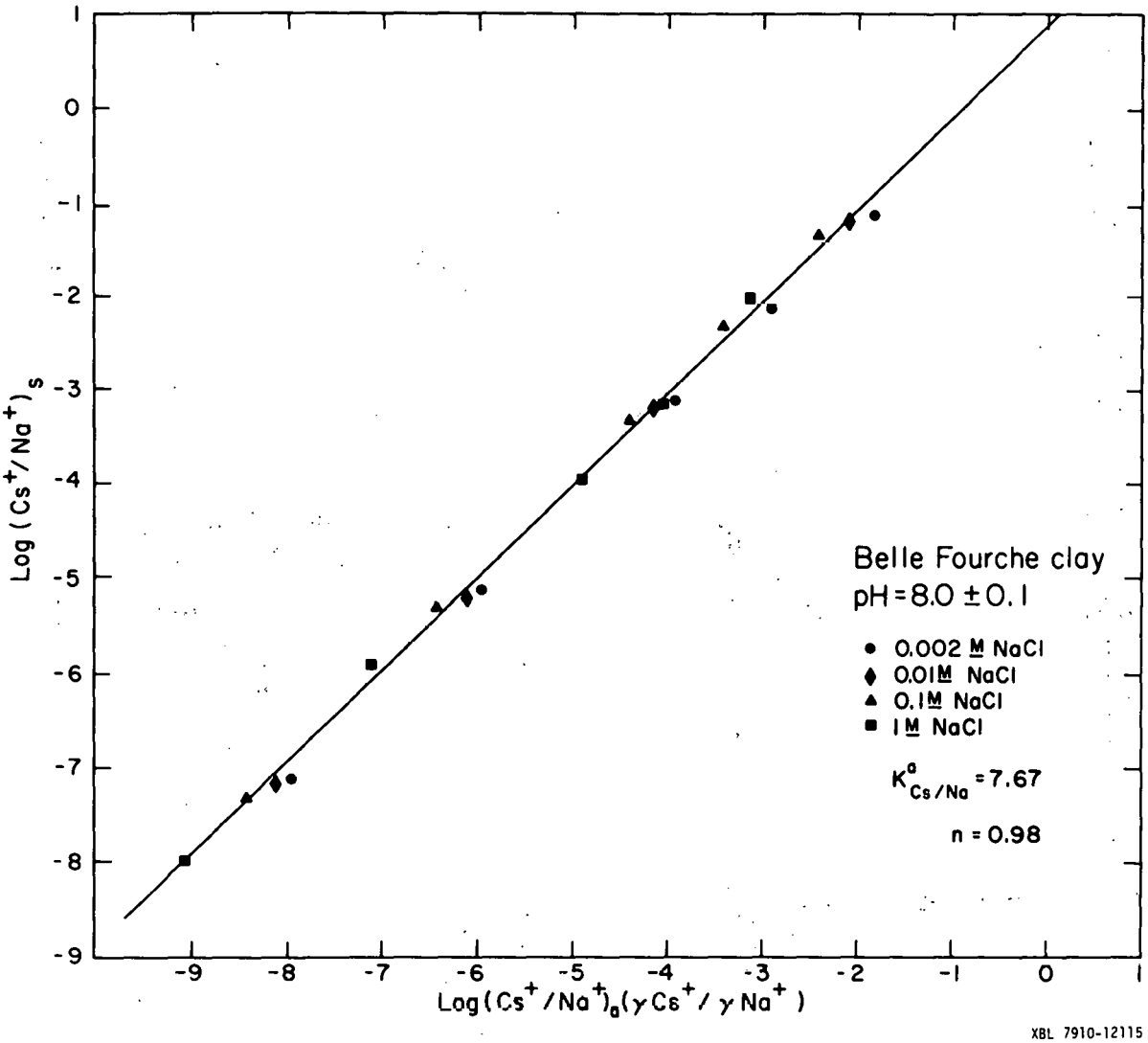

FIGURE 11. Mass-action law representation (equation 41) of the exchange of Cs^+ for Na^+ on the Belle Fourche clay at pH 8 and several NaCl concentrations. The solid line is a least squares fit to experimental points from which an estimate of the Cs/Na exchange constant, $K^a_{Cs/Na}$, can be obtained. The slope, n, should be 1 for the exchange of monovalent ions.

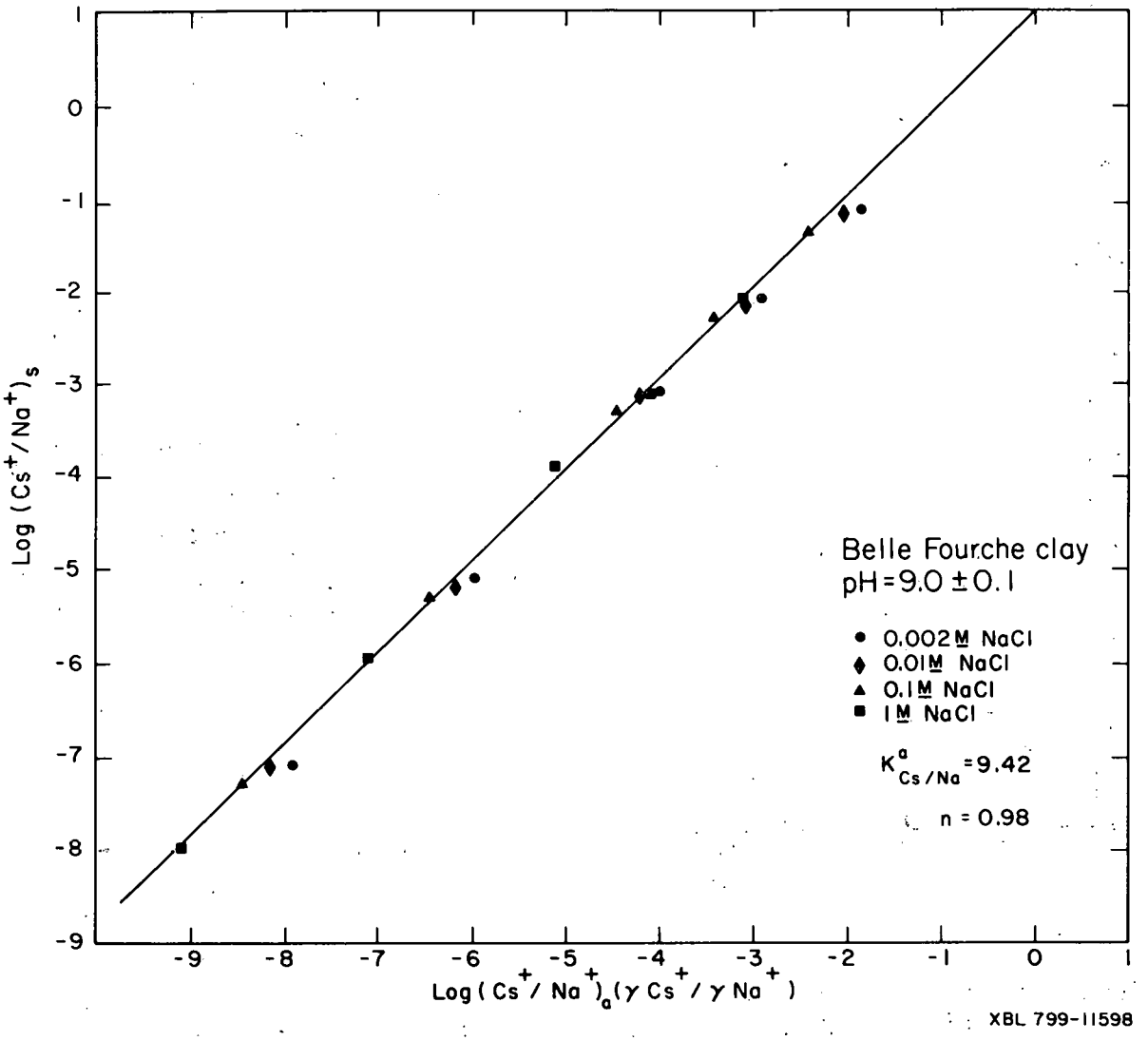

FIGURE 12. Mass-action law representation (equation 41) of the exchange of Cs^+ for Na^+ on the Belle Fourche clay at pH 9 and several NaCl concentrations. The solid line is a least squares fit to experimental points from which an estimate of the Cs/Na exchange constant, $K^a_{Cs/Na}$, can be obtained. The slope, n, should be 1 for the exchange of monovalent ions.

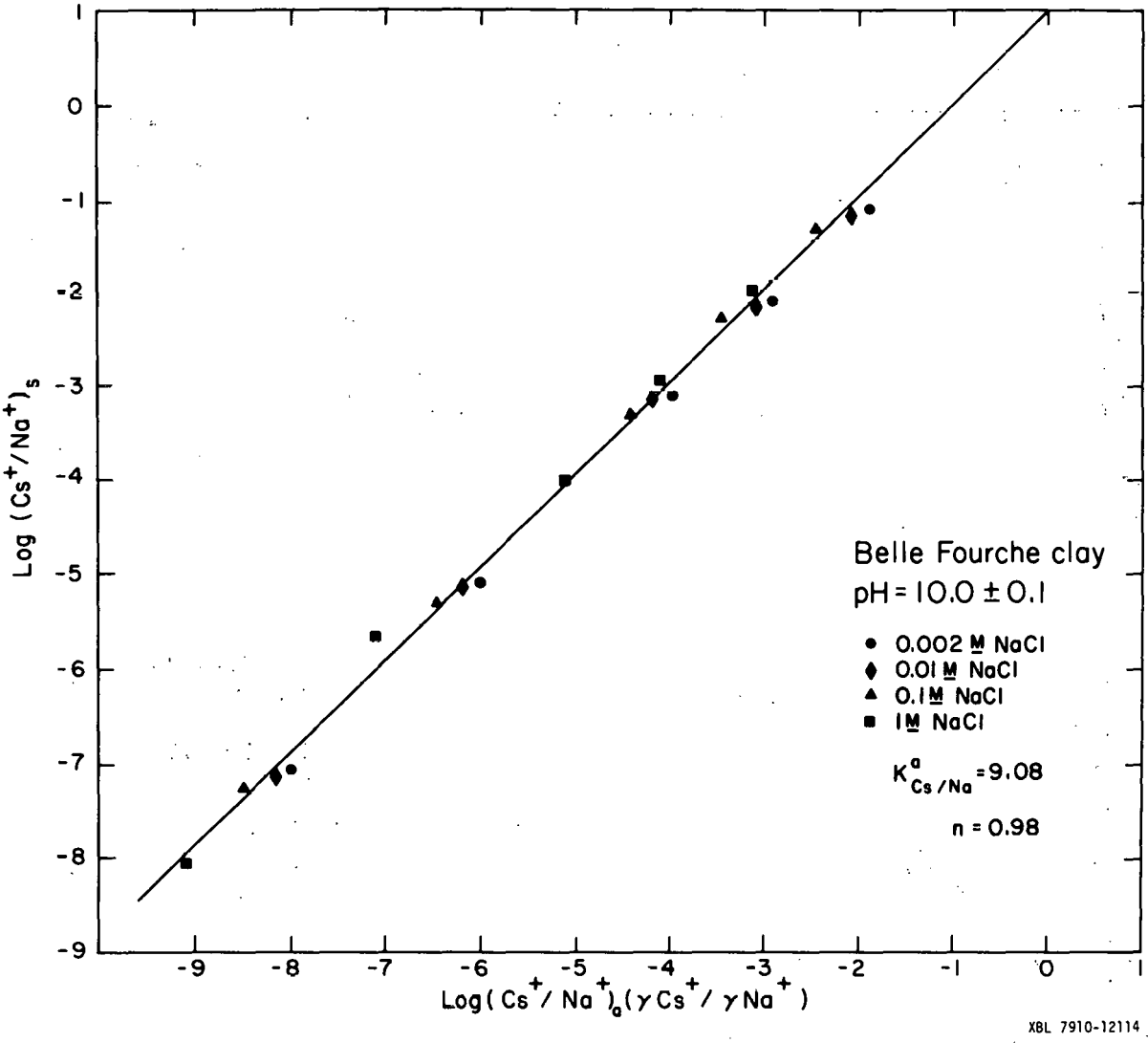

FIGURE 13. Mass-action law representation (equation 41) of the exchange of Cs^+ for Na^+ on the Belle Fourche clay at pH 10 and several NaCl concentrations. The solid line is a least squares fit to experimental points from which an estimate of the Cs/Na exchange constant, $K^a_{Cs/Na}$, can be obtained. The slope, n, should be 1 for the exchange of monovalent ions.

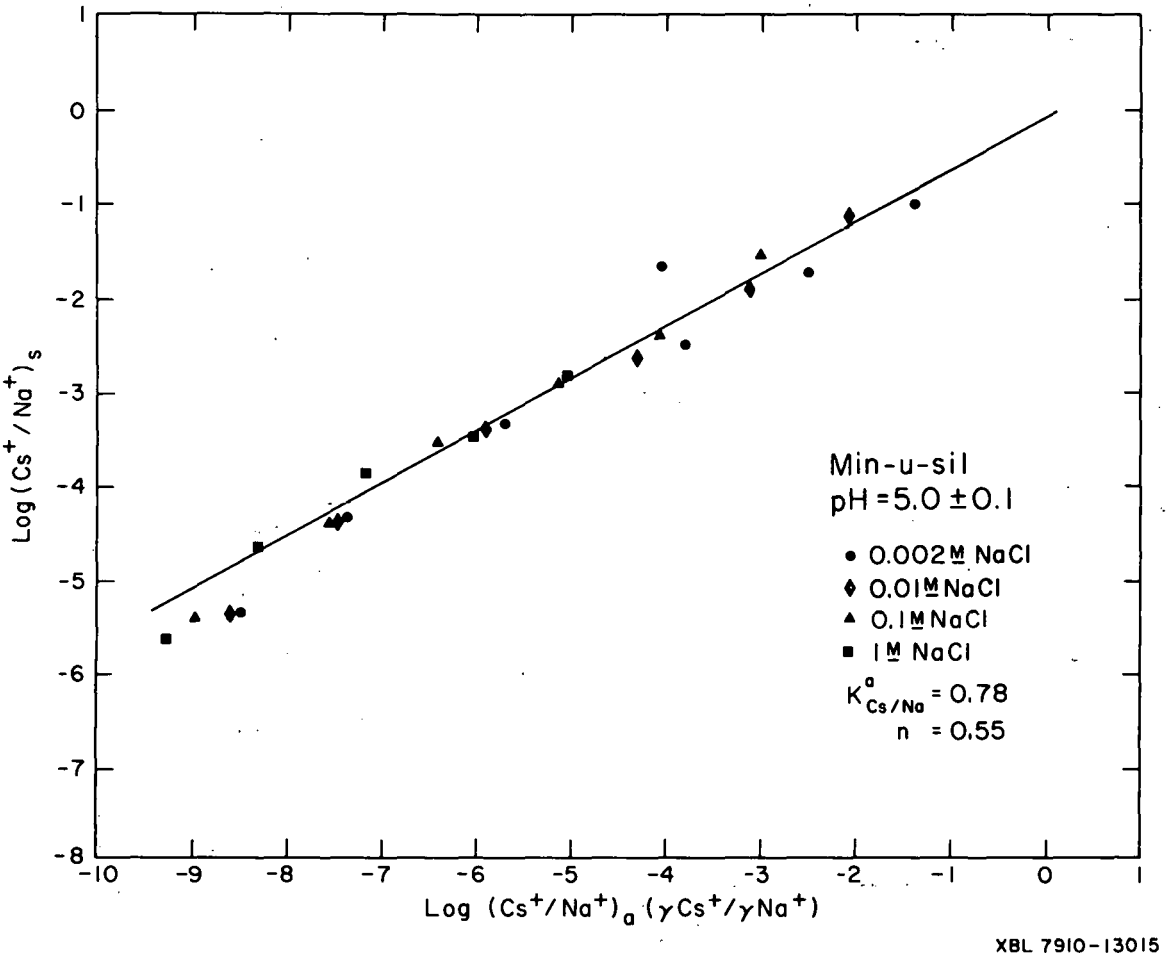

FIGURE 14. Mass-action law representation (equation 41) of the exchange of Cs^+ for Na^+ on the Min-u-sil at pH 5 and several NaCl concentrations. The solid line is a least squares fit to experimental points from which an estimate of the Cs/Na exchange constant, $K^a_{Cs/Na}$, can be obtained. The slope, n, should be 1 for the exchange of monovalent ions.

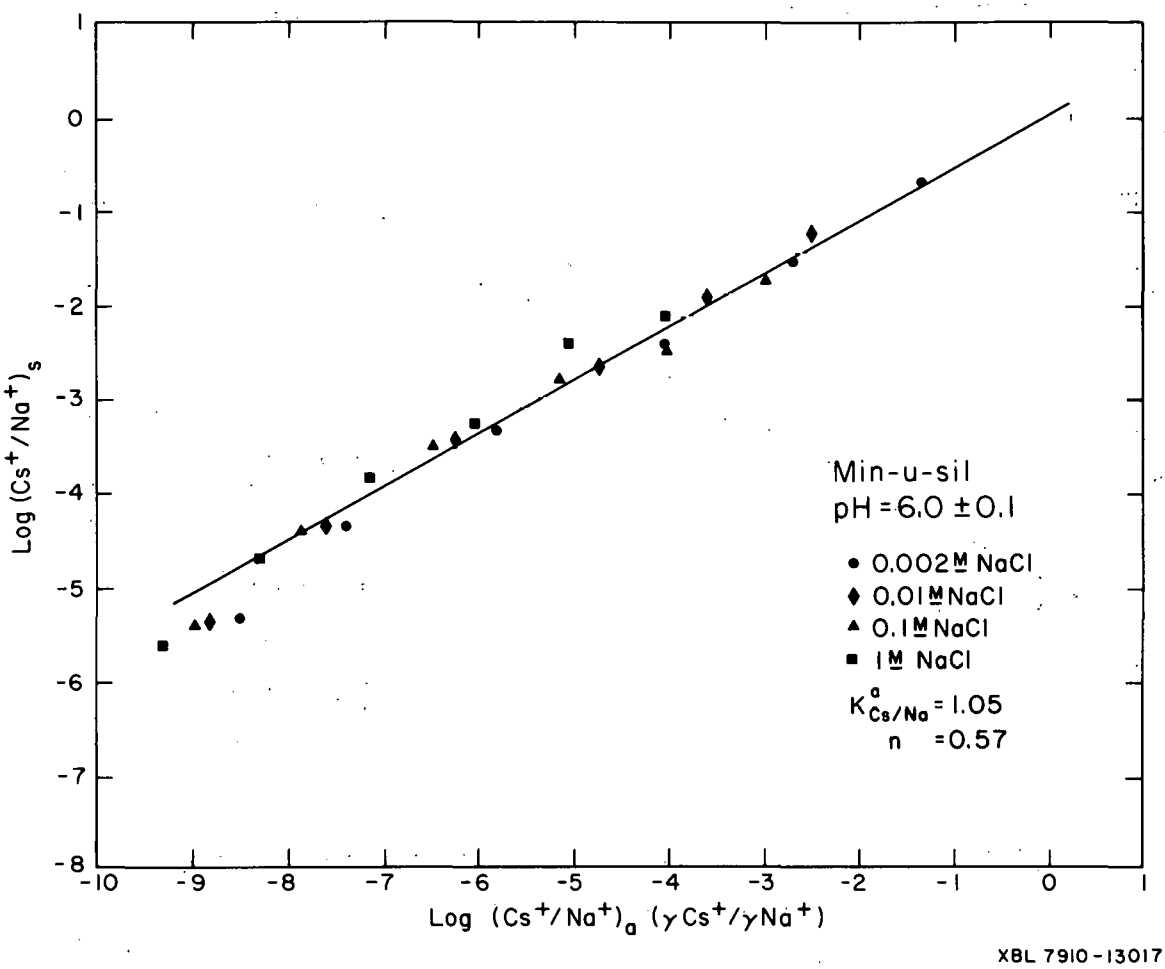

FIGURE 15. Mass-action law representation (equation 41) of the exchange of Cs^+ for Na^+ on the Min-u-sil at pH 6 and several NaCl concentrations. The solid line is a least squares fit to experimental points from which an estimate of the Cs/Na exchange constant, $K^a_{Cs/Na}$, can be obtained. The slope, n, should be 1 for the exchange of monovalent ions.

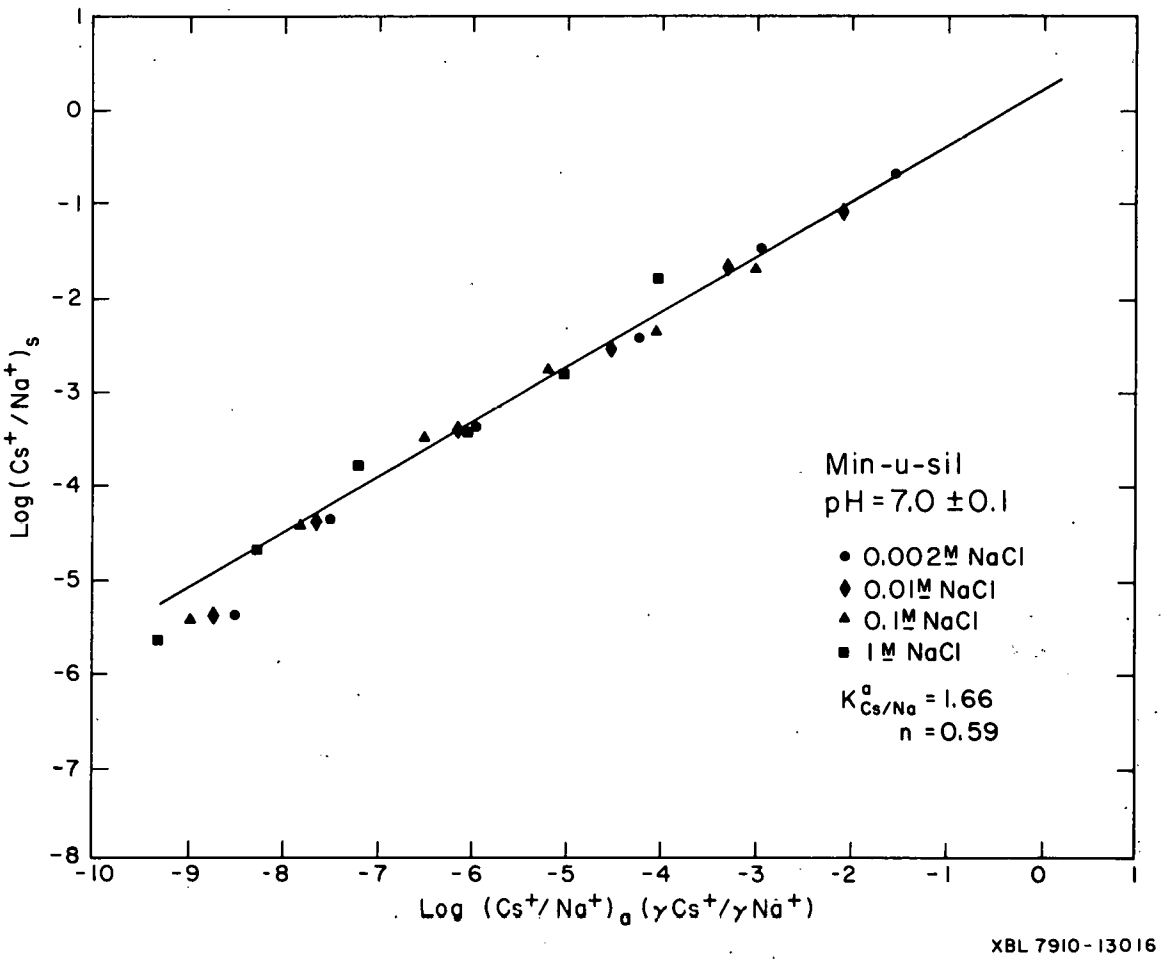

FIGURE 16. Mass-action law representation (equation 41) of the exchange of Cs^+ for Na^+ on the Min-u-sil at pH 7 and several NaCl concentrations. The solid line is a least squares fit to experimental points from which an estimate of the Cs/Na exchange constant, $K^a_{Cs/Na}$, can be obtained. The slope, n, should be 1 for the exchange of monovalent ions.

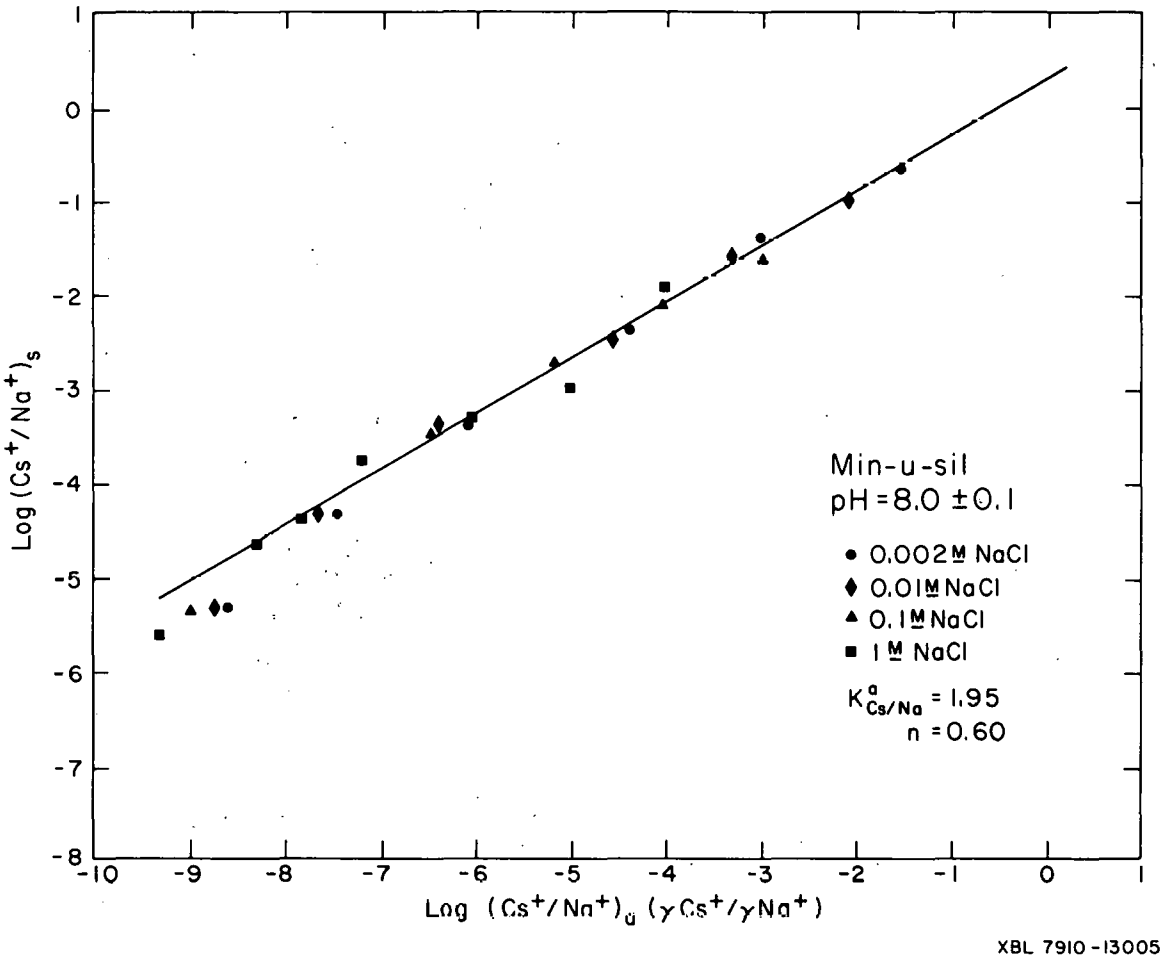

FIGURE 17. Mass-action law representation (equation 41) of the exchange of Cs^+ for Na^+ on the Min-u-sil at pH 8 and several NaCl concentrations. The solid line is a least squares fit to experimental points from which an estimate of the Cs/Na exchange constant, $K^a_{Cs/Na}$, can be obtained. The slope, n, should be 1 for the exchange of monovalent ions.

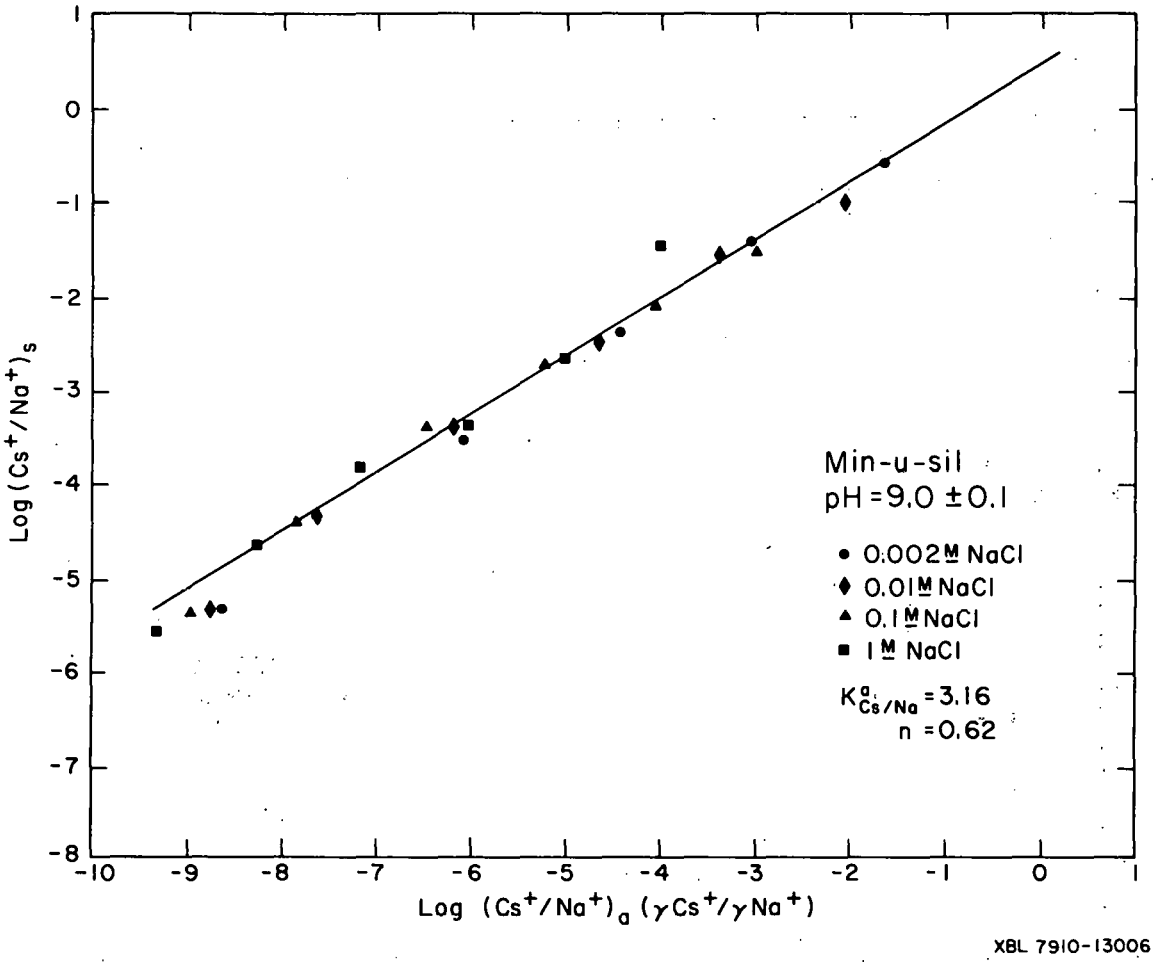

FIGURE 18. Mass-action law representation (equation 41) of the exchange of Cs^+ for Na^+ on the Min-u-sil at pH 9 and several NaCl concentrations. The solid line is a least squares fit to experimental points from which an estimate of the Cs/Na exchange constant, $K^a_{Cs/Na}$, can be obtained. The slope, n, should be 1 for the exchange of monovalent ions.

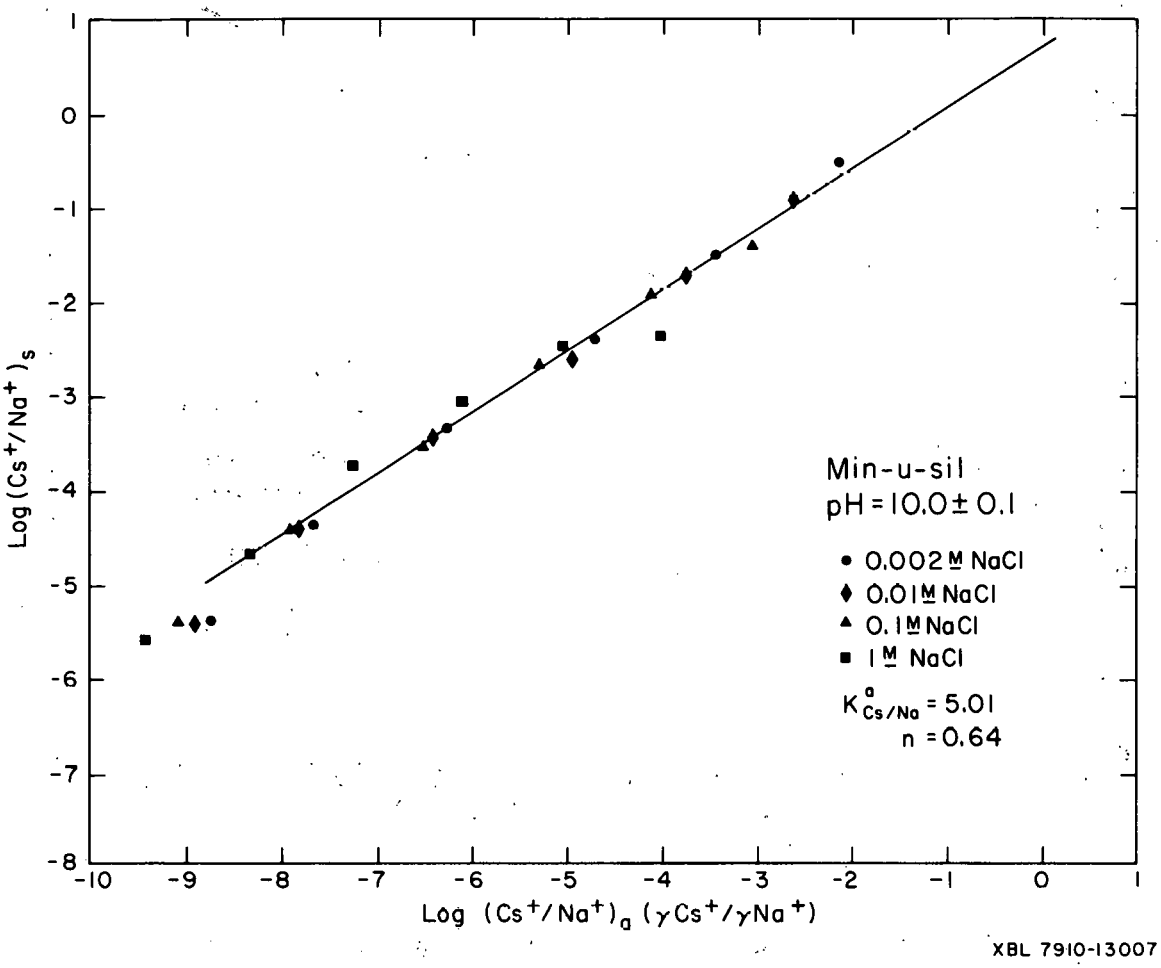

FIGURE 19. Mass-action law representation (equation 41), of the exchange of Cs^+ for Na^+ on the Min-u-sil at pH 10 and several NaCl electrolyte concentrations. The solid line is a least squares fit to the experimental points from which an estimate of the Cs/Na exchange constant, $K^a_{Cs/Na}$, can be obtained. The slope, n, should be 1 for the exchange of monovalent ions.

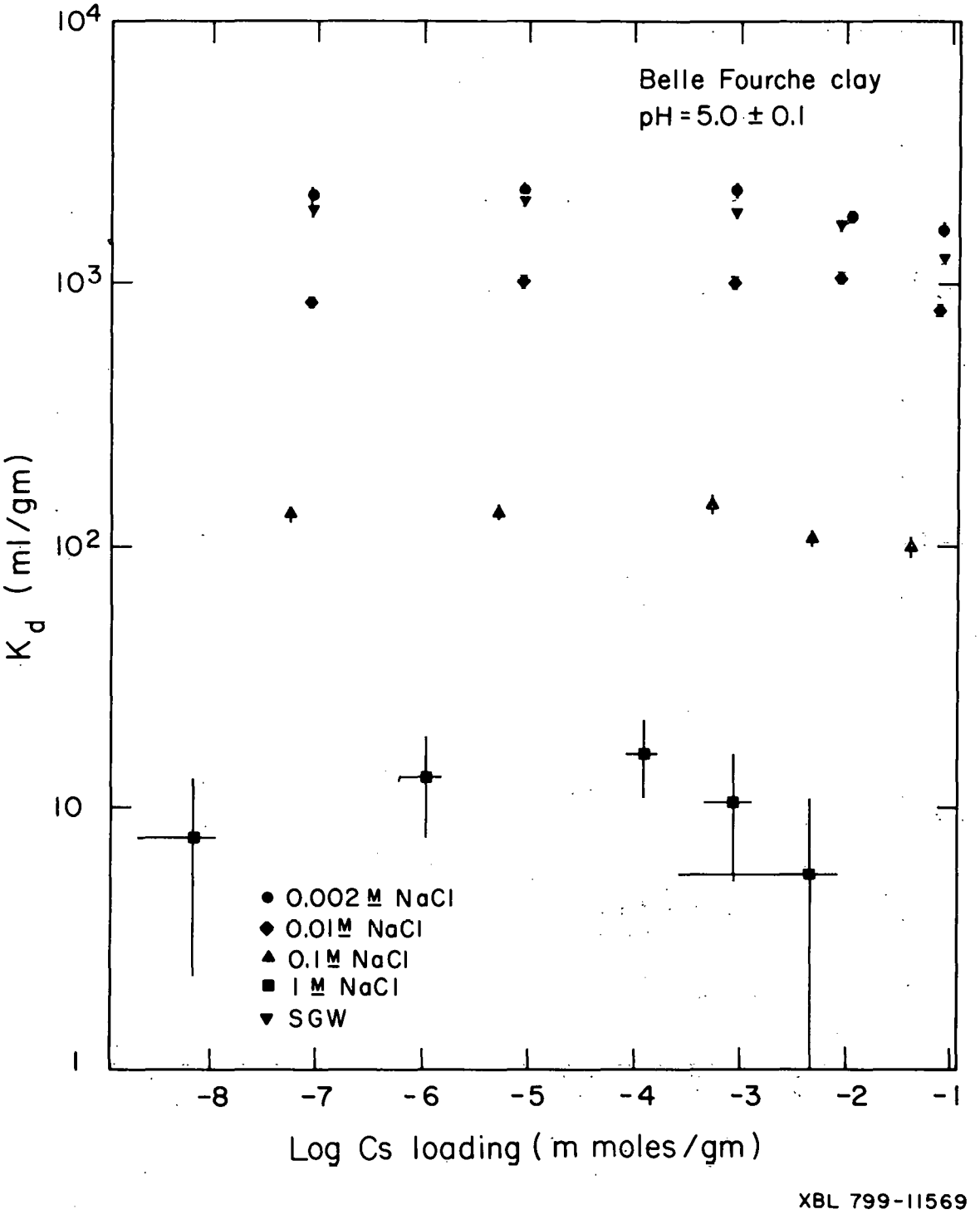

FIGURE 20. Distribution coefficients, K_d, for cesium measured at 26°C for the Na form of the Belle Fourche clay as a function of Cs loading at pH 5 for several electrolyte compositions. SGW = simulated basalt groundwater.

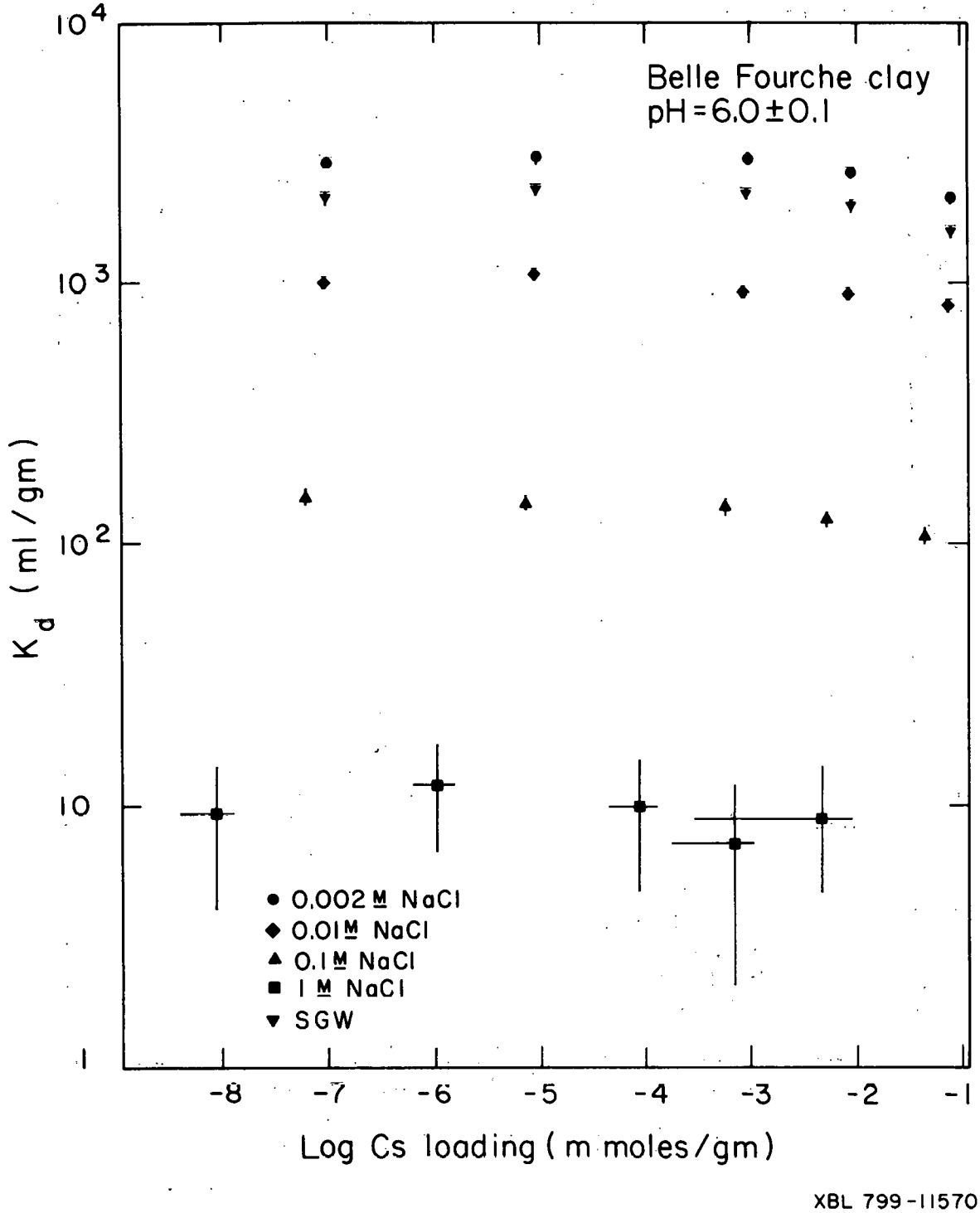

FIGURE 21. Distribution coefficients, K_d, for cesium measured at 26°C on the Na form of the Belle Fourche clay as a function of Cs loading at pH 6 for several electrolyte compositions. SGW = simulated basalt groundwater.

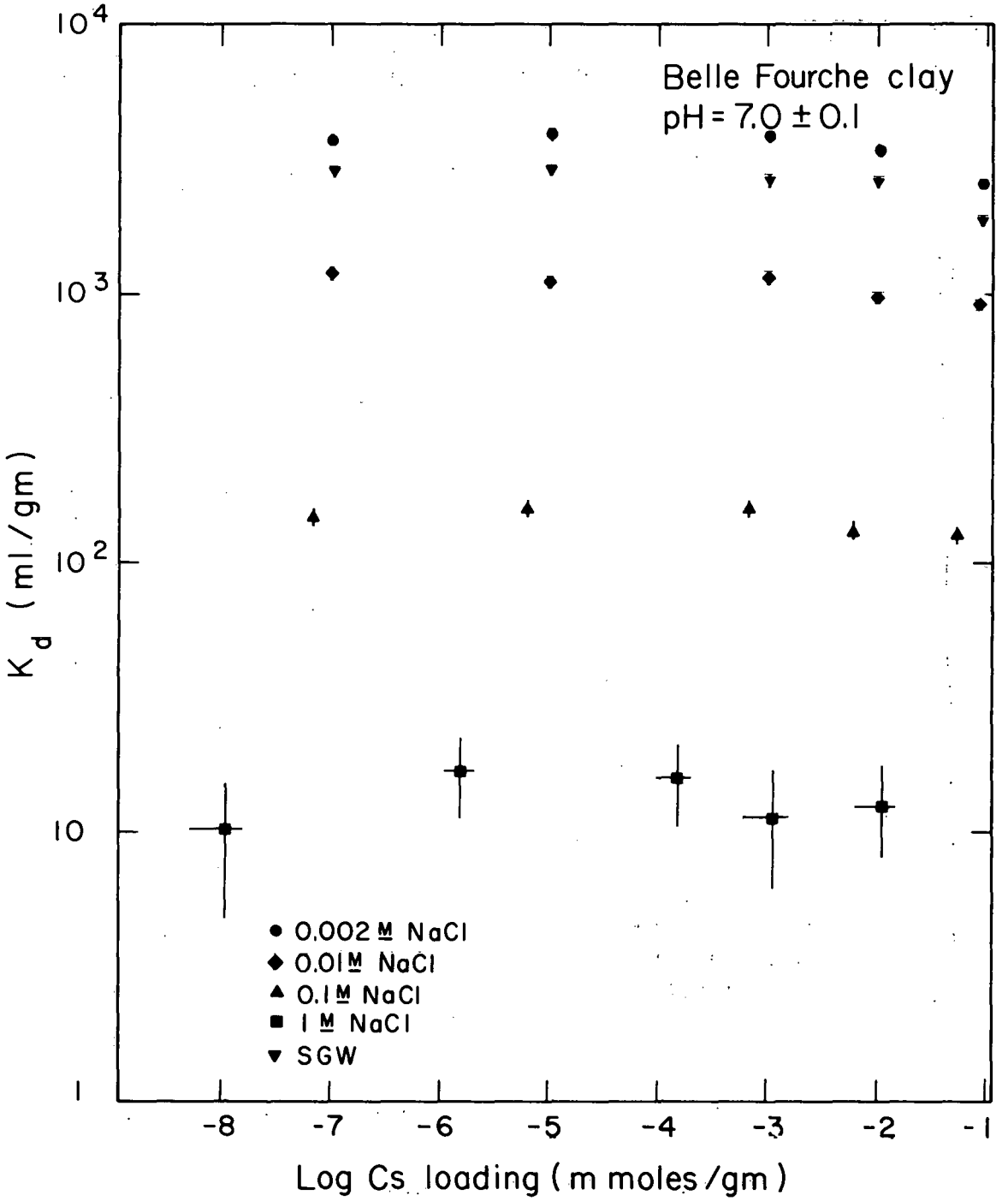

FIGURE 22. Distribution coefficients, K_d, for cesium measured at 26°C on the Na form of the Belle Fourche clay as a function of Cs loading at pH 7 for several electrolyte compositions. SGW = simulated basalt groundwater.

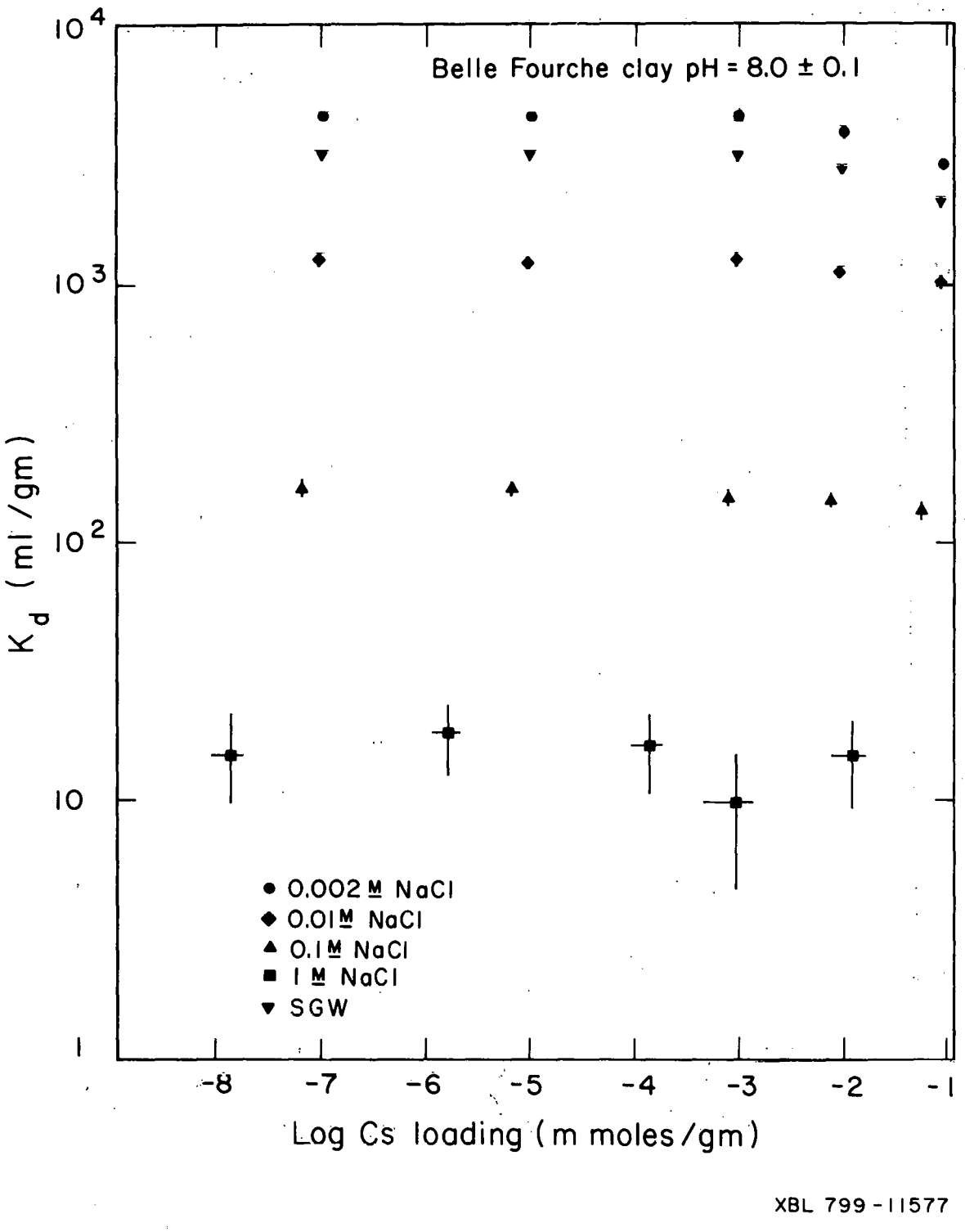

FIGURE 23. Distribution coefficients, K_d, for cesium measured at 26°C on the Na form of the Belle Fourche clay as a function of Cs loading at pH 8 for several electrolyte compositions. SGW = simulated basalt groundwater.

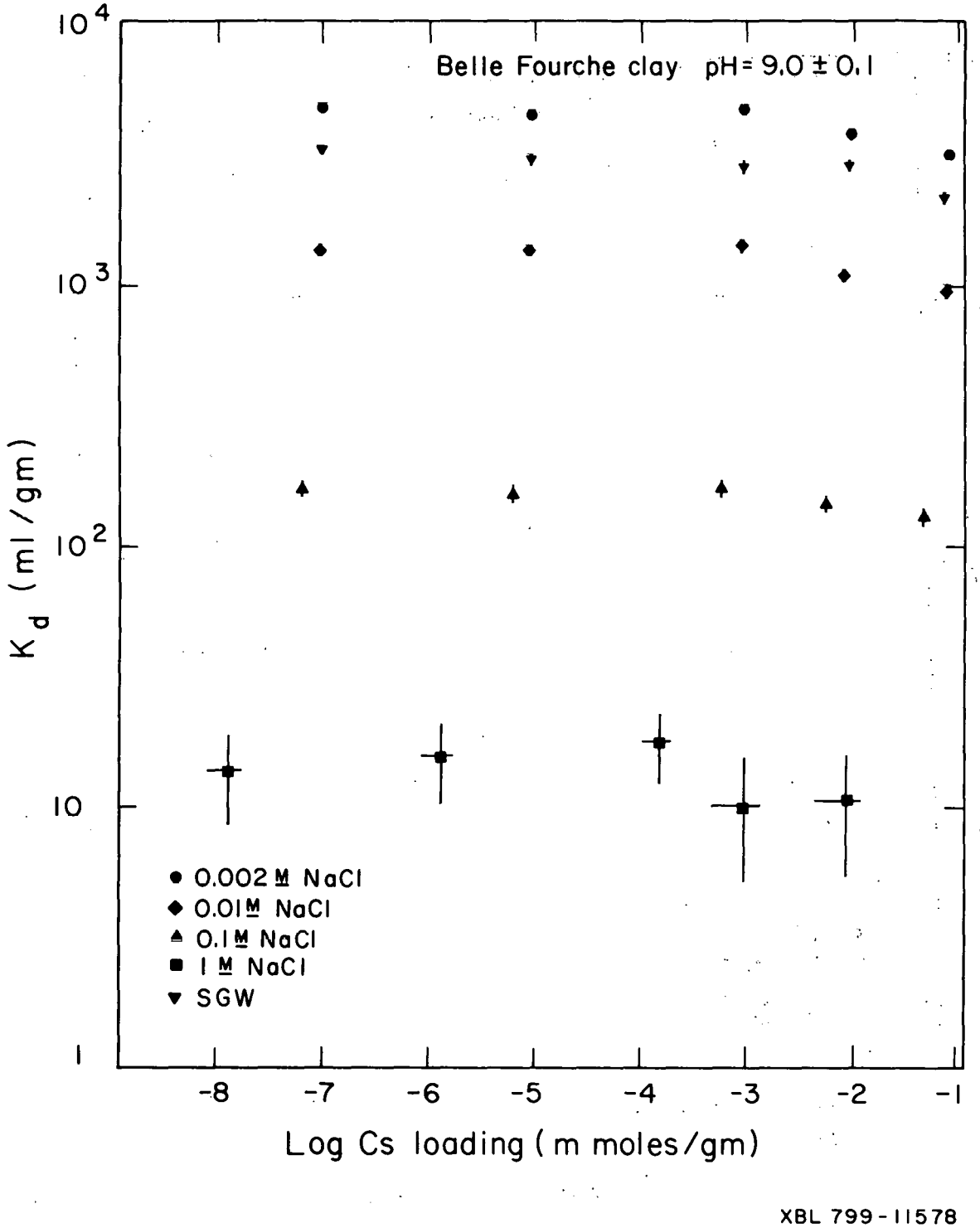

FIGURE 24. Distribution coefficients, K_d, for cesium measured at 26°C on the Na form of the Belle Fourche clay as a function of Cs loading at pH 9 for several electrolyte compositions. SGW = simulated basalt groundwater.

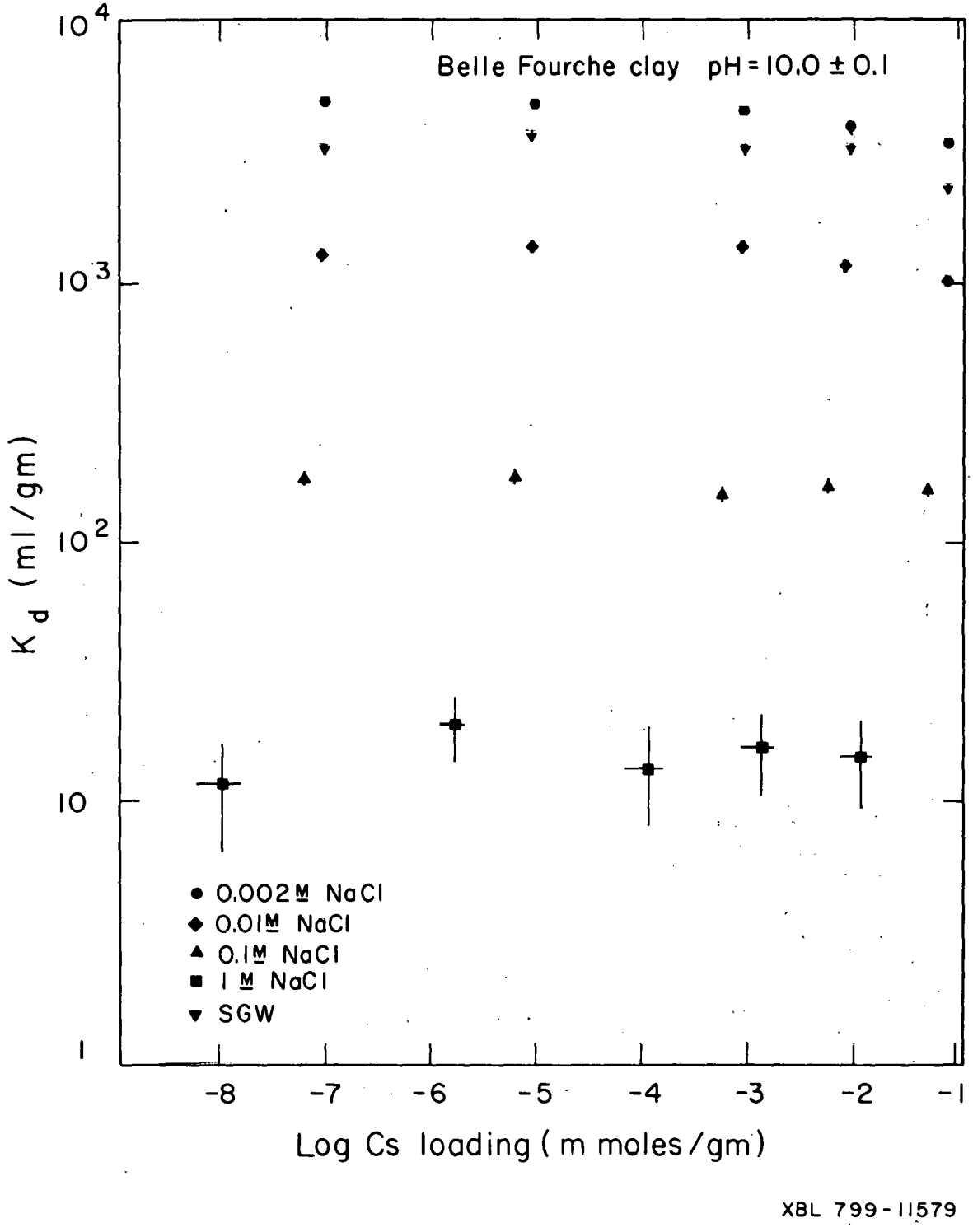

FIGURE 25. Distribution coefficients, K_d, for cesium measured at 26°C on the Na form of the Belle Fourche clay as a function of Cs loading at pH 10 for several electrolyte compositions. SGW = simulated basalt groundwater.

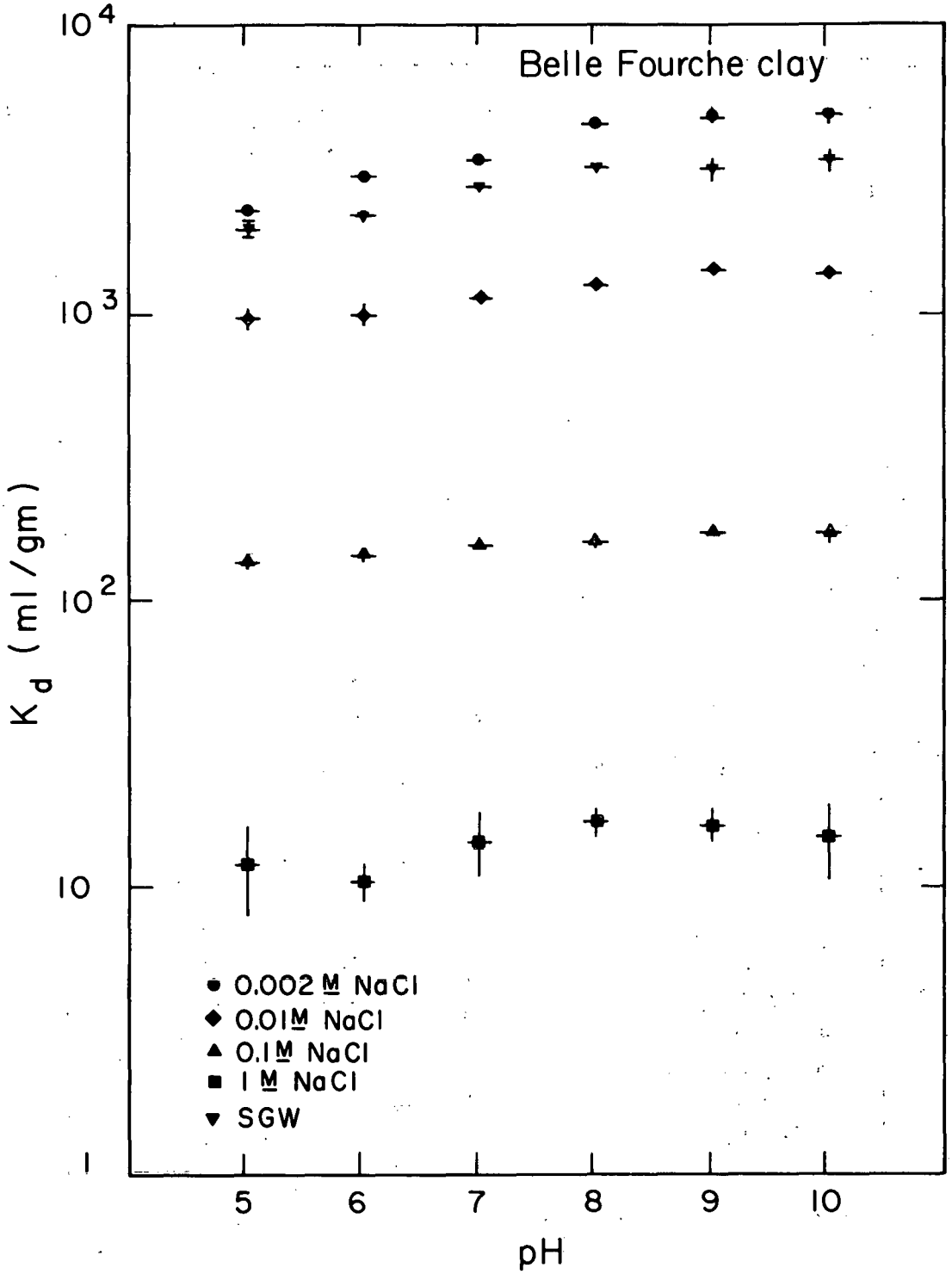

FIGURE 26. Average distribution coefficients, K_d, for cesium loadings less than 10^{-3} m moles/gm on the Belle Fourche clay as a function of pH for several electrolyte compositions. SGW = simulated basalt groundwater.

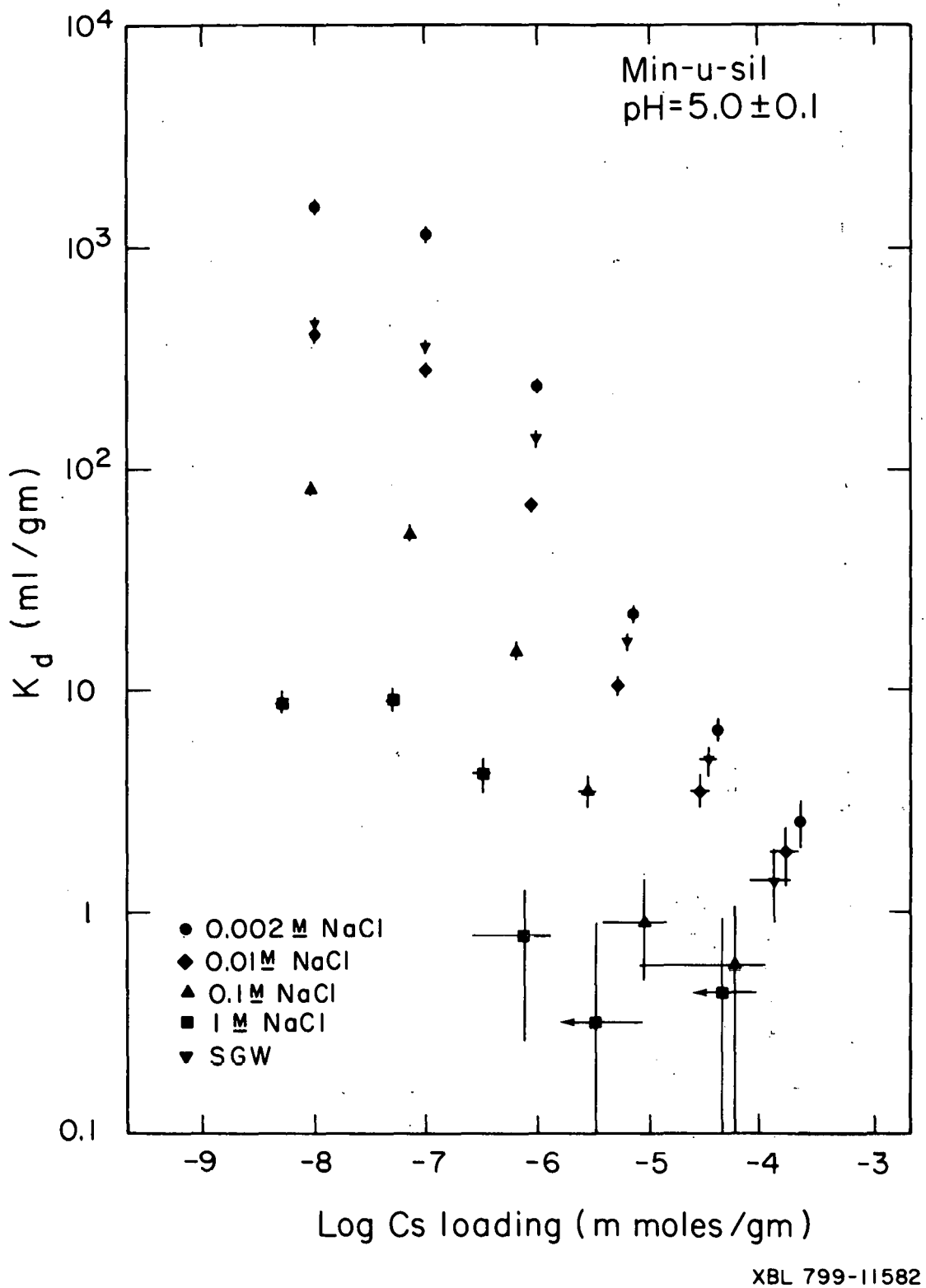

FIGURE 27. Distribution coefficients, K_d, for cesium measured at 26°C on Min-u-sil as a function of Cs loading at pH 5 for several electrolyte compositions. SGW = simulated basalt groundwater.

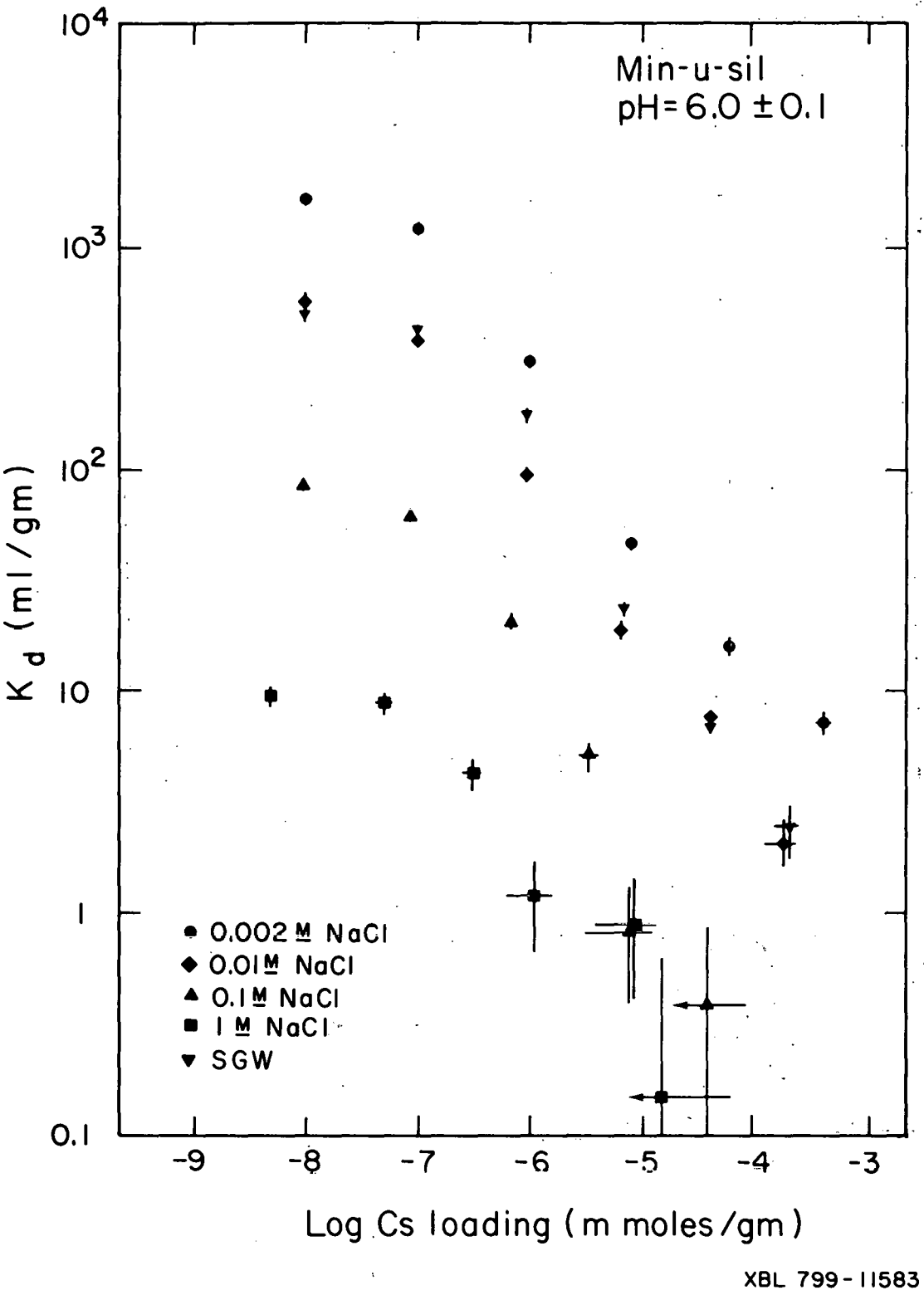

FIGURE 28. Distribution coefficients, K_d, for cesium measured at 26°C on Min-u-sil as a function of Cs loading at pH 6 for several electrolyte compositions. SGW = simulated basalt groundwater.

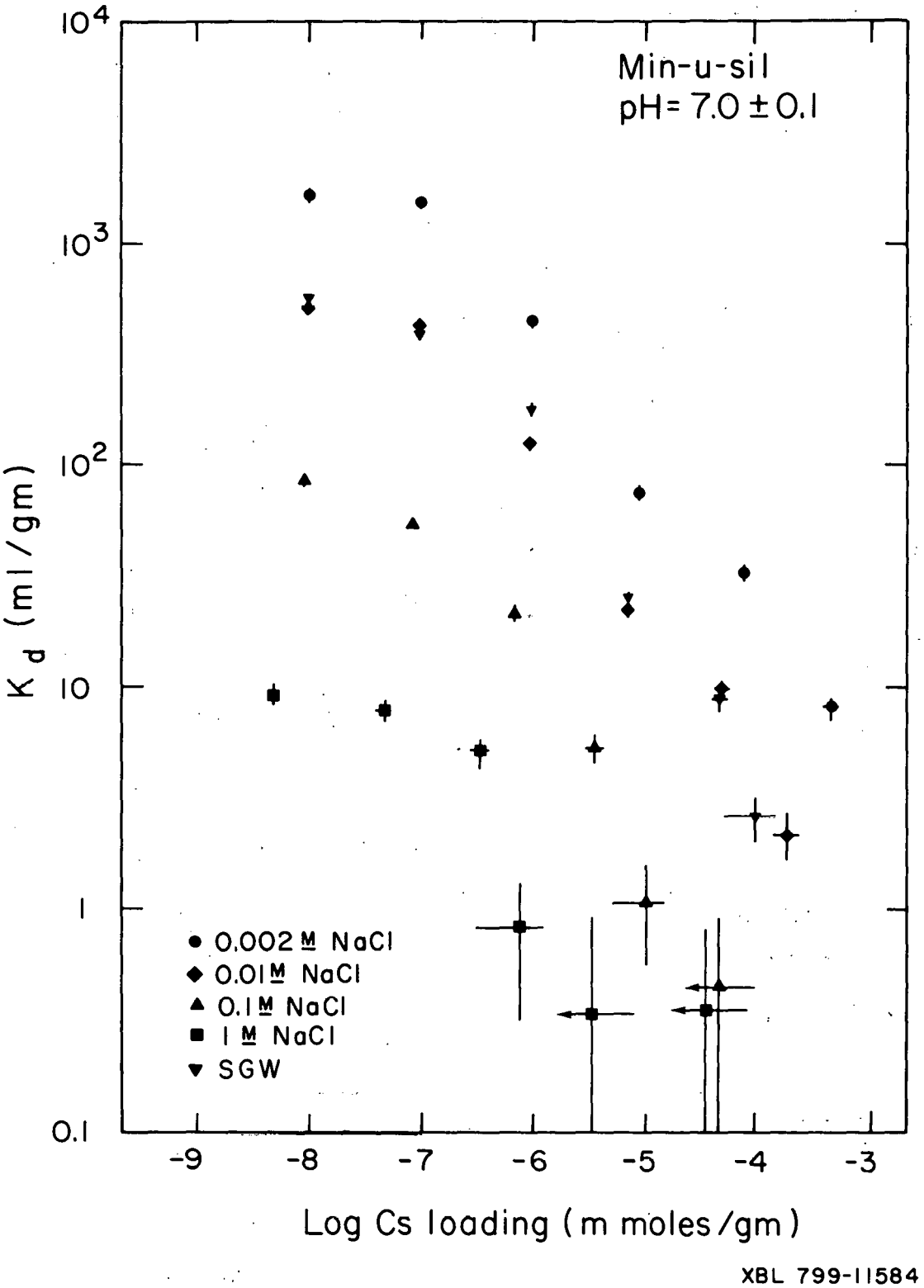

FIGURE 29. Distribution coefficients, K_d, for cesium measured at 26°C on Min-u-sil as a function of Cs loading at pH 7 for several electrolyte compositions. SGW = simulated basalt groundwater.

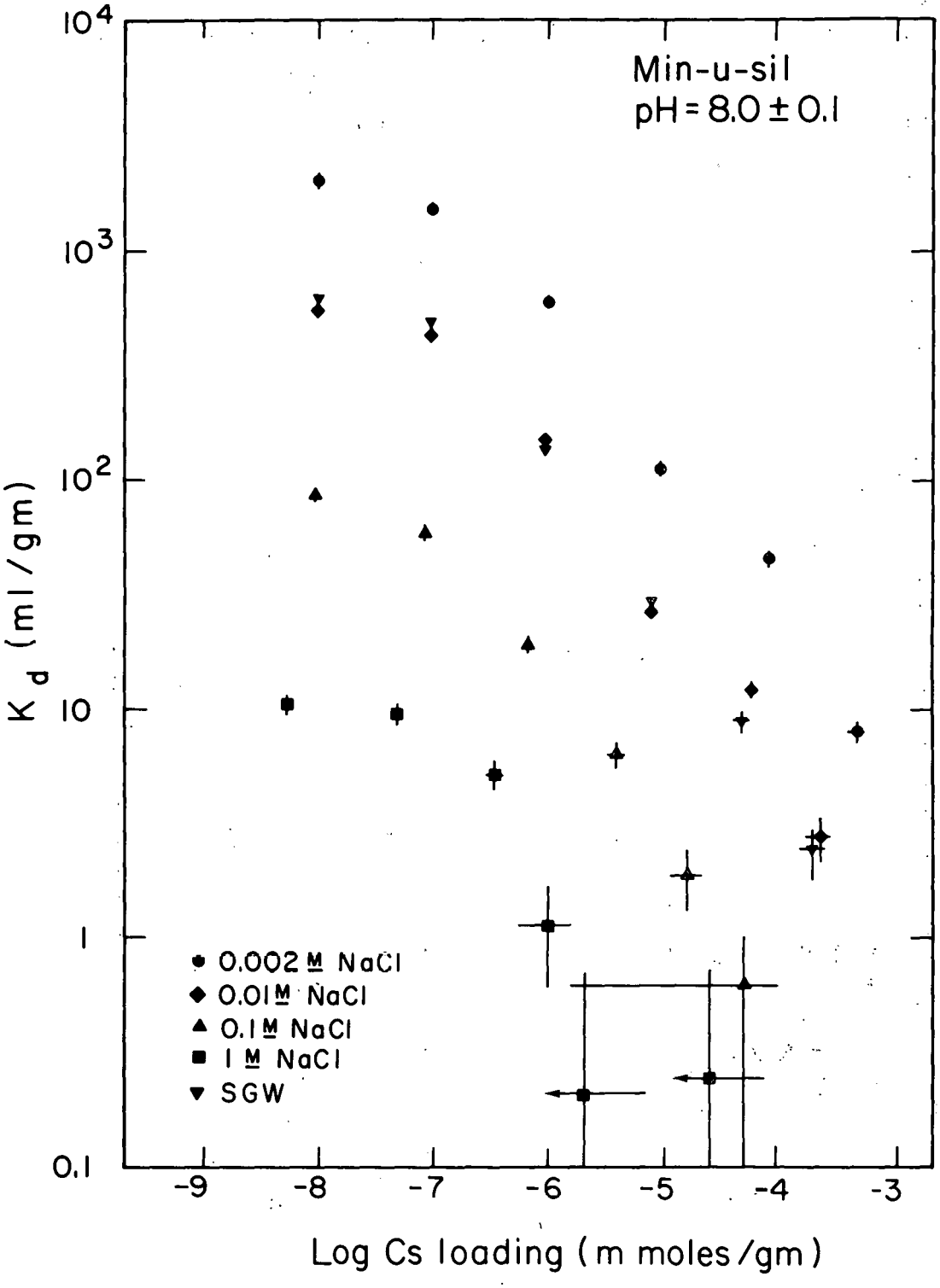

FIGURE 30. Distribution coefficients, K_d, for cesium measured at 26°C on Min-u-sil as a function of Cs loading at pH 8 for several electrolyte compositions. SGW = simulated basalt groundwater.

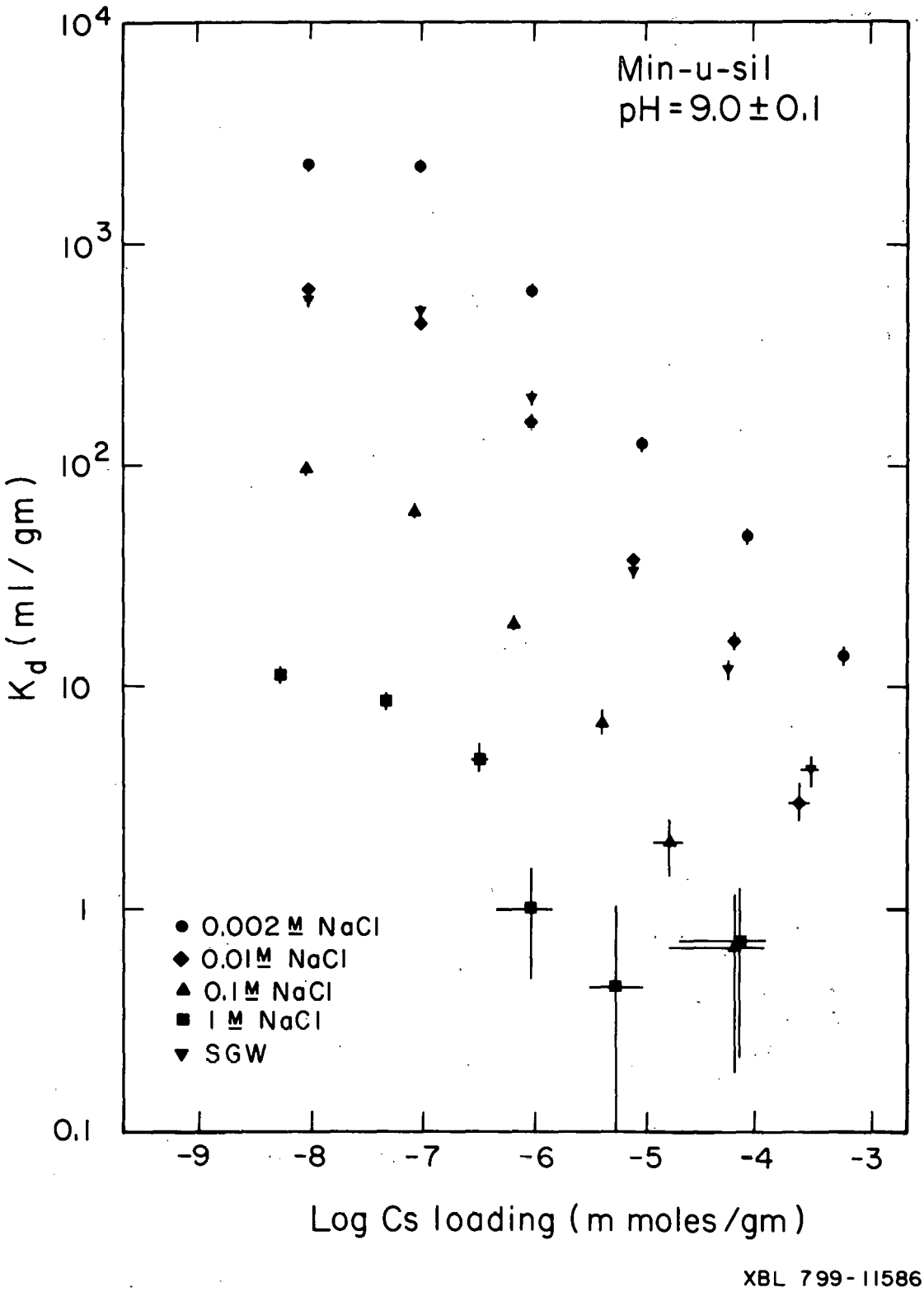

FIGURE 31. Distribution coefficients, K_d, for cesium measured at 26°C on Min-u-sil as a function of Cs loading at pH 9 for several electrolyte compositions. SGW = simulated basalt groundwater.

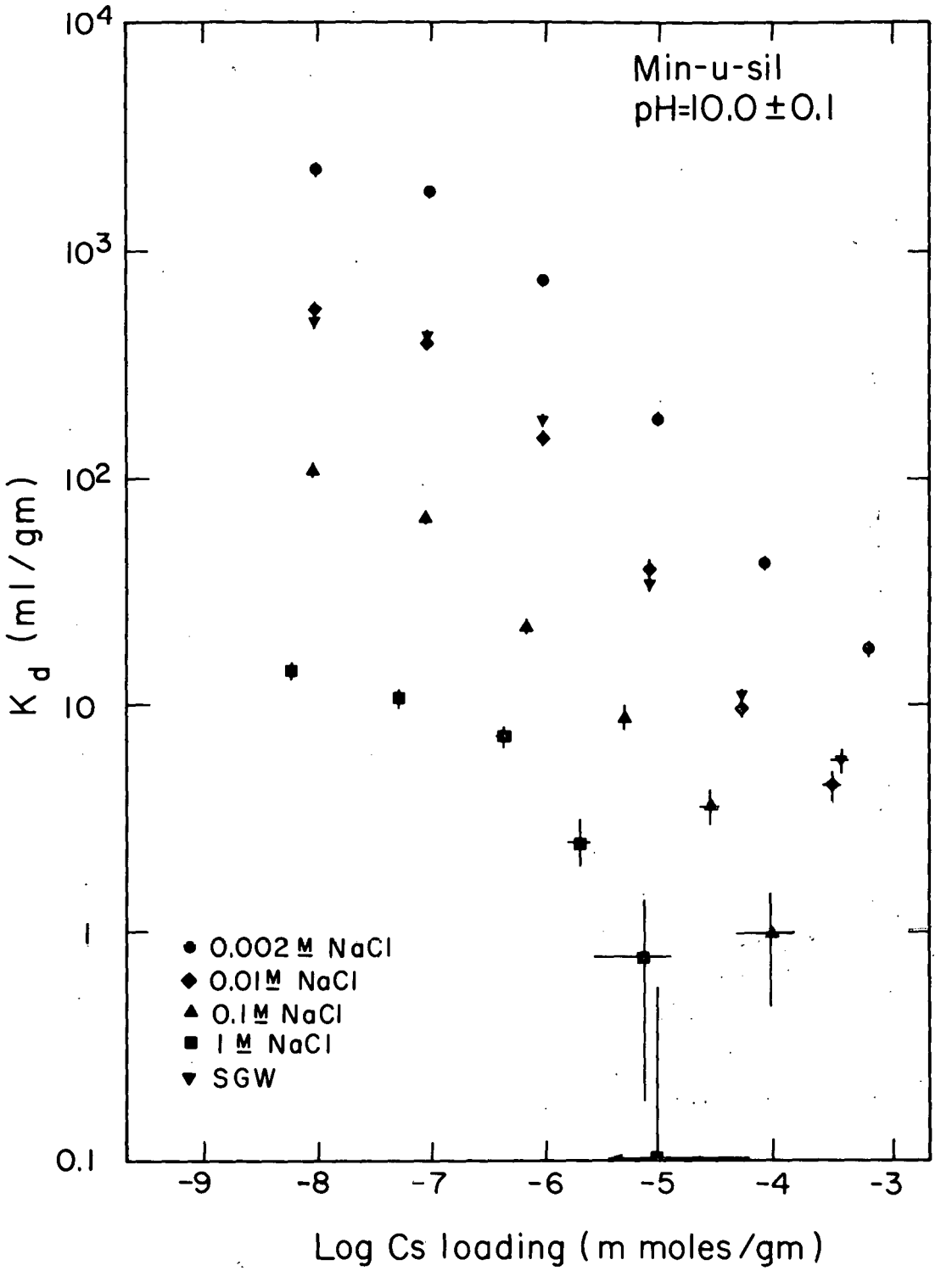

FIGURE 32. Distribution coefficients, K_d, for cesium measured at 26°C on Min-u-sil as a function of Cs loading at pH 10 for several electrolyte compositions. SGW = simulated basalt groundwater.

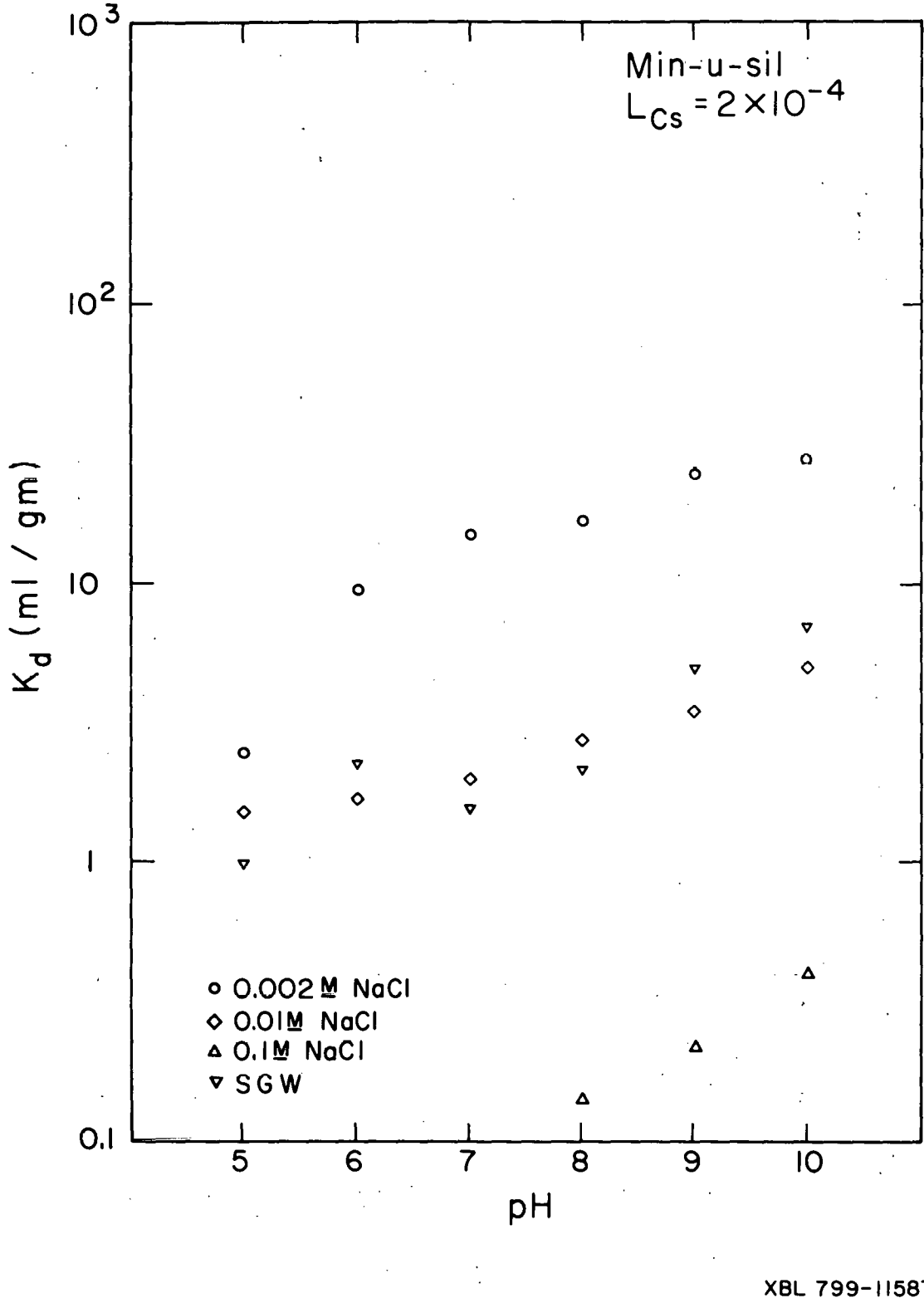

FIGURE 33. Distribution coefficients, K_d, for cesium on Min-u-sil as a function of pH for several electrolyte compositions. SGW = simulated basalt groundwater. Open points result from slicing through smooth curves through the points given in figures 27-32 at a Cs loading of 2×10^{-4} m moles/gm.

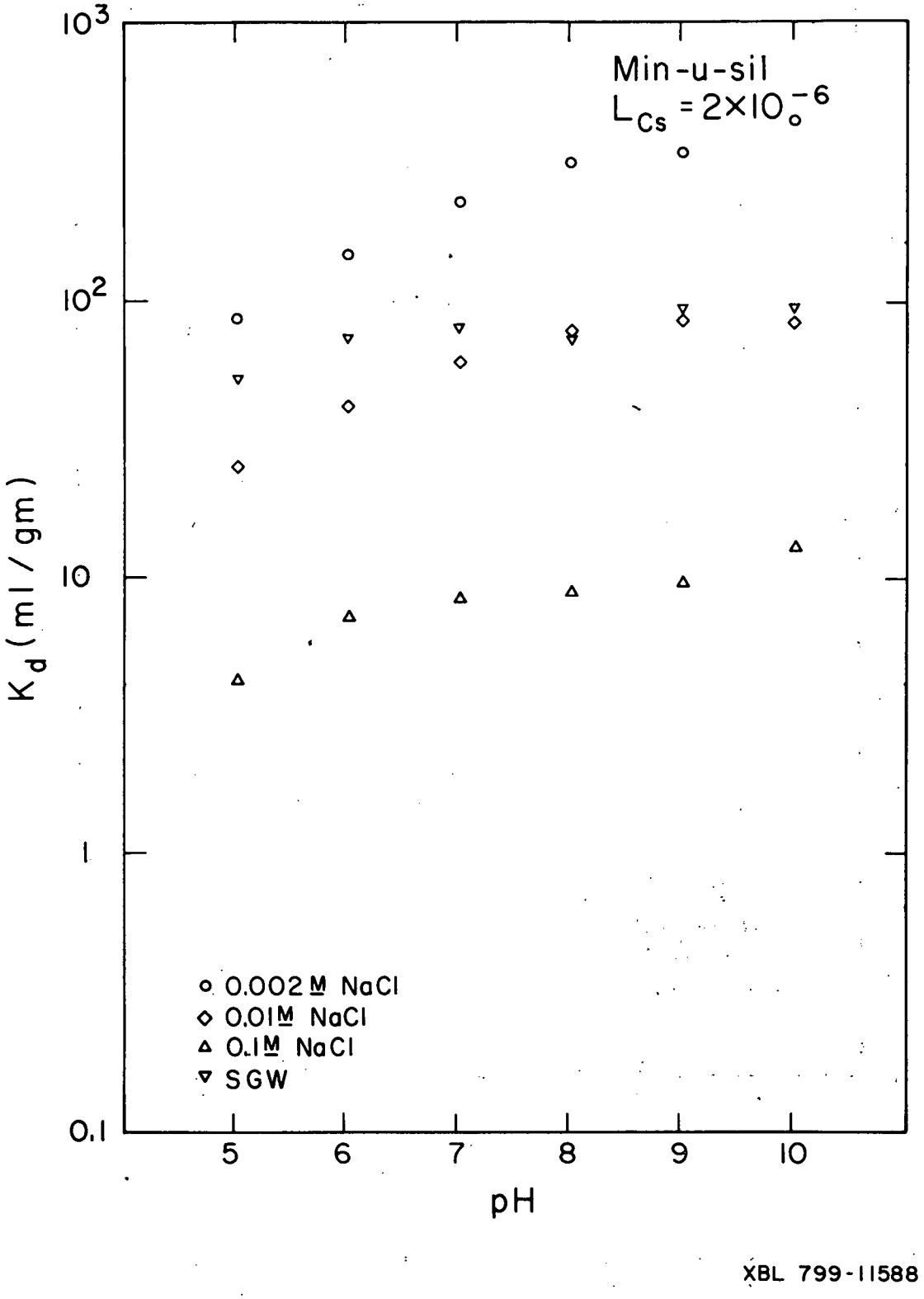

FIGURE 34. Distribution coefficients, K_d, for cesium on Min-u-sil as a function of pH for several electrolyte compositions. SGW = simulated basalt groundwater. Open points result from slicing through smooth curves through the points given in figures 27-32 at a Cs loading of 2×10^{-6} m moles/gm.

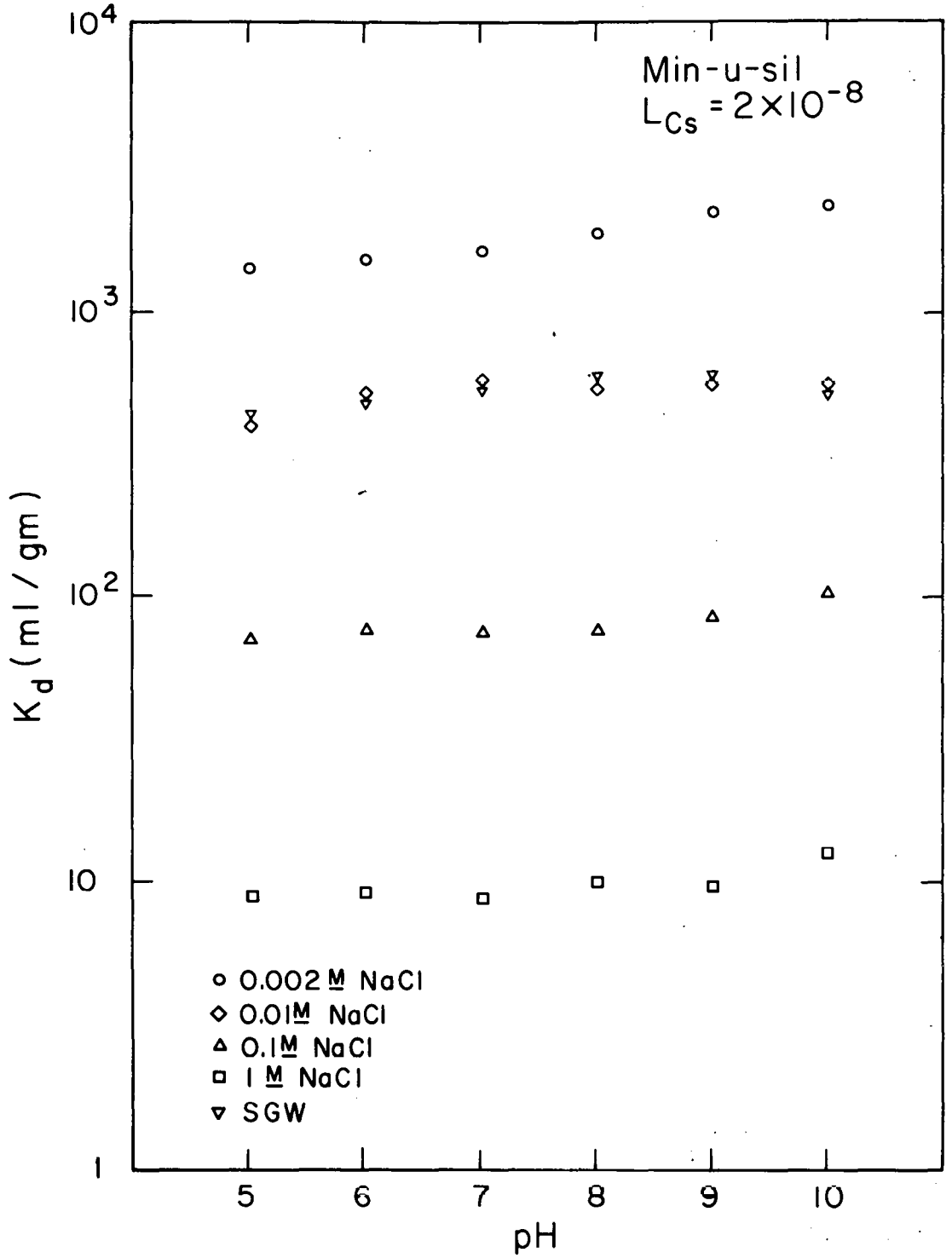

XBL 799-11589

FIGURE 35. Distribution coefficients, K_d, for cesium on Min-u-sil as a function of pH for several electrolyte compositions. SGW = simulated basalt groundwater. Open points result from slicing through smooth curves through the points given in figures 27-32 at a Cs loading of 2×10^{-8} m moles/gm.

analysis. At the higher loadings, the dependence of K_d on pH is rather large but this dependence decreases rapidly with decreased loading. For Min-u-sil, the results for the SGW are more nearly like the 0.01M NaCl solution than the 0.002M NaCl solution as was the case with the clay.

For the Belle Fourche clay, the K_d values showed only a small dependence on pH and Cs loading but a large dependence on electrolyte concentration. For the Min-u-sil, the K_d values showed a large dependence on all three parameters.

TESTING OF THE MODEL

SORPTION OF Cs ON BELLE FOURCHE CLAY

Several investigators (Garrels and Christ 1956; Blackman 1958; Truesdell and Christ 1968) have found from acid/base titrations that a single hydrogen clay behaves like a mixture of at least two distinct weak acids, i.e., two energetically different uniform sets of exchange sites. The possible nature of these sites have been discussed by Grim (Grim 1968, p.198) and James (James and Parks 1979). Our titration curves for the Belle Fourche clay also suggest the presence of two sites and, therefore, we have used a two-site model in our analysis.

Determination of MINEQL Modeling Parameters

Surface Ionization and Sodium Exchange Constants

In principle, the double extrapolation method should be applicable for determining the intrinsic surface ionization and sodium exchange constants from the titration data. As discussed previously, in practice the presence of a second site confuses the problem and long extrapolations make the results suspect. Instead, we were obliged to use a graphic method of fitting calculated curves to the titration data to obtain approximate values for these constants which ignores the changes in the constants due to surface charge. Therefore, the superscript, int, has been omitted from the symbols.

Since neither a positively charged surface nor a point of zero charge were observed for the clay in the pH region studied, the surface should be dominated by the species SO^-, TO^-, SO^-Na^+, TO^-Na^+, SOH and TOH, and the surface charge determined by the concentrations of the four charged species. For the SOH type site, we assume

$$SOH \rightleftarrows SO^- + H^+; \quad K_{a_2} = \frac{(SO^-)(H^+)_{aq}}{(SOH)} \tag{42}$$

$$SOH + Na^+ \rightleftarrows SO^-Na^+ + H^+; \quad {}^*K_{Na^+} = \frac{(SO^-Na^+)(H^+)_{aq}}{(SOH)(Na^+)_{aq}} \tag{43}$$

and,

$$(SO^-) + (SO^-Na^+) = \frac{K_{a_2}(SOH)}{(H^+)_{aq}} + \frac{{}^*K_{Na^+}(SOH)(Na^+)_{aq}}{(H^+)_{aq}} \tag{44}$$

or in logarithmic form,

$$\log[(SO^-) + (SO^-Na^+)] = \log(SOH) + pH + \log[K_{a_2} + {}^*K_{Na^+}(Na^+)] \tag{45}$$

Similar equations can be written for the TOH type sites.

At low pH values, little surface ionization occurs and $(SOH) \simeq N_s$, the total concentration of the SOH-type sites. In this pH region for constant Na^+ activity, a plot of $\log[(SO^-) + (SO^-Na^+)]$ versus pH should yield a curve which has a slope approaching +1 with decreasing pH. At high pH values, the surface is nearly completely ionized and $[(SO^-) + (SO^-Na^+)] \simeq N_s$. In this region, the slope of the curve should approach zero with increasing pH. The overall shape of the curve produced by plotting $\log[(SO^-) + (SO^-Na^+)]$ versus pH for a given value of Na^+ activity is independent of the actual values of N_s, K_{a_2}, and ${}^*K_{Na^+}$ (assuming they are constants) and, therefore, a generalized curve may be constructed. However, the position of the curve along the $\log[(SO^-) + (SO^-Na^+)]$ axis is determined by N_s, while the position along the pH axis is determined by $[K_{a_2} + {}^*K_{Na^+}(Na^+)]$. Thus, estimates for N_s, K_{a_2}, and ${}^*K_{Na^+}$ can be obtained by fitting the generalized curves to the experimental points calculated from the titration data.

The estimates for the surface ionization and Na exchange constants from this analysis are in actuality the fixed or average value of the reaction quotients, Q_{a_2} and ${}^{*}Q_{Na^+}$ of equations 9 and 10, that result in the best fit of the calculated curves to the experimental data over the entire titration range rather than the values of the quotients at zero surface charge. Therefore, one would expect these estimates to differ somewhat from the intrinsic constants.

Figures 36, 37, 38, and 39 show plots of $\log[(SO^-) + (SO^-Na^+)]$ versus pH for the four different electrolyte concentrations used in the titrations. The solid points were calculated from the titration data by assuming $[(SO^-) + (SO^-Na^+)] = \sigma_o / \beta$, where $[(SO^-) + (SO^-Na^+)]$ represents the sum of the contributions from both SOH and TOH sites. The solid curves, labeled SOH and TOH, are generalized curves so positioned that their sum, the dashed curves, gave the best fit to the experimental points. Since the data did not allow an accurate placement of the SOH curve along the pH axis at the low pH range for the 0.1M NaCl solution, it was arbitrarily set with the same spacing relative to the TOH curve as was observed for the other NaCl solutions, i.e., ~ 2 pH units. The limiting values that $\log[(SO^-) + (SO^-Na^+)]$ approached at high pH by the individual SOH and TOH curves, after adjusting their positions in this way, were taken as estimates for N_s for these two sites for the four different electrolyte concentrations. At one-half these limiting values, where $\log [(SO^-) + (SO^-Na^+)] = \log (SOH) = 1/2 \log N_s$, $[K_{a_2} + {}^{*}K_{Na^+}(Na^+)] = -pH$. Thus, estimates of the $[K_{a_2} + {}^{*}K_{Na^+}(Na^+)]$ can be obtained for the SOH and TOH sites for the four electrolyte concentrations from the corresponding SOH and TOH curves by identifying the pH values that satisfy this condition. The values of N_s and $[K_{a_2} + {}^{*}K_{Na^+}(Na^+)]$ estimated from the SOH and TOH curves are given in the figures. For each type of site, the four equations, one for each electrolyte concentration, relating K_{a_2} and ${}^{*}K_{Na^+}$ were solved simultaneously to give the best values for these parameters. These values are given in Table 16.

TABLE 16. MINEQL Modeling Parameters for the Belle Fourche Clay.

	SOH	TOH
N_s (meq./100 gm)	36	84
pK_{a_2}	4.0	7.1
$p^*K_{Na^+}$	0.24	2.9
$p^*K_{Cs^+}$	- 0.84	1.8

Total surface area = 800 m^2/gm

Total C.E.C. = 120 meq/gm

$K^a_{Cs/Na} = 12$

$C_1 = 500\ \mu F/cm^2$

$C_2 = 20\ \mu F/cm^2$

Site Concentrations

When using a two-site model in MINEQL, the concentrations of the two sites must be entered separately. The apparent ratio of the concentrations of SOH to TOH sites was nearly constant for the 0.001M, 0.01M and 0.1M NaCl solutions, i.e., ~ 0.43, however, the ratio for the 0.0002M NaCl solution was 0.80. A repeat of the titrations yielded essentially the same results. The reason for the difference in the (SOH) to (TOH) ratio between the 0.0002M and the other NaCl concentrations is not known. Since the Cs sorption isotherms were measured over a NaCl concentration range of 0.002M to 1M, a ratio of 0.43 was used to calculate the concentrations of the SOH and TOH sites from the C.E.C. value of 120 meq/100 gms measured for Cs and Na. These values are given in Table 16.

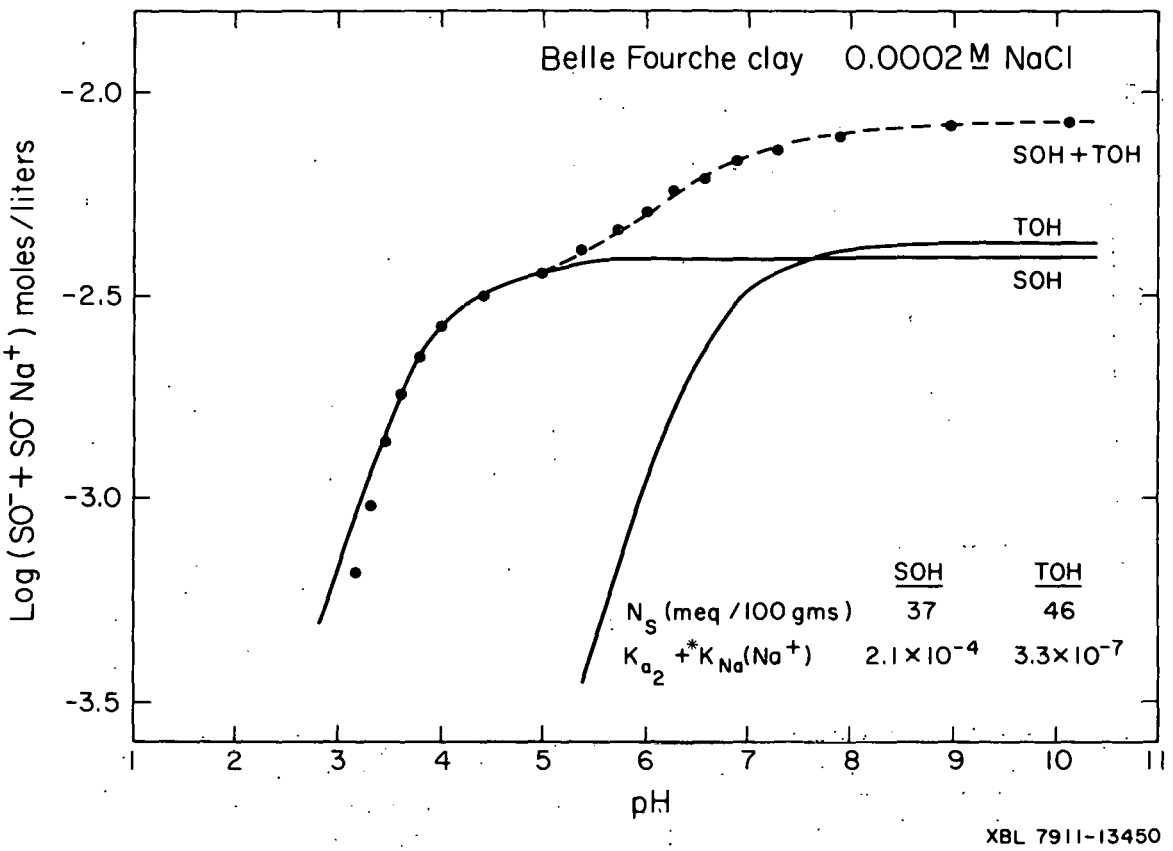

FIGURE 36. The concentration of negative sites, where $[(SO^-) + (SO^-Na^+)]$ represent contributions from both the SOH and TOH sites, as a function of pH for a NaCl electrolyte concentration of 0.0002M. The solid points were calculated from the titration data using equations 36 and 44. The lines result from the fitting of generalized curves based on equation 45 (see text for explanation). Also shown are the site concentrations, N_s, and the values of $[K_{a2} + {}^*K_{Na} + (Na+)]$ for the SOH and TOH sites that result from the fitting analysis.

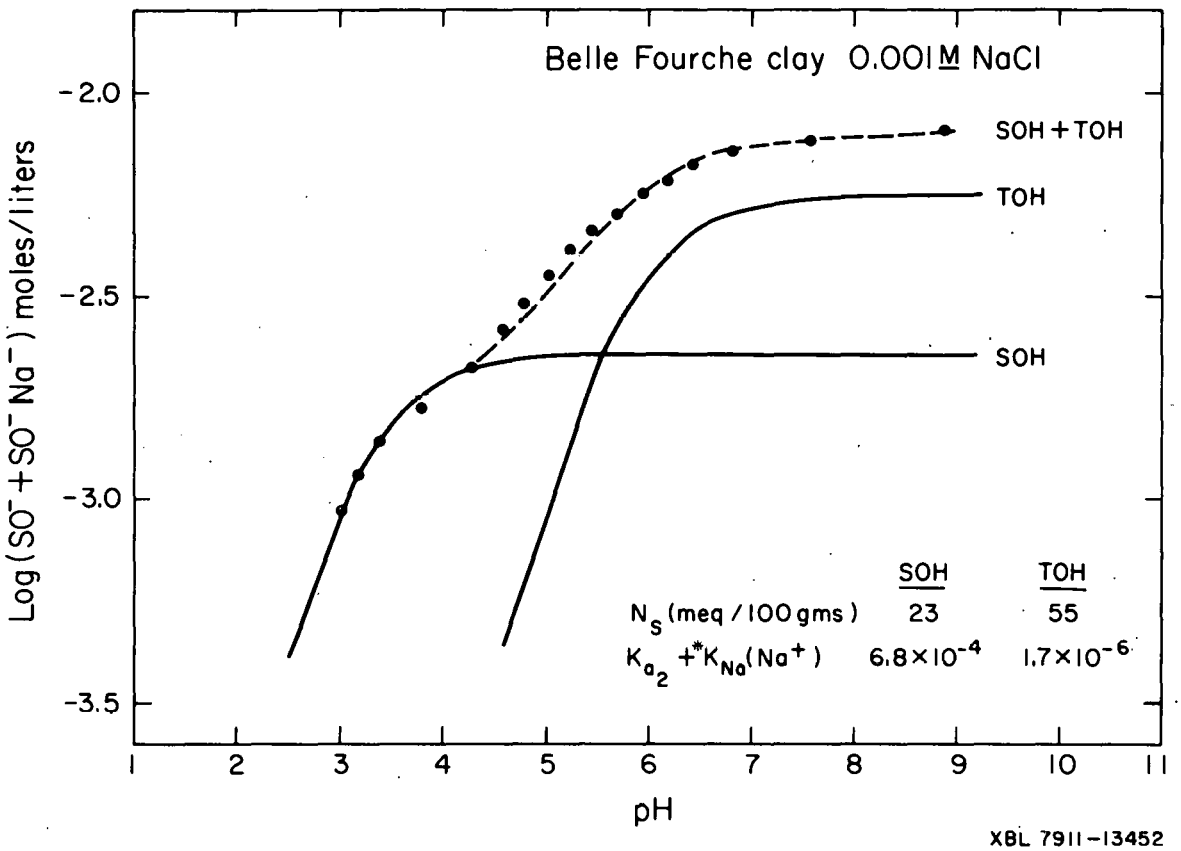

FIGURE 37. The concentration of negative sites, where $[(SO^-) + (SO^-Na^+)]$ represent contributions from both the SOH and TOH sites, as a function of pH for a NaCl electrolyte concentration of 0.001M. The solid points were calculated from the titration data using equations 36 and 44. The lines result from the fitting of generalized curves based on equation 45 (see text for explanation). Also shown are the site concentrations and the values of $[K_{a2} + {}^*K_{Na} + (Na^+)]$ for the SOH and TOH sites that result from the fitting analysis.

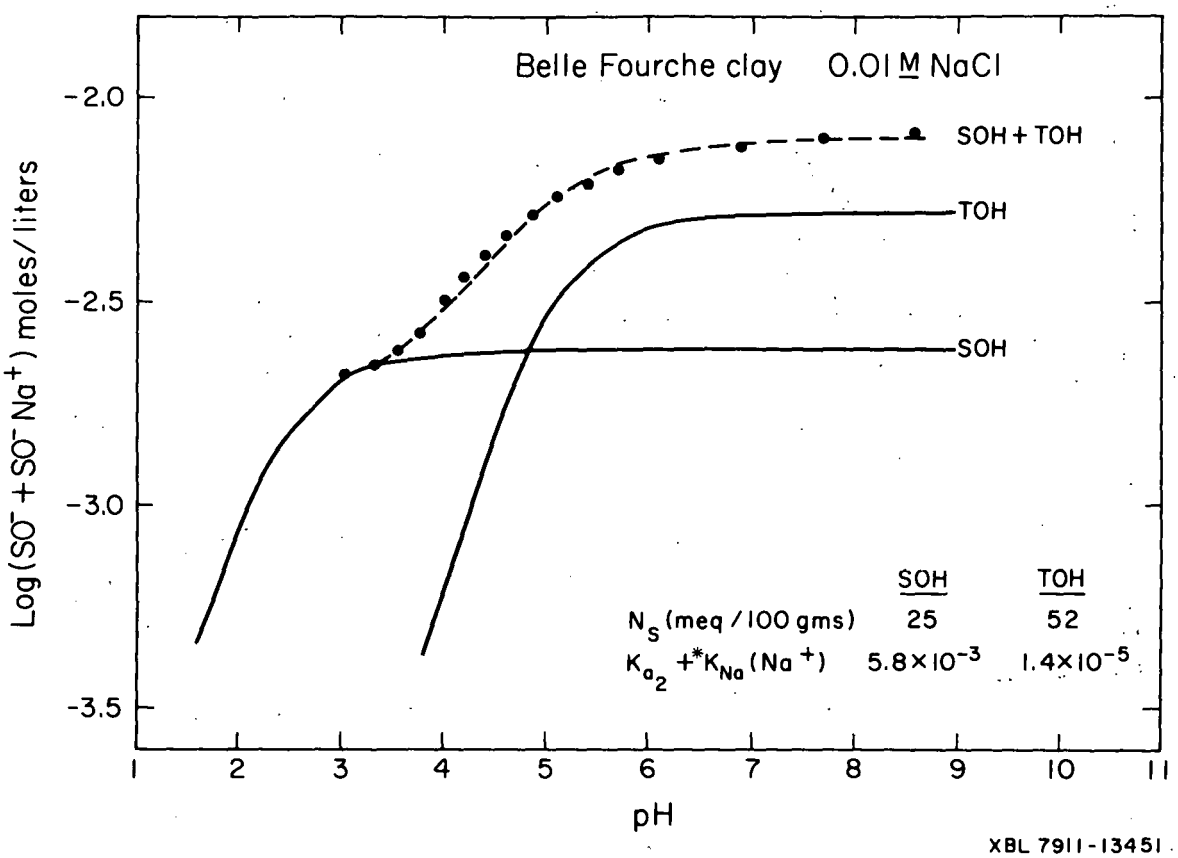

FIGURE 38. The concentration of negative sites, where $[(SO^-) + (SO^-Na^+)]$ represent contributions from both the SOH and TOH sites, as a function of pH for a NaCl electrolyte concentration of 0.01M. The solid points were calculated from the titration data using equations 36 and 44. The lines result from the fitting of generalized curves based on equation 45 (see text for explanation). Also shown are the site concentrations, N_S, and the values of $[K_{a_2} + {}^*K_{Na} + (Na^+)]$ for the SOH and TOH sites that result from the fitting analysis.

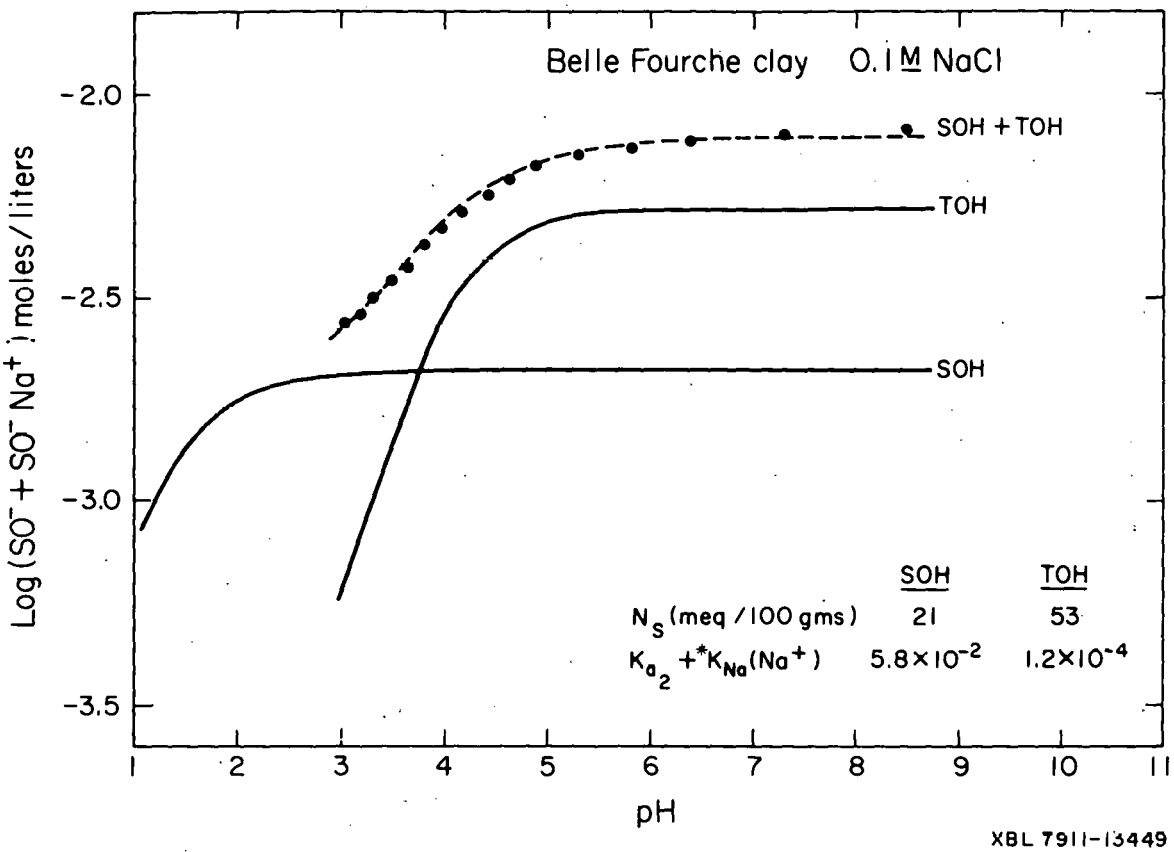

FIGURE 39. The concentration of negative sites, where $[(SO^- + SO^-Na^+)]$ represent contributions from both the SOH and TOH sites, as a function of pH for a NaCl electrolyte concentration of 0.1M. The solid points were calculated from the titration data using equations 36 and 44. The lines result from the fitting of generalized curves based on equation 45 (see text for explanation). Also shown are the site concentrations, N_S, and the values of $[K_{a2} + {}^*K_{Na^+}(Na^+)]$ for the SOH and TOH sites that result from the fitting analysis.

The Cesium Exchange Constant

Given the values of ${}^*K_{Na^+}$ estimated in the preceding section, the Cs exchange constant, ${}^*K_{Cs^+}$, can be calculated from the values of $K^a_{Cs/Na}$ given in Figures 8-13 through the relationship

$$\frac{{}^*K_{Cs^+}}{{}^*K_{Na^+}} = K^a_{Cs/Na} \qquad (46)$$

The values of $K^a_{Cs/Na}$ varied from 6.3 to 9.4 over the pH range 5 - 10. Using an average value of 8 and assuming that $K^a_{Cs/Na}$ is the same for both types of site, values for ${}^*K_{Cs^+}$ were calculated from the corresponding values of ${}^*K_{Na^+}$ for the SOH and TOH sites. The first attempts to simulate the Cs sorption isotherms for the clay using these values in MINEQL resulted in calculated K_d values consistently lower than the experimental ones by a factor of about 2 under all conditions. Better overall agreement was obtained using a value of 12 for $K^a_{Cs/Na}$. The values for ${}^*K_{Cs^+}$ given in Table 16 were obtained using this number. We do not as yet know the reason for this discrepancy.

Integral Capacitances

The integral capacitances of the electrical double layer, C_1 and C_2 in equation 20, are required as input parameters to MINEQL. A value of about 20 $\mu F/cm^2$ has been found for the diffuse layer capacitance, C_2, for Hg (Stumm 1970), AgI (Lyklema 1961), and a number of oxide surfaces (Yates 1974), and has been used successfully for simulated titrations of latexes and clays (James 1979). We have used this value for C_2 in our analysis.

The value of C_1 is customarily taken as an adjustable parameter. It affects the slope of the σ_0 versus pH curves. MINEQL calculates σ_0 for a given set of parameters and thus it is possible to obtain calculated values of σ_0 as a function of pH and electrolyte concentration. Using the other parameters given in Table 16, σ_0 was calculated for electrolyte concentrations

of 0.0002M, 0.001M, 0.01M and 0.1M as a function of pH over the range 3 to 10 for C_1 values of 120, 250, 500, and 750 $\mu F/cm^2$. The calculated curves were compared with the appropriate experimental ones shown in Figure 4. A value of 500 $\mu F/cm^2$ gave the best simulation over the pH range used in the Cs sorption measurements, i.e., 5 to 10, and was used in the subsequent calculations to simulate the Cs sorption isotherms.

Calculations of the Cs Sorption Isotherms

Using the parameters listed in Table 16, Cs sorption isotherms were calculated for the same values of initial Cs concentrations, pH and NaCl concentrations as used in the experimental measurements. The results of these calculations are shown in Figures 40 through 45 (curves) along with the experimental values (points). The solid curves were calculated without including the electrical double layer effects while the dashed curves resulted when they were included. The dashed and solid curves occur in pairs, the top-most pair corresponds to the 0.002M NaCl solution, the next lower pair to the 0.01M NaCl solution, the next lower to 0.1M NaCl, and the lowest to 1M NaCl. Where the solid and dashed curves coincide, only the solid curve is shown.

Comparisons of the calculations with the experimental data shown in the figures demonstrates that MINEQL is able to simulate the Cs sorption isotherms rather well for the most part. The data for the 0.1M and 1M NaCl solutions is fit for all Cs loadings and pH values. However, the MINEQL calculations underestimate the K_d values at the lowest pH for both the 0.002M and 0.01M NaCl solution and overestimate the K_d values for the 0.002M NaCl solution at high pH values. These trends are more easily seen in Figure 46 which shows the variation of K_d with pH for an initial Cs concentration of 10^{-7}M. Again, the points are the experimental values and the curves are the MINEQL simulations. The cause of the deviation between experiment and calculation is being investigated so that corrections can be made. The calculations with and without the inclusion of the electrical double layer effects give essentially the same results for the 0.1M and 1M NaCl solutions. There is a difference for the other NaCl concentrations but the difference decreases with increasing pH. Inclusion of the electrical double layer effects does not improve the overall

There is a difference for the other NaCl concentrations but the difference decreases with increasing pH. Inclusion of the electrical double layer effects does not improve the overall quality of the fit of the calculations to the experimental data. However, it should be remembered that the acid dissociation and sodium exchange constants were extracted from the titration data by essentially ignoring surface charge effects. They represent average values for the entire titration range rather than the actual intrinsic constants for zero surface charge, i.e., there is some average electrical double layer effect included in the constants. Other methods for obtaining the intrinsic constants from the experimental data are being investigated.

There were difficulties in obtaining values for some of the input parameters required by MINEQL in a straightforward manner and further efforts to improve our understanding of the nature of these problems is needed. However, these first attempts to use MINEQL to simulate the Cs sorption isotherms are very encouraging and further testing of the model with other substrates and radionuclides is in progress.

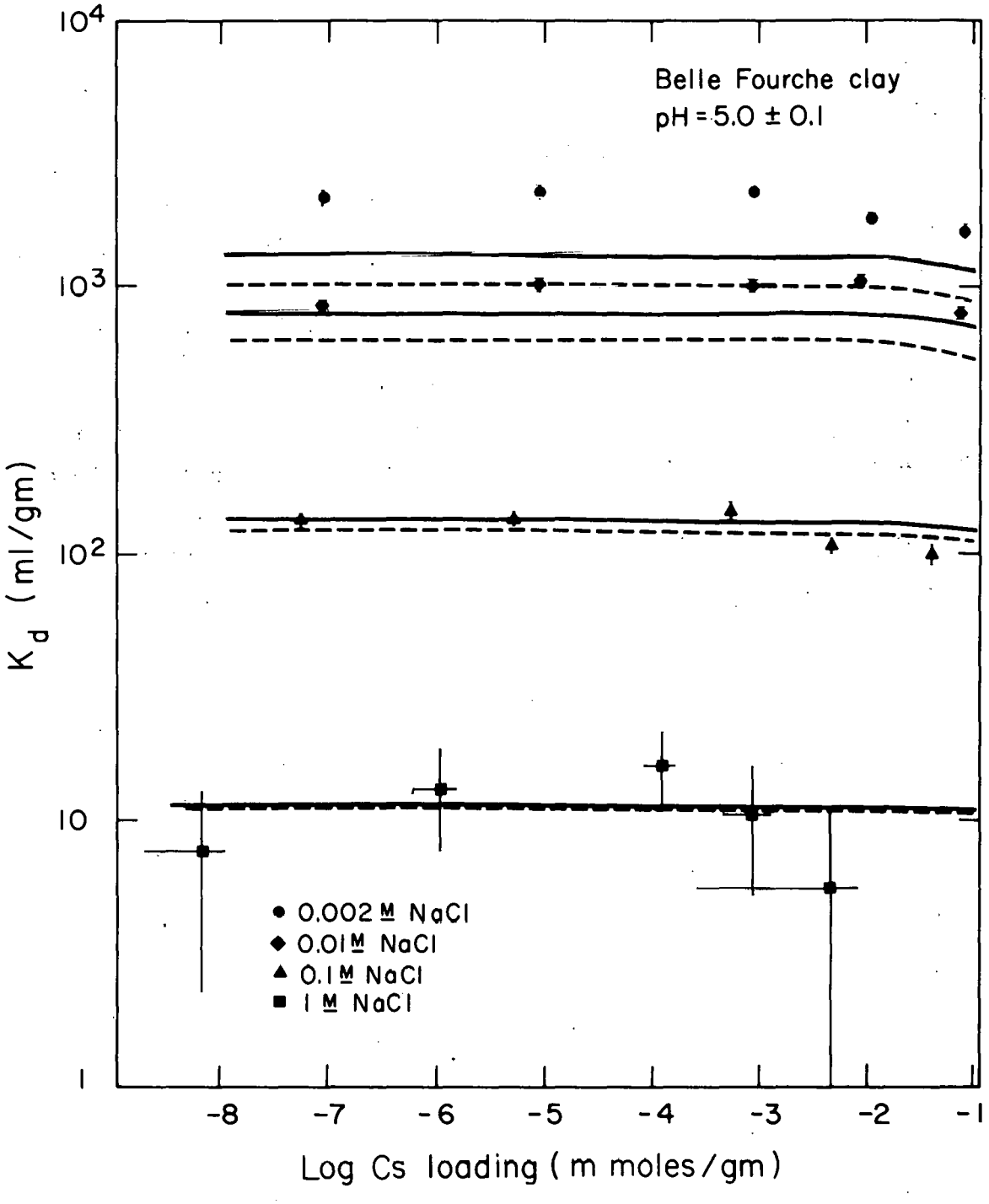

FIGURE 40. Cs sorption isotherms (26°C) for the Belle Fourche clay for several NaCl electrolyte concentrations at pH 5. The solid points represent the experimental data given in Table 4. The solid and dashed curves were calculated using MINEQL without and with the inclusion of the electrical double layer effects, resp. Upper most pair of solid and dashed curves for 0.002M NaCl.

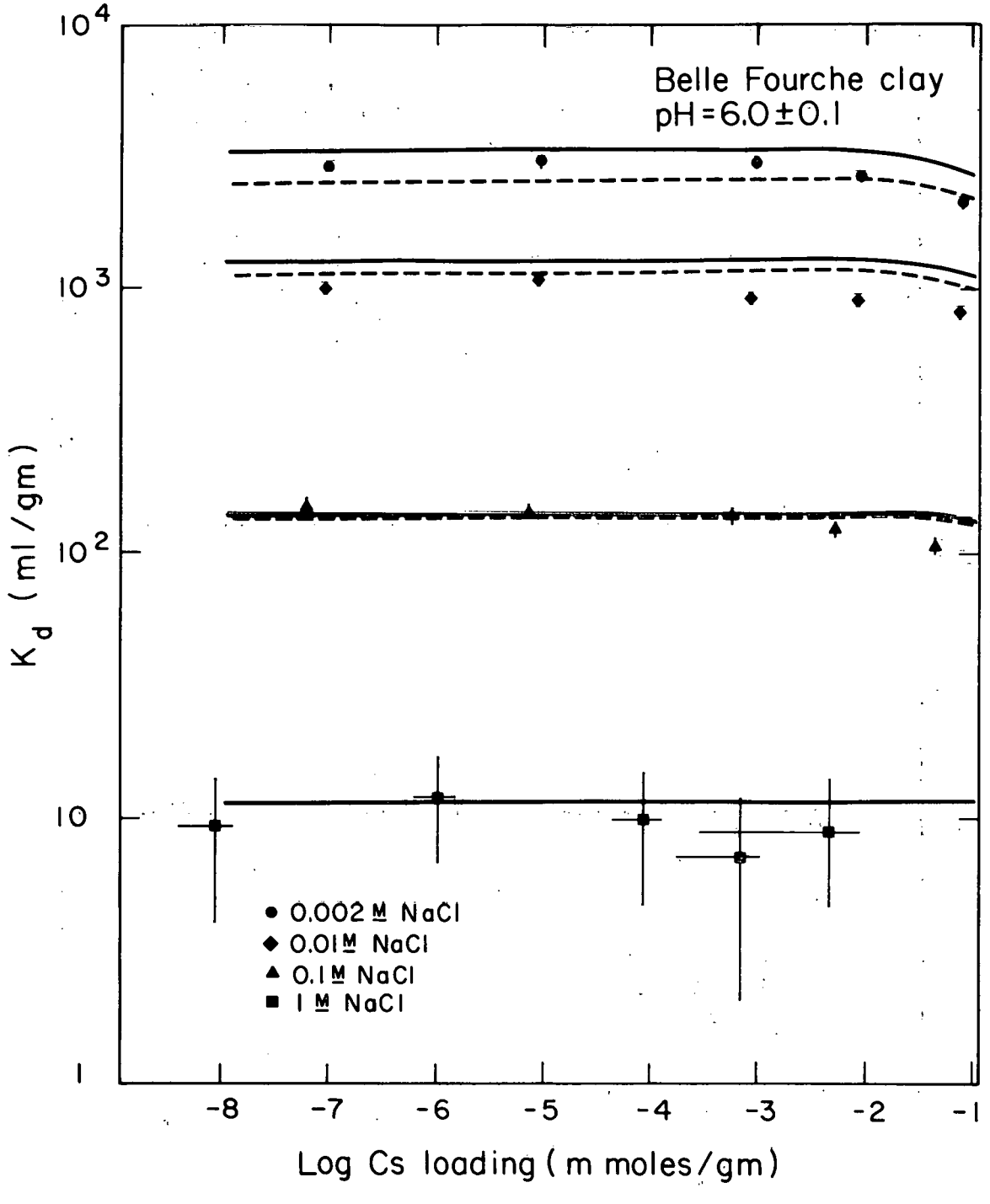

XBL 799-11570A

FIGURE 41. Cs sorption isotherms (26°C) for the Belle Fourche clay for several NaCl electrolyte concentrations at pH 6. The solid points represent experimental data given in Table 4. The solid and dashed curves were calculated using MINEQL without and with inclusion at the electrical double layer effects, resp.

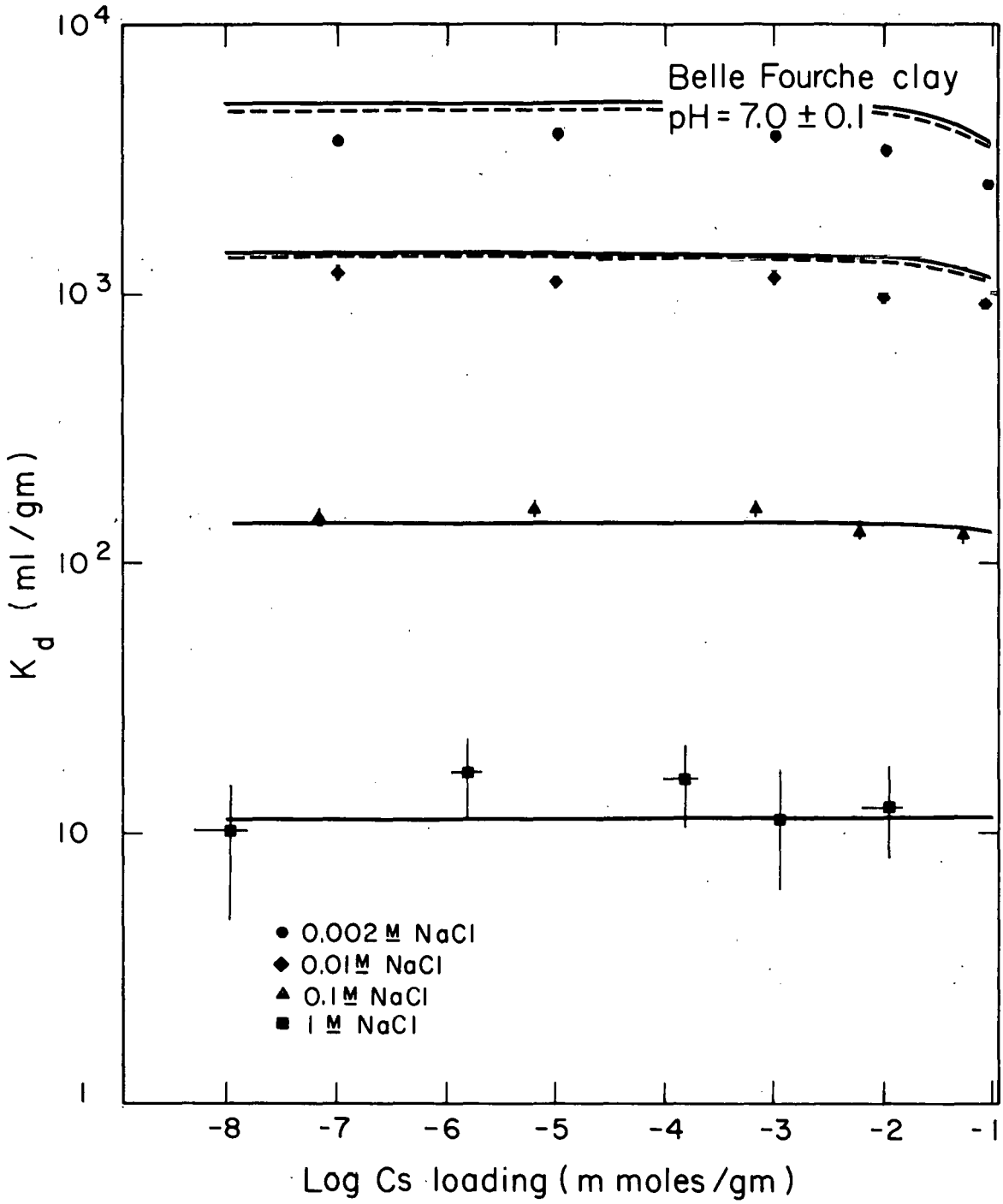

XBL 799-11576A

FIGURE 42. Cs sorption isotherms (26°C) for the Belle Fourche clay for several NaCl electrolyte concentrations at pH 7. The solid points represent experimental data given in Table 4. The solid and dashed curves were calculated using MINEQL without and with inclusion of the electrical double layer effects, resp.

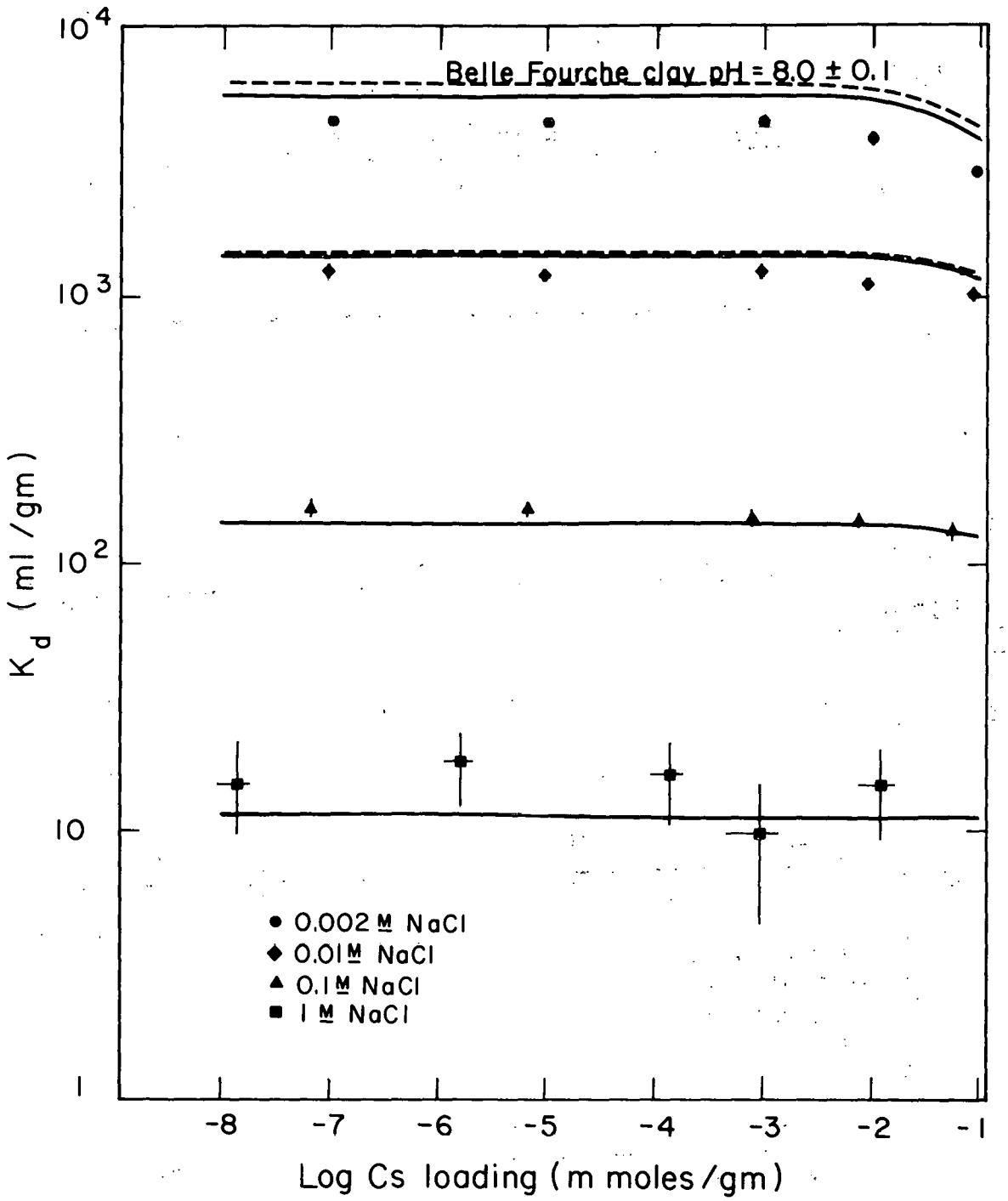

XBL 799-11577A

FIGURE 43. Cs sorption isotherms (26°C) for the Belle Fourche clay for several NaCl electrolyte concentrations at pH 8. The solid points represent experimental data given in Table 4. The solid and dashed curves were calculated using MINEQL without and with inclusion of the electrical double layer effects, resp.

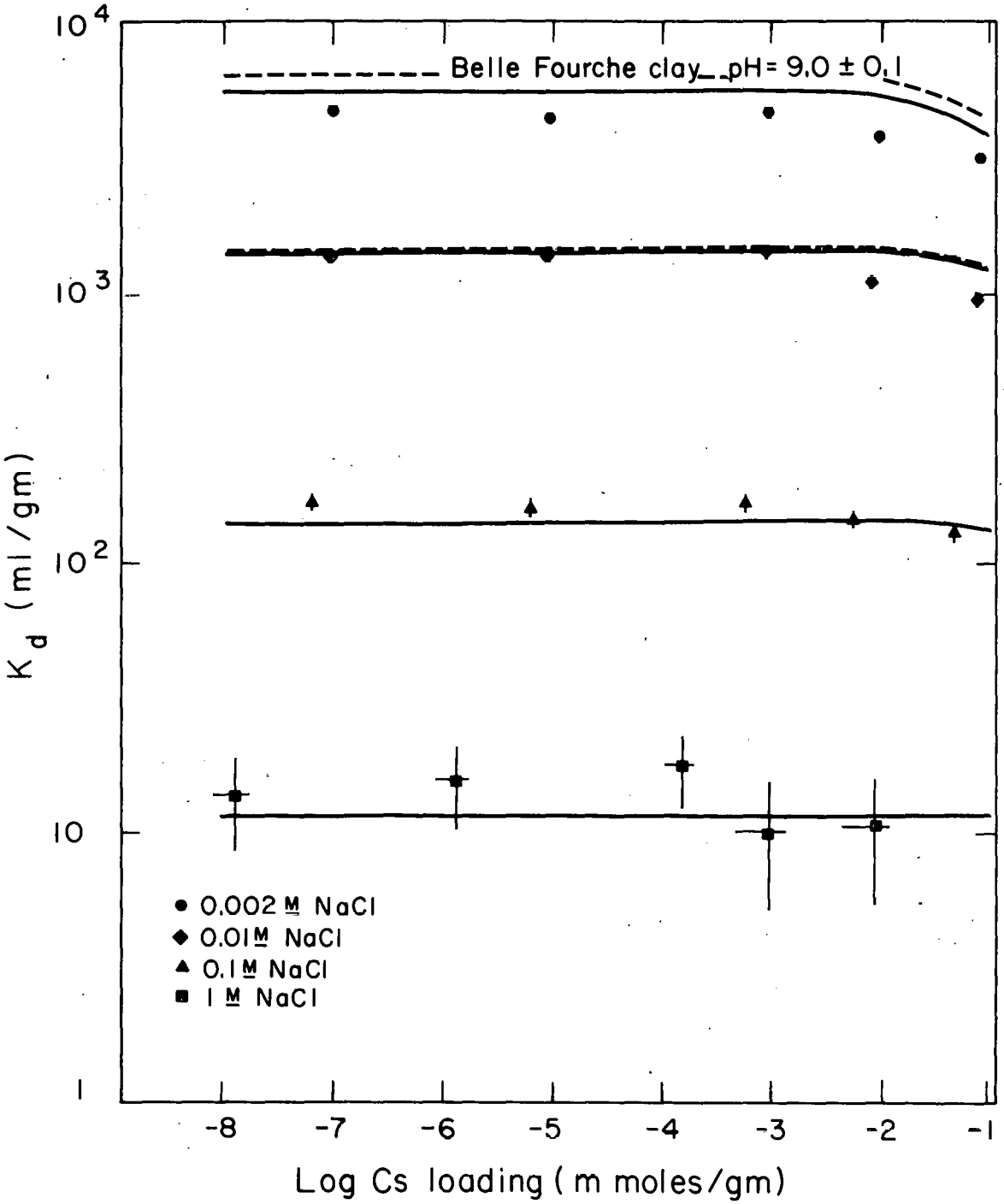

XBL 799-11578A

FIGURE 44. Cs sorption isotherms (26°C) for the Belle Fourche clay for several NaCl electrolyte concentrations at pH 9. The solid points represent experimental data given in Table 4. The solid and dashed curves were calculated using MINEQL without and with inclusion of the electrical double layer effects, resp.

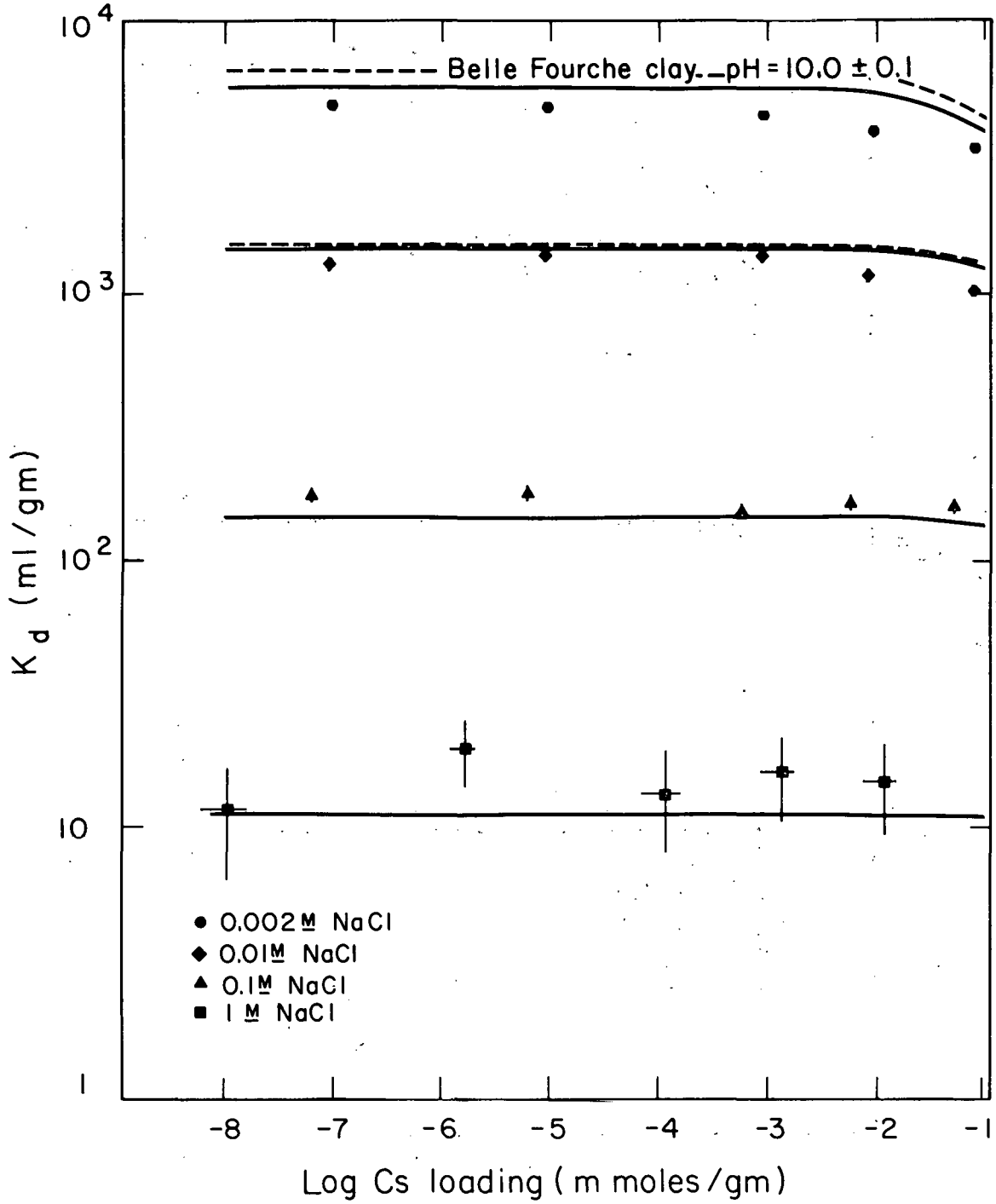

XBL 799-11579A

FIGURE 45. Cs sorption isotherms (26°C) for the Belle Fourche clay for several NaCl electrolyte concentrations at pH 10. The solid points represent experimental data given in Table 4. The solid and dashed curves were calculated using MINEQL without and with inclusion of the electrical double layer effects, resp.

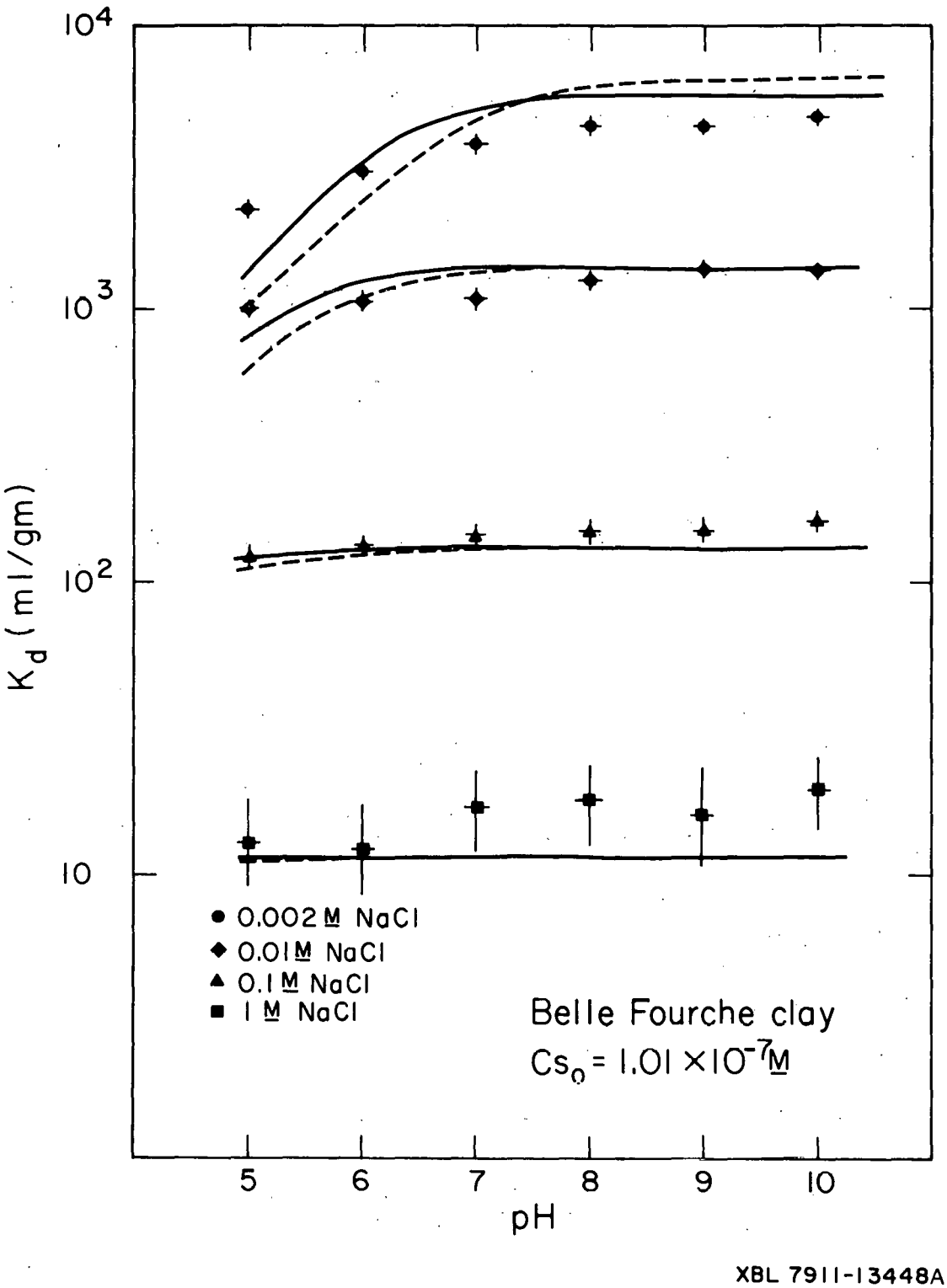

FIGURE 46. Variation of distribution coefficients for cesium with pH for an initial Cs solution concentration of 1.01×10^{-7} M for several NaCl electrolyte concentrations. Solid points represent the experimental data given in Table 4. The solid and dashed curves result from calculations using MINEQL without and with the inclusion of the electrical double layer effects, resp.

BIBLIOGRAPHY

REFERENCES SITED

Allen, L. H., E. Matijevic, and L. Meites, 1971. "Exchange of Na^+ for the silanolic protons of silica." J. Inorg. Nucl. Chem. 33: 1293-1299.

Apps, J. A., J. Lucas, A. K. Mathur, and L. Tsao, 1977. Theoretical and Experimental Evaluation of Waste Transport in Selected Rocks: 1977 Annual Report. Lawrence Berkeley Laboratory Report No. 7022, Lawrence Berkeley Laboratory, Berkeley, California.

Aylmore, L. A. G., 1977. "Microporosity in montmorillonite from nitrogen and carbon dioxide sorption." Clay and Clay Minerals. 25: 148-154

Blackman, P. D., 1958. "Neutralization curves and the formulation of monovalent cation exchange properties of clay minerals." Am. J. Sci. 256: 733-743.

Butler, J. N., 1964. Ionic Equilibrium. Addison-Wesley, Reading, Mass.

Chapman, D. L., 1913. "A contribution to the theory of electrocapillarity." Phil. Mag. 25(6): 475-481.

Davis, J. A., R. O. James, and J. O. Leckie, 1978. "Surface ionization and complexation of the oxide/water interface." J. Colloid Interface Sci. 63(3):480-499.

Deer, W. A., R. A. Howie, and J. Zussman, 1963. Rock Forming Minerals. Vol. 4, Framework silicates. John Wiley, New York, N. Y.

Edwards, D. G. and H. P. Quirk, 1962. "Repulsion of chloride by montmorillonite." J. Colloid Sci. 17: 872-882.

Garrels, R. M. and C. L. Christ, 1956. "Application of cation exchange reactions to the beidellite of the putnam silt soil." Amer. Jour. Sci. 254: 372-379.

Gouy, G., 1910. "Sur la constitution de la charge electrique a la surface d'un electrolyte." Ann. Phys. (Paris). 9(4): 457-468.

Gouy, G., 1917. "Sur la fonction electrocapillaire." Ann. Phys. (Paris). 7(9): 129-184.

Grahame, D. C., 1947. "The electrical double layer and the theory of electrocapillarity." Chem. Rev. 41: 441-501.

Greeland, D. J. and J. P. Quirk, 1962. "Adsorption of 1-n-alkylpyridinium bromides by montmorillonites." Clays and Clay Minerals. 9: 484-499.

Grim, R. E., 1968. Clay Minerology. McGraw-Hill, New York, New York.

Hawk, P. B., B. L. Oser, and W. H. Summerson, 1965. Practical Physiological Chemistry. McGraw-Hill, New York, New York.

Helfferich, F., 1962. Ion Exchange. McGraw-Hill, New York, New York.

Hunter, R. J. and H. J. L. Wright, 1971. "The determination of electrokinetic potential on concentration of electrolyte." J. Colloid Interface Sci. 37: 564-580.

Husler, J., 1972. Instrumental Analysis Laboratory Procedures. University of New Mexico, Department of Geology, Albuquerque, New Mexico.

Jackson, M. L., 1975. Soil Chemical Analysis - Advanced Course. published by author, Madison, Wisconsin.

James, R. O., J. A. Davis, and J. O. Leckie, 1978. "Computer simulation of the conductometric and potentiometric titrations of the surface groups on ionizable latexes." J. Colloid Interface Sci. 65(2): 331-344.

James, R. O. and G. A. Parks, 1979. "Characterization of aqueous colloids by their electrical double layer and intrinsic surface chemical properties." Submitted for publication to J. Surface and Colloid Sci.

Jones, B. F. and C. J. Bowser, 1977. "The minerology and related chemistry of lake sediments." Lakes: Chemistry, Geology, Physics, pp. 179-235, Springer Verlag, New York, New York.

Keren, R., R. G. Gast and R. I. Barnhisel, 1977. "Ion exchange reactions in nondried chambers montmorillonite hydroxy-aluminum complexes." Soil Sci. Soc. Am. J. 41: 34-39.

Koltoff, I. M., E. B. Sandell, E. J. Meeham and L. S. Bruckenstein, 1952. Quantitative Chemical Analysis, Macmillan, New York, New York.

Lyklema, J. and J. Th. G. Overbeek, 1961. "Electrochemistry of silver iodide, the capacity of the double layer at the silver iodide-water interface." J. Colloid Interface Sci. 16: 595-608.

McKeague, J. A. and J. H. Day, 1966. "Dithionite- and oxalate-extractable Fe and Al as aids in differentiating various classes of soils." Can. J. Soil Sci. 46: 13-22.

Morin, R. E. and H. S. Jacobs, 1964. "Surface area determination of soils by adsorption of ethylene glycol vapor." Proc. Am. Soil Science Soc. 28: 190-194.

Seidell, A. and W. F. Linke, 1958. Solubilities of Inorganic and Metal Organic Compounds. American Chem. Soc., Washington, D. C.

Sillen, L. G. and A. E. Martell, 1964. Stability Constants and Metal Ion Complexes, Spec. Pub. 17. The Chemical Society, London.

Silva, R. J., L. V. Benson and J. A. Apps, 1978. Theoretical and Experimental Evaluation of Waste Transport in Selected Rocks: 1978 Annual Report. Lawrence Berkeley Laboratory Report No. 8904, Lawrence Berkeley Laboratory, Berkeley, California.

Smith, R. M. and A. E. Martell, 1976. Critical Stability Constants, Vol. 4: Inorganic Complexes. Plenum, New York, New York.

Stumm, W., C. P. Huang, and S. R. Jenkins, 1970. "Specific chemical interactions affecting the stability of dispersed systems." Croat. Chem. Acta., 42: 223-225.

Stumm, W. and J. J. Morgan, 1970. Aquatic Chemistry. Wiley-Interscience, New York, New York.

Truesdell, A. H. and C. L. Christ, 1968. "Cation exchange in clay interpreted by regular solution theory." Am. J. Sci., 266: 402-412.

van Olphen, H., 1977. Clay Colloid Chemistry. Wiley-Interscience, New York, New York.

Westfall. J. C., J. I. Zachary, and F. M. M. Morel, 1976. MINEQL - A Computer Program for the Calculation of Chemical Equilibrium Composition of Aqueous Solutions. Note No. 18, EPA Grant R803738. Dept. Civil Eng., Mass. Inst. Tech. Cambridge, Massachusetts.

Yates, D. E., 1975. PhD. Thesis, Research in Collois and Surface Chemistry: The structure of the oxide/aqueous electrolyte interface. University of Melbourne, Melbourne, Australia.

Yates, D. E., S. Levine, and T. W. Healy, 1974. "Site binding model of the electrical double layer at the oxide/water interface." J. Chem. Soc. Faraday Trans. I. 170: 1807-1818.

THIS PAGE

WAS INTENTIONALLY

LEFT BLANK

QUESTIONS AND ANSWERS

LBL

Prediction of Kd from Mineralogical Analysis

Q: This may be anticipating tomorrow's paper but I think all of us have seen loading curves like this for the past 20 years on sorption on cesium from clay sands and they all come up with about the same results.

A: I haven't seen any that covered as broad a range as our data.

Q: Many of us have conducted similar expriments. Are we any closer to a point where we can predict Kds now on the basis of mineral analysis, for instance, for this type of process.

A: You mean on an actual mix?

Q: Yes. In order words, can you take a site-specific clay, for instance, of this general type? Can we, in fact, predict these?

A: I'm not quite sure what the question is; but in the modeling, you can put in as many components as you like. If you want to use a mixed mineral, you could put in each specific component as a specific site with a measured cation exchange capacity or what-have-you for that particular component. You could, in principle, put this into the program and allow the program to tell you.

Q: No, my question is really that considering the wealth of data on cesium adsorption on clays, can you explain the differences that people might have observed on the basis of the minor differences in the composition of clay, for instance?

A: As far as the minor composition of the clays, I'm not sure.

A: What we can do is explain the variation of Kd with the solution phase parameters. We can predict that to a pretty good extent. The type of modeling we're using has just gotten started in the last few months but already it looks as though there will be some mineralogical predictive capabilities. I can't say "yes" yet, but it looks promising.

A: That seems to be tied in more with the cation exchange capacities than with the surface areas.

Different Exchange Sites in Model

Q: I was wondering what your feeling is to getting involved in more natural materials which are more heterogeneous than say the Belle Fourche clay. Do you think this is a matter of isolating components, or talking about 2-binding sites, or increasing its scale to 5 or 10 binding sites, or is there a way to experimentally determine all necessary constants, etc. What's your projection as to where this model might go before it's all over?

A: It is just another component. So if you know the components there you can put them in the code; it is like putting in another site. If you put in another component you put in another site. Now the problem is, of course, getting the constants in. They come from a titration curve. It gets very complicated and it is difficult to extract them all. But chances are they're going to be dominant components and that you'll see in the curves. And you'll be able to get out the sorption constants.

C: I think if you integrate our thinking you'll come up with pretty much what you've been thinking. For instance, among the silicates, the behavior of the whole family of the silicates is going to be dominated by certain classes or certain minerals themselves. But the code, the way it is written can accommodate any number up to 40 or 50 minerals if you like. We don't expect that to be necessary. What we are expecting is that real materials will be dominated by a relatively small number of phases and that we'll be able to determine the constants we need for each for those phases. Or maybe an average constant with relatively narrow ranges for types of phases, and then put them in.

A: You could get your constants and titrations of the individual minerals rather than do the mixture.

Q: Iron oxide and silica, say hematite and silica, are what we call poly-acrylic acid and show different nonconstant acid constants and saturation. My intuition suggests that you have only one kind of site -- can you account for that -- handle it.

A: One kind of site is no problem. It depends on what kind of nonconstant you mean. In my experience with iron oxide, the acid constant changes with time for the first couple of days.

Q: But also with acid concentration?

A: No, that's accounted for. I believe that would be accounted for by taking into account the NaCl binding. I'm not certain but we haven't had any trouble with that. And we've been using mostly the Australian data of Quirk and Atkinson.

THIS PAGE

WAS INTENTIONALLY

LEFT BLANK

UCRL-52929

GEOCHEMICAL STUDIES OF SORPTION AND TRANSPORT OF RADIONUCLIDES IN ROCK MEDIA

Annual Report

FY 1979 -

David G. Coles
Homer C. Weed
John D. Tewhey

September 18, 1979

Revised

March 21, 1980

Battelle/ONWI Contract No. 23173

P. O. Box 808
Livermore, California 94550

THIS PAGE

WAS INTENTIONALLY

LEFT BLANK

GEOCHEMICAL STUDIES OF SORPTION AND TRANSPORT OF RADIONUCLIDES IN ROCK MEDIA
Annual Report
FY 1979

David G. Coles
Homer C. Weed
John D. Tewhey

ABSTRACT

Four studies, which supported the goals of the WISAP Program at Battelle PNL, were undertaken by the Lawrence Livermore Laboratory during FY 1979. These were: 1) Batch K_d experiments, 2) Dynamic sorption experiments on rock cores, 3) Feasibility study for an in situ tracer test at the Climax Stock, NTS, and 4) Geochemical equilibrium code development. Only the equilibrium code development was not funded by the WISAP during FY 1979.

The emphasis for the batch K_d studies was on various (15) sandstones in brine using ^{75}Se, ^{85}Sr, ^{125}Sb, ^{137}Cs, ^{141}Ce, and ^{237}Pu tracers. These sandstone samples were well-characterized for their physical and mineralogical nature. Complex K_d behavior was observed for the radionuclides studied but ^{85}Sr showed K_d values near zero for all samples. Both ^{141}Ce and ^{239}Pu K_d values ranged from 20 to upper limits of $\geq$ 17,000.

Dynamic sorption studies were done on NTS tuff and St. Peter sandstone cores using ^{3}H, ^{85}Sr, and ^{95m}Tc. These radionuclides were injected as a short pulse into the rock-equilibrated water that was flowing through the core. Tracer-free water was then continually flowed through the core until elution curves for the mobile radionuclides were established. Tritium and ^{95m}Tc both traveled through the cores at the same rate, indicating no sorption for the mobile fraction of ^{95m}Tc ($^{95}TcO_4^-$). Strontium-85 did not exit the tuff cores but did exit the sandstone core although the elution cures showed definite retardation relative to the movement of ^{3}H and ^{95m}Tc. Post-elution sectioning of the cores indicated that a fraction of the ^{95m}Tc remained in the cores and was evenly distributed through the tuff cores. Strontium-85 showed a generally decreasing distribution from the inlet side to the outlet side of the tuff cores.

INTRODUCTION

An important goal of the WISAP program is the capability of calculating the rate of radionuclide transport in the groundwater surrounding waste repositories. Sorption of radionuclides on rock material is a very important factor to be taken into account in understanding subsurface migration away from a repository. Four types of sorption-related studies were conducted at LLL during FY 79 in support of Task 4 of the WISAP Program. They were

(1) batch K_d experiments on a variety of rock types with an emphasis on sandstones,

(2) sorption experiments on rock cores which are "dynamic" in the sense that they simulate the flow of groundwater through intact rock,

(3) a small effort devoted to a study of the feasibility for field tracer studies in NTS granite in order to measure sorption characteristics in a natural environment, and

(4) geochemical equilibrium code development undertaken to determine radionuclide reactions in a rock-water regime from a theoretical point of view. The code development work was not funded by WISAP.

The relationship of these four studies to one another and to WISAP goals is shown in Fig. 1.

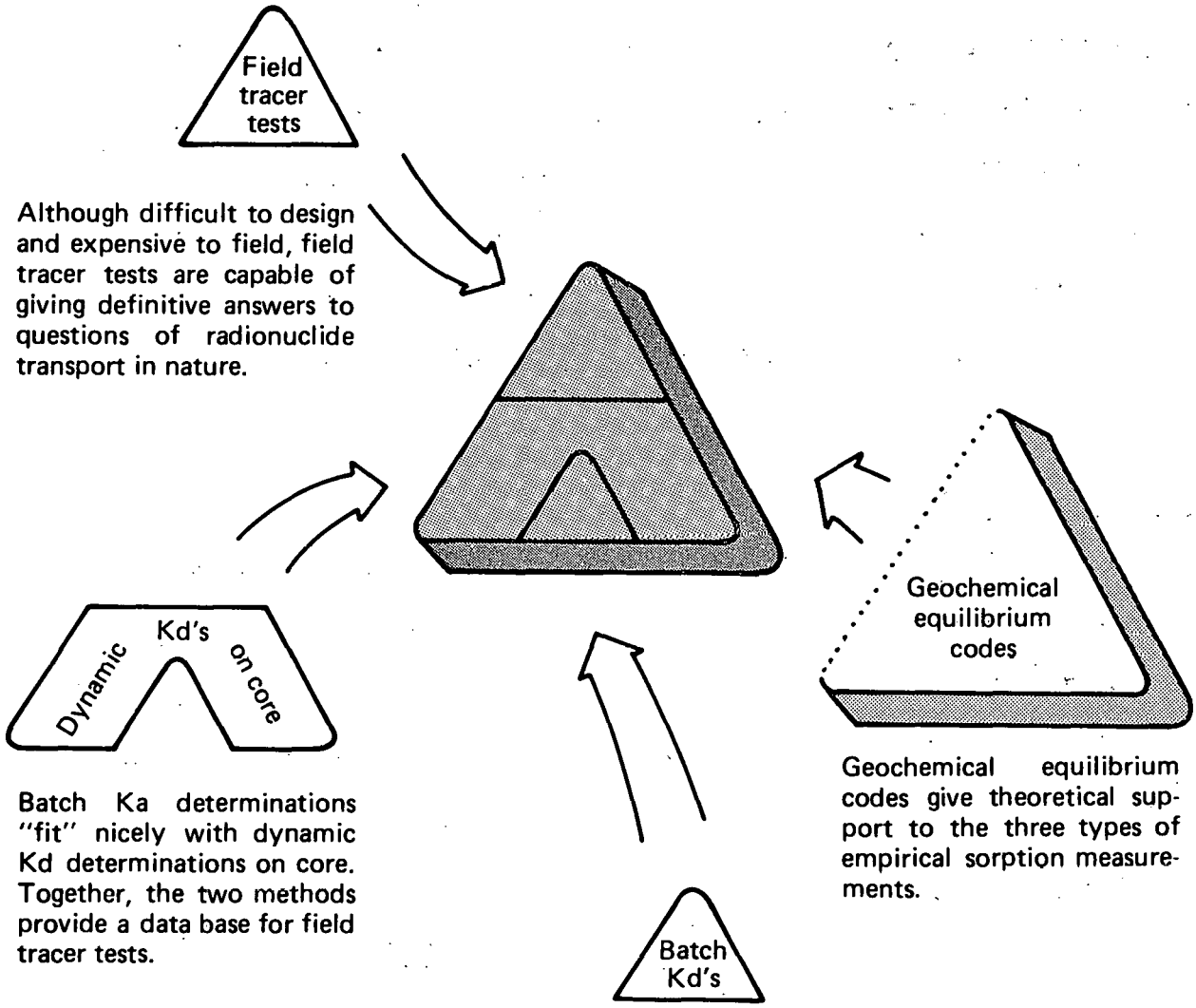

Fig. 1. LLL sorption-related studies in support of WISAP TASK 4. The four separate areas of investigation are complimentary and represent successively closer approximations to the "truth" from batch Kd's,to dynamic determination, to field studies.

The thrust of these activities is not only to understand sorption processes but also to investigate the scaling factors, from simplistic laboratory dynamic sorption studies on rock cores, to actual field in situ tests. Geochemical codes provide the theoretical support to this progression in sorption methodology. It is the investigation of scaling factors which will show whether inexpensive laboratory data can be validly extrapolated to an actual repository environment. Understanding scaling factors is of profound importance for assessment of the safety of a waste repository.

PERSONNEL INVOLVED IN THE PROGRAM DURING FY 79

Below are listed the individuals involved in Task 4 during FY 79 and their areas of involvement. Only a fraction of these people's full time effort was directed toward WISAP Task 4 and that amount varied for each individual. Scientific effort for WISAP Task 4 at LLL was funded at about 1.5 man-years.

John Tewhey - - - - - - - -	Geologist Project Leadership for FY 79/1, FY 79/2, FY 79/3, and involvement in all elements of Task 4.
David Coles - - - - - - - -	Nuclear Chemist/Geochemist Project Leadership for FY 79/4 and involvment in all elements of Task 4 with emphasis on batch sorption studies.
Homer Weed - - - - - - - -	Physical Chemist Sorption studies with emphasis on core sorption studies.
Janet Garrison - - - - - -	Chemist Batch sorption studies
Susan MacLean - - - - - -	Chemist Batch sorption studies

James Schweiger - - - - - Technician
Core sorption studies

Susan Schultz-McKinley - - Geologist
Petrography and x-ray diffraction analysis of sandstones. Some effort on core sorption studies.

Various others provided service work on characterization of the sandstone samples, etc.

ELEMENTS OF THE LLL PROGRAM

The LLL program consists of the four elements listed above. The code development was not funded by WISAP during FY 79. The batch K_d and dynamic K_d elements were given most of the funded effort, divided about equally between them. The *in situ* tracer test feasibility study received only a very small percentage of the total funded effort.

BATCH SORPTION STUDIES

LLL is one of nine laboratories involved in the program to assess empirically the methodology of batch K_d determinations. A systematic evaluation of the sorption characteristics of sandstones in brine solutions was carried out in FY 79. Since sandstones are expected to be the most permeable strata in a bedded salt or salt dome geology, their sorption characteristics were studied in a brine medium. These data will provide useful information for understanding radionuclide migration from a salt repository.

Also, K_d values were determined for Pu on Climax Stock shear zone materials, WISAP-controlled sample program shale, and Thirsty Canyon tuff in early FY 79. These samples completed FY 78 efforts (as reported in

UCID-17928[1]) which could not be finished because of a lack of ^{237}Pu tracer at the end of FY 78.

These batch K_d studies serve three purposes. The first is to help establish batch K_d methodology, the second is to provide K_d data to the WISAP data bank, and the third is to provide batch K_d data for comparison to K_d data generated on the same rocks with the dynamic core sorption apparatus.

DYNAMIC CORE SORPTION STUDIES

These studies are conducted in two systems, one of which can be operated up to 80°C. Each system is designed to measure the dynamic distribution of soluble and suspended species between the exchange medium (a rock core) and a flowing aqueous solution. The rock cores can be subjected to confining pressures up to 34.8 MPa (6000 psi) to simulate lithostatic pressures in the field. Measurements during FY 79 were made on cores of Thirsty Canyon tuff and St. Peter sandstone. Results from these studies are compared with those for the corresponding static batch K_d determinations. Since retardation factors are measured directly, they can be used directly for nuclide transport calculations.

IN SITU TRACER TEST FEASIBILITY STUDY

A small effort was expended on studying the feasibility for conducting a small scale, modest cost, *in situ* tracer experiment in the Climax Stock granite at the NTS. One result of the study was a proposal for an *in situ* tracer test which was submitted to WISAP/ONWI during FY 79/3. The main

goals of this proposed test are to

(1) produce data that will permit assessment of the merits of extrapolating lab K_d data to actual field conditions, and

(2) develop the technology for meaningful in situ testing in a fracture flow medium, that can be applied to other media being proposed for a waste repository.

GEOCHEMICAL EQUILIBRIUM CODE DEVELOPMENT

LLL is developing geochemical equilibrium codes that are capable of predicting the potential rock-water interactions associated with nuclear waste isolation in geologic media. A very limited amount of WISAP funding was allocated during late FY 78 for the development of a geochemical code by Dr. Howard Levine of Jaycor Corp. of La Jolla, California, in cooperation with LLL. The code development work was begun in FY 77 and was 90% complete at the end of FY 78. No WISAP funding was available for this work during FY 79; most of the funding for this code development was borne by other programs. Another LLL code that has been funded outside of WISAP is the EQ3/6 geochemical code[2] written by T. J. Wolery of the LLL Earth Sciences Division. Given adequate funding, one or both of these codes could be brought to bear on the general problem of understanding the geochemical interaction of radionuclides with various geologic media.

LABORATORY STUDIES

BATCH SORPTION STUDIES

Batch sorption studies at LLL are conducted using modifications of the WISAP Task 4 Controlled Samples Program procedure as described in UCID-

17928[1]. Modifications include

(1) drying the tracers in a plastic bottle at 85°C, then adding the simulated groundwater of interest;

(2) filtration of the tracer doped groundwater before use;

(3) filtration after centrifugation as the final phase separation technique; and

(4) calculating the K_d values in two ways. The first method used the concentration of radionuclide in the blank vials as the "influent" value. The second method used the concentration of radionuclides in the original stock solution as the "influent" value. Figure 2 shows diagrammatically the batch procedure used at LLL.

Controlled Sample Program and Miscellaneous Samples

Early in FY 79, Pu K_d values were determined for two Controlled Sample Program shales, Climax Stock shear zone materials, and Thirsty Canyon tuff. These determinations completed work begun in FY 78 which could not be finished because of a lack of ^{237}Pu tracer. The results consequently supplied the missing data for Pu in Table VIII of UCID-17928[1]. Data for Pu sorption on Thirsty Canyon tuff were obtained during FY 78 but with a basalt groundwater instead of a granite groundwater. The Pu sorption ratio was redetermined for this tuff but with a granitic groundwater. Since it is a rhyolite tuff, the groundwater in contact with it is probably more granitic than basaltic in composition.

The filtration sequence followed in batch K_d experiments is shown schematically in Fig. 3. The final filtration is preceded with a centrifigation step conducted at 4000 RPM for a minimum duration of 20 minutes.

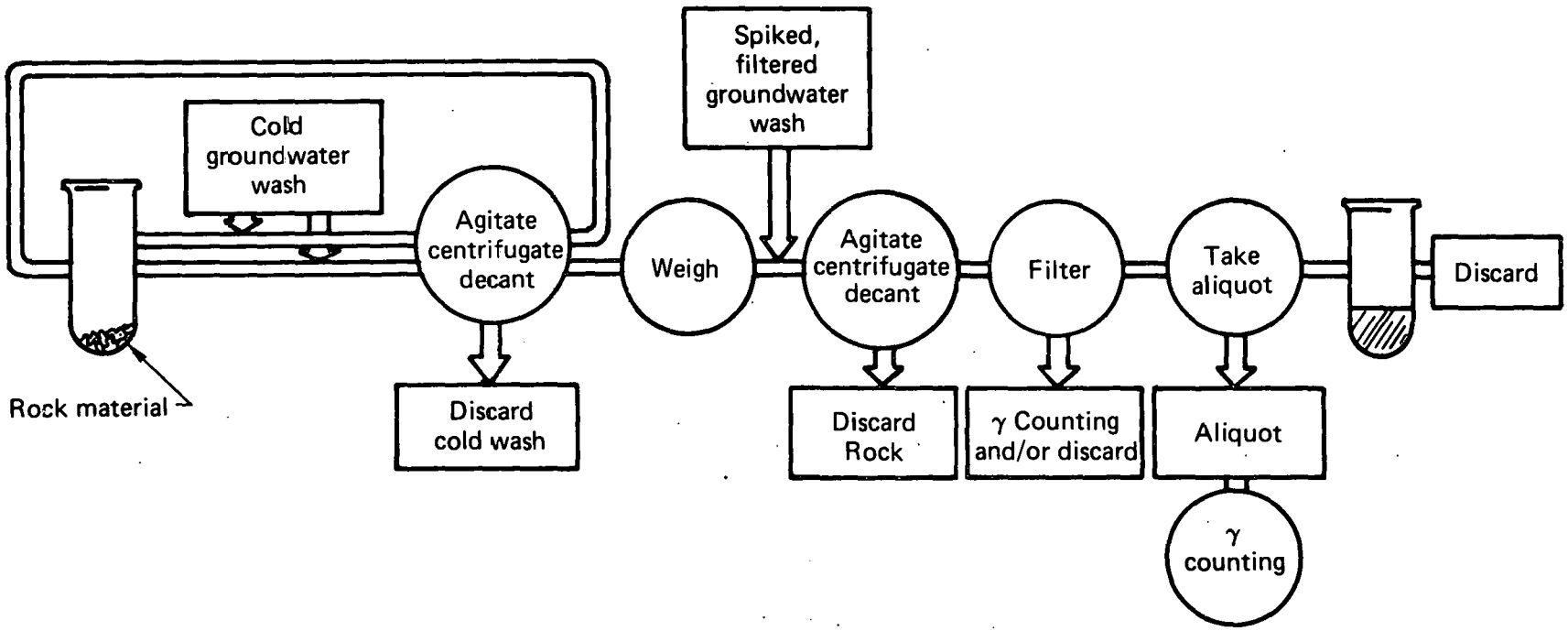

Fig. 2. Schematic of batch-type sorption experiments.

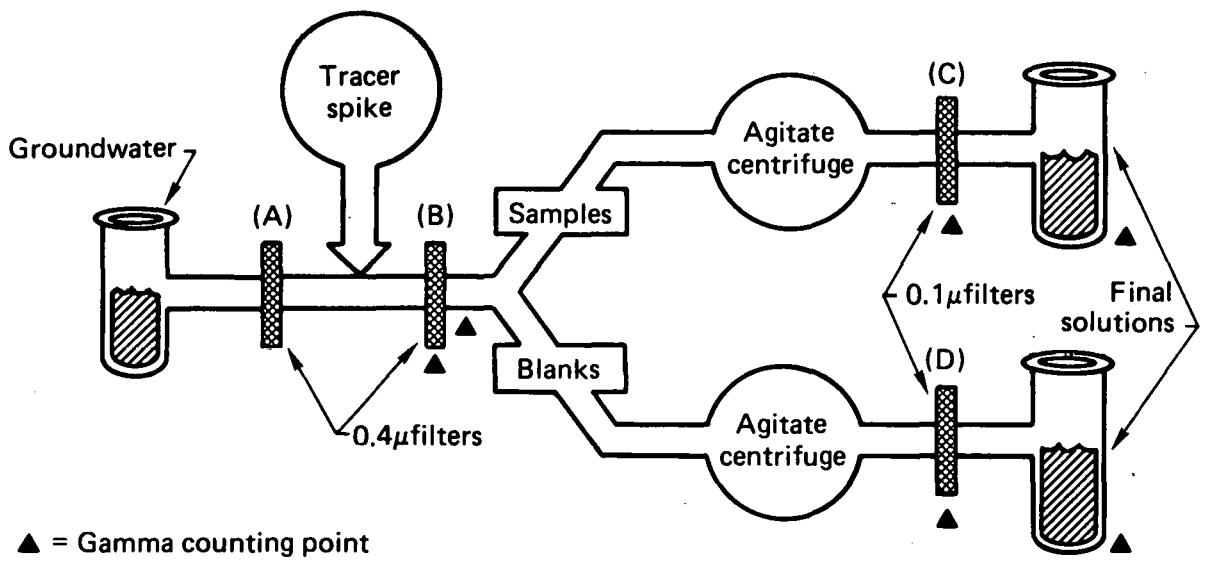

Fig. 3. Filtration sequence in batch Kd experiments.

A systematic analysis of Pu sorption was made as the equilibrated, spiked solution transited the system during sorption determinations on granite and shale. The results of this analysis are given in Tables 1 and 2. Table 3 gives the compositions of the three simulated groundwaters used in this study. The Pu concentration based on ^{237}Pu activity, is about 1 x 10^{-12}M. The concentrations for all tracers used in the batch K_d study are given in Table 4. These solutions were air equilibrated which should result in mildly oxidizing conditions where Pu^{4+} would be stable.

It is quite apparent from Table 2 that a considerable fraction of the Pu which was added to the blank containers becomes sorbed onto those containers. This also appears to be related to the groundwater composition as 97% of the Pu is lost to the container with the granite groundwater while only 45% of the Pu is lost with the bicarbonate groundwater. The primary difference between these two compositions is that the granite water (before contact with the rock) contains no SiO_2 but more HCO_3^{2-}. One might expect that the bicarbonate may complex the Pu ion and thus help keep it in solution but the great loss upon filtration of the initial spiked groundwater (96.5% retained on 0.4 μm filter, Table 1) contradicts this explanation. For the initial spiked water filtration, the loss of Pu to the filter from the bicarbonate water is much greater than from the granite water, but for the blank losses, the reverse is true. These data are confusing but what is clear is that Pu is very difficult to work with near neutral pH values. Also it is not certain whether the absorption on the container walls is the same for both the blanks and for containers holding rock samples.

The K_d data were calculated two ways. The use of Method 1 corrects for the blank by using the blank liquid as the "influent" solution. By using this method, it is assumed the container sorption is the same for both blank

Table 1. Loss of ^{237}Pu upon Filtration of Spike-Equilibrated Groundwater (filtered through 0.4 μm Nucleopore Filter (B) in Fig. 3) Expressed as % of ^{237}Pu in Original Unfiltered Spike Equilibrated Groundwater.

Granite Groundwater

25% obtained on filter (B), Fig. 3

77% remain with the filtrate

*102%

Bicarbonate Groundwater (used with shale samples)

** 95 - 100 % obtained on filter (B), Fig. 3

3.5% remained with the filtrate

100 %

*The 102% is an artifact of counting these two sample types with quite different geometries. The filter is a 2.5 cm, very thin disc and the liquid is a 10 ml volume-extended geometry.

**This number is inexact since it was also counted at a different geometry than the filtrate. The filter was also much hotter.

Table 2. Analytical Results for Pu Which Indicate Adsorption on Blank Containers[1]

Blank	% Pu on 0.1 μm Filter (D) in Fig. 3[2]	% of Pu in Final Solution (Post Filter D)	% of Total Pu Accounted for on Filter D & Final Solution[3]
Granite Blank 4	0.03%	2.5%	2.53%
" " 5	0.07%	2.6%	2.67%
" " 6	0.06%	2.6%	2.66%
			$\bar{X}$ 2.62 3%
Shale Blank 4	2.07%	51.2%	53.3%
" " 5	2.09%	53.8%	55.9%
" " 6	2.51%	52.4%	54.9%
			$\bar{X}$ 54.7 2%

[1] % Pu data based on amount of Pu in post filter B solution (Fig. 3).

[2] It is noteworthy how little loss occurs in this post-centrifugation filtration step.

[3] The remainder must be on the blank vial-by difference

and sample. The other calculation (Method 2) employs a formula which makes no attempt at a blank correction.

Method 1:

$$K_d = \frac{\frac{A_{blank}}{A\ sample} \times C_{blank} - C_{sample}}{C\ sample} \times \frac{A\ sample}{B\ sample}$$

where A = liquid volume

B = sample weight

C = DPM/ml at an arbitrary zero time, T_o

Table 3a. SIMULATED "LIMESTONE" GROUNDWATER COMPOSITION

	mg/l	Analytical Reagents	mg/l
Ca^{+2}	50.	$Ca(OH)_2$	92.5
Mg^{+2}	3.6	$MgSO_4$ anhyd.	18.
Na^{+}	2.3	NaCl	5.8
K^{+}	0.4	KCl	0.8
HCO_3^{-}	153.		
SO_4^{-2}	14.4	pH 8.2 $\pm$ 0.2	
Cl^{-}	3.5		

Table 3b. WIPP BRINE B (SLIGHTLY ALTERED) COMPOSITION

	mg/l	Analytical Reagents	
Na^{+}	115,000.	NaCl	287. g/l
K^{+}	15.	Na_2SO_4	6.2 g/l
Mg^{+2}	10.	$Na_2B_4O_7.10\ H_2O$	16. mg/l
Ca^{+2}	900.	$NaHCO_3$	14. mg/l
Sr^{+2}	1.5	NaBr	520. mg/l
Cs^{+}	1.	KCl	29. mg/l
Cl^{-}	175,000.	$MgCl_2.6\ H_2O$	85.4 mg/l
SO_4^{-2}	3,500.	$CaCl_2$ anhyd.	2.49 g/l
BO_3^{-3}	10.	$SrCl_2.6\ H_2O$	4.52 mg/l
HCO_3^{-}	10.	CsCl	1.3 mg/l
Br^{-}	400.		

pH 6.5 $\pm$ 0.5

Table 3c. SIMULATED "GRANITE" GROUNDWATER COMPOSITION

	mg/l	Analytical Reagents	mg/l
SiO_2	26.2	$MgSO_4.7\ H_2O$	6.88
Ca^{+2}	8.3	KCl	2.83
Mg^{+2}	1.5	$MgCl_2.6\ H_2O$	3.85
Na^+	6.7	MgO	0.60
K^+	1.5	$Ca(OH)_2$	15.5
HCO_3	47.7	$Na_2SiO_3.9\ H_2O$	125.
SO_4^{2}	2.7		
Cl^-	2.1		

pH 7.8 $\pm$ 0.3

Table 4. CHEMICAL CONCENTRATION OF TRACERS (CARRIERS) IN SPIKED GROUNDWATER[1]

Tracer		Molarity
^{75}Se	With Carrier	5×10^{-8} M Se
^{85}Sr	With Carrier	1×10^{-5} M Sr
^{125}Sb	Carrier-Free	2×10^{-8} M Sb
^{137}Cs	Carrier-Free	2×10^{-7} M Cs
^{141}Ce	With Carrier	2×10^{-6} M Ce
^{237}Pu	Carrier-Free	1×10^{-12} M Pu

[1] Simulated groundwaters as made from formulas in Table 3.

Method 2:

$$K_d = \frac{rCo-Ce}{Ce} \times \frac{A}{B}$$

where r = ratio of tracer solution to total solution

C_o = dpm/ml at T_o for influent stock solution

C_e = dpm/ml at T_o for effluent solution

As can be observed from K_d data in Table 5, where values from the two methods of calculation are presented, very great differences exist. We suspect that sorption on the container is different for blank versus sample but did not assess the extent of that difference for our experiments. Studies were performed at LASL[3] which indicated that the blank container preferentially absorbed a greater amount of tracer than the sample container did. Using a blank solution for the Co value in the K_d calculation would therefore result in an erroneously low K_d value. This is consistant with our observations based on the data in Tables 5, 13, and 15. As a result of our work and that of the LASL group, we recommend use of the non-blank corrected Co value since LASL observed very little container absorbtion for the sample containers. At least this error was usually small in comparison to the error obtained when using the blank corrected Co values. It might also be pointed out that even for Pu, the 0.1 μm post-centrifugation filtration does not perturb the system significantly as can be observed in Table 2. Apparently, most of the filterable Pu is removed with the 0.4 μm stock solution filterations. As a result, it is critical that samples be filtered before assaying the liquid phase for radioactivity since any tiny portion of a high K_d solid (such as shale), which might get into the aqueous phase after centrifugation, could result in erroneous K_d values.

For the shale samples, the K_d values reported were upper limit calculations. No ^{237}Pu was observable in the aqueous phase above the analytical detection limit. This implies very high K_d values for Pu on shale samples.

Table 5

Pu K_d Values on Shales, Climax Stock Shear Zone Material, and Thirsty Canyon Tuff

SAMPLE	GROUNDWATER	K_d FOR ^{237}Pu[1] METHOD 1 CALCULATION[2]	METHOD 2 CALCULATION[3]
Thirsty Canyon Tuff	"Granite"	190 ± 20%	8,000 ± 18%
Green Argillaceous Shale (20 - 50 Mesh)	"Limestone"	≥ 10,000	≥ 20,000
Conasauga Shale (20 - 50 Mesh)	"Limestone"	≥ 6,000	≥ 72,000
Climax Stock Shear Zone 1 (100-325 Mesh)	"Granite"	400 ± 83%	20,000 ± 80%
Shear Zone 2 (100-325 Mesh)	"Granite"	470 ± 18%	19,000 ± 17%
Shear Zone 2 (50-100 Mesh)	"Granite"	500 ± 58%	20,000 ± 56%
Shear Zone 3 (< 325 Mesh)	"Granite"	80 ± 30%	3,700 ± 25%
Shear Zone 3 (100-325 Mesh)	"Granite"	30 ± 65%	1,700 ± 43%
Shear Zone 3 (50-100 Mesh)	"Granite"	8 ± 72%	900 ± 24%

1 Mean ± 1σ S.D. of 3 replicates. All experiments run for 7 days.

2 Using blank as "influent" solution.

3 Using filtered stock solution as "influent" solution.

The shale samples were counted and they contained from 95-102% of the Pu added in the spike. In other words, the shales adsorbed essentially all the Pu from the solution. No attempt has been made to determine K_d as a function of Pu concentration, or oxidation state.

The plutonium K_d reported in UCID-17928 for Thirsty Canyon tuff in basalt groundwater was 420 $\pm$ 4.8%, using calculation method 1. The value for granite groundwater shown in Table 5 is 190 $\pm$ 20%.

X-ray diffraction studies were completed for the various size fractions of rock from the three prominent shear/fracture zones at the 1400 foot level in the Climax Stock. These are the same samples that were used for the K_d studies mentioned earlier. The purpose was to ascertain whether there were differences in clay mineralogy in the various size fractions which might be induced by the sieving process. The results are presented in Table 6. In this table, only montmorillonite and calcite are determined quantitatively. The meanings of the other symbols are as follows:

T = trace (< 1%)
VW = very weak (< 5%)
W = weak (< 15%)
M = moderate (up to 50%)

The data show no significant trends as a function of size fraction; therefore fine sieving is not expected to have a measurable effect on mineralogy-related variations in K_d determinations.

Table 6. X-ray Diffraction Analyses of Various Size Fractions of Rock from Climax Stock Shear Zones at the 1400 Foot Level.

	SIZE FRACTION (SIEVE MESH NO.)	CHLORITE	MONTMORILLONITE	ILLITE-MUSCOVITE	CLINOPTILOLITE	QUARTZ	CRISTOBALITE	K & Na FELDSPAR	CALCITE	DOLOMITE	GLASS	GYPSUM
Shear Zone 1	>100	VVW	10%	VW	--	M	VW	M	>1<5%	--	--	T
	<100>325	VVW	15%	VW	--	M	VW	M	>1<5%	--	--	T
	<325	VW	15%	W	--	M	VW	M	>1<5%	--	--	T
Shear Zone 2	>100	VVW	25%	VW	--	M	VW	W	>1<5%	--	--	--
	<100>325	VVW	25%	VW	--	M	VW	W	>1<5%	--	--	--
	<325	VVW	20%	W	--	M	VW	W	>1<5%	--	--	--
Shear Zone 3	>100	W	25%	M	--	M	VW	M	<1%	--	--	--
	<100>325	W	25%	M	--	M	VW	M	<1%	--	--	T
	<325	W	20%	W	--	M	W	M	<1%	--	--	T

Sandstone K_d Study with Brine

A systematic study of sorption of Se, Sr, Sb, Cs, Ce, and Pu on sandstones in brine solutions was done during FY 79. See Table 3 for the brine composition. A variety of sandstones were collected (15) and they were characterized by means of x-ray diffraction, SEM*, and optical petrography in order to assess their mineralogical, chemical and physical characteristics. The goal of the project was to attempt to correlate sandstone properties with sorption characteristics as a first step in understanding the rock

*Scanning Electron Microscopy

properties which most affect K_d values. The ultimate goal is to be able to establish a preliminary model for sorption on sandstones in the vicinity of salt repositories. The list of sandstones to be evaluated can be found in Table 7.

The 15 sandstones listed in the table were ground so that the minimal quartz grain breakage occurred. They were then sieved into two size fractions. A 48-100 mesh fraction was chosen because the samples in this size range showed the least breakage of the quartz grains. Thus, this fraction is felt to represent the "disaggregated" sandstone. The resultant particle surface ought to represent the same surfaces that groundwater would encounter as it moves through a sandstone stratum. The < 100 mesh fraction is felt to be representative of the sandstone cement as well as some fractured quartz grains.

The 30 samples (15 sandstones, 2 size fractions each) have undergone x-ray diffraction analysis (Table 8), particle size analysis (Table 9), BET surface area analysis (Table 10), and SEM. Optical petrography with photomicrography was done on thin sections of each sandstone. The optical petrography descriptions, photomicrographs, and SEM photomicrographs are too voluminous to include in this report but will be published early in FY 80 as a UCID report to provide a complete account of the characterization of these sandstones.

Four batch K_d experiments were carried out on these 30 samples using the Livermore modification of the WISAP procedure discussed earlier. For

TABLE 7

Sandstone used for Batch K_d Study

SANDSTONE	SOURCE LOCATION	PETROGRAPHICAL CLASSIFICATION	NON-QUARTZ CONTENT EXPRESSED AS VOL % OF ROCK
St. Peter sandstone	Illinois	Quartz Arenite	1%
Nugget sandstone	Colorado	Quartz Arenite	2%
Medina gray sandstone	New York	Quartz Arenite	3%
Mt. Tom Arkose	Massachusetts	Arkose	5%
Portland brownstone micaceous sandstone	Connecticut	Subarkose	<9%
Berea sandstone	Ohio	Quartz Arenite	10%
Kayenta sandstone	Colorado	Quartz Arenite	10%
Mojave Co. ferruginous sandstone	Arizona	Quartz Arenite	5-23%
Manhattan Arkose	Montana	Arkose	15%
Tick Canyon sandstone	California	Arkose	18%
Masonville argillaceoous sandstone	New York	Quartz Arenite	23%
Grafton Graywacke	New York	Arkose	25%
Portageville argillaceous sandstone	New York	Quartz Arenite	30%
Buffalo Gap banded sandstone	South Dakota	Quartz Arenite	40%
San Felipe sandstone	California	Subarkose	45%

TABLE 8a

Description of Sandstone Samples Based On X-Ray Diffraction data

Sandstone	Minerals		Fine fraction has (more, less) (species than the coarse fraction
	Major	Minor (<10%)	
Berea	Quartz	Clays Kaolinite, Palygorskite) Mica (Musc.) Microcline	More clay, mica, microcline Less quartz
Kayenta	Quartz (95%)*	Calcite (4%)* (Cement)	More calcite Less microcline, mica, clay
St. Peter	Quartz	K-Feldspar Clay <1%*	Less K-feldspar, clay
San Felipe	Quartz	Plagioclase (Oligoclase) Calcite (Cement) Mica (< 19%)*	More calcite Less quartz, plag., mica
Nugget	Quartz	Microcline Mica (< 1%)	More microcline

*Optical Data

TABLE 8b

Description of Sandstone Samples Based on X-Ray Diffraction Data

Sandstone	Minerals		Fine fraction has (more, less) (species) than the coarse fraction
	Major	Minor (<10%)	
Buffalo Gap	Quartz	K-felspar Muscovite Calcite Hematite Chlorite	More calcite
Grafton Graywacke	Quartz Na-Plagioclase	Chlorite Muscovite Calcite	More calcite Less muscovite, chlorite
Mojave Co.	Quartz	K-feldspar Calcite Muscovite Chlorite Clay (palygorskite)	More chlorite Less muscovite, calcite, K-feldspar
Manhattan	Quartz Na-Plagioclase Chlorite	Muscovite Calcite	Less chlorite, muscovite
Masonville	Quartz Chlorite	Muscovite Na-Plagioclase Calcite Clay ?	Less calcite
Medina	Quartz	Na-Plagioclase Calcite Muscovite Chlorite	Less muscovite, calcite
Mt. Tom	Quartz Na-Plagioclase K-Feldspar	Muscovite Calcite Hematite	Less muscovite, feldspar

TABLE 8c

Description of Sandstone Samples Based on X-Ray Diffraction Data

Sandstone	Minerals		Fine fraction has (more, less) (species) than the coarse fraction
	Major	Minor (<10%)	
Portageville	Quartz Chlorite	Na-Plagioclase Muscovite Calcite	More muscovite, chlorite
Portland Brownstone	Quartz	Ca-Plagioclase Muscovite Calcite Chlorite Hematite	More muscovite
Tick Canyon	K-Feldspar Quartz	Chlorite Calcite Muscovite Epidote	More chlorite, epidote

TABLE 9

Sieve Analysis of Sandstone Fractions

SANDSTONE	DIAMETERS AT WHICH 10, 50 and 90% OF MATERIAL FALL BELOW					
	-100 MESH			48 - 100 MESH		
	D/10 Microns	D/50 Microns	D/90 Microns	D/10 Microns	D/50 Microns	D/90 Microns
Mojave Co.	45	90	160	140	200	310
Manhattan Arkose	40	82	160	160	220	330
Tick Canyon	32	75	150	140	190	300
Buffalo Gap	48	99	145	140	180	280
Portageville	37	62	140	160	220	350
Mt. Tom	38	85	140	145	195	310
Grafton Graywacke	38	65	140	150	210	310
Medina	38	105	175	145	190	300
Masonville	45	90	160	145	195	300
Portland Brownstone	35	75	150	155	210	320
St. Peter	62	130	175	160	210	310
San Felipe	20	70	150	170	220	320
Nugget	32	90	160	155	210	310
Berea	70	140	175	150	200	250
Kayenta	36	95	160	180	230	330

TABLE 10

B.E.T. Surface Area of Sandstone

SANDSTONE SOURCE	SURFACE AREA M^2/G -100 MESH (A)	48 - 100 MESH (B)	A/B
Mojave Co.	6.18	2.68	2.31
Manhattan Arkose	2.95	1.97	1.50
Tick Canyon	3.25	2.30	1.41
Buffalo Gap	4.44	4.45	1.00
Portageville	4.15	3.77	1.10
Mt. Tom	0.87	0.65	1.34
Grafton Graywacke	1.46	0.64	2.28
Medina	1.74	1.04	1.67
Masonville	3.45	2.03	1.70
Portland Brownstone	4.29	3.45	1.24
St. Peter	1.01	0.46	2.20
San Felipe	4.45	2.14	2.08
Nugget	1.64	1.21	1.35
Berea	1.34	0.87	1.54
ayenta	4.58	1.58	2.90

each sandstone, a run on each fraction for ^{75}Se, ^{85}Sr, ^{125}Sb, ^{137}Cs, and ^{141}Ce as well as a pair of similar runs using ^{237}Pu are required. Each run generated 45 samples of water (15 sandstones x 3 replicates), plus an equal number of 0.1 μm final filters, plus three liquid standards, plus three filter standards, plus another sample (0.4 μm filter) generated from a pre-run filtration of the stock solution. The total number of samples was thus 97 for each of the four runs or 388 samples for the entire sandstone experiment. This was a very large number of samples. Half (194) of these samples contained ^{75}Se, ^{85}Sr, ^{125}Sb, ^{137}Cs, and ^{141}Ce and could be counted with the automatic sample-changing equipment. The other half of the samples which contained ^{237}Pu had to be hand-changed and counted on a small minicomputer-driven Ge(Li) gamma-ray spectrometer system. Only two samples could be counted on this system each day because of the low level of ^{237}Pu in the liquid phase. Much of the ^{237}Pu (49.4%) was lost during the 0.4 μm prefiltration of the stock solution. The chemical concentration of ^{237}Pu (as Pu) was approximately $1x10^{-12}M$. This loss was observed in previous experiments and was reported in UCID-17928 as well as earlier in this report. Also, Table 11 shows that 31.9% of the ^{75}Se, 15.4% of the ^{125}Sb, and 18.8% of the ^{141}Ce are lost during the initial filtration step. Strontium-85 and ^{137}Cs do not suffer significant losses upon filtration. The complex aqueous chemistries of these variable valence elements apparently render some fraction of each in filterable states. Consequently, if K_d values are to be understood in terms of soluble species, then the removal of insoluble species before contacting the spiked groundwater with the rock material is essential.

Table 12 presents data for the amount of the original filtered and spiked groundwater that is retained on the final 0.1 μm filter during the

TABLE 11

Percent of Tracer Retained by Initial
Filtration of Spiked Groundwater Through a 0.4 μm Filter
For 48 - 100 Mesh Samples

	^{75}Se	^{85}Sr	^{125}Sb	^{137}Cs	^{141}Ce	^{237}Pu
PERCENT OF TRACER ON 0.4 μm FILTER	31.9%	1.0%	15.4%	0.1%	18.8%	49.4%

TABLE 12a

Percent of Stock Tracer Remaining on
0.1 μm (Final) Filters for 48 - 100 Mesh Samples

Expressed As Percent of Filtered (Filter B in Fig. 3) Stock Solution Activity[1]

	^{75}Se	^{85}Sr	^{125}Sb	^{137}Cs	^{141}Ce	^{237}Pu
Blanks	0.04 - 0.06	0.02 - 0.06	0.04 - 0.06	0	0.26 - 0.64	0.2 - 0.5
St. Peter	0.24 - 0.36	0.08 - 0.36	0.10 - 0.38	0 - 0.44	0.30 - 0.42	0.2[2]
San Felipe	0.30 - 0.36	0.04 - .32	0.14 - 0.34	0 - 0.38	0.58 - 0.76	0.4
Berea	0.18 - 0.30	0.02 - 0.04	0.06 - 0.08	0	0.56 - 0.74	0.3
Kayenta	0.18 - 0.30	0.06 - 0.30	0.08 - 0.32	0 - 0.24	0.26 - 0.44	0.2
Nugget	0.12 - 0.18	0.12 - 0.46	0.12 - 0.34	0.10 - 0.40	0.14 - 0.14	0.1
Masonville	0.12 - 0.16	0.04 - 0.24	0.03 - 0.20	0	0.12 - 0.22	0.2
Portageville	0.10 - 0.18	0.08 - 0.40	0.08 - 0.36	0 - 0.04	0.14 - 0.24	0.3
Portland Brownstone	0.10 - 0.12	0.04 - 0.10	0.06 - 0.10	0 - 0.14	0.12 - 0.14	0.3
Buffalo Gap	0.02 - 0.14	0.04 - 0.24	0.04 - 0.12	0 - 0.26	0.04 - 0.12	0.01
Medina	0.40 - 0.48	0.06 - 0.08	0.12 - 0.14	0 - 0.12	0.52 - 0.66	0.3
Grafton Graywacke	0.08 - 0.26	0.06 - 0.08	0.08 - 0.18	0 - 0.06	0.08 - 0.30	0.2
Tick Canyon	0.18 - 0.22	0.10 - 0.14	0.12 - 0.14	0 - 0.10	0.24 - 0.34	0.2
Mt. Tom	0.20 - .36	0.08 - 0.12	0.10 - 0.14	0.10 - 0.12	0.28 - 0.64	0.4
Mojave Co.	0.16 - 0.56	0.06 - 0.14	0.10 - 0.16	0 - 0.14	0.20 - 0.74	0.2
Manhattan Arkose	0.08 - 0.24	0.04 - 0.06	0.06 - 0.08	0 - 0.4	0.10 - 0.30	0.2

1 Range of three replicate samples. Data based on amount of tracer in post Filter B solution (filtered stock solution) in Fig. 3.
2 Only one third of Pu filters were counted - one from each triplicate set.

TABLE 12b

PERCENT OF STOCK TRACER REMAINING ON 0.1 μm (FINAL) FILTERS FOR < 100 MESH SAMPLES
Expressed as Percent of Filtered (Filter B in Fig. 3) Stock Solution Activity[1]

	^{75}Se	^{85}Sr	^{125}Sb	^{137}Cs	^{141}Ce
St. Peter	0.19 - 0.22%	0.03 - 0.05%	0.07 - 0.10%	0.03 - 0.05%	0.43 - 0.50
San Felipe	0.09 - 0.14%	0.05 - 0.06%	0.06 - 0.08%	0.05 - 0.05%	0.18 - 0.27
Berea	0.17 - 0.32%	0.04 - 0.10%	0.12 - 0.15%	0.05 - 0.11%	0.48 - 0.85
Kayenta	0.10 - 0.15%	0.03 - 0.04%	0.06 - 0.07%	0.03 - 0.04%	0.21 - 0.24
Nugget	0.16 - 0.19%	0.04 - 0.07%	0.10 - 0.12%	0.05 - 0.10%	0.31 - 0.37%
Masonville	0.04 - 0.06%	0.03 - 0.07%	0.04 - 0.07%	0.03 - 0.07%	0.09 - 0.13%
Portageville	0.06 - 0.10%	0.03 - 0.11%	0.05 - 0.10%	0.03 - 0.11%	0.13 - 0.21%
Portland Brownstone	0.07 - 0.14%	0.04 - 0.06%	0.07 - 0.08%	0.05 - 0.06%	0.17 - 0.32%
Buffalo Gap	0.02 - 0.04%	0.03 - 0.05%	0.04 - 0.06%	0.03 - 0.05%	0.03 - 0.05%
Medina	0.07 - 0.17%	0.04 - 0.06%	0.07 - 0.11%	0.04 - 0.06%	0.14 - 0.40%
Grafton Graywacke	0.05 - 0.08%	0.13 - 0.17%	0.09 - 0.10%	0.12 - 0.16%	0.08 - 0.15%
Tick Canyon	0.05 - 0.13%	0.04 - 0.05%	0.05 - 0.08%	0.04 - 0.05%	0.20 - 0.71%
Mount Tom	0.07 - 0.13%	0.02 - 0.11%	0.04 - 0.11%	0.02 - 0.11%	0.12 - 0.22%
Majave Co.	0.10 - 0.15%	0.04 - 0.17%	0.07 - 0.14%	0.05 - 0.16%	0.21 - 0.31%
Manhatton Arkose	0.07 - 0.13%	0.02 - 0.20%	0.05 - 0.16%	0.02 - 0.19%	0.15 - 0.26%
Blanks	0.06 - 0.06%	0.03 - 0.04%	0.06 - 0.07%	0.03 - 0.04%	0.85 - 12.1%

[1] Range of three replicate samples.

final filtration step. This filtration step occurs after centrifugation of the samples and is done to assure separation between the liquid and solid phases at the end of the seven-day contact period. If radioactivity is observed on the filter, it can come from one of three sources. They are 1) suspended rock material containing sorbed radioactivity which remained suspended after centrifugation, 2) reformation of insoluble, filterable species after the initial filtration, 3) insoluble filterable material smaller in size than the 0.4 μm initial filter but larger than the 0.1 μm final filter. Values in Table 12 are constantly low for all radionuclides, which tend to support 1) above since individual chemistries of the nuclides apparently don't play a major role in their behavior at this stage of the procedure.

Table 13 presents K_d data for all nuclides on all sandstone samples in the coarse size range (48-100 mesh). Table 14 presents these data for the <100 mesh samples. As in Table 5, the data are calculated according to both Method 1 and Method 2. K_d values for ^{75}Se, ^{85}Sr, ^{125}Sb, and ^{137}Cs differ for each calculation method but generally agree within a factor of 2. Strontium-85 K_d values are all less than zero or very near zero. Negative values can occur if the tracer in the stock solution or blank preferentially deposits on the container, compared to a sample where the rock provides a much greater surface for sorption. One value for ^{125}Sb (METHOD 2 calculation) and many values for ^{137}Cs are also negative. Precision for all the ^{75}Se, ^{125}Sb, and ^{137}Cs values is very poor. These data probably reflect experimental variations for radionuclides with K_d values very near zero. We interpret the ^{85}Sr and ^{137}Cs data to indicate K_d values of zero for all the sandstone samples.

TABLE 13a

K_d VALUES FOR SANDSTONES IN BRINE (48-100 MESH)[1]

	K_d for ^{75}Se		K_d for ^{85}Sr		K_d for ^{125}Sb	
	METHOD 1 CALCULATIONS[2]	METHOD 2 CALCULATIONS[3]	METHOD 1 CALCULATIONS[2]	METHOD 2 CALCULATIONS[3]	METHOD 1 CALCULATIONS[2]	METHOD 2 CALCULATIONS
St. Peter	6.9 ± 3.7%	18.6 ± 2.2%	-0.11 ± 3.6%	-0.87 ± 0.8%	0.17 ± 31.%	-0.15 ± 36%
Nugget	48 ± 13%	81 ± 12%	-0.21 ± 35%	-0.97 ± 7.2%	10 ± 33%	9.0 ± 34%
Medina	37 ± 9%	65 ± 8.0%	-0.15 ± 26%	-0.90 ± 4.1%	2.3 ± 24%	1.9 ± 28%
Mt. Tom	7 ± 39%	19 ± 23%	-0.28 ± 22%	-1.05 ± 6.8%	4.8 ± 2.7%	4.3 ± 3.0%
Portland Brownstone	23 ± 23%	42 ± 18%	-0.158 ± 1.1%	-0.92 ± 0.9%	2.9 ± 10%	2.5 ± 12%
Berea	34 ± 5.4%	59 ± 4.8%	-0.12 ± 21%	-0.87 ± 3.6%	1.42 ± 5.3%	1.08 ± 6.6
Kayenta	12 ± 12%	26 ± 8.2%	-0.13 ± 65%	-0.88 ± 8.5%	0.8 ± 16%	0.5 ± 26%
Mojave Co.	19 ± 22%	36 ± 17%	-0.2 ± 51%	-0.94 ± 9.8%	2.2 ± 9.1%	1.9 ± 11%
Manhattan Arkose	42 ± 16%	70 ± 14%	-0.16 ± 11%	-0.91 ± 3.0%	4.6 ± 10%	4.2 ± 11%
Tick Canyon	8 ± 36%	20 ± 22%	-0.20 ± 33%	-0.96 ± 7.0%	1.2 ± 23%	0.9 ± 30%
Masonville	63 ± 12%	100 ± 9.1%	-0.16 ± 24%	-0.91 ± 5.2%	8 ± 1.5%	7.5 ± 1.6%
Grafton Graywacke	26 ± 24%	48 ± 19%	-0.06 ± 76%	-0.81 ± 6.5%	14 ± 10%	14. ± 9.6%
Portageville	47 ± 3.3%	79 ± 3.0%	-0.05 ± 276%	-0.8 ± 16%	2 ± 7.2%	1.7 ± 8.8%
Buffalo Gap	17 ± 13%	34 ± 9.6%	-0.16 ± 48%	-0.93 ± 8.2%	1.2 ± 11%	0.9 ± 14%
San Felipe	43 ± 4.9%	74 ± 4.4%	0.01 ± 538%	-0.76 ± 7.3%	6.2 ± 6.5%	5.8 ± 6.8%

1 Mean ± 1σ S.D. of 3 replicates
2 Using blank as "influent" solution
3 Using filtered stock solution as "irfluent" solution

TABLE 13b

K_d VALUES FOR SANDSTONES IN BRINE (48-100 mesh)[1]

	K_d for ^{137}Cs		K_d for ^{141}Ce		K_d for ^{237}Pu	
	METHOD 1 CALCULATIONS[2]	METHOD 2 CALCULATIONS[3]	METHOD 1 CALCULATIONS[2]	METHOD 2 CALCULATIONS[3]	METHOD 1 CALCULATIONS[2]	METHOD 2 CALCULATIONS[3]
St. Peter	1 ± 122%	-1. ± 443%	20 ± 16%	260 ± 9.4%	60 ± 10%	130 ± 9.2%
Nugget	2 ± 93%	-0.3 ± 600%	1100 ± 14%	8000 ± 13%[4]	1300 ± 51%	2000 ± 51%
Medina	1.9 ± 46%	0.2 ± 132%	500 ± 31%	4000 ± 30%	430 ± 6.1%	850 ± 6%
Mt. Tom	1 ± 1780%	-2 ± 62%	600 ± 47%	5000 ± 46%	800 ± 9.1%	1500 ± 9%
Portland Brownston	6 ± 40%	3. ± 63%	400 ± 60%	3000 ± 58%	310 ± 27%	600 ± 27%
Berea	-.01 ± 11,200%	-2 ± 79%	20 ± 19%	260 ± 12%	600 ± 26%	1100 ± 25%
Kayenta	1 ± 238%	-1 ± 332%	60 ± 33%	500 ± 27%	280 ± 23%	500 ± 234%
Mojave Co.	2 ± 84%	-0.3 ± 366%	700 ± 15%	5500 ± 15%	180 ± 51%	400 ± 49%
Manhattan Arkose	1.7 ± 42%	-0.4 ± 158%	≥ 2300	≥ 17,000	1670 ± 5%	3200 ± 5%
Tick Canyon	-.01 ± 13,200%	-2 ± 66%	80 ± 18%	700 ± 15%	800 ± 15%	1600 ± 15%
Masonville	1 ± 363%	-1 ± 116%	≥ 1940	≥ 14,800	1900 ± 44%	4000 ± 44%
Grafton Graywacke	-.4 ± 371%	-2 ± 60%	≥ 1930	≥ 14,700	350 ± 26%	700 ± 25%
Portageville	2 ± 186%	-.5 ± 559%	120 ± 24%	1000 ± 21%	5000 ± 102%	9000 ± 101%
Buffalo Gap	1 ± 167%	-1 ± 99%	80 ± 40%	700 ± 34%	186 ± 120%	400 ± 115%
San Felipe	-.2 ± 965%	-2 ± 98%	≥ 2100	≥ 16,000	4000 ± 70%	7000 ± 70%

1 Mean ± 1σ S.D. of 3 replicates
2 Using blank as "influent" solution
3 Using filtered stock solution as "influent" solution
4 Mean of two values only

TABLE 14a

K_d VALUES FOR SANDSTONES IN BRINE (<100 MESH)[1]

	K_d for ^{75}Se		K_d for ^{85}Sr		K_d for ^{125}Sb	
	METHOD 1 CALCULATIONS[2]	METHOD 2 CALCULATIONS[3]	METHOD 1 CALCULATIONS[2]	METHOD 2 CALCULATIONS[3]	METHOD 1 CALCULATIONS[2]	METHOD CALCULATIONS[3]
St. Peter	26.2 ± 25%	27.8 ± 2.4%	-0.13 ± 31%	-0.16 ± 25%	2.0 ± 6.2%	3.2 ± 4.2
Nugget	350. ± 7.9%	370. ± 7.8%	-0.09 ± 19%	-0.12 ± 14%	10. ± 11%	12. ± 10%
Medina	170. ± 2.6%	178. ± 2.8%	-0.21 ± 16%	-0.24 ± 14%	6.2 ± 5.9%	7.6 ± 5.1
Mt. Tom	96. ± 1.6%	100. ± 1.5%	-0.05 ± 116%	-0.07 ± 73%	10. ± 1.4%	11.7 ± 1.
Portland Brownstone	130. ± 2.3%	136. ± 2.4%	-0.32 ± 12%	-0.35 ± 11%	5.83 ± 1.0%	7.25 ± 0.
Berea	119. ± 3.0%	124. ± 3.0%	-0.10 ± 32%	-0.13 ± 25%	5.6 ± 6.3%	7.0 ± 5.3
Kayenta	140. ± 9.6%	150. ± 9.6%	-0.05 ± 42%	-0.10 ± 16%	6.9 ± 1.5%	8.4 ± 1.3
Mojave Co.	176. ± 2.4%	183. ± 2.4%	-0.2 ± 57%	-0.2 ± 50%	6.1 ± 2.9%	7.6 ± 3.1
Manhattan Arkose	280. ± 9.9%	290. ± 9.7%	-0.08 ± 74%	-0.11 ± 54%	11.8 ± 6.2%	13.6 ± 5.
Tick Canyon	22. ± 7.9%	23. ± 7.8%	-0.04 ± 35%	-0.07 ± 22%	3.15 ± 2.3%	4.40 ± 1.
Masonville	430. ± 19%	450. ± 19%	-0.26 ± 24%	-0.29 ± 22%	19. ± 16%	21. ± 15%
Grafton Graywacke	360. ± 11%	370. ± 11%	-0.03 ± 104%	-0.06 ± 57%	18. ± 11%	20. ± 10%
Portageville	191. ± 0.8%	199. ± 0.8%	-0.39 ± 11%	-0.41 ± 10%	6.96 ± 1.4%	8.5 ± 1.2
Buffalo Gap	33. ± 6.3%	35. ± 6.3%	0.2 ± 448%	0.2 ± 534%	3. ± 37%	4. ± 28%
San Felipe	460. ± 6.9%	480. ± 7.0%	0.3 ± 70%	0.3 ± 79%	34. ± 3.0%	37.7 ± 2.

1 Mean ± 1σS. D. of 3 replicates
2 Using blank as "influent" solution
3 Using filtered stock solution as "influent" solution

TABLE 14b

K_d VALUES FOR SANDSTONES IN BRINE (<100 MESH)[1]

	K_d for ^{137}Cs		K_d for ^{141}Ce		K_d for ^{237}Pu	
	METHOD 1 CALCULATIONS[2]	METHOD 2 CALCULATIONS[3]	METHOD 1 CALCULATIONS[2]	METHOD 2 CALCULATIONS[3]	METHOD 1 CALCULATIONS[2]	METHOD 2 CALCULATIONS
St. Peter	0.2 ± 69%	0.01 ± 34%	1000 ± 46%[4]	4000 ± 46%[4]	72 ± 7.9%	240 ± 6.8%
Nugget	1.12 ± 0.5%	0.947 ± 0.2%	≥2997	≥13,010	360 ± 26%	1100 ± 25%
Medina	0.16 ± 55%	-0.01 ± 905%	≥1818	≥7900	600 ± 32%	1700 ± 32%
Mt. Tom	0.15 ± 46%	-0.02 ± 324%	≥2932	≥12,730	700 ± 70%[4]	2000 ± 70%[4]
Portland Brownstone	3.17 ± 2.4%	2.97 ± 2.5%	≥2011	≥8750	948 ± 1.5%	≥2797
Berea	0.2 ± 78%	-0.001 ± 12,670%	1200 ± 14%[5]	5000 ± 14%	380 ± 18%[5]	1100 ± 17%[5]
Kayenta	0.77 ± 9.2%	0.59 ± 12%	≥2945	≥12,780	300 ± 64%[5]	1000 ± 62%[5]
Mojave Co.	0.81 ± 5.2%	0.63 ± 7.8%	3000 ± 63%	11,000 ± 63%	300 ± 49%	1000 ± 47%
Manhattan Arkose	0.40 ± 9.2%	0.23 ± 16%	3000 ± 65%	11,000 ± 65%	470 ± 44%[4]	1400 ± 44%[4]
Tick Canyon	0.84 ± 5.8%	0.66 ± 7.2%	≥2407	≥10,460	≥957	≥2830
Masonville	0.62 ± 23%	0.4 ± 31%	≥2112	≥9180	≥1189	≥3500
Grafton Graywacke	1.14 ± 3.0%	0.96 ± 4.0%	≥3072	≥13,340	500 ± 29%[5]	1400 ± 28%[5]
Portageville	0.8 ± 15%	0.6 ± 19%	≥2034	≥8850	≥948	≥2797
Buffalo Gap	1. ± 146%	1. ± 192%	900 ± 45%[4]	4000 ± 45%[4]	86 ± 5.3%	280 ± 4.7%
San Felipe	0.2 ± 138%	0.04 ± 641%	≥2536	≥11,000	≥1194	≥3517

1 Mean ± 1σ S.D. of 3 replicates
2 Using blank as "influent" solution
3 Using filtered stock solution as "influent" solution
4 One sample with counting statistic error
5 Mean of two values only

The original intent of this study was to assess the extent to which mineralogical variability of sandstones effected their K_d values in brine for the radionuclides used. To that end, the 15 sandstones listed in Table 7 were chosen for their wide range of mineralogical compositions and then K_d measurements were taken with sandstone composition as the only variable. For the individual sandstones the effects of particle size was also investigated by measuring K_d on two size fractions. For the purpose of further discussions, K_a values from Table 15 will be used. These values were obtained by taking the most reliable K_d values from Tables 13 and 14 (calculation method #2) and dividing by the corresponding BET surface area measurements from Table 10. The resultant distribution coefficients are based on surface area rather than weight. Since sorption is likely to be a function of surface area rather than weight, this treatment should result in a more realistic measure of sorption character for these sandstones. The authors recognize that surface area measurements based on the BET technique (N_2 absorption) may not represent the same surface which radionuclides see in a aqueous system. We intend to measure surface area by the ethylene glycol method during FY80. Until a comparison is made between the two techniques, we have used the BET data for the preliminary interpretations presented here.

Table 7 lists the sandstones in terms of decreasing quartz content. Since quartz is the primary constituent for all these sandstones (99%-55% by volume), possible correlations of K_a with respect to quartz content was investigated. From Table 15, it can be seen that no trend exists between K_a and quartz content for any of the six radionuclides investigated. The K_a values observed are more likely a result of high K_d minerals (with respect to quartz) in the various sandstones. Table 8 presents the bulk mineralogical content of the samples as determined by an x-ray diffraction study. This technique provides only a

TABLE 15a

K_a VALUES FOR SANDSTONES IN BRINE (48-100 MESH)[1]

	^{75}Se	^{85}Sr	^{125}Sb	^{137}Cs	^{141}Ce	^{237}Pu
St. Peter	46	-0-	-0-	-0-	570	280
Nugget	67	-0-	7.4	-0-	6600	1650
Medina	62	-0-	1.8	-0-	3850	820
Mt. Tom	29	-0-	6.6	-0-	7690	2310
Portland Brownstone	12	-0-	0.72	0.87	870	170
Berea	68	-0-	1.2	-0-	300	1260
Kayenta	16	-0-	0.32	-0-	320	320
Mojave Co.	13	-0-	0.72	-0-	2050	150
Manhattan Arkose	36	-0-	2.1	-0-	$\geq$8630	1630
Tick Canyon	8.7	-0-	0.39	-0-	300	690
Masonville	49	-0-	3.7	-0-	$\geq$7310	1970
Grafton Graywacke	75	-0-	22.	-0-	$\geq$23,100	1100
Portageville	21	-0-	0.45	-0-	270	2390
Buffalo Gap	7.6	-0-	0.20	-0-	160	90
San Felipe	34	-0-	2.7	-0-	$\geq$7470	3270

1. K_a are K_d values converted from units of ml/gm to ml/m^2 as based on BET surface area measurements (see Table 10 for BET surface area values). All negative values from Tables 13 and 14 are considered as zero K_a. Only data from the #2 calculation method are presented.

TABLE 15b

K_a VALUES FOR SANDSTONES IN BRINE (<100 MESH)[1]

	^{75}Se	^{85}Sr	^{125}Sb	^{137}Cs	^{141}Ce	^{237}Pu
St. Peter	28.	-0-	3.2	0.010	3970	240
Nugget	230.	-0-	7.3	0.58	≥7930	670
Medina	100.	-0-	4.4	-0-	≥4550	980
Mt. Tom	110.	-0-	14.	-0-	≥14,700	2300
Portland Brownstone	32.	-0-	1.7	0.69	≥2040	650
Berea	93.	-0-	5.2	-0-	3740	820
Kayenta	33.	-0-	1.8	0.13	≥2790	220
Mojave Co.	30.	-0-	1.2	0.10	1780	160
Manhattan Arkose	98.	-0-	4.6	0.078	3720	470
Tick Canyon	7.1	-0-	1.4	0.20	≥3220	≥870
Masonville	130.	-0-	6.1	0.12	≥2660	≥1010
Grafton Graywacke	250.	-0-	14.	0.66	≥9170	960
Portageville	48.	-0-	2.0	0.14	≥2130	≥670
Buffalo Gap	7.9	0.045	0.90	0.22	3250	63
San Felipe	110.	0.067	8.5	0.009	≥2470	≥790

1. K_a are K_b values converted from units of ml/gm to ml/cm^2 as based on BET surface area measurements (see Table 10 for BET surface area values). All negative values from Tables 13 and 14 are considered as zero K_a. Only data from the #2 calculatin method are presented

qualitative accounting of the minerals present. In order to correlate K_a with mineral content, a more accurate method is required. Optical petrography analysis has been done on these samples and further correlation studies will be done during FY80 using this analysis. For this report it can be concluded that K_a values for the sandstones investigated here are not simply a function of quartz content but are relate to as yet unknown factors.

For individual sandstones, some comments can be made concerning the effect of size separated samples on K_a. For ^{75}Se, the <100 mesh fractions show higher K_a values than the 48-100 mesh fractions for all samples except St. Peter. Tick Canyon and Buffalo Gap (within the experimental errors) show nearly equal values for both size fractions. Strontuim-85 values are essentially zero for all samples of both size fractions. For ^{125}Sb, only the 48-100 mesh sample for Grafton Graywacke has a higher K_a than for the <100 mesh sample. All other ^{125}Sb K_a values (within experimental error) show higher values for the <100 mesh samples except for Nugget where they are nearly equal. All ^{137}Cs values are either both zero or the <100 mesh samples are larger. Many of the ^{141}Ce values are upper limits, but where they are based on observed ^{141}Ce in the solution, the <100 mesh samples show a higher K_a than the 48-100 mesh samples with the exception of Mojave Co. Errors are large for many of the ^{237}Pu values. For five of the <100 mesh samples only upper limit values are reported. Because of the large errors and limit values, only the Manhattan Arkose 48-100 mesh sample shows a value (within the errors) which is higher than the <100 mesh sample. Otherwise, little can be said about the size effect on the ^{237}Pu K_a values.

In general, then, the <100 mesh samples show higher K_a values than the 48-100 mesh samples. This is consistant with the assumption that the samples were prepared by "disaggragating" the sandstone rather than grinding it and that the resultant finer fraction was richer in non-quartz minerals. These non-quartz

minerals could be cement or alteration minerals located between the quartz grains in the original rocks. Table 8 presents x-ray diffraction data which show that for many of the samples, the finer fraction contained more clay, mica, calcite, chlorite, and microcline than the coarser fraction. These minerals generally have higher K_a values than quartz.

The sorption behavior of the radionuclides can be addressed by comparison of K_a values to one another rather than by rock sample or size fraction. Selenium-75 resulted in K_a values ranging from 7.1 to 254. Except for two very small values, ^{85}Sr had a K_a of zero. Antimony-125 K_a values ranged from 0.20 to 22. Cesium-137 K_a values ranged from 0 to 0.87. Cerium-141 K_a values ranged from 160 to $\geq$ 23,100. Finally, ^{237}Pu K_a values ranged from 63 to 3270. From the K_a values in Table 15, a general trend can be inferred for K_a values as follows: $^{141}Ce > {}^{237}Pu > {}^{75}Se > {}^{125}Sb > {}^{137}Cs > {}^{85}Sr$. The behavior of ^{85}Sr and ^{137}Cs can be understood since these elements were in high concentration in the brine (see Table 3) relative to the radiotracer concentrations (see Table 4). Their K_a values of zero to near zero would be expected merely from the competition for exchange sites by the nonradioactive Sr and Cs in solution. Since the salt content in the brine is very high it might even be expected that <u>all</u> the tracers would not be sorbed since they have very low chemical concentrations themselves (see Table 4). However, for Ce, Pu, Se, and to some extent Sb, exchange sites were available in spite of the massive competition by the ions making up the brine. It can be concluded that the unique chemistry of these elements plays a critical role in their sorption behavior under these intense solution conditions.

The specific aqueous geochemistry for Ce, Pu, Se, and Sb in a saturated salt brine under mildly oxidizing laboratory conditions cannot be understood from these studies. It is hoped that with the completion of ethylene glycol surface area measurements and cation exchange capacity measurements during

FY80 coupled with the observations reported in this document, an understanding of the effect of sandstone mineralogy on radionuclide sorption behavior in salt brine will result.

DYNAMIC CORE SORPTION STUDIES

The dynamic core sorption apparatus was built during FY 78 and was ready for debugging during early FY 79. A schematic diagram of one unit of the apparatus is shown in Fig. 4. The initial runs on the dynamic sorption apparatus were made with Thirsty Canyon tuff, a partially welded rhyolitic ash-flow tuff from Pahute Mesa, NTS (Fig. 5). The Thirsty Canyon tuff was the rock that was used in early core-sorption experiments conducted at LLL[3]. The first runs were made with distilled water in order to debug the apparatus and evaluate the permeability characteristics of the cores.

Subsequent experiments consisted of calibration runs on standard samples, and experiments to determine the radionuclide transport velocities in rock cores. The standard samples were high density Al_2O_3 cylinders with negligible sorption and accurately known pore volumes. The results of the calibration runs gave numerical values for the dead volume of the system; this is the total system volume from the spike injection valve to the end of the effluent discharge line, not including the pore volume of the standard samples or the rock core. Transit times determined in the experiments on the rock cores were corrected for transit through the dead volume before the transport velocities and retardation factors were calculated from them.

In the experiments on Thirsty Canyon tuff and St. Peter sandstone, the transport solution and spike solution were prepared from distilled water which had been pre-equilibrated with the 100-325 mesh fraction of the appropriate rock for at least 75 hours. Solution compositions are shown in Table 16.

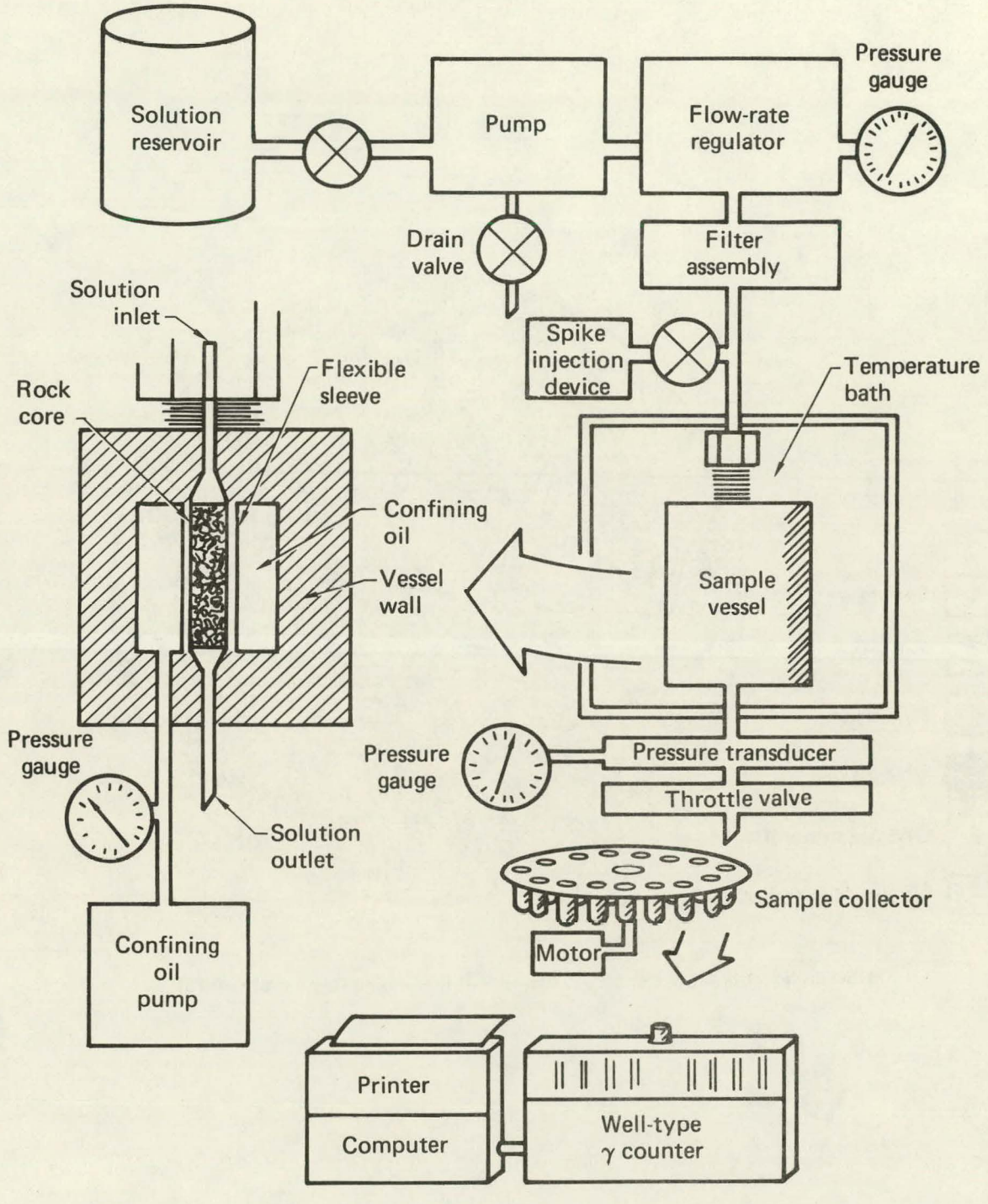

Fig. 4. High pressure "dynamic" sorption apparatus.

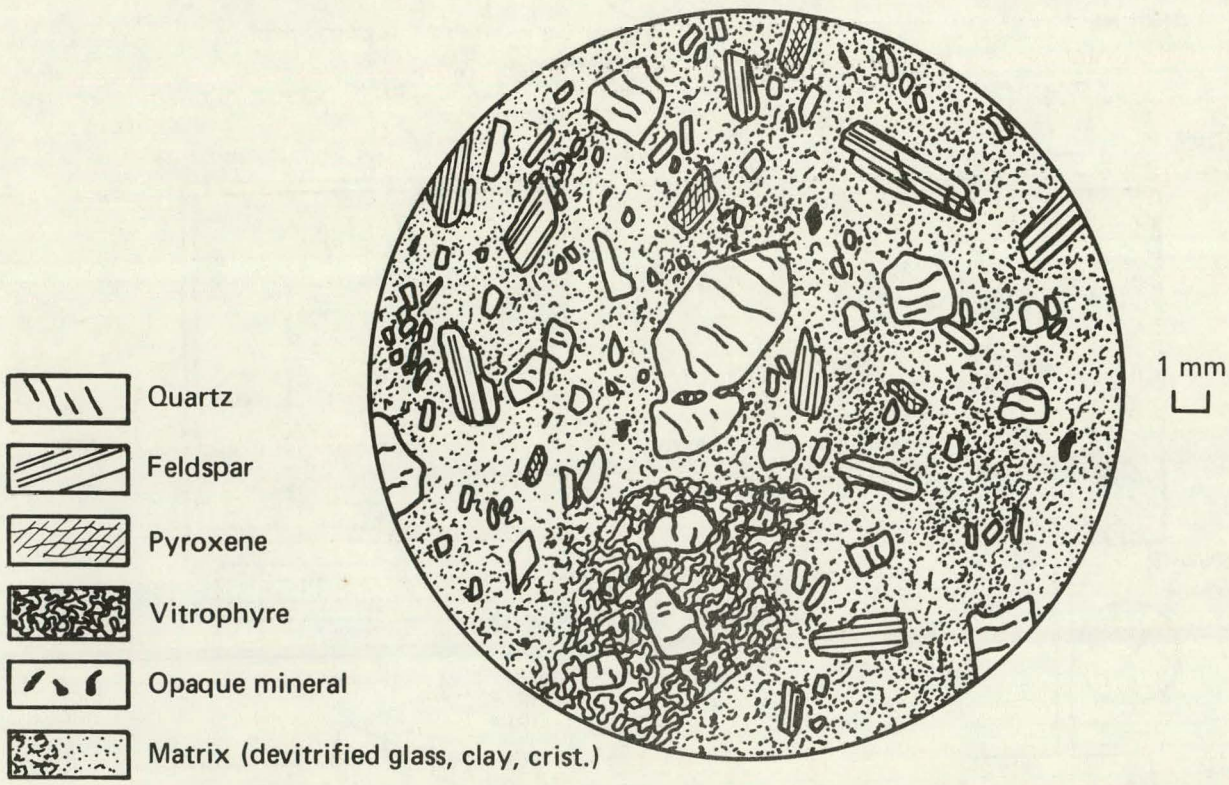

Fig. 5. Thin-section of the Trailridge member of the Thirsty Canyon tuff (NTS).

TABLE 16

COMPOSITION OF STOCK SOLUTIONS FOR MEASUREMENTS ON RADIONUCLIDE TRANSPORT IN ROCK CORES

COMPONENT	SYSTEM TYPE	
	St. Peter Sandstone, 200 g/l, No. 1 Micromoles/Liter	Thirsty Canyon Tuff, 100 g/l, No. 1 Micromoles/Liter
Al	8.5	0.22
As	0.3	0.
B	14.	1.4
Cd	0.	0.
Co	0.	0.
Cu	0.46	0.04
Fe	0.	0.
Li	1.0	0.
Mn	0.02	0.
Mo	0.58	0.
Ni	0.	0.
P	<5.	<5.
Pb	<0.14	<0.14
Se	<0.09	<0.9
Si	68.	210.
Sr	0.70	<0.14
Ti	<0.04	<0.04
V	<0.06	<0.06
Zn	0.06	<0.08
Ca	342.	0.4
K	190.	69.
Mg	103.	0.45
Na	1590.	300.
H+	0.007 - 0.0105	0.011

The St. Peter sandstone was a quartz arenite with about 1% clay and a porosity of 15%. Spike solutions contained ^{85}Sr and ^{95m}Tc in early experiments on tuff; and ^{85}Sr, ^{95m}Tc and ^{3}H in later runs on tuff and on sandstone. Results are shown in the form of plots of activity vs. time and number of pore volumes for the effluent, and concentration profiles for the solid core.

The experiments were conducted under the following conditions:

- temperature, 25°C
- confining pressure, 10 MPa (1470 psig)
- flow rates, 0.006 to 0.031 cm^3/min for tuff and 0.092 cm^3/min for sandstone
- linear Darcy velocities, 6 to 30 m/yr for tuff and 91 m/yr for sandstone.

(For comparison, flow velocities beneath Pahute Mesa range from 2 to 76 m/yr.) After establishment of steady flow through the rock core, a short pulse of spike solution was injected at the inlet face, transported along the core, and monitored in the effluent solution as a function of time. Effluent curves are obtained during the run as indicated schematically in Fig. 6. Concentration profiles were obtained after the run by drying the core with compressed air, impregnating it with Epon 815 resin, slicing the impregnated core with a thin diamond wafering saw, and γ-counting the slices. Transit times (τ) were read from the effluent curves as indicated in Fig. 6 and migration velocities (v) were calculated from the formulas in Table 17.

Thirsty Canyon Tuff and Equilibrated Water

The results of runs on Tuff Samples 5, 6, and 3 are shown in Table 17, Figs. 7 to 9 for the effluent activity, and Figs. 10 to 12 for the core concentration profiles. The effluent activity curves in Fig. 9 show that ^{95m}Tc and ^{3}H have the same transit time (τ) within the limits of accuracy of the measurements. The ^{95m}Tc peak shows much more tailing than the ^{3}H peak, though they both have the same rise rates.

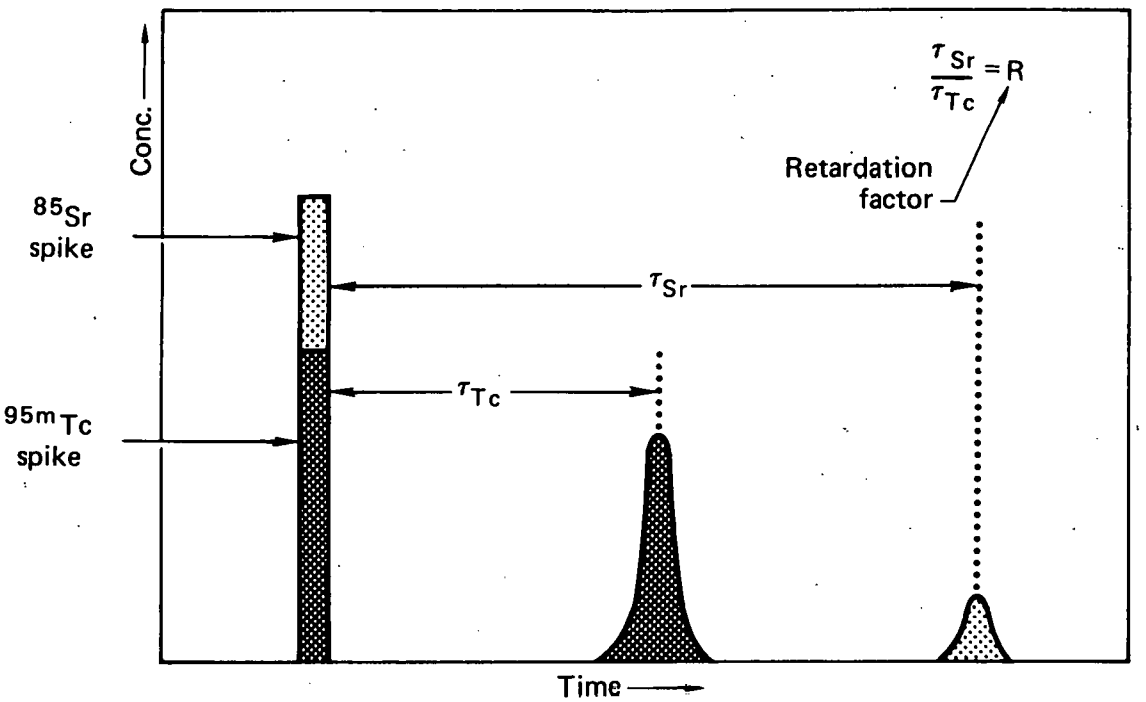

Fig. 6. Transit time behavior for radionuclides in an ideal core run.

TABLE 17. Retardation Factors, Sorption Ratios, and Activity Balance in Thirsty Canyon Tuff

Figure	Core	L	ρ	Atom	f_j	τ	t_m	$\overline{X}$	v_j	R	K_d
7,10b	5	2.713	2.181	^{95m}Tc	0.0114	262			0.1035	1	0
10a				^{85}Sr	0.0062		8295	.424	5.1 E-5	110	13
8,11b	6	2.497	2.143	^{95m}Tc	0.0152	155			0.01611	1	0
11a				^{85}Sr	0.0113		8260	.234	2.8E-5	567	66
9,12b	3	2.684	2.147	^{95m}Tc	0.0305	80			0.0335	1	0
9				^{3}H	0.0305	80			0.0335	1	0
12a				^{85}Sr	0.0194		11915	.274	2.30 E-5	928	108

Table 17 (Continued)

Activity			Fraction of Spike			Spike Conc.		V_p	t_{in}	ϕ'
Ac	Ae	As	Core	Effluent	r	dpm/cm^3	M/l			
1.74 E4	-	1.78 E6	.010	-	-	3.55 E6	7.53 E-10	2.98	44	.234
1.29 E6	0	1.26 E6	1.02	0	1.02	2.51 E6	5.62 E-10			
1.00 E4	-	1.78 E6	.006	-	-	3.55 E6	7.53 E-10	2.40	32	.184
9.23 E5	0	1.26 E6	0.73	0	0.73	2.51 E6	5.62 E-10			
1.93 E4	1.24 E6	1.36 E6	.014	.91	0.92	2.71 E6	5.74 E-10	2.43	16	.174
-	-	1.11 E3	-	-	-	2.23 E3	3.48 E-11			
1.00 E6	0	9.60 E5	1.04	0	1.04	1.92 E6	4.30 E-10			

a) Volume of trace solution = 0.500 cm^3

(Continued Table 17)

DEFINITIONS:

L = length of core in cm

ρ = bulk density in g/cm^3

f_j = solution flowrate in cm^3/min which applies to the transport of the jth species

τ_j = observed transit time through the core for the jth species, in min

t_m = total experiment time, in min

X_j = location of the centroid of the concentration in the core for the jth species in cm

v_j = transport velocity for the jth species, in cm/min

R = the retardation factor, corrected for flowrate effects

K_d = the sorption ratio in cm^3/g

A_c = activity in the core, in disintegrations/minute (dpm), corrected for radioactive decay

A_e = activity in effluent solution (dpm), corrected for radioactive decay

A_s = activity in spike solution (dpm), corrected for radioactive decay

r = fraction of nuclide recovered

V_p = pore volume in cm^3

V = solution volume in cm^3

V_t = total effluent volume during t_m, in cm^3

ϕ = fractional porosity = 0.25 for Thirsty Canyon Tuff

t_{in} = injection time for the spike solution, in min

V_c = volume of core sample, in cm^3

A_{ij} = activity in the ith section of the core, dpm, for the jth species

x_i = location of the ith section

(Continued Table 17)

FORMULAS:

$f = V/t$; $f_{sr} = V_t/t_m$

$\overline{X}_j = \Sigma_i X_i A_{ij} / \Sigma_i A_{ij}$

$v_{sr} = \overline{X}/t_m$

$v_{3_H} = L/\tau_{3_H}$

$v_{Tc} = L/\tau_{Tc}$

$v = v_r(f_j/f_r)$; $v_r = v_{3_H}$ or v_{Tc}

$R = (v/v_j)$

$K_d = (\phi/\rho)\ (R-1)$

$r = (A_c + A_e)/A_s$

$V_p = \tau_{Tc} f_{Tc}$ or $\tau_{3_H} f_{3_H}$

$t_{in} = 0.5/f$

$\emptyset' = Vp/Vc$

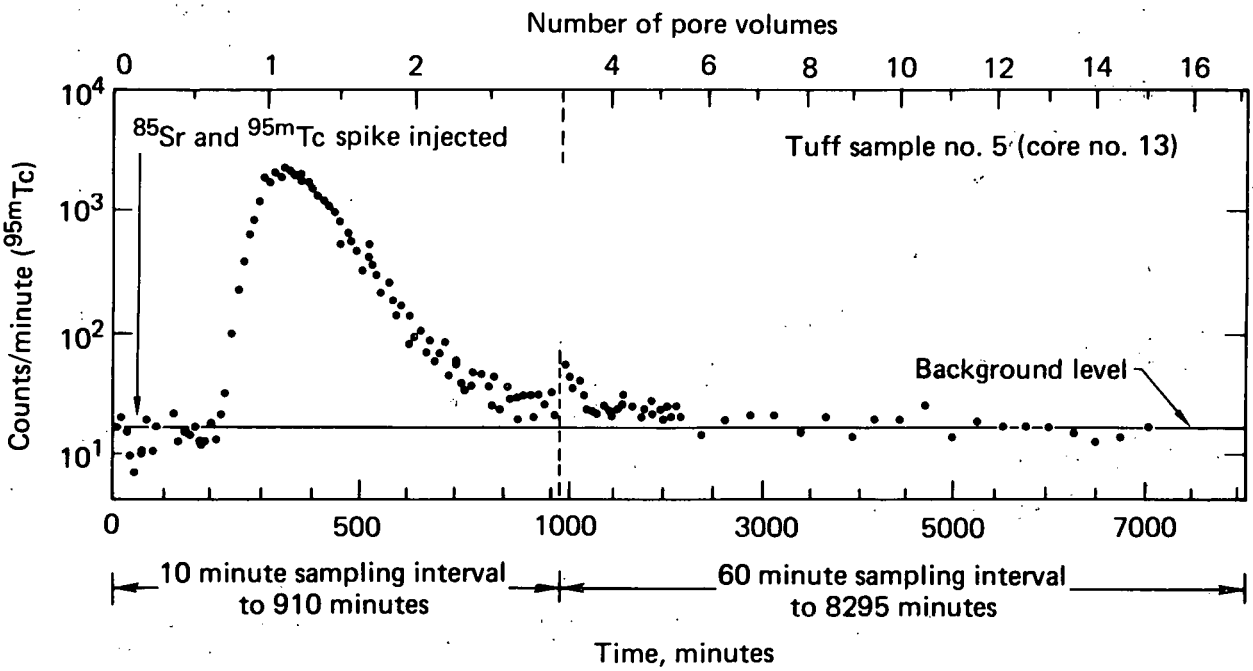

Fig. 7. Counts per minute vs. time for ^{95m}Tc.

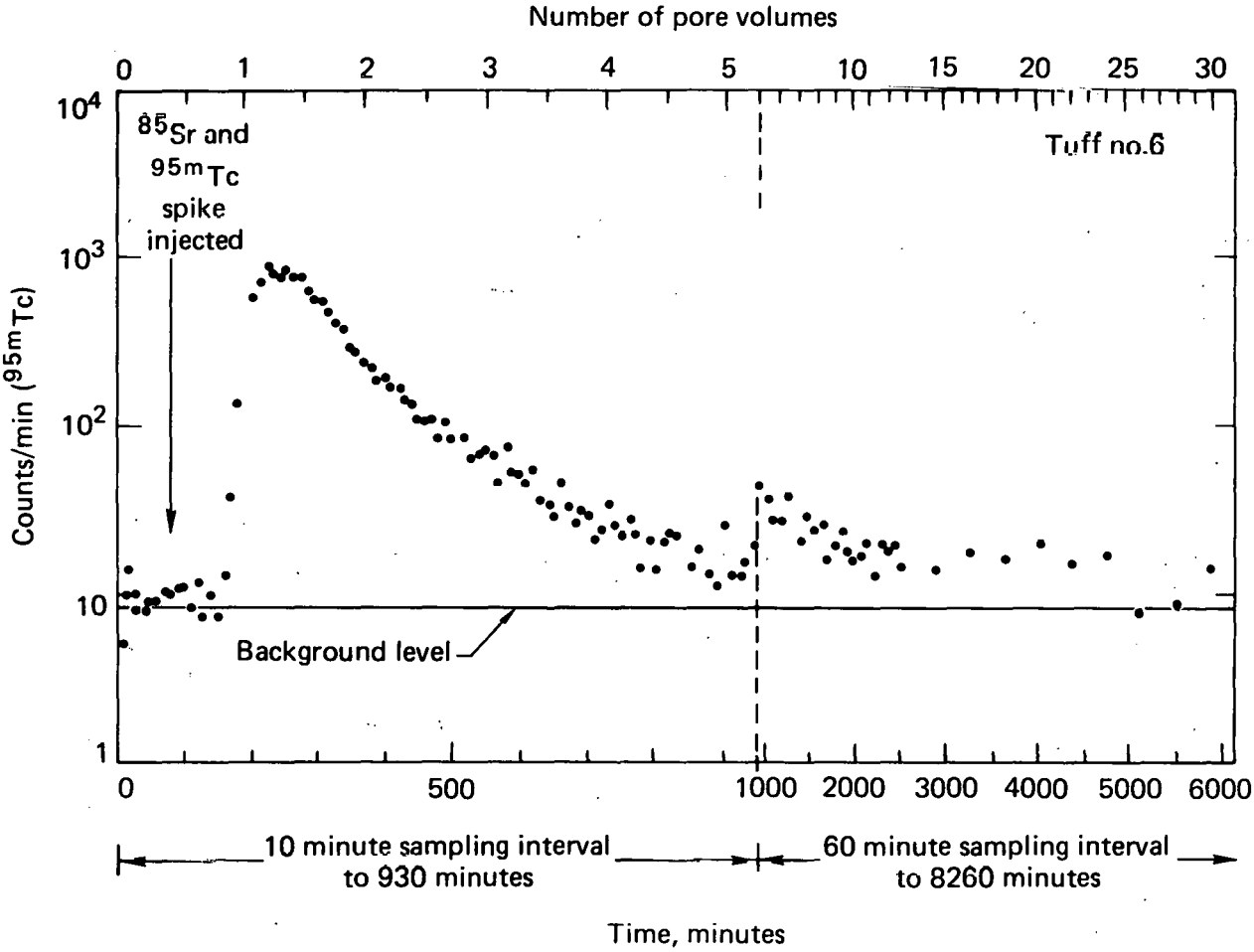

Fig. 8. Counts per minute vs. time for ^{95m}Tc.

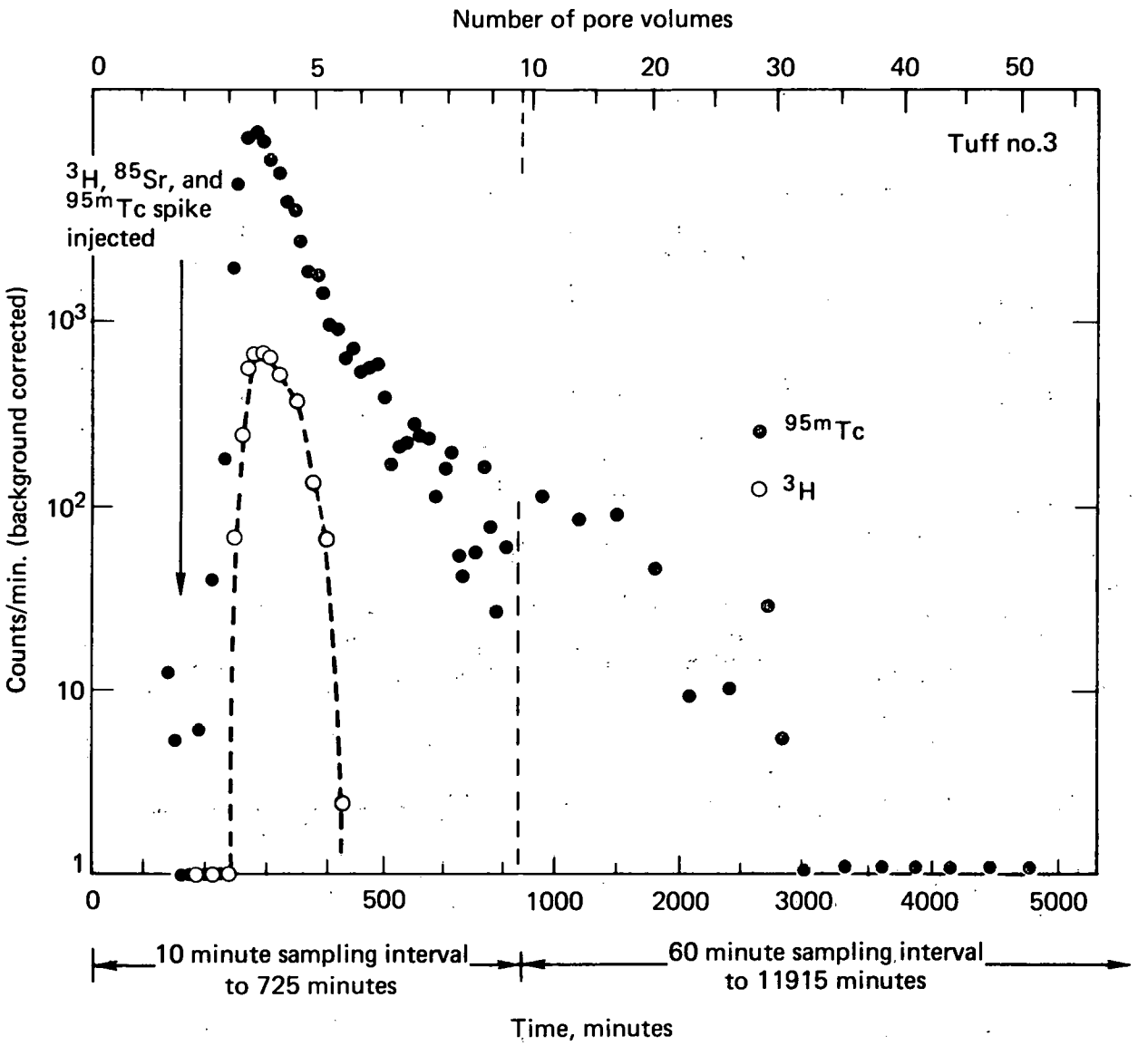

Fig. 9. Counts per minute vs. time for ^{3}H and ^{95m}Tc.

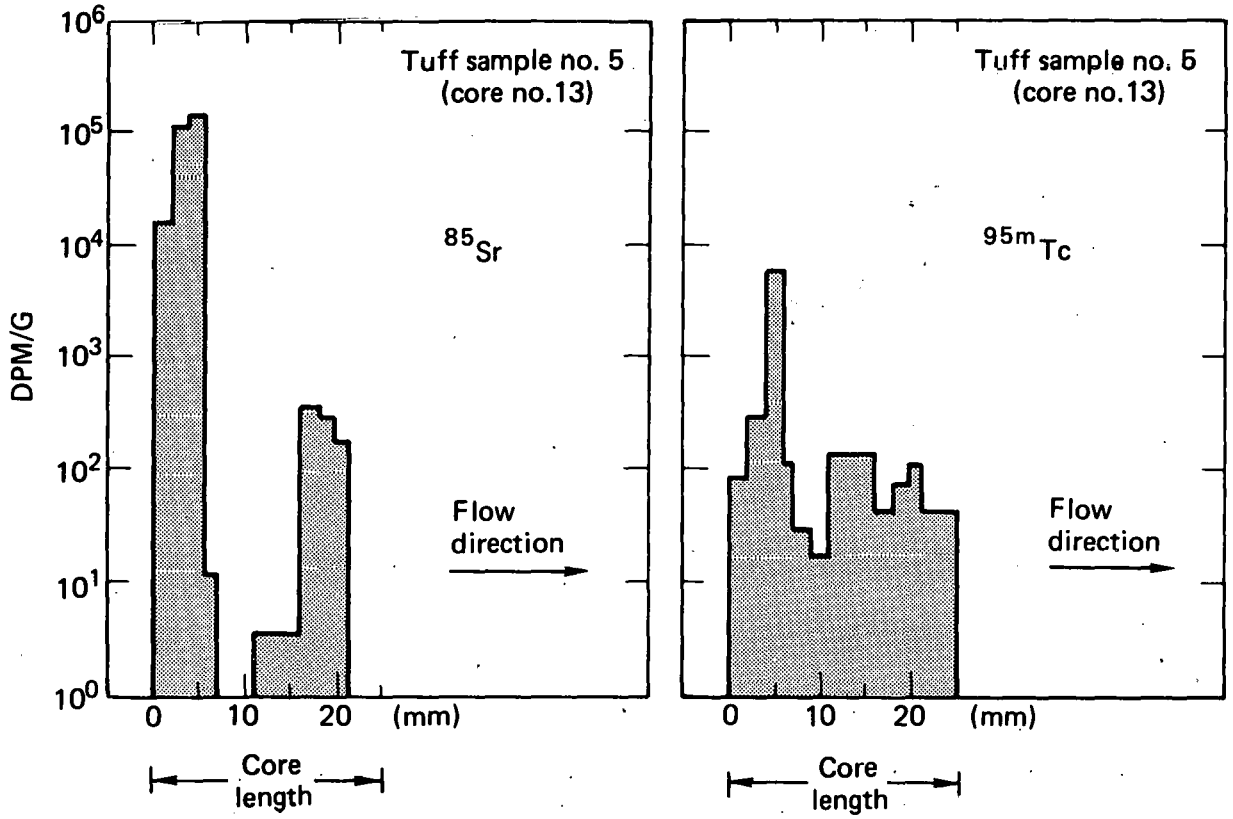

Fig. 10-a.

Fig. 10-b.

Concentration profiles for ^{85}Sr and ^{95m}Tc in Thirsty Canyon tuff sample no. 5.

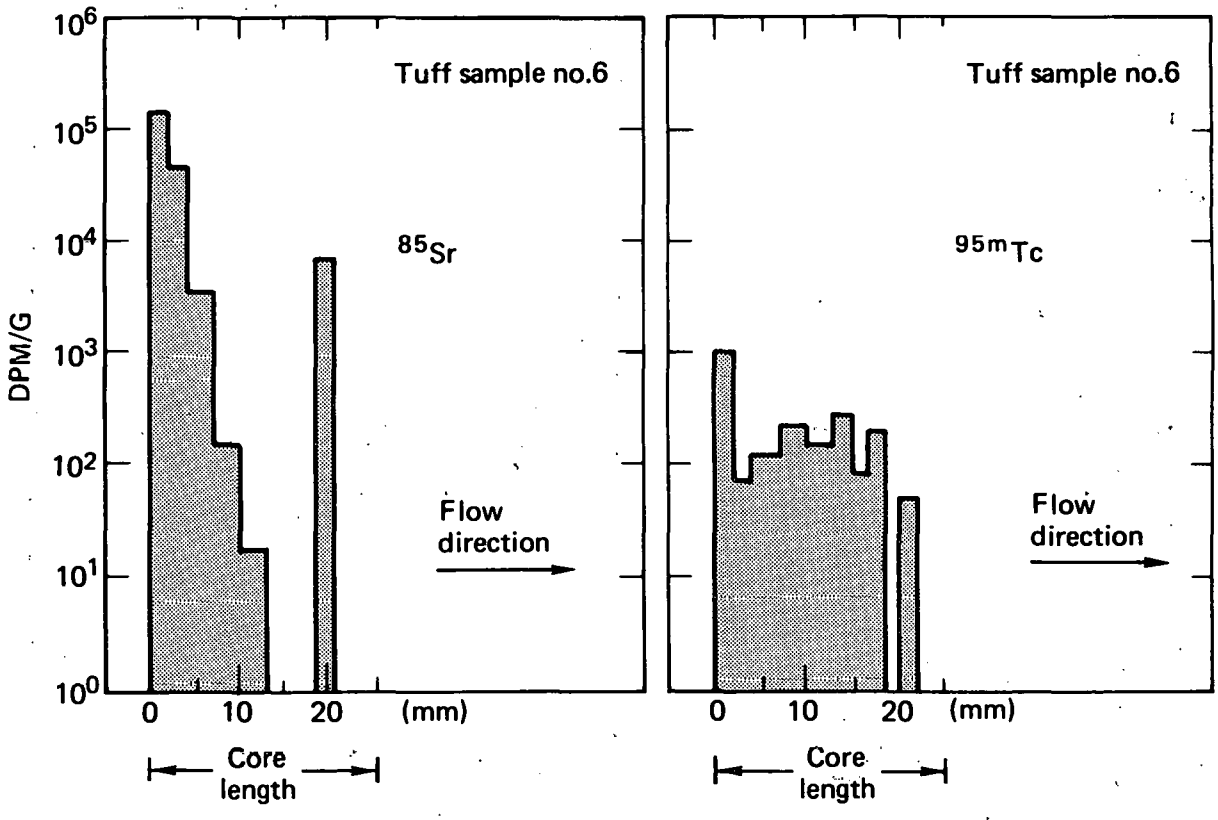

Fig. 11-a.

Fig. 11-b.

Concentration profiles for ^{85}Sr and ^{95m}Tc in Thirsty Canyon tuff sample no. 6.

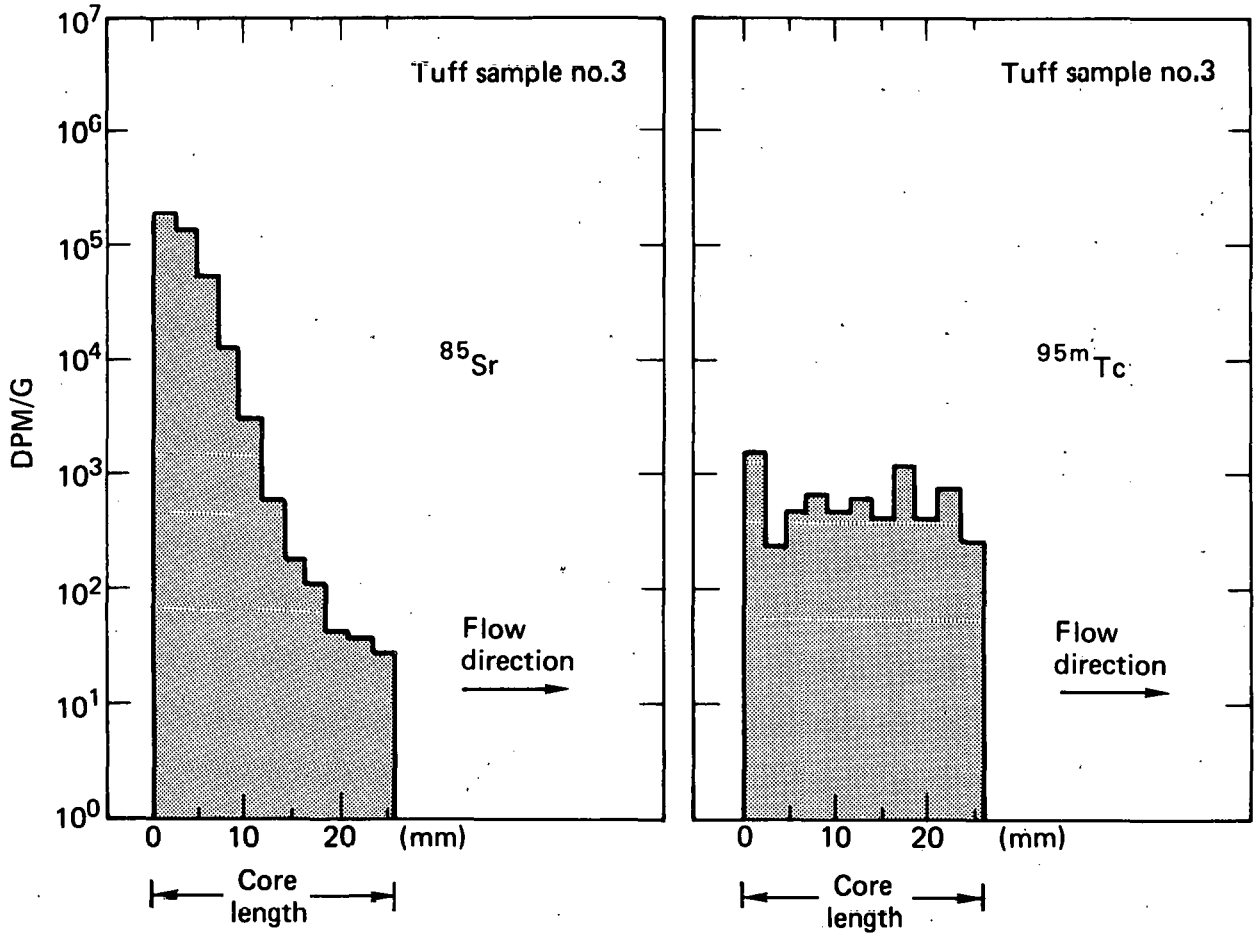

Fig. 12-a.

Fig. 12-b.

Concentration profiles for ^{85}Sr and ^{95m}Tc in Thirsty Canyon tuff sample no. 3.

In the core concentration profiles, two of the ^{85}Sr profiles are bimodal and the third, unimodal. This together with the relatively long run time for the unimodal distribution suggests that the smaller ^{85}Sr peak may have been eluted from the core at around 60000 min. No ^{85}Sr has been observed in the effluent from any tuff sample, but we expect to look for it more intensively in the effluent from Tuff Sample 3 as time permits. Most of the ^{85}Sr is near the inlet faces of the cores. In order to be consistent in the calculation of the transport velocity v_{Sr} for all samples, the location (X) of the ^{85}Sr centroid was determined by averaging over the gross activity distribution.

The values of R (the retardation factor in Table 17) are calculated for each nuclide from $R = (v/v_j)$ where v is the pore fluid velocity of the solution which transports the j-th nuclide. For an experiment at constant flow rate, $v = v_r$ the velocity of the reference nuclide chosen for the particular experiment. For experiments in which the flow rate is not constant, $v = v_r\ (f_j/f_r)$, where f_j is the flow rate of the solution which transports the j-th nuclide and f_r is the flow rate of the solution which transports the reference nuclide. In general, f_j and f_r are calculated for different time intervals during the experiment and therefore will not be equal in an experiment where the flow rate varies. The resulting values of K_d for ^{85}Sr are correlated with solution flow rate as shown in Fig. 13. In this correlation, the flow rate is the total volume during each experiment divided by the total run time, which is shown in Table 17 as f_{Sr} since it applies to the transport of ^{85}Sr a distance X in the core during the experiment. Additional experiments will be needed in order to determine whether or not the correlation is significant. The static K_d value is near the middle of the range of the dynamic values (Fig. 13).

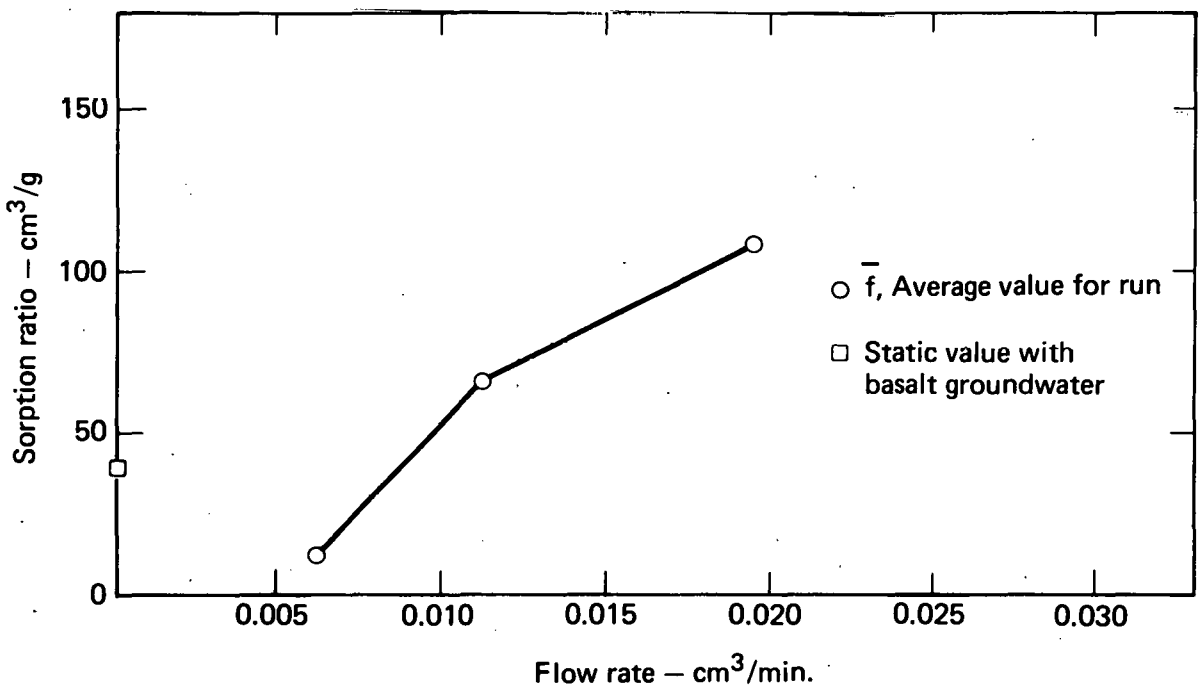

Fig. 13. Sorption ratio vs. flow rate for ^{85}Sr on Thirsty Canyon tuff.

In the runs on Tuff Sample 5 and 6, no attempt is made to obtain an activity balance on ^{95m}Tc since the counting efficiency was not determined on the counting equipment used to count the effluent samples. Spikes and cores were analyzed in the LLL γ-counting facility for ^{95m}Tc and ^{85}Sr so these results are corrected for decay and counter efficiency. As shown in Table 17, the ^{85}Sr activity balance is satisfactory.

In the run of Tuff Sample 3, the core, effluent, and spike samples were all counted using a Canberra 30 Pulse Height Analyzer and NaI(Tl) well counter for which the counting efficiency was determined in separate calibration experiments. No attempt was made to obtain an activity balance for ^{3}H since only enough of the peak was analyzed to establish it as a transit time reference. In this run the activity balance is satisfactory for both ^{85}Sr and ^{95m}Tc.

Only a small fraction of the ^{95m}Tc introduced in the spike was retained on the tuff cores (0.6% to 1.4%). This suggests that most of the ^{95m}Tc was transported through the core (presumably as $^{95m}TcO_4^-$), and that the small fraction left was reduced and irreversibly sorbed or precipitated, possibly as $^{95m}TcO_2$. In the experiment on Tuff Sample 3, the fraction of ^{95m}Tc which is first transported through the core has a transit time for the concentration peak which is the same as the transit time for ^{3}H. Tritium is chosen as the reference nuclide in this experiment, so that $K_d(^{3}H)=0$. Assuming that $^{95m}TcO_4^-$ is the mobile species, $K_d(^{95m}TcO_4^-)=0$, an important result for studies in which ^{95m}Tc is chosen as the reference nuclide. Another important result is that ^{85}Sr is much more strongly retained on Thirsty Canyon Tuff then either $^{95m}TcO_4^-$ or ^{3}H.

St. Peter Sandstone and Sandstone Equilibrated Water

Results of the run on St. Peter Sandstone Sample No. 11 are shown in Table 18 and Figs. 14 and 15. In Fig. 14, the effluent activity peaks for ^{95m}Tc and ^{3}H occur at the same time within the limits of accuracy of the measurements. In both cases there is much less tailing in effluent curves from sandstone than from tuff (Figs. 7 to 9). The effluent peak for ^{85}Sr is much broader than those for ^{95m}Tc and ^{3}H, with a maximum corresponding to a transit time of 283.6 min.

As shown in Table 18, no ^{95m}Tc activity and less than 1% of the ^{85}Sr spike activity are left in the core. The activities shown in the table are corrected for decay and for counter efficiency, and the activity balance is satisfactory for ^{95m}Tc and ^{85}Sr. As in the case of Tuff Sample 3, the ^{3}H peak is used as a time reference marker and no attempt is made to check the ^{3}H activity balance.

Since so little ^{85}Sr is left in the core, K_d is calculated only for the major fraction which showed a transit time of 283.6 min for the peak. This value is 0.83 cm^3/g. There is no corresponding batch K_d value for St. Peter sandstone with sandstone-equilibrated water, so a direct comparison cannot be made at this time. Tritium is used as the reference nuclide in this experiment, with $K_d(^{3}H) = 0$. Since the transit time for ^{95m}Tc is the same as that for ^{3}H, $K_d(^{95m}Tc) = 0$ within the limits of accuracy of the measurements. The behavior of all three nuclides on St. Peter sandstone is consistent with the petrological characterization of it as mostly quartz with about 1% clay.

In summary, ^{95m}Tc and ^{3}H show $R = 1$, $K_d = 0$ in both Thirsty Canyon tuff and St. Peter sandstone, using pre-equilibrated water solutions. In tuff, 0.6 to 1.4% of the ^{95m}Tc remains in the core. The ^{85}Sr remains mostly at the inlet end of the tuff core. In the sandstone core, both ^{85}Sr and ^{95m}Tc are distributed in low concentrations,

TABLE 18. Retardation Factors and Sorption Ratios on St. Peter Sandstone

Figure	Core	L	ρ	Atom	f_j	τ	t_m	$\overline{X}$	v_j	R	K_d
14	11	2.7152	2.265	^{95m}Tc	.0917	22.89	6398	-0.04	.1186	1.0	0
14				^{3}H	.0917	22.89		-	.1186	1.0	0
				^{85}Sr	.0974	283.6		1.66	.00957	13	0.81

----->

Table 18 (Continued)

Activity			Fraction of Spike			Spike Conc.				
Ac	Ae	As	Core	Effluent	r	dpm/cm^3	M/l	V_p	t_{in}	ø′
-1.19 E4	2.81 E6	2.70 E6	0	1.04	1.04	5.41 E6	1.14 E-9	2.325	49	.1458
-	-	1.90 E4	-	-	-	3.79 E4	5.91 E-10	-	-	-
3.36 E4	2.93 E6	2.93 E6	.010	.91	.92	6.43 E6	1.44 E-9			

a) Volume of tracer solution = 0.500 cm^3.

ø = 0.15 for St. Peter sandstone.

$V_{Sr} = L/\tau_{Sr}$.

Other terms are defined in Table 17.

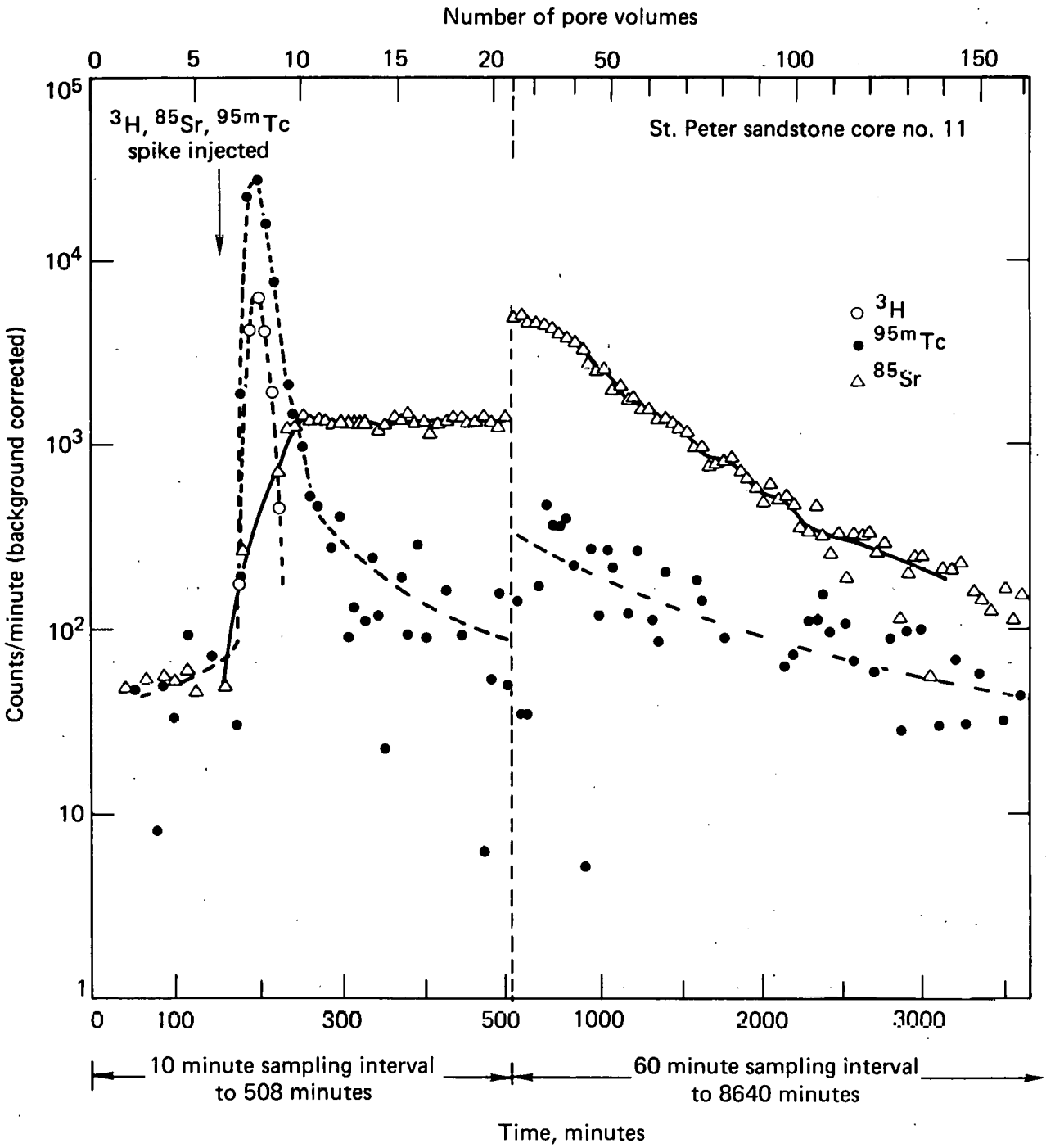

Fig. 14. Counts per minute vs. time for ^3H, ^{85}Sr, and ^{95m}Tc.

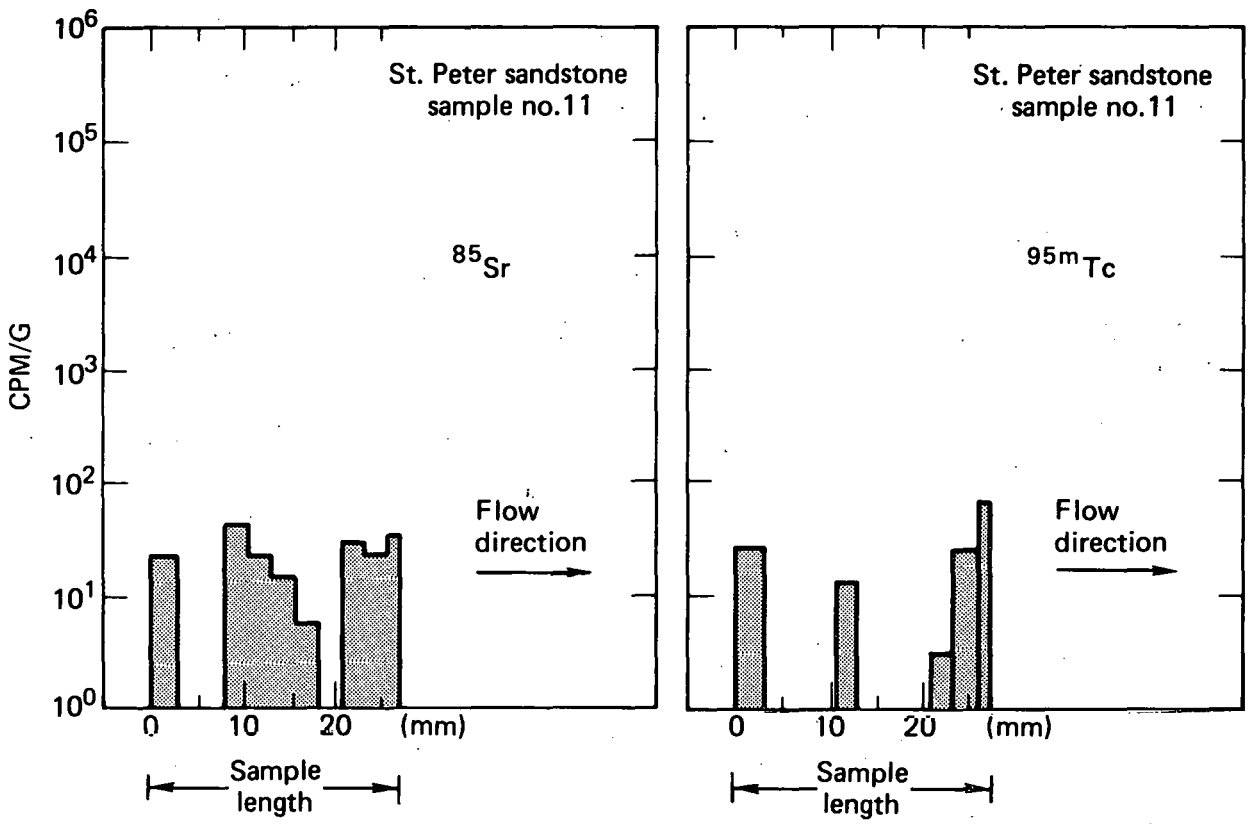

Fig. 15-a.

Fig. 15-b.

Concentration profiles for ^{85}Sr and ^{95m}Tc in St. Peter sandstone. (from sandstone-water solution)

between 0 and 1%. Most of the ^{85}Sr is transported through the sandstone core because the clay concentration is very low and ^{85}Sr is not strongly sorbed on the quartz.

The present investigation gives retardation factors for conditions similar to those encountered in the field. The St. Peter sandstone results should be of interest in connection with repositories located in or near sandstone formations.

REFERENCES

[1] S. C. MacLean, D. G. Coles, and H. C. Weed, "The Measurement of Sorption Ratios for Selected Radionuclides on Various Geologic Media," UCID Report 17928 (1978).

[2] T. J. Wolery, "Calculation of Chemical Equilibrium between Acqueous Solution and Minerals: The EQ3/6 Software Package," UCRL Report 52658 (1979).

[3] W. R. Daniels and B. R. Erdal, LASL, Private Communication, October, 1979.

[4] J. D. Tewhey, "Preliminary Results of Experimental Work in the Radionuclide Migration Program," UCID Report 17964 (Feb. 24, 1976).

NOTICE

This report was prepared as an account of work sponsored by the United States Government. Neither the United States nor the United States Department of Energy, nor any of their employees, nor any of their contractors, subcontractors, or their employees, makes any warranty, express or implied, or assumes any legal liability or responsibility for the accuracy, completeness or usefulness of any information, apparatus, product or process disclosed, or represents that its use would not infringe privately-owned rights.

Reference to a company or product name does not imply approval or recommendation of the product by the University of California or the U.S. Department of Energy to the exclusion of others that may be suitable.

"Work performed under the auspices of the U.S. Department of Energy by the Lawrence Livermore Laboratory under contract number W-7405-ENG-48."

QUESTIONS AND ANSWERS

LLL - Questions to Dave Coles and Homer Weed

Speciation of Tc and Precipitation

Q: In your tuff experiments, does the fact that you show the black curve for the technetium indicate that you get some technetium with precipitation within your plug.

A: We don't know. It is certainly true that the technetium is retained. Whether it's retained because it's irreversibly sorbed or because it's precipitated as TcO_2 we cannot tell without some auxiliary information. I suggest that it may well be reduced and just stay there as TcO_2. It's obvious that it partitions between the rocks.

Q: Would this be classified as a solution study or solution chemistry study where you're looking at the tracer feed solution?

A: I think I wouldn't classify it as a study unless I set out specifically to study it rather than as an after thought. Yes to what you're saying, it's a solution study.

C: One thing we see just in the attempt to measure a Kd is that many nuclides in their feed solution disappear and there are processes going on before we ever get it to the rocks or to the minerals and there are some things we need to understand about the solubilities.

C: I don't think we understand what species are present and it is obvious that we really can't interpret the Kd values very well.

Kd Measuring Techniques

Q: You said that for the Kds, you only had 1 or 2% in the post centrifugation filter (relative to the original stock solution) and it wasn't that important. It could be important if you have a high adsorption material and you're just looking at maybe 50% of what's left in the solution being taken out by the filter.

A: I'm not sure what you mean.

Q: If you run your sample through and you get 90% taken out of your tracer, say you have 10% left in your solution and you take out 2-1/2% then, a quarter of it. And if you make your Kd by looking at the solution alone; that can make a big difference.

A: I think that's right. I don't feel comfortable with batch Kd. But I think that's a problem shared by many of us.

Applicability to a Site

Q: We need to clarify a statement that was made. In general, these results will have nothing to do with WIPP site for three reasons. First, the hydrologic evidence is that the water will not go down into the Bell Canyon but will come up from the Bell Canyon. Secondly, St. Peter's sandstone is a far cry from the Bell Canyon sandstone which contains a large amount of feldspars (two kinds at least), some fluorides and even the mineral polyhallites. The third reason is a question: Is anyone who's mentioned the WIPP Brine B, as it's called, aware of the origin of this brine?

A: Yes. At least, I think I am. My impression is that this is intended to simulate a composition of the solid material taken from a core.

Q: Brine B is intended to simulate what you get when you throw out a chunk of core in distilled water and probably has very little to do with any ground water that has so far been found in southeastern New Mexico.

A: I think that insofar as I am able to reply to the observations, I will do so in three parts. The first is that we would welcome suggestions about the appropriate composition of solution to be used if we want to simulate conditions at the WIPP site. The second is that we hope eventually to be able to get samples of core material from the WIPP site and try these types of experiments on them. It really is relevant to the field. So, I think your objections to the experiment as conducted are valid. In the immediate future, I think we probably will repeat them just to find out something about the level of precision.

C: I wasn't objecting to the experiment.

A: Tomorrow I will talk more about samples that are more applicable to WIPP, but we're not picking on WIPP because we have no bones to pick there. It's just an example of a repository in salt, and a salt dome works equally well.

A: I would like to emphasize, however, that if we could get a sample of material from the WIPP site, we would be interested in running a test like this upon a material which is considered to be realistically chosen.

Q: What bothers me about all these Kd values, not your particular measurements, is the implication that if you measured the adsorption and moles per gram you're really dealing with a permeable medium, permeable to the solution. Whereas, it seems to me the much bigger source of error is the variability in surface area for these particles. And to that extent, it seems the kind of correlation the data was describing and looking for is quite insignificant in comparison with variation and surface areas in samples of different types.

A: What you actually measure is retardation factors, not Kds. So this means that you don't have to worry about surface area considerations, per se, because the surface area that interacts with the nuclide that you're using is the surface area that is going to be seen in the field. So, the essential feature of the core method that makes it nice is that you measure directly the kind of factors that the hydrologists are interested in for field work. Also you can think of the experiment this way. You have this core and you put solution through it but you have confining pressure on it. That entire system can be thought of as a little analog computer for the situation in the field. If you have troubles in the system; that is, if you get extra peaks where you don't expect them, what this does is to give a warning to the hydrologist. If you want to interpret your results in the field, you might have an anomaly.

Speciation of Tc Precipitation

Q: What was the mass balance of this technetium that you found that hung up on the core as opposed to what came through? You showed that you had a pretty even distribution and that the dPm per gram was rather small. But are we talking about the fractional percent of overall technetium that you injected of 1% or 10% or --?

A: I will have that answer when we finish all the counting on the technetium that came out and the technetium that stayed in. But as it is right now it looks as though the level of technetium that remains in the core is on the order of a tenth of a percent to 1%.

Q: A question on those results of technetium. Last year we heard that technetium migration is dependent on valence state or its anion/cation relationship in the solutions, some results by Bondietti. Do your results agree with that, or don't they compare with that?

A: What I'm guessing is that technetium partitions itself between the rock and the solution and that part of the technetium that remains in the plus seven state as the pertechnetate moves with the speed of water. The rest of the technetium that sets down on rock, I surmise, has been reduced to maybe +4 valence state so that it sets down as say, TcO_2. One of our problems in connection with details of this is that we don't know anything about the speciation of the technetium that's sitting there on the rock. We know it's there, but we don't know what the valence state is. When I suggest TcO_2 it's on the basis, really, of guess. Sherm Fried suggested that -- I hope we have time to do it within the next month -- we try an experiment with tuff in which we pre-flush the tuff with an oxidizing agent. He suggested permanganate; another possibility is H_2O_2. If the technetium stays there because it gets reduced and if you pre-oxidize the tuff core before you do the experiment, you ought to see a difference in the amount of technetium that you get in the concentration profile in the core. And, furthermore, you shouldn't see any difference in the effluent wave.

Q: But you could do post-oxidizing, take the technetium that's stuck on the core and run some peroxide through it.

A: Yes, I never thought of that.

Q: The technetium has a retardation factor of one, which applies to the technetium that moves with the water front. Yet there was technetium left behind, that is, a continuous distribution of the technetium left behind. How do you reconcile that?

A: The way I reconcile it is that there is not one species but two. That's all.

Q: Basically, you've got two retardation factors.

A: Yes. And if you were to calculate the retardation factor for the reduced technetium around the core, you would take the core distribution, get an average value which would be half-way through the core for the technetium, take the total run time, and use that to estimate an average velocity and an effective velocity for the technetium. For the technetium that sets down on the core, you would get a pretty big Kd and a pretty large retardation factor.

Q: But if it's precipitation you can't call it Kd and use equations in which ion exchange is involved. It's a totally different situation.

A: I'm not arguing about the difference in the situation. All I'm saying is, this method would provide information for a hydrologist. I think that from the point of view of using these results to predict migration in the field, what's important is the retardation factor, the numerical value and the details of why the technetium has the particular retardation factor, although very interesting scientifically, may be something that a hydrologist doesn't need to know.

Q: But I think when precipitation is put into a hydraulic model, it would add sink terms in which retardation is treated separately from precipitation.

A: Then in that case, one of the things that we're going to have to do is some auxiliary experimentations, and I frankly do not know how to go about it. The question is whether or not the technetium that stays in the core, stays there as a precipitate TcO_2, or whether it is for some reason or another, say, irreversibly sorbed as Tc in the +2 valence state. At this stage, those are possibilities, but I can't distinguish between them.

Q: Well, I think the question deals with having an infinitely long core in the experiment and not having technetium spilling out the end. That's an important philosophical question: how do you treat this problem of prediction? You've got two different species, almost like two different elements.

Q: Are you getting reduction of technetium by ferrous iron on minerals, some surface effect?

A: We don't know. It sounds like an interesting possibility.

Q: There is a very large difference between how the hydrologist will treat transport when there is retardation due to precipitation, and if we have a Kd value which implies a concentration of the solutions proportional to the salt. In the precipitation case, if we only have that mechanism we would just have one constant concentration coming out of the core. From the hydrologist's point of view, or we would say the safety analysis point of view, that is of prime importance. Now if you could tell, or anybody could measure this example, the reduction capacity of that solid for example expressed as how many moles per gram or how many equilavents per gram we have of ferrous iron or some reactive material, this might just give us the total sorption capacity, and as John indicated, I think, say the length of the core which would be needed to just pick up all the things we have in the repository.

A: We already have enough information from the technetium concentration profile to tell the numbers of moles of technetium per cubic centimeter of tuff that stays there. Now, whether or not it can be interpreted in the way that you're talking about, I'm not sure, but I have the feeling that it can be. Suppose you assume the technetium that is there as TcO_2. Right away you will get a measure of what's reduced from technetium plus seven to technetium plus four. This gives you a measure of the total reducing power per gram for the tuff. It doesn't tell you what did the reduction, however. That's a different problem, and I fear it's a much more difficult one.

Q: I wonder if it's safe to assume that it's only the tuff, that we don't also have to consider reducing potential of the solution flowing through. I want to warn you that tuff alone may be the answer.

A: Yes.

Q: How much was left on the column from the solution? Less than 1% or what?

A: It isn't very much. I think it's probably less than a percent.

Q: Well, we don't want to ignore it. I think we're emphasizing the wrong issue here. You're talking about 99% is going on through. In one sense that's hardly of any consequence. Surely, we have a very long problem. You may say, well, we'll get it all sorbed. We have a very small problem. You are passing through 99% technetium plus. We have the same experiment you have a column of flushed granitic rock. It all comes out except for a little bit. Now that's what we are dealing with. Now the 1% that stays behind is sorbed, or precipitated out, so what?

A: Again, it's partly a question of how you want to use the results. For example, if you're visualizing a field situation in which you are concerned with technetium, a long distance away from source, so that the total column through which transport occurs is very long, then a relatively small amount of technetium, a relatively small fraction of technetium, that's retained on the column may really have considerable practical importance. If the column is short, if you're concerned with the near-field problem, then the big concentration wave that comes through as TcO_2^- is what you have to watch out for.

Q: Let's worry about the 99% that made it through.

Precipitation and Solubility

Q: If we try to use the solubility constraint, when you think eons ahead in time, as long as you're going to use a solubility constraint, one thing you've got to remember is you're always going to have something in solution. So that you just can't draw this conclusion and say, well, all I need is a longer piece of rock and then nothing comes out. If you're going to go to solubility-product rules, you've still got to talk about that at equilibrium, that there is something in solution dribbling out. So, it's not an all-or-nothing proposition. What we're probably doing here is bantering back and forth over how long is the lag time before you reach equilibrium in the precipitation process or something. It buys us some time that it doesn't totally make the problem disappear.

Q: Well, Jeff made my point. Do we, in fact, know that TcO_2 is that insoluble? I don't know if anybody knows anything about solubility. Everything has a solubility.

Kd Measurement Techniques

Q: Could it be possible that, as you said, the problem is so long-lived so you have a slope from the material deposited but it's not within the precision of the analytical technique to see that. So you're measuring very, very low Kd, on technetium.

A: One of our concerns about the concentration profiles of the cores is that they don't have as good a spacial resolution as we would like. We've tried impregnating the cores with plastic in order to be able to section them at smaller intervals. But what we'd really like to have is a thin section that can saw about half a micron thick that doesn't remove substantial chunks of the core every time it is cut, but we have yet to find such an instrument.

High Ionic Strength - Questions to Tom Woolery

Q: How, with these various models, do we treat solution with a very high ionic strength such as up in the 5 molar range and maybe even higher?

A: Well, I'll answer that one and if Dr. Parks has a different answer, he can add on to it. We need to get a better description and understanding of the activity coefficients of aqueous species in more concentrated solutions, and the need is not just for 25 but for elevated temperatures as well. One possibility is to use Pfitzer's equation. Pfitzer's equations have been shown to give reasonable reproduction of reality for ionic species for at least the case of low valance. They don't work quite as well for species of higher valence, probably because complexing is treated implicitly in these equations. Consequently, in this approach you don't normally compute the concentrations of the complexes and you don't have the mass action equations that correspond with this association, but that might be one way of looking at it. There may be some other approaches developed in the next few years that will allow us to do some meaningful calculations at a higher ionic strength.

Q: Are there any models currently in existence that try to deal with high ionic strengths?

A: There are several different ones with different shortcomings. Pfitzer's is currently the most advanced (mainly equilibrium model). None of these are in any of the programs that I am aware of. There is one program that has been recently written by John Weir which uses Pfitzer's equations to permit modeling of this sort. In a brine evaporate type environment, but as to whether or not you would have quick success in adding nuclear waste forms into that system -- that is something that would be a ways down the road.

I might mention that using Pfitzer's equations are very good when the information is available on the activity coefficients of various supporting electrolytes. When it comes to finding out how various individual trace species behave in those supporting electrolytes, you need the same kind of coefficients. However, the information is just not available. So similar difficulties with the use of Pfitzer's model ultimately is involved in conventional models that currently exist.

Mineral Stability

Q: Is there enough information on the behavior of mineral solubility to be able to now write these models as the more realistic incongruent dissolution reactions rather than congruency of previous models?

A: While the reaction progress codes explicitly permit you to model incongruent dissolution, you might be thinking of the problem of modeling solid solutions. The major problem there is a lack of data and theoretical equations.

Q: Does that derth of information really hinder you?

A: I think in some systems it does. And in others you can sometimes get away with estimating the thermodynamic parameters for specific compositions, some of which can be equivalent to analytical measurements and others which are for idealized end members. This is not the most satisfactory treatment, but it does give you a reasonable first-order picture in a number of systems. I had to do this with my study of the reaction of sea water with ocean crust basalt, in which smectite is the dominant product. I had to use approximately 18 different smectite compositions. But it turned out that they correspond fairly well with Seigfried's experimental results and to some extent as with geologic reality in that there were some very low temperatures. I might point out that reaction progress calculations that I showed for the lowest temperatures, 0°, don't correspond too well with the situation of weathering on the deep sea floor because there you have a different type of alteration from the glass leaching type problem.

Water Composition and Rocks

Q: How close are you predicting what sort of water would be in equilibrium with say a fairly simple rock type like anorthosite? 1 year, 5 years, 10 years?

A: It could probably be done now. The question is if you go out to some anorthosite and drill a sample ground water, how well will that correspond to code predictions. I am always somewhat leary about writing a code as a black box and then immediately running out and comparing it

with something from the real world without doing a careful study of what happened in the real world and how that may relate to the code.

A: The reason I'm asking is that we are doing some adsorption studies on anorthosite and it would be nice to know what sort of rock/ground-water composition we have to use.

A: This approach has been used in the past to model some ground-water and stream-water evolutions and in those cases has apparently been quite satisfactory.

I might just mention that we've been doing studies like this with respect to albite at elevated temperatures with very good agreement. We've made the actual solubility measurement on albite and modeled it using a similar approach to Tom's.

Q: That's a mineral?

A: Yes. Anorthosite is dominantly anorthite.

Rock Mineral Characterization - Questions for Dave Coles and Homer Weed

Q: Could you define what volume matrix means, please?

A: The petrographer says that that is everything that's not quartz, if I remember correctly. Now, that may not be true.

Oxidation State of Species

Q: Do you have any idea of the oxidation state of the plutonium, and I assume for selenium?

A: Yes, I think so. We had made no measurements of plutonium oxidation states, so it is whatever one might guess would be the range and then the technique we used. I would like to be able to say we do, but unfortunately that is not the case.

Mineral Rock Characterization

Q: You say that you have made a fairly complete characterization of your sandstones, but one of the things you didn't have on the slides is checks for organic matter. I don't know that much about chemistry and some of the particular nuclides that you worked with here, but I know that some material such as mercury will very strongly complex and dissolve solid organic matter, and that is something you won't detect simply by doing petrography or X-ray diffraction.

A: Yes, I agree, and given an infinite budget I could characterize it for everything. What you are saying is characterization should be a top priority.

Q: Well, yes, that for some nuclides a tiny bit of organic matter could be much more important in accounting for the work than some of the other things that you did characterize.

A: We still have samples, splits of the samples we used and we could continue to do characterization work as we find the time. Of course, if the organics is a problem we should be able to see a direct correlation with organic matter in the sandstones. Something ought to show up, because there is such a wide range of compositions in these things. But we have to just do a lot of work trying to figure out or see if there is any one thing or two things or whatever that could correlate with Kd.

LABORATORY STUDIES OF RADIONUCLIDE DISTRIBUTION BETWEEN SELECTED GROUNDWATERS AND GEOLOGIC MEDIA

Compiled by

B. R. Erdal

Los Alamos Scientific Laboratory

Contributors

R. D. Aguilar
B. P. Bayhurst
G. E. Bentley
W. R. Daniels
S. J. DeVilliers
B. R. Erdal
F. O. Lawrence
S. Maestas
P. Q. Oliver
J. L. Thompson
E. N. Vine
K. Wolfsberg

ABSTRACT

Extensive studies of the behavior of plutonium and americium in pH ≈ 8 groundwaters were made, particularly with respect to container sorption, filtering, and centrifugation. Significant improvements in the method used for measuring sorption ratios for these elements were developed, and their sorption-desorption ratios on argillite and tuff were measured. Effects of particle size, temperature, sampling location, mineralogy, and time were investigated for these elements. The chemical composition of the water was found to be a major factor that governs sorption behavior for some elements. Studies of the sorption of strontium, cesium, barium, cerium, europium, uranium, and americium on Hainesville salt dome materials were made under aerobic and anoxic (<0.2 ppm oxygen) conditions using two synthetic groundwaters: One represented the Wilcox aquifer in the Hainesville region and the second was a dilute brine. Studies of the sorption of strontium, cesium, barium, cerium, europium, and uranium(VI) on granite and argillite were made under anoxic (<0.2 ppm oxygen) conditions and the results were compared to earlier measurements made under aerobic conditions. The sorption of uranium(VI) on argillite under atmospheric conditions was investigated. Measurements of migration rates in crushed granite, argillite, and tuff were made and compared with batch results. Infiltration experiments involving the forced injection of activity into intact and fractured cores were also performed. Microautoradiographic techniques were used to detect specific sorption sites. This latter technique was also used to characterize the sorption of plutonium and neptunium on polished thin-sections of alluvium, granite, tuff, and argillite and to assess the amount of "aggregation" that occurred. Additional physical and chemical characterizations of the materials used in these studies were made, and new analytical techniques were developed.

INTRODUCTION

The Los Alamos Scientific Laboratory (LASL) contribution to the Waste Isolation Safety Assessment Program (WISAP), Task 4, in FY-79 had five principal objectives. The first was to perform migration rate studies using three different types of columns: 1) crushed rock, 2) whole cores, and 3) cores containing natural fractures. Second, the LASL batch sorption methodology (Erdal-1 1979; Erdal-2 1979; Wolfsberg 1979) was used to obtain data on several additional variables that influence sorption-desorption behavior and to perform studies on several new radionuclide-geomedia systems. Third, the microautoradiographic technique currently utilized at LASL (Thompson 1979) was used for further studies of the sorption of radionuclides on polished or ground surfaces of mineral grains and for identification of the specific sorbing surfaces in natural (nonpulverized) systems. Fourth, studies of sorption behavior in systems related to salt domes were performed. Finally, studies of the chemistry of several radionuclides in the pH $\approx$ 8 solutions that frequently occur in natural environments were performed.

Most of these studies were limited to three geologic types - granite, argillite, and tuff - usually from, but not limited to, the Nevada Test Site (NTS). Natural groundwaters or waters having a chemical composition related to the phreatic water were used for all studies. Detailed analytical and mineralogical analyses of all materials were made.

SORPTION OF PLUTONIUM AND AMERICIUM ON ARGILLITE

The measurement of the sorption behavior of americium and plutonium on argillite under atmospheric conditions involved geologic materials and groundwaters described earlier (Erdal-1 1979).

MEASUREMENT TECHNIQUES

Preparation of Tagged Solutions

Most of the traced waters used in these studies were prepared using the pre-equilibrated synthetic groundwater described in Erdal-1 1979, ^{237}Pu

tracer produced at Argonne National Laboratory under contract with Battelle (PNL), and isotopically pure ^{241}Am tracer obtained from Oak Ridge National Laboratory. Tracer purities were checked by both alpha and gamma spectroscopy. (Feed solutions were prepared so as to contain $\approx 10^{-12}$ M Pu or $\approx 10^{-6}$ M Am at 100% yield of tracer in water; actual concentrations can be calculated from the yields given in Table 1.) Stock tracer solutions were in 3 M HCl, which resulted in an added chloride concentration of $<10^{-2}$ M. The ^{237}Pu tracer was treated with $NaNO_2$ so that the plutonium was in the IV oxidation state at the beginning. This step resulted in the addition of $\approx 10^{-4}$ M sodium to the feed solutions containing plutonium. In general, feed solutions were prepared by drying the tracers at room temperature and then dissolving them in the appropriate groundwater. The chloride added with the tracers was normally $\approx 5 \times 10^{-3}$ M.

Some samples were run using one of two feed solutions containing both ^{241}Am and ^{239}Pu, partially in order to examine the effect of a large change in Pu concentration. (The concentration at 100% yield would have been $\approx 10^{-6}$ M Am and $\approx 10^{-5}$ M Pu; actual concentrations can be estimated using the data in Table 1.) One such feed solution was prepared by drying the tracer, and one was prepared by adding the tracer solution directly to the water and then readjusting the pH to its original value by adding NaOH solution. The latter step resulted in the addition of $\approx 1 \times 10^{-3}$ M sodium to the feed solution.

In order to examine the difference in apparent sorption resulting from filtering the feed solutions, solutions were centrifuged for one hour at 12 000 rpm (28 000 g) and then portions were used in the batch experiments both before and after filtering through a 0.4-μm Nuclepore filter (all plastic parts). The filters always retained activity which had not been removed by centrifuging. The tracer yields in the feed solutions were determined by gamma-counting aliquots and are given in Table 1.

Sorption Measurements

Crushed rock from cores 1 (548 m) and 2 (717 m) from the Eleana formation at the NTS were used for batch sorption studies at both ambient (22 ± 2°C) and elevated (70 ± 1°C) temperatures. Three particle sizes were used: 106-150, 150-180, and 355-500 μm. The material was pretreated by shaking

TABLE 1. Tracer Yields in Feed Solutions

Tracer	Temperature(°C)	Yield (%)	
		Unfiltered	Filtered
^{237}Pu	22	54	48
^{237}Pu	70	30	6
^{241}Am	22	38	22
^{241}Am	70	42	15
$^{241}Am+^{239}Pu$	22	11[b]	0.2[b]
$^{241}Am+^{239}Pu$[a]	22	19[b]	0.4[b]

[a]Tracer was not dried; pH readjusted with NaOH.

[b]Am yield; other experiments indicated that the plutonium yield was probably approximately the same, at least for the unfiltered solutions.

weighed one-gram quantities with 20-mℓ portions of synthetic groundwater for periods of at least two weeks. The samples were contained in pre-washed, capped 40-mℓ polypropylene tubes. The phases were separated by centrifuging at 12 000 rpm for one hour. The weight of the wash solution remaining with the solid phase was obtained by weighing the tube and solid before and after pre-equilibration.

Twenty-mℓ portions of traced feed solution of known pH were added to the tubes containing crushed rock. The solutions were dispersed by vigorous shaking and the mixtures were agitated gently for selected times: 1, 2, 4, and 8 weeks. The shaking rates were 200 oscillations per minute for the ambient temperature samples and 80 oscillations per minute for the 70°C samples.

At the end of a shaking period, the aqueous phases were separated from the solids by centrifuging, usually four times, each time transferring the water to a new tube, for one hour at 12 000 rpm (28 000 g). Usually the final solution was aliquoted and the remainder was then passed through a 0.4-μm Nuclepore filter, sometimes twice, and aliquoted again, in order to observe the effect of filtering on the observed sorption ratio. An improved technique

was used for later measurements (see below). Any errors in the data for unfiltered solutions in the argillite measurements would result in the reported R_d values being too low.

A number of rock-water mixtures were transferred to clean tubes before the first centrifuging. The original tubes were then checked for activity in order to determine the gamma activity sorbed on the walls. This was found to be negligible (<2% of total input activity). All other solid phases were left in the original tubes and counted directly, after centrifuging.

Earlier comments (Erdal-1 1979; Erdal-2 1979; Wolfsberg 1979) concerning the use of "control" samples with traced aqueous phase but no solid are applicable here. The activity in the control samples was found to sorb on the walls much more readily than when rock was also present.

Desorption experiments were performed by adding pre-equilibrated synthetic groundwater to the solid phases from the sorption experiments and continuing as for the sorption measurements.

Assay of Radioactivity

Solid samples were normally gamma-counted for ^{241}Am or ^{237}Pu on a NaI(Tl) detector utilizing a single-channel analyzer and a scaler. Counting standards were prepared using known amounts of ^{241}Am or ^{237}Pu in the same geometries and conditions as the experimental samples.

Liquid samples were usually gamma-counted with a NaI well counter(Packard Auto-gamma Scintillation Spectrometer). Standards were prepared in the appropriate geometry.

The ^{239}Pu was determined radiochemically (Smith 1975) after sample dissolution.

Calculations

Since both solid and liquid phases were counted directly for ^{241}Am and ^{237}Pu, or analyzed separately for ^{239}Pu, the sorption ratio, R_d, can be calculated directly as

$$R_d = \frac{\text{activity in solid phase per unit mass of solid}}{\text{activity in solution per unit volume of solution}} .$$

The activities in the control tubes were not used in the calculations; container

effects are considered negligible (see above).

RESULTS AND CONCLUSIONS

The results for the batch measurements of the sorption behavior of ^{241}Am, ^{237}Pu, and ^{239}Pu on argillite under atmospheric conditions are given in Tables 2-5. Data for the desorption of ^{239}Pu from four argillite samples are not yet available.

Observations made later during sorption measurements with tuff (see below) tend to confirm that little or no sorption (at least for plutonium) occurs on the filter membranes and to suggest that most of the activity removed by filtering the final solutions during the argillite experiments consisted of particulates. The "unfiltered" data, therefore, probably provide lower limits for the sorption ratios since particulates remaining with the solutions after centrifuging would tend to lower the calculated R_d values. The "filtered" data perhaps provide more accurate sorption ratios; however, the use of "unfiltered" data would err in the conservative direction. The later experiments (see below) showed that the large differences between results from unfiltered and filtered final solutions and the large variations between replicate samples can be greatly reduced by use of a very cautious technique for transferring solutions between centrifugings.

For the argillite experiments, sorption ratios based on data from unfiltered solutions tended to decrease with increasing temperature, but for filtered solutions the calculated ratios tended to increase with increasing temperature. This effect is probably related to the size of the particles which form at the different temperatures and which behave differently when centrifuged or filtered. Less activity was removed by centrifuging solutions contacted at 70°C but more activity was removed by filtering these same solutions.

Several general conclusions can be made for the plutonium and americium results: Very little americium or plutonium sorbs on the container walls when crushed argillite is present (see below). There was no significant effect related to particle size or core sample within the ranges examined. Filtering the initial feed solutions appears to have had little effect except possibly with filtered final solutions which had been contacted at 70°C. At ambient

TABLE 2. ^{241}Am Sorption Ratios (Argillite)

Core Sample	Fraction (μm)	Temp. (°C)	Filtered[a] Feed ?	Sorp. Time (d)	Desorp. Time (d)	R_d (mℓ/g) Unfilt.	Filt. 1[a]	Filt. 2[a]	pH Initial	pH Final
1	106-150	22	yes	6.8		b	57 000		8.65	8.57
					28.7	24 000	450 000		8.3	8.58
			yes	12.7		b	100 000		8.65	8.61
					28.7	51 000	540 000		8.3	8.60
			yes	27.6		91 000[b]	320 000		8.65	8.66
					28.7	71 000	740 000		8.3	8.65
			yes	27.6		54 000[b]	170 000		8.65	8.57
					28.7	59 000	520 000		8.3	8.59
			yes	54.7		99 000[b]	420 000		8.65	8.21
					28.7	53 000	930 000		8.3	8.59
1	355-500	22	yes	12.7			62 000		8.65	8.69
					31.7	21 000	400 000		8.3	8.67
			yes	27.6		26 000[b]	120 000		8.65	8.59
					28.7	28 000	270 000		8.3	8.59
			yes	27.6		54 000	180 000		8.65	8.63
					31.7	33 000	280 000		8.3	8.68
			yes	54.7		35 000[b]	210 000		8.65	8.47
					28.7	36 000	280 000		8.3	8.53
			yes	54.7		28 000	260 000		8.65	8.66
					31.7	76 000	590 000		8.3	8.66

TABLE 2 (cont). ^{241}Am Sorption Ratios (Argillite)

Core Sample	Fraction (μm)	Temp. (°C)	Filtered[a] Feed ?	Sorp. Time (d)	Desorp. Time (d)	R_d (mℓ/g) Unfilt.	Filt. 1[a]	Filt. 2[a]	pH Initial	pH Final
1	355-500	70	yes	6.8			55 000		8.33	8.39
					32.9	14 000	$> 10^6$		8.3	8.69
			yes	12.7			67 000		8.33	8.44
					32.9	31 000	$> 10^6$		8.3	8.71
			yes	26.7		1 600	410 000		8.33	8.53
					32.9	40 000	$> 10^6$		8.3	8.64
			yes	55.7		7 300	810 000		8.33	8.02
					32.9	33 000	$> 10^6$		8.3	8.61
2	355-500	22	yes	6.8		b	52 000		8.65	8.56
					28.7	61 000	330 000		8.3	8.56
			yes	12.7		b	62 000		8.65	8.61
					31.7	60 000	210 000		8.3	8.65
			yes	12.7			85 000		8.65	8.68
					33.9	47 000	470 000		8.3	8.65
			no	13.0		12 000	83 000		8.65	8.78
					31.9	68 000	400 000		8.3	8.67
			yes	26.7		34 000	270 000		8.65	8.65
					33.9	79 000	450 000		8.3	8.63
			yes	27.6		12 000[b]	77 000		8.65	8.63
					31.7	160 000	400 000		8.3	8.54

TABLE 2 (cont). ^{241}Am Sorption Ratios (Argillite)

Core Sample	Fraction (μm)	Temp. (°C)	Filtered[a] Feed ?	Sorp. Time (d)	Desorp. Time (d)	R_d (mℓ/g) Unfilt.	Filt. 1[a]	Filt. 2[a]	pH Initial	pH Final
			yes	27.6		57 000[b]	190 000		8.65	8.58
					31.7	180 000	420 000		8.3	8.67
			no	27.9		25 000	210 000		8.65	8.72
					33.9	69 000	490 000		8.3	8.63
			yes	29.7		70 000	280 000	330 000	8.65	8.72
					33.9	59 000	450 000		8.3	8.64
			yes	54.7		84 000[b]	270 000		8.65	8.39
					31.7	71 000	650 000		8.3	8.67
			yes	54.7		140 000	560 000	790 000	8.65	8.36
					33.9	59 000	520 000		8.3	8.64
			no	54.9		150 000	620 000		8.65	8.68
					33.9	110 000	730 000		8.3	8.63
			yes	55.6		230 000	590 000		8.65	
					33.9	77 000	420 000		8.3	8.63
2	355-500	70	no	12.7		3 300	130 000		8.33	8.50
					32.9	7 300	$> 10^6$		8.3	8.63
			yes	12.7			94 000		8.33	8.41
					32.9	26 000	$> 10^6$		8.3	8.66
			no	26.7		10 000	150 000		8.33	8.16
					32.9	27 000	$> 10^6$		8.3	8.45
			yes	26.7		1 700	160 000		8.33	8.48
					32.9	38 000	450 000		8.3	8.33

TABLE 2 (cont). ^{241}Am Sorption Ratios (Argillite)

Core Sample	Fraction (μm)	Temp. (°C)	Filtered[a] Feed ?	Sorp. Time (d)	Desorp. Time (d)	R_d (mℓ/g) Unfilt.	Filt. 1[a]	Filt. 2[a]	pH Initial	pH Final
			no	55.7		15 000	370 000		8.33	7.88
					32.9	60 000	170 000		8.3	8.37
			yes	55.7		5 800	760 000		8.33	7.78
					32.9	20 000	$> 10^5$		8.3	8.39
			yes	55.7		3 700	300 000	380 000	8.33	7.73
					32.9	250 000	$> 10^6$		8.3	8.42

[a]Through 0.4-μm polycarbonate membrane.

[b]Crushed rock was pre-equilibrated with groundwater for ≈276 d, as opposed to the usual 14 d.

TABLE 3. ^{237}Pu Sorption Ratios (Argillite)

Core Sample	Fraction (μm)	Temp. (°C)	Filtered[a] Feed ?	Sorp. Time (d)	Desorp. Time (d)	R_d (mℓ/g)[b] Unfilt.	Filt. 1	Filt. 2	pH Initial	Final
1	355-500	22	yes	13.7		c	37 000	63 000	8.47	8.49
					14.9	11 000	68 000		8.27	8.60
			no	13.7			15 000		8.47	8.56
					14.9	3 800	41 000		8.27	8.64
			yes	13.7			15 000		8.47	8.53
					14.9	1 400	25 000		8.27	8.65
			no	13.7			19 000	19 000	8.47	8.57
					14.9	2 500	17 000		8.27	8.66
			no	27.6		3 300	7 000		8.47	8.55
					14.9	3 300	41 000		8.27	8.58
			yes	27.6		2 300	6 100		8.47	8.59
					14.9	2 300	27 000		8.27	8.61
			yes	27.6		2 400	31 000	33 000	8.47	8.60
					14.9	3 200	4 800		8.27	8.64
			no	55.7		4 700	69 000		8.47	8.64
					21.0	2 900	36 000		8.20	8.43
			yes	55.7		1 300	2 100		8.47	8.64
					21.0	3 600	35 000		8.20	6.98
			yes	56.7		2 700	41 000	46 000	8.47	8.56
					21.0	1 700	33 000		8.20	8.39

TABLE 3 (cont). ^{237}Pu Sorption Ratios (Argillite)

Core Sample	Fraction (μm)	Temp. (°C)	Filtered[a] Feed ?	Sorp. Time (d)	Desorp. Time (d)	R_d (mℓ/g)[b] Unfilt.	Filt. 1	Filt. 2	pH Initial	pH Final
			no	56.7		2 200	36 000		8.47	8.60
					21.0	2 700	30 000		8.20	8.54
			yes	56.7		33 000[c]	27 000	47 000	8.47	8.56
					21.0	1 300	44 000		8.20	8.52
1	355-500	70	no	13.7			100 000		8.26	8.50
					15.9	1 100	>100K		8.19	8.63
			yes	13.8			15 000		8.26	8.46
					15.9	3 000	40 000		8.19	8.64
			no	27.6		2 600	>100K		8.26	8.52
					15.9	1 700	>100K		8.19	8.42
			yes	27.6		2 500	6 000		8.26	8.55
					15.9	2 000	15 000		8.19	8.57
			no	56.7		1 900	>100K		8.26	8.46
					21.1	1 300	67 000		8.25	8.42
			yes	56.7		1 800	18 000	>100K	8.26	
					21.1	2 200	>100K		8.25	8.39
2	150-180	22	yes	13.7			11 000	38 000	8.47	8.54
					14.9	7 200	38 000		8.27	8.62
			yes	55.7		8 000	22 000		8.47	8.54
					21.0	19 000	>100K		8.20	8.52

TABLE 3 (cont). ^{237}Pu Sorption Ratios (Argillite)

Core Sample	Fraction (μm)	Temp. (°C)	Filtered[a] Feed ?	Sorp. Time (d)	Desorp. Time (d)	R_d (mℓ/g)[b] Unfil.	Filt. 1	Filt. 2	pH Initial	Final
2	355-500	22	yes	13.7			22 000		8.47	8.53
					15.9	8 100	28 000		8.27	8.43
			yes	55.7		11 000	>100K		8.47	8.65
					21.0	17 000	44 000		8.20	8.44
3	355-500	70	yes	13.7			3 600		8.26	8.40
					15.9	1 700	33 000		8.19	8.58
			yes	56.7		1 500	23 000		8.26	8.33
					21.1	3 000	21 000		8.25	8.32

[a]Through 0.4-μm polycarbonate membrane.

[b]All calculated R_d values >100 000 indicated as >100K because of poor counting statistics on the ^{237}Pu solutions, which had very low count rates.

[c]Crushed rock was pre-equilibrated with groundwater for ≈276 d, as opposed to the usual 14 d.

TABLE 4. ^{239}Pu Sorption Ratios for Argillite Core #2, 150-180 μm, Ambient Temperature, Filtered Feed[a]

Tracer Prep	Sorp. Time (d)	R_d (mℓ/g)[b]	pH	
			Initial	Final
dried	14.7	8 200	8.60	8.53
	30.6	27 000	8.60	8.59
	55.6	39 000	8.60	8.45
pH adjust	14.7	5 100	8.39	8.45
	30.6	16 000	8.39	8.42
	55.6	81 000	8.39	8.10

[a]Through 0.4-μm polycarbonate membrane.

[b]Values from unfiltered final solutions were used.

TABLE 5. Representative Sorption Ratios for Am and Pu

	R_d (mℓ/g)[a]	
	22°C	70°C
Am sorption		
unfiltered[b]	75 000(15 000)[c]	6 500(1 900)
filtered	300 000(42 000)	450 000(120 000)
Am desorption		
unfiltered	68 000(8 100)	29 000(4 300)
filtered	480 000(35 000)	> 10^6
^{237}Pu sorption		
unfiltered	4 200(1 100)	2 100(220)
filtered	37 000(12 000)	75 000(38 000)
^{237}Pu desorption		
unfiltered	5 700(1 400)	2 000(250)
filtered	34 000(3 700)	97 000(50 000)
^{239}Pu sorption		
unfiltered	25 000(9 000)	

[a]All data are for feed solutions prepared by drying the tracers (see text).

[b]Indicates whether final solutions were filtered after centrifuging and before counting.

[c]Values in parentheses are standard deviations of the means (absolute values).

temperature, americium R_d values for desorption are roughly the same as the values for sorption, while the R_d values for the elevated temperature appear to be higher for desorption than for sorption. Within the rather large errors in the data, there is no significant difference in ^{237}Pu R_d values for sorption and desorption at a given temperature. The data in Table 4 indicate that there was little difference in the observed R_d values for ^{239}Pu between the two methods of preparing the traced feed solutions, i.e., drying the tracer or adding an acid tracer solution and readjusting the pH. The average values are 25 000 ± 9 000 and 34 000 ± 24 000, respectively. The results for ^{237}Pu and ^{239}Pu indicate that there is a difference in R_d values, which probably results from the $\approx 10^7$ difference in plutonium concentration and may well be a solubility effect. Based on data from unfiltered final solutions the average R_d value for the more concentrated ^{239}Pu was significantly higher than for ^{237}Pu, 25 000 ± 9 000 vs. 4 200 ± 1 100. The ^{237}Pu data for filtered solutions, however, give an average R_d value for sorption of 37 000 ± 12 000. No ^{239}Pu data are available for filtered final solutions.

SORPTION OF PLUTONIUM AND AMERICIUM ON TUFF

The measurement of the sorption behavior of americium and plutonium on tuff under atmospheric conditions involved geologic materials and groundwater described in Wolfsberg 1979.

MEASUREMENT TECHNIQUES

Preparation of Traced Feed Solutions

The traced waters used in these studies were prepared using the pre-equilibrated waters described earlier (Wolfsberg 1979), isotopically pure ^{241}Am tracer obtained from Oak Ridge National Laboratory, ^{239}Pu tracer (weapons grade) from Los Alamos Scientific Laboratory, and ^{237}Pu tracer produced at Argonne National Laboratory under contract with Battelle (PNL). Tracer purities were checked by both alpha and gamma spectroscopy. The ^{237}Pu tracer was treated with $NaNO_2$ so that the plutonium was in the IV oxidation state at the beginning; this resulted in the addition of $\approx 10^{-4}$ M sodium to the feed solu-

tions containing ^{237}Pu. Feed solutions were prepared* by two methods: Most of the solutions for Experiments 1, 2, and 3 were prepared by drying the tracers at room temperature and then dissolving them in the appropriate groundwater. This operation resulted in the addition of $\approx 5 \times 10^{-3}$ M chloride to the feed solutions. In Experiment 4 the traced feed solutions were prepared by adding ^{237}Pu or ^{241}Am tracer solution to the pre-treated groundwater and readjusting the pH to the original value by adding NaOH solution. This step added $\approx 1 \times 10^{-3}$ M sodium and $\approx 5 \times 10^{-3}$ M chloride to the feed solutions. Feed solutions were prepared so as to contain (at 100% yield) $\approx 1 \times 10^{-6}$ M americium, $\approx 1 \times 10^{-5}$ M plutonium when ^{239}Pu was used, and $\approx 4 \times 10^{-13}$ M plutonium when ^{237}Pu was used. After allowing for the yield through preparation of the traced feed solutions, the concentrations were $\approx 4 \times 10^{-7}$ M americium, $\approx 1 \times 10^{-13}$ M plutonium with ^{237}Pu, and $\approx 4 \times 10^{-7}$ M plutonium with ^{239}Pu, but these varied significantly from one feed solution to another.

Sorption Measurements

Crushed rock (Wolfsberg 1979) from cores JA-18, JA-32, and JA-37 was used for sorption studies at both ambient (22 ± 2°C) and elevated (70 ± 1°C) temperatures. The material was pretreated by shaking weighed one-gram quantities with 20-mℓ portions of water from well J-13 for periods of at least two weeks. The samples were contained in prewashed, capped, 40-mℓ polypropylene tubes. The phases were separated by centrifuging at 12 000 rpm (28 000 g) for one hour. The weight of the wash solution remaining with the solid phase was obtained by weighing the tube and solid before and after the pre-equilibration.

Twenty-mℓ portions of traced feed solution of known pH were added to the tubes containing crushed rock. The solids were dispersed by vigorous shaking, and the mixtures were agitated gently for selected times: 1, 2, 4, and 8 weeks. A few contacts are being continued for ≈6 months to examine long-term effects. The shaking rates were 200 oscillations per minute for the ambient temperature samples and 80 oscillations per minute for the 70°C samples.

At the end of a shaking period, the aqueous phases were separated from the solids by four centrifugings, each in a new tube, for one hour at 12 000 rpm. Solutions were transferred by decanting the first three times and by

*Additional details are given in Erdal-3 1979 and Erdal-5 1979.

transferring with a plastic pipet the last time. In Experiment 4 three centrifugings were normally used (1, 1, and 2 h), and the solutions were transferred by pipet each time. Extreme care was taken to avoid transferring any particulates from the bottoms of the tubes or in surface films. Aliquots of the final solutions were taken for pH measurements, gross gamma counting, and gamma spectroscopy. The solid phases were left in the tubes and counted directly. The activity sorbed on the walls is considered negligible (see below). The comments (Erdal-1,2 1979; Wolfsberg 1979) concerning control samples with a traced aqueous phase but no solid are applicable here. Such samples run with plutonium and americium showed much higher wall sorption on the container when no solid was present.

Desorption experiments were performed by adding pre-equilibrated synthetic groundwater to the solid phases from the sorption experiments and continuing as for the sorption experiments.

In Experiment 4, the effects of a number of different variables related to experimental technique were examined. The results are described below.

Assay of Radioactivity

Solid samples were normally gamma-counted for ^{241}Am or ^{237}Pu on a NaI(Tl) detector utilizing a single channel analyzer and a scaler. Liquid samples were usually gamma counted with a NaI well counter (Packard Auto-gamma Scintillation Spectrometer). Both liquid and solid samples were sometimes counted using a calibrated, 23%, coaxial Ge(Li) detector. The 1024-channel spectra were recorded in a multichannel analyzer connected to a PDP-9 computer.

A minimum of two counts were taken for each sample. Counting standards were prepared using known amounts of ^{241}Am or ^{237}Pu in the same geometries and conditions as the experimental samples.

The ^{239}Pu was determined radiochemically (Smith 1975) after sample dissolution. Some analyses are not yet complete.

Calculations

Since both solid and liquid phases were counted directly for ^{241}Am and ^{237}Pu, or analyzed separately for ^{239}Pu, the sorption ratio, R_d, can be calculated directly as

$$R_d = \frac{\text{activity in solid phase per unit mass of solid}}{\text{activity in solution per unit volume of solution}} .$$

The activities in the control tubes were not used in the calculations; container effects are considered negligible (see below).

RESULTS AND CONCLUSIONS

The results to date for the batch measurements of the sorption behavior of ^{241}Am, ^{237}Pu, and ^{239}Pu on tuff under atmospheric conditions are given in Tables 6-10. Data for samples that were contacted for six months and for some samples that were traced with ^{239}Pu are not yet available. The initial and final pH values are also listed in the tables.

The quoted R_d values were calculated from direct counts of the solids and aliquots of the aqueous phases after they were centrifuged but before they were filtered. Average sorption ratios for both "dried" and "pH adjusted" methods of preparing the traced feed solutions are listed in Table 10. These ratios were averaged over 1-, 2-, 4-, and 8-week contact times, 106-150 and 355-500 μm particle sizes, and $\approx 10^{-6}$ and $\approx 10^{-13}$ M plutonium concentrations. The errors quoted are the standard deviations of the means.

For comparison purposes, the results for Experiment 4 are presented in Table 11. Although more limited in scope, these data are probably more reliable than those from earlier experiments because of an improved experimental technique (minimal transfer of particulates).

Several general conclusions can be made for the plutonium and americium results: The sorptive properties tend to vary with the mineralogy; the R_d values are highest for the zeolitized tuff (JA-37). At least qualitatively the americium R_d value for sorption or desorption tends to increase slightly with increasing particle size, while the plutonium value shows a slight decrease. The R_d values show very little increase with longer contact times; the plutonium values tend to increase more than do the americium values. The R_d values for sorption tend to increase with increasing temperature, while those for desorption tend to decrease with increasing temperature, at least for americium. The method of preparing the traced feed solutions appears to have influenced the observed sorption ratios, the "pH adjusted" method giving

TABLE 6. Am and Pu Sorption Ratios, Sample JA-18, Ambient Temperature

Experiment Number	Fraction (μm)	Tracer Prep	Time (d)		R_d		pH	
			Sorp	Desorp	Am	Pu	Initial	Final
1	106-150	dried	7.0		200	170[a]		8.19
1			7.0		250			8.29
				14	270	160[a]	8.30	
2			7.6		96	70[a]	8.56	7.43
2			7.6		310			7.52
				59.8	810		8.51	8.58
3			13.8			110[b]	8.38	8.30
				13.7		710[b]	8.43	8.51
2			14.6		86		8.56	8.42
				34.7	440		8.51	8.53
2			14.6		310			8.29
				59.8	710		8.51	8.57
2			28.6		120	81[a]	8.56	8.55
2			28.6		200		8.53	8.58
				34.7	1 200		8.51	8.15
2			28.6		360			8.60
				59.8	790		8.51	8.58
2			28.6		220		8.52	8.60
3			28.9			120[b]	8.38	8.41
				14.0		450[b]	8.44	8.56
3			55.7			220[b]	8.38	8.42
				17.8		97[b]	8.35	8.45
2			56.6		57	68[a]	8.56	8.36
2			56.6		100		8.52	8.57
				34.7	2 000		8.51	8.36
2			56.6		85			8.57
				59.8	2 300		8.51	8.52
2			56.6		85		8.53	8.49
4	106-150	pH adjust	32.9		450		8.55	8.42
				41.8	1 000		8.50	8.59
4			32.9		440		8.55	8.43
				41.8	930		8.50	8.64
4			60.9		420		8.55	8.27
				43.8	950		8.50	8.62
4			61.9		430		8.55	8.44
				44.8	970		8.50	8.65

[a]Approximately 10^{-6} M ^{239}Pu.
[b]Approximately 10^{-13} M ^{237}Pu.

TABLE 7. Am and Pu Sorption Ratios[a], Sample JA-32, Ambient Temperature

Experiment Number	Fraction (μm)	Tracer Prep	Time (d)		R_d		pH	
			Sorp	Desorp	Am	Pu	Initial	Final
2	106-150	dried	7.6		110		8.50	7.60
				34.7	2 800		8.58	8.56
2			14.6		110	110	8.50	8.60
2			28.6		140		8.50	8.63
2			28.6		230		8.50	8.63
				34.7	1 500		8.58	8.34
2			56.6		79		8.50	8.64
1	106-150	pH adjust	7		1 600	1 200	7.92	8.26
1			14		1 000	1 800	7.92	8.19
1			28		1 100		7.92	8.32
				14	2 100	920	8.30	
1	355-500	pH adjust	7		890	1 000	7.92	8.19
4			13.0		1 300		8.59	8.49
				47.8	2 100		8.46	8.64
1			14		640		7.92	7.94
				14	920	580	8.30	
4			14.0		1 400		8.59	8.45
				47.8	3 900		8.46	8.69
1			28		490	820	7.92	8.23
4			61.9		1 200		8.59	8.50
				44.8	2 100		8.46	8.67
4			62.9		1 700		8.59	8.52
				47.8	2 600		8.46	8.69

[a]Approximately 10^{-6} M ^{239}Pu.

TABLE 8. Am and Pu Sorption Ratios, Sample JA-37, Ambient Temperature

Experiment Number	Fraction (μm)	Tracer Prep	Time (d)		R_d		pH	
			Sorp	Desorp	Am	Pu	Initial	Final
2	106-150	dried	7.6		430	390[a]	8.64	7.53
2			14.6		365		8.64	8.52
				34.7	14 000		8.60	8.47
2			28.6		430	180[a]	8.64	8.67
2			28.6		1 500		8.64	8.62
				34.7	21 000		8.60	8.28
2			56.6		640		8.64	8.56
1	106-150	pH adjust	7		7 200	7 200[a]	7.92	8.53
1			14		5 200		7.92	8.23
				14	2 700	890[a]	8.30	
4			14.0		11 000		8.60	8.48
				47.8	12 000		8.58	8.64
4			14.7		10 000		8.59	8.44
				47.8	8 900		8.58	8.63
1			28		7 500	12 000[a]	7.92	7.94
				14	5 200	1 600[a]	8.30	
4			27.7			750[b]	8.35	8.33
				40.8		5 300[b]	8.58	8.60
4			27.7			720[b]	8.35	8.33
				40.8		8 600[b]	8.58	8.59
4			33.9		14 000	1 900[b]	8.60	8.52
				42.8	11 000		8.58	8.56
4			34.7		14 000		8.59	8.57
				42.8	9 500		8.58	8.55
4			54.7			1 900[b]	8.35	8.30
				43.8		5 500[b]	8.58	8.56
4			60.9		12 000		8.60	8.31
				43.8	12 000		8.58	8.57
4			62.6		11 000		8.59	8.54
				44.8	10 000		8.58	8.59
4			63.6		13 000		8.59	8.56
				47.8	9 700		8.58	8.61
4							8.60	
1	355-500	pH adjust	7		3 700	5 400[a]	7.92	8.38
1			14		2 800	7 200[a]	7.92	8.19
1			28		3 800		7.92	8.29
				14	5 800	670[a]	8.30	
4			32.9		12 000		8.60	8.50
				41.8	17 000		8.58	8.58

TABLE 8 (cont). Am and Pu Sorption Ratios, Sample JA-37, Ambient Temperature

Experiment Number	Fraction (μm)	Tracer Prep	Time (d)		R_d		pH	
			Sorp	Desorp	Am	Pu	Initial	Final
4			33.9		13 000		8.60	8.51
				42.8	17 000		8.58	8.55
4			60.9		14 000		8.60	8.37
				43.8	18 000		8.58	8.58
4			62.9		12 000		8.60	8.53
				47.8	33 000		8.58	8.60
4			27.7			280[b]	8.38	8.40
				40.8		6 500[b]	8.58	8.61
4			27.7			320[b]	8.38	8.40
				40.8		3 600[b]	8.58	8.59
4			54.7			450[b]	8.38	8.28
				43.8		1 000[b]	8.58	8.59
4			54.7			470[b]	8.38	8.46
				43.8		1 900[b]	8.58	8.56

[a] Approximately 10^{-6} M ^{239}Pu.
[b] Approximately 10^{-13} M ^{237}Pu.

somewhat higher R_d values than the "dried" method for sorption but approximately the same for desorption. However, the improved procedure used in Experiment 4 (pH adjusted) for centrifuging and transferring solutions after contact may have resulted in the removal of more particulates from solution, which would result in the observation of higher R_d values. Five different feed solutions of ^{241}Am and two of ^{237}Pu were used in Experiment 4 with no observable differences in their behavior for a given element. This indicates that the feed preparation, at least for the pH-adjusted method, is fairly reproducible. For americium, the R_d values were greater for desorption than for sorption, except possibly at 70°C.

Comparison of results for ^{239}Pu ($\approx 4 \times 10^{-7}$ M) and ^{237}Pu ($\approx 1 \times 10^{-13}$ M) at least for "pH adjusted" feed solutions, shows higher sorption R_d values for ^{239}Pu but higher desorption R_d values for ^{237}Pu. Also, for ^{239}Pu the sorption R_d values are greater than the desorption but for ^{237}Pu the desorption R_d values are greater than the sorption.

TABLE 9. Am and Pu Sorption Ratios[a], Samples JA-18, -32, and -37, 70°C

Core Sample	Experiment Number	Fraction (μm)	Tracer Prep	Time (d)		R_d		pH	
				Sorp	Desorp	Am	Pu	Initial	Final
JA-18	2	106-150	dried	7.6		220			7.19
					33.9	3 100		8.35	8.48
	2			7.6		190			7.32
	2			14.6		190			7.57
					33.9	3 600		8.35	8.42
	2			14.6		170			8.08
	2			28.6		290			8.61
	2			28.6		150			8.62
	2			28.6		340		8.60	
	2			28.6		370		8.57	8.50
	2			56.6		300			
	2			56.6		76			
JA-32	2	106-150	dried	7.6		120		8.46	7.33
	2			14.6		160		8.46	8.14
	2			28.6		130		8.46	8.57
	2			56.6		46		8.46	
JA-37	2	106-150	dried	7.6		520	240	8.58	7.33
	2			14.6		680		8.58	8.06
	2			14.6		2 100		8.58	8.18
	2			28.6		960		8.58	8.67
	2			56.6		800		8.58	
	2			56.6		730		8.58	8.52
JA-37	4	355-500	pH adjust	32.9		32 000		8.37	8.23
					41.7	3 800		8.41	8.59
	4			33.9		48 000		8.37	8.25
					42.7	7 200		8.41	8.46
	4			61.8		19 000		8.37	8.51
					44.7	5 500		8.41	8.58
	4			62.8		37 000		8.37	8.64
					47.8	4 800		8.41	8.58

[a]Approximately 10^{-6} M ^{239}Pu.

TABLE 10. Average Sorption Ratios (mℓ/g) for Am and Pu on Tuff[a]

Element	Core	Temp (°C)	Dried		pH Adjusted	
			Sorption	Desorption	Sorption	Desorption
Am	JA-18	22	180(30)	1 100(260)	435(6)	960(15)
		70	230(30)	3 400(300)		
	JA-32	22	130(30)	2 200(650)	1 100(120)	2 300(310)
		70	110(30)			
	JA-37	22	670(210)	17 000(3 500)	8 800(1 100)	12 000(2 000)
		70	970(240)		34 000(6 000)	5 300(720)
Pu	JA-18	22	140(30)	350(140)		
	JA-32	22	≈110		1 200(210)	750(170)
	JA-37	22	280(100)		3 300(1 200)	3 800(950)

[a]Sorption ratios are given for both "dried" and "pH adjusted" methods of preparing the traced feed solutions. They are averaged over 1-, 2-, 4-, and 8-week contact times, 106-150 and 355-500 μm particle sizes, and $\approx 10^{-6}$ and $\approx 10^{-13}$ M plutonium concentrations. Values in parentheses are the standard deviations of the means (absolute values).

BEHAVIOR OF PLUTONIUM AND AMERICIUM IN GROUNDWATER AT pH ≈ 8

Although a considerable number of procedural variables were examined during batch sorption experiments with tuff (Wolfsberg 1979), argillite (Erdal-3, 5 1979), and granite (Erdal-2 1979), the following discussion will be primarily based upon tuff Experiment 4 (see the previous section). In this experiment improvements were made in the method used for separating solid and liquid phases after contact, presumably reducing the amount of particulates present in the aqueous phases and giving more accurate results. A few operations were added to examine container sorption for samples and controls, the fraction of centrifugible species in the controls, the effect of filtering successive portions of the same after-contact solution through the same filter membrane, the

TABLE 11. Average Sorption Ratios for Am and Pu on Tuff, Experiment 4 Data[a]

Element	Core	Temp (°C)	R_d (mℓ/g) Sorption	R_d (mℓ/g) Desorption
Am	JA-18	22	425(5)	960(15)
	JA-32	22	1 450(250)	2 900(380)
	JA-37	22	12 000(500)	14 000(2 100)
		70	28 000(9 000)	5 300(720)
^{237}Pu	JA-37	22	700(210)	4 600(1 000)

[a]Sorption ratios are given for the "pH adjusted" method of preparing the traced feed solutions. They are averaged over 1-, 2-, 4-, and 8-week contact times and 106-150 and 355-500 μm particle sizes. Values in parentheses are the standard deviations of the means (absolute values).

effects of filtering after-contact solutions through filter membranes with different pore sizes, and the effects of centrifuging after-contact solutions a different number of times and for different durations. A few contacts will be continued for ≈6 months to examine long-term effects. The procedure used for phase separation after contact was usually three centrifugings, for 1, 1, and 2 hours, at 12 000 rpm (28 000 g). Extreme care was taken to avoid transferring any particulates from the bottoms of the tubes or in surface films. The centrifuged solutions were then filtered in various ways. In some cases, aliquots were taken for counting after each centrifuging and each filtering.

Sorption on container walls during tuff contacts was measured by transferring the contents after contact, without centrifuging, to new tubes and counting the original tubes. Sorption on the container walls when solids were present was measured for twenty-four ^{241}Am and seven ^{237}Pu samples. The amount of activity sorbed on the container, with the possibility of retention of a small amount of solid even after transfer, averaged 2.1% for americium and 2.5% for plutonium. For the controls, container sorption averaged 24% for nine americium solutions at room temperature, 74% for four americium solutions at 70°C, and 16% for two plutonium solutions at room temperature. The amount of

plutonium or americium activity remaining on the container is obviously much lower for the samples than for the controls.

During earlier experiments container sorption for argillite samples was examined in essentially the same way except that the control samples were centrifuged and the aqueous phase was transferred to another tube. The activity observed in a control tube therefore represented the sum of wall sorption and centrifugable species. Sorption on the container walls when solids were present was measured for thirteen ^{241}Am and nine ^{237}Pu samples. The amount of activity sorbed on the container, with the possibility of retention of a small amount of solid even after transfer, averaged 1.2% for americium and 0.6% for plutonium. For the controls, the americium activity remaining with the container averaged 13% for thirteen solutions at ambient temperature and 90% for four solutions at 70°C. For two plutonium controls at each temperature the values were 43% at ambient and 88% at elevated temperature. Again, container sorption was much higher for the controls than for samples containing crushed rock.

The ratio of the activity on the bottom of a tube to that on the wall was measured for both tuff and argillite control tubes. For six tubes used with tuff controls, this ratio varied from 0.3 to 1.1 with an average of 0.7. Results for nine argillite controls gave a value of 1.2 for this ratio. The activity on both sets of control tubes appears to have been sorbed fairly evenly on the surface.

The above results for container sorption suggest that sorption is dependent on available surface area so when crushed argillite or tuff is present container sorption is negligible.

For the tuff controls described above, the fraction of centrifugable species was measured by centrifuging the contents of the new tubes after the first transfer, again transferring the liquid, and counting the activity left in the tubes. The average fraction of the activity in the solution after contact that was removed by one 1-h centrifuging was 17% for nine americium controls at room temperature, 37% for four americium controls at 70°C, and 13% for two plutonium controls at room temperature. Since there was a significant amount of centrifugable species in the control solutions, presumably a similar fraction of the activity was also present with the samples where it would have been combined with the crushed rock and counted with the sorbed activity.

Each of three centrifugings (1h, 1h, 2h) removed additional activity from americium solutions after contact and, therefore, would appear to be necessary. (Such measurements were not made with plutonium solutions.)

In an experiment to see if effects related to the filtering process result in a change in the activity concentration of solutions after contact, three ≈3-mℓ portions of an after-contact solution were passed through the same 0.4-μm polycarbonate membrane. Each portion was aliquoted and counted after passing through the membrane. The averages for a number of samples of the relative concentrations of the solutions after filtering in this way are given in Table 12. Filtering successive portions of the same after-contact solution through the same filter membrane does not appear to result in a significant difference in the concentration of plutonium or americium in the solution.

The effects of centrifuging the solutions after contact and then passing them through filters with various pore sizes were examined by counting aliquots of the solutions after each step. Data for a number of samples and controls are given in Table 13. Filter sequences used were 1.0-0.4-0.05, 0.4-0.4, and 0.05-0.05 μm. The results indicate that the most recent procedure for centrifuging and transferring after contact gave plutonium solutions from which no additional plutonium was removed by filtering. This was not true for americium, where a factor of two or more of the activity was sometimes removed by filtering the centrifuged solutions, the results varying with the contact temperature.

TABLE 12. Effect of Consecutive Filtering of Traced Solutions Through 0.4-μm Membranes

	Ratio of Activity Concentrations of Different Portions	
	Second/First	Third/First
Sample		
^{241}Am		
22°	0.98	0.97
70°	0.97	0.93
Controls		
^{241}Am		
22°	0.94	0.92
70°	0.99	0.98
^{237}Pu		
22°	0.98	0.97

to establish a lower limit to the sorption ratio since particulates remaining with the solution would tend to lower the calculated R_d.

In an attempt to clarify the mechanism by which americium is retained on filter membranes, 38 filters from the sequential filterings listed in Table 13 were examined by a microautoradiograpic technique. Approximately one-half to one-third of each filter membrane was mounted on a glass slide by coating with a thin layer of parlodion (a 2% solution in isopentanyl acetate). The slide was then alpha counted to determine the length of exposure time needed (calculated to give $\approx 10^7$ disintegrations) and clamped together with a second slide on which a Kodak AR.10 strippable emulsion had been mounted. It was found that mounting the emulsion directly onto the coated filter made visualization of single tracks very difficult. To get a good adherence of the emulsion on blank glass slides, the slides were first etched with a dilute solution of HF, then dried and coated with a 2% parlodion in isopentanyl acetate, dried again and finally coated with a thin gelatin layer by dipping the slide in a water solution containing 0.5% gelatin and 0.06% $CrK(SO_4)_2 \cdot 12H_2O$.

Microautoradiography of the "sorption" membranes showed not only single-alpha tracks but also clusters and stars, indicating the presence of large complex species or polymers in the so-called solutions even after multiple centrifugings. Some "sorption" solutions were filtered through several membranes with the same or decreasing pore sizes (see Table 13). In general, all of these membranes were found to retain americium in clusters, stars, and single tracks. Americium species in these solutions probably exist in a broad range of particle sizes. In contrast, the "desorption" membranes generally showed only single-alpha tracks, suggesting that some americium sorbed on the membranes but that large particulates were not removed from the solids during desorption nor did they form in the aqueous phases during contact.

In related work B. M. Allard (Chalmers University, Göteborg, Sweden, personal communication) observed sorption ratios for Millipore filter paper comparable to those for rock-forming minerals during "batch" sorption experiments with americium in simulated groundwater.

Considering the above results, we have decided to take the conservative approach in calculating americium sorption ratios and use the results from the solutions after they have been centrifuged but not filtered.

TABLE 13. Average Activity Removed[a] from Solution by Centrifuging and Filtering (in percent)

Treatment	Samples			Controls		
	^{237}Pu(22°)	^{241}Am(22°)	^{241}Am(70°)	^{237}Pu(22°)	^{241}Am(22°)	^{241}Am(70°)
Centrifuge[a] 1 h (2nd)		22	51		14	8
Centrifuge 2 h (3rd)		24	26		6	8
Filter 1.0 μm	0	10		3	28	0
Filter 0.4 μm	0	13		2	26	0
Filter 0.05 μm	0	27		1	8	48
or						
Filter 0.4 μm		22		2	26	6
Filter 0.4 μm		11		-	24	3
or						
Filter 0.05 μm	0	39	70		40	
Filter 0.05 μm	0	21	6		32	

[a]Decreases in activity are in percent of input activity (just before addition to the rock) for a given operation removed by that operation.

[b]All centrifugings were at 12 000 rpm.

This plutonium result suggests that plutonium does not significantly sorb on polycarbonate filter membranes, at least in the time required for filtering. The activity present in a plutonium solution after it has been centrifuged three times is, therefore, probably the "true" value for calculating sorption ratios. For americium, centrifuging the solution after contact would appear

It is important to emphasize that the measured sorption ratios for plutonium and americium include effects other than sorption. There may well be differences in the behavior of plutonium or americium even in supposedly identical solutions at pH ≈ 8 to 8.5 e.g., in the degree of polymerization and radiocolloid formation, and hydrolysis resulting in variations in species (including charge) and particle size. Grebenshchikova and Davydov (1965) reported that the charge on colloidal Pu(IV) species may be either positive (at low pH values) or negative (at high) and that the isoelectric pH, or point of zero charge, is in the pH region 8.0 to 8.5. Polzer and Miner (1976) presented a plot of effective charge (due to hydrolysis) of the americium species vs. pH for a 0.1 M $LiClO_4$ solution. Between pH 8.0 and 8.5 the average effective positive charge per atom of americium varied from ≈1.3 to essentially zero. Therefore, large variations in the behavior of both plutonium and americium could be expected in this pH range.

EFFECTS OF GROUNDWATER COMPOSITION ON SORPTION RATIOS

Since the composition of the groundwater may have a pronounced effect on the sorption ratio for many radionuclides, the first experiments to assess this dependence for granite and argillite have been initiated. The compositions of the two waters being used in the study were selected to represent extremes for the media being used. While the dependence of the sorption ratio on specific major ion concentrations cannot be determined in these experiments since the concentrations of several ions were varied, the overall effects can be distinguished. The same sieve fraction was used in all experiments. All measurements were made under aerobic conditions.

MEASUREMENT TECHNIQUES

The approximate initial compositions of two waters selected for study are given in Table 14. The dilute groundwater (labeled I) was prepared by adding 2.2 mℓ KCl solution (17.2 mg/mℓ), 13.2 mℓ NaOH solution (4.0 mg/mℓ), and 1.24

TABLE 14. Approximate Initial Groundwater Composition

Constituent	μg/mℓ Water I	μg/mℓ Water II
Na	10	50
K	5	5
Ca	10	50
Mg	2	20
SO_4	5	70
Cl	4.5	15

mℓ Na_2SO_4 solution (23.9 mg/mℓ) to 74 mg $Ca(OH)_2$ plus 19.2 mg $Mg(OH)_2$. The mixture was diluted to 4.0 ℓ with deonized water and then sparged with carbon dioxide for about 36 h. After the solution was sparged with nitrogen until a pH ≈ 8 was reached, it was allowed to air-equilibrate for 2 d prior to use. The more concentrated groundwater (labeled II) was prepared in a similar manner using 370 mg $Ca(OH)_2$, 192 mg $Mg(OH)_2$, 2.2 mℓ KCl solution, 17.9 mℓ NaOH solution, 17.3 mℓ Na_2SO_4 solution, and 9.1 mℓ NaCl solution (7.3 mg/mℓ).

The 250-355 μm sieve fractions prepared earlier (Erdal-1,2 1979; Wolfsberg 1979) were used. They were the Climax Stock quartz monzonite (CS5 and CS7) and the Eleana argillite (CN1 and CN2). Weighed 1-g quantities of these materials were pretreated for two weeks with 20 mℓ of each of the appropriate waters described earlier. The phases were then separated by centrifugation at 12 000 rpm (28 000g).

Four different rock-treated waters were prepared by shaking each of the two waters with the 250-355 μm fractions of CS5 and CN1. A 20 mℓ/g solution to solid ratio was used. The phases were separated by centrifugation at 6 000 rpm (20 000 g) for 1 h followed by filtration through 0.45-μm Millipore filter membranes.

The ^{85}Sr, ^{137}Cs, ^{133}Ba, ^{141}Ce, and ^{152}Eu tracers were added to these rock-treated waters using the technique described earlier (evaporation to dryness followed by dissolution) (Erdal-1,2 1979, Wolfsberg 1979). The concentrations due to the carrier added with the tracer are given in Table 15.

TABLE 15. Estimated Element Concentrations

Material	Water	Molarity				
		Sr	Cs	Ba	Ce	Eu
Granite	I	5.8×10^{-8}	4.9×10^{-10}	1.0×10^{-8}	3.3×10^{-8}	1.9×10^{-8}
	II	6.4×10^{-8}	6.6×10^{-10}	1.2×10^{-8}	6.0×10^{-9}	3.5×10^{-8}
Argillite	I	5.1×10^{-8}	6.2×10^{-10}	6.4×10^{-9}	1.8×10^{-8}	1.5×10^{-8}
	II	6.4×10^{-8}	7.2×10^{-10}	8.3×10^{-9}	1.6×10^{-8}	1.8×10^{-8}

Each granite and argillite sample was treated with each of the corresponding tagged waters by the procedures described earlier (Erdal-1,2 1979, Wolfsberg 1979) for measuring sorption ratios. All solutions and solids were assayed for radioactivity, and our standard calculation methods (Erdal-1,2 1979) were used. Contact times of 4 and 8 weeks were used.

Determination of the actual composition of the waters before and after contact with the rock is in progress.

RESULTS AND CONCLUSIONS

The results from these measurements are given in Table 16. The initial and final pH values are given in Table 17.

There is a strong general tendency for the sorption ratios for cesium, strontium, and barium to decrease when the more concentrated water is used. This is undoubtedly due to the effect of the increased amount of competing ions.

There is a large increase in the R_d values for cerium and europium when water II is used, especially for the granite samples. Since water II had an increased concentration of sulfate ions, perhaps the higher R_d values for cerium and europium can be explained by the greater tendency to form radiocolloids with increasing sulfate concentration. The values also increase greatly between 4 and 8 weeks. All of this is a further indication that the sorption mechanism for cerium and europium is quite different than that for strontium, cesium, and barium.

TABLE 16. Granite and Argillite Sorption Ratios, Ambient Temperature

Sample	Water	Sorption Ratio, R_d (mℓ/g)[a] Cs	Sr	Ba	Ce	Eu
		27.63-d Contact Time				
CS5	I	179(4.2)	8.2(7.3)	63.1(2.4)	184(7.1)	195(6.8)
	II	234(3.3)	5.0(10)	28.3(2.8)	>10 000	4 770(7.0)
CS7	I	160(4.2)	10.3(6.2)	52.8(2.5)	130(6.7)	133(6.4)
	II	214(3.3)	6.4(8.6)	33.9(2.6)	>13 000	30 100(18)
CN1	I	1 460(5.2)	227(2.5)	1 030(3.2)	1 890(9.6)	2 580(9.5)
	II	1 010(4.6)	91.7(2.6)	396(2.4)	2 760(14)	1 990(8.7)
CN2	I	2 390(6.3)	703(2.8)	2 300(3.8)	5 810(12)	8 340(13)
	II	1 630(3.5)	173(2.4)	703(2.1)	12 400(13)	10 700(7.8)
		59.63-d Contact Time				
CS5	I	591(3.7)	6.6(8.3)	59.4(2.4)	5 200(14)	3 290(6.1)
	II	366(3.4)	4.8(11)	39.7(2.5)	>13 000	17 800(17)
CS7	I	409(3.7)	10.0(6.2)	74.2(2.2)	1 690(7.6)	1 550(5.2)
	II	289(3.4)	4.4(12)	31.6(2.7)	>9 500	20 600(20)
CN1	I	1 410(3.8)	143(2.5)	822(2.4)	>68 000	>55 000
	II	1 070(3.4)	83.6(2.6)	428(2.1)	>55 000	>56 000
CN2	I	2 980(4.2)	144(2.5)	2 570(2.7)	>73 000	>54 000
	II	1 760(3.6)	83.2(2.6)	767(2.1)	>60 000	>62 000

[a]Standard deviations of the means expressed in percent are given in parentheses.

TABLE 17. pH Values in the Water Composition Studies

Solid	Water	pH Initial	pH 28 d	pH 60 d
CS5	I	8.08	8.01	8.17
	II	8.58	8.44	8.50
CS7	I	8.08	8.03	8.13
	II	8.58	8.50	8.50
CN1	I	8.66	8.59	8.69
	II	8.76	8.72	8.76
CN2	I	8.66	8.65	8.75
	II	8.76	8.65	8.78

Assuming that uncontrolled variables are not important, the composition of the water seems to be a major factor that governs the observed sorption ratio. The possible influence of anions, other than in a complexing role, must be taken into account in future studies.

SORPTION MEASUREMENTS ON HAINESVILLE SALT DOME MATERIALS

Since salt systems are considered to be important as potential sites for nuclear waste repositories, it is necessary to begin sorption studies on materials from such areas. Two samples from the Hainesville area in east Texas have been received from Battelle Pacific Northwest Laboratories (BPNL). These samples are representative of two strata surrounding the dome. Recipes for two "typical" groundwaters were also supplied by BPNL.

Studies of the sorption of strontium, cesium, barium, cerium, europium, uranium, and americium were made under aerobic and anoxic (<0.2 ppm oxygen) conditions.

MEASUREMENT TECHNIQUES

Preparation of Materials

The two different solid samples "representative" of the materials around the Hainesville salt dome were used as received from BPNL. According to R. J.

Serne and J. F. Relyea (BPNL), these are mixtures of materials from the pertinent strata. The "aquifer" sample was a 50/50 mixture of the Calvert Bluff and Carrizo strata, while the "aquitard" sample was a 50/50 mixture of Hooper and Simsboro materials. The preliminary mineralogy indicated that all the samples were mainly quartz with minor amounts of secondary clays. Appreciable discoloring was observed. The detailed mineralogy will be done at BPNL.

The groundwater compositions used were selected (R. J. Serne, J. F. Relyea) to represent two different scenarios for breach of the dome. The first water represents the Wilcox aquifer which is in the Hainesville region. It was made up to contain 1260 ppm $NaHCO_3$ and 7 ppm $CaSO_4$ (12.6 g $NaHCO_3$ plus 0.0885 g $CaSO_4 \cdot 2H_2O$ per 10.0 ℓ deionized water). The second water represents the high density brine as diluted by the Wilcox aquifer, and contains 10 000 ppm NaCl and $\approx$7 ppm $CaSO_4$ (100 g NaCl plus 0.0885 g $CaSO_4 \cdot 2H_2O$ per 10.0 ℓ deionized water).

The materials were pretreated by shaking weighed 1-g quantities with 30 mℓ of the appropriate groundwater for 4 d. The phases were separated by centrifuging at 12 000 rpm (28 000 g) for 20 m. A second pretreatment using 20 mℓ was then done for 3 d, followed by a centrifugation at 12 000 rpm for 20 m. The weight of solution remaining with the solid phase was obtained by weighing the tube and solid before and after the pre-treatment.

Preparation of Tagged Solutions

The appropriate volumes of the tracer solutions for ^{85}Sr, ^{137}Cs, ^{133}Ba, ^{141}Ce, and ^{152}Eu needed for a set of measurements were evaporated to dryness in a washed polyethylene bottle overnight on a steam bath. Concentrated hydrochloric acid was added and the mixture was taken dry again in order to convert the salts to chlorides. The appropriate volume of groundwater was added and the mixture was mixed for 3 d in an orbit shaker. The mixture was centrifuged for one hour at 7 000 rpm, followed by filtration through a 0.4-μm Nuclepore filter. The resulting tracer solution was used for the sorption measurements within 0.2 day. An aliquot of the final solution was also removed for assay of the initial activity of each of the tracers in the solution. This aliquot was acidified with hydrochloric acid before assaying in order to stabilize the solution.

The ^{237}U used in these measurements was made by the $^{236}U(n,\gamma)^{237}U$ reaction in the HFIR at the Oak Ridge National Laboratory. The purification chemistry was done at Oak Ridge. It consisted of a dissolution in HCl-HNO_3, a conversion to the nitrate, an extraction with ethyl acetate, an anion column washed with 5M HCl-0.1M HF, and an elution with water. The ^{237}U thus prepared was used, after dilution, by simply adding an aliquot to the desired volume of the appropriate groundwater, and then the remainder of the procedure given earlier was followed.

The isotopically pure ^{241}Am tracer used in this study was obtained from Oak Ridge National Laboratory. For each preparation, the desired amount of tracer solution was evaporated at room temperature in a polypropylene tube. The dried activity was then contacted several times with 20-mℓ volumes of groundwater for a few minutes. The mixture was transferred to a large polyethylene bottle. Contacts were continued until no significant decrease in gamma-ray activity in the tube was observed. Generally three contacts were made. Groundwater was added to the bulk of the feed solution in the bottle to give the desired final volume. The solution was shaken in the bottle in an orbit shaker for >24 h and then passed through a 0.4-μm Nuclepore filter. An aliquot of the final solution was assayed to determine the initial ^{241}Am activity. The traced feed solution was used for the sorption measurements within about 1 h.

In all cases, the original evaporation of the tracers was done in air. The evaporated samples needed for the measurements under reduced oxygen conditions were then transferred to the anoxic boxes. The groundwaters used in the anoxic boxes were sparged with high-purity nitrogen gas prior to transfer to the glove box.

Table 18 gives the estimated molarities for the tracers.

Sorption Measurements

Batch sorption experiments were performed by shaking the 1-g quantities of pretreated material with 30 mℓ of the tagged water, dispersing the solid by vigorous shaking, and agitating the mixture for about 20 d. At the end of the shaking period, the aqueous phase was separated from the solids by a single centrifuging for one hour at 12 000 rpm. An aliquot of the final solution was

TABLE 18. Tracer Concentrations

	Concentration (molarity)			
	Wilcox		Dilute Brine	
Tracer	Aerobic	Anoxic	Aerobic	Anoxic
^{85}Sr	5.3×10^{-8}	6.2×10^{-8}	6.2×10^{-8}	6.4×10^{-8}
^{137}Cs	1.8×10^{-9}	2.7×10^{-9}	2.7×10^{-9}	2.7×10^{-9}
^{133}Ba	1.3×10^{-8}	1.2×10^{-8}	1.8×10^{-9}	1.6×10^{-8}
^{141}Ce	7.5×10^{-8}	4.0×10^{-8}	5.3×10^{-8}	6.9×10^{-8}
^{152}Eu	1.1×10^{-7}	1.4×10^{-7}	1.4×10^{-8}	3.0×10^{-8}
^{237}U	$\approx 1 \times 10^{-7}$	$\approx 1 \times 10^{-7}$	$\approx 1 \times 10^{-7}$	$\approx 1 \times 10^{-7}$
^{241}Am	4.9×10^{-7}	4.4×10^{-7}	4.3×10^{-7}	1.4×10^{-7}

then removed and placed in a standard scintillation counting polyvial. This solution was acidified with hydrochloric acid, and it was then assayed for the remaining activities. The pH of the solution before and after contact with the rock was also recorded. Three samples for each groundwater-solid combination were used.

The same sorption procedure was also preformed using three tubes for each water type that did not have a solid phase present. These control samples were used to indicate if any of the radionuclides were likely to be removed by the containers.

The samples were all assayed for radioactivity using the techniques described earlier (Erdal-1,2 1979).

The following equation was used to calculate the sorption ratios for strontium, cesium, barium, and uranium:

$$R_d = \frac{R \cdot A_c - A_t}{A_t} \cdot \frac{V}{W} \quad , \qquad (1)$$

where A_c is the average activity per mℓ of a given radionuclide in the control samples, A_t is the activity per mℓ in the supernatant solution after the required contact time, W is the weight (grams) of solid material used, V is the total final volume of supernatant solution, and R is the dilution factor to take into account the residual solution from the wash that remains with the solid. The amount of residual solution (V_r) left with the solid material was calculated from the weight increase of the sample plus container (g_r) after the two prewashes and the measured density (ρ_r) of the solutions used ($V_r = g_r/\rho_r$).

For the barium and cerium cases, a different calculational method was used. Since sorption on the container has never been observed for cesium, the R_d value for cesium was used as in internal monitor. The activity of the element of interest and of cesium in the solid and liquid was measured. The sorption ratio is

$$R_d = \frac{A_s}{A_t} \cdot \frac{1}{W} \qquad (2)$$

where A_s is the activity on the solid. If a ratio of R_d values is calculated using Eq. 2 one has, after rearrangement,

$$R_{dx} = \frac{\left(\frac{A_{sx}}{A_{sm}}\right)}{\left(\frac{A_{tx}}{A_{tm}}\right)} R_{dm}$$

where the x and m refer to the element of interest and cesium, respectively. This equation was used to calculate the R_d value for the element of interest since the sorption ratio for cesium was measured in the same experiment and calculated using Eq. 1.

Eq. 2 was used to calculate the sorption ratio values for americium.

The standard deviation for each measurement was obtained from the errors associated with the activity measurements (usually less than 5%), 3% uncertainty assumed for g_r, a 10 mg uncertainty in W, and 0.5% uncertainty in the volumes, and, where applicable, the uncertainty associated with the reproducibility of the control measurements (A_c). The errors were propagated using the rule for change of variables in a moment matrix assuming independence of the variables.

RESULTS AND CONCLUSIONS

The results for the sorption ratio measurements under aerobic and anoxic conditions are given in Tables 19-24. The percent of the feed activity remaining in solution in the control samples is given in Tables 25 and 26, while Tables 27 and 28 give the pH values observed.

On examining Tables 19-24 one can make several general conclusions. The sorption ratios for a given element are, with a few exceptions, significantly higher for the aquifer solid than for the aquitard samples. The R_d values for cesium are all rather high, independent of the medium, water, or atmospheric conditions. This may indicate that there is a mineral present which has a high capacity and selectivity for cesium. The values for strontium, cesium, and barium are not affected by the atmospheric conditions in the brine solutions the strontium and barium values are generally low. However, the R_d values for these elements in the bicarbonate water generally decrease when the measurements are performed under anoxic conditions. This may be a function of the absence of carbon dioxide in the anoxic studies which resulted in higher pH values (Tables 27 and 28). The R_d values for cerium and europium are not strongly affected by the atmospheric conditions except for the aquifer solid with the bicarbonate water. In this case, the sorption ratios decreased strongly when anoxic conditions were used.

The most surprising result from these measurements is the rather significant R_d values obtained for uranium(VI). The values obtained using the brine solutions are always high, independent of the atmospheric conditions. Those for the aquifer solid and the bicarbonate water are also larger than observed in other systems studied (Erdal-2; see below). Anoxic conditions, however, do result in somewhat lower sorption ratios. The reasons for these observations are not understood.

TABLE 19. Aerobic Measurements for Cesium, Strontium, and Barium

Solid	Water	Sample	Sorption Ratio, R_d (mℓ/g)[a] Cs	Sr	Ba
Aquifer	Wilcox	1	14 400 (3.8)	472 (1.9)	2 200 (2.2)
		2	13 900 (3.3)	451 (2.0)	2 120 (2.0)
		3	14 100 (3.1)	465 (2.0)	2 200 (1.9)
		Average[b]	14 100 [1.9]	463 [1.4]	2 170 [1.2]
Aquitard	Wilcox	1	5 960 (7.2)	418 (2.5)	837 (3.1)
		2	4 540 (6.2)	419 (2.6)	839 (3.1)
		3	4 260 (6.2)	409 (2.6)	821 (3.1)
		Average[b]	4 650 [9.1]	415 [1.5]	832 [1.8]
Aquifer	Brine	1	3 670 (3.0)	7.13 (8.8)	22.3 (3.7)
		2	3 730 (3.0)	7.84 (8.0)	24.2 (3.5)
		3	3 750 (3.0)	8.17 (7.9)	24.0 (3.5)
		Average[b]	3 720 [1.7]	7.70 [4.7]	23.5 [2.6]
Aquitard	Brine	1	4 810 (6.0)	9.18 (8.1)	15.7 (4.7)
		2	5 000 (3.3)	10.1 (6.9)	16.5 (4.4)
		3	5 940 (3.4)	11.2 (6.9)	18.4 (4.3)
		Average[b]	5 280 [6.3]	10.1 [5.6]	16.8 [4.6]

[a] The values in parentheses are the standard deviations for a single measurement of the R_d values expressed in percent; these were obtained from the errors associated with the activity measurements and estimated uncertainties for the various parameters entering into the calculation; these estimated uncertainties were propagated using the rule of change of variables in a moment matrix assuming independence of the variables.

[b] Weighted average; the error (%) given is the standard deviation of the mean for the three replicate experiments.

TABLE 20. Anoxic Measurements for Cesium, Strontium, and Barium

Solid	Water	Sample	Sorption Ratio, R_d (mℓ/g)[a] Cs	Sr	Ba
Aquifer	Wilcox	1	8 950 (2.9)	657 (2.2)	3 400 (3.1)
		2	7 670 (2.9)	608 (2.3)	3 280 (3.0)
		3	9 090 (5.2)	635 (2.4)	3 290 (3.7)
		Average[b]	8 310 [5.6]	633 [2.3]	3 320 [1.9]
Aquitard	Wilcox	1	3 420 (2.1)	441 (1.9)	871 (1.8)
		2	3 200 (2.4)	427 (2.1)	822 (1.8)
		3	3 450 (2.3)	432 (2.1)	844 (1.8)
		Average[b]	3 360 [2.3]	434 [1.2]	845 [1.7]
Aquifer	Brine	1	3 800 (2.8)	7.91 (7.7)	25.7 (3.5)
		2	3 790 (2.8)	7.38 (8.3)	24.9 (3.6)
		3	3 200 (2.8)	7.62 (8.2)	24.5 (3.6)
		Average[b]	3 550 [5.8]	7.64 [4.7]	25.0 [2.1]
Aquitard	Brine	1	4 470 (3.1)	10.1 (6.6)	16.0 (4.6)
		2	4 170 (2.9)	9.98 (6.6)	15.8 (4.8)
		3	4 120 (2.9)	9.24 (7.7)	15.2 (4.9)
		Average[b]	4 230 [2.4]	9.80 [4.0]	15.7 [2.7]

[a]The values in parentheses are the standard deviations for a single measurement of the R_d values expressed in percent, these were obtained from the errors associated with the activity measurements and estimated uncertainties for the various parameters entering into the calculation; these estimated uncertainties were propagated using the rule of change of variables in a moment matrix assuming independence of the variables.

[b]Weighted average; the error (%) given is the standard deviation of the mean for the three replicate experiments.

TABLE 21. Aerobic Measurements for Cerium and Europium

Solid	Water	Sample	Sorption Ratio, R_d (mℓ/g)[a] Ce	Eu
Aquifer	Wilcox	1	37 400 (18)	27 900 (11)
		2	40 700 (20)	32 600 (11)
		3	36 300 (19)	25 400 (11)
		Average[b]	37 900 [11]	28 000 [7.2]
Aquitard	Wilcox	1	5 860 (8.2)	2 780 (7.3)
		2	4 940 (7.2)	2 530 (6.6)
		3	6 440 (8.5)	3 020 (7.4)
		Average[b]	5 520 [7.9]	2 730 [5.2]
Aquifer	Brine	1	965 (5.1)	1 820 (11)
		2	1 190 (6.9)	2 640 (16)
		3	943 (5.0)	1 640 (9.4)
		Average[b]	988 [6.0]	1 780 [10]
Aquitard	Brine	1	300 (7.8)	333 (8.3)
		2	317 (7.6)	323 (8.2)
		3	333 (7.6)	364 (8.2)
		Average[b]	316 [4.4]	338 [4.8]

[a]The values in parentheses are the standard deviations for a single measurement of the R_d values expressed in percent; these were obtained from the errors associated with the activity measurements and estimated uncertainties for the various parameters entering into the calculation; these estimated uncertainties were propagated using the rule of change of variables in a moment matrix assuming indenpendence of the variables.

[b]Weighted average; the error (%) given is the standard deviation of the mean for the three replicate experiments.

TABLE 22. Anoxic Measurements for Cerium and Europium

Solid	Water	Sample	Sorption Ratio, R_d (mℓ/g)[a] Ce	Eu
Aquifer	Wilcox	1	17 100 (11)	15 200 (7.5)
		2	24 900 (16)	27 900 (9.3)
		3	25 100 (15)	23 700 (9.2)
		Average[b]	19 600 [13]	18 500 [19]
Aquitard	Wilcox	1	8 970 (6.5)	2 670 (5.8)
		2	8 790 (11)	3 970 (9.4)
		3	8 480 (10)	3 900 (8.2)
		Average[b]	8 810 [4.9]	3 030 [13]
Aquifer	Brine	1	956 (5.2)	1 730 (6.0)
		2	1 000 (5.2)	1 800 (6.0)
		3	967 (4.8)	1 650 (5.2)
		Average[b]	973 [2.9]	1 710 [3.3]
Aquitard	Brine	1	332 (5.4)	359 (5.4)
		2	330 (5.5)	354 (5.5)
		3	326 (5.2)	344 (5.2)
		Average[b]	329 [3.1]	352 [3.1]

[a]The values in !arentheses are the standard deviations for a single measurement of the R_d values expressed in percent; these were obtained from the errors associated with the activity measurements and estimated uncertainties for the various parameters entering into the calculation; these estimated uncertainties were propagated using the rule of change of variables in a moment matrix assuming independence of the variables.

[b]Weighted average; the error (%) given is the standard deviation of the mean for the three replicate experiments.

TABLE 23. Aerobic Measurements for Uranium(VI) and Americium

Solid	Water	Sample	Sorption Ratio, R_d (mℓ/g)[a] U(VI)	Am
Aquifer	Wilcox	1	233 (8.1)	89 000
		2	86 (9.6)	134 000
		3	141 (8.6)	108 000
		Average	118 [29][b]	110 000 [12][c]
Aquitard	Wilcox	1	3.82 (67)	19 900
		2	3.37 (75)	17 400
		3	2.89 (85)	21 400
		Average	3.34 [43]	19 500 [5.6][c]
Aquifer	Brine	1	10 900 (7.2)	2 160
		2	9 320 (7.2)	2 190
		3	8 150 (7.2)	2 510
		Average	9 200 [8.3]	2 290 [4.9][c]
Aquitard	Brine	1	594 (7.5)	336
		2	566 (7.5)	319
		3	571 (7.6)	325
		Average	577 [4.4]	326 [1.5][c]

[a]The values in parentheses are the standard deviations for a single measurement of the R_d values expressed in percent; these were obtained from the errors associated with the activity measurements and estimated uncertainties for the various parameters entering into the calculation; these estimated uncertainties were propagated using the rule of change of variables in a moment matrix assuming independence of the variables.

[b]Weighted average; the error (%) given is the standard deviation of the mean for the three replicate experiments.

[c]The error (%) given is the standard deviation of the simple mean.

TABLE 24. Anoxic Measurements for Uranium(VI) and Americium

Solid	Water	Sample	Sorption Ratio, R_d (mℓ/g)[a] U(VI)	Am[a]
Aquifer	Wilcox	1	7.13 (40)	96 800
		2	7.35 (37)	107 400
		3	7.10 (40)	76 800
		Average	7.20 [22][b]	93 500 [9.6][c]
Aquitard	Wilcox	1	1.48 (150)	19 600
		2	1.68 (140)	18 900
		3	1.17 (200)	21 400
		Average	1.44 [92][b]	19 900 [3.8][c]
Aquifer	Brine	1	7 300 (10)	3 790
		2	5 250 (10)	1 910
		3	5 390 (10)	2 330
		Average	5 730 [10][b]	2 680 [2.1][c]
Aquitard	Brine	1	232 (11)	334
		2	235 (11)	306
		3	244 (11)	319
		Average	237 [6.4][b]	319 [2.5][c]

[a]The values in parentheses are the standard deviations for a single measurement of the R_d values expressed in percent; these were obtained from the errors associated with the activity measurements and estimated uncertainties for the various parameters entering into the calculation; these estimated uncertainties were propagated using the rule of change of variables in a moment matrix assuming independence of the variables.

[b]Weighted average; the error (%) given is the standard deviation of the mean for the three replicate measurements.

[c]The error (%) given in the standard deviation of the simple mean.

TABLE 25. Percent Recovery of Cesium, Strontium, and Barium in the Control Samples

Condition	Water	Sample	Percent in Solution		
			Cs	Sr	Ba
Aerobic	Wilcox	1	100	100	99.0
		2	101	101	99.6
		3	100	99.4	99.1
Anoxic	Wilcox	1	100	98.8	96.9
		2	101	99.5	97.8
		3	101	99.3	98.5
Aerobic	Brine	1	98.6	98.4	97.1
		2	99.0	98.5	97.7
		3	98.9	98.3	96.9
Anoxic	Brine	1	99.7	99.4	98.9
		2	101	99.2	98.9
		3	99.3	98.7	98.1

TABLE 26. Percent Recovery of Cerium, Europium, Uranium(VI), and Americium in the Control Samples

Condition	Water	Sample	Percent in Solution			
			Ce	Eu	U(VI)	Am
Aerobic	Wilcox	1	3.11	53.7	96.3	93.9
		2	7.04	55.9	95.7	92.1
		3	8.57	58.0	96.7	93.6
Anoxic	Wilcox	1	48.0	83.0	101	11.1
		2	56.8	85.9	101	7.2
		3	49.1	84.7	101	8.1
Aerobic	Brine	1	94.7	93.2	78.1	77.1
		2	94.6	92.4	77.2	75.6
		3	94.0	91.8	78.9	75.9
Anoxic	Brine	1	29.3	19.1	39.9	0.20
		2	52.9	40.6	35.6	0.30
		3	0.4	1.1	35.5	0.21

TABLE 27. pH Values, Aerobic Conditions[a]

Solid	Water	Sample	pH		
			Sr, etc.	U(VI)	Am
Aquifer	Wilcox	1	8.79	9.09	8.82
		2	8.75	8.54	8.86
		3	8.82	8.46	8.84
Aquitard	Wilcox	1	8.51	8.64	8.94
		2	8.72	8.77	8.89
		3	8.70	8.85	8.89
	Wilcox	1	8.98	9.05	9.05
		2	9.04	9.09	9.02
		3	9.16	9.17	9.01
	Wilcox[b]		8.72	9.07	9.32
Aquifer	Brine	1	7.60	8.15	5.12
		2	7.86	7.58	5.09
		3	7.44	7.26	5.12
Aquitard	Brine	1	5.94	7.42	4.43
		2	5.20	6.59	4.40
		3	4.92	6.07	4.40
	Brine	1	7.16	7.24	6.02
		2	6.86	7.10	5.91
		3	6.75	6.93	6.00
	Brine[b]		6.94	5.65	6.14

[a]Unless otherwise indicated the values are those obtained at the end of the measurement.

[b]The value for the feed solution.

TABLE 28. pH Values, Anoxic Conditions[a]

Solid	Water	Sample	pH		
			Sr, etc.	U(VI)	Am
Aquifer	Wilcox	1	9.30	9.32	9.58
		2	9.30	9.43	9.58
		3	9.32	9.44	9.59
Aquitard	Wilcox	1	9.34	9.39	9.66
		2	9.31	9.37	9.52
		3	9.31	9.40	9.63
	Wilcox	1	9.45	9.39	9.66
		2	9.45	9.43	9.69
		3	9.45	9.40	9.64
	Wilcox[b]		9.47	9.52	
Aquifer	Brine	1	6.32	6.50	5.35
		2	5.20	6.43	4.93
		3	5.07	6.33	4.93
Aquitard	Brine	1	4.36	4.46	4.28
		2	4.34	4.08	4.30
		3	4.32	4.39	4.27
	Brine	1	6.24	6.09	6.53
		2	6.16	6.06	6.55
		3	6.32	6.11	6.51
	Brine[b]		7.97	5.83	6.42

[a]Unless otherwise indicated the values are those obtained at the end of the measurement.

[b]The value for the feed solution.

The sorption ratios for americium are all rather large. There does not seem to be any observable dependence on atmospheric conditions.

It is also important to further emphasize the need to assay both the solution and solid for radioactivity in order to obtain proper answers for some elements. For example, some of the americium numbers reported here are more than a factor of ten larger than those calculated using Eq. 1. Somewhat lesser effects were found for cerium and europium.

SORPTION OF URANIUM(VI) ON ARGILLITE

MEASUREMENT TECHNIQUE

The measurement of the sorption behavior of uranium(VI) on argillite under atmospheric conditions involved geologic materials and groundwaters described earlier (Erdal-1 1979). The procedure used for these measurements at ambient temperature was described before (Erdal-2 1979) except that the amount of wash solution left with the solid was measured. The estimated uranium(VI) concentration was $\approx 4.3 \times 10^{-7}$ M.

RESULTS AND CONCLUSIONS

The results of the uranium(VI) sorption ratios and the final pH values are presented in Tables 29 and 30. The pH of traced feed for sorption was 8.58; that of the untraced feed for desorption was 8.59. The fraction of ^{237}U in the control samples for 1, 2, and 3 week contact times were 100%, 107%, and 98%, respectively.

As expected, uranium(VI) is poorly sorbed on argillite under the conditions used. This is presumably due to the rather high carbonate concentration in these waters, which would strongly complex the uranyl ion. For the smaller particle size (<75 μm) there is a decided increase in sorption ratio. This observation is not understood. However, one should note that the <75-μm particle size material is not a sieve fraction. It was prepared by repeated grindings of the material until the entire sample passed through the sieve. No iron was introduced in the grinding procedure (see below).

TABLE 29. Uranium(VI) Sorption Ratios, Eleana Argillite, CN1, Ambient Temperature[a]

Fraction (μm)	Sorption Time (d)	Desorption Time (d)	R_d (mℓ/g)[a]	Final pH
<75	6.810		21.5(14)	8.78
		19.703	21.3(24)	8.62
	13.807		24.9(12)	8.61
		13.734	31.3(17)	8.52
	20.804		21.2(14)	8.58
		7.905	34.1(18)	8.58
106-150	6.810		2.1(72)	8.56
		19.703	- 2.0(510)	8.13
	13.807		1.7(87)	8.53
		13.734	- 4.6(210)	8.56
	20.804		3.4(43)	8.64
		7.905	6.7(130)	8.62
250-355	6.810		1.9(81)	8.60
		19.703	- 2.4(460)	8.67
	13.807		1.4(105)	8.55
		13.734	- 5.9(180)	8.56
	20.804		3.1(48)	8.63
		7.905	7.4(140)	8.55
355-500	6.810		1.9(82)	8.67
		19.703	- 2.5(440)	8.59
	13.807		1.2(121)	8.50
		13.734	- 6.6(180)	8.52
	20.804		3.1(51)	8.66
		7.903	7.7(150)	8.66

[a]The values in parentheses are the standard deviations for a single measurement of the R_d values expressed in percent; these were obtained from the errors associated with the activity measurements and estimated uncertainties for the various parameters entering into the calculation; these estimated uncertainties were propagated using the rule of change of variables in a moment matrix assuming independence of the variables.

TABLE 30. Uranium(VI) Sorption Ratios, Eleana Argillite, CN2-4, Ambient Temperature[a]

Core and Fraction (μm)	Sorption Time (d)	Desorption Time (d)	R_d (mℓ/g)[a]	Final pH
CN2, <75	6.810		15.4(16)	8.61
		19.703	16.2(31)	8.65
	13.807		13.6(17)	8.61
		13.734	15.7(34)	8.51
	20.804		16.8(15)	8.69
		7.905	22.8(25)	8.54
CN2,355-500	6.810		5.5(31)	8.62
		19.703	7.0(100)	8.61
	13.807		5.1(31)	8.61
		13.734	5.0(123)	8.53
	20.804		7.1(25)	8.69
		7.905	14.5(50)	8.59
CN3, <75	6.810		95.5(8)	8.52
		19.703	84.2(11)	8.59
	13.807		94.9(8)	8.58
		13.734	86.9(11)	8.57
	20.804		107(8)	8.66
		7.905	108(10)	8.68
CN4, <75	6.810		83.2(9)	8.61
		19.703	72.6(11)	8.67
	13.807		74.4(9)	8.61
		13.734	69.0(11)	8.88
	20.804		77.2(9)	8.61
		7.905	89.6(11)	8.62

[a]The values in parentheses are the standard deviations for a single measurement of the R_d values expressed in percent; these were obtained from the errors associated with the activity measurements and estimated uncertainties for the various parameters entering into the calculation; these estimated uncertainties were propagated using the rule of change of variables in a moment matrix assuming independence of the variables.

MEASUREMENTS UNDER CONTROLLED ATMOSPHERE CONDITIONS

SYSTEM INSTALLATION

The equipment needed to perform sorption measurements under reduced oxygen conditions or conditions having a specific atmosphere was purchased and made operational. The two-station controlled atmosphere boxes were manufactured by Vacuum/Atmospheres Co. (model DL-002-S-P). The oxygen concentration is measured by use of a Teledyne trace-oxygen analyzer (model 317-X, special modifications for LASL). The nitrogen gas is cleaned by a Vacuum/Atmospheres Co. gas purification system (model MO-40-2-H). The equipment works very reliably and the oxygen concentration is less than 0.2 ppm. Only measurements under ambient temperature conditions can presently be made.

PREPARATION OF MATERIALS

The solids being used are the same as those previously described. These are the Climax Stock quartz monzonite (core CS7, Erdal-1 1979) and Eleana argillite (core CN3, Erdal-2 1979). Solid samples of these materials were ground under anoxic conditions in a non-iron system using an agate mortar with a 50- or 70-mm agate ball (Tekmar Co., Pulverisette). Each material was graded by use of Tyler sieves (ASTM E-11 specification) into two size fractions, <75 μm and 75-500 μm. The entire sample was ground until it passed into one of these fractions.

The same groundwaters as previously described (Erdal-1,2 1979) were used to prepare the rock-treated waters for granite and argillite. The rock-treated waters were prepared by contacting batches of the groundwater, which had been sparged with high purity nitrogen for at least 1 h with pulverized material (20 to 40 g) that had not been sieved. The contact time was at least two weeks at ambient temperature with a solution volume to solid ratio of 50 mℓ/g. The phases were separated by centrifugation at 7 000 rpm for 1 h followed by filtration through a 0.4-μm Nuclepore filter membrane. All operations were performed in the controlled atmosphere boxes.

The solid samples were also pretreated with the appropriate oxygen-free groundwater by shaking weighed 1-g quantities of the crushed rock with 20 mℓ

of the water for a period of two weeks at ambient temperature under anoxic conditions. The samples were contained in stoppered 40-mℓ polypropylene (Oak Ridge) screw-cap centrifuge tubes. All tubes were washed with deionized water prior to use. The phases were separated by centrifuging at 12 000 rpm (28 000g) for 1 h. The weight of the wash solution remaining with the solid phase was obtained by weighing the tube and solid before and after the pretreatment.

SORPTION OF STRONTIUM, CESIUM, BARIUM, CERIUM, AND EUROPIUM

The sorption of strontium, cesium, barium, cerium, and europium on argillite and granite under anoxic conditions (<0.2 ppm oxygen) was studied. This was done to see if there was any effect of reduced oxygen concentration on the solid since one would not expect any major effect of oxygen on these elements. However, there was also a reduction in the amount of carbon dioxide in the solutions used.

Preparation of Tagged Solutions

The appropriate volumes of the tracer solutions for ^{85}Sr, ^{137}Cs, ^{133}Ba, ^{141}Ce, and ^{152}Eu needed for a set of measurements were evaporated to dryness in a washed polyethylene bottle overnight on a steam bath. Concentrated hydrochloric acid was added and the mixture was taken dry again. The appropriate volume of groundwater was added to the bottle inside the anaerobic box and the mixture was mixed for about 2 d in an orbit shaker. The mixture was filtered through a 0.45-μm Millipore filter and the resulting tracer solution was used for the sorption measurements within about 0.2 d. An aliquot of the final solution was also removed for assay of the initial activity of each of the tracers. This aliquot was acidified with hydrochloric acid before assaying in order to stabilize the solution. The estimated molarities of the tracers were Sr(7.9×10^{-8} M), Cs(3.3×10^{-9} M), Ba(2.4×10^{-8} M), Ce(3.1×10^{-8} M), and Ba(6.3×10^{-8} M) for the argillite samples, and Sr(8.3×10^{-8} M), Cs(1.8×10^{-9} M), Ba(2.5×10^{-8} M), Ce(9.5×10^{-10} M), and Eu (1.3×10^{-9} M) for the granite samples.

Sorption Measurements

Batch sorption measurements were performed using the techniques described earlier (Erdal-1,2 1979). The contact times were 3, 6, and 12 weeks. At the end of the shaking period the samples were centrifuged for one hour at 12 000 rpm (28 000 g). The solid and aqueous phases were separated by transferring the liquid into a clean tube with a plastic transfer pipet. After centrifuging for another hour at 12 000 rpm, the solutions were again tranferred into a clean tube by pipet and centrifuged for 2 h. An aliquot was then taken for assay of the radioactivity. The pH measurements were made on the remainder of the solution. A small amount of the solid was tranferred to a counting vial for activity assay. All the handling of the solid or solution samples was made inside the anaerobic boxes. The assay and calculational methods described earlier (Erdal-1,2 1979) were used.

Results and Conclusions

The results from the 3 week contact time measurements are given in Table 31. The other measurements are still in progress. The initial pH values were all 8.43 and the final granite pH values were 8.56 and 8.52 for the <75 μm and 75-500 μm samples, respectively, while the corresponding final argillite pH values were 8.55 and 8.68, respectively.

The R_d values obtained for strontium, cesium, and barium on the granite are all consistent with the values obtained under aerobic conditions (Erdal-2 1979), particularly when the differences in the particle sizes used are taken into account. However, the values for cerium and europium are significantly larger. Perhaps this is due to the absence of carbon dioxide in the anaerobic studies.

Similarly, the values for cerium and europium on the argillite are also larger than those observed under aerobic conditions (Erdal-1 1979). However, the values for strontium and barium are lower. This must be due to the absence of carbon dioxide in the anaerobic boxes. The values for cesium are consistent with the measurements under aerobic conditions.

TABLE 31. Measurements Under Anoxic Conditions, 20.63-d Contact Time[a]

Sample	Fraction (μm)	R_d (mℓ/g) Cs	Sr	Ba	Ce	Eu
CS7	<75	1 780(2.7)	69.8(2.5)	1 720(1.7)	>2 600	>1 100
	75-500	752(2.4)	19.4(3.8)	245(1.4)	>1 400	>5 300
CN3	<75	1 190(2.2)	32.1(3.1)	288(1.4)	>110 000	>400 000
	75-500	1 020(2.6)	31.9(3.2)	209(1.6)	>128 000	>440 000

[a]The values in parentheses are the standard deviations for a single measurement of the R_d values expressed in percent; these were obtained from the errors associated with the activity measurements and estimated uncertainties for the various parameters entering into the calculation; these estimated uncertainties were propagated using the rule of change of variables in a moment matrix assuming independence of the variables.

SORPTION OF URANIUM(VI)

The measurement of the sorption behavior of uranium(VI) on argillite and granite under anaerobic conditions (<0.2 ppm oxygen) utilized the same geologic materials described earlier (see above). The only change in the experimental method from that used in the aerobic studies (see earlier) was that the tracers were evaporated to dryness before being brought into the anoxic system.

The results from these measurements are given in Table 32. The ambient temperature for the anoxic boxes was 32°C. The desorption measurements are in progress. No loss of ^{237}U from solution was observed in the control samples. It is surprising that no sorption of uranium(VI) was observed under these conditions since it was felt that the reducing potential of these materials could have resulted in the formation of uranium(IV), which could be expected to sorb. This reduction must not be taking place. All values are consistent with the values obtained earlier (Erdal-2,3 1979).

TABLE 32. Uranium(VI) Sorption Ratio Measurements Under Anoxic Conditions, 32°C

Sample	Fraction (μm)	Contact Time (d)	R_d (mℓ/g)
CS7	<75	6.755	0.99 (150)
		13.774	1.20 (130)
		20.803	1.28 (120)
	75-500	6.755	0.97 (150)
		13.774	-0.51 (270)
		20.803	0.35 (400)
CN3	<75	6.755	6.61 (29)
		13.774	8.43 (24)
		20.803	8.91 (23)
	75-500	6.755	5.26 (35)
		13.774	5.76 (32)
		20.907	7.26 (27)

[a]The values in parentheses are the standard deviations for a single measurement of the R_d values expressed in percent; these were obtained from the errors associated with the activity measurements and estimated uncertainties for the various parameters entering into the calculation; these estimated uncertainties were propagated using the rule of change of variables in a moment matrix assuming independence of the variables.

CRUSHED ROCK COLUMN MIGRATION RATE STUDIES

MEASUREMENT TECHNIQUES

Preparation of Columns

Crushed rock column studies have been made on three types of media from the Nevada Test Site: tuff, argillite, and granite. The geologic materials chosen were those on which batch R_d measurements had previously been made in order to provide a comparison with results obtained using columns. The pretreated waters used for the infiltration were prepared using techniques described elsewhere (Erdal-1,2 1979; Wolfsberg 1979).

Water delivery rates were controlled by syringe pumps (Sage Instruments, Model 352). Initially the columns, 0.5 cm inside diameter by 2 to 4 cm long (Bio-Rad Econo-Columns), were run by gravity flow and the syringe pumps were used only to control the delivery rate of water to the top of the column. The actual flow rate through the column was not known. A simple, upflow, 0.4-0.5 cm x 2 cm column was then developed to maintain a known, steady flow rate controlled by the syringe pump. The columns were modified from Bio-Rad Econo-Columns by shortening them to ~2 cm, lining them with Teflon tubing, and placing polyethylene bed supports and a polypropylene Luer fitting on each end.

A summary description of the crushed rock columns studied and the parameters measured are given in Table 33. Each column was characterized in terms of the total column volume (the size of the column calculated from the dimentions of the column), the free column volume (FCV) (measured and used to calculate the effective column porosity), the dry bulk density, the particle size, and the flow rate. Flow rates were determined by weighing the eluate sample delivered in a known time period. Gravity flow columns tended to decrease in flow rate before a steady flow rate was maintained. For example, the first and third YM54 columns began with flow rates of ≈0.08 and 0.07 mℓ/h and decreased to ≈0.04 and 0.03 mℓ/h, respectively. However, the flow rates of the upward-flow columns were found to be relatively constant for a given column, syringe, and pump setting. Upward flow rates ranged from 0.041 to 0.082 mℓ/h. A flow rate of 0.045 mℓ/h for a 2.1-cm long column with a free column volume of 0.224 mℓ would correspond to a flow of ~34 m/y.

The free column volumes of approximately one-third of the columns studied were determined by use of both HTO and $^{131}I^-$. In the iodide case, the ^{131}I breakthrough (leading edge) curve and the rinse (trailing edge) were both used. There was essentially no difference in the values obtained with HTO or with $^{131}I^-$ and all measurements for a given column were averaged irrespective of the method used. For example, the FCV for YM54 obtained with iodide (breakthrough) was 0.177 mℓ and with HTO was 0.182 mℓ. On YM22, the iodide breakthrough method gave 0.249 mℓ and the iodide rinse gave 0.239 mℓ. Another YM22 column (not yet used or included in Table 33) gave 0.208 mℓ with HTO, 0.205 mℓ by the iodide breakthrough method, and 0.199 mℓ by the water rinse method. The values for the CS5 and CS7 granite columns, the CN1 and CN2 argillite columns, and

the JA18, JA37, and YM45 tuff columns were measured using ^{131}I only.

The radionuclides studied were usually added to the column in a minimal (5 to 15 μℓ) volume or "spike." The radionuclides used were primarily ^{85}Sr, ^{137}Cs, and ^{133}Ba, although studies using ^{141}Ce and/or ^{152}Eu were recently begun. Rickert et al. (personal communication, Argonne National Laboratory) had previously noted a cesium concentration dependence for ^{137}Cs sorption on limestone, where the R_d value decreased with increasing concentration. The concentration of cesium in the batch measurements ($\approx 10^{-9}$ M) was $\approx 10^{-3}$ times less than that of the cesium spike added to two YM54 columns. Another YM54 column was, therefore, run with a continuous feed of ^{137}Cs at a concentration comparable to that of the batch measurements in order to determine if the cesium concentration effect also existed for tuff.

In addition to varying the radionuclide loading concentration (of ^{137}Cs) on crushed core columns, the flow rates were also varied for three JA32 tuff columns loaded with ^{85}Sr. Flow rates were varied from 0.082 mℓ/h to 18 mℓ/h. Two of these columns were run by gravity flow and the third was run by the upward flow technique.

Data Acquisition and Analysis

Eluate fractions from each column were collected in closed pre-tared vials. The vials were replaced daily and weighed immediately after removal for determination of the eluate volume. At flow rates of ~0.03 to 0.08 mℓ/h, this represented ≤ 1 to 2 mℓ/d. Each sample was diluted to a known volume, sealed, and saved for measurement of radioactivity. Samples from a given column were counted with a NaI(Tl) detector until activity was observed. If more than one radioisotope had been placed on the column, all samples, beginning with the one in which activity was first detected, were counted on a calibrated, 14%, coaxial Ge(Li) detector. The 4096 channel spectra were recorded in multichannel analyzers and analyzed on-line with a PDP-9 computer by our in-house gamma-ray spectroscopy program, RAYGUN. If only one radioisotope had been added to a column, all eluate fractions were counted with a NaI(Tl) detector.

The activity per mℓ of each fraction collected (and of each tracer, if more than one was used) was plotted against the total volume which had been

eluted at the time the sample was taken. An example of these plots is given in Figure 1 (YM54, third column). A main reason for utilizing column studies is that the behavior of a radionuclide can be observed directly as it flows through the rock. The relative velocity of the radionuclide with respect to the groundwater velocity, or the retardation factor, R_f, can then be related to the distribution coefficient, K_d:

$$R_f = K_d (\rho/\epsilon) + 1$$

where ρ is the bulk density and ϵ is the porosity (FCV/V). Thus, the total volume eluted which corresponded to the peak of each radioisotope was compared to the free column volume (the volume corresponding to the peak of the $^{131}I^-$ or HTO curve) to obtain the retardation factor and, subsequently, the sorption ratio. Since K_d implies reversible equilibrium and batch studies have shown that equilibrium is frequently not attained in a few weeks or months for many cases, it may not be entirely correct to use this equation. However, for calculational purposes it is assumed that the sorption ratio R_d is the same as the distribution coefficient K_d.

Such data can also be represented by a breakthrough curve where the (cumulative) fraction of the total activity is plotted against eluate volume. If the breakthrough curve is symmetrical, the volume where 50% of the activity has been eluted should correspond to the peak of the elution curve. The ^{85}Sr elution and breakthrough curves from the first JA32 column are plotted in Figures 2 and 3.

RESULTS AND CONCLUSIONS

The columns for which data are available are those begun initially to develop techniques. Seventeen columns are described in Table 33. Ten of the columns are still running, with one or more isotopes yet to be eluted. Thus, the conclusions to date should be considered preliminary. The materials and isotopes chosen initially were those for which batch R_d values were known to be low. The exception, ^{85}Sr on YM38, where the R_d values are about ≈14 000 and 22 000 mℓ/g for sorption and desorption, respectively, was begun before the batch

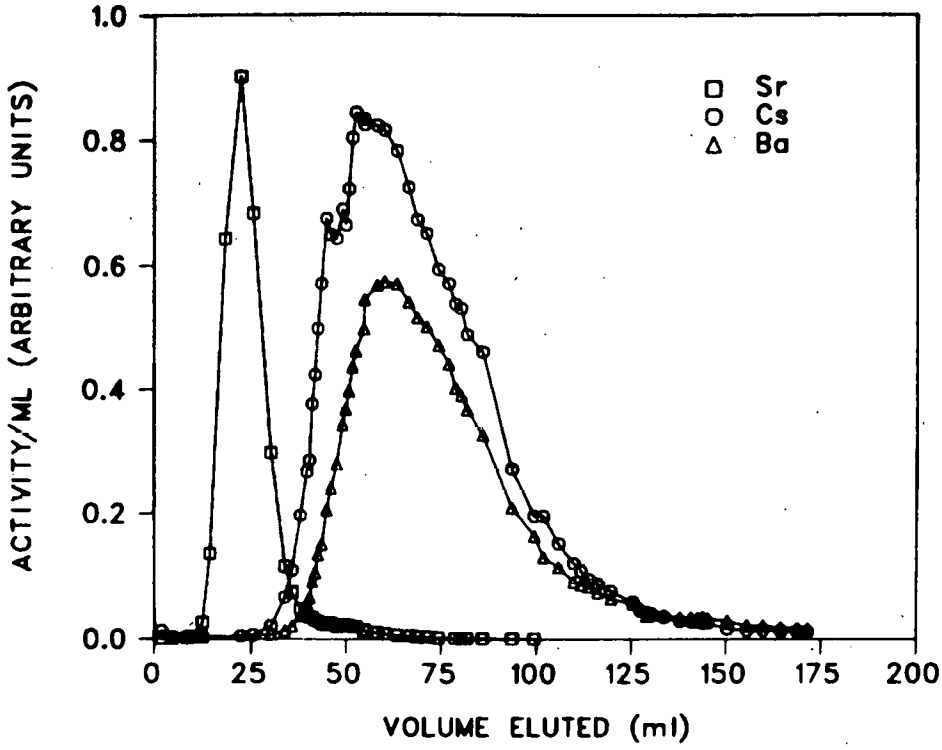

Fig. 1. ^{85}Sr Elution Curve, First JA-32 Column.

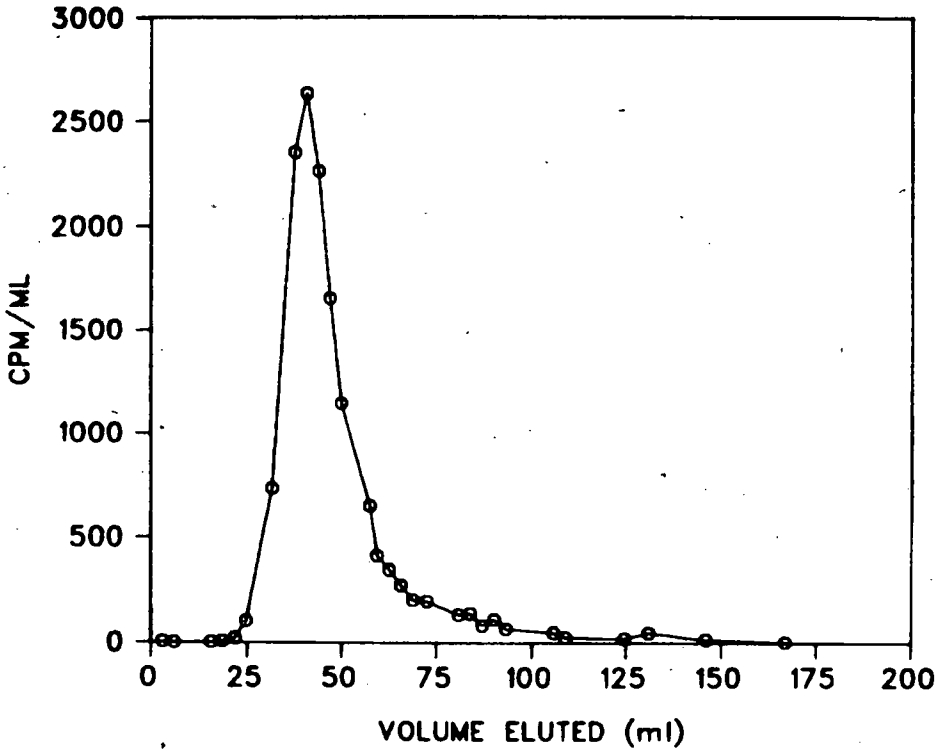

Fig. 2. ^{85}Sr Breakthrough Curve, First JA-32 Column.

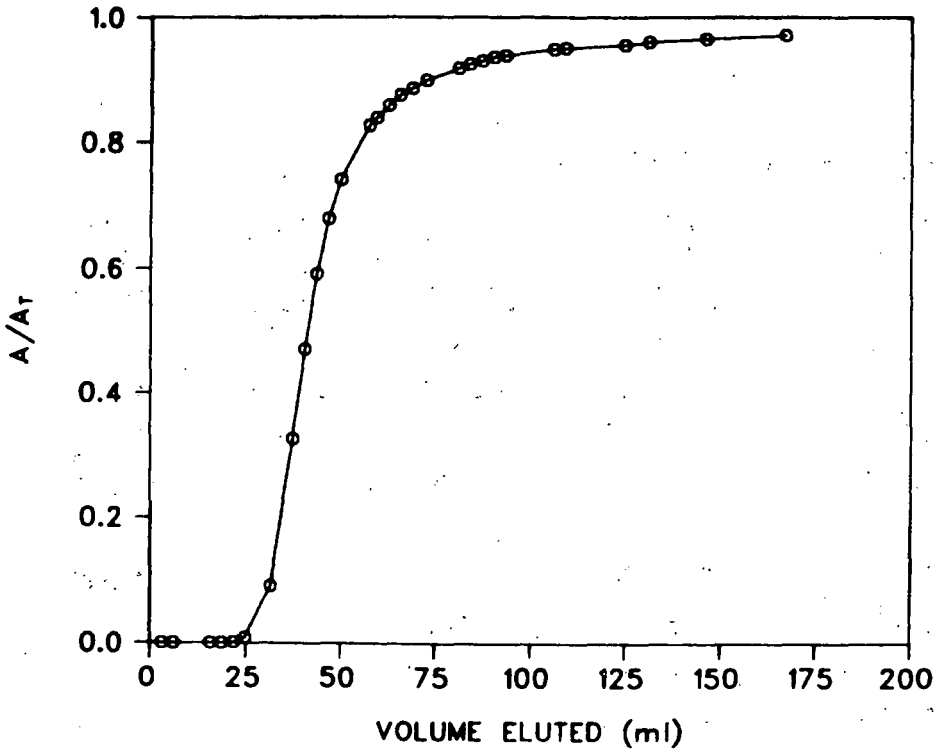

Fig. 3. Breakthrough Curve, First JA32 Column.

measurements had been completed. It is therefore not surprising that no ^{85}Sr has been eluted in ≈240 days. The initial pH values for the waters were 8.12 (YM54), 8.17(JA37), 7.76(JA18), 7.90(argillite), and 7.99(granite). There was little or no pH change of the waters due to flow through the columns.

The R_d values which have been calculated from the column data are given in Table 34. Generally, the peak shapes of the elution curves were reasonably symmetric and the point where 50% of the activity had been eluted corresponded closely to the peak of the elution curve. For example, in Figures 2 and 3 for ^{85}Sr on the first JA32 column, the 50% point was 41.5 mℓ and the peak of the elution curve was at 39.0 mℓ. For all three JA32 columns, the average R_d value calculated from peak volumes was 41.6 mℓ/g and that obtained from the volumes at the 50% point was 43.3 mℓ/g. Since the other columns studied to date also had relatively symmetric peak shapes, the peak volumes were used for convenience to calculate the retardation factors. This made it unnecessary to rely on an external standard as a monitor of total activity, A_t, or to wait until all the activity had been eluted from a column to calculate A_t.

TABLE 33. Descriptions of the Crushed Rock Columns

Material	Particle Size (μm)	Column Size (cm)	Porosity	Bulk Density (g/mℓ)	Flow Rate (mℓ/h)	Expt. Type[a]
Tuff						
YM54	35-106	1.50x0.50	0.793	0.98	0.037	S,G
	35-106	1.50x0.50	0.612		0.067	CF,G
	35-106	2.60x0.50	0.669		0.033	S,G
YM45	106-500	2.10x0.40	0.318			S,U
YM38	35-106	4.00x0.50			0.060	S,G
	106-500	2.12x0.40	0.357			S,U
	106-500	2.45x0.45	0.390			S,U
YM22	35-106	1.90x0.50	0.654	1.16	0.077	S,U
JA37	106-150	2.15x0.45	0.444			S,U
JA32	35-106	4.40x0.49	0.549	0.89	0.131	S,G
	35-106	2.20x0.50	0.678		18.0	CF,G
	35-106	1.80x0.50	0.635		0.082	S,U
JA18	106-150	2.00x0.40	0.562			S,U
Argillite						
CN1	180-250	2.40x0.45	0.592	1.11	0.053	S,U
	180-250	2.43x0.45	0.644	1.18	0.054	S,U
Granite						
CS5	35-106	2.15x0.50	0.597	1.25	0.041	S,U
	35-106	2.10x0.50	0.592	1.26	0.045	S,U

[a]U(upward flow); G(gravity flow); S(spike loading); CF(continuous feed).

TABLE 34. Comparison of Batch and Column Sorption Ratio (mℓ/g) Values

	Sr		Cs		Ba	
Column	Column[a]	Batch[b]	Column[a]	Batch[b]	Column[a]	Batch[b]
YM54	44	84,82	92	247,321	126	652,632
			80			
	44		113		122	
YM22	30	50,57	122	287,365	335	899,824
JA32	52	56,47				
	37					
	35					
CN1	43	138,133	NA	1830,3110	NA	4270,5530
CN2	52	156,131	NA	1580,3810	NA	4900,5650
CS5	8.5	14,19	NA	328,734	32	154,176
CS7	15	18,22	NA	347,533	44	

[a]If no entry appears the corresponding element was not loaded onto the column; NA means that the elution is not yet complete.

[b]The two numbers for the batch results are the mean values obtained under ambient temperature conditions for sorption and desorption, respectively. They were obtained from the following sources: CS5 and CS7 granite, Erdal-2 1979 (106-150, 250-355, and 500-850 μm fractions, ⩽ 4 weeks contact time); CN1 and CN2 argillite, Erdal-1 1979 (<75, 106-150, and 355-500 μm fractions, ⩽ 8 weeks contact time); JA32 tuff, Wolfsberg 1979 (106-150 μm fraction, ⩽ 8 weeks contact time time for sorption and ⩽ 11.5 weeks for desorption); YM54 and YM22 tuff, Erdal-3 1979 (⩽ 106 μm fraction, ⩽ 6 week contact time).

Three general conclusions can be drawn from the results: The ^{85}Sr column R_d value, at least for JA32 tuff is relatively independent of flow rate. Sorption ratios of 37 and 35 mℓ/g were obtained for the first JA32 (gravity flow) column where the delivery rate was 0.131 mℓ/h. (The actual flow rate although unknown, was probably on the order of several mℓ/h.) The higher R_d value obtained for the first JA32 column could perhaps be due to the column being twice as long as the other two, although two YM54 columns, which also varied in length by close to a factor of two, gave identical R_d values for ^{85}Sr. Variations in rate constants and distribution coefficients with bed depth have been noted in the literature (see, for example, Boyd 1947).

The effect of the cesium ion concentration on the R_d value appears to be negligible for the tuff crushed core studied (YM54). Two columns, where ^{137}Cs was loaded at $\approx 10^{-6}$ M, gave R_d values of 113 and 92 mℓ/g. A third column, where the ^{137}Cs concentration was $\approx 10^{-9}$ M, gave an R_d value of 80 mℓ/g. All three values are approximately three times lower than the sorption ratio obtained by a batch technique.

The sorption ratio obtained using the columns analyzed so far were always found to be less than those obtained using the batch technique. The ratios of batch to column sorption ratios are given in Table 35. The biggest differences are factors of about five for ^{133}Ba. In most cases, the agreement between batch and column R_d values are within a factor of two to three. Given the variations in batch measurements themselves, this is fairly good agreement. The flow rates and column sizes used correspond to $\approx 10^{-4}$ cm/sec or ~30 m/y, which, although not slow by geologic standards, are within a reasonable range for flow rates in geologic media ($\sim 10^{-3}$ to 10^{-7} cm/sec). The fact that column sorption ratios (for materials with low R_d values) tend to be smaller could in part be due to the shorter residence times (about 1 d). Perhaps in batch experiment lasting weeks or months, diffusion contributes significantly in cases of low R_d values. This effect would be negligible in a comparatively short column

TABLE 35. R_d (batch) / R_d (column)

Column	Sr	Cs	Ba
YM54	2.0	3.6	5.1
		3.1	
	2.0	2.5	5.3
YM22	1.8	2.7	2.6
JA32	1.0		
	1.4		
	1.4		
CN1	3.1		
CN2	2.8		
CS5	1.9		4.8
CS7	1.3		4.0

experiment. (In fact, a significant difficultly with small crushed core columns, even given good agreement with batch R_d data, will be in relating such data, obtained over small distances in short contact times, to long distances and long contact times.)

Since preliminary data indicated that increasing flow rate did not significantly alter results, experiments were begun to look at isotopes having high R_d values on tuff. The elution of ^{85}Sr on a column of YM38 (average batch R_d ≈18 000) should be done in ≈38 days at a flow rate of ≈3 mℓ/h. Since several liters of water will be required, the column has been prepared; however, ^{85}Sr has not been loaded, since the water is still being pretreated. It will also be important to measure how closely cerium and europium column R_d data agree with batch R_d values since sorption of these elements is most likely not by ion-exchange mechanisms. Such experiments are in progress (YM38 and YM45).

MICROAUTORADIOGRAPHY

Microautoradiography has been employed at LASL as an adjunct to other techniques for studying the sorption properties of certain elements on selected types of rocks. Whereas column or batch sorption methodologies yield information on sorption properties of gross rock, microautoradiography can indicate the specific mineral phase responsible for the sorption. Furthermore, this technique can give insight into the state of aggregation of the sorbed material. Since many of the transuranic elements tend to form polymeric or colloidal species in solution at groundwater pH values, observation of the amount of aggregation in adhering species is very important.

SORPTION OF PLUTONIUM AND NEPTUNIUM ON THIN-SECTIONS

Techniques had been developed earlier (Thompson 1979) for preparing autoradiograms of ^{233}U and ^{241}Am on thin sections of rocks derived from NTS alluvium, tuff, granite and argillite. In general, the same techniques were employed with ^{239}Pu and ^{237}Np.

An effort was made to prepare ^{239}Pu solutions of groundwaters with activity levels which would remain constant with time. All water used for these solutions was filtered through 0.4- and 0.05-μm filters, and the solutions

were stored in capped Teflon tubes. The original plutonium stock solution (in $HClO_4$) was evaporated to dryness, the plutonium was dissolved in distilled water, taken to dryness, and redissolved in the groundwater derived from the alluvial, tuff or granite formation or, in the case of argillite, synthesized to represent the natural groundwater. It was found that plutonium disappeared from these solutions in a period of several days, but could be reproducibly reintroduced (probably in a colloidal form) by placing the Teflon tubes in an ultrasonic bath for a short time. It was thought that this "colloidal" plutonium would settle out on the thin sections under the force of gravity, but experiments conducted with droplets of plutonium solution hanging suspended from the thin section did not produce less activity on the rock surface than when the droplets were sitting on top of the thin-section.

Microautoradiograms were prepared of ^{239}Pu on alluvium, JA25 and JA26 tuff, Climax Stock granite, and Eleana argillite. Complete petrographic analyses of these have not yet been done, but strong sorption by specific minerals seemed to be lacking. Generally the alpha track distribution was fairly uniform, with a number of stars present (indicating aggregated species). It appears that plutonium sorbs rather indiscriminately on rock thin-sections and even on glass. However, it is also true that the amount of sorption on the various rock types varied significantly, with the tuffs showing the least sorption and granite the most. Perhaps some unidentified variable, such as the dissolved species in the groundwaters, is controlling the quantity of deposition on the thin-sections.

Attempts to sorb ^{237}Np on rock thin-sections were hampered by the rather low tendency of the neptunium to sorb (estimated to be lower than plutonium by at least a factor of ten) and by the presence of large amounts of the ^{233}Pa daughter in the radioactive source solution. The ^{233}Pa sorbed strongly on the thin-sections, and the beta radiation from this nuclide exposed the emulsions to the point of obscuring the alpha tracks generated by the ^{237}Np. Two procedures were exployed to purify the Np: a TTA extraction (Burney 1974), and a fluoride precipitation followed by extraction on an ion exchange column. Neither of these procedures gave a very complete separation. Autoradiograms were prepared with alluvium, JA26 tuff, Eleana argillite, and granite thin-sections using a high specific activity solution ($\sim 7 \times 10^6$ dps/mℓ) with the ^{233}Pa in secular equilibrium with the ^{237}Np. In general, the neptunim seemed

to deposit in some aggregated form, as dense clumps of tracks were present on all the thin sections. In the case of the JA26 tuff and the alluvium, there is possibly some association of the tracks with specific minerals. As always, individual alpha tracks were difficult to see against the dark background of the Eleana argillite, but with intense illumination a large number of dense clumps of tracks were visible. The granite showed a broad distribution of tracks and clumps, with no apparent tendency to sorb on specific minerals.

BETA MICROAUTORADIOGRAPHY

A number of autoradiograms were prepared using ^{85}Sr, ^{63}Ni, ^{233}Pa, and ^{90}Sr. Kodak AR.10 strippable emulsion, Kodak liquid emulsions NTB-2 and NTB-3, and a film-backed emulsion "Ultrafilm ^{3}H" (manufactured by LKB, Rockville, Md.) were utilized. Beta tracks (generally spots) were readily visible at moderate surface densities against a clear background, but were difficult or impossible to identify except at very high densities against the mottled backgrounds typical of rock thin-sections. Thus it appears that beta autoradiography may be limited in geologic applications to situations in which high resolution is not required and in which rather large track density can be tolerated.

INFILTRATION OF ROCK CORES

Several experiments involving solutions of radionuclides pumped through solid rock cores were performed. An apparatus similar to the equipment used in FY-78 for permeability measurements was constructed for use as a high-pressure column apparatus. This may be somewhat of a misnomer because the net difference between the confining pressure and the delivery pressure (which equals the effective pore pressure) is normally in the 50- to 100-psi range. The equipment design is based on that of Brace et al. (1968) as modified by Potter (1978) and is shown schematically in Fig. 4. The right circular cylindrical core sample 15.9 mm high and 25.4 mm in diameter is placed in a Teflon sleeve and a porous disk of pressed stainless steel fiber is placed on each end of the sample. Steel cylinders of the same diameter as the sample, with pressure lines attached, are then inserted into the ends of the Teflon

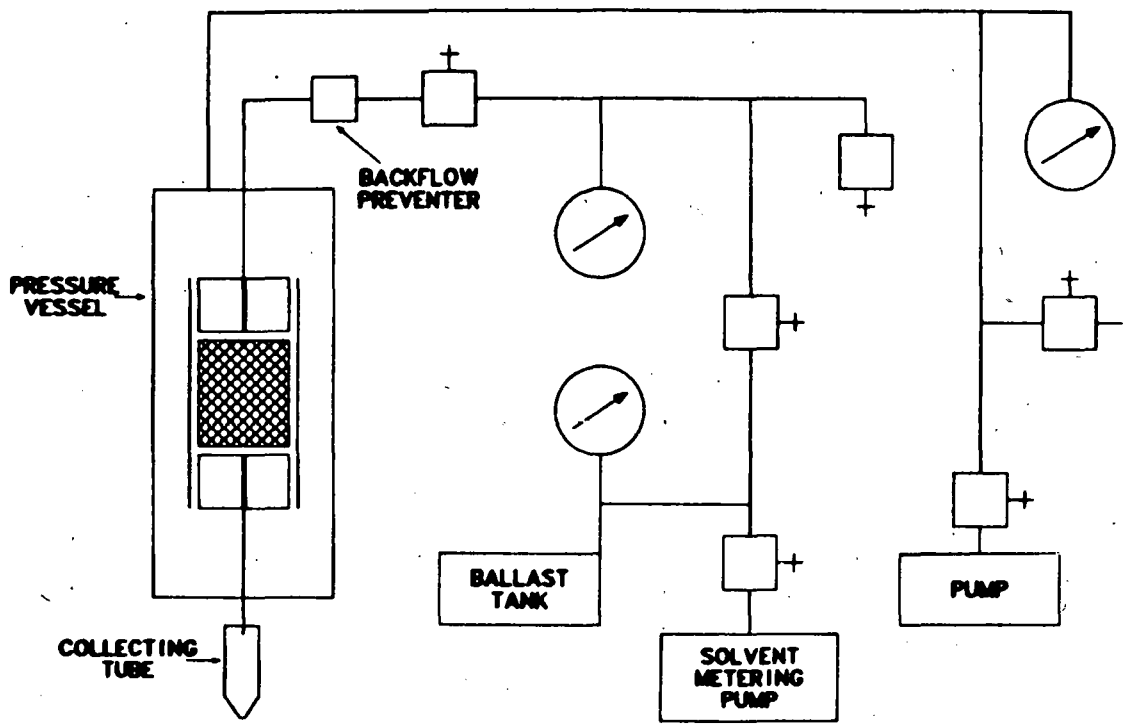

Fig. 4. Schematic of the High-pressure Column Apparatus.

cylinder and the assembly is placed in a pressure vessel, which then is pressurized by a miniaturized air-driven hydraulic pump (Haskel, MCP-88). The stainless steel capillary tubing leading to the collecting tube has a 0.048-cm internal diameter. The delivery pressure is supplied by a metering pump (Altex, model 100A) capable of operation either as a constant-flow metering pump or as a constant-pressure source up to 10^4 psi. It has a minimum metered flow rate of 0.01 mℓ/m and is pressure limiting within the operating range without shut-off. Currently all tubing is stainless steel rated at 60 000 psi. Water was forced through the core at a controlled rate and "pumping pressure" significantly lower than the confining pressure. After the core had been flushed with the appropriate type of groundwater (filtered through 0.4- and 0.05-μm filters), the core was removed, and a small volume of high specific activity solution was placed on the top face. The core was again placed in the pressure assembly, and the rate of transport of the radioactive material through the core was determined by monitoring the activity in the effluent water.

POROSITY MEASUREMENTS

The system described above for studying high-pressure columns was utilized for some preliminary measurements of connected pore space (i.e., free column volume or effective porosity) of tuff and granite cores. The volume of tritiated water required to fill the available pore space of a rock core 2.54 cm in diameter and 1.6 cm thick was measured by liquid scintillation counting. By comparison with the total core volume, the fraction of free space was determined. Three measurements on a tuff core from well J-13 at the NTS, JA35, Core #3, gave values fo 0.233, 0.247, and 0.239 for an average of 0.240 with a spread of ±3%. Measurements on two Climax granite cores gave values of 0.0015 for Core #6A and 0.0050 and 0.0081 for two measurements on Core #2A.

The tritiated water method appears to give satisfactory results for the available pore space in tuff and granite. Limited data suggest that measurement of the low values for granite is less reproducible than for the higher tuff values.

^{233}U in JA26 Tuff

Two experiments were conducted with ^{233}U in the JA26 tuff cores from the Jackass Flats area of the NTS. These experiments were undertaken to allow development of techniques for handling the rock and preparing autoradiograms, rather than to yield much information on sorption characteristics of the rock. After placing the ^{233}U solution on the core and reassembling the pressure apparatus, water was pumped through the core only until appreciable amounts of activity appeared in the effluent. In the first experiment, using mixed isotopes of uranium, 4.8 mℓ of effluent passed through the core. In the second measurement, using isotopically pure ^{233}U, 13.4 mℓ of effluent passed through the column. The pumping rates were 0.3 to 0.7 mℓ/h. The rock core were then sliced perpendicular to the direction of water flow using a small rock saw (Isomet, Model 11-1180).

Several pieces of information were obtained from these two experiments: The ^{233}U activity, which was placed at the center of the top faces of the tuff cores, was found to be spread laterally so that at a depth of about 1 mm there

were no obvious concentration gradients across the diameter of the core. A substantial fraction of the activity was still on the top surface when some of the ^{233}U had passed completely through the core.

The stainless steel frits in contact with the top and bottom surfaces of the core showed some activity, though the amount relative to the total activity was small (see, however, the ^{233}U on granite experiments described below).

The surface activity on the rock cross-sections was measured using emulsions in one of two ways. In the first technique, a microscope slide was coated with Kodak NTB-2 or NTB-3 liquid emulsion, dried, placed against the rock for an appropriate time (until about 10^6 to 10^7 disintegrations had occurred), and developed using standard procedures. This yielded a transparent slide with the alpha tracks readily visible. However, it was difficult to correlate the tracks with their points of origin on the rock with a certainty of better than a few mm. Even with the use of a jig constructed to align the rock core and microscope slide, it was not possible to improve the registration significantly. A second technique involved coating the emulsion directly on the rock, then exposing and developing it while in place. To insure good adhension of the emulsion, an undercoating of parlodion and gelatin had to be applied. The liquid emulsions worked better than the strippable emulsion (Kodak AR.10) for this application. With the emulsion developed in place, registry with the underlying surface was no problem, but viewing the tracks was difficult against the opaque background. The tracks could be illuminated with reflected, polarized light, but the underlying minerals could not be seen well. Thus neither emulsion technique proved to be very useful for identifying specific sorption sites by mineral composition.

It proved to be impractical to slice the tuff cross-sections thinner than about 1.2 mm, as the saw tended to dislodge grains at lesser thicknesses. It was necessary to cool and lubricate the saw blade with a liquid which would not dissolve the uranium sorbed on the rock. Benzene was found to be satisfactory for this purpose.

^{85}SR IN CLIMAX STOCK GRANITE

About 2×10^5 cpm of ^{85}Sr in 50 $\mu\ell$ of solution was placed on the top face of a Climax Stock granite core on February 15, 1979, and filtered synthetic

granite ground water was pumped through the core until July 5, 1979, at an average rate of 0.17 mℓ/d. During the first few days the effluent had a specific activity of about 10^3 cpm/mℓ, and then it fell to about 10^2 cpm/mℓ and was more or less constant (allowing for the decay of ^{85}Sr) until the elution was stopped. The core had what appeared to be a crack running lengthwise through it, so attempts were made using a NaI(Tl) scintillation detector and collimated lead shields to measure enhanced radiation levels in the region of the crack. These efforts were not successful and showed only that the top of the core still contained more activity than other regions. It was found that ^{85}Sr could be detected with a proportional counter and with emulsions, probably because of Auger electron emission initiated by the electron capture decay. Kodak NTB-3 emulsions were used to determine the ^{85}Sr on the surfaces of several cross-sectional slices of this core. No pattern of high concentrations in the vicinity of the "crack" or elsewhere could be found. The tracks produced in the emulsion were generally dots, and were rather difficult to identify unless they were present in high concentrations. The granite could be cut in very thin slices ($\leq$ 0.5 mm), and even slices several mm thick were translucent. The distribution of activity through the core as measured with the NaI(Tl) detector is shown in Fig. 5. It appeared that this activity was distributed through the length of the core with a linear concentration gradient.

^{233}U IN CLIMAX STOCK GRANITE

Climax granite core "2d-3" was placed in the pressure apparatus and flushed with filtered synthetic granite water (about 0.7 mℓ) at a pumping pressure of 550 psi and confining pressure of 1000 psi. Then about 75 µℓ of isotopically pure ^{233}U solution containing about 7.6 µg of uranium and yielding nearly 10^8 disintegrations/m was applied to the top of the core and pumping was resumed at the same pressures previously used. The flow rate varied from 0.1 to 0.3 mℓ/d. About 60% of the activity was eluted in the first 0.5 mℓ, and about 35% in the next 0.6 mℓ. This effluent was concentrated to about 200 µℓ, and reintroduced on the top of the core. Pumping was continued as before until about 0.2 mℓ of effluent was collected and the specific activity began to increase rapidly. The core was removed, several slices were taken

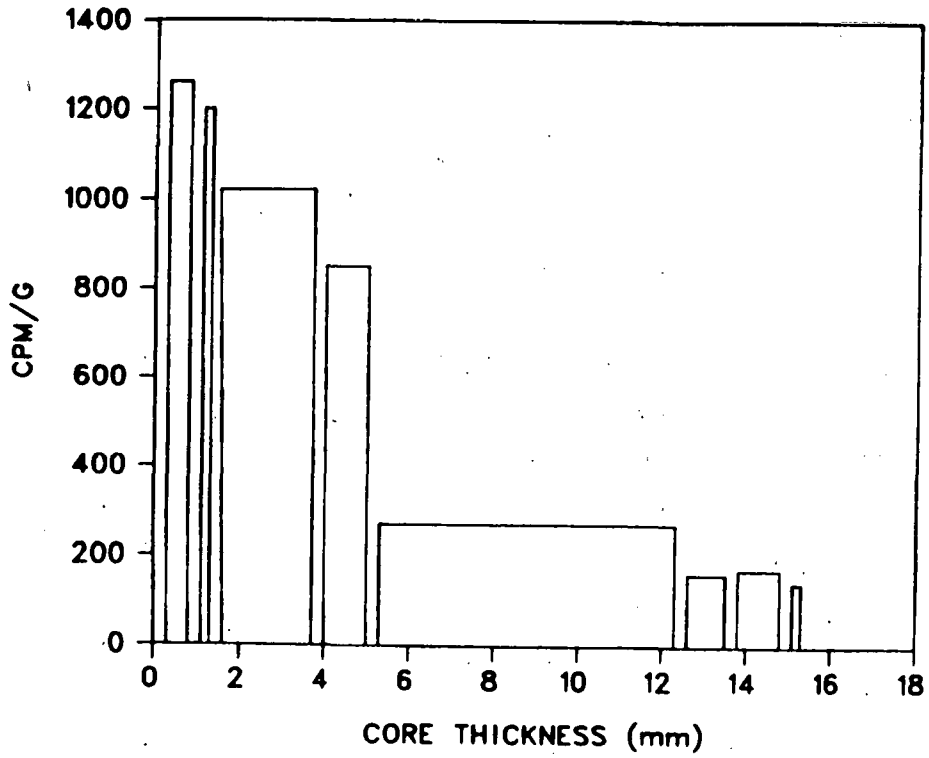

Fig. 5. Strontium Distribution in a Climax Stock Granite Core.

from the top and bottom ends, and the surface activity on the slices was measured with both a proportional counter and with emulsions. Both the top and bottom surfaces of the core showed a high level of activity, as did the stainless steel frits in contact with them. Also, the sides of the core cylinder yielded a high count rate, indicating that some of the radioactive solution had penetrated the sleeve-core boundary. This activity appeared to be evenly distributed over the surface. The activity in the frits was slowly released by rising by a large volume (about 170 mℓ) of water. Some radioactive contamination of the exit tube of the pressure apparatus was observed, though at a much lower activity level than the contamination of the frits.

The emulsions revealed that flow through the core was by means of a very few small cracks, with the majority of the rock mass not coming in contact with the radioactive solution. Some sorption by minerals along the path of flow was indicated (but not yet confirmed by petrographic examination). An apparent radiocolloid was detected at a site along a crack several mm into the core. These observations were documented on 35 mm color film.

A second experiment was performed as an attempt to measure an R_d value for a solid granite core which could be compared with R_d values determined on

crushed granite. No activity peak in the eluate was observed, and there is considerably doubt that all of the eluent actually ran through the core. Climax core C-79-9a-1 was mounted in the pressure apparatus and about 0.15 mℓ of synthetic granite water was flushed through the core at 540 psi. The core was removed from the pressure apparatus and about 50 μℓ of ^{233}U solution was placed on the top surface. This solution had been prepared by taking to dryness 45 mℓ of isotopically pure ^{233}U solution containing about 47 μg of uranium (about 10^7 disintegrations per min), then redissolving it in filtered synthetic granite water. A 1-mm thick disc of the granite was placed on top of the core to provide a barrier between the radioactive material and the metal endpiece. (Unfortunately, some of the ^{233}U solution squeezed up around the edges of the disc.) This material was dried in air, the pressure apparatus was reassembled, checked for leaks, and pumping was initiated at the previous setting of 540 psi. No flow was observed until the pumping pressure was raised to 850 psi. The eluate was collected dropwise using a fraction collector (ISCO Model 1200) contained in a plastic bag with a water-saturated atmosphere. Without this container, it was found that the drops would evaporate rather than fall. The drop rate was about 5 drops per day for several days, then it increased to about 12 drops per day. The drops were collected in small glass cups, dried, and the activity measured with a methane flow proportional counter. Nearly 1.5 mℓ of effluent was collected, and the dropwise distribution of activity is shown in Fig. 6. Although there are a number of fluctuations in the activity level for individual drops, these may be due to uncertainties in the counting procedure used. In any event, there is no well-defined activity peak. The core was examined for residual activity, and it was found that the top, bottom, and sides had high levels of activity (about 10^4 counts per min). At a depth of about 1 mm inside from either the top or bottom, the activity level was reduced by a factor of about 30. The activity was spread more or less uniformly over the exterior surfaces, but seemed to be confined to small crack systems in the interior. It was not possible to tell whether activity found in the interior had entered through the top face of the core or from the side. It appears that the confining pressure of 1000 psi was not sufficient to keep the eluting water (at 850 psi) from penetrating

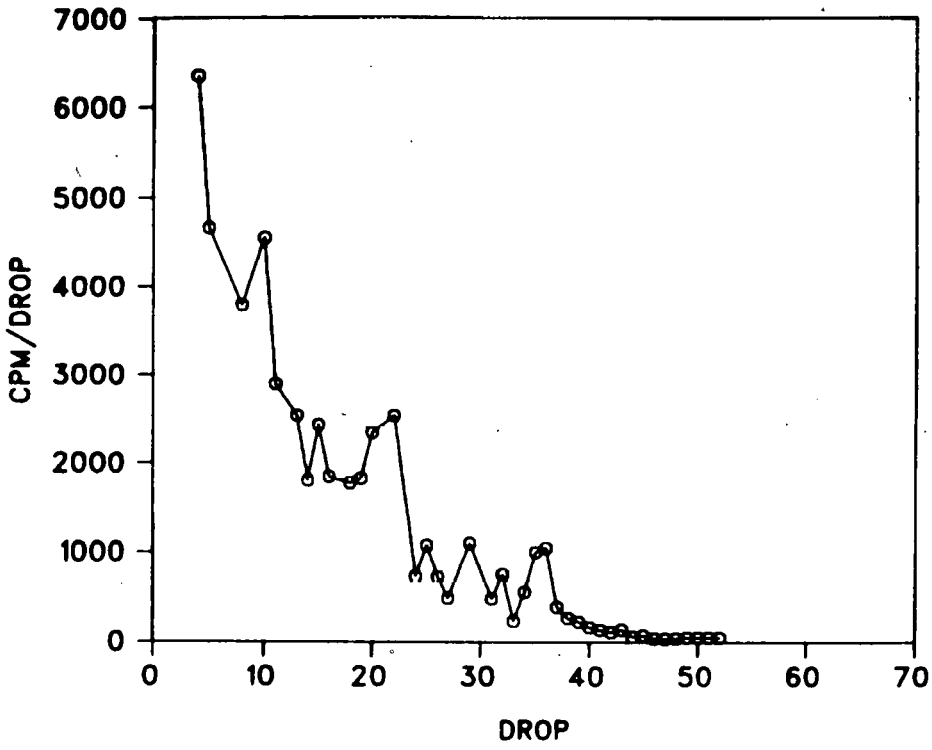

Fig. 6. ^{233}U from a Climax Stock Granite Core.

the Teflon-granite interface. Probably more than half of the activity initially introduced remained on the exterior surfaces of the core when the experiment was ended.

Since pentration of solutions into small crack systems in granite cores had been observed, it was decided to attempt to study flow through a large crack known to extend through the core. An intact core, C-79-16a-3, was selected because it had an apparent fracture plane extending the length of the core. A sharp rap with a hammer and chisel caused it to split cleanly along the old fracture. The inner surfaces of the fracture contained a number of small gold-colored particles (some of which fell out when the core split) which X-ray analysis showed to be iron pyrite. The core sections were recombined, inserted in a Teflon sleeve, and placed in the pressure apparatus as usual. The confining pressure was increased to the point (5000 psi) where water would not flow through the core under the force of gravity. About 3 mℓ of filtered synthetic granite water was then flushed through the core at a rate of 0.3 mℓ/hr. At this point the Teflon sleeve ruptured along the bottom edge of the core where a chip was missing (not near the crack). The core was placed in a new Teflon sleeve, the chip void filled in with epoxy cement, a 1 mm

granite disc inserted as a top endpiece, and about 4 mℓ more of granite water flushed through it, again with a confining pressure of 5000 psi. A ^{233}U solution of the same composition as that used in the two previous experiments was again employed. About 50 μℓ was dried in the center of the top of the core, a distance of several mm from the crack. After reassembly in the pressure apparatus and pressurization to 5000 psi, pumping of water through the core was resumed. Activity was detected in the first 0.5 mℓ of effluent, so the flow was stopped and the core held in this condition for 3 days. Then the core was removed and slices (about 2 to 3 mm thick) were sawed from each end, with the Teflon sleeve holding the fracture pieces together. The slices, as well as the fracture surface of the smaller fragment, were coated with NTB-2 emulsion. The larger fragment was sawed so as to remove the fracture surface with about 2 mm of supporting rock, and it too was coated with emulsion. The top surface of the core showed regions of high track density in the middle and along one segment of the crack. At a depth of several mm tracks were found only along the large crack and along a small crack branching from the large crack and running almost the width of the core. The bottom surface of the core had activity distributed fairly uniformly over it. The interior surfaces of the large crack were difficult to observe with the microscope because of their roughness, but alpha tracks were found spread over most of this surface. There were several regions of very dense tracks on this surface. Identification of the minerals on the surface which appear to sorb ^{233}U strongly is in progress.

MATERIALS CHARACTERIZATION

In order to be able to use the data bank of sorption information for the estimation of the migration behavior of a nuclide in any geologic material and type of water, one must gather the appropriate supporting information for the materials used. A method for rapidly analyzing the groundwaters for the major and minor elements was developed. Similarly, techniques were developed for determination of trace constituents of solids and solutions. Final determinations of surface areas by the ethylene glycol technique were also completed.

X-RAY FLUORESCENCE ANALYSES

Our in-house capability for chemical analysis via tube-excited X-ray fluorescence spectrometry has been used for samples utilized in previous studies (see above; Erdal-3,4,5 1979). This technique is relatively simple and gives results for most major and semi-major elements. In our analysis system, either a tungsten or molybenum target can be chosen as the target for X-ray production by high-voltage electrons. The X-rays from the sample are detected with a Si(Li) detector which is sensitive down to the 1-keV line of sodium. The linear data from the detector is stored in a multichannel analyzer from where it is read into a small computer (PDP-11/04) at the termination of a run. Data reduction programs to perform the analytical calculations have been written locally (T. Bornhorst) for both qualitative and quantitative analysis. The system is calibrated using samples having compositions similar to the unknowns. The results are given in Tables 36-39.

It is interesting that the total iron concentration is these materials does not change with the fraction used. One explanation for the observation (Erdal-1,2 1979) that Tc(VII) sorbed on the finer particle size material was that iron was concentrated in these fractions. This could still be the case if the fine fractions were enriched in the non-Fe(III) materials. This could happen if a clay fraction had some preference for Fe(II) and this clay was concentrated in the finer sieve fraction.

The observation that the total iron (Table 39) concentration in the <75-μm fractions prepared by grinding in an agate system (see earlier) are not appreciably different than those prepared by grinding in a pulverizer is encouraging. This means that the iron introduced during the grinding operation was not significant and that the earlier measurements (Erdal-1,2 1979) were not perturbed by the addition of iron.

ETHYLENE GLYCOL SURFACE AREA MEASUREMENTS

Many sorption ratios are expected to scale with surface area. Table 40 summarizes the measurements performed to date for all materials studied in the first year of the LASL program. The equilibrium glycol procedure (Dyal and

TABLE 36. CS5 Granite X-ray Fluorescence Analyses

Element	Fraction (μm)[a]			
	106-150	250-355	500-850[b]	
K_2O	4.63	4.23	4.67	4.63
CaO	2.98	3.20	3.33	3.32
TiO_2	0.50	0.40	0.44	0.43
Fe_2O_3	3.72	2.96	2.56	2.56
	μg/g			
V	58(9)	51(8)	46(7)	48(8)
Cr	19(11)	14(9)	11(7)	11(6)
Mn	495(7)	379(6)	403(6)	378(6)
Ni	16(5)	10(4)	10(4)	9(3)
Cu	31(6)	24(5)	30(6)	27(6)
Zn	78(9)	75(9)	74(9)	73(9)
Ga	<25	<25	<25	<25
Ge	1.29(0.06)	1.27(0.06)	1.28(0.06)	1.27(0.06)
As	<100	<100	<100	<100
Se	0.05(0.02)	0.04(0.02)	0.05(0.02)	0.04(0.02)
Pb	16(8)	16(8)	<16	18(9)
Rb	193(6)	169(5)	179(6)	181(6)
Sr	564(8)	626(9)	660(9)	657(9)
Y	25(9)	22(8)	24(9)	24(8)
Zr	196(20)	186(19)	178(18)	177(18)
Ba	1 181(118)	1 083(108)	1 103(110)	1 112(111)

[a]The numbers in parentheses are the errors given in μg/g. If no error is listed then it is less than 0.1%.

[b]Duplicate analyses are reported.

TABLE 37. CS7 Granite X-ray Fluorescence Analyses

Element	Fraction (μm)[a]				
	106-150[b]		250-355[b]		500-850
	Percent				
K_2O	3.46	3.42	3.25	3.25	3.93
CaO	3.23	3.20	3.29	3.29	3.14
TiO_2	0.35	0.35	0.29	0.29	0.43
Fe_2O_3	2.82	2.82	2.33	2.33	2.88
	μg/g				
V	46(7)	45(7)	42(7)	42(7)	45(7)
Cr	18(11)	19(11)	14(8)	13(8)	13(8)
Mn	358(5)	347(5)	401(6)	369(6)	659(10)
Ni	11(4)	12(4)	10(3)	9(3)	9(3)
Cu	18(4)	21(4)	19(4)	16(3)	18(4)
Zn	76(9)	76(9)	75(9)	75(9)	78(9)
Ga	<25	<25	<25	<25	<25
Ge	1.29(0.06)	1.30(0.06)	1.29(0.06)	1.28(0.06)	1.28(0.06)
As	<100	<100	<100	<100	<100
Se	0.04(0.02)	0.05(0.02)	0.04(0.02)	0.05(0.02)	0.04(0.02)
Pb	<16	19(9)	<16	<16	<16
Rb	126(4)	124(4)	124(4)	122(4)	167(5)
Sr	547(8)	543(8)	585(8)	587(8)	601(8)
Y	24(8)	24(8)	20(7)	20(7)	23(8)
Zr	184(18)	184(18)	179(18)	180(18)	188(19)
Ba	690(69)	664(66)	770(77)	735(74)	860(86)

[a]The numbers in parentheses are the errors given in μg/g. If no error is present then it is less than 0.1%.

[b]Duplicate analyses are reported.

TABLE 38. Argillite X-ray Fluorescence Analyses

	CN1		CN2	
	Fraction (μm)		Fraction (μm)	
	150-180	355-500	150-180	355-500
	Percent			
K_2O	1.11	1.12	1.79	1.78
CaO	0.99	0.94	0.85	0.84
TiO_2	1.31	1.30	1.20	1.18
Fe_2O_3	7.09	6.76	5.94	5.90
	μg/g			
V	66(11)	58(9)	52(8)	51(8)
Cr	51(31)	47(28)	44(27)	44(27)
Mn	1 236(19)	1 153(17)	507(8)	504(8)
Ni	29(10)	30(11)	29(10)	29(10)
Cu	45(9)	45(9)	47(9)	42(8)
Zn	94(11)	89(11)	96(12)	93(11)
Ga	<25	<25	<25	<25
Ge	1.33(0.06)	1.31(0.06)	1.26(0.06)	1.27(0.06)
As	<100	<100	<100	<100
Se	0.06(0.03)	0.05(0.03)	0.04(0.02)	0.04(0.02)
Pb	72(7)	60(6)	44(22)	51(5)
Rb	57(2)	59(2)	103(6)	124(4)
Sr	153(2)	154(2)	224(3)	222(3)
Y	36(12)	38(13)	35(12)	35(12)
Zr	272(27)	294(29)	176(18)	176(18)
Ba	<25	32(3)	<25	<25

[a]The numbers in parentheses are the errors given in μg/g. If no error is quoted then it is less than 0.1%.

TABLE 39. X-ray Fluorescence Analyses for the <75-μm Fractions

Element	Sample[a] CN3	CS7
	Percent	
K_2O	1.58	3.55
CaO	0.60	3.55
TiO_2	1.39	0.38
Fe_2O_3	6.16	2.32
	μg/g	
V	30(5)	42(7)
Cr	40(24)	13(8)
Mn	399(6)	469(7)
Ni	31(11)	10(3)
Cu	77(15)	29(6)
Zn	85(10)	74(9)
Ga	<25	<25
Ge	1.30(0.06)	1.31(0.06)
As	<100	<100
Se	0.05(0.02)	0.05(0.02)
Pb	55(6)	23(12)
Rb	91(3)	141(4)
Sr	186(3)	589(8)
Y	35(12)	23(8)
Zr	201(20)	206(21)
Ba	180(18)	769(77)

[a]The numbers in parentheses are the errors given in μg/g. If no error is quoted then it is less than 0.1%.

TABLE 40. Surface Area Measurements

Identification	Core	Fraction (μm)	Treatment[a]	Surface Area(m^2/g)
Climax granite	5	106-150	W	8
		250-355	W	4
		500-800	W	7
	7	106-150	W	7,11
		250-355	W	3
		500-850	W	3
Westerly granite			U	<1
Eleana argillite	1	106-150	W	50,47
		250-355	W	63
		355-500	W	45,49
		106-150	U	51,48
		355-500	U	64,64
	2	<75	U	75
	3	<75	U	99
	4	<75	U	92
Argillacious shale NY			U	46
Jackass Flats tuff	18	106-150	W	31
		355-500	W	46
	32	106-150	W	8,8
		355-500	W	9
	37	106-150	W	94,115
Umtanum basalt		355-500	U	3
Oolitic limestone			U	2

[a]W implies that the samples were briefly washed with distilled water to remove dust; U implies that the sample was not washed with distilled water.

Hendricks 1950; Bower and Goertzen 1959; McNeal 1964) was used. Briefly, this procedure consists of wetting a dried and weighed sample of calcium-saturated material with glycol. This is then followed by equilibration in an evacuated desiccator containing an anhydrous calcium chloride-ethylene glycol solvate. The equilibration is repeated until the weights become constant, presumably indicating that only a monolayer remains.

Generally, the granites or granite-type material (Jackass Flats tuff JA18) have low surface areas relative to argillites and tuff. This is presumably due to the high clay/zeolite content in the latter materials, which have considerable internal surface area. The surface areas do not scale strongly with particle size except perhaps for the granites. This is consistent with the observation (Erdal-1,2 1979; Wolfsberg 1979) that the amounts of the various minerals in the sieve fractions are relatively constant.

EMISSION SPECTROMETRY

The Spectrometrics Inc. twenty-channel direct-current plasma-source emission spectrometer allows the simultaneous determination, in a liquid sample, of up to twenty preselected elements. The suite of elements to be determined is selected by inserting a cassette into the instrument so that only certain atomic emission wavelengths are permitted to impinge upon the instrument's elements.

Four multielement cassettes are currently operational,. The cassettes are set up for the following elements: 1) Si, Al, Fe, Mg, Ca, K, Ti, Mn, Au, Ag, Ba, Rb, Sr, Li, V, Ga, and Sn; 2) Li, K, Na, Mg, Al, Rb, Mo, Ti, V, Sc, Bi, Pb, Tl, Hg, Cd, Sb, W, and Ga; 3) Li, K, Na, Mg, Al, Si, B, Be, Se, As, Ge, Ga, Zn, Cu, Ni, Co, Sr, and In; and 4) La, Ce, Pr, Nd, Sm, Eu, Gd, Dy, Tb, Ho, Er, Tm, Yb, Lu, Hf, Ta, Y, and Ga. If it is desired to determine an element not included in one of the multielement cassettes, it is possible to do so by using a variable single-element cassette.

Five water samples which had been analyzed by the USGS (Erdal-1,2 1979; Wolfsberg 1979) by atomic absorption (AA) spectrophometry were subjected to analysis using the plasma emission spectrometer (ES). The results obtained by the two different methods are given in Table 41. The sample identification

numbers are those assigned to a Climax Stock (W-10) and Eleana Argillite (W-5) ambient temperature pretreated water, ambient temperature pretreated waters for JA-32 (W-14) and JA-37 (W-16) tuffs, respectively, and a 70°C pretreated water for JA-37 (W-17) tuff.

Regression calculations were performed for each set of analyses for each of the five samples. Perfect agreement between the two sets (AA and ES) is indicated by a correlation coefficient and slope of the regression line equal to one and an intercept of the regression line equal to zero. The values obtained are given in Table 42.

It would appear that the USGS uses charge balance between major cations and anions as a primary quality control mechanism for the analysis of water samples. The ions used are Ca, Mg, K, and Na for the cations, and HCO_3, CO_3, Cl, F, and SO_4 as the anions. The milliequivalents per liter of each species is calculated, and the anions and cations are summed separately. An average of the sums is taken and a percent difference is calculated by dividing the deviation from the average by the average and multiplying by 100. This was done for each of the five water samples compared in this study, using the USGS values for the anions, and the ES values for the cation values. These are also shown in Table 42. A perfect analysis would have a percent difference equal to 0.

From these data, one may conclude that the emission spectroscopy technique gives results for these waters that are quite consistent with those achieved by the much more laborious atomic absorption method of analysis. Of the nine elements listed only barium was significantly different by the two methods. It may be speculated that this is due to an change in the water, as they were not preserved in any manner, or to an unknown deficiency in one or both techniques.

TABLE 41. Comparison of Atomic Absorption and Emission Spectroscopy Analyses

	Sample[a]									
	W-5		W-10		W-14		W-16		W-17	
	ES	AA	ES	AA	ES	AA	ES	AA	ES	AA
Mg	2.1	2.0	2.1	2.0	0.92	0.8	0.91	0.9	0.40	0.30
SiO_2	18	22	61	58	51	39	33	27	45	39
Ca	10.1	11	12.8	13	6.2	7.2	7.7	8.9	4.4	5.2
Fe	0.2	0.1	0.06	0	0.6	0.5	0.05	0.04	0.04	0.02
Sr		0.03	0.04	0.06[b]	0.05	0.05	0.1	0.1	0.06	0.07
				0.04						
Ba		0.30	0.04	0.2	0.12	0.3	0.12	0.08	0.08	0.20
Li	0.06	0.02	0.05	0.05	0.04	0.06	0.03	0.06	0.03	0.05
K	3.6	2.9	4.6	4.7	5.6	6.0	8.4	8.6	5.1	5.6
Na	8.9	7.7	41	47	50	60	52	65	53	64

[a]All values are in ppm.

[b]Two values were reported by the USGS.

TABLE 42. Regression Data and Equality Control Data

	W-5	W-10	W-14	W-16	W-17
R[a]	0.990	0.994	0.967	0.981	0.984
Slope	1.196	1.004	0.974	1.142	1.068
Intercept	-0.808	0.321	0.259	-0.657	-0.112
Σ meq$^+$	0.93	2.71	2.70	2.89	2.68
Σ meq$^-$	1.09	2.88	2.88	3.35	3.05
$(\Sigma+) + (\Sigma-)/2$	1.01	2.80	2.79	3.12	2.86
% Diff.	7.8	3.0	3.2	7.4	6.6

[a]Correlation coefficient.

REPORTS AND PUBLICATIONS

1. B. R. Erdal, R. D. Aguilar, B. P. Bayhurst, W. R. Daniels, C. J. Duffy, F. O. Lawrence, S. Maestas, P. Q. Oliver, and K. Wolfsberg, "Sorption-Desorption Studies on Granite," Los Alamos Scientific Laboratory report LA-7456-MS (1978).

2. B. R. Erdal, R. D. Aguilar, B. P. Bayhurst, P. Q. Oliver, and K. Wolfsberg, "Sorption-Desorption Studies on Argillite," Los Alamos Scientific Laboratory report LA-7455-MS (1978).

3. J. L. Thompson and K. Wolfsberg, "Applicability of Microautoradiography to Sorption Studies," Los Alamos Scientific Laboratory report LA-7609-MS (1979).

4. B. R. Erdal, Ed., "Laboratory Studies of Radionuclide Distributions Between Selected Groundwaters and Geologic Media, October 1 - December 31, 1978," Los Alamos Scientific Laboratory progress report LA-7638-PR (1979).

5. B. R. Erdal, W. R. Daniels, D. C. Hoffman, F. O. Lawrence, and K. Wolfsberg, "Sorption and Migration of Radionuclides in Geologic Media," Scientific Basis for Nuclear Waste Management (Plenum, NY, 1979), p. 423.

6. B. R. Erdal, Ed., "Laboratory Studies of Radionuclide Distribution Between Selected Groundwaters and Geologic Media, January 1 - March 31, 1979," Los Alamos Scientific Laboratory progress report LA-7780-PR (1979).

7. B. R. Erdal, Ed., "Laboratory Studies of Radionuclide Distributions Between Selected Groundwaters and Geologic Media, April 1 - June 30, 1979," Los Alamos Scientific Laboratory report LA-7893-PR (1979).

8. B. R. Erdal, B. P. Bayhurst, B. M. Crowe, W. R. Daniels, D. C. Hoffman, F. O. Lawrence, J. R. Smyth, J. L. Thompson, and K. Wolfsberg, "Laboratory Studies of Radionuclide Transport in Geologic Media," IAEA/OECD Symposium on the Underground Disposal of Radioactive Wastes, Otaniemi, Finland, July 2-6, 1979 (to be published).

9. J. R. Smyth, J. L. Thompson, and K. Wolfsberg, "Microautoradiographic Studies of the Sorption of U and Am on Natural Rock Samples" (submitted to the Journal of Radioactive Waste Management.)

10. B. R. Erdal, B. P. Bayhurst, W. R. Daniels, S. J. DeVilliers, F. O. Lawrence, E. N. Vine, and K. Wolfsberg, "Parameters Affecting Radionuclide Migration in Geologic Media," Symposium on the Scientific Basis for Nuclear Waste Management, Materials Research Society, Boston, MA, November 26-29, 1979 (to be published).

11. B. R. Erdal, B. P. Bayhurst, W. R. Daniels, S. J. DeVilliers, F. O. Lawrence, J. L. Thompson, E. N. Vine, and K. Wolfsberg, "Parameters Affecting Radionuclide Migration in Argillaceous Media," Workshop on the Use of Argillaceous Materials for the Isolation of Radioactive Waste, OECD Nuclear Energy Agency, Paris, France, September 10-12, 1979 (in press).

ORAL PRESENTATIONS

1. B. R. Erdal, W. R. Daniels, D. C. Hoffman, F. O. Lawrence, and K. Wolfsberg, "Sorption and Migration of Radionuclides in Geologic Media," Symposium on Science Underlying Radioactive Waste Management, Materials Research Society, Boston, Massachusetts, Nov. 28 - Dec. 1, 1978.

2. W. R. Daniels, F. O. Lawrence, P. Q. Oliver, and S. Maestas, "Sorption of Pu and Am on Tuff, Granite, and Argillite," Joint ACS/CSJ Symposium on Radioactive Waste Disposal, Honolulu, Hawaii, April 1-6, 1979.

3. J. R. Smyth, K. Wolfsberg, and J. L. Thompson, "Microautoradiographic Studies of U and Am Sorption on Minerals," Joint ACS/CSJ Symposium on Radioactive Waste Disposal, Honolulu, Hawaii, April 1-6, 1979.

4. B. R. Erdal, "Studies of the Behavior of Radionuclides in Geologic Media," University of Oslo, Oslo, Norway, June 21, 1979.

5. B. R. Erdal, "Radionuclide-Geologic Media Interactions," Chalmers University of Technology, Göteborg, Sweden, June 25, 1979.

6. B. R. Erdal, "A Field Study of Radionuclide Migration," Studsvik Energiteknik AB, Studsvik, Sweden, June 27, 1979.

7. B. R. Erdal, B. P. Bayhurst, B. M. Crowe, W. R. Daniels, D. C. Hoffman, F. O. Lawrence, J. R. Smyth, J. L. Thompson, and K. Wolfsberg, "Laboratory Studies of Radionuclide Transport in Geologic Media," IAEA Symposium on the Underground Disposal of Radioactive Wastes, Otaniemi, Finland, July 2-6, 1979.

8. B. R. Erdal, B. P. Bayhurst, W. R. Daniels, S. J. DeVilliers, F. O. Lawrence, J. L. Thompson, E. N. Vine, and K. Wolfsberg, "Parameters Affecting Radionuclide Migration in Argillaceous Media," Workshop on the Use of Argillaceous Materials for the Isolation of Radioactive Waste, OECD Nuclear Energy Agency, Paris, France, September 10-12, 1979.

9. B. R. Erdal, B. P. Bayhurst, W. R. Daniels, S. J. DeVilliers, F. O. Lawrence, E. N. Vine, and K. Wolfsberg, "Parameters Affecting Radionuclide Migration in Geologic Media," Symposium on the Scientific Basis for Nuclear Waste Management, Materials Research Society, Boston, MA, November 26-29, 1979.

VISITORS

1. Prof. Ivars Neretnieks, Royal Institute of Technology, Stockholm, Sweden (University of California, Berkeley); Feb. 6-7, 1979.

2. Prof. Jan Rydberg, Chalmers Institute of Technology, Göteborg, Sweden; March 30, 1979.

3. W. R. Davison and D. Hanson, General Atomic Co., San Diego, CA; May 1, 1979.

4. T. T. Vandergraaf, Whiteshell Nuclear Research Establishment, AECL, Pinawa, Manitoba, Canada; May 14-15, 1979.

5. P. J. Shirvington, Environmental and Public Health Unit, Australian Atomic Energy Commission, Cliffbrook, Coogee, NSW, Australia; July 16-18, 1979.

6. B. M. Allard, Chalmers Institute of Technology, Göteborg, Sweden; August 16-17, 1979.

BIBLIOGRAPHY

Brace, W. R., J. B. Walsh, and W. T. Frangos. 1974. "Permeability of Granite Under High Pressure." J. Geophys. Res. 73:2225.

Bower, C. A., and J. O. Goertzen. 1959. "Surface Area of Clays and Soils by an Equilibrium Ethylene Glycol Procedure." Soil Sci. 87:289.

Boyd, G. E., L. S. Myers, Jr., and A. W. Adamson. 1974. "The Exchange Adsorption of Ions from Aqueous Solutions by Organic Zeolites. III. Performance of Deep Adsorbent Beds Under Non-equilibrium Conditions." J. Am. Chem. Soc. 69:2849.

Burney, G. A., and R. M. Harbour. 1974. Radiochemistry of Neptunium. NAS-NS-3060. National Academy of Sciences - National Research Council.

Dyal, R. S., and S. B. Hendricks. 1950. "Total Surface of Clays in Polar Liquids as a Characteristic Index." Soil Sci. 69:421.

Erdal, B. R., R. D. Aguilar, B. P. Bayhurst, P. Q. Oliver, and K. Wolfsberg. 1979. Sorption-Desorption Studies on Argillite. LA-7455-MS. Los Alamos Scientific Laboratory. Los Alamos, NM. (Erdal-1 1979).

Erdal, B. R., R. D. Aguilar, B. P. Bayhurst, W. R. Daniels, C. J. Duffy, F. O. Lawrence, S. Maestas, and K. Wolfsberg. 1979. Sorption-Desorption Studies on Granite. LA-7456-MS. Los Alamos Scientific Laboratory. Los Alamos, NM. (Erdal-2 1979).

Erdal, B. R. (Ed.). 1979. Laboratory Studies of Radionuclide Distributions Between Selected Groundwaters and Geologic Media, October 1 - December 31, 1978. LA-7638-PR. Los Alamos Scientific Laboratory. Los Alamos, NM. (Erdal-3 1979).

Erdal, B. R. (Ed.). 1979. Laboratory Studies of Radionuclide Distributions Between Selected Groundwaters and Geologic Media, January 1 - March 31, 1979. Los Alamos Scientific Laboratory. Los Alamos, NM. (Erdal-4 1979).

Erdal, B. R. (Ed.). 1979. Laboratory Studies of Radionuclide Distributions Between Selected Groundwaters and Geologic Media, April 1 - June 30, 1979. Los Alamos Scientific Laboratory. Los Alamos, NM. (Erdal-5 1979).

Grebenshchikova, V. I., and Yu. P. Davydov. 1965. "State of Pu(IV) in the Region of pH = 1.0-2.0 at a Plutonium Concentration of $2 \cdot 10^{-5}$ M." Radiokhimiya 7:191.

McNeal, B. L. 1964. "Effect of Exchangeable Cations on Glycol Retention by Clay Minerals." Soil Sci. 97:96.

Polzer, W. L., and F. J. Miner. 1976. Plutonium and Americium Behavior in the Soil/Water Environment. BNWL-2117. Battelle Pacific Northwest Laboratories. Richland, WA.

Potter, J. M. 1978. Experimental Permeability Studies at Elevated Temperature and Pressure of Granite Rocks. LA-7224-T. Los Alamos Scientific Laboratory. Los Alamos, NM.

Smith, H. L. (Ed.) 1975. Collected Radiochemical Procedures. LA-1721, 4th Ed. Los Alamos Scientific Laboratory. Los Alamos, NM.

Thompson, J. L., and K. Wolfsberg. 1979. Applicability of Microautoradiography to Sorption Studies. LA-7609-MS. Los Alamos Scientific Laboratory. Los Alamos, NM.

Wolfsberg, K., B. P. Bayhurst, B. M. Crowe, W. R. Daniels, B. R. Erdal, F. O. Lawrence, A. E. Norris, and J. R. Smyth. 1979. Sorption-Desorption Studies on Tuff. LA-7480-MS. Los Alamos Scientific Laboratory. Los Alamos, NM.

QUESTIONS AND ANSWERS

LASL

Kd Measuring

Q: What was the container?

A: Polypropylene Oak Ridge type.

Q: Under what conditions would you centrifuge?

A: 12,000 RPM.

Q: One hour or two hours? For how long?

A: Three times for one hour, and one hour and two hours. If you do a rough calculation you find out you should remove the particles down to pretty small particle size, certainly less than 0.02 microns.

Kd Experimental Parameters

Q: You had an equation earlier relating to the distribution coefficients of the column volumes flowing through and used the word "density". What did you mean by the "density"? Is that the bed density or is it the density of the material?

A: Bulk density.

Q: Well, I think that may account for the small error there.

A: I'm not talking about whole density. I'm talking about the crushed rock density, per unit volume.

Q: I'm wondering about the form of the effluent curve for the Jackass Flat tuffs in these experiments in which you used a wide variation in flow rate. Did you notice any narrowing of the width of the effluent curve at high flow rate?

A: The curve shape was just about identical in the two experiments. If I plotted them they would look just about the same. There wasn't very much difference at all.

Q: How were the columns saturated with water? Did you add the spike to the dry crushed column?

A: No, the columns were prepared first. The pre-equilibrated water was passed through the columns for a few days. Then the tritium or iodide elutions were made. The same pre-equilibrated water was passed through the column. For the upflow columns actually the spike was loaded and the columns were flipped over and then run out. The columns were definitely wet.

Q: I wonder if Silvia Devilliers could tell us if she has a working hypothesis for either cerium or europium isotopes?

A: Well, we established the formation of colloids under high sodium and sulfate concentrations and these colloids would take them out with the solids. We went from 7 to 70 ppm of sulfate in those waters, and sulfate is known to enhance the formation of colloids.

Q: In all types of materials? Who knows?

Q: You had a pretty large increase in your carbonate concentration, too. That was the major anion in those solutions, wasn't it?

A: Yes, that's true.

Colloid Formation and Transport

With reference to a radiocolloid 0.2 mm in diameter, deposited in a cracked system, 0.3 mm down from the surface from the initial rock core, 0.3 mm in from one surface edge. Thompson believes this colloid to have been carried that far into the rock core. This, he believes, has interesting applications regarding the transport of radionuclides through very small crack systems in hard rock types.

Q: Are you saying that a colloid of this size will move as an entity?

A: I believe that's the case. Now, the colloid isn't that size, the tracks are 0.2 mm - the colloid is much smaller. The rock distribution from this colloid is an enormous entity.

Q: But the colloid has to move as a body?

A: Yes.

Autoradiography

Q: Can I direct a question to Joe Thompson? This technique of microautoradiography helps me with the radioassay of thin sections if I can get my detector down low enough. I'm also considering looking at this and using this in conjunction with an ion probe. It will take a couple of months before I know if it will work. I'll take that thin section and put some radionuclides on it and see where they go by means of the ion probe.

C: I'm kind of glad to see somebody is using this technique. I've been thinking about this for a while myself. I don't know if I'll get to do it. But it looks like in the case that you have here, you told me that your flow was because of the physical structure in the cracks in terms of sorption/desorption. I think that's a characterization of something in the rocks and you use that technique to tell me something about the characteristic of the rock bed.

C: Along the same lines, there has been considerable work in the last 5 years -- much has come out of Carnegie in Washington out of their geophysical laboratory, where they have used tracers to experimentally determine properties of phase crystallization. In a sense they worked with spiked crystalline batch materials and at the end of their experiment they used tracking techniques to determine partitioning (I do not want to get it confused with the Kds), but partitioning coefficients for trace elements in fission materials -- and these have been successfully used for many years, especially the last 2 or 3 years, and there is a whole batch of literature that you might find very helpful.

Q: First of all, I think that your work has shown us very well once again that we cannot expect to take a bunch of pure minerals from Wards or wherever, shake them up in a jar, and get something as good as a rock. I'm wondering now, do you intend to try to identify by microprobe or whatever what those phases were actually doing during sorbing?

A: I don't intend to, but that work is being conducted.

DISTRIBUTION

No. of Copies

OFFSITE

A. A. Churm
DOE Patent Division
9800 S. Cass Avenue
Argonne, IL 60439

27 DOE Technical Information Center

John A. Apps
Lawrence Berkeley Laboratory
University of California
One Cyclotron Road
Building 90/1140C
Berkeley, CA 94720

Charles Baes
Oak Ridge National Laboratory
P. O. Box X
Oak Ridge, TN 37830

S. J. Basham
Office of Nuclear Waste Isolation
Battelle Memorial Institute
505 King Avenue
Columbus, OH 43201

Randy L. Bassett
Bureau of Economic Geology
University of Texas
University Station, Box X
Austin, TX 78712

Chuck Bazan
Lawrence Livermore Laboratory
P.O. Box 808
Livermore, CA 94550

Gary Beall
Radian Corporation
8500 Shoal Creek
Austin, TX 78766

No. of Copies

Larry Benson
Lawrence Berkeley Laboratory
University of California
1 Cyclotron Road
Building 90/1140G
Berkeley, CA 94720

Dr. Ernest A. Bondietti
Oak Ridge National Laboratory
P. O. Box X, Bldg. 3504
Oak Ridge, TN 37830

J. Braithwaite
Sandia Laboratories
Nuclear Waste Experimental Programs
Division 4512
Albuquerque, NM 87115

Gary Brock
Battelle, Human Affairs Research Center
4000 NE 41st St.
Seattle, WA 98105

Doug G. Brookins
University of New Mexico
Department of Geology
Albuquerque, NM 87131

Steve Brown
Lawrence Berkeley Laboratory
University of California
One Cyclotron Road
Building 90/1140C
Berkeley, CA 94720

H. B. Brugger
Office of Nuclear Waste Isolation
Battelle Memorial Institute
505 King Avenue
Columbus, OH 43201

No. of
Copies

Jerry Bucher
Lawrence Berkeley Laboratory
University of California
70A-2223
One Cyclotron Road
Berkeley, CA 94720

H. C. Burkholder
Office of Nuclear Waste
Isolation
Battelle Memorial Institute
505 King Avenue
Columbus, OH 43201

J. L. Burnett
Office of Basic Energy Sciences
U.S. Department of Energy
Washington, D.C. 20545

Wayne A. Carbiener
Office of Nuclear Waste
Isolation
Battelle Memorial Institute
505 King Avenue
Columbus, OH 43201

W. T. Carnall
Argonne National Laboratory
Chemistry Division
9700 South Cass
Argonne, IL 60439

H. Clyde Claiborne
Oak Ridge National Laboratory
P. O. Box X
Oak Ridge, TN 37830

Jess M. Cleveland
U.S. Geological Survey
Box 25046, MS-412
Denver Federal Center
Lakewood, CO 80225

David G. Coles
Lawrence Livermore Laboratory
L-233
P. O. Box 808
Livermore, CA 94550

No. of
Copies

Pete Colombo
Brookhaven National Laboratory
Dept. of Applied Science
Upton, NY 11973

Carl R. Cooley
Office of Waste Management
U.S. Department of Energy
Washington, D.C. 20545

Rex Couture
Chemical Engineering Division
Argonne National Laboratory
9700 S. Cass Ave.
Argonne, IL 60439

Williams R. Daniels
Los Alamos Scientific Laboratory
MS-514
Los Alamos, NM 87545

Jared Davis
Nuclear Regulatory Commission
Washington, DC 20555

George DeBuchananne
U.S. Geological Survey
Reston, VA 22092

Sylvia DeVilliers
Los Alamos Scientific Laboratory
MS-514
Los Alamos, NM 87545

R. G. Dosch
Sandia Laboratories
P. O. Box 5800
Albuquerque, NM 87115

Norm Edelstein
Lawrence Berkeley Laboratory
1 Cyclotron Road
Berkeley, CA 94720

Dr. Geoffrey G. Eichholz
School of Nuclear Engineering
Georgia Institute of Technology
Atlanta, GA 30332

No. of Copies

Merril Eisenbud
New York University
Medical Center
Box 817
Tuxedo, NY 10987

W. Eister
Office of Waste Management
U.S. Department of Energy
Washington, D.C. 20545

Dr. Bruce R. Erdal
Los Alamos Scientific Laboratory
CNC-11, MS-514
P. O. Box 1663
Los Alamos, NM 87545

Fred Ernsberger
Box 11472
Pittsburgh, PA 15238

D. R. Fortney
Sandia Laboratories
P. O. Box 5800
Albuquerque, NM 87115

Chet W. Francis
Environmental Sciences Division
Oak Ridge National Laboratory
Building 1505
Oak Ridge, TN 37830

Sherman Fried
Argonne National
9700 S. Cass Ave.
Argonne, IL 60439

Steven Fritz
E. I. duPont De Nemours Co.
Savannah River Laboratory
Aiken, SC 29801

A. J. Gancarz
Los Alamos Scientific Laboratory
P. O. Box 1663
Los Alamos, NM 87545

No. of Copies

Robert G. Garvin
E. I. duPont DeNemours Co.
Savannah River Laboratory
Aiken, SC 29801

Richard L. Hahn
Oak Ridge National Laboratory
P. O. Box X
Oak Ridge, TN 37830

R. J. Hall
Office of Nuclear Waste
Isolation
Battelle Memorial Institute
505 King Avenue
Columbus, OH 43201

M. A. Harwell
P. O. Box 667
Cannon Beach, OR 97110

Colin A. Heath
Office of Waste Management
U.S. Department of Energy
Washington, D.C. 20545

William M. Hewitt
Office of Nuclear Waste
Isolation
Battelle Memorial Institute
505 King Avenue
Columbus, OH 43201

Peter L. Hoffmann
Office of Nuclear Waste
Isolation
Battelle Memorial Institute
505 King Avenue
Columbus, OH 43201

H. H. Holland
Department of Geological Sciences
Harvard University
Cambridge, MA 02138

No. of
Copies

Norman Hubbard
Office of Nuclear Waste
Isolation
Battelle Memorial Institute
505 King Avenue
Columbus, OH 43201

Dana Isherwood
Lawrence Livermore Laboratory
MS L-224
P.O. Box 808
Livermore, CA 94550

G. Jenks
Oak Ridge National Laboratory
P. O. Box X
Oak Ridge, TN 37830

Greg Jones
Columbia Bank Bldg.
3rd Floor
P.O. Box 800
Richland, WA 99352

Muzaffer Kehnemuyi
Office of Nuclear Waste
Isolation
Battelle Memorial Institute
505 King Avenue
Columbus, OH 43201

James Keith
Mail Code - SN7
Johnson Space Center
Houston, TX 77058

John F. Kircher
Office of Nuclear Waste
Isolation
Battelle Memorial Institute
505 King Avenue
Columbus, OH 43201

Mel Knapp
Division of Waste Management
Nuclear Regulatory Commission
Washington, DC 20555

No. of
Copies

G. A. Kolstad
Office of Basic Energy Sciences
U.S. Department of Energy
Washington, D.C. 20545

Dr. Kurt A. Kraus
110 Ogontz Lane
Oak Ridge, TN 37830

Daniel Lam
Argonne National Laboratory
Materials Science Division
Building 212
9700 South Cass Avenue
Argonne, IL 60439

S. J. Lambert
Sandia Laboratories
P. O. Box 5800
Albuquerque, NM 87115

R. B. Laughon
Office of Nuclear Waste
Isolation
Battelle Memorial Institute
505 King Avenue
Columbus, OH 43201

Darrell Leap
Denver Federal Center
U.S. Geological Survey WRD
P.O. Box 25046
MS-416
Denver, CO 80225

S. Y. Lee
Oak Ridge National Laboratory
Environmental Studies Division
Buiding 1505
Oak Ridge, TN 37830

Linda Lehman
U.S. Nuclear Regulatory Commission
Division of Waste Management
Washington, D.C. 20555

No. of Copies

David H. Lester
Scientific Applications, Inc.
P. O. Box 2351
1200 Prospect Street
La Jolla, CA 92037

Paul W. Levy
Brookhaven National Laboratory
Upton, NY 11973

Stan E. Logan
Los Alamos Technical Associates, Inc.
P. O. Box 410
Los Alamos, NM 87544

R. W. Lynch
Sandia Laboratories
P. O. Box 5800
Albuquerque, NM 87115

I. D. MacGreagor
Office of Basic Energy Sciences
U.S. Department of Energy
Washington, D.C. 20545

I. W. Marine
E. I. duPont DeNemours Co.
Savannah River Laboratory
Aiken, SC 29801

J. B. Martin
Asst. Director for Radioactive Waste Management Branch
NRC Division of Materials and Fuel Cycle Facility Licensing
Washington, DC 20555

S. C. Matthews
Office of Nuclear Waste Isolation
Battelle Memorial Institute
505 King Avenue
Columbus, OH 43201

No. of Copies

Jeff L. Means
Battelle Memorial Institute
505 King Avenue
Columbus, OH 43201

Dr. Robert E. Meyer
Oak Ridge National Laboratory
P. O. Box X
Bldg. 4500, MS-C18
Oak Ridge, TN 37830

Don Moak
Office of Nuclear Waste Isolation
Battelle Memorial Institute
505 King Avenue
Columbus, OH 43201

Martin Molecke
Sandia Laboratories
Nuclear Waste Experimental Programs
Division 4512
Albuquerque, NM 87185

Anthony N. Mucciardi
Adaptonics, Inc.
1750 Old Meadow Road
McLean, VA 22102

Bob Nebeker
Exxon Nuclear Idaho
P.O. Box 2800
Idaho Falls, ID 83401

J. O. Neff
Department of Energy
Columbus Program Office
505 King Avenue
Columbus, OH 43201

Ivars Nerentnieks
Lawrence Berkeley Laboratory
University of California
Earth Sciences Bldg. 90
1 Cyclotron Road
Berkeley, CA 94720

No. of Copies

E. Norris
Los Alamos Scientific Laboratory
CNC-11, MS-514
P. O. Box 1663

Clyde Northrup
Chemicl Technology Division
Sandia Laboratories
P.O. Box 5800
Albuquerque, NM 87185

E. J. Nowak
Sandia Laboratories
Division 5824
Albuquerque, NM 87115

Edward O'Donnell
Nuclear Regulatory Commission
Washington, D.C. 20005

Office of Radiation Programs
Technical Assessment Division
Environmental Protection Agency
Washington, DC 20460

W. M. Pardue
Office of Nuclear Waste Isolation
Battelle Memorial Institute
505 King Avenue
Columbus, OH 43201

George A. Parks
Department of Applied Earth Sciences
Stanford University
Stanford, CA 94305

M. A. Penneman
Los Alamos Scientific Laboratory
P. O. Box 1663
Los Alamos, NM 87545

Kent Peterson
U.S. Bureau of Mines
P.O. Box 1660
Twin Cities, MN 55111

No. of Copies

Gil Raines
Office of Nuclear Waste Isolation
Battelle Memorial Institute
505 King Ave.
Columbus, OH 43201

B. A. Rawles
Battelle Memorial Institute
Office of Nuclear Waste Isolation
505 King Avenue
Columbus OH 43201

Terry F. Rees
Denver Federal Center
U.S. Geological Survey
P.O. Box 25046
MS-412
Lakewood, CO 80225

Paul Rickert
Argonne National Laboratory
Building 200
9700 S. Cass Ave.
Argonne, IL 60439

Gary Robbins
Nuclear Regulatory Commission
Division of Waste Management
Washington, DC 20555

John Robertson
Office of Radio Hydrology
U.S. Geological Survey
MS-410
Reston, VA 20092

D. M. Rohrer
Nuclear Regulatory Commission
Division of Waste Management
Washington, DC 20555

D. R. Roy
Materials Research Laboratory
Pennsylvania State University
University Park, PA 16802

No. of
Copies

L. Santos
Nuclear Regulatory Commission
Mail Stop 1130-SS
Washington, DC 20555

Dr. Martin G. Seitz
Argonne National Laboratory
9700 South Cass Avenue
Argonne, IL 60439

Barry E. Scheetz
Materials Research Laboratory
Pennsylvania State University
University Park, PA 16802

Hank Schilling
Battelle Human Affairs Research Centers
4000 NE 41st Street
Seattle, WA 98105

Genevieve Segol
Bechtel Corporation
P.O. Box 3965
San Francisco, CA 94119

Martin Seitz
Argonne National Laboratory
9700 S. Case Ave.
Argonne, IL 60439

C. G. Shirley
Los Alamos Technical Association
P.O. Box 410
Los Alamos, NM 87544

Dr. Robert J. Silva
Lawrence Berkeley Laboratory
1 Cyclotron Road
Bldg. 70A/1160
Berkeley, CA 94720

D. R. Simpson
Lehigh University
Bethlehem, PA 18001

No. of
Copies

Bruce Staples
Exxon Nuclear Idaho
P.O. Box 2800
Idaho Falls, ID 83401

David B. Stewart
U.S. Geological Survey
National Center 959
Reston, VA 22092

H. P. Stephens
Sandia Laboratories
Albuquerque, NM 87115

Joseph L. Thompson
Department of Chemistry
Idaho State University
P.O. Box 8397
Pocatello, ID 83209

Daryl Tweeton
U.S. Bureau of Mines
P.O. Box 1660
Twin Cities, MN 55111

Elizabeth R. Vine
Los Alamos Scientific Laboratory
CNC-11, MS-514
Los Alamos, NM 97545

R. L. Watters
Department of Energy
Office of Biomedical and Environmental Research
Washington, DC 20545

Homer C. Weed
Lawrence Livermore Laboratory
MS-L350
P.O. Box 808
Livermore, CA 94550

Allen Weiss
Brookhaven National Laboratory
Building 830
Upton, NY 11973

No. of
Copies

William B. White
Materials Research Laboratory
Pennsylvania State University
University Park, PA 16802

W. A. Williams
Office of Radiation Programs
Environmental Protection Agency
Washington, DC 20460

Willste Library
Nuclear Regulatory Commission
Washington, DC 20555

Tom Wolery
Lawrence Livermore Laboratory
P.O. Box 808 MS-L224
Livermore, CA 94550

Kurt Wolfsberg
Los Alamos Scientific Laboratory
CNC-11, MS-514
Los Alamos, NM 87545

R. Wunderlich
Department of Energy
Columbus Program Office
505 King Avenue
Columbus, OH 43201

H. Tom Yolken
National Bureau of Standards
Physics Building 1B230
Washington, DC 20234

FOREIGN

B. Allard
Chalmers University
S-402
20 Goteborg 5
SWEDEN

No. of
Copies

D'Allessandro Avogadro
Commission of European
Communities
Joint Research Centre
I-21020 Ispra (Varese)
ITALY

L. R. Dole
Institut fur Tieflagerung
Wissenschaftliche Abteilung
Berliner Strasse 2
3392 Clansthal Zellerfeld
F.R. of GERMANY

Ferruccio Gera
Radiation Protection and
Waste Management Division
Nuclear Energy Agency/OECD
38 boulevard Suchet
75016 Paris
FRANCE

David Grey
Institute of Geologic Sciences
Exhibition Road
S. Kensington
London, SW7-2DE
UNITED KINGDOM

Owe Landstrom
Studsvik Emergiteknik AB
S-611 82 Nykoping
SWEDEN

H. Lang
Inst. F. Radiohydrometrie der
Gesellschaft Fuer Strahlen-
und Umweltfopschung
Ingolstaedter Landstrasse 1
8042 Neuherberg
GERMANY

No. of Copies

Hans W. Levi
Hahn-Meitner-Institut fur Kernforschung
Glienicker Strasse 100
1000 Berlin 39
F.R. of GERMANY

Ian McKinley
Environmental Pollution Section
Building 151
Harwell Laboratory
Oxfordshire, Ox 11 ORA
UNITED KINGDOM

Franz Peter Oesterle
Physikalisch-Chemische Bundesanstalt
Bundesallee 100
D-3300 Braunschweig
F.R. of GERMANY

Peter Sargent
Atomic Energy of Canada
Whiteshell Nuclear Research Establishment
Storage and Disposal Branch
Pinawa, Manitoba, REO 1LO
CANADA

T. Chuck Vandergraff
Atomic Energy of Canada
Whiteshell Nuclear Research Establishment
Pinawa, Manitoba REO 1LO
CANADA

ONSITE

4 DOE Richland Operations Office

O. J. Elgert
H. E. Ransom
J. J. Schreiber
F. R. Standerfer

No. of Copies

3 Hanford Engineering Development Laboratory

D. A. Cantley
D. E. Clark
A. C. Leaf

8 Rockwell Hanford Operations

G. Scott Barney
G. E. Brown
W. Coons
S. A. Gallagher
R. E. Johnston
R. Reitz
R. A. Deju
M. J. Smith

62 Pacific Northwest Laboratory

L. L. Ames
D. J. Bradley
A. Brandstetter
A. C. Campbell
D. B. Cearlock/G. W. Dawson
T. D. Chikalla
M. O. Cloninger
W. J. Deutsch
F. H. Dove
H. Drucker
C. E. Elderkin
R. W. Fulton
J. K. Gower
C. R. Hann
D. D. Hostetler
J. H. Jarrett
C. G. Jordan
Y. B. Katayama
M. R. Kreiter
K. M. Krupka
W. L. Kuhn
L. T. Lakey
D. E. Larson/E. Wheelright
J. L. McElroy/R. E. Nightingale

No. of Copies

G. L. McVay
W. J. Martin
D. A. Moore
R. D. Nelson/W. A. Ross/O. F. Hill
J. M. Nielson
C. R. Palmer/R. O. Lokken/
A. D. Chockie/G. B. Mellinger
H. M. Parker
A. M. Platt
D. Rai
J. F. Relyea
J. L. Ryan
J. M. Rusin/R. P. May
R. J. Serne
J. W. Shade
D. J. Silviera

No. of Copies

R. G. Strickert
A. M. Sutey
J. L. Swanson
R. P. Turcotte/D. M. Strachen
H. H. VanTuyl
B. E. Vaughn
R. Wang
C. D. Washburne
R. E. Westerman/L. A. Charlot/
L. A. Chick
J. H. Westsik
L. D. Williams
Water and Land Resources
Library (6)
Technical Information (5)
Publishing Coordination (SH)(2)